REVEALING THE ART AND SCIENCE OF SELF-REPLICATING ROTAXANES

Nurul Izzaty Hassan

A Thesis Submitted for the Degree of PhD
at the
University of St Andrews

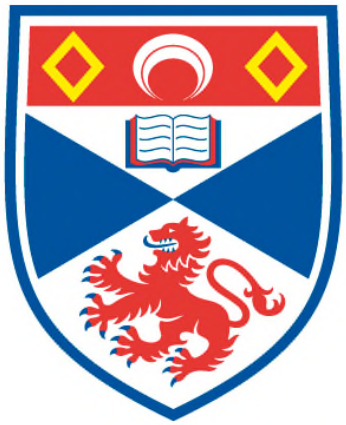

2012

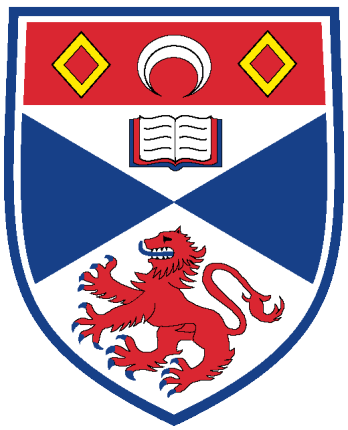

University
of
St Andrews

Revealing the art and science of self-replicating rotaxanes

by

Nurul Izzaty Hassan

A Thesis presented for the
Degree of Doctor of Philosophy
in the
School of Chemistry
University of St Andrews

December 2011

1. Candidate's declarations:

I, Nurul Izzaty Hassan hereby certify that this thesis, which is approximately……. words in length, has been written by me, that it is the record of work carried out by me and that it has not been submitted in any previous application for a higher degree.

I was admitted as a candidate for the degree of PhD in January, 2008; the higher study for which this is a record was carried out in the University of St Andrews between 2008 and 2011.

Date …….. signature of candidate ……..

2. Supervisor's declaration:

I hereby certify that the candidate has fulfilled the conditions of the Resolution and Regulations appropriate for the degree of PhD in the University of St Andrews and that the candidate is qualified to submit this thesis in application for that degree.

Date …….signature of supervisor ……..

3. Permission for electronic publication: (*to be signed by both candidate and supervisor)*

In submitting this thesis to the University of St Andrews I understand that I am giving permission for it to be made available for use in accordance with the regulations of the University Library for the time being in force, subject to any copyright vested in the work not being affected thereby. I also understand that the title and the abstract will be published, and that a copy of the work may be made and supplied to any bona fide library or research worker, that my thesis will be electronically accessible for personal or research use unless exempt by award of an embargo as requested below, and that the library has the right to migrate my thesis into new electronic forms as required to ensure continued access to the thesis. I have obtained any third-party copyright permissions that may be required in order to allow such access and migration, or have requested the appropriate embargo below.

The following is an agreed request by candidate and supervisor regarding the electronic publication of this thesis:

(iii) Embargo on both [all] of printed copy and electronic copy for the same fixed period of 1 year on the following ground(s):

publication would be commercially damaging to the researcher, or to the supervisor, or the University;
publication would preclude future publication;

Date ……signature of candidate ……..signature of supervisor ……

Table of contents

Synopsis ix-xi

Acknowledgements xii-xiv

Abbreviations xv-xvi

Chapter 1 – Introduction 1-39

1.1	Supramolecular chemistry	1
1.2	Minimal model of self-replication	3
1.3	Reciprocal model of self-replication	5
1.4	The do's and the don'ts in self-replication	6
1.4.1	What usually goes wrong?	6
1.4.2	What happens if it works well?	11
1.4.3	The need for control experiments	12
1.4.4	How to optimize the conditions?	15
1.5	Examples of self-replicating systems	16
1.5.1	Self-replicating systems based on oligonucleotides	16
1.5.2	Self-replicating systems based on RNA	20
1.5.3	Self-replicating systems based on polypeptides	22
1.5.4	Self-replicating systems based on small organic molecules	26
1.5.5	Self-replicating systems based on Diels-Alder reaction	33
1.6	Outlook	39

Chapter 2 - Chemical topology and mechanically interlocking molecules 41-61

2.1	Nomenclature for mechanically interlocked system	42
2.2	The chemistry of the mechanical bond	43
2.3	Pseudorotaxanes	44
2.4	How to synthesise a [2]-rotaxane?	46
2.4.1	Clipping mechanism	48
2.4.2	Threading and stoppering mechanism	48
2.4.3	Slippage mechanism	49
2.5	Template synthesis of interlocked molecules	50
2.5.1	Transition metal templates	51
2.5.2	π-donor or π-acceptor templation	52
2.5.3	Hydrogen bond templation	53
2.6	Applications in devices	56

Chapter 3 - Integrating self-replication process within rotaxane formation 63-76

3.1	Introduction	63
3.2	Essential requirements	63
3.2.1	Recognition site	64
3.2.2	Reactive site	65
3.2.3	Binding site	67
3.3	Association constant, K_a	68
3.3.1	High association constant is crucial	69
3.4	Minimal replication model of self-replicating rotaxanes	70
3.4.1	Replication model 1	70

3.4.2 Replication model 2 73
3.4.3 Replication model 3 74
3.5 Summary 76

Chapter 4 - Design, synthesis and binding properties of macrocycles 77-109

4.1 Introduction 77
4.2 First generation macrocycles 77
4.2.1 Ethylene urea macrocycle (**MEU**) 78
4.2.2 Binding studies – **MEU** 80
4.2.3 Acyclic urea macrocycle (**MAU**) 88
4.2.4 Symmetrical macrocycle (**SM**) 92
4.3 Second generation of macrocycles – Alternative synthesis 93
4.3.1 Alkyne ethylene urea macrocycle (**MAEU**) 94
4.3.2 Diethylene glycol macrocycle (**MDG**) 95
4.3.3 Binding studies – **MDG** 97
4.3.4 Pyridine macrocycle (**MP**) 103
4.3.5 Binding studies – **MP** 104
4.4 Conclusion 109

Chapter 5 - Replication model 1 111-143

5.1 Introduction 111
5.2 Structural invariances of thread component 112
5.3 Improving the synthesis of the nitrone **115** 114
5.4 Synthesis of the model maleimides 114
5.5 Kinetic analysis of thread 116
5.5.1 Reaction with short CH_3 maleimide **108** 116
5.5.2 Reaction with long CH_3 maleimide **109** 117
5.5.3 Reaction with CF_3 amide maleimide **110** 118
5.5.4 Reaction with CF_3 urea maleimide **111** 119
5.6 Synthesis of the control nitrone 120
5.7 Kinetic analysis of simple rotaxane formation 120
5.7.1 Comparison of the analysed systems 130
5.8 Kinetic analysis of simple rotaxane formation 2 133
5.8.1 Synthesis of the control nitrone 2 133
5.9 Computational study 138
5.10 Conclusion 142

Chapter 6 - Low temperature capture of pseudorotaxanes 145-155

6.1 Introduction 145
6.2 An alternative stoppering reaction 147
6.3 Conclusion 155

Chapter 7 - Replication model 2 157-212

7.1 Introduction 157
7.2 Synthesis of control macrocycles 158
7.3 Binding studies – **cMDG** and **cMP** 163

7.4 Synthesis of a potential self-replicating rotaxane 169
7.5 Synthesis of acid recognition macrocycles 169
7.5.1 Synthesis of acid recognition macrocycles with ethynylbenzene spacer 172
7.5.2 Synthesis of acid recognition macrocycles with phenyl spacer 174
7.6 Binding studies with maleimides 176
7.7 Design of a potential self-replicating rotaxane 187
7.7.1 Synthesis of first generation nitrones 187
7.7.2 Binding studies with first generation nitrones 190
7.7.3 Improving the design for second generation nitrones 191
7.7.4 Binding studies with second generation nitrones 193
7.7.5 Synthesis and binding study with third generation nitrone 195
7.8 Design of a potential self-replicating rotaxane 2 198
7.9 Design of a potential self-replicating rotaxane 3 198
7.9.1 Binding study with maleimide **198** 199
7.9.2 Kinetic study of the thread 201
7.9.3 Kinetic study of the rotaxane 204
7.10 Conclusion 212

Chapter 8 - Replication model 3 213-239

8.1 Introduction 213
8.2 Design of a potential self-replicating rotaxane 214
8.2.1 Binding study 215
8.2.2 Kinetic study of the thread 215
8.2.3 Kinetic study of the rotaxane 218
8.3 Modified design of a potential self-replicating rotaxane 222
8.4 Synthesis of the nitrone 224
8.5 Binding study with CF_3 nitro **209** 229
8.6 Binding study with OC_8H_{17} nitro **213** 233
8.7 Conclusion 239

Chapter 9 - General conclusion 241-242

Chapter 10 - Experimental and synthetic procedures 243-311

10.1 General experimental procedures 243
10.2 General NMR spectroscopy procedures 244
10.3 ^{1}H NMR spectroscopy : Preparation, kinetic measurements and deconvolution data 245
10.4 ^{19}F NMR spectroscopy : Preparation, kinetic measurements and deconvolution data 249
10.5 Determination of binding constants 251
10.6 Computational methods 251
10.7 Kinetic simulation and fitting 251
10.8 Synthetic procedures 252

References 313-321

Appendixes A-C

Synopsis

This Thesis reveals the strategies for the construction and replication of mechanically interlocked molecules, particularly rotaxanes, which consist of a macrocyclic ring that encircles a linear component terminated with bulky groups. The work highlights our recent research activities in exploring the recognition-mediated synthesis of this class of interlocked molecule and its amplification by replication. Our starting point is the minimal model of self-replication.

The introductory chapters (**Chapter 1** and **2**) provide some background and significance to the study, which presents comprehensive review of the published work carried out in the area of self-replication with existing examples from biomimetic and discrete synthetic assemblies. In **Chapter 1**, we mainly discuss the do and the don'ts in designing successful self-replicating systems based on our own experience in previous work. Our chief concerns in **Chapter 2** are the understanding of the chemistry of the mechanical bond and the synthesis of rotaxanes by three means of approaches (clipping, threading and stoppering, and slippage). Attractive and useful examples are illustrated for each mechanism. Moreover, the definition and the roles of templated-synthesis of interlocked molecules are described. Recent advances in the understanding of the nature of the mechanical bond have also been introduced into molecular electronic devices.

Emphasis is placed in **Chapter 3** upon the essential requirements for the design of self-replicating rotaxanes, namely a recognition site, a reactive site and a binding site. These aspects are explained in the designed minimal model chosen in the past (**Replication model 1**) and the alternate proposed models (**Replication model 2** and **Replication model 3**). The importance of high association constant to provide substantial amount of pseudorotaxane [**L•M**] precursors is exemplify in the simple kinetic model of rotaxane formation. The advantages and disadvantages of each independent minimal replication model are also summarized.

In the self-replicating rotaxane frameworks, the principal strategy involves a selection of an efficient macrocycle to accommodate the guest unit. Thus, **Chapter 4** exclusively describes the design, synthesis and binding properties of a series of

macrocycle incorporating the hydrogen bond donors and/or hydrogen bond acceptors motif. In particular, the guests were designed and synthesised based on the mutual interactions with the macrocycle framework and the binding experiments is described in details. An account is provided of the problems faced in the synthetic attempts towards the formation of these macrocycles. The novel macrocycle **MEU** demonstrated a deficient binding performance with amide and urea compounds, and thus abandoned in later stages. The developed macrocycle **MDG** and **MP** have been selected as our workhorse macrocycles, which successfully increase the binding strength in the pseudorotaxanes formation. We have learnt that the association constant, K_a can be manipulated by the changing the binding site of the guest or redesign the framework of the macrocycle itself.

An exhaustive investigation of the performance of self-replicating rotaxanes focuses on **Replication model 1** is demonstrated in **Chapter 5**. It was evident now that as a consequence of low K_a, a substantial amount of thread is present over rotaxane. The implementation of the simple kinetic model of rotaxane formation is prevailed through out this chapter. The position of the central reversible equilibrium in this model effectively resulted in a different reactivity of thread and rotaxane. Therefore, it is concluded that the ratio of rotaxane and thread is sensitive to both the association constant for the [**L•M**] complex and to the ratio of $k_{rotaxane}/k_{thread}$.

The key marker for the efficiency of the rotaxane-forming protocol is the ratio of rotaxane, **R** to thread, **T**. In previous chapter, the K_a for the [**L•M**] complex was around 100 M^{-1} and $k_T = 3\ k_R$, which led to an unacceptably small [**R**]/[**T**] ratio. We demonstrated for the first time in **Chapter 6**, that it is possible to manipulate the K_a for the [**L•M**] complex by means of a change in temperature. Yields of a rotaxane can be improved by employing a two-step capture protocol. Cooling a solution of the linear and macrocyclic components required for the rotaxane increases the population of the target pseudorotaxane, which is then captured by a rapid capping reaction between an azide and PPh_3. The resulting iminophosphorane rotaxane can then be manipulated synthetically at elevated temperatures. Following this, these imines could be reduced readily to afford the stable amine rotaxane.

Replication model 2 is subsequently proposed as alternate replication framework in **Chapter 7**, which realised significant advantages over the first model. A number of designs of a potential self-replicating rotaxane have been fabricated in order to integrate self-replication with the formation of rotaxanes. An account is provided of the problems faced with the unanticipated larger cavity of the newly prepared acid recognition macrocycles, and hence, force us to search for a new scaffold of the nitrone structures. Pleasingly, a substantial amount of rotaxane was present, mostly as *trans* diastereoisomer. It is concluded that the resulting rotaxane structures may be self-replicating through the recognition-mediated pathways from the preliminary kinetic experiments. Nonetheless, the remainder of the full kinetic analysis are prevented given a small quantity of the necessary building block.

Chapter 8 reveals our recent efforts to demonstrate the notions behind the final replication scheme, **Replication model 3**. We have become aware that the reactive site must be placed sufficiently far away from the binding site to inhibit the remote steric effect through the proximity of the macrocyclic component. The design of novel nitrone structures is described in details. We bring together conclusions that can be drawn from three designated replication models in **Chapter 9**. Experimental and synthetic procedures of the target compounds and appropriate spectroscopic analysis of the products are elaborated in **Chapter 10**.

Acknowledgements

Praise be to Allah, the most Beneficient and the most Merciful and salutations be upon His messenger Muhammad (peace upon him), his family and his companions.

I have greatly enjoyed the years (2008 – 2011) I have spent at University of St Andrews and it will be hard to express my thanks to the many people to whom I am indebted to for such unforgettable experiences.

First, I was fortunate to have Professor Douglas Philp as my supervisor. I appreciate the energy, enthusiasm and support that Doug provided during my graduate career. The door of his office was always open for me, he always welcomed new ideas, and would have an interesting suggestions when the experiment did not work. Most of all, I value the freedom that Doug gave me in conducting research.

When I joined the DP group, I was working closely on the experiments with Dr Annick Vidonne about mechanically interlocked architectures and learned many useful things about lab management and experimental techniques. The DP group was an interesting place to work and I would like to thank some of its former and current members for providing a friendly working environment, and for lending a hand or a good word when I needed them: Dr Jürgen Huck, Dr Ilaria Bottero, Dr Craig Robertson, Dr Vicente del Amo, Dr Jan Sadownik and Harry Mackenzie.

Technical staffs of the School of Chemistry for their quality work on the parts of my experiment, Caroline Horsburgh for mass spectrometry analyses, Catherine Botting for the MALDI spectrometry, Dr Tomas Lebl and Melanja Smith was helpful with all the NMR experiments. With (Dr) Noor Akmal Shareela Ismail, (Dr) Nurul Liyana Berahim, (Dr) Siti Marwanis Anuar and (Dr) Mazlina Musa, my long time friends, I had many discussions about science and life in general. And to my St Andrews's junior doctors and physiologist - (Dr) Eddy Shah Razdi Baharuddin, (Dr) Leyla Nadia Kamil, (Dr) Nur Atiqah Ramli, (Dr) Nasrul Asyraf Saiful Yazan and Siti Sabariah Ahmad Murtazam : The hope, the struggle and the hard work towards a goal itself is part of the rewards. Achieving goal itself is not the whole rewards. All best wishes!!

Finally, I would like to my family, especially my parents, Hj Hassan Puteh and Hjh Che Puteh Mohd Noor and my three brothers, Mohd Fahmi, Mohd Fairus Naqim and Mohd Fauzal Hassan. They always provided me with freedom of choice and supported my interest in science, even when that interest led me to distant shores.

And it is to my parents that I dedicate this thesis.

Abbreviations

A	Hydrogen bond acceptor
B3LYP	Becke, 3 parameters, Lee, Yang and Parr
C	Cytidine
$CBPQT^{4+}$	cyclobis (paraquat-*p*-phenylene) tetracation
CI	Chemical Ionisation
conc.	concentrated
d	doublet
D	Hydrogen bond donor
DB24C8	dibenzo-24-crown-8
decomp.	decomposed
DEPTQ	Distorsionless Enhancement by Polarization Transfer including the detection of Quarternary nuclei
DFT	Density Functional Theory
DMF	Dimethylformamide
DMSO	Dimethyl sulfoxide
DNA	Deoxyribonucleic acid
DNP	1,5-dioxynaphthalene
EDC/EDCI	*N*'-(3-dimethylaminopropyl)-*N*-ethyl-carbodiimide
EI	Electron Impact
ES	Electrospray
EXSY	Exchange SpectroscoPY
g	gram(s)
G	Guanosine
h	hour(s)
HMDS	Hexamethydisilazane
HPLC	High-Performance Liquid Chromatography
HRMS	High Resolution Mass Spectrometry
K_a	Association constant
K_d	Dissociation constant
lit.	literature
M	Molar

m	multiplet
m	meta
MALDI	Matrix Assisted Laser Desorption/Ionization
Me	Methyl
mg	miligram
MHz	Megahertz
min	minute(s)
mL	milileter
mM	milimolar
mmol	milimol
M.p.	Melting point
MPTTF	Monopyrrolo Tetrathiafulvalene
MS	Mass Spectroscopy
NMR	Nuclear Magnetic Resonance
NOE	Nuclear Overhauser Effect
o	ortho
p	para
Pd/C	Palladium on activated carbon
Rh/C	Rhodium on activated carbon
ROESY	Rotating frame Overhauser Effect SpectroscopY
RNA	Ribonucleic acid
rt	room temperature
s	second(s) / singlet
sat.	saturated
t	time / triplet
TFA	Trifluoroacetic Acid
THF	Tetrahydrofuran
TLC	Thin Layer Chromatography
TS	transition state
TTF	Tetrathiafulvalene
UV	Ultraviolet
wt.	weight

1

Introduction

1.1 Supramolecular chemistry

Supramolecular chemistry has been defined as chemistry beyond the molecule[1,2] more than three decades ago as one of the most active fields of science, and has grown enormously in importance. The initial motivation in the early history[3,4] of supramolecular chemistry was to design chemical systems that mimic[5] biological processes. Biological phenomenal exploited the wide range of weak, non-covalent interactions[6,7] which are responsible for the selective transport of ions and small molecules across membranes, nucleic acid's transcription and translation, virus assembly and action, and the tertiary and quaternary structure of proteins. Nowadays, much work in supramolecular chemistry has been focusing on molecular design to achieve complementarity between molecule hosts and their guests.

The principle of complementarity follows that to complex, a host must have binding sites that can simultaneously contract and attract the binding sites of guest without generating internal strains or strong non-bonded repulsions[4,8]. Thus, complementarity is the key determinant of structural recognition. Besides complementarity, self-assembly[9], recognition[10,11], preorganisation[12-14] and even self-replication[15] represent important key words in the armoury of the supramolecular chemist[16].

Self-assembly may be defined as the process by which a supramolecular entity forms spontaneously from its components. For the majority of synthetic systems it appears to be a beautifully simple convergent process which give rise to the assembled target in a straightforward[9] manner. Like self-assembly, molecular recognition are widespread phenomena both in nature and synthetic systems. The birth of molecular recognition in the supramolecular sense can be traced back to Pedersen's work on

crown ethers and the discovery[17] of their affinities for Group 1 metal cations. In that case, selectivity was determined[18] by the size of the metal cation and the diameter of the crown ether. It needs to be noted that it is the degree of electronic and steric complementarity between host and guest that dictates the magnitude of any molecular recognition that occurs for a given supramolecular system. Essentially, it is instructive to consider the relationship between molecular preorganisation[4,12-14], recognition and self-assembly in relation to the formation of supramolecular complex. Fundamentally, all three will play a sequential role in complexation. Specifically, appropriate preorganisation of the binding sites in the host to receive the guest thus predisposes the former for guest recognition. This predisposition, in turn, promotes spontaneous self-assembly of the required supramolecular entity. There is no doubt that self-assembly can be utilized to construct[5] a wide diversity of structural types with apparent ease.

In addition to the above, this new chemistry has provided synthetic systems capable of self-replication[19-21] by examining the way nature accomplishes these objectives and demonstrated these in a chemical context. The ability of nucleic acids to act as templates for self-replication is a fundamental process in Nature's chemistry. Synthetic self-replicating system are of special interest in bioorganic and supramolecular chemistry since these fields may contribute[15] experimentally to the understanding of the Origin of Life. This fascinating idea that a molecule can generate or catalyse its own formation by acting the same way as nucleic acids[22] to act as templates for self-replication are well introduced in both the natural and synthetic models in recent years.

Additionally, an understanding of molecular replication may be also helpful to simulate self-replication, mutation, and evolution in non-natural environments[15] such as computers or other technical devices. In the following section, the two elementary models of replication are described and evaluated. We will then mainly focus on development and design of synthetic replication processes to produce artificial self-replicating systems in order to provide a sufficient background in this thesis.

1.2. Minimal model of self-replication

The simplest published[23] framework of non-enzymatic systems can be conceptualized in a simple three pathways model. The initial pathway can be regarded as the uncatalysed bimolecular reaction composed of two substrate molecules, **A** and **B**, that become joined to form the template molecule, **T** (**Figure 1.1**). This reaction is facilitated by random collisions and, hence, slow and unselective pathway in the system. However, as a consequence of the presence of the recognition sites (green cartoons), reagents **A** and **B** can associate with each other to form a binary complex, [**A**•**B**]. The formation of this complex open the second pathway, the binary complex [**A**•**B**] pathway, in which this complex has the ability to bring the reactive sites (blue cartoons) in **A** and **B** into close proximity and the reaction is rendered pseudointramolecular.

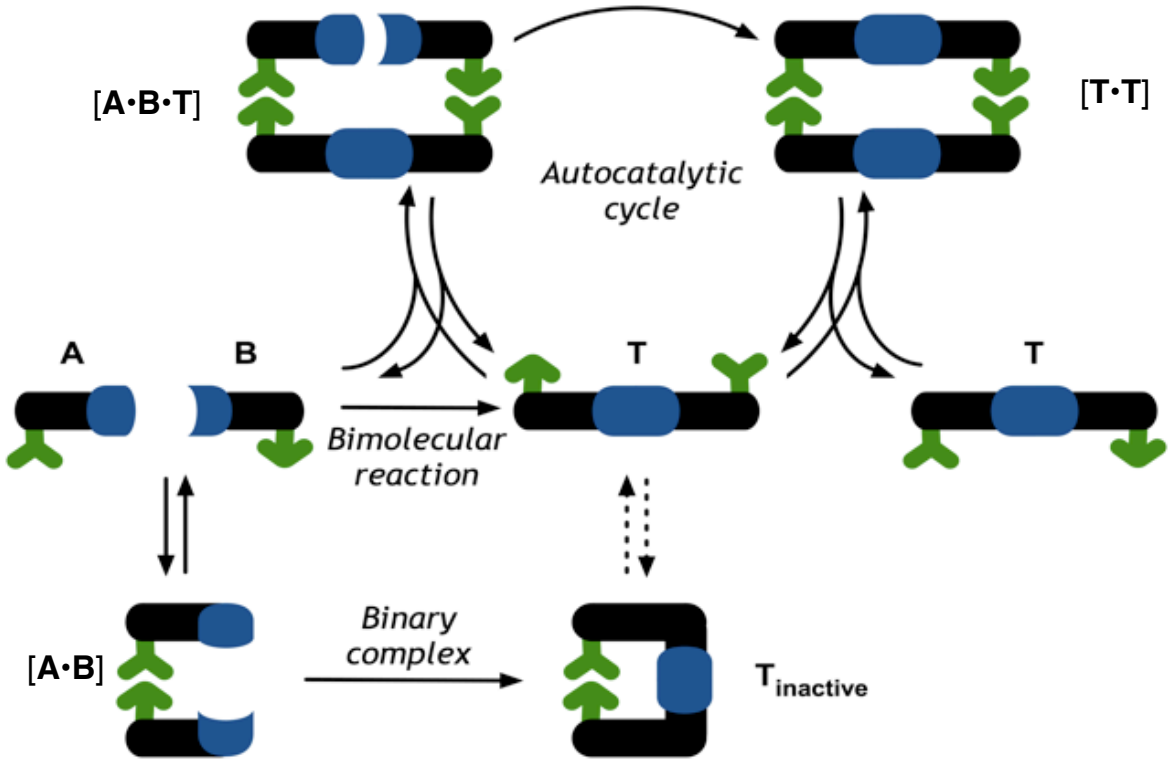

Figure 1.1. The minimal model of self-replication. Molecules **A** and **B** can react through three pathways, namely an uncatalysed bimolecular reaction, a recognition-mediated psseudounimolecular pathway mediated by a binary complex [**A**•**B**] and a recognition-mediated pseudounimolecular autocatalytic cycle mediated by a ternary complex [**A**•**B**•**T**].

Consequently, reaction through this pathway leads to the closed template $\mathbf{T}_{\text{inactive}}$ in which the recognition sites used to assemble the binary complex remain associated together. Therefore, although rate acceleration[24,25] is achieved by this mechanism

relative to the background bimolecular rate, this product is catalytically inert. The third reaction channel available in the system is the autocatalytic cycle. In contrast to $\mathbf{T}_{inactive}$, the template **T** formed through the bimolecular reaction has its recognition sites open to the solution. In this channel, **A** and **B** binds reversibly to the open template **T** to form a catalytic ternary complex [**A•B•T**]. In a manner similar to the [**A•B**] complex, the reaction between **A** and **B** is also rendered pseudointramolecular. Bond formation occurs between **A** and **B** to give the product duplex [**T•T**], which then dissociates to return two molecules of **T** to initiate a new autocatalytic cycle. The dissociation of [**T•T**] duplex is a key consideration in the design of replicating systems and for efficient autocatalytic turnover as its stability must be lower or comparable to that of the ternary complex [**A•B•T**]. Thus, the autocatalytic function of self-replicating template is only completed, when the product duplex dissociates to return two free templates to the reaction mixture. The autocatalytic cycle can potentially lead to exponential growth of **T** as two templates makes four, four make eight and so on, until reagents **A** and **B** are consumed. Thus, the important property of the template **T** is to catalyse the formation of additional template, which results in an autocatalytic behavior.

In this respect, the template **T** is capable of transmitting the molecular information such as stereo or regiochemistry through the formation of identical template molecules. Even so, such ideal acceleration is hardly illustrated in real closed systems and remained to be challenging. In essence, a system in which self-replication is operating can be defined[26] as an autocatalytic reaction. The characteristic of self-replicating reaction is apparent from the concentration *vs* time profile, which displays a non-linear sigmoidal growth profile consisting of a lag period in the early stages of the reaction (**Figure 1.2a**). The product is formed slowly through the bimolecular process because there is no product **T** available to catalyse the reaction.

As soon as the critical concentration of **T** is reached, the autocatalytic cycles can start to operate and the reaction achieve the maximum autocatalytic rate before the starting reagents are fully consumed (reactant limiting stage). Accordingly, the rate *vs* time profile can be constructed (**Figure 1.2b**) by extracting the first derivative of the concentration *vs* time profile. Whilst the minimal self-replication scheme in **Figure 1.1**

illustrates the basic action of this type of system, more intricate model is required to illustrate the many other interactions inherent in this system. These additional considerations will be highlighted in the next section.

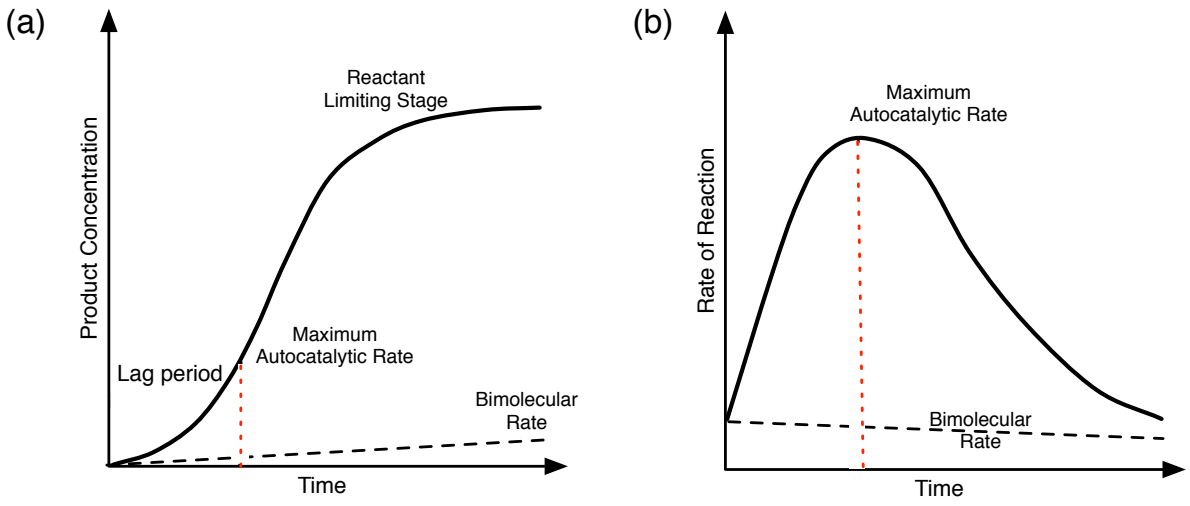

Figure 1.2. (a) Concentration *vs* time profile for the formation of replicators (solid line) and the corresponding bimolecular rate reaction (dashed line) and (b) Rate *vs* time profile of replicators (solid line) and the corresponding bimolecular reaction (dashed line). Red dashed line point out the maximum autocatalytic rate in each profile.

1.3 Reciprocal model of self-replication

The intrinsic concept in this type of replication is a crosscatalytic reaction, in which one strand acts as a catalyst for the formation of another strand and *vice versa*. Therefore, two interlinked crosscatalytic cycles in this reciprocal model rely on each other, in which the two templates catalyse the formation of each other. The implementation model of such crosscatalytic self-replicating system can be illustrated in **Figure 1.3**.

It is, however, important to note that the complexity of this system can increase dramatically depending on the nature of the chemical reaction that forms the two templates. In the case where the reaction between **C** and **D** and the reaction between **E** and **F** are orthogonal, only one reciprocal replication cycle is present in the system. However, if **C** can react with **E** and **D** with **F**, four replication cycles can be envisaged, namely two minimal replication cycles – $\mathbf{T_{CE}}$ and $\mathbf{T_{DF}}$ may self-replicate and the original reciprocal replication cycle, $\mathbf{T_{CD}} \rightarrow \mathbf{T_{EF}}$ and $\mathbf{T_{EF}} \rightarrow \mathbf{T_{CD}}$. Eventually, the minimal replicators $\mathbf{T_{CE}}$ and $\mathbf{T_{DF}}$ may cross-catalyse the formation of each other.

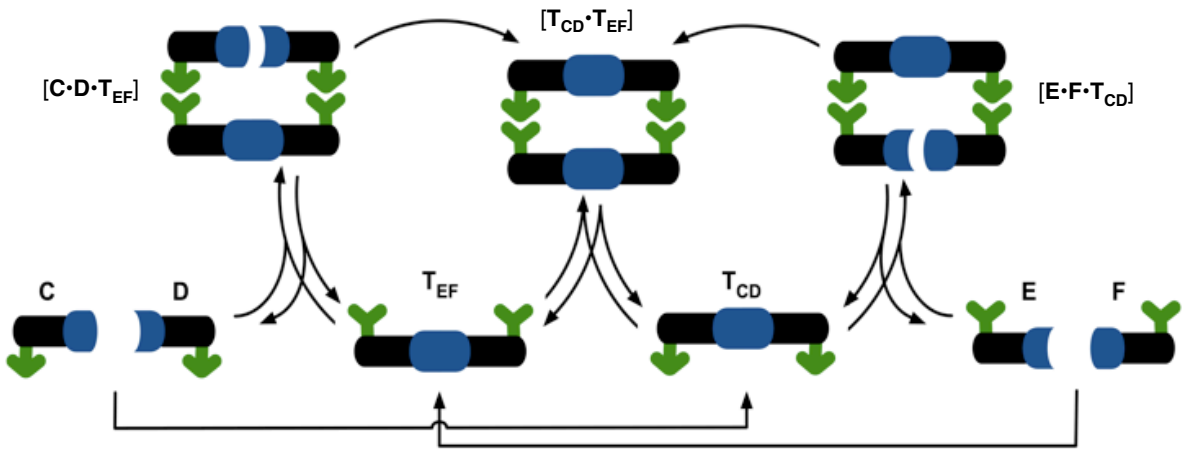

Figure 1.3. The reciprocal model of self-replication comprised two interlinked crosscatalytic cycles. In these systems, compounds **C** and **D** can react to form the template $\mathbf{T_{CD}}$, and, similarly, compounds **E** and **F** can react to form template $\mathbf{T_{EF}}$. Since the four reactive partners bear recognition sites (green coloured cartoons) and since $\mathbf{T_{CD}}$ and $\mathbf{T_{EF}}$ are mutually complementary, $\mathbf{T_{CD}}$ is capable of assembling **E** and **F** into the ternary complex [**E**•**F**•$\mathbf{T_{CD}}$]. This ternary complex intramolecularizes the reaction between **E** and **F** and hence, catalyses the formation of $\mathbf{T_{EF}}$. Similarly, $\mathbf{T_{EF}}$ is capable of assembling **C** and **D** into the ternary complex [**C**•**D**•$\mathbf{T_{EF}}$] and catalyse the formation of $\mathbf{T_{CD}}$.

1.4 The do's and the don'ts in self-replication

Self-replicating systems usually are limited in their ability to undergo efficient autocatalytic self-replication. One of the factors relies on the design of the replicator itself. Therefore, we will try to justify the ideal conditions attempted to improve the systems. All these observations are demonstrated from the self-replicating systems developed in our laboratory. We have investigated different reactions, building block geometries and substitution patterns which leads to a concise understanding of the mechanism of self-replication and successfully discover some efficient replicators.

1.4.1 What usually goes wrong?

We noticed that there are two recognition-mediated pathways exist in the minimal model of self-replication (see **Figure 1.1**), namely the [**A**•**B**] complex pathway and the autocatalytic cycle accomplishing the same target, that is the acceleration of a chemical reaction. In principle, given sufficient conformational freedom and the location of complementary recognition sites on two reagents **A** and **B** permits the association of **A** and **B** through their mutually compatible recognition site to form a complex, [**A**•**B**]. Within the [**A**•**B**] complex, the chemical reaction between **A** and **B** is effectively intramolecular, and thus, we would then expect the formation of the [**A**•**B**]

complex to accelerate the transformation involving reagents **A** and **B** significantly.

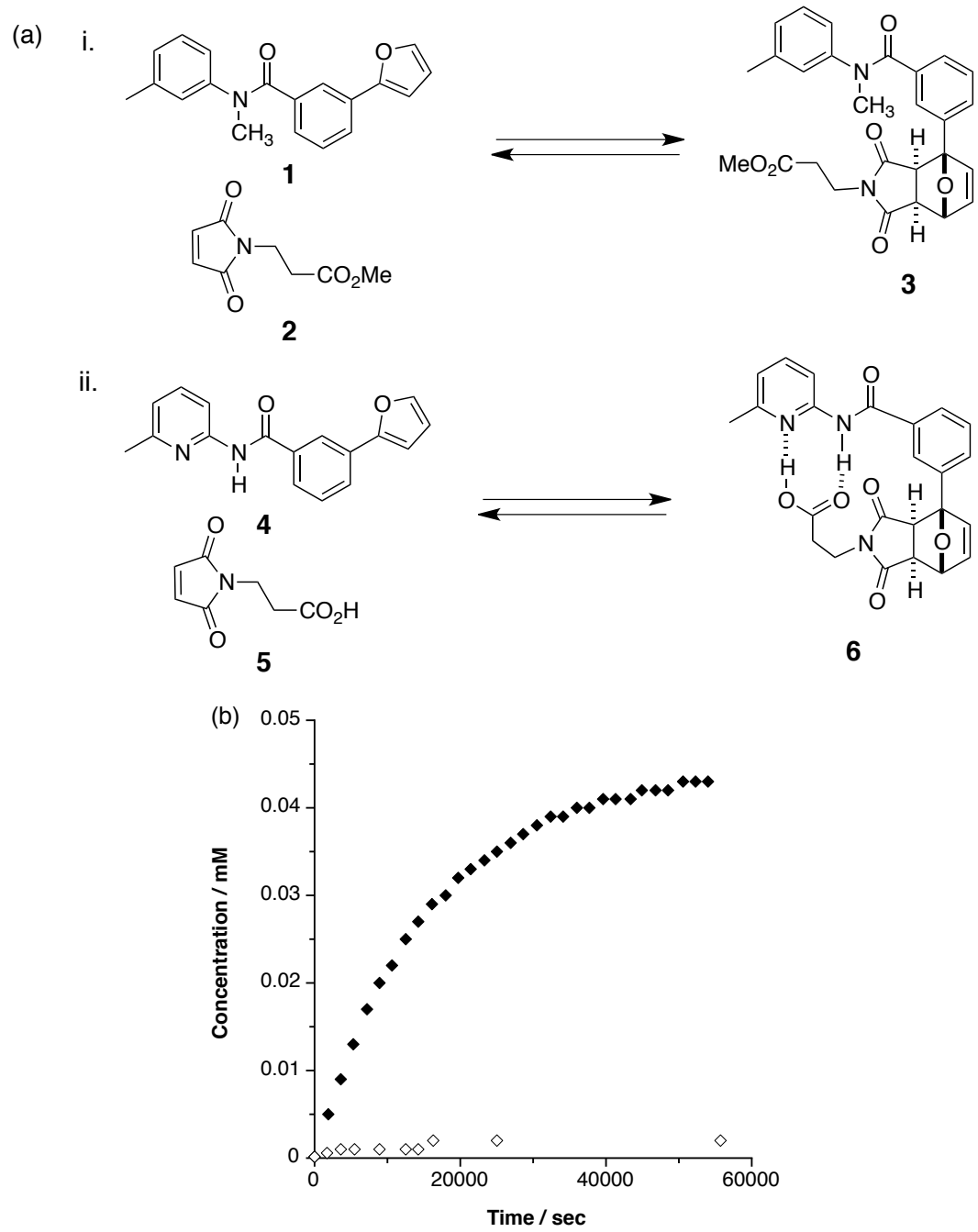

Figure 1.4. (a) i. Scheme reaction between diene **1** and maleimide **2** in $CDCl_3$ at 50 ˚C and ii. Scheme reaction between diene **4** and maleimide **5** in $CDCl_3$ at 50 ˚C. In both cases, the starting concentrations of the reactants were 100 mM; (b) The filled squares represent the concentration of the *exo* cycloadduct **6** and the open squares represent the concentration of the *exo* cycloadduct **3**. Figure taken from reference 27.

The [**A**•**B**] complex pathway however differ from latter pathway, as such it does not involve any form of *recognition-mediated catalysis* because the closed template $\mathbf{T}_{inactive}$ does not play any further role in the reaction process. In comparison, the autocatalytic cycle in the self-replicating system has become an appealing aim to amplify a targeted structure over others in the design systems. We have described a

recognition-based systems which can accelerate the rate and control the stereochemical outcome of Diels-Alder reaction between a maleimide and furan[27-29] (**Figure 1.4**). When a 100 mM solution of diene **1** and maleimide **2** in $CDCl_3$ was heated at 50 ˚C, only very small amounts of the *exo* cycloadduct **3** could be detected after 15 hours. In order to investigate the recognition-mediated facilitation of this cycloaddition reaction, diene **4** bearing an amidopyridine recognition site, and maleimide **5** bearing a complementary carboxylic acid recognition site were then prepared. When a 100 mM solution of diene **4** and maleimide **5** was heated at 50 ˚C in $CDCl_3$, a significant quantity of the disfavoured *exo* cycloadducts **6** are detected after 15 hours. From these results, it is clear that the introduction of the recognition elements within the diene **4** and dienophile **5** has increased the extent of reaction dramatically. From the concentration profile, it is clearly visible that the maximum rate can be found at the start of the reaction (**Figure 1.4b**). This enhancement is indicative of the [**A•B**] complex pathway. Since the template is in its closed structure, the recognition sites are associated through intramolecular hydrogen bonds and hence, the template does not possess any catalytic activity. Moreover, adding pre-synthesised product template **6** at the start of the reaction has no effect on the shape of the curve. For that reason, the suppression of the binary complex [**A•B**] pathway is an important limitation within the minimal model to ensure an efficient self-replicating enterprise.

This problem can be resolved by careful design of the building blocks. The angle at which the reactive site and the recognition site relatively to each other is one of the main factors determining whether the reaction will follow the [**A•B**] complex or the autocatalytic pathway. If the bond angles in the product structure allow for intramolecular recognition of the complementary recognition sites, than the resulting closed template will be inactive for autocatalysis. We have demonstrated[30] that by introduction of length segregation using substrates with sufficiently different length of linkers connecting the recognition and reactive sites, we enable to preclude this reaction pathway. Thus, upon recognition the reactive sites are inaccessible to stabilize the transition state.

The second significant problem associated with the catalytic efficiency of ternary complex [**A•B•T**] (see **Figure 1.1**). The template molecule **T** must accelerate the rate

of reaction between the substrates **A** and **B** substantially compared to the rate of reaction in the absence of **T**. The presence of pre-synthesised template **T** at the beginning of the reaction should result in the loss of the initial lag period, providing evidence for the existence of a self-replicating system. Additionally, the maximum rate of the reaction should instantly occur at the start of the reaction. In order to demonstrate this expectation, we reacted nitrone **7** and malemide **8** at starting concentration of 25 mM in $CDCl_3$ at 10 ˚C, giving rise to major formation of *trans* **9** in a ratio 6:1 relative to *cis* **9** (**Figure 1.5b**) demonstrating the sigmoidal growth[31].

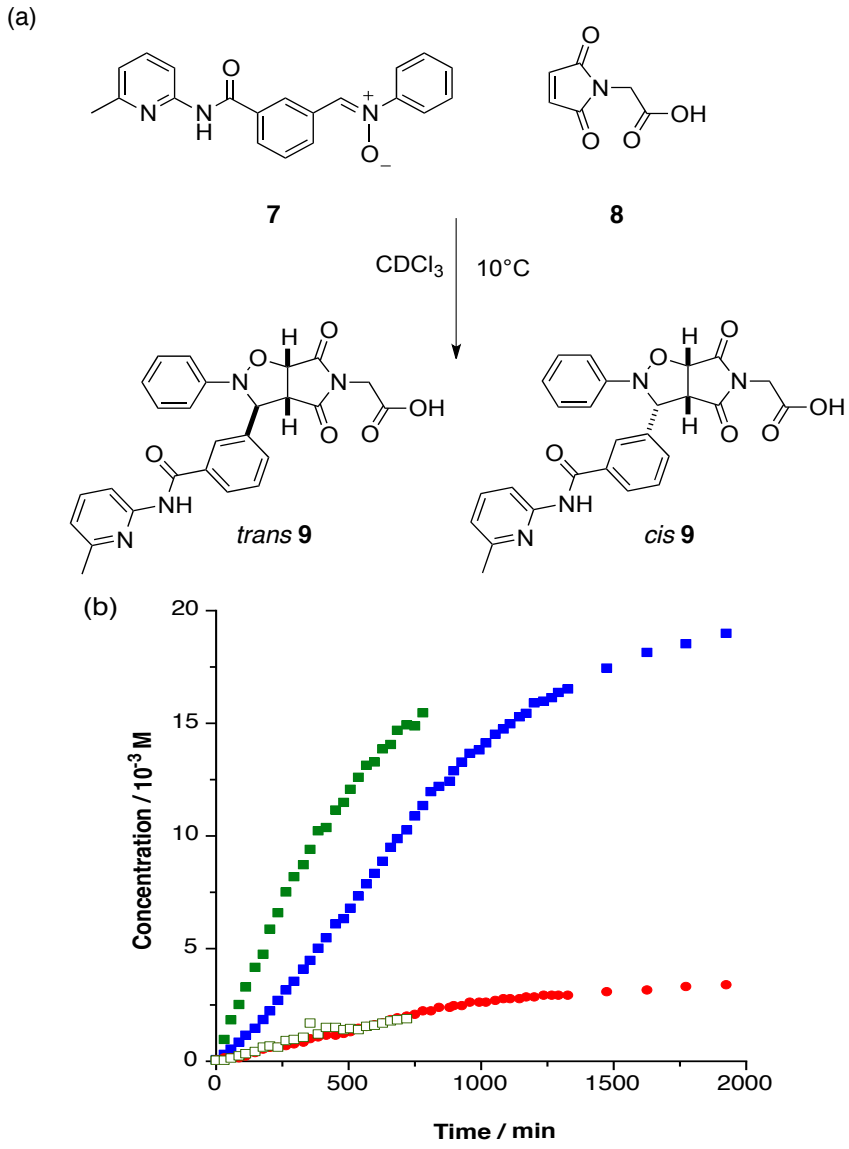

Figure 1.5. (a) Scheme reaction between nitrone **7** and maleimide **8** in $CDCl_3$ at 10 ˚C at 25 mM starting concentration; (b) Concentration *vs* time profile for nitrone **7** and maleimide **8** demonstrating the sigmoidal growth of the *trans* **9** (blue filed diamonds) and *cis* **9** (red filled circles). The template directed nature of the reaction was demonstrated by addition of preformed *trans* **9** to reagents **7** and **8** removed the lag period and the maximum autocatalytic rate was achieved at $t = 0$ (green filled boxes). By contrast, the addition of pre-synthesised template *cis* **9** at the beginning of the reaction has no effect on the rate of production of *trans* **9** or *cis* **9** (green open circles). Figure adapted from reference 31.

In the presence of 40 mol% preformed template *trans* **9**, the reaction revealed the absence of the lag period. It is clear from the experimental results presented here that *trans* **9** exerts a significant level of stereocontrol on the reaction between **7** and **8** in the [**7**•**8**•*trans* **9**] complex. By contrast, the addition of pre-synthesised template *cis* **9** at the beginning of the reaction has no effect on the rate of formation of *trans* **9**, indicating that this diastereoisomer is inactive to influence self-replication either in an autocatalytic or crosscatalytic context.

In other cases, if the product molecules bind the component molecules too tightly, the product duplex [**T**•**T**] (see **Figure 1.1**) may be slow to dissociate and raise the product inhibition, reducing the number of available product molecules and eventually hampered the autocatalytic cycle. We have demonstrated that the reaction between azide **10** and maleimide **11** at 30 ˚C in $CDCl_3$ at 25 mM starting concentration forms a template **12** (**Figure 1.6a**) that is capable of self-replication[32] but form a strong template duplex [**12**•**12**] in the solid state (**Figure 1.6c**). The autocatalytic behavior of this system can be described using von Kiedrowski analysis[23] to determine the type of the autocatalytic growth curve using the reaction order *p*.

In this case, the kinetic simulation revealed a *p* value of 0.4, which indicates that the replicating system obeys the square root law. These results suggest strongly that the [**12**•**12**] duplex is very stable in our system, in which case leads to almost no turnover in the autocatalytic cycle. Such a system may be termed self-replicating because it constructs one copy of itself, but not autocatalytic, as it does not return significant amounts of free template to the reaction mixture.

This effect can be reduced by reducing the alkyl spacer placed between the carboxylic acid and the maleimide, the reactive sites are prohibited to accelerate within the binary [**A**•**B**] complex pathway. Despite that, if the product duplex [**T**•**T**] dissociates too readily, then the product template may not bind the components very well. Either case reduces the number of functional products that can serve as the template. Therefore, a delicate balance has to be achieved between strong binding of the components and facile release of the newly formed template.

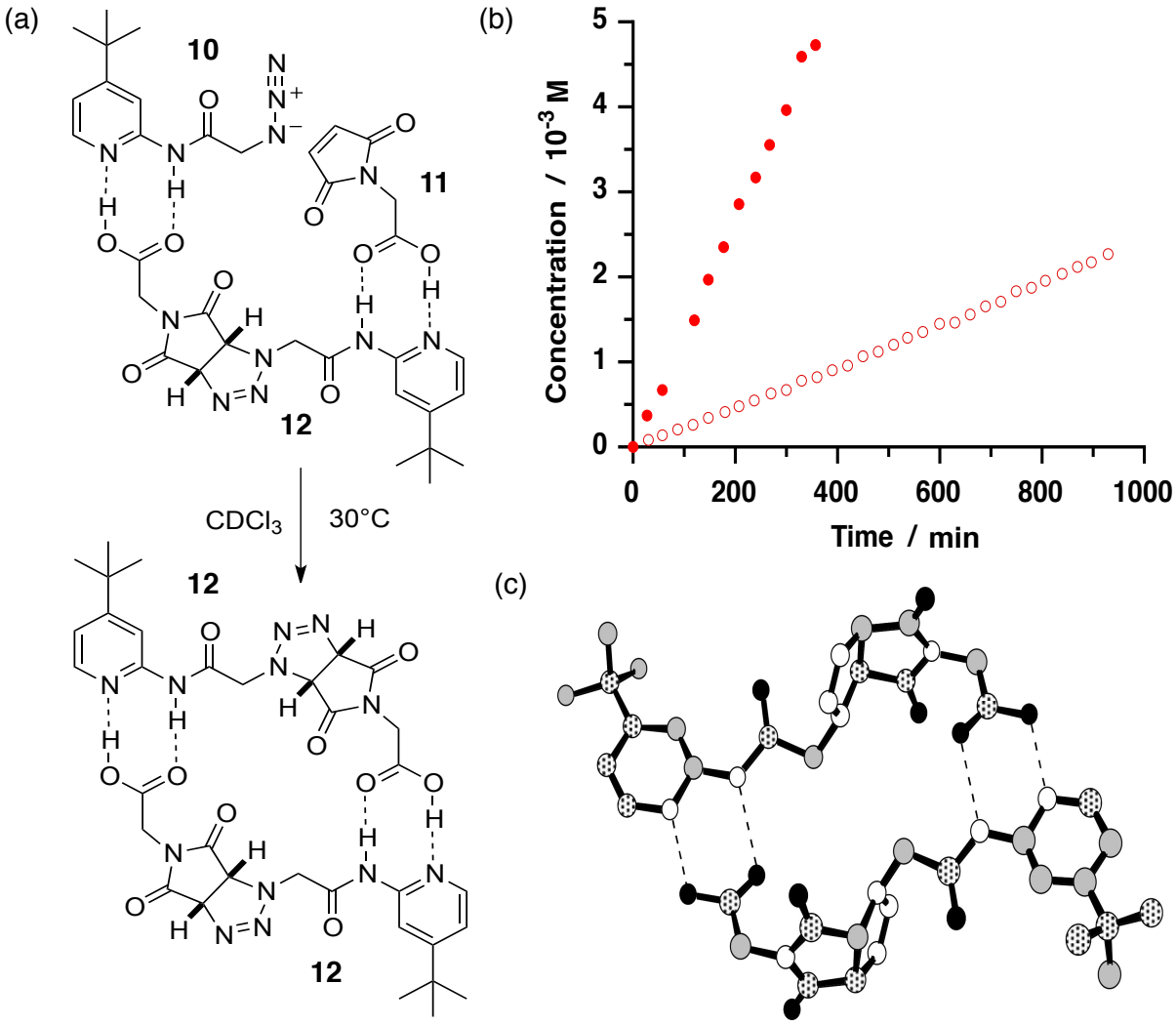

Figure 1.6. (a) Template **12** can assemble maleimide **10** and azide **11** in $CDCl_3$ at 30˚C and accelerate the reaction between them; (b) Concentration *vs* time profiles for the formation of **12** in the recognition-mediated reaction (red open circles) between and in the presence of 50 mol% preformed **12** (red filled circles); (c) Solid-state structure of the [**12**•**12**] duplex as determined by single-crystal X-ray diffraction. Figure taken from reference 32.

1.4.2 What happens if it works well?

In an efficient self-replicating system, the template **T** molecules will contribute to the formation of new product template by binding the available reagent components, **A** and **B** (see **Figure 1.1**). After the reaction, the product duplex [**T**•**T**] comes apart readily so that additional component molecules can be assembled. If the template molecules capable to participate in multiple replication cycles, sustained exponential growth can occur, before reaching the steady state when all the starting reactants has been consumed.

In principal, we should be able to observe a sigmoidal or 'S' shaped growth in the concentration *vs* time profile (**Figure 1.7a**) in the investigated systems. Theoretically, the behavior of the replicators can be evaluated by the reaction order, ρ as such the value normally lies between 0.5 and 1.0, depending on how close the reaction is to exponential growth and the extent of product inhibition[23,33]. In the case of rapid dissociation of the template duplex [**T•T**], an exponential growth would be observed from concentration *vs* time profile with reaction order of 1.0. However, when the product inhibition is a significant problem, the concentration *vs* time profile displays a parabolic growth with reaction order of 0.5 as shown in **Figure 1.7b**.

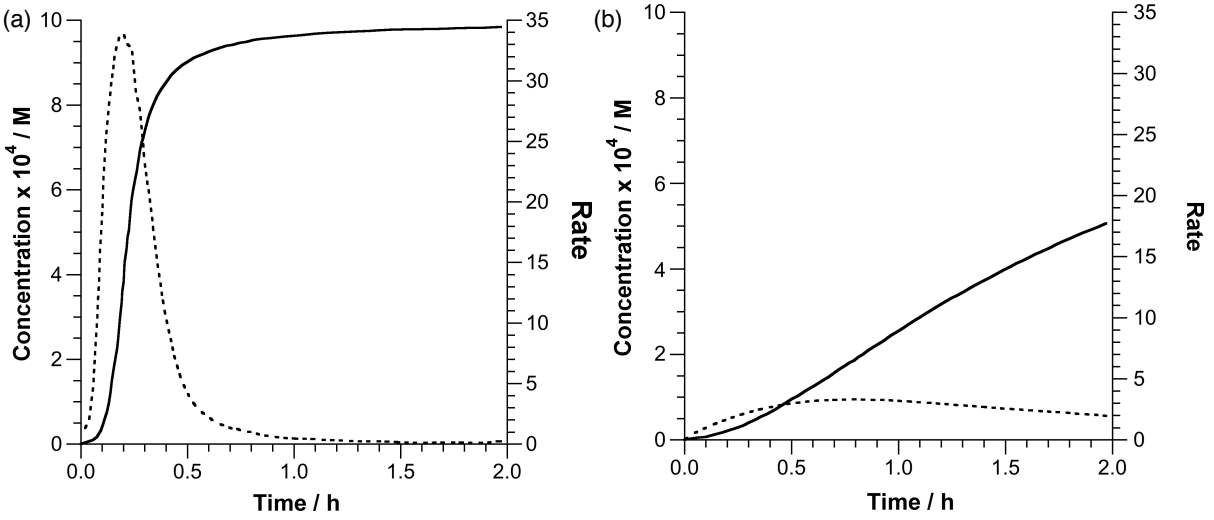

Figure 1.7. Simulated concentration *vs* time (solid line) and rate *vs* time (dashed line) profiles for a reaction with reaction order of (a) ρ = 1.0 (exponential growth) and (b) ρ = 0.5 (parabolic growth). Figure adapted from reference 33.

In consequence, we have to make sure that the reaction preferentially went through the autocatalytic pathway. Our own approach to distinguish a replicator's behavior whether it is exponential or parabolic is by following the formation of template **T** in the presence of three different amounts of preformed template at the start of the reaction. In the case of exponential growth, the initial rate of formation of **T** scales as 1:2:4 whereas the initial rate of formation of **T** scales as 1:√2:√4 in parabolic growth.

1.4.3 The need for control experiments

On that account, it is essential to perform several control experiments to indicate that the formation of a product template is a consequence of self-replicating behavior. We will discuss in detail the previous cycloaddition reaction (**Figure 1.5a**) to illustrate the

example of how we carried out the control experiments. Initially, a control compound **13** is identified, which possess the same chemical functionality as the building blocks of the replicator. Practically, the recognition site is removed in this control compound. In this case, the carboxylic group of maleimide **8** is substituted with the corresponding methyl ester, giving the maleimide **13**, which eventually obstruct the formation of the hydrogen bonds with nitrone **7** and thus, incapable to participate in any recognition-mediated processes (**Figure 1.8a**).

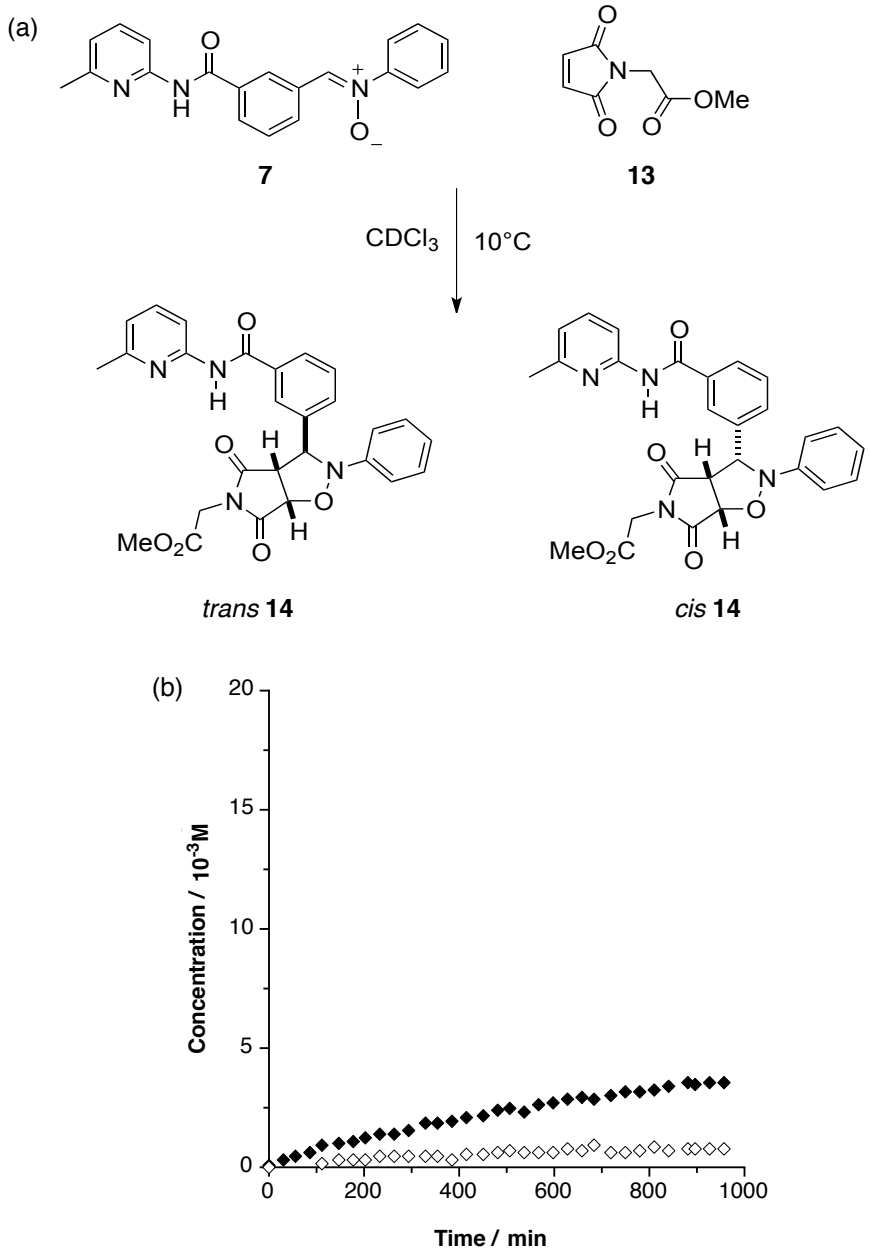

Figure 1.8. (a) Scheme reaction between nitrone **7** and malemide **13** at 25 mM at 10 ˚C in $CDCl_3$. The formation of *trans* **14** is shown as filled diamonds and of *cis* **14** as open diamonds. Figure adapted from reference 31.

The kinetic data measured using this control compound provide a comparative baseline for kinetic studies and will be termed the background reaction. The rate

enhancement in the formation of one of the diastereoisomer in comparison with the background reaction will indicate the dominant pathway whether it is replicating cycle or the [**A**•**B**] complex. Subsequently, it is also crucial to establish the dependency of the reaction on molecular recognition since the efficient enterprise of a self-replicating system revolves around the reversible recognition events that occur in the autocatalytic cycle. Secondly, the previous developed replicating systems shown in **Figure 1.5a** were allowed to react in the presence of an unreactive carboxylic acid, for example benzoic acid.

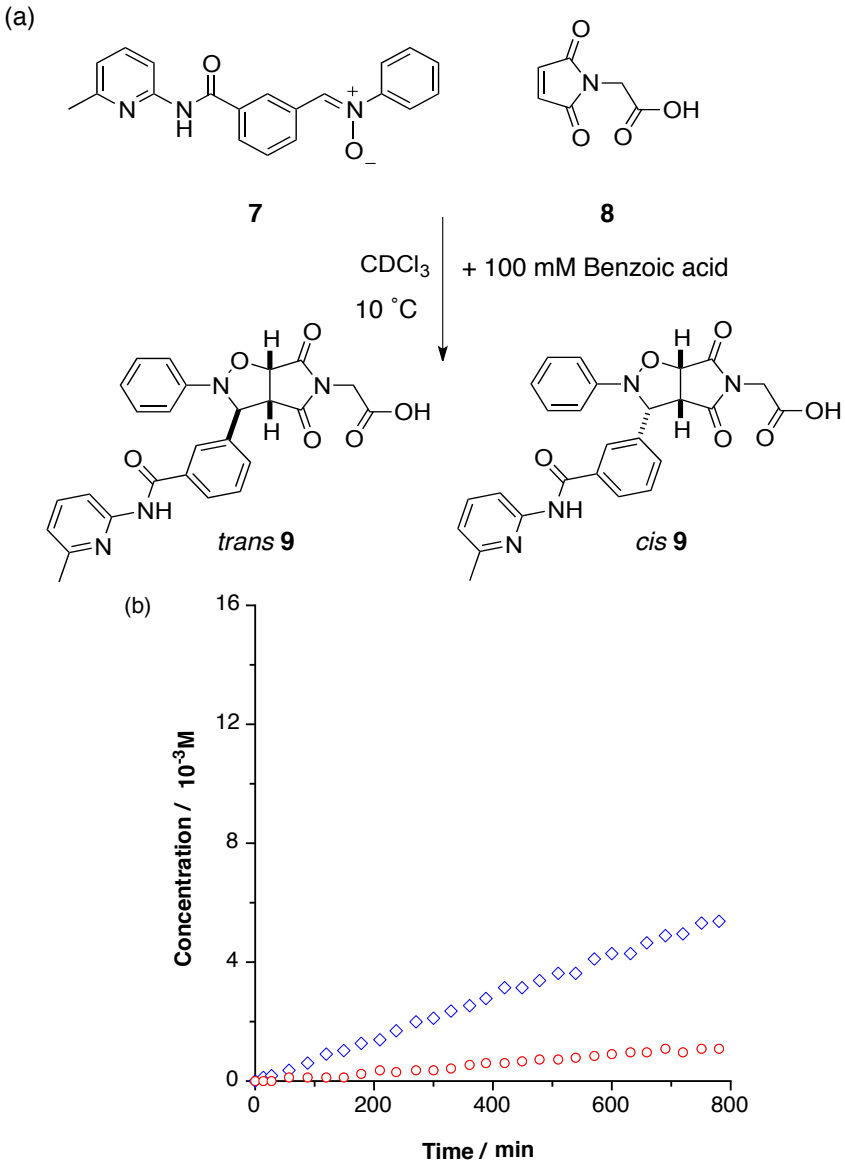

Figure 1.9. (a) Scheme reaction between nitrone **7** and maleimide **8** in $CDCl_3$ in the presence of 100 mM benzoic acid at 10 ˚C at 25 mM starting concentration as shown in **Figure 1.5a**; (b) Concentration *vs* time profile for the formation of *trans* **9** (blue open diamonds) and *cis* **9** (red open circles) at 10 ˚C in the presence of 100 mM benzoic acid in $CDCl_3$. Figure adapted from reference 31.

This competitive inhibitor is capable of binding to the recognition sites present in compound **7** and, hence, interfere the crucial recognition processes. Consequently, the autocatalytic cycle is disrupted, resulting in a decrease in the rate and/or selectivity in the rate of the reaction, which often accompanied by disappearance of the sigmoidal curve (**Figure 1.9b**).

The final experiment that provides the evidence of self-replicating operating within a system can be obtained by seeding the reaction with the product **T** itself. The presence of pre-synthesised template **T** at the beginning of the reaction should result in a loss of the initial lag period in the concentration *vs* time profile for the reaction, indicating the reaction is now template-directed (as demonstrated in **Figure 1.5b**). The rate of the reaction should be highest from the start of the experiment and comparable to the maximum rate of the formation of the products in the absence of template **T**. Such behavior is only observed for the self-replicating pathway. If the reaction proceeds *via* [**A•B**] complex channel (as depicted in **Figure 1.4b**), the addition of the template to such system will not affect the rate of the product formation.

1.4.4 How to optimize the conditions?

The conditions chosen must suppress the bimolecular pathway but still allow for efficient autocatalytic turnover of the replicator. The involvement of this reaction can only be influenced by the changes in concentration and temperature. For instance, by reducing the concentration by a half reduces the rate of bimolecular reaction by four times. However, if the concentration drops[33] below the dissociation constant, K_d for the recognition process used to assemble the ternary complex, replication will effectively be shut down. It is also noteworthy that a reduction in the reaction temperature will strengthen the binding and facilitate the formation of the product through recognition. Nonetheless, the association constant of the product duplex will also increased, resulting in the increased product inhibition. Therefore, the lowering of either of the parameters will slow down the bimolecular channel to a much greater extent than any of the recognition-mediated pathways.

1.5 Examples of self-replicating systems

Over the last twenty-five years, a various investigations on chemical self-replicating systems has make use of oligonucleotide analogues[34], polypeptides[35] and small organic molecules[36] as templates. However, a common problem of these systems is product inhibition. In the next section, we will illustrate the examples of each replicating systems including our own work based on small organic molecules.

1.5.1 Self-replicating systems based on oligonucleotides

The successful evidence for self-replication in non-enzymatic reaction utilizing oligonucleotides was demonstrated by von Kiedrowski in 1986[19] (**Figure 1.10**). 5'-terminally protected trideoxynucleotide **15** with base sequence 5'-CCG-3' and complementary 3'-protected **16** with base sequence 5'-GGC-3' were reacted in the presence of EDC to yield the self-complementary hexadeoxynucleotide **17**, 5'-CCGCGG-3'. In addition, the CDI activated intermediate **15b** underwent rapid hydrolysis to unreactive **15a** which was itself reactive with **15b** forming the side product, pyrophosphate $^{5'}$-MeCCG$^{3'}$pp$^{3'}$GCC-Me$^{5'}$ (**pp**) through self-condensation.

The course of the reaction was followed by HPLC and revealed two parallel pathways, both autocatalytic and non-autocatalytic pathway contributing to the formation of the hexameric templates. The latter pathway has been found to be predominant. In order to demonstrate autocatalysis in template production, the reaction mixtures differing in the initial concentration of template were prepared as shown in **Figure 1.11**.

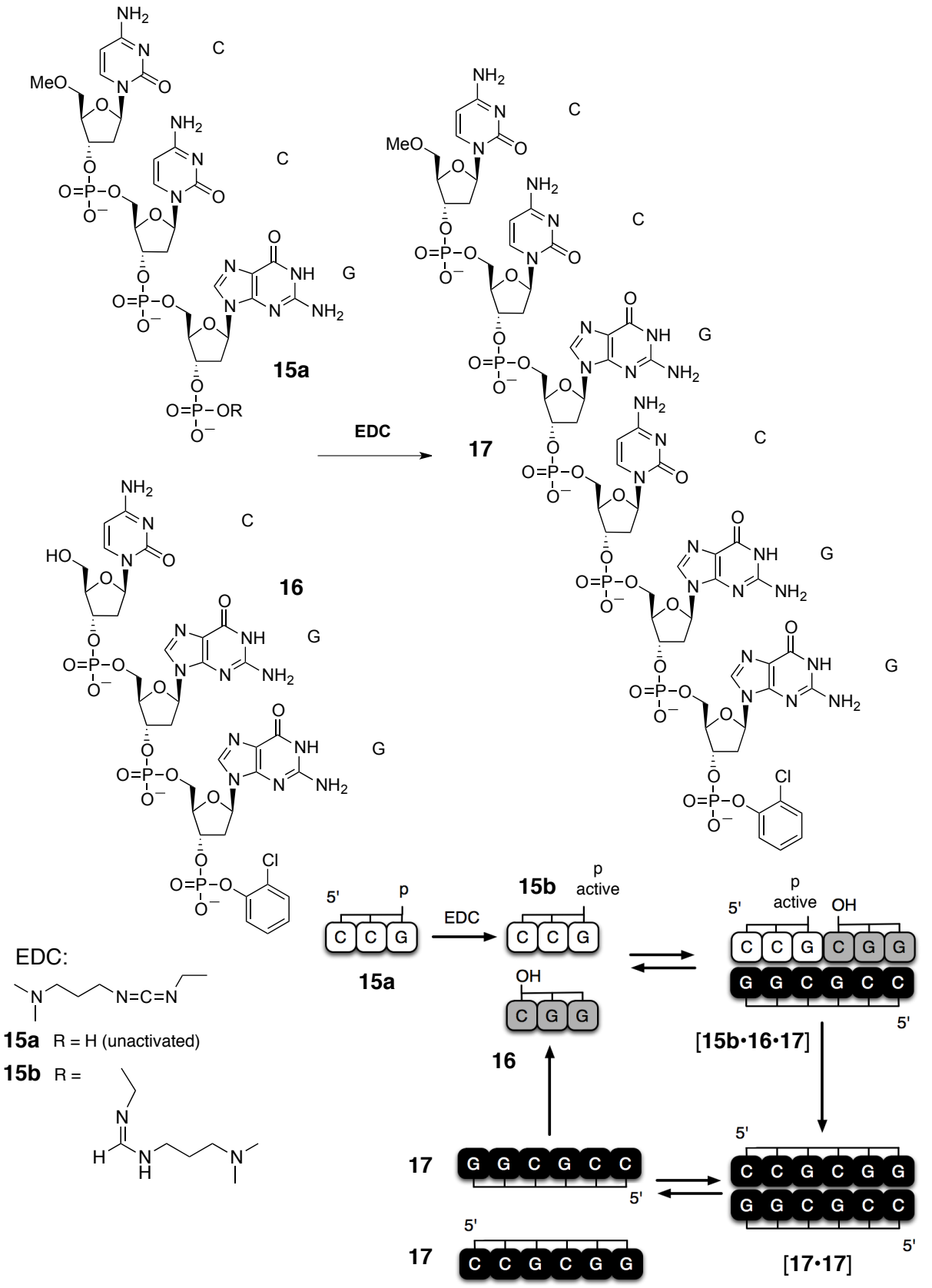

Figure 1.10. Reaction of two trinucleotide substrates at 10 mM in aqueous solution is initiated by EDC activation of **15a** to form the intermediate **15b**. Subsequent condensation reaction with the 5' hydroxyl group on **16** leads to phosphoester formation and yields the self-complementary hexanucleotide **17** with base sequence 5'-CCGCGG-3' with the 5'-terminus protected as a methyl ester and the 3' terminus protected with the *o*-chlorophenyl group.

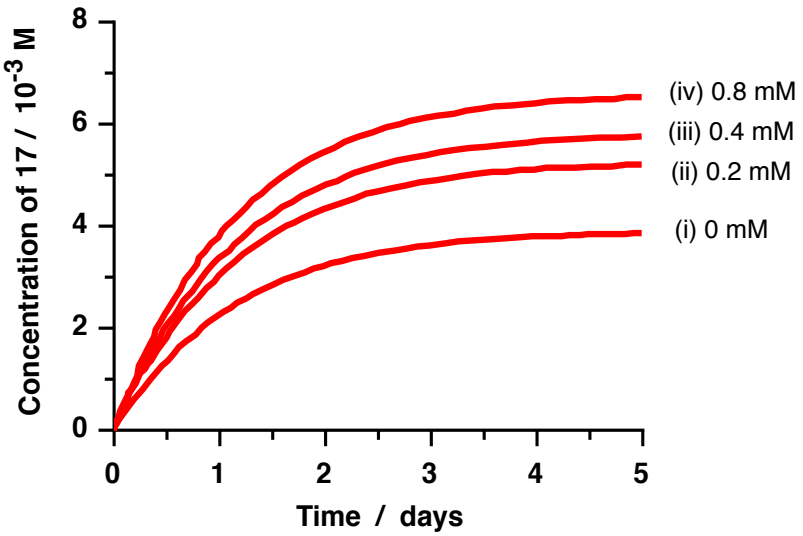

Figure 1.11. The progress of the reaction without pre-synthesised template **17** at the start of the reaction (i) 0 mM and with the presence of template **17** (ii), (iii) and (iv), respectively. In the absence of template **17**, the reaction proceeds slowly and by increasing the initial concentration of preformed template **17** (0.2, 0.4 and 0.8 mM) had the effect on the rate formation of template **17**. Figure taken from reference 19.

When the preformed template product was added at the start of the reaction, it did not increase the rate of autocatalytic template formation in a linear sense. Instead, the initial rate of autocatalytic synthesis was found to be proportional to the square root of the template concentration with the reaction order was found to be 0.48. They expected that most of the product template remained in their double helical forming a strong association and prevents the systems from an exponential growth[37]. It was first pointed out that the rate of formation of **pp** is almost independent of the initial concentration of template **17**. However, it was revealed that the presence of **pp** template in solution is in similar concentrations to template **17**. The increase of the initial concentration of template **17** would slightly decrease the rate of formation of **pp**, simply because template **T** and **pp** compete for the same activated trinucleotide. Further investigations were directed to the base pairs sequence dependency[38] in the self-replication of hexamer which led to significant decrease of catalytic activity when one of the bases in trimer **15** is varied from C to G and *vice versa*. The effect is most pronounced if the missmatch base pair is closer to the reactive site.

The first recognition of sigmoidal growth[39] of template molecules in non-enzymatic reaction has been achieved by reacting trinucleotide **18** and 5'-amino group trinucleotide **19** which led to the formation of a 3'-5'-phosphoramidate bond in hexamer template **20** (**Figure 1.12a**).

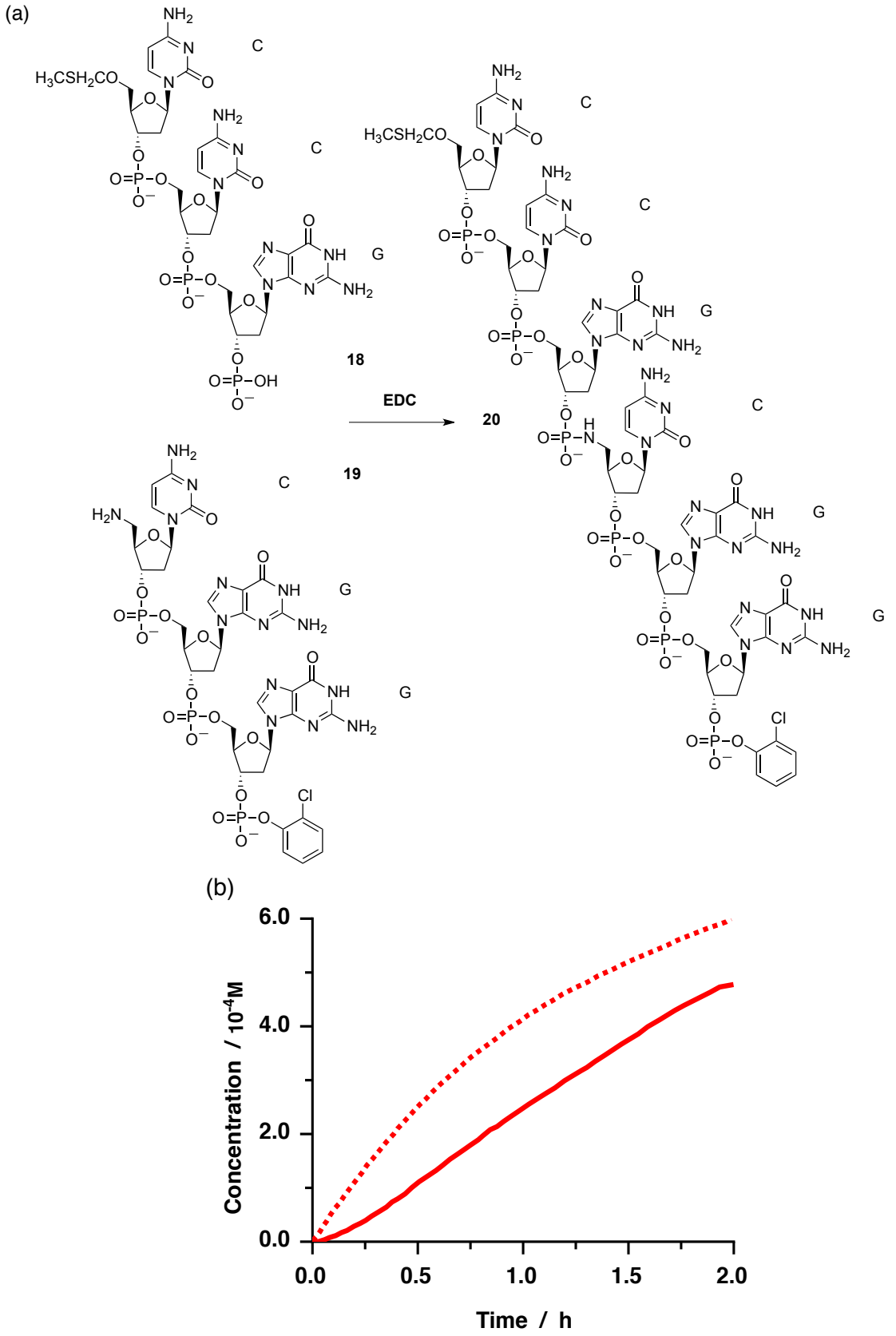

Figure 1.12. (b) Concentration *vs* time profile for the formation of the (a) hexameric 3'-5' phosphoamidate **20** from trinucleotide **18** and **19** the absence of preformed template **20** (red solid line) and in the presence of 32 mol% preformed template **20** (red dashed line) as measured by HPLC. The yield of **20** is 50% after 2 hours. Figure taken from reference 39.

The time course for template formation was followed by HPLC (**Figure 1.12b**). The rate formation of template **20** is higher than template **17** with almost 50% conversion after 2 hours with sigmoidal rate profile. Addition of 32 mol% preformed template **20** at the start of the reaction increase the yield of template **20**, which indicates that the autocatalytic process is operating in this system. The author later described a parabolic growth with the reaction order, *p* was found to be 0.5 as a consequence of product inhibition. By far, the reported self-replicating system only composed of two constituents. Therefore, more complex systems with three or more starting materials are also envisioned[40]. Further developments of oligonucleotide self-replicating system aimed on the development of crosscatalytic[41] replication systems.

1.5.2 Self-replicating systems based on RNA

Some scientists believe that the early forms of life may be hiding in our cells, in molecules known as RNA. RNA, DNA and other nucleic acid like compounds are informational macromolecules that have inherent template properties and so lend themselves in a straightforward way to both storing information and replicating[42]. The discovery[43] of ribozymes as both genetic material and catalyst provided an empirical basis for the concept of the RNA world. An example of self-replication developed based on ribozyme[44], catalyses the assembly of additional copies of itself through an RNA-catalysed RNA ligation reaction (**Figure 1.13a**). The ribozyme catalyses attack of a 3'-hydroxyl of the substrate on the α-phosphate of the 5'-triphosphate of the ribozyme, with concomitant release of inorganic pyrophosphate. The R3C ligase **23** was redesigned as a symmetrical dimer, so that it would ligate two substrates **21** and **22** to generate an exact copy of itself (**Figure 1.13b**).

The main consideration is to ensure the template and substrates interact with minimal base pairing so that the ligated product could easily dissociate from the template and, thus be available to catalyse subsequent ligation reactions. The ligation reaction involving **21** and **22** in the absence of **23** was very slow, with less than 1% product formed after 3 hours (**Figure 1.14**).

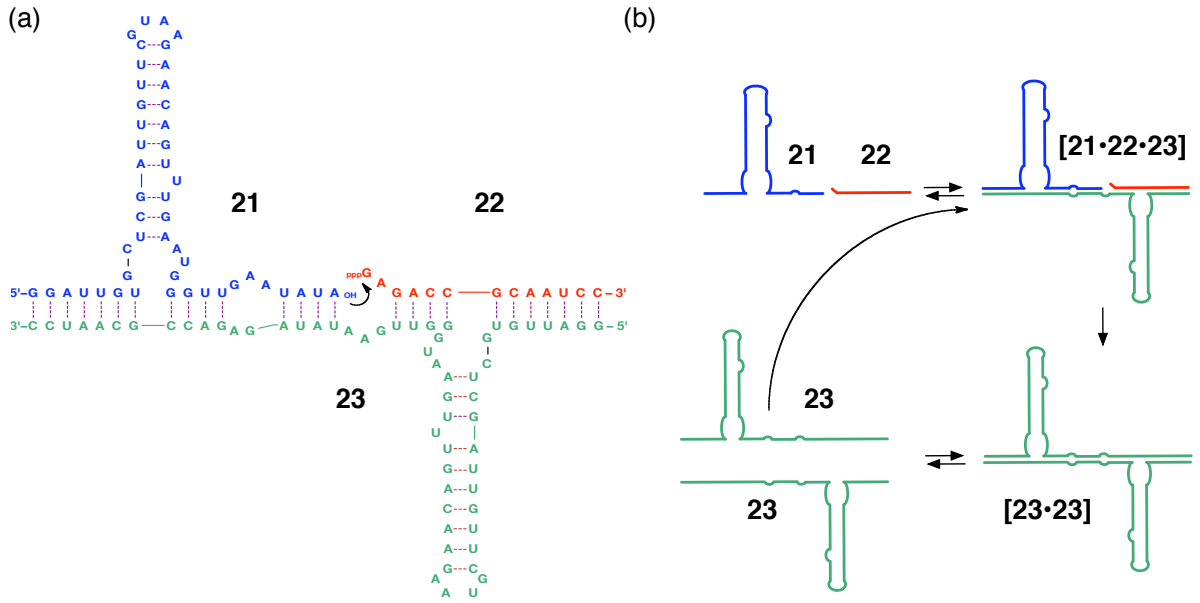

Figure 1.13. (a) Secondary structure of the self-replicating ligase ribozyme. The template molecule **23** binds the two substrate molecules **21** and **22**, which then undergo RNA-catalyzed ligation (black arrow) to generate another copy of template **23**; (b) Schematic presentation of the ribozyme-based self-replicating cycle. Figure adapted from reference 44.

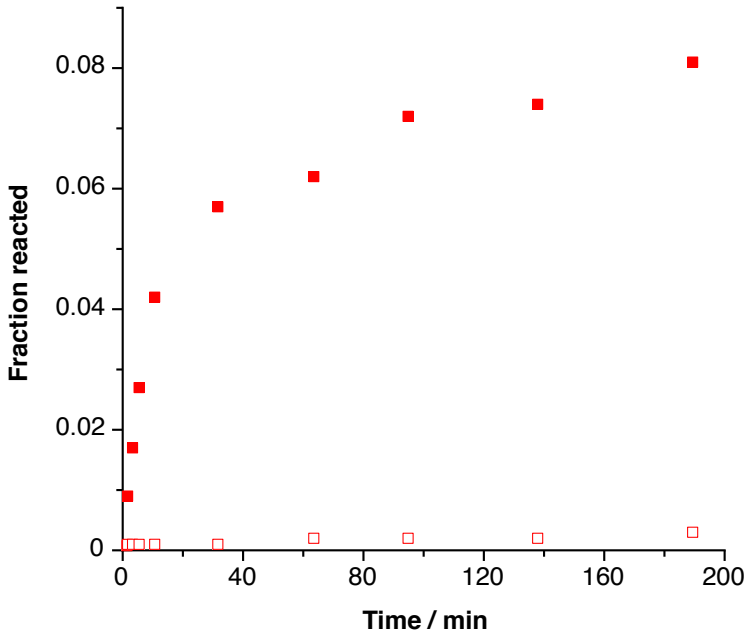

Figure 1.14. Concentration *vs* time profile for the production of template **23** in reaction mixtures consisting the **21** and **22** substrates in the absence of **23** (red open boxes) and in the presence of template **23** (red filled boxes). Figure adapted from reference 44.

When 0.5 equivalents of **23** were added to a reaction mixture, 400 folds increase in the initial rate of ligation was observed. Therefore, the template dependence of the reaction between **21** and **22** was considered to be significant because the rate enhancement achieved by the introduction of template **23** could not be achieved by the use of more substrates alone. A linear dependency between the initial rate of reaction and the starting concentration of template consistent with the reaction order of 1.0, which indicates that the availability of template **23** at the start of the reaction is not limited by dissociation of [**23•23**] complexes, allowing for product turnover. Despite the fact that the ternary complex [**21•22•23**] dissociated readily, exponential amplification was limited by a tendency for the substrate molecules to form a binary complex [**21•22**]. The authors reasoned that the remaining free substrates **21** and **22** capable of forming [**21•22**] complex before template **23** becomes available to initiate a new autocatalytic cycle and hence, further disrupted the recognition-mediated reaction.

1.5.3 Self-replicating systems based on polypeptides

The feasibility of peptide self-replication system[45-49] has been established experimentally[46] such that the preliminary report based on the peptide replicator[46] utilized the α-helical coiled coils with 32-residue polypeptide as the template **T** in the replication strategy. These structures are distinguished by their amphiphilic primary sequence of heptad repeats $(abcdefg)_n$.

The molecular recognition is based on hydrophobic interface (residues at *a* and *d* positions) and electrostatic interactions (residues at *e* and *g* positions) in the coiled-coil structure. Residues at the *b*, *c*, and *f* positions are exposed to the solvent and do not participate directly in the self-assembly of the coiled-coil structure and capable of tolerating a substantial variation of amino acid substitutions. The ligation site was chosen to lie on the solvent exposed surface of the α-helical structure to avoid interference with the hydrophobic recognition surface (**Figure 1.15**).

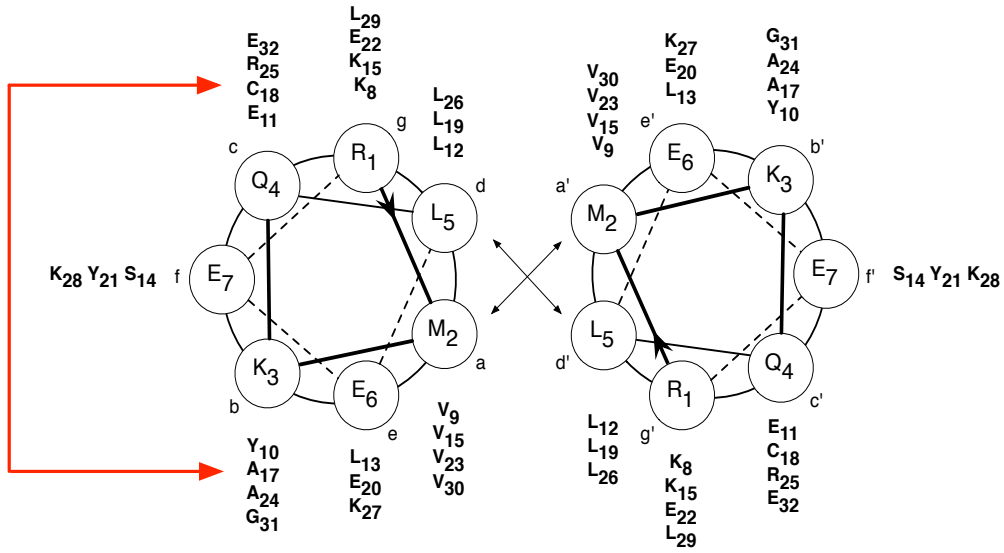

Figure 1.15. Helical-wheel diagram of the template peptide in the dimeric α-helical coiled-coil configuration emphasising the heptad repeats motif. The interhelical recognition surface consists of amino acids allowing for hydrophobic packing interactions (positions *a* and *d*) and electrostatic interactions (positions *e* and *g*). Amino acids at positions *b*, *c* and *f* lie on the solvent-exposed surface of the helical structure and do not participate in the molecular recognition processes. Red arrows indicate the ligation site between a cysteine residue 18 at position *c* and alanine residue 17 at position *b* on the solvent exposed face. Figure adapted from reference 45.

Ghadiri *et al.* employed the Kent ligation[50] as the peptide fragment coupling strategy. The coupling reaction proceeds through an initial *trans* thioesterification between *C* terminal thioester of electrophile polypeptide **E** and the *N* terminal cysteine sulfhydryl group of nucleophile polypeptide **N**. The resulting thioester intermediate rapidly rearranges *via* intramolecular S to N acyl transfer to give the final amide bond. The association of polypeptide **E** and **N** to the template **T** produce the ternary complex [**E**•**N**•**T**] (illustrated in **Figure 1.16**). The reactive sites are now in close proximity to allow the Kent ligation reaction pseudo-intramolecular to form duplex [**T**•**T**]. Subsequent dissociation of two molecules of **T** to the start of the reaction completed the autocatalytic cycle.

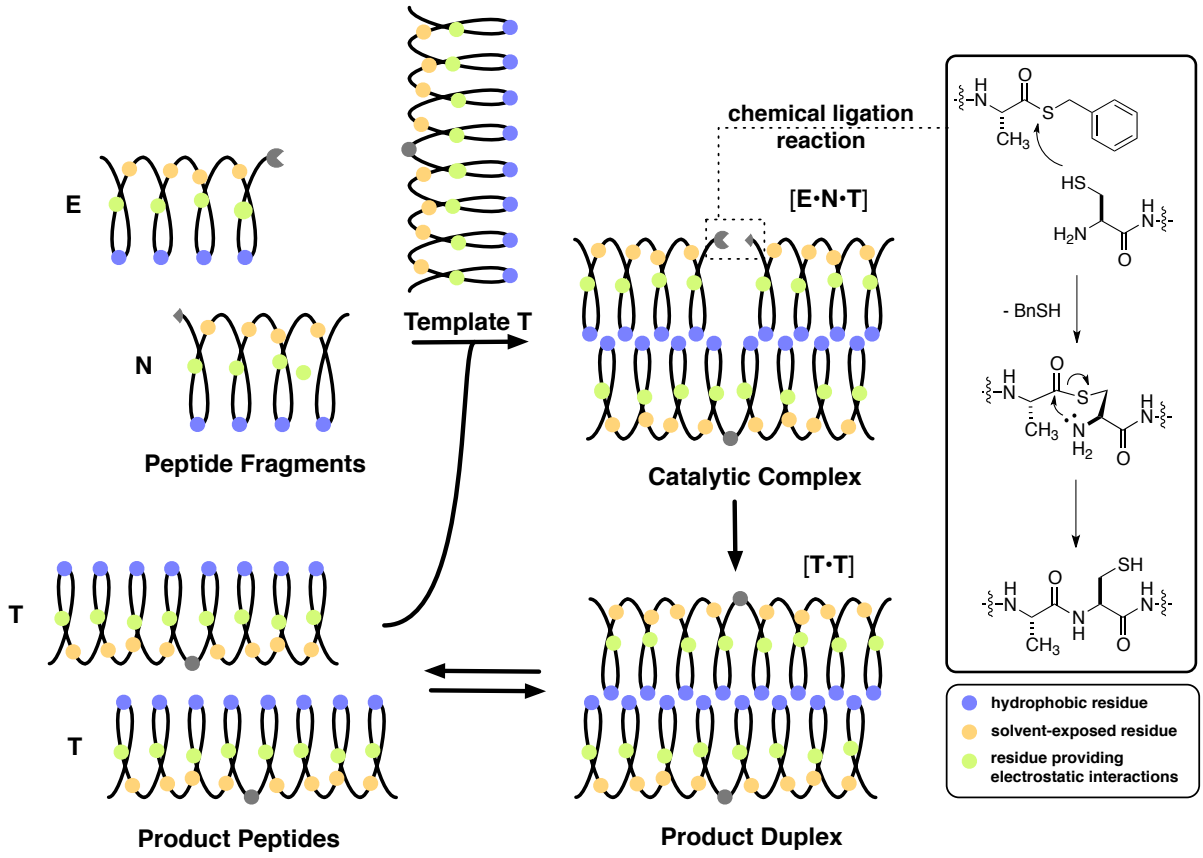

E : ArCONH–RMKQLEEKVYELLSKVA–COSBn

N : H_2N–CLEYEVARLKKLVGE–$CONH_2$

T : ArCONH–RMKQLEEKVYELLSKVA–CLEYEVARLKKLVGE–$CONH_2$

Figure 1.16. Schematic representation of the minimal replication model for self-replicating α-helical peptide. The electrophilic and nucleophilic peptide fragments **E** and **N** are recognised by template **T** through interhelical hydrophobic interactions to form catalytic complex, [**T**·**E**·**N**]. Subsequent chemical ligation produces an identical copy of the template, which remains bound in the product duplex [**T**·**T**]. Dissociation allows the two templates to undergo further catalytic cycles. The inset depicts the amide bond forming process based on thioester promoted peptide fragment condensation strategy of Kent.

An equimolar mixture of both electrophile and nucleophilic fragments were reacted in the absence or presence of various amounts of template (**Figure 1.17**). Autocatalysis in template production is established with pronounced increases as the initial concentration of the template is increased. At higher concentrations of peptides, an increase in autocatalytic growth was observed with reaction order, *p* of 0.63. It was also attributed from the contribution of quaternary complex [**E**•**N**•**T**•**T**] (the association of two substrates **E** and **N** with the duplex [**T**•**T**]) to the autocatalytic pathway despite the inhibition from duplex [**T**•**T**] complex. Therefore, the reaction order as well as the autocatalytic efficiency is strongly dependent on the relative thermodynamic stability

of the ternary complex [**T**•**E**•**N**] with respect to the template duplex [**T**•**T**]. Control reactions with single mutant peptide support the contribution of the autocatalytic pathways to the overall product formation, which must proceeds through the ternary and/or quarternary complex. Furthermore, these experiments reveal a remarkable sequency selectivity, as evidenced by the loss of the autocatalytic activity as a result of a single replacement of leucine or valine residue with an alanine at the recognition interface.

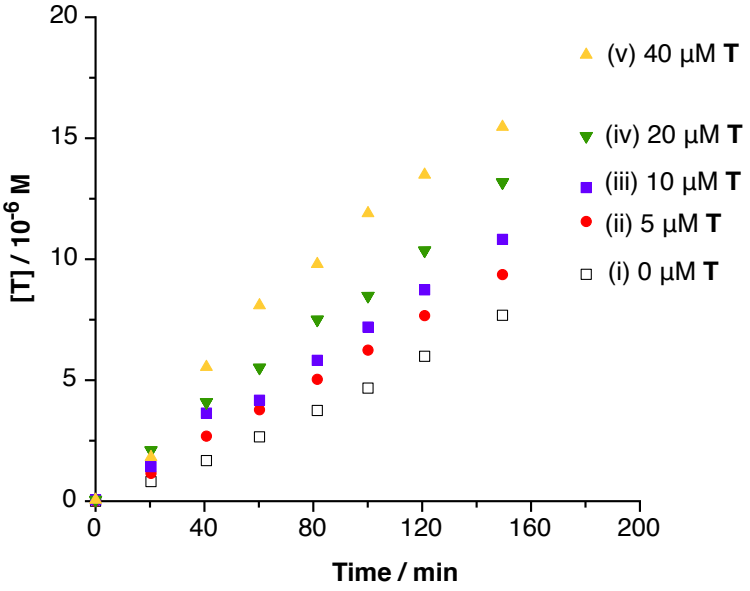

Figure 1.17. Concentration *vs* time profile for the formation of template **T** in the absence of preformed template **T** (i) and in the presence of different initial concentrations of template (ii), (iii), (iv) and (v). Figure adapted from reference 46.

Further progress towards exponential growth in self-replicating peptides was aimed through the destabilisation of template duplex. Chmielewski *et al.* have implemented two strategies to achieve a reaction order of 0.91, indicative of exponential amplification. In 2001, this was accomplished by shortening the coiled coil from 35 to its minimum length of 26 amino acids[51]. In shortening the peptide, the number of leucine residues was reduced and the overall hydrophobicity of the templating surface was decreased. These resulted in more efficient product release, therefore facilitating successive cycles of replication[52].

Alternatively, in 2003, they documented that the insertion of one proline amino acid for the change of glutamate (Glu20) in the building blocks of the replicating peptides leads to a 30˚ kink in the α-helix (**Figure 1.18**). The position of the proline substitution, located on the hydrophilic face of the helix, was found to be critical for

this improved behaviour. The substitution did not disrupt the hydrophobic templating face, allowing efficient complexation between the template and substrates, while the kink results in the reduced coiled-coil stability[53].

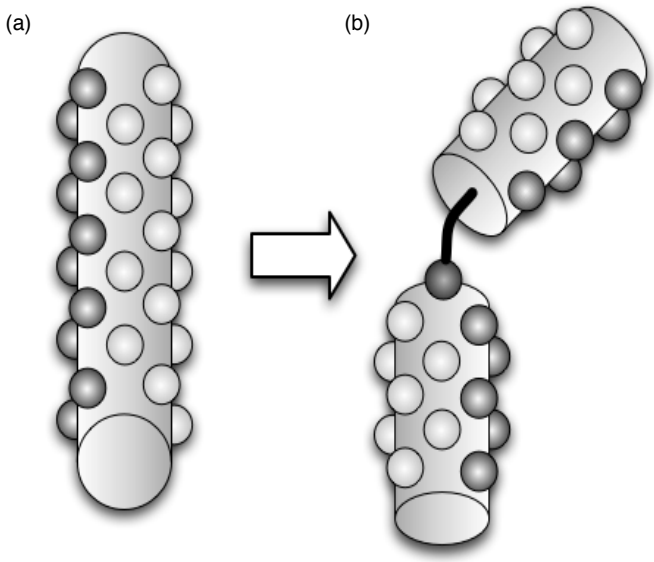

(a) **Ac–ELYALEKELGALEKELACL^{19}E^{20}KELGALEKELYALEK–CONH$_2$**

(b) **Ac–ELYALEKELGALEKELACL^{19}P^{20}KELGALEKELYALEK–CONH$_2$**

Figure 1.18. The effect of proline substitution in the replicating peptide-based template with respect to the hydrophobic surface of leucine residues. The 30˚ kink destabilises the template duplex and thus enhancing replication.

1.5.4 Self-replicating systems based on small organic molecules

A further exciting field in bioorganic chemistry is development of synthetic replicators. It seems feasible to invent new replicators based on truly artificial replicators since molecular recognition and catalysis are common features among organic molecules. Rebek and co-workers first reported wholly synthetic system, which involves the formation of amide bond with relatively small organic molecules for the production of an assembled system. This system could promote replication by employing both templating and base pairing effects. They have set out to prepare two components bearing both complementary reactive functionality and a complementary hydrogen bonding surfaces. Their initial attempts[36] employed the Kemp's triacid **24** incorporating a phenyl spacer and adenosine **25** through the formation of amide bond by aminolysis of a pentafluorophenolate ester by the primary amine (**Figure 1.19**). An unfavourable [**A**·**B**] complex with subsequent intramolecular binding resulted in the product, which remain closed as a consequence of the short phenyl spacer and the

flexible chain. Alternative template was subsequently developed[54] to include the naphthyl-ribose spacer to separate the recognition sites and destabilise the product duplex.

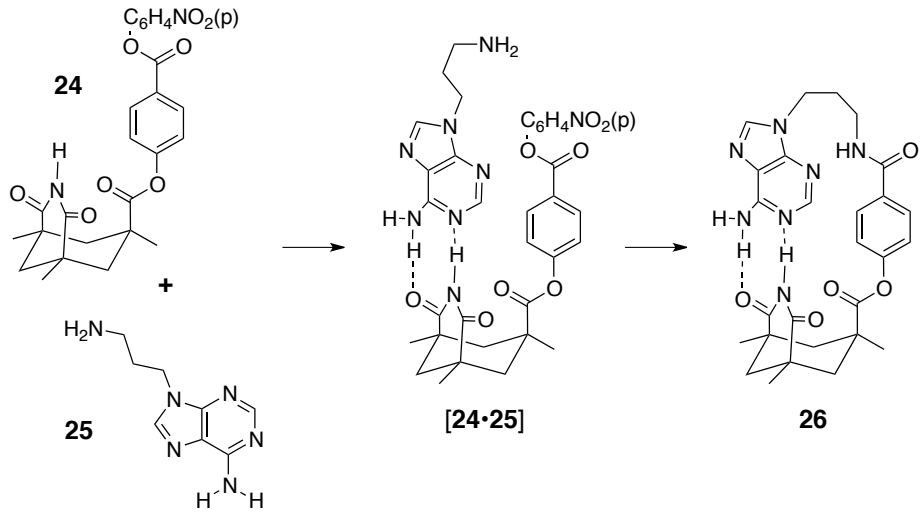

Figure 1.19. Rebek's initial design of a minimal replicator utilised a phenyl spacer in Kemp's substrate **24** was too short as well as flexible chain in adenosine substrate **25**, which resulted in the formation of unfavourable [**A•B**] complex.

Accordingly, a new replicator consisting of the amino adenosine **28** and its coupling reactions to imides bearing 2,6-napthalene surfaces **27a** were examined to form template **29'** in its *cis* amide formation. Isomerisation to the more stable *trans* amide **29** occurs rapidly allowing hydrogen-bonding surfaces to be exposed for dimerisation or autocatalysis.

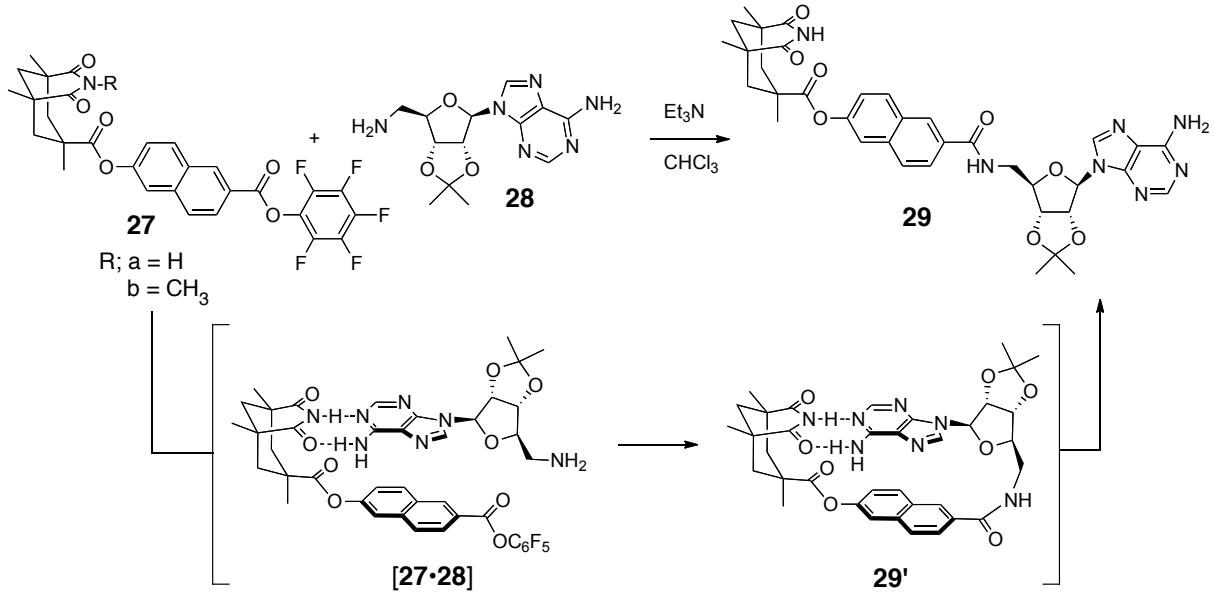

Figure 1.20. Synthetic self-replicating system illustrated by Rebek. Template **29** incorporates a longer naphthalene spacer on the Kemp's acid **27** and the amino adenosine **28** now contain a ribose ring.

As shown in **Figure 1.20**, the reactive ends of the **27a** and **28** come into spatial proximity when the reactants interact with the template **29**. Nucleophilic attack of the primary amine of **28** on the activated carboxyl ester of **27a** leads to amide bond formation, generating the template **29**. Dissociation of the resulting template duplex closes the first replication cycle with the released free template. The control experiments rate with *N*-methyl imide **27b** is substantially slower the formation of the product, than that of the parent NH imide, **27a** under the same conditions, thus provides strong evidence for base pairing. The inhibition of the reaction **28** and **27a** by the competitive inhibitor, 2,6-bis(acetylamino)pyridine provides additional evidence. A decrease in the rate of reaction corresponds with the decrease in the percentage of base paired complex (**Figure 1.21**).

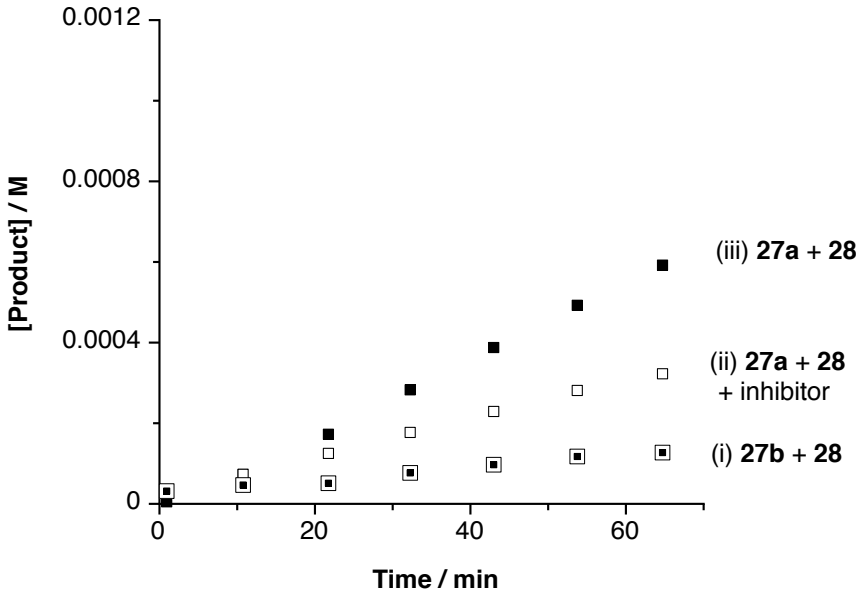

Figure 1.21. Initial rates of template formation as determined by HPLC. All reactions were performed with initial concentration of [**27a**] = [**28**] = 8.2 mM in $CHCl_3$ with four equivalent of Et_3N added as a general base. (i) Reaction of **28** and the *N*-methylated **27b**, (ii) Reaction of **28** and **27a** with one equivalent of 2,6-bis(acylamino)pyridine, (iii) Reaction of **28** and **27a**. Data taken from reference 54.

The authors demonstrate "autocatalysis" by the rate enhancement of the initial reaction upon seeding the prefabricated template **29** to coupling mixture, although the observation of a sigmoidal curve was hampered by the action of reactive [**A•B**] complex (**Figure 1.22**). The formation of [**A•B**] complex is as a result of the association of both substrates **27a** and **28** which promotes the formation of *cis* **29'** by intramolecular reaction before *cis* to *trans* amide isomerisation furnish the open template **29**. Thus, the principal step in producing a predominantly autocatalytic

system would therefore lie in removing the possibility of binary complex. In coexistence with the reactive [**A•B**] complex described in the system, Rebek groups computed that only 2% of the building blocks are assembled in the ternary complex. Therefore their estimation of the population of the ternary complex is highly questionable and posed significant controversial feedback.

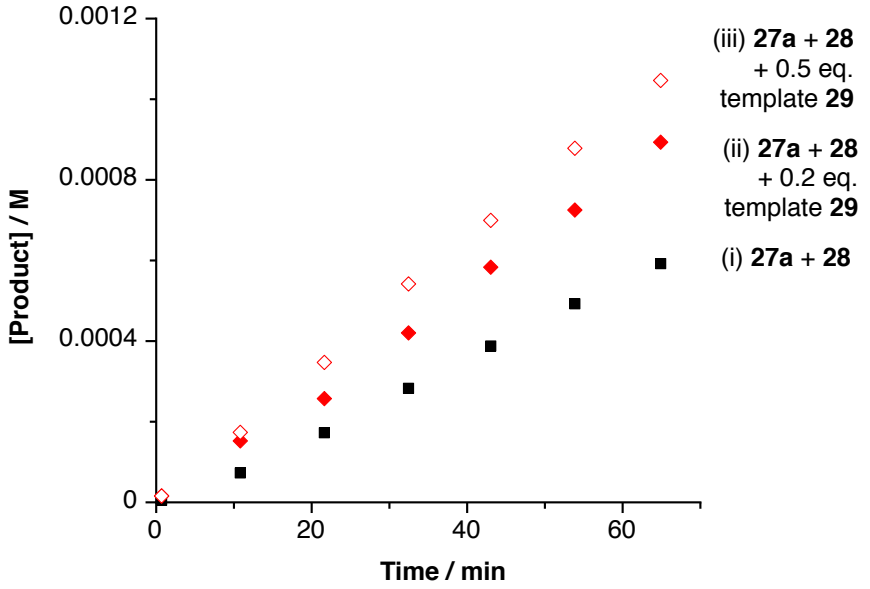

Figure 1.22. Initial rates of template formation as determined by HPLC. All reactions were performed with initial concentration of [**27a**] = [**28**] = 8.2 mM in $CHCl_3$ with 4 equivalent of Et_3N added as a general base. (i) Reaction of **28** and **27a**, (ii) Reaction of **28** and **27a** with 0.2 equivalent of preformed template **29** and (iii) Reaction of **28** and **27a** with 0.5 equivalent of preformed template **29**. Data taken from reference 54.

Menger and co-workers reinvestigated[55] the claims of autocatalytic self-replication in these systems. Menger *et al.* proposed a mechanism (**Figure 1.23**) explaining the rate enhancement found in this system, based on a bimolecular reaction between the bound amine building block and the non-binding ester, which led to a tetrahedral intermediate stabilised by the amide bond of the template. This mechanism directly questioned the replicative nature of Rebek's system as there was no obvious purpose for simultaneous recognition of both the ester and amide moieties, and, therefore the turnover could not be attributed to the ternary complex.

Thus, the methylated imide control compound **27b** used in original studies to prove the need for molecular recognition would not be expected to behave as a catalyst for this reaction. Whilst the scheme presented in this case might not be considered as autocatalytic, it is not self-replication in the sense of a selective autocatalyst as it

could, as it theoretically catalyse the reaction between amine building block and any activated ester. Rebek and co-authors discredited[56] this new evidence and the two groups participated in an open discussion by publishing new evidence[57,58] to support their own theories. The final comment on the controversial discussion was published by Reinhoudt *et al.* They utilized an intricate and detailed kinetic scheme[59] to quantify various different species and the reaction paths available to the components of a self-replicating system

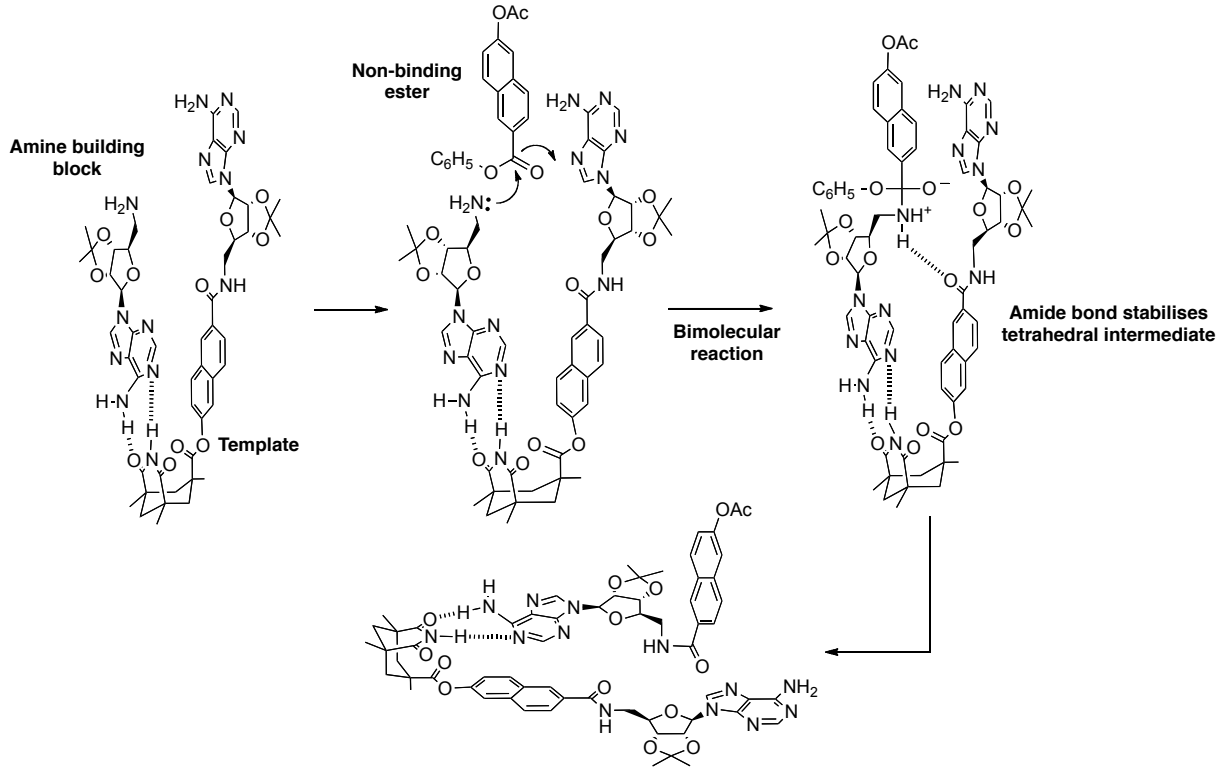

Figure 1.23. Menger's proposed amide catalysis mechanism. The mechanism involves the assembly of the amine building block upon the template followed by a simple bimolecular reaction with non-bonding ester to produce the tetrahedral intermediate, which is stabilised by the amide bond of the template.

The study demonstrates that these different pathways could obscure the simple picture of a single pathway as the only responsible of rate enhancement. They concluded that both the Rebek and Menger interpretations are correct as such the mechanism of self-replication originally proposed by Rebek was operating in the system however its observation was also hampered by alternative pathway described by Menger.

Although the reaction between **27a** and **28** in the presence of preformed template **29** can operate through self-replication, the major pathway in its absence is the [**A•B**]

complex. Given the debate from the initial publication of synthetic replicating molecules, this event serve to demonstrate and emphasize the usefulness of full kinetic modeling in characterising the autocatalytic reaction.

Throughout the time that these discussions were taking place, the Rebek research group improved its system to present evidence of sigmoidal growth and render the [**A•B**] pathway less important by preparing a longer spacer, 4,4'-biphenyldiyl spacer[60] in compound **30**. This adaptation separates the reactive centres in the [**A•B**] complex rendering it less reactive in the intramolecular sense (**Figure 1.24**).

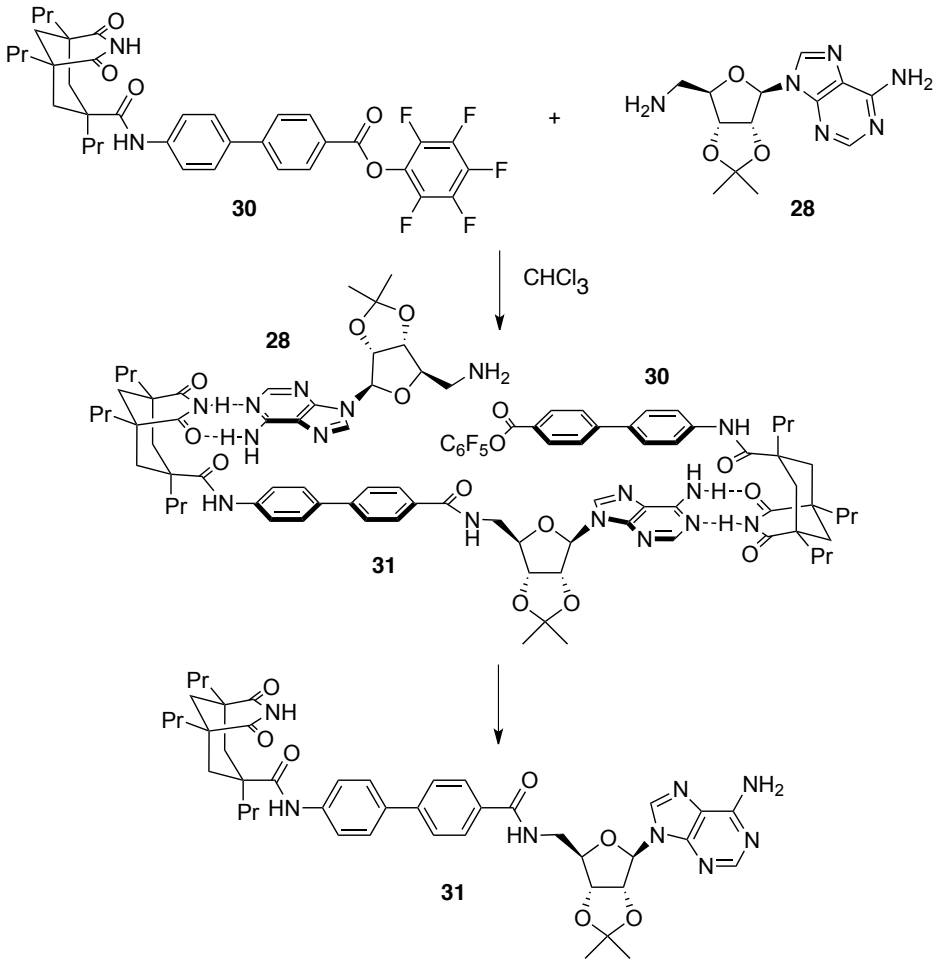

Figure 1.24. Compound **31** was prepared by acylation of the 5'-aminoadenosine derivative **28** with the biphenyl ester **30** in $CHCl_3$.

This adenine-imide conjugate **31** possesses self-complementary that can acts as templates for their production (**Figure 1.25**). It was clear that the sigmoidality of the autocatalysed reaction curve is a contribution of the self-replicating pathway *via* ternary complex even though the mechanism involving bimolecular base paired species is still operative.

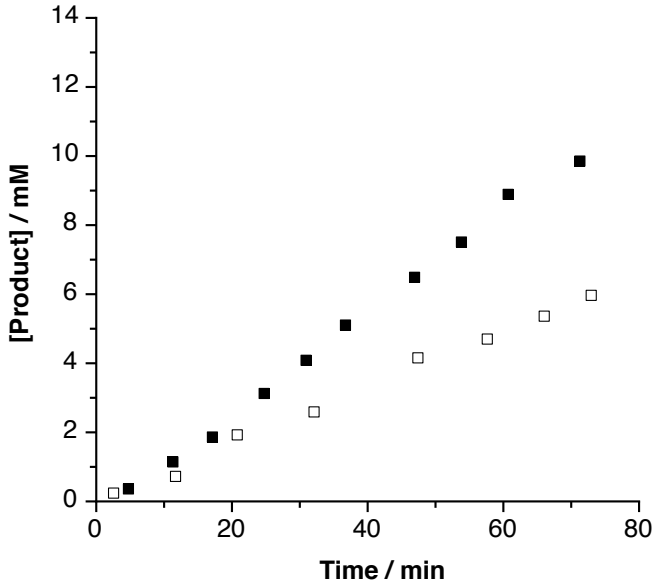

Figure 1.25. Initial concentration of template production in second generation of Rebek's replicator with a clear sigmoidal character (filled squares). Original data taken from reference 60.

Furthermore, the Rebek laboratory has also reported a novel design based around a xanthene scaffold with recognition between a diaminotriazine and a thymine with amide formation for the bond forming[61]. Then, they combined the imide/adenosine and thymine/diaminotriazine systems to generate two hybrid systems, both capable of self-replication[62].

Majority of the systems demonstrated earlier follow a half reaction order, which display a parabolic growth. Attempts to realise this principle have utilized the reversible covalent reaction with even simpler organic constituents. Terfort and von Kiedrowski[63] used the amidinium-carboxylate salt bridge to replace the base pairing for molecular recognition. Condensation of aniline **32** with aldehyde **33** yielded imine **34**, which can exist in conformations in which the recognition sites are aligned roughly parallel to each other (**Figure 1.26**).

These molecules should act as autocatalysts since they should be able to bind components **32** and **33** more easily due to preorganisation effect within the ternary complex [**32•33•34**]. In this case, the autocatalytic cycle was observed as such the higher addition of the initial concentration of **34** in the reaction mixture, the faster its formation. From the experimental evidence, the condensation follows the square-root law.

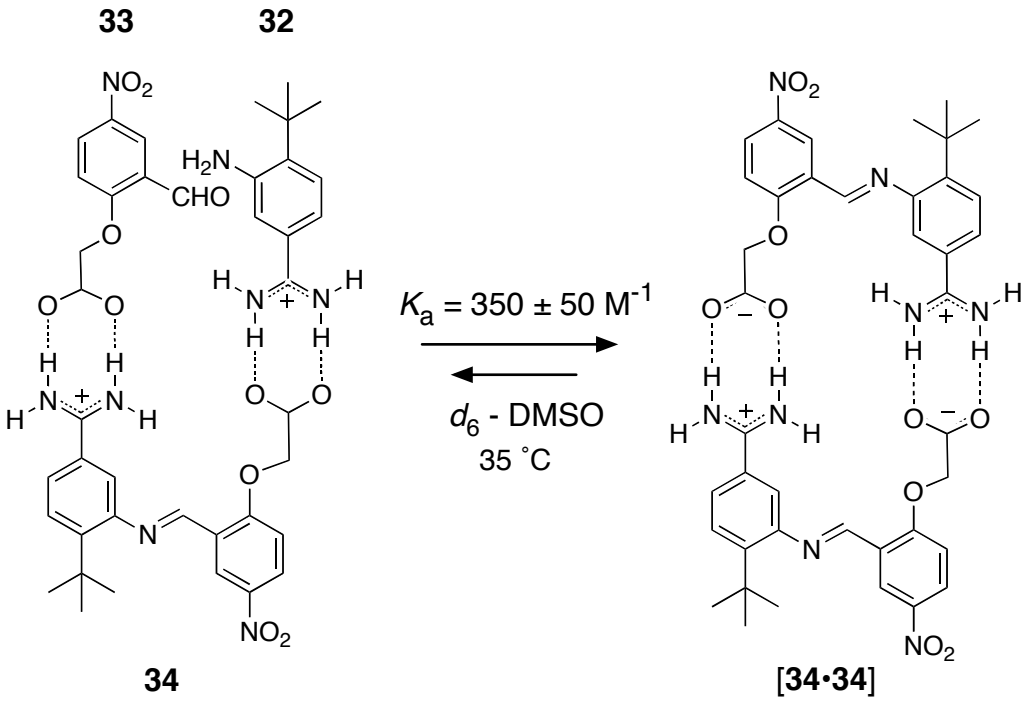

Figure 1.26. Template **34** bind amine **32** and aldehyde **33** within the ternary complex to give the subsequent template duplex [**34**•**34**].

1.5.5 Self-replicating systems based on Diels-Alder reaction

Other examples have been developed based on Diels-Alder reaction, studied by Wang and Sutherland[64] in 1997. The 2-acylaminonaphthyridine **35** and the 6-acylamino-2-pyridone derivative **36** were selected as target ene and diene systems with both the naphtyridine and 2-pyridone as the complementary recognition site (**Figure 1.27)**.

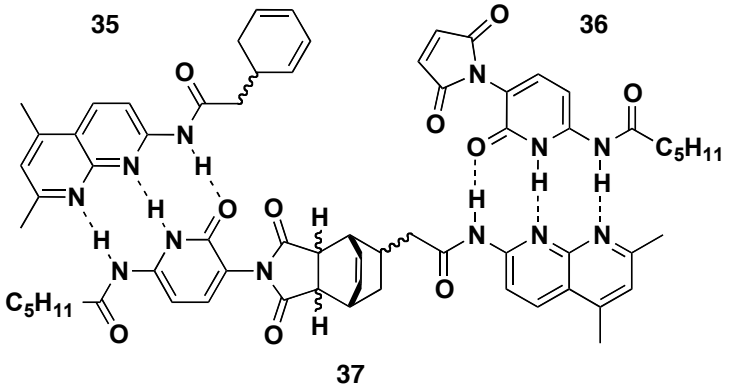

Figure 1.27. Diels–Alder cycloadduct **37** can assemble the diene **35** and maleimide **36** in a catalytically-active ternary complex in CD_2Cl_2.

The course of the product formation **37** were followed by ^{1}H NMR spectroscopy and revealed an autocatalytic reaction order of 0.8 with sigmoidal character. This was

further confirmed by treatment of up to 10% of preformed template **37**, which validate that the reaction was template-dependent with the loss of induction (**Figure 1.28**) period. They remarked that this reaction is the very first example of nearly exponential growth and could offers the basis of efficient self-replicating systems capable of chemical information transfer in terms of regio- and stereoselectivity of template catalysed bond formation.

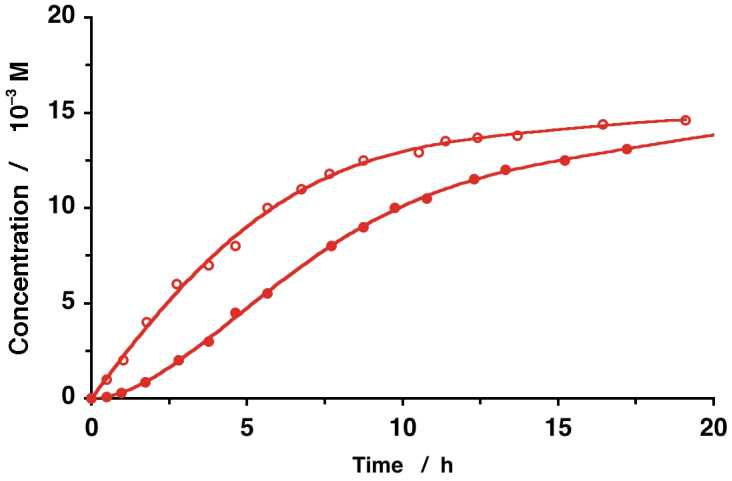

Figure 1.28. Concentration *vs* time profile for the formation of **37** in CD_2Cl_2 at 25 ˚C (open circles in graph). The addition of 5 mol% preformed template **37** to the reaction mixture (filled circles in graph) removes the lag period from the initial concentrations demonstrating that **37** is a catalyst for its own formation. Figure taken from reference 64.

It also has the potential to exhibit homochiral autocatalysis and heterochiral cross-catalysis, because a chiral diene **35** was employed as a racemic mixture, this opens the possibility of many diastereoisomeric reaction pathways. However, consideration of the stereochemical implications of the bond forming reaction and the presence of a chiral building block reveals some unexplained aspects and have not yet been completed in their paper. The [4+2] cycloaddition reaction is reported to produce an *endo* stereochemistry but no unambiguous assignment of the stereochemistry of the template has been made.

On that account, Kinderman and Stahl from the von Kiedrowski lab[65] in 2005 has decided to reassess the Wang-Sutherland system with respect to its stereochemical aspect. It is evident that their variants resembled Wang-Sutherland system with a further increase of reaction order of 0.89 and 0.9 denoting the operation of homochiral autocatalytic and heterochiral crosscatalytic reaction channels operating

in the systems. Self-replication with the ability of chiral instruction has recently received considerable attention from its relevance to the question of breaking of chiral symmetry on the early earth[66]. Further examples of self-replication developed within our research groups also focussed on the cycloaddition[67,68,69] reactions. In previous example[27], the Philp laboratory exploited the Diels-Alder reaction between furan and maleimide as the means of forming covalent bonds while maintaning the similar recognition motif. The Diels-Alder reaction gives two diastereoisomer products, namely the *endo* and *exo* cycloadduct. Only one of two possible diastereoisomers formation is being accelerated through the reactive binary [**A•B**] complex as described previously in **Section 1.4.1**.

We then become interested[70,71] to employ this reaction and carried out a series of potential replicators with structurally related system in von Kiedrowski[65] replicator. We examined the role that systematic structural variation plays in determining the recognition-mediated reactivity in order to probe the relationship between structure and function in minimal self-replicating systems. A clear take home message[72] is that a small structural changes can make huge differences of function that are not entirely foreseeable.

In addition, the design and characterization of a minimal self-replicating system based on 1,3-dipolar cycloaddition has also been well investigated[31,32,73]. Typically, this reaction affords a pair of racemic diastereoisomeric cycloadducts, *trans* and *cis*, depending on the relative orientation of the nitrone and the maleimide. The two products provide the means of exposing the efficiency of information transfer in any replicating system as the *trans* to *cis* ratio observed is always close to 3:1 in the absence of molecular recognition. These two products have markedly different geometries. The *trans* diastereoisomer has an open geometry compatible with acceleration through the ternary complex and the *cis* diastereoisomer has a closed geometry compatible with acceleration through the [**A•B**] complex pathway.

The initial reaction between nitrone **7** and maleimide **8** reacted at 10 ˚C in $CDCl_3$ affording the corresponding *trans* **9** and *cis* **9** (as depicted in **Figure 1.5a**). It is clear that the introduction of the recognition motif has significantly increased the rate of the reaction with sigmoidal growth, particularly for the formation of the major, *trans* **9**

(blue filled diamonds in **Figure 1.5b**) with reaction order, *p* of 0.9. The result clearly shows that the high *p* value is a result of efficient autocatalytic cycle. Further optimization on the performance of replicating system was carried out by screening a series of compounds computationally[73] and we identified nitrone **38** (*para* position) and maleimide **39** as suitable precussors (**Figure 1.29**). The calculated structure on the two possible diastereoisomers reveals that *trans* **40** has an open structure, in which the two recognition sites are available to interact with other complementary species in solution, while the structure of *cis* **40** is folded with the recognition sites are placed in proximity to each other, thus rendering this product inert in a catalytic sense. These computational studies indicate that *trans* **40** should be capable of templating its own formation through the transition state of the ternary complex [**38**•**39**•*trans* **40**].

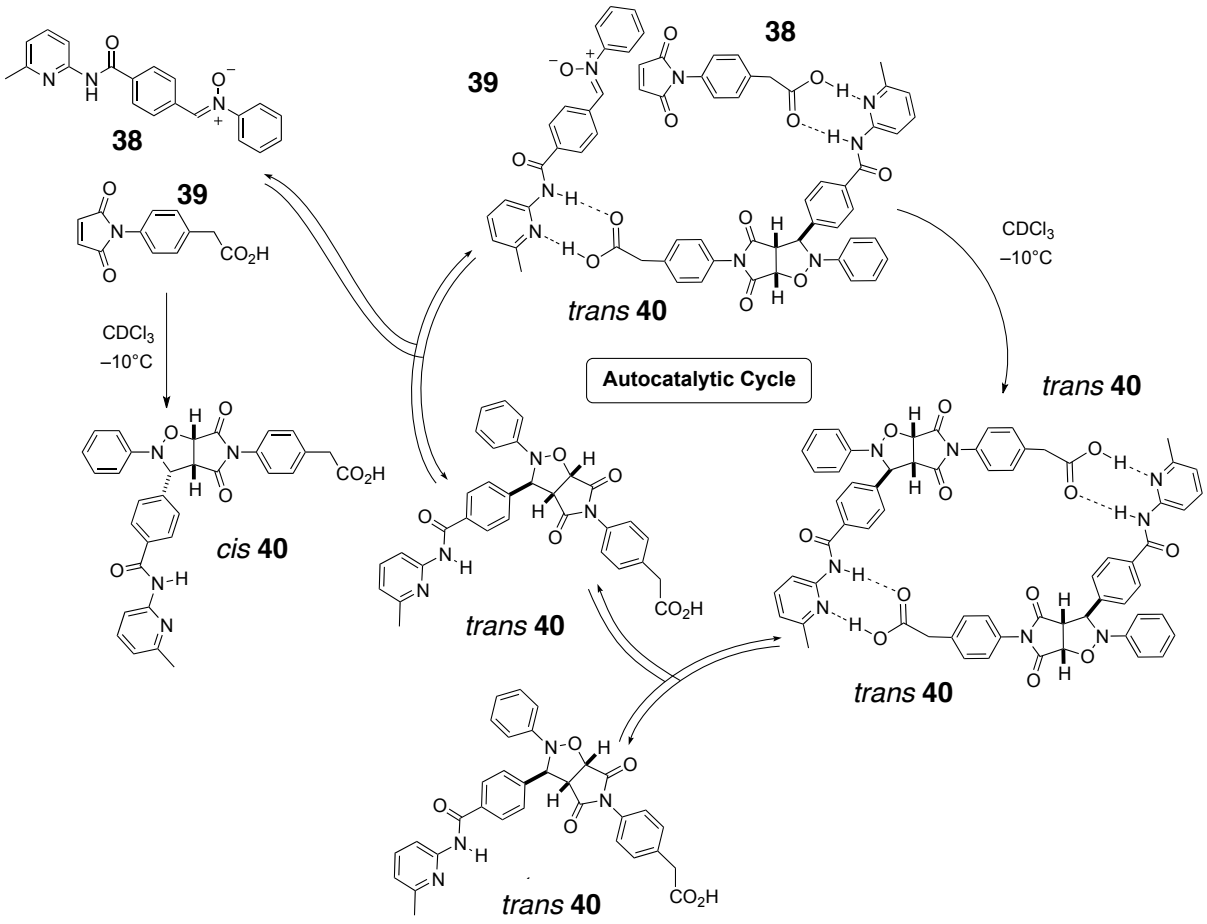

Figure 1.29. Reaction of nitrone **38** with maleimide **39** in $CDCl_3$ at –10 ˚C gives rise to two diastereoisomeric cycloadducts – *trans* **40** and *cis* **40**. The exclusive formation of cycloadduct *trans* **40** is mediated by the formation of ternary complex [**38**•**39**•*trans* **40**].

Experiments conducted with **38** and **39** in $CDCl_3$ at –10 ˚C revealed that the recognition-mediated reaction were uniformly fast, reaching more than 85% overall

conversion after 16 hours and the diastereoselectivity was 115:1 with the formation of the major product *trans* **40** (blue filled diamonds in **Figure 1.30**) in comparison to the *cis* diastereoisomer (red filled circles in **Figure 1.30**). Furthermore, the concentration *versus* time profile reveals the classical sigmoidal shape characteristics of an autocatalytic process and the rate of reaction are higher than that observed in the absence of recognition.

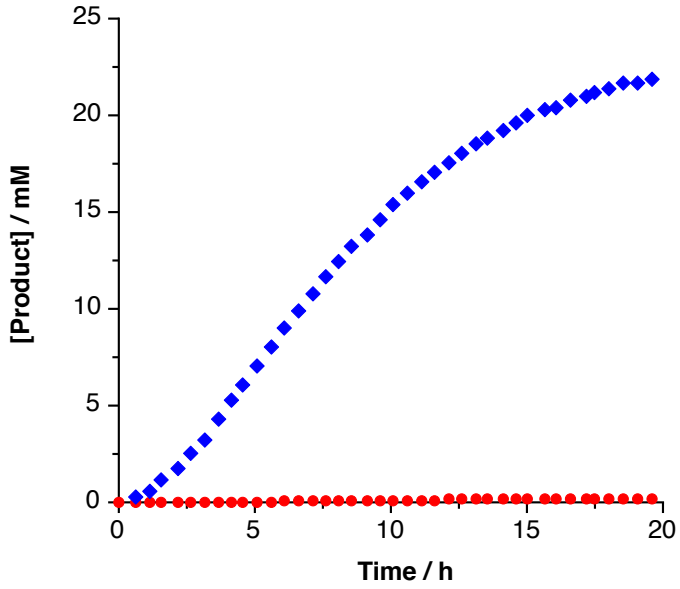

Figure 1.30. Concentration *vs* time profile for the reaction between nitrone **38** and maleimide **39** demonstrating the sigmoidal growth for exclusive formation of *trans* **40** (blue filled diamonds) with a ratio of 115:1 to *cis* **40** (red filled circles) at –10 ˚C in $CDCl_3$.

The injection of substoichiometric amounts (10 mol%) of *trans* **40** at the start of the reaction between **38** and **39** accelerate the maximum autocatalytic rate formation of *trans* **40** immediatedly at t = 0. The *trans* to *cis* ratio is now at least 250:1. By contrast, the addition of 10 mol% of *cis* **40** has no effect on the rate profile. Therefore, the *cis* cycloadduct is completely incapable of competing with the efficient replication cycle for *trans* **40**.

As part of the ongoing studies on self-replicating systems, our focus has shifted toward exploiting the implications of replication events in dynamic and reactive chemical systems and networks. We became intrigued by the possibility of introducing a reversible covalent bond forming reaction into our own replicating systems. The central design involved the condensation reaction[74] between an aniline derivative **41** and an aromatic aldehyde **42** to form an imine **43**. Imine **43** is capable of directing its own formation through recognition-mediated pathways (**Figure 1.31**).

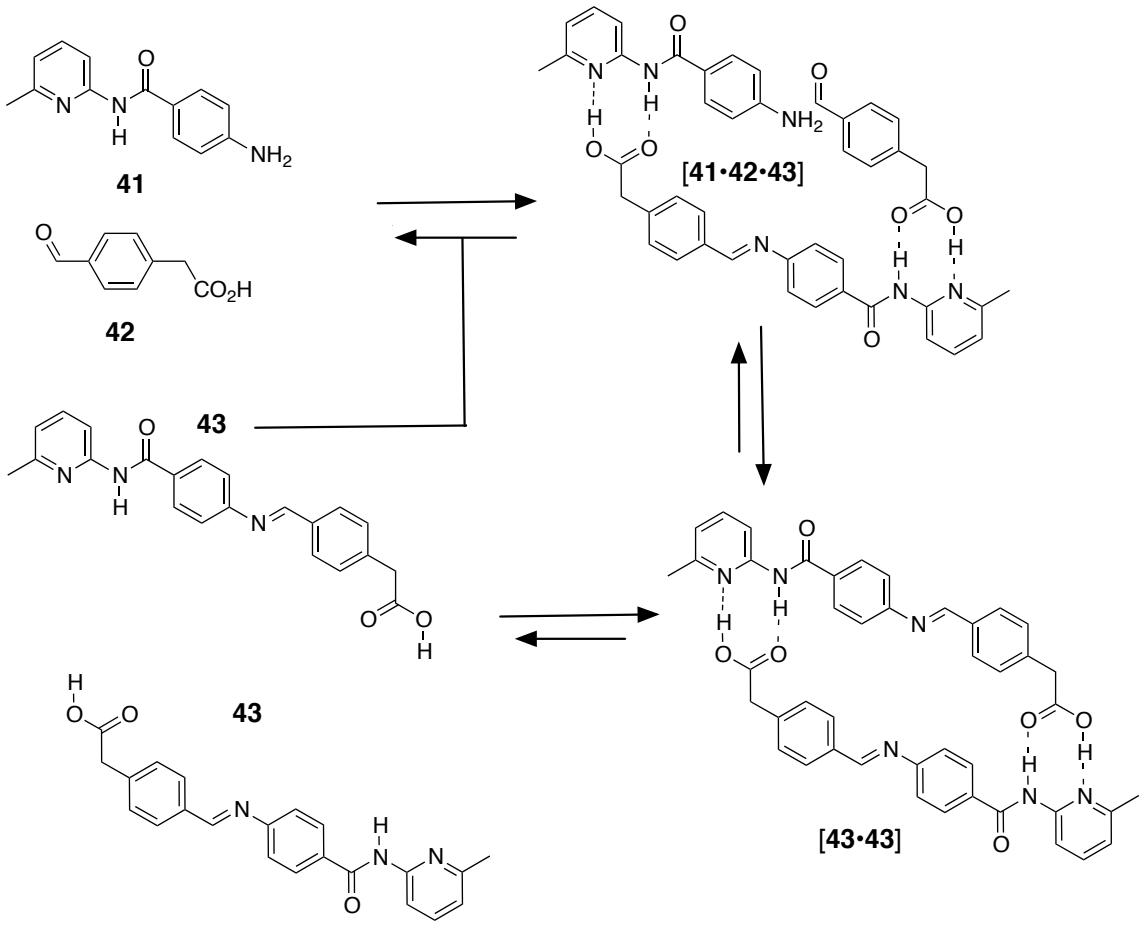

Figure 1.31. Imine **43** capable to assemble amine **41** and aldehyde **42** in $CDCl_3$ at 25 ˚C and accelerate the reaction between them through the autocatalytic cycle, which is mediated by the ternary complex [**41**•**42**•**43**].

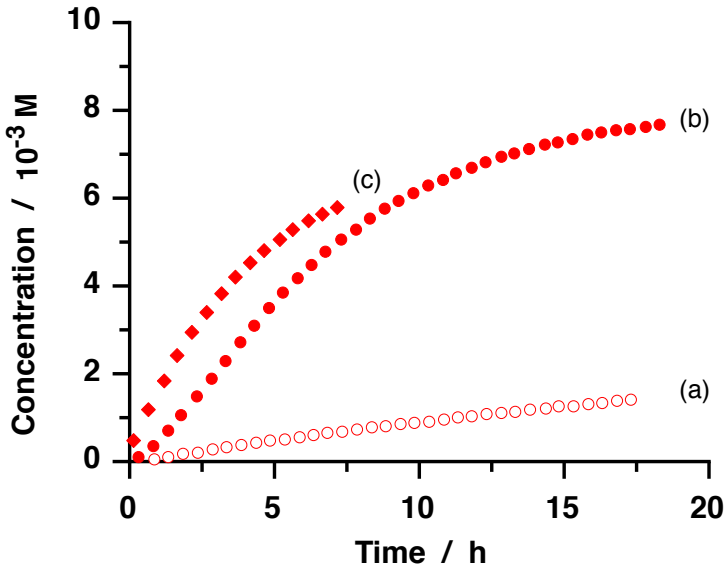

Figure 1.32. Concentration *vs* time profile for (a) non-recognition-mediated reaction between **41** and 4-methylbenzaldehyde (open circles); (b) formation of imine **43** (filled circles) and (c) in the presence of 15 mol% of **43** at the start of the experiment (filled diamonds). All experiments were conducted in dry $CDCl_3$ at 25 ˚C from starting concentrations of the appropriate reagents of 15 mM. Figure adapted from reference 74.

In the case of recognition-mediated reaction between **41** and **42**, the rate of reaction was relatively fast with more than 50% conversion, which clearly manifested the sigmoidal characteristics for the rate profile (**Figure 1.32b**). In the absence of recognition (**Figure 1.32a**), the rate of the reaction was very slow with lower conversions. Addition of 15 mol% of preformed imine **43** at the start of the reaction, results in the disappearance of the lag period and the maximum rate was reached at the beginning of the reaction (**Figure 1.32c**).

1.6 Outlook

The design and implementation of chemical entities capable of replication by either autocatalytic or crosscatalytic pathways has engaged and challenged synthetic chemistry for the past twenty-five years. The demonstration of molecular replication implied that a replication is possible for chemical information transfer and amplification with notable obstacles have been disclosed in **Section 1.4**. The idea that a molecule could catalyse its own formation has been long associated with the Origin of Life. In order to reach the ultimate goal of creating functional chemical systems using synthetic tools that is capable of directing its own synthesis and cooperating with other similar systems to create an organized network, a much higher level of design is therefore required. These ideas will be explored in subsequent chapters.

2

Chemical topology and mechanically interlocking molecules

In general, chemical topology[75] describes the connectivity and linkage of atoms and molecules in space. This connectivity and linkage play vital roles in determining[76] the chemical and physical characteristics of the molecules. The concept of chemical topology is highly relevant[77] when considering interlocked[78] structures. A compound regarded[79] as significantly topological, if, by a continuous deformation of the bonds between the atoms, it cannot be converted into another isomer of the compound albeit having the similar connectivity and occupy a non-planar molecular graph when embedded in three-dimensional space.

For instance, a [2]-catenane (**Figure 2.1a**) needs at least two crossing points when drawn on a pieces of paper, which illustrates the structure has a non-planar graph when embedded in three-dimensional space. Thus, a [2]-catenane cannot be converted into the constituent rings without physically breaking one of the macrocycles and reforming the ring in the absence of others. Conversely, deformation of the macrocyclic component of a [2]-rotaxane (**Figure 2.1b**) allows it to be removed from the dumbbell component. Therefore, the [2]-rotaxane can be drawn as a planar graph when embedded in three-dimensional space and, hence, are not topological isomers[80] of their component parts.

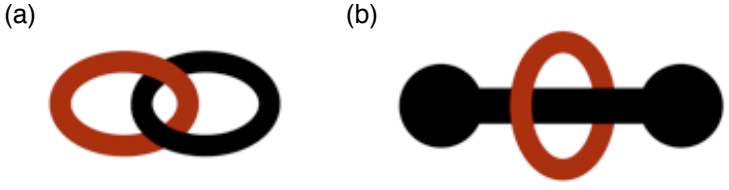

Figure 2.1. Cartoon representation of mechanically interlocked molecules : (a) [2]-catenane and (b) [2]-rotaxane.

In other words, if we could imagine stretching out the ring component of the [2]-rotaxane with both hands more than its average width, at some extent the ring is going to slip over the thread, but not in the case of [2]-catenane. The astonishing developments in synthetic methodology in the field of supramolecular chemistry have allowed the creation and characterization of complex molecular topologies which are the supreme targets for chemical synthesis[81] of artificial products.

Over the past 40 years, chemists have sought to create complex interlocking molecular structure, in which the synthesis of intricate interwoven molecules has been taken to an advanced level from rudimentary structure[82] of rotaxane and catenane to trefoil knot[83], Solomon link[84], Borromean ring[85,86], the synthesis of the molecular equivalent of the Olympic rings, olympiadane[87] and ultimately to the molecules[88] in a suits, the suit[5]ane. The flurry of activity directed toward new topologically complex molecules will not only provide aesthetically attractive structure, but may exploit their functional potential in applications such as nanotechnology. The area of interlocked molecules is broad and therefore in the light of part of the research carried out in this thesis, focus will be lay down on recent advances in research into [2]-catenane and in particular, [2]-rotaxane molecular architectures which has been chosen to integrate the replication processes.

The first reported attempt in catenane synthesis were discussed[89] by Lüttringhaus *et al.* in 1958, whereas rotaxanes were put forward[79] in 1961 and shown to exist[90] in 1967. The introduction of template synthesis of catenanes and rotaxanes by Sauvage *et al.* in 1984 and by Stoddart *et al.* in 1989 opened up a new era. According to the IUPAC compendium of chemical terminology, rotaxane was defined as molecules in which a ring encloses another rod-like molecule having end groups too large to pass through the ring opening, which holds the rod-like molecule in position without covalent bonding. Generally speaking, a rotaxane is a chemical substance comprising one or more macrocyclic species threaded onto one or more linear species.

2.1 Nomenclature for mechanically interlocked system

In 1971, Schill was the first to introduce a nomenclature[82] system for rotaxane, which latterly offer a good basis to develop a more comprehensive nomenclature system.

The nomenclature employed with interlocked molecules involves placing in square brackets the total number of components before the name of the compounds or complexes. Thus, a [3]-catenane is comprised of three interlocked macrocycles, and a [3]-rotaxane is comprised of one dumbbell component and two macrocycles. The nomenclature for polymeric systems is described in **Figure 2.2**.

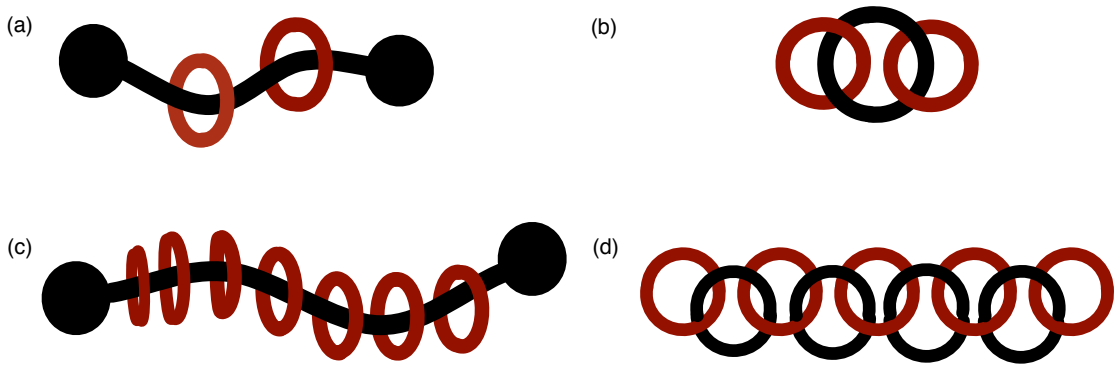

Figure 2.2. Cartoon representation of higher order rotaxane and catenane species. For examples: (a) [3]-rotaxane; (b) [3]-catenane; (c) [8]-rotaxane; and (d) [9]-catenane.

The extended version of nomenclature system proposed by Vögtle and co-workers included the information about mechanical or covalent linkages between the components of rotaxane[91]. As the authors themselves imply, creation of a complete systematic nomenclature system for these substances will be a formidable task.

2.2 The chemistry of the mechanical bond

This type of chemical bond found exclusively in mechanically interlocked molecules architectures in which two or more molecular components become mechanically interlocked, one with another, and so on, in some manner or another[75] such as catenanes and rotaxanes. Each component are not connected by conventional covalent bond but intrinsically linked to each other, resulting in mechanical bond, which prevents dissociation without cleavage of one or more covalent bonds. The first reported synthesis, by Wasserman[92] in 1960, of a catenane in a yield of 1% by statistical threading introduced mechanical bonds into chemical compounds.

Some years later, the Harrison and Harrison described[90] the synthesis of a polymer-bound rotaxane in a 6% yield after numerous treatment of column chromatography. Nevertheless, the absence of any appearance of templation was evidenced in the very low yield of these first catenanes and rotaxanes. Mechanical

bonds present[93] chemists with both the worlds of the molecular and supramolecular, since they contain all the intricacies and subtleties associated with coordinative and covalent bonding, rendering the molecules ideal for the control of function at single molecule to the macroscopic levels.

Therefore, the presence of geometrically precise coordination and non-covalent bonds are key[94,95] to the introduction of mechanical bonds *via* template effects into molecules with any kind of proficiency and efficiency. In addition, the fact that these weaker bonds live on inside these mechanically interlocked molecules after their template-directed synthesis[96] give the molecules much added value when it comes to exploiting their physical and chemical properties. Therefore, the fundamental understanding of the nature of the mechanical bond is paramount in the challenge to make more sophisticated compounds and can be employed to do complex systems chemistry in very different environments where emergent phenomena[97] become the order of the day.

2.3 Pseudorotaxanes

A common retrosynthetic disconnection shared by generic [2]-rotaxane and [2]-catenane structures revolves around [2]-pseudorotaxane precursor[98], in which a linear molecule is threaded through a macrocyclic unit. Thus, they are similar to rotaxane structure with the exception that the linear molecule not terminated by the two bulky stoppers. Further modification of the this precursor can possibly proceed in two ways, by virtue of (a) stoppering the end linear component with sufficiently large groups, results in the formation of [2]-rotaxane or (b) macrocyclisation of the linear component to affords to [2]-catenane (**Figure 2.3**).

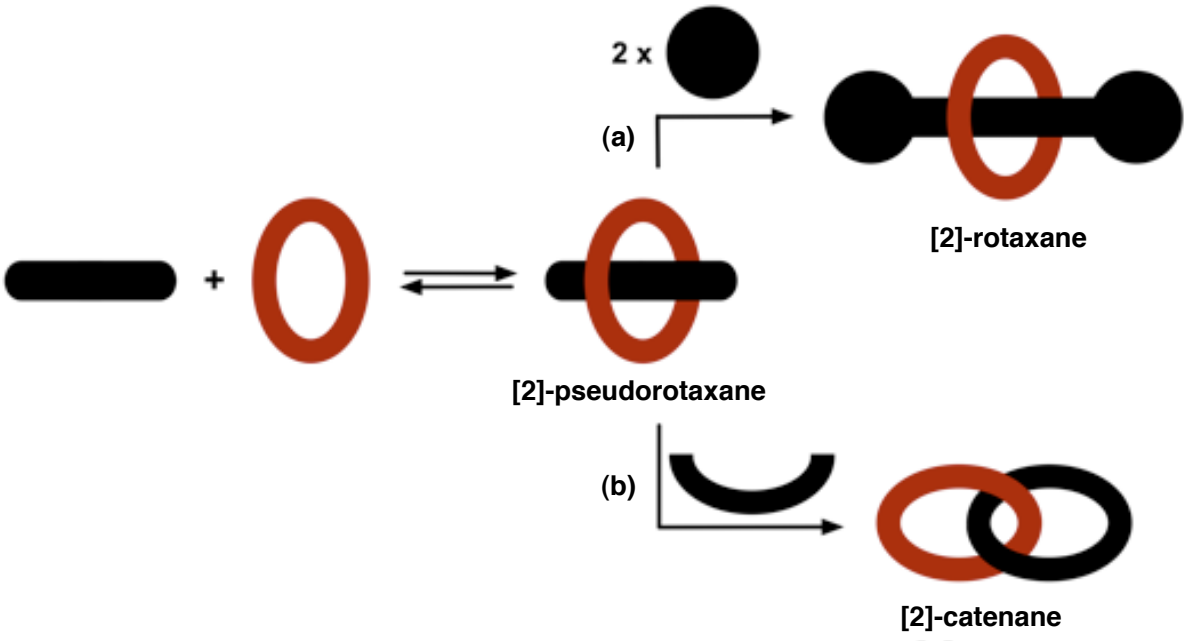

Figure 2.3. Cartoon representation of the synthesis of (a) [2]-rotaxane by means of stoppering the linear component with two bulky end groups and (b) [2]-catenane by means of macrocyclisation of the linear component of the similar precursor.

It should be noted that a considerable number of [2]-pseudorotaxane[99,100] have been investigated. The successful directed self-assembly of the [2]-pseudorotaxane utilized cyclobis (paraquat-*p*-phenylene) tetracation **44** and linear polyether **45**, incorporating two tetraethyleneglycol units alternating between three hydroquinone derivatives was carried out and isolated[101] (**Scheme 2.1**). The structure of this 1:1 product displays a large degree of self-ordering in the solid state, largely based around π-π stacking.

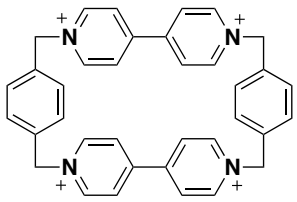

44

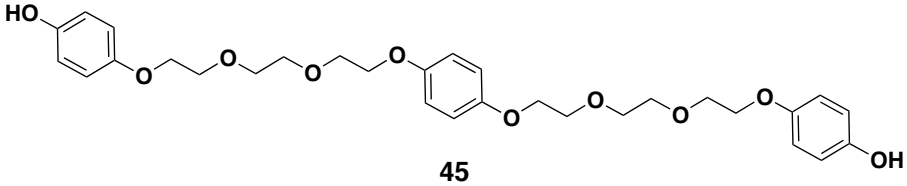

45

Scheme 2.1. Self-assembly of the [2]-pseudorotaxanes utilized tetracationic cyclophane **44** and linear polyether **45**.

Similar ordering process also has been established by the further synthesis of higher pseudorotaxanes such as the [3]-pseudorotaxane[102] with the formation of a

tightly-packed, π–π structure. Alternatively, an anion-directed pseudorotaxanes has been reported by Beer and co-workers[103]. The zwitterion **46** comprised Crabtree-type pyridinium cleft binding a chloride[104,105] with macrocycle **47** results in the formation of a pseudorotaxane [**46•47**] in acetone-d_6 with an association constant, K_a of 2400 M^{-1} (**Scheme 2.2**).

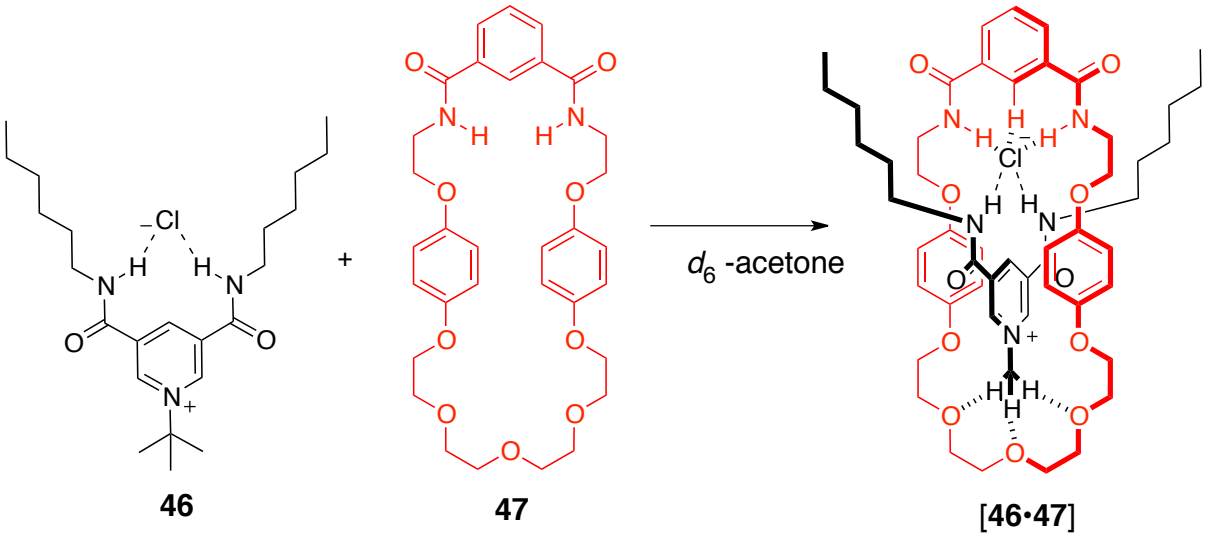

Scheme 2.2. An anion-directed [2]-pseudorotaxane [**46•47**] consists of a Crabtree-type pyridinium cleft **46** binding a chloride with macrocycle **47** reported by Beer and co–workers.

The pseudorotaxane is stabilized by chloride–NH hydrogen bonds, π–π stacking interaction and C-H•••O hydrogen bonds. A vast consideration has been given to the potential use of pseudorotaxanes in molecular devices[106] such as switches by means of external stimulus such as light. We will look into more detail on the switching experiment later in this chapter.

2.4 How to synthesise a [2]-rotaxane?

Theoretically, [2]-rotaxane can be constructed by three[107] different approaches. The first clipping strategy[108-110] (**Figure 2.4a**) initiated when an acyclic precursor is cyclised around a linear dumbbell-shaped template. This mode requires a recognition site within the linear component acting as a template for the formation of the macrocyclic component. The macrocycle is assembled in the correct formation to the binding site by means of non-covalent interactions.

Threading and stoppering[111-115] (as previously depicted in **Figure 2.3a**), involves a two steps strategy. Initially, a [2]-pseudorotaxane complex is formed between the

linear component and the macrocyclic component, whereas a sufficient interaction between both hydrogen bond donors and acceptors takes place. Subsequently, a bulky stopper will be inserted at both ends of the linear component by covalent bond formation preventing the dissociation of the macrocyclic ring (**Figure 2.4b**).

The stoppering groups are usually larger in size than the inner diameter of the ring to assure it did not slip off from the linear component. An alternative approach[116,117] to construct rotaxanes, called slippage (**Figure 2.4c**). In this procedure, the macrocycle and the dumbbell were prepared separately prior to self-assembly before heated together in an appropriate solvent permitting the macrocycle slips over the dumbell stopper by overcoming the associated free energy of activation. The resulting [2]-rotaxane is stabilised by non-covalent bonding interactions. The solution is then cooled down to ambient temperature, whereby the rotaxane comes into existence as the free energy barrier to its dissociation back into its components becomes insurmountable. It was reasoned[118] that careful size adjustment of the stoppers could permit the synthesis of the corresponding rotaxane directly at elevated temperature.

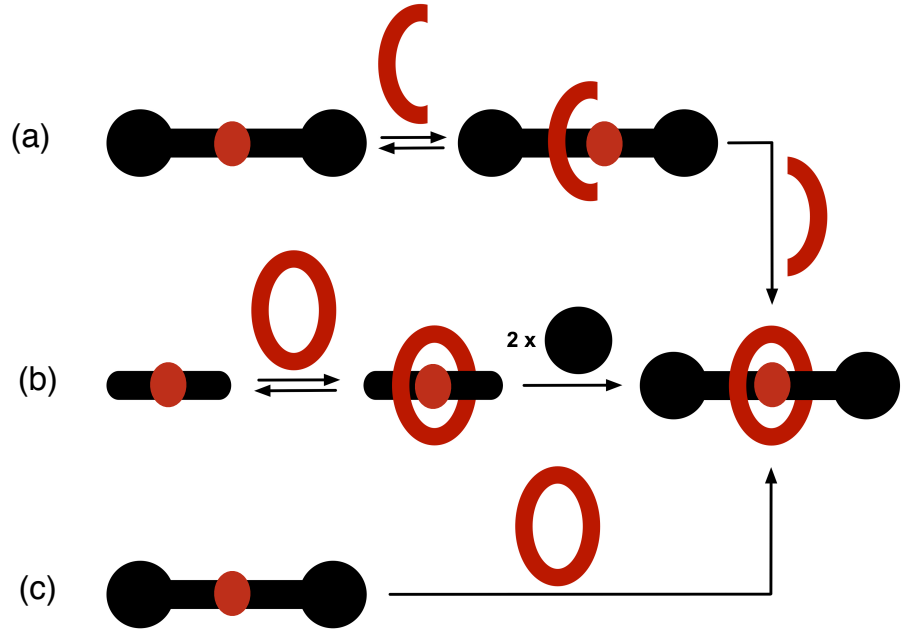

Figure 2.4. Three possible approaches in the formation of [2]-rotaxane: (a) clipping, (b) threading and stoppering and (c) slippage.

2.4.1 Clipping mechanism

The first [2]-rotaxane prepared to act as a molecular shuttle (**Scheme 2.3**) involved the clipping route[119] starting with the preformed triisopropyl silylated **48** polyether together with tetracation cyclophane **44** (from tetracationic precursor **44a** and *p*-dibromoxylene **44b**) as illustrated in Scheme **2.3**. The dynamic ^{1}H NMR 500 MHz behaviour of the resulting [2]-rotaxane [**44•48**] and [**44•48**]' indicated that the cyclophane bead shuttles to and fro between the two hydroquinone derivative sites approximately 500 times a second at room temperature.

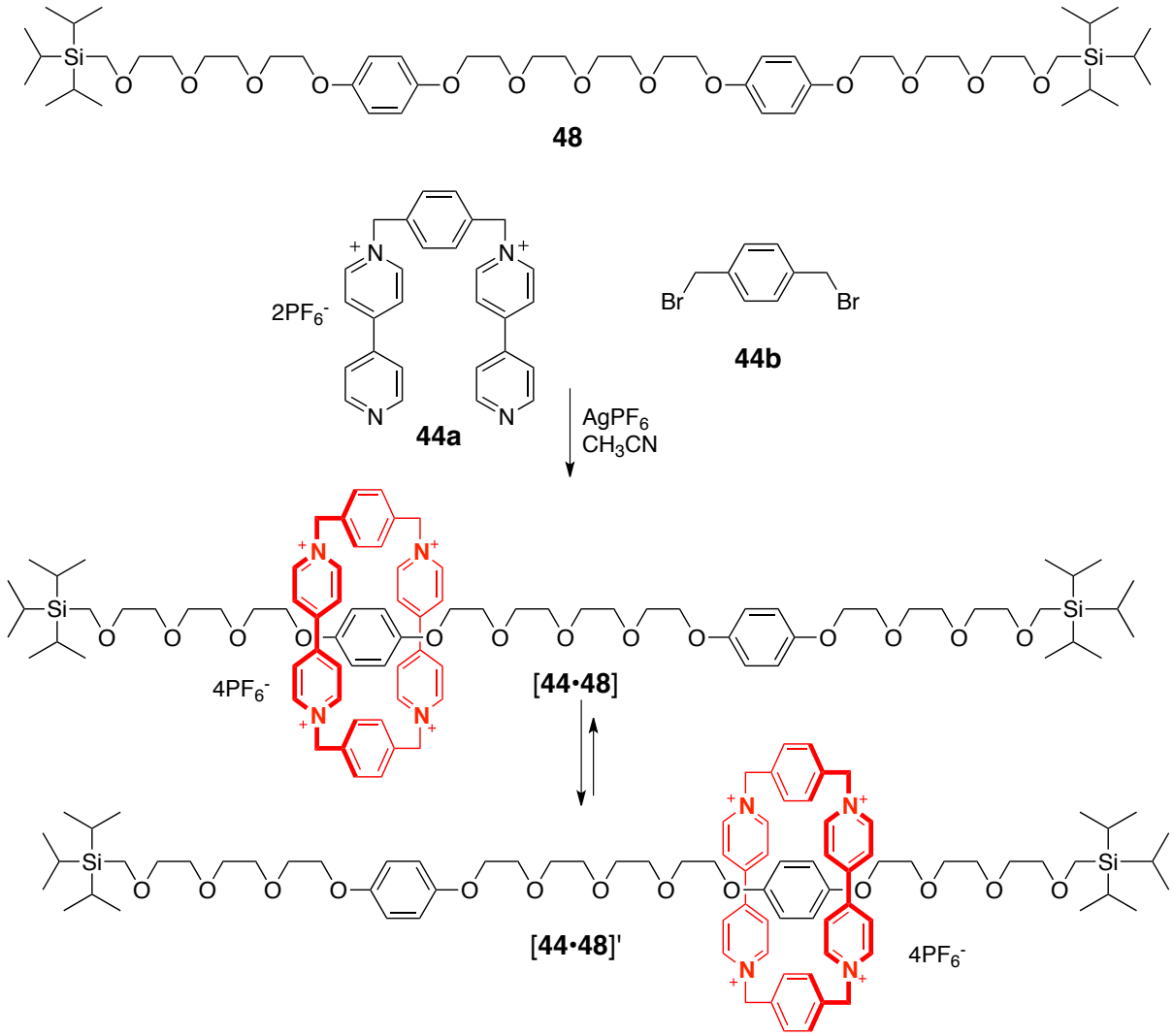

Scheme 2.3. A [2]-rotaxane prepared by the clipping mechanism, [**44•48**] and [**44•48]'** act as molecular shuttles. The tetracationic cyclophane **44** exchanges between two hydroquinone detivative sites approximately 500 times a second at room temperature.

2.4.2 Threading and stoppering mechanism

An example[120] which illustrates this methodology is the synthesis of [2]-rotaxane illustrated in **Scheme 2.4** which exploited the supramolecular assistance provided by

hydrogen bond interactions between secondary dialkylammonium centers and the macrocyclic polyether dibenzo-24-crown-8 (**DB24C8**). As a result of these hydrogen bond interactions, the functionalised diaklyammonium cation **49**$^+$ infiltrates the **DB24C8** cavity to give the pseudorotaxane [**DB24C8•49**]$^+$, which subsequently stoppered when its azido termini react with a bulky acetylenedicarboxylate by means of 1,3-dipolar cycloaddition to afford [2]-rotaxane **50**$^+$. The first amide-based rotaxanes were also have been described[121] employing the similar strategies.

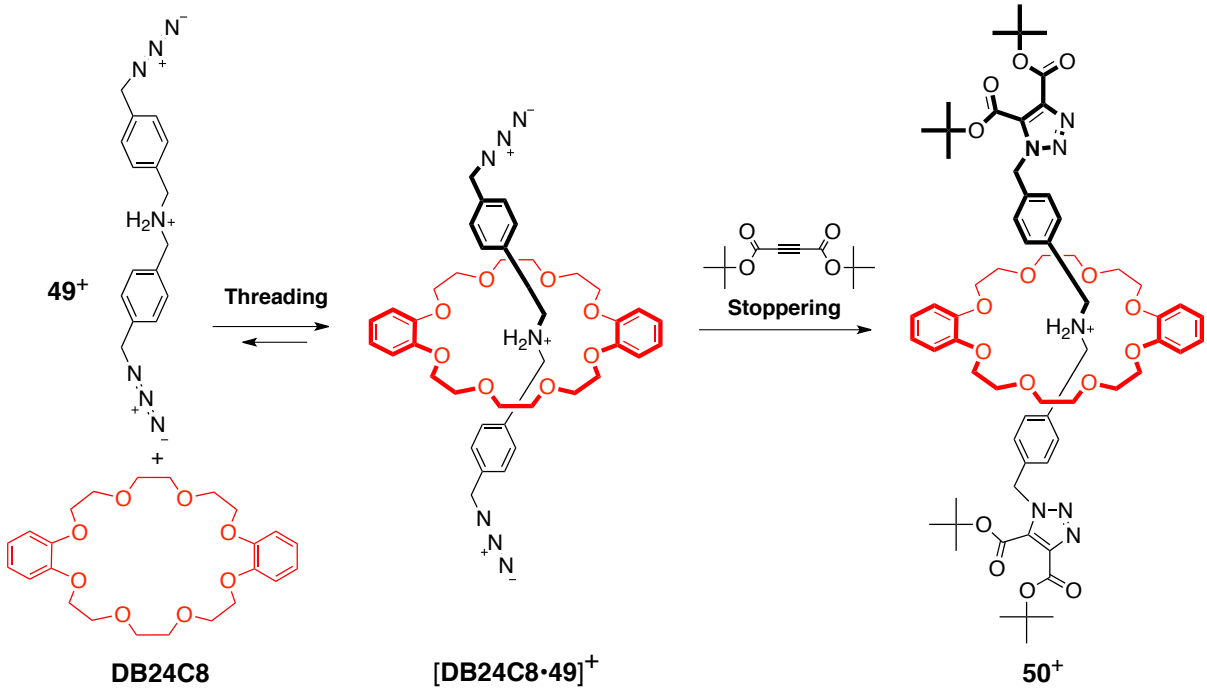

Scheme 2.4. Formation of [2]-rotaxane **50**$^+$ *via* threading and stoppering mechanism, which incorporates both **DB24C8** and secondary dialkylammonium cation **49**$^+$.

2.4.3 Slippage mechanism

The slippage procedure lends itself to the preparation of [*n*]-rotaxanes[122] that are based on longer linear fragments incorporating more than one dicationic binding site and fitted with stoppers of appropriate size. A kinetic investigation revealed[123,124,] that the free energies of activation associated with the slipping on and slipping off processes are correlated with the size of cavity of the macrocyclic component, as well as with the size of the stoppers attached to the dumbbell shaped component. The free energy of activation was observed to increase upon reducing the size of the cavity of the macrocycle and/or enlarging the bulk of the stoppers[125].

The successful synthesis of the [3]-rotaxane **51** has been achieved by this means[126] and provides a useful technique for the preparation of oligo- and poly-rotaxanes including ones in which many recognition sites along the linear component are encircled by different macrocyclic components (shown in **Scheme 2.5**).

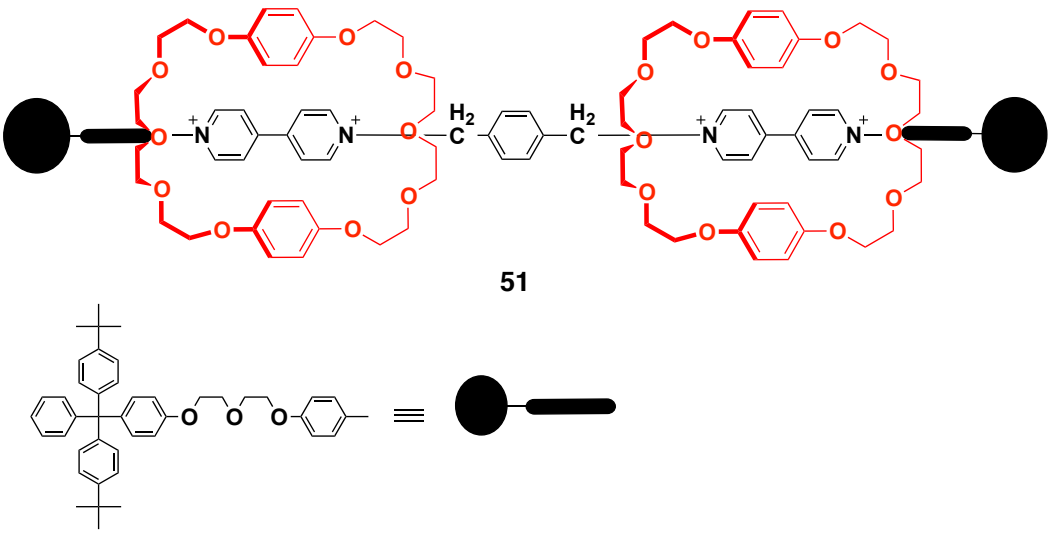

Scheme 2.5. Synthesis of [3]-rotaxane **51** by slippage mechanism based on longer linear fragments incorporating two dicationic binding site and fitted with stoppers of appropriate size (denoted by black circle).

In particular, the slippage approach leads to rotaxane that only stable under certain conditions as a consequence of elevated temperature imposed during the process. As a matter of fact, an increase in temperature, solvent polarity or acidity can substantially affect the stability[118] of rotaxanes.

2.5 Template synthesis of interlocked molecules

The term template[96] effect was first defined[127] and used in the beginning of late 1960s. A chemical template organises[128] an assembly of atoms with respect to one or more geometric point, in order to achieve a particular linking of atoms. The template provides instructions for the formation of a single product from a substrate, which otherwise have the potential to assemble and react in a variety of ways. By changing the template resulted in a different substrate assembly and consequently a different product. After the template has directed the formation of the product, it is removed to yield the template-free product. The emergence of supramolecular chemistry has allowed the exploitation of metal-ligand binding, hydrogen bonding and π–π interaction in the synthesis of larger molecules with a remarkable degree of

control. For instance, mechanically interlocked molecules can be synthesised in high yield using template-directed assistance to covalent synthesis.

Schill *et al.* have introduced[129] the first directed synthesis of catenanes, rotaxanes and knots with the use of covalent template. The multiple-step synthesis were employed in the preparation of [2]-catenane[130], [2]-rotaxane[131] as well as of molecular knots[132]. The covalent-directed synthesis also capable of delivering characterized mechanically interlocked molecular compounds although in small yields as a consequence of the many steps required in the synthesis. Furthermore, this protocol also give rise to the use of metal templates and subsequently, noncovalent templates for the efficient and practical synthesis of molecular catenanes, rotaxanes and knots in one or two steps in good yields from available precursors.

The seminal contribution[133] made by Sauvage in 1983 of the use of copper(I) cations as a template to form mechanically interlocked macrocyclic phenanthroline derivatives provided a facile and efficient means of making metallo-catenanes. A range of different templates has been utilized such as transition metals[134-137], π–donor or π–acceptors[138-140] and hydrogen bonding motifs[141-147]. The following section highlighted the formation of catenanes and rotaxanes under kinetic regimes.

2.5.1 Transition metal templates

Seeing the first reported metal-templated protocols[133], the efficient synthesis of catenanes and rotaxanes has now been well demonstrated[148,149] by employing a wide range of transition metals as synthetic templates. Sauvage and co-authors reported[150] a Cu(I)-templated [2]-rotaxane **55**•BF_4 with the aid of threading and stoppering approach (**Scheme 2.6**). In this case, a 2,2'-bipyridine derivative **52** is treated with a phenanthroline terpyridine containing macrocycle **53** in the presence of Cu(I) ions, resulting in the formation of a tetrahedral coordination complex.

The subsequent alkylation of the complex with the stoppering reagent **54** affords the desired Cu(I) templated rotaxane **55**•BF_4 in 20% yield for the final two steps. It was pointed out that **55**•BF_4 capable to undergo controllable rotary motion (pirouetting) of the macrocycle around the dumbbell axis following the oxidation and reduction of the

Cu metal center. Cu(I) ion opts for four coordinate ligand set in a tetrahedral geometry with the 2,2'-bipyridine and phenanthroline ligands while Cu(II) ion favors a five coordinate geometry with 2,2'-bipyridine and terpyridine ligands (as illustrated in **Scheme 2.6**).

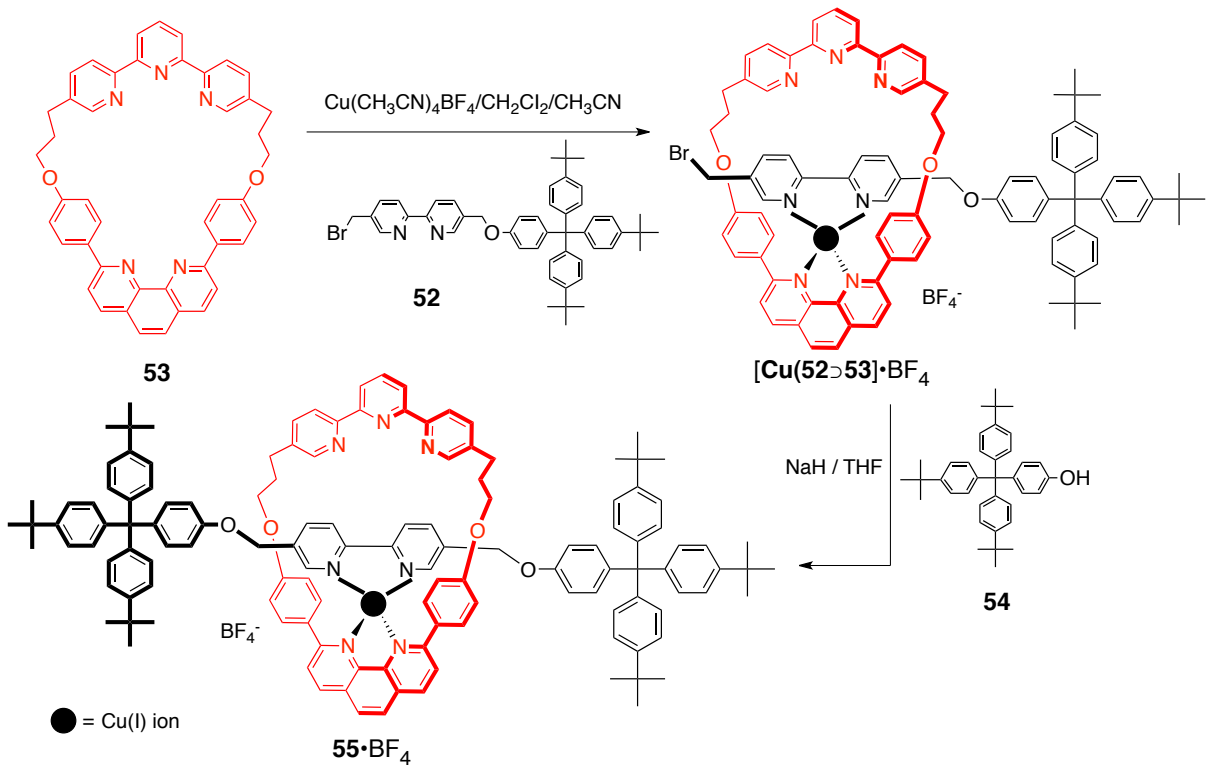

Scheme 2.6. Synthesis of the metal-templated [2]-rotaxane **55**•BF_4 by means of threading and stoppering approach.

2.5.2 π–donor or π–acceptor templation

Stoddart *et al.* initiated the templating effects of charged π–donor or π–acceptor[151] non-covalent bonding interaction in the synthesis of a [2]-catenane. The preparation of catenanes and rotaxanes[94,152] has benefited from charged π–donor or π–acceptor templates[153] on account of their high self-assembling efficiency. By far, the most effective π–donors for the preparation of charged catenanes and rotaxanes are those[154] based on tetrathiafulvalene (**TTF**) **56** and mutual recognition by the π–electron deficient tetracationic cyclophane **44**, (**CBPQT**$^{4+}$).

The binding affinities of 1:1 pseudorotaxane complex was determined to be aproximately 10 000 M^{-1} in CH_3CN at 298 K, which is driven by π–π stacking[155] and charge transfer interactions[156]. The mutual recognition was incorporated[157] in a bistable, electrochemically switchable, [2]-rotaxane **57**•$4PF_6$ in 23% yield by

employing the template directed clipping process (**Scheme 2.7**) with the dicationic salt **44a**•2PF_6 and dibenzylbromide **44b** around the dumbbell component, consist of two alternative donors site, monopyrrolo tetrathiafulvalene (**MPTTF**) and 1,5-dioxynaphthalene (**DNP**). Interestingly, when the clipping reaction is performed under high pressure (for example, 10 kbar), the yield of [2]-rotaxanes increased dramatically to 50%. Contemporaneously, the Sanders group[158] constructed the [2]-catenanes structure with high efficiencies by employing the neutral π–stacking motifs.

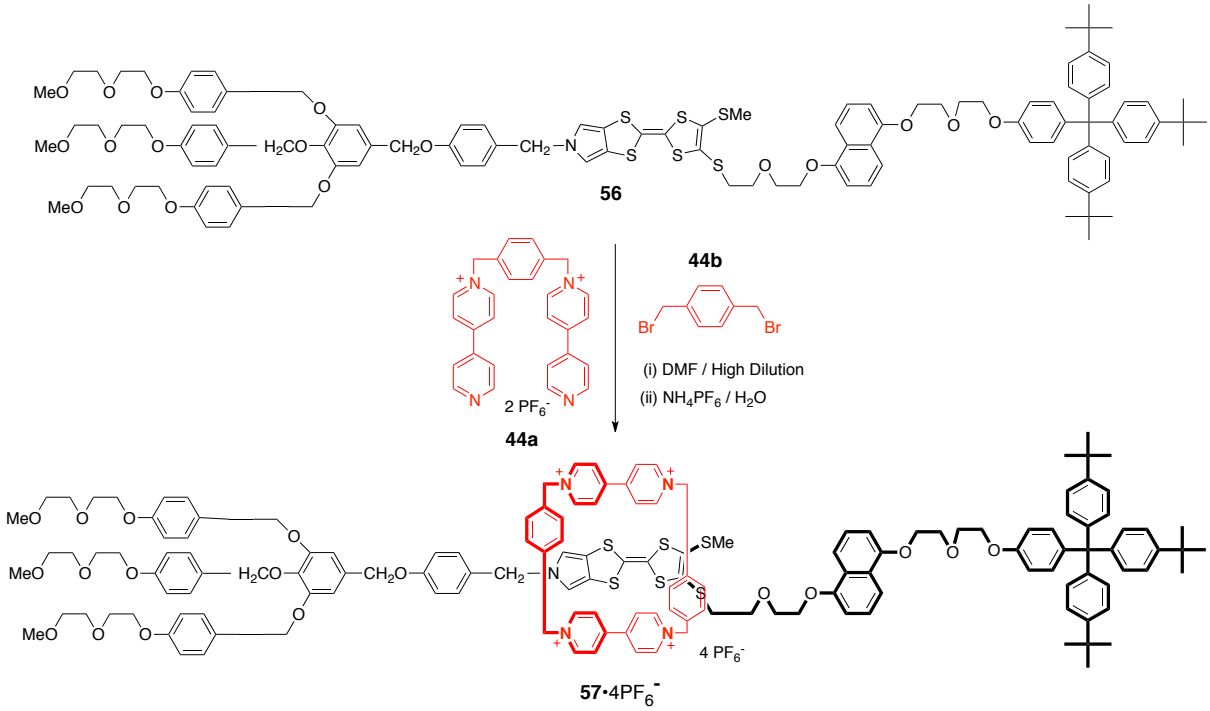

Scheme 2.7. Template directed synthesis of the charged π–donor or π–acceptor [2]-rotaxanes **57**•4PF_6 by virtue of clipping strategies around **MPTTF** units.

2.5.3 Hydrogen bond templation

Hunter[159] and Vögtle[160] independently reported the synthesis of [2]-catenanes in a satisfactory yield using amide forming reactions back in 1992. The intermediates[161] are held in place by strong [C=O•••H-N] hydrogen bond. Next, Leigh published[162-168] a various amide-based [2]-rotaxanes. One example[162] is that [2]-rotaxane **61** can be synthesised in a 59% yield from succinamide and naphthalimide-containing compound **58** with a standard one pot formation of the macrocyclic lactam ring from both compound **59** and **60**. The [2]-rotaxane **61** displays bistable switching behaviours in which the macrocyclic lactam ring moves from the succinamide station to the naphthalimide station (**Scheme 2.8**).

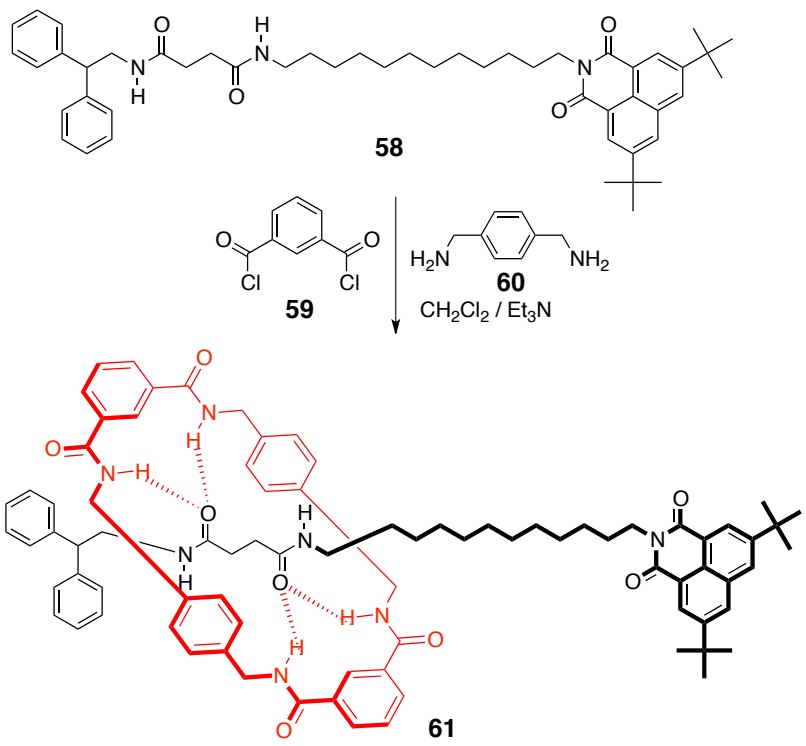

Scheme 2.8. Template directed synthesis of the amide-based [2]-rotaxane **61** from succinamide and naphthalimide-containing thread **58** with one-pot formation of the macrocyclic ring from the acyclic starting materials **59** and **60**.

Furthermore, a strong [N^+-H•••O] hydrogen bonding, resulting from the interaction between the published crown ethers, such as 18-crown-6 and 24-crown-8 with primary alkyl and secondary dialkylammonium ions can also be exploited in the hydrogen-bonding motif templates. Stoddart laboratory has published[169] that ammonium-containing [2]-rotaxanes **63-H**•2PF_6 and **65-H**•PF_6 can be prepared by templation between **DB24C8** and dialkylammonium salts **62-H**•PF_6.

The synthesis involves[170,171] threading and stoppering approach, whereas the stopper-end dialkylammonium salt **62-H**•PF_6 is threaded into **DB24C8**, followed by stoppering with triphenylphosphine, PPh_3 to afford [2]-rotaxane **63-H**•2PF_6 in 80% yield. The subsequent Wittig reaction with aldehyde **64** modified the triphenylphosphonium stoppers to an aryl stoppers. Such reactions, followed by catalytic hydrogenation provide new [2]-rotaxane **65-H**•PF_6 in about 50% yield (outlined in **Scheme 2.9**).

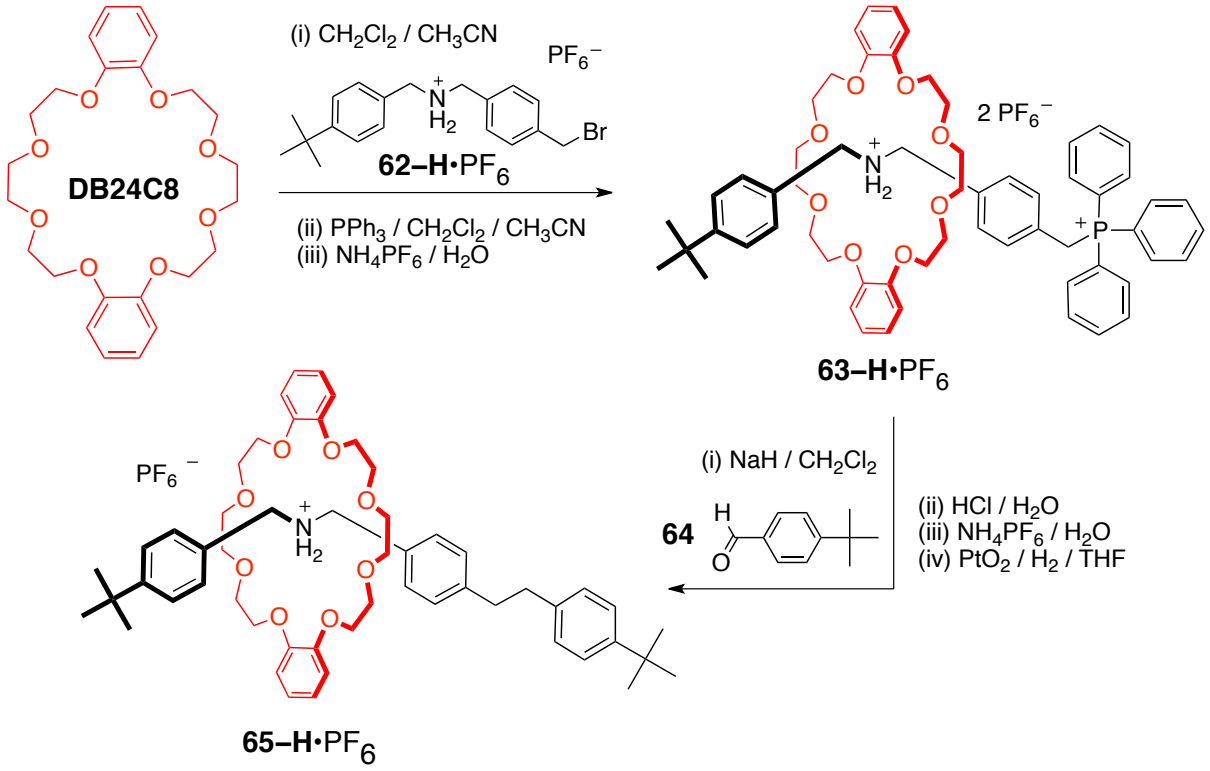

Scheme 2.9. Template directed synthesis of ammonium-containing [2]-rotaxane **63-H**•$2PF_6$ and **65-H**•PF_6 between **DB24C8** and dialkylammonium salts **62-H**•PF_6.

Alternatively, it was pointed out that the use of phenoxy anion templates[172-177] effectively directs the synthesis of [2]-rotaxanes in excellent yield. Vögtle has demonstrated[172] that the macrocyclic lactam **66** is a good acceptor for a *p*-triphenoxy anion as a results of forming [N-H•••O]$^-$ hydrogen bonds. As shown in **Scheme 2.10**, an intermediate complex [**66**•**67**]$^-$ is subsequently reacted with a trityl end-stoppered alkylbromide **68**, affording an amide-containing [2]-rotaxane **69** in 95% yield.

In conclusion, mechanically interlocked molecules, such as catenanes and rotaxanes can be efficiently prepared by utilizing organic or inorganic templates under kinetic control. The efficiency of these template directed strategies immensely depend upon the supramolecular approach that combine the cooperative non-covalent bonding interactions such as metal-ligand interactions, π–π stacking and hydrogen bonding motif to form intermediates, result in the irreversible formation of mechanically interlocked molecules by the formation of a final covalent bond under kinetic control. However, as a result of the irreversible nature of this approach, unbound dumbbell components and unbound macrocycles formed during the final step invariably reduce the yield of the mechanically interlocked compounds.

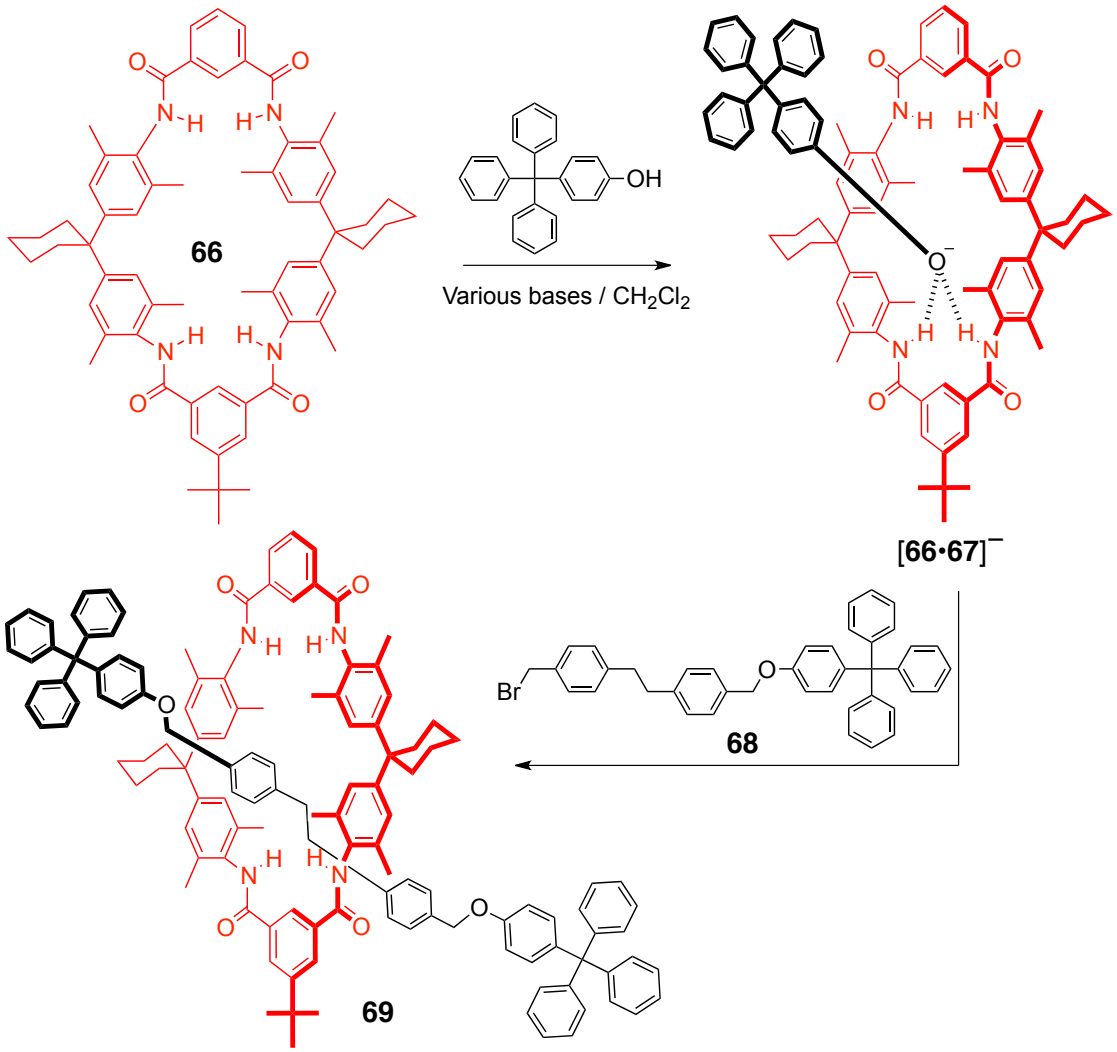

Scheme 2.10. Anion-templated synthesis of the [2]-rotaxane **69** using threading and stoppering approach.

2.6 Applications in devices

Research on supramolecular chemistry has shown that molecules are convenient nanometre scale building blocks in a bottom-up approach, to construct ultra miniaturised devices and machines capable of storing information[178] at the molecular level. Performing macroscopic mechanical tasks with the early generations of synthetic molecular machines has proved to be quite elusive. Molecules with mechanically interlocked architectures are particularly suited for these types of applications because they permit the controlled, large amplitude movement and positioning of one mechanically interlocked component with respect to another. Through the pioneering work[179-183] of Stoddart, Sauvage and Vögtle, it has become clear that rotaxanes have the ability to change the relative positions of their interlocked components by means of external stimulus such as chemical[184-186], electrochemical[183,187,188] or photochemical[189-191].

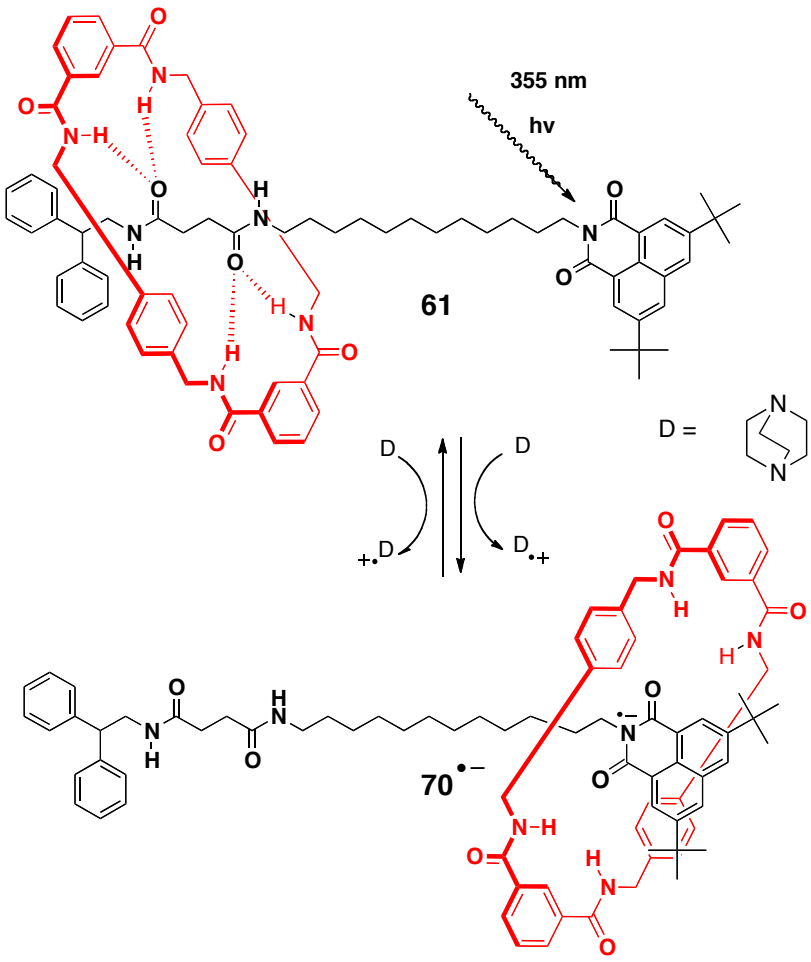

Scheme 2.11. Linear motion in the photoactive [2]-rotaxane **61** can be driven by light in the presence of the secondary electron donor 1,4-diazabicyclo[2.2.2]octane (symbolized as D).

A bistable light driven switch[162] in the form of a [2]-rotaxane **61** has been designed so that the hydrogen-bond accepting ability of a photoactive naphthalimide is turned on by a photochemical reaction with a secondary electron donor (**Scheme 2.11**). The benzylic amide macrocycle is located preferentially at the succinamide site in the electronic state in CH_3CN at 298 K. Electrochemical reduction drives the translocation of the macrocycle to encircle the newly reduced naphthalimide unit. The reduced form of the rotaxane can be now regarded as a possible candidate for photo-induced electron transfer. In this case, the photo-excited (355 nm) naphthalimide unit of **70** accepts an electron from the triplet transfer agent 1,4-diazabicyclo[2.2.2]octane (D), generating the reduced state and turn on the contemporary site for the macrocycle.

Thus, the photo-induced translational motion is achieved. The linear motions of the moving components typically were distributed randomly in the solution state.

Additional organization and integration onto surfaces either as self-assembled monolayers or Langmuir-Blodgett films are presently being addressed to express the motions coherently in a mechanical context. By taking advantage of the intramolecular disulfide bonding motif, [2]-rotaxane **71**$^{4+}$ was prepared. The rotaxane structure display[192,193] a redox controlled motion of the tetracationic cyclophane **44** from the tetrathiafulvalene (**TTF**) unit to the **DNP** ring system (**Scheme 2.12**).

Over the past few years, the progress toward devices for molecular electronics[194] based computing systems has becoming increasingly important to overcome the fundamental limitations of top-down lithographic techniques. Molecular switches[195-197] based on mechanically interlocked and movable components have been fabricated into nanowire crossbar arrays, producing working, defect tolerant memory devices of revolutionary densities. The amphiphilic bistable [2]-rotaxane **72**[198] has also been utilized in molecular electronic devices, which consist of similar cyclophane **CBPQT**$^{4+}$, encircling a linear component containing π–electron rich **MPTTF** and **DNP** units and terminated with the hydrophilic dendron stopper (**Figure 2.5**).

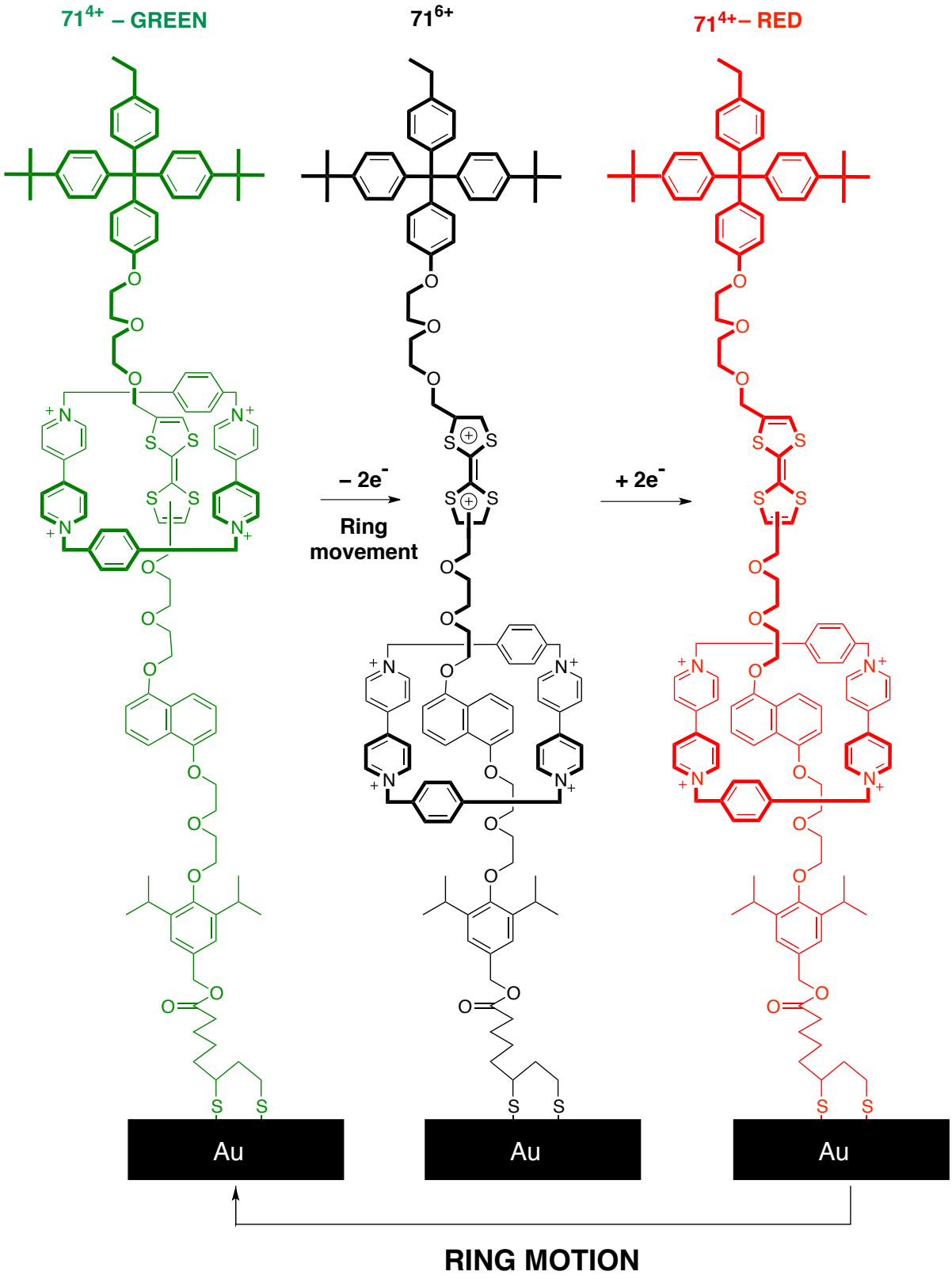

Scheme 2.12. The interlocked macrocycle of a surface-bound bistable [2]-rotaxane **71** displays electrochemically driven linear motions between two recognition sites – tetrathiafulvalene (**TTF**) and 1,5-dioxynaphthalene (**DNP**). The binding of the macrocycle to the weaker donor, **DNP** in the metastable state is sufficiently strong to prevent the reformation of the ground state, following electrochemical reset.

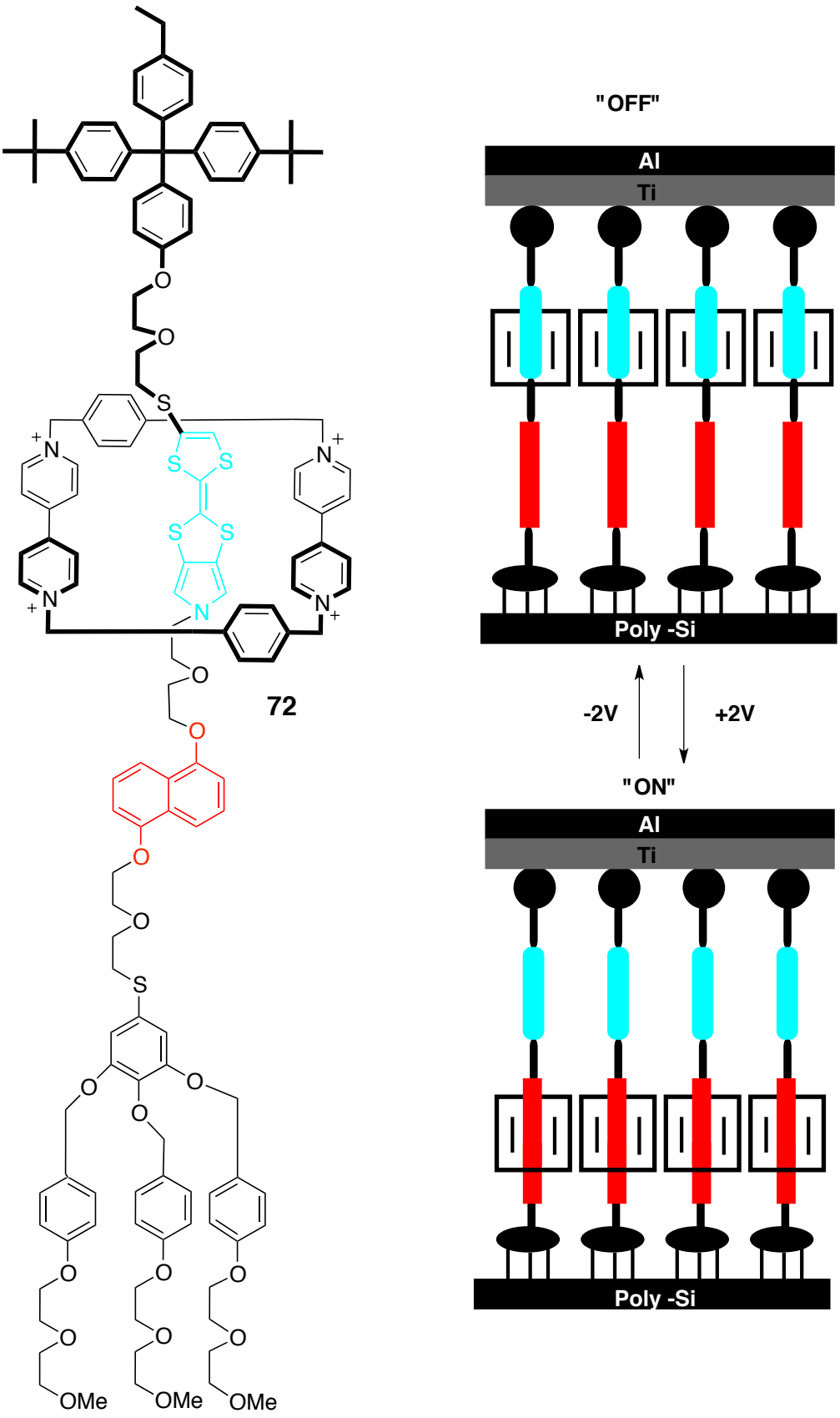

Figure 2.5. The amphiphilic bistable [2]-rotaxane **72** has been integrated into a crossbar device between two electrodes as Langmuir-Blodgett monolayers. The ON and OFF states of the device are accessed at +2 V and –2 V, respectively, and are assigned to two different translational isomers, the metastable and the ground states, respectively.

The molecular device depicted in **Figure 2.5** displays binary switching between high and low conductance states. The ON state is accessed at +2 V, which is equivalent to net oxidizing conditions, whereas the OFF state is triggered at –2 V, or net reducing conditions. The OFF state corresponds to the translational isomer, with the tetracationic cyclophane **44** encircling the **MPTTF** unit. In the device, application of a +2 V bias generates an oxidize form of the **MPTTF** unit in the rotaxane. The resulting charge-charge repulsive force drives a linear movement of the cyclophane along the dumbbell component to a position encircling the **DNP** ring system. This new metastable translational isomer is responsible for the high-conductance ON state. Alternatively, applying a reverse bias of –2 V causes the electrochemical reduction of the tetracationic cyclophane **44**, allowing the facile reformation to the most stable translational isomer.

Additionally, an effort in the Heath group have been focusing on the fabrication and testing of a 160-kbit memory[199] at 10^{11} bits cm^{-2}, a density that correlates to the 2020 node of the International Techonology Roadmap for Semiconductors published in 2005. This challenge have been met, consequently prove that a simple demonstration of a molecular electronics involves logic and memory talking to each other and to the outside world are thus possible.

3

Integrating self-replication process within rotaxane formation

3.1 Introduction

With the previous literature review in hand, we are now in position to experiment using our own expertise in the design and evaluation of highly efficient self-replicating system in the mechanically-interlocked molecules architectures. The research described in this thesis is a part of an extension of the preceding investigation on integrating self-replication process within the [2]-rotaxane structure. In the course of these investigations, the first minimal model of self-replicating rotaxanes has been outlined.

In that respect, the succeeding work should be built on the improvement of the previous designed replication model (**Replication model 1**) and work through the alternative options, namely **Replication model 2** and **Replication model 3**. Additionally, the basic features of the self-replicators are discussed and the current knowledge in the formation of self-replicating rotaxanes is evaluated. Threading and stoppering strategy has been selected[200] for rotaxane formation given that it is the only one that can be combined with the synthesis of a linear template through replication.

3.2 Essential requirements

Principally, in designing a self-replicating rotaxanes, the prerequisite design criterion consists of a recognition site, a reactive site and a binding site (shown in **Figure 3.1**). In the following section, these features are explained on each representation minimal model for self-replicating rotaxanes.

3.2.1 Recognition site

The preference for the choice of the recognition event between carboxylic acid and amidopyridine in the two building blocks of **A** and **B** (as depicted in **Figure 1.1**) has been selected considerably in our laboratory based on the work[201-203] of Hamilton research group and utilized in both minimal and reciprocal self-replicating systems. The recognition sites between the two building blocks **A** and **B** will enable the association of the catalytically active ternary complex [**A**•**B**•**T**]. Despite that, a considerably weak recognition must be ensured to allow the dissociation of the product duplex [**T**•**T**] and hence, remove the product inhibition.

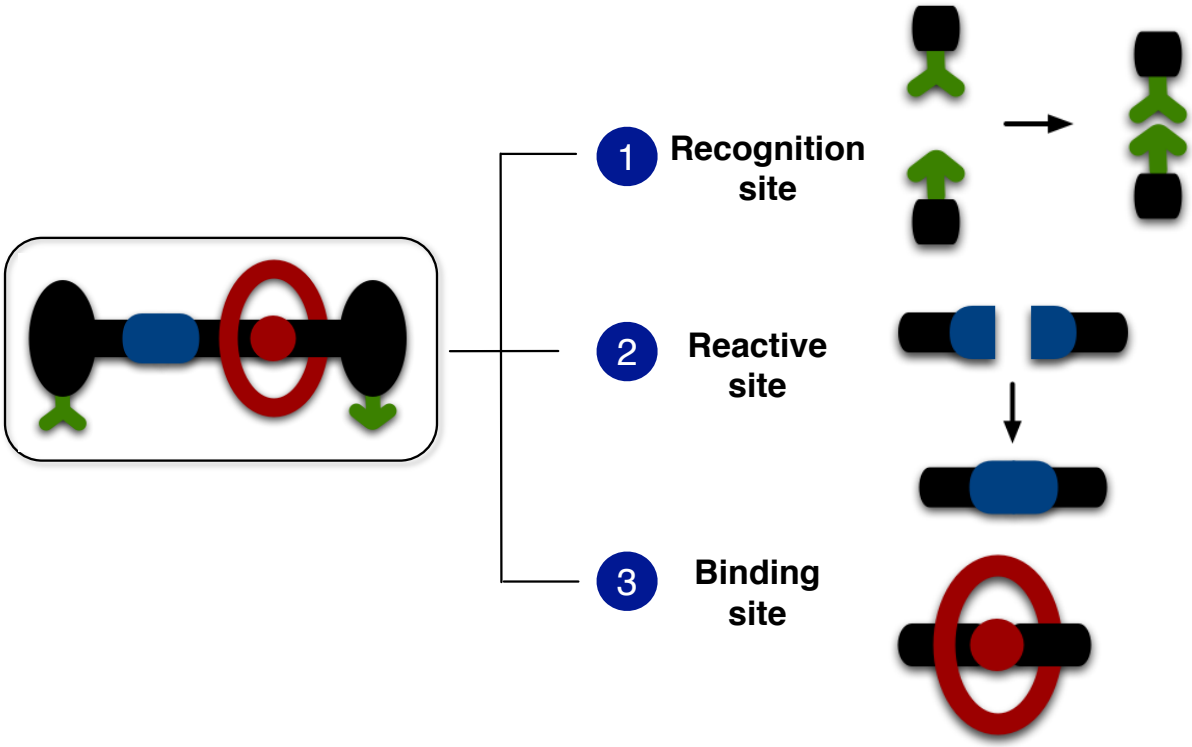

Figure 3.1. Three design criteria in designing a self-replicating rotaxane based on **Replication model 1**, namely the recognition site (allow the building blocks to associate to the template molecule), the reactive site (connect the two parts of the thread by forming a covalent bond) and the binding site (essential features of self-replicating rotaxanes). The green cartoons represent the recognition site, the blue cartoons represent the reactive site and the red cartoons represent the binding site.

The association takes place *via* hydrogen bonding of the carboxylic acid hydrogen **74** to the pyridine nitrogen **73** and between the amide proton **73** and the carbonyl group of the acid **74** (**Scheme 3.1**). The established design[73] includes the 6-methyl substituent to prevent self-association between the amidopyridine moieties by bringing in the steric hindrance. Recently, in the development of self-replicating

rotaxanes, 4,6-dimethyl moiety is utilised for a notable steric barrier, in which case acted as blocking group as well as to regulate the strength of the recognition motif.

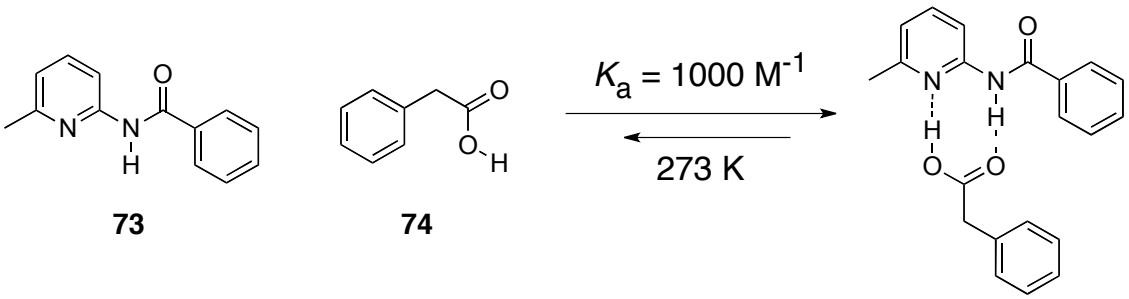

73 **74** [**73•74**]

Scheme 3.1. The recognition event between amidopyridine **73** and carboxylic acid **74** assisted *via* hydrogen bonding and the association constant, K_a was determined in $CDCl_3$ at 273 K as 1000 M^{-1}.

An exhaustive investigation of the structural variations appended on the amidopyridine unit is described and evaluated in **Chapter 7** of this thesis. Additionally, the utilization of polar solvent (which acts as good hydrogen bond acceptor and/or donor) consequently leads to strong solvation of the recognition sites and hence, disrupted the crucial binding processes. Thus, a solvent that is incapable of participating in hydrogen bonding must be chosen, such as chloroform.

3.2.2 Reactive site

The second design criteria in the self-replicating rotaxane framework is the reactive site, which is useful to attach the two building blocks **A** and **B** to give template **T** through the formation of covalent bond. This stage is equivalent to the stoppering reaction in the formation of [2]-rotaxanes and hence, an efficient and irreversible reaction is compulsory. During the course of prior investigations, the 1,3-dipolar cycloaddition between a maleimide and nitrone has been successfully incorporated in the self-replicating rotaxanes scheme. The preferential formation of the 5-substituted isoxazolidine structure proceeds through a concerted[204] mechanism, in which the bonds between the dipolarophile (in this case, maleimide) and the dipole (in this case, nitrone) are created simultaneously.

As well as being regioselective, 1,3-dipolar cycloadditions[205] can be highly stereoselective. The stereochemistry of nitrone cycloadditions has been the subject[206] of several studies. Reaction between the asymmetric nitrone **75** and

maleimide derivatives **76** proceeds through a bimolecular pathway in the absence of any recognition events to give the diastereoisomeric products, namely the *trans* and *cis* isomer with respect to the *endo* and *exo* transition states (see **Scheme 3.2**). In the case of *cis* isomer, all protons are positioned on the same side with regards to the isoxazolidine ring while in the *trans* isomer, the nitrone-derived hydrogen atom is rendered *trans* to the two hydrogen atoms originally located on the maleimide group. Frequently, mixture of diastereoisomers are obtained with a *trans*:*cis* ratio between 1.4:1 and 3.9:1 depending on the electronic nature of the substituents appended on the two reagents. In other words, the outcome depends on the interplay of two generally opposing forces in the transition state – attractive π-orbital overlap of unsaturated substituents favouring an *endo* transition state (**Scheme 3.2a**), and repulsive van der Waals steric interactions favouring an *exo* transition state (**Scheme 3.2b)**.

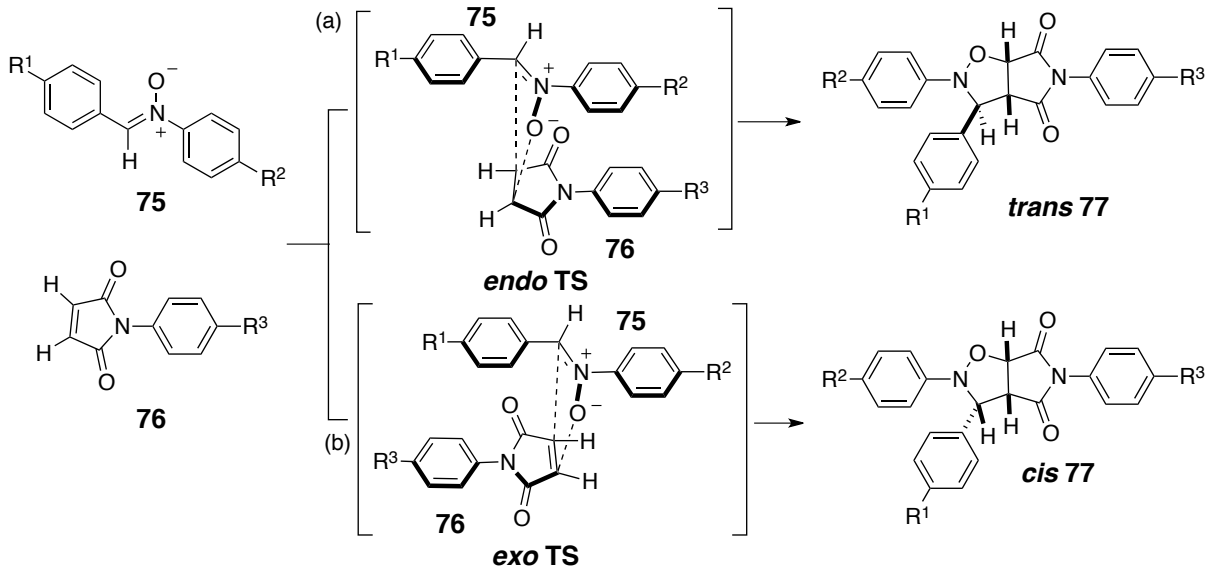

Scheme 3.2. 1,3-dipolar cycloaddition between the nitrone **75** and maleimide **76**. (a) The *endo* approach leads to the *trans* **77** (b) The *exo* approach leads to the *cis* **77**.

In order to connect the reactive site with the recognition site, careful consideration in selecting the spacer is required to control the geometry of the substrates. The suitable spacer can be altered by means of the length and angle. The spacer length could induce notable flexibility in the system and consequently render the recognition site and reactive site at a correct distance to eliminate excessively stable duplex [**R•R**] and to avoid the binary complex pathway. Furthermore, the angle could be modified with different substitution patterns on the benzene ring. The angle at which

the reactive site and the recognition motif are relatively to each other will eventually determine whether the reaction will follow the [**A**•**B**] complex or the autocatalytic pathways.

3.2.3 Binding site

The final prerequisite element embedded into the building block **B** is the binding site between the ring and the linear component (see **Figure 3.1**), which is the key feature in self-replicating rotaxanes. The importance of the association of the ring component *via* hydrogen bond to the conserved binding site can be envisaged in[207] the simple kinetic model of rotaxane formation (**Figure 3.2**). There are two parallel kinetic pathways operating either side of equilibrium. Upon addition of a guest in the **L** component and macrocycle **M** with the complementary binding motifs, the equilibrium is established. The macrocycle **M** is constantly being displaced from the binding site in the linear component, which resulted in two species, namely the [2]-pseudorotaxane complex [**L**•**M**] and guest **L** distinguishable *in situ*. The subsequent stoppering reaction with the stopper reagent **S** affords the important rotaxane **R** alongside with the undesired thread **T**.

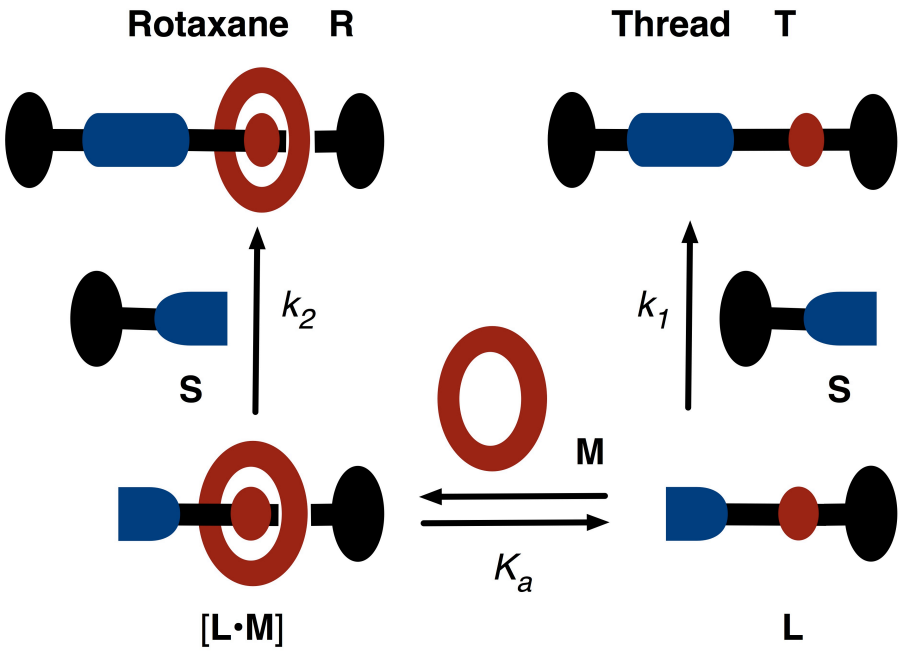

Figure 3.2. The simple kinetic model for rotaxane formation. The stopper **S** can react either with the unbound linear component **L** (k_1) or the [2]-pseudorotaxane complex [**L**•**M**] (k_2). The stability of the [2]-pseudorotaxane complex is defined by K_a. Ratio of rotaxane **R** to thread **T** can be obtain by assuming $k_1 = k_2$. At increased temperature, the K_a value decrease, therefore [2]-pseudorotaxane formation is disfavoured. At lower temperature, [2]-pseudorotaxane formation is favoured as the K_a value increase leading to higher yields of rotaxane **R**. Figure taken from reference 207.

The rate constants for thread **T** and rotaxane **R** formation (k_1 and k_2) are assumed to be equivalent and, hence, the amount of rotaxane **R** formed is dependent upon the amount of [2]-pseudorotaxane [**L•M**] present, which in turn related to the association constant, K_a. On that account, a high association constant for the [**L•M**] complex is mandatory. The association constant relates to the affinity of the macrocycle to associate the binding site of the guest and can be varied by manipulating the temperature, based on the free energy Gibbs, $\Delta G = -$ RT In K_a.

In the case of low temperature, substantial amount of [2]-pseudorotaxane [**L•M**] are obtained as a results of increase value of K_a and, hence, force the equilibrium to the left-hand side. The stoppering reaction usually involves elevated temperature, thus lowering the K_a value and consequently lowering the yield of pseudorotaxane. Raising the temperature will diminished the K_a value for the complexes by increasing the magnitude of the TΔS term in the free energy of binding. On the whole, this simple kinetic model heavily relies on a high association constant of [**L•M**] complex to ensure that a significant amount of rotaxane is synthesised.

3.3 Association constant, K_a

The thermodynamic stability of a complex between host and guest in a given solvent at a given temperature is quantified by measurement of the association constant, K_a. The binding constant is calculated using concentrations and thus has units of M^{-1} for a given 1:1 complex. For the binding equilibrium for the reaction shown in **Equation 3.1** (*e.g.* between a guest, G and host, H), the association constant is given by:

$$H + G \rightleftharpoons [H \bullet G]$$

$$K_a = \frac{[H \bullet G]}{[H][G]} \qquad \textbf{Equation 3.1}$$

On that account, a large association constant corresponds to a high equilibrium concentration of bound guest, and hence a more stable or tighter the preorganisation of the [**H•G**] complex. Moreover, the association constants is also related to the free energy of the association process according to the Gibbs equation: $\Delta G^\circ = -$ RT In K (R = gas constant, 8.314 J K^{-1} mol^{-1}, T = temperature in Kelvin). Thus, the general affinity of a host for a guest under specific conditions (solvent, temperature and *etc.*)

may be given either in terms of K or $-\Delta G^{\circ}$ values as we have seen earlier in the simple kinetic model of rotaxane formation.

3.3.1 High association constant is crucial

Strong association is crucial to attain substantial amount of [**L**•**M**] complex. In the previous simple kinetic model in **Figure 3.2**, we assumed both linear component **L** and [2]-pseudorotaxane [**L**•**M**] hold a similar reactivity, and hence, the ratio of rotaxane **R** to thread **T** component in the reaction mixture are evaluated across a series of association constant values for the [**L**•**M**] complex through kinetic simulation. Assuming the rate of k_1 and k_2 to be 1.67×10^{-3} M^{-1} s^{-1} and the concentrations of starting reagents **L**, **S** and **M** at concentration of 20 mM, it is clearly evident that the [rotaxane]/[thread] composition in the final mixture varies with respect to the K_a values (**Figure 3.3**).

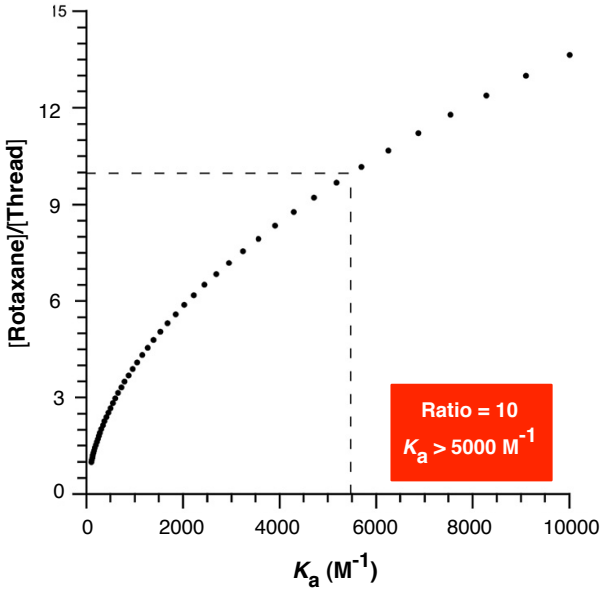

Figure 3.3. The kinetic simulation depicts the selectivity of rotaxane **R** to thread **T** in the reaction mixture as a function of K_a by assuming the $k_1 = k_2 = 1.67 \times 10^{-3}$ M^{-1} s^{-1}. Ratio of rotaxane to thread of 10:1 gives a K_a value of [**L**•**M**] complex higher than 5000 M^{-1}. Figure taken from reference 207.

The kinetic simulation reveals a selectivity of rotaxane to thread of 10:1, which corresponds to a K_a value of greater than 5000 M^{-1} for the [**L**•**M**] complex. The association constant for the [2]-pseudorotaxane complex required to be as high as possible since the formation of this complex will suppress the kinetic pathways involving free compound **L**, which eventually lead to thread **T** formation. As a

consequence of decrease free **L** species, thus concentrates the kinetic flux in the autocatalytic cycle involving the rotaxane **R**. Undoubtedly, [2]-pseudorotaxane [**L•M**] unit is the main concern for a success within a self-replicating rotaxane framework.

3.4 Minimal replication model of self-replicating rotaxanes

One of the main objectives of the research described in this thesis is the exploration of replicating system within the rotaxane architecture. Prior studies acknowledged the essence of the three stages required in the formation of self-replicating rotaxanes by virtue of threading and stoppering strategy, commencing from the association of the macrocycle to the guest binding site, the stoppering reaction yielding the simple rotaxane and ultimately the recognition event, which enable the rotaxane to self-replicate by autocatalytic means. In order to accomplish this aim, three different minimal replication models has been proposed and described. On that account, each minimal model employed is presented in the following section to comprehend the objective of each designed scheme. In each case, the advantages and disadvantages of each replication model are further emphasised.

3.4.1 Replication model 1

The primary model contemplated for the formation of self-replicating rotaxanes linked four mutual catalytic cycles. Both autocatalytic and crosscatalytic cycles of thread and rotaxane synthesis equally emerged as a consequence of the reversible reaction between the **L** component and the macrocyclic **M** unit (represent as central solid box in **Figure 3.4**). The probability that the thread and rotaxane to act as a replicator in autocatalytic and crosscatalytic manner has been kinetically investigated which suggests[200] that the thread and rotaxane are not mutually complementary templates. These evidence shows that rotaxane and thread are unable to catalyse the formation of each other. On that account, there are only two pathways accessible in the **Replication model 1**, which related to the innermost binding event, the reversible formation of the [2]-pseudorotaxane [**L•M**] complex (see **Figure 3.5**). In the case of rotaxane synthesis, the [**L•M**] complex react with the stoppering reagent **S** to afford rotaxane **R**. Subsequently, rotaxane **R** enable to enter the autocatalytic cycle by collecting the [**L•M**] complex and the stoppering reagent **S** and hence, catalyse the formation of a second molecule of rotaxane, **R**.

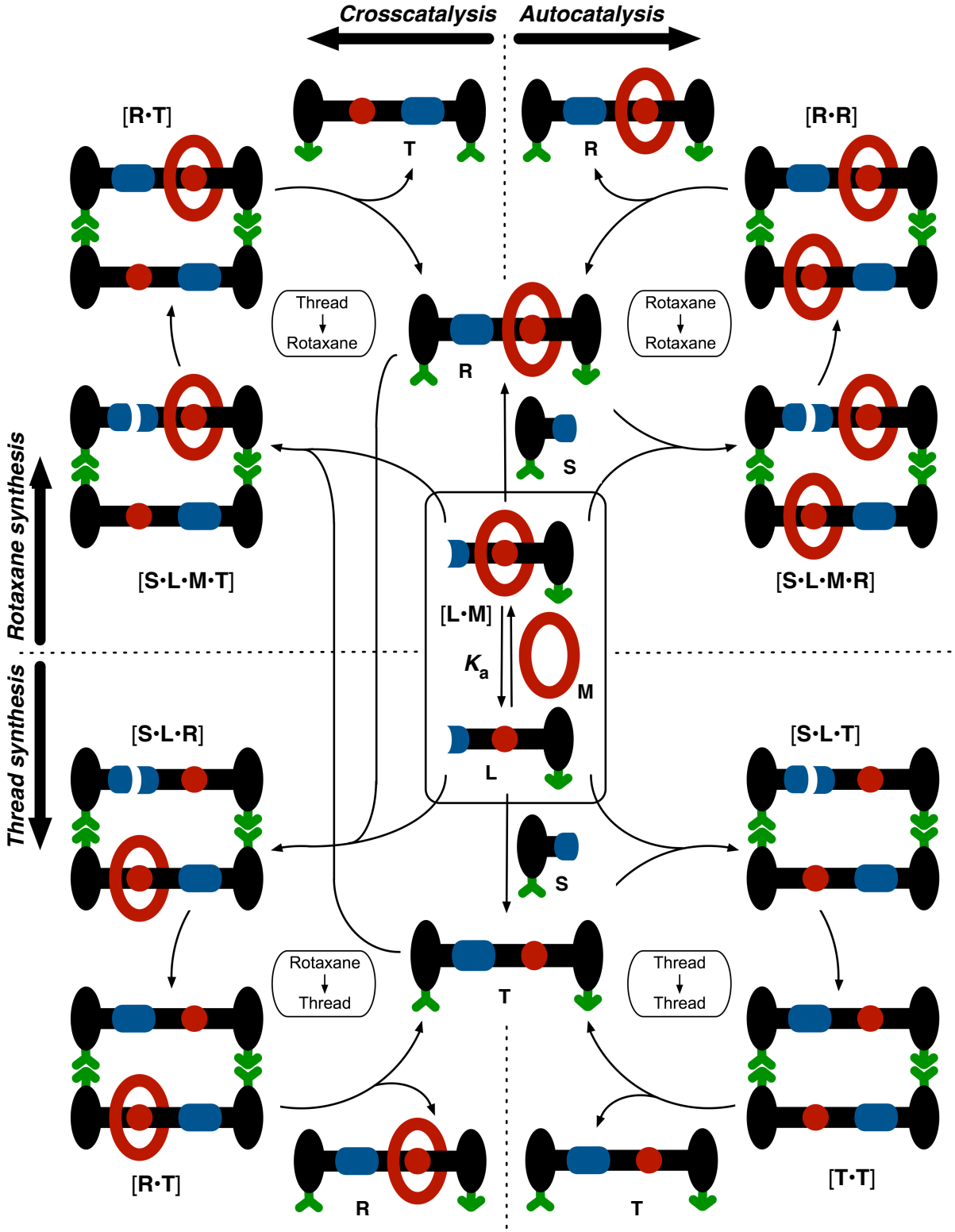

Figure 3.4. **Replication model 1** (***Extended version***) – based on the threading and stoppering strategy with the placement of one recognition site (green cartoons) on both stoppers of the rotaxane. The catalytic cycles operate emanating from the reversible formation of the [**L**•**M**] pseudorotaxane complex. On the top, the synthesis of rotaxane is accomplished either through autocatalysis (right) by rotaxane **R** or crosscatalysis (left) by thread **T**. On the bottom, the synthesis of thread is achieved either through autocatalysis (right) by thread **T** or crosscatalysis (left) by rotaxane **R**. Reactions through binary complexes are not shown here for clarity. The blue cartoons represent the reactive sites, the green cartoons represent the recognition sites and the red cartoons represent the binding site.

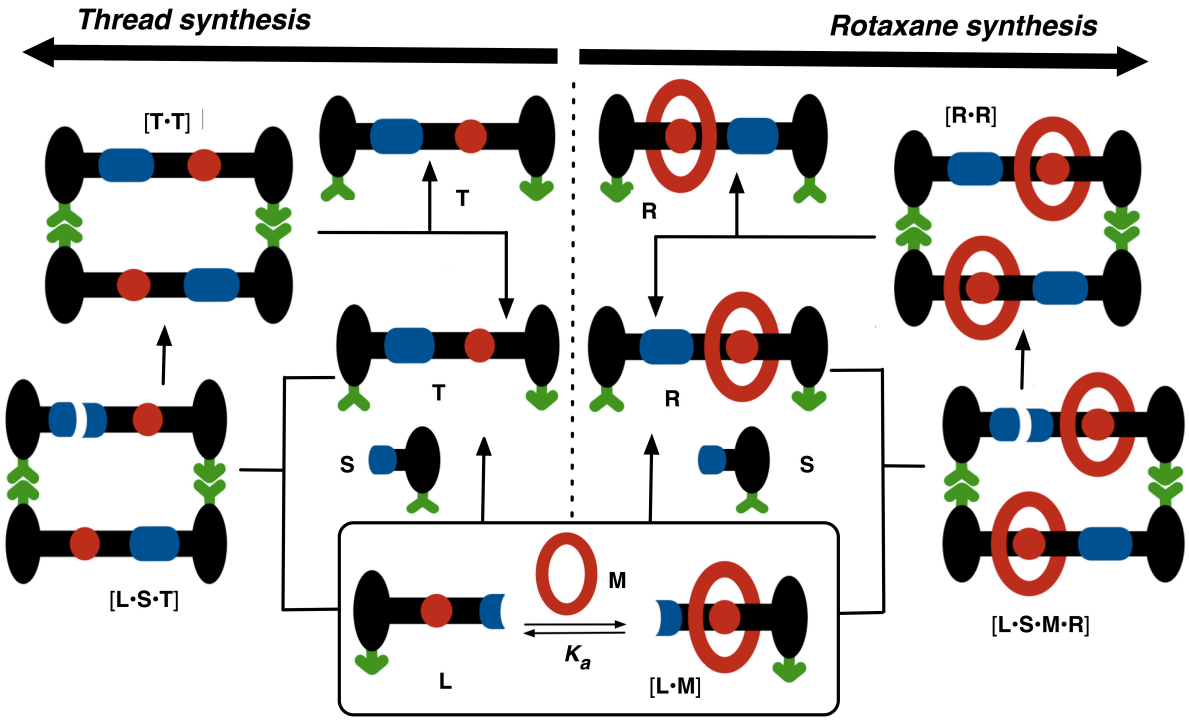

Figure 3.5. **Replication model 1** (***Simplified version***) - consists of two autocatalytic cycles emanating from the central binding event (boxed), the reversible formation of the [**L•M**] complex. (Right – Rotaxane synthesis) The association between macrocycle **M** with the linear component **L** afforded the [**L•M**] species. Reaction between [**L•M**] complex and stoppering reagent **S** gives the rotaxane **R**. [**L•M**] complex and **S** can bind reversibly to the rotaxane **R** to form a catalytically quarternary complex [**S•L•M•R**]. Bond formation occurs between **S** and [**L•M**] to give duplex [**R•R**] which then withdraw two molecules of **R** to start a new replicating cycle. (Left – Thread synthesis). Unbound linear component **L** react with the stoppering reagent **S** to form thread **T**. Thread **T** can then enter the autocatalytic cycle similarly by collecting the unbound species **L** and **S** to catalyse the formation of a second molecule of thread **T**. The blue cartoons represent the reactive sites, the green cartoons represent the recognition sites and the red cartoons represent the binding site.

In parallel, unbound linear component **L** also react with the stoppering reagent **S** to form thread **T**. Following this, thread **T** can then enter the autocatalytic cycle similarly by collecting the unbound species of linear component **L** and stoppering reagent **S** and, hence, catalyse the formation of a second molecule of thread **T**. It is now demonstrated that the rotaxane **R** and the thread **T** capable of replicating. Regardless that, significant quantity of thread **T** was present as a result of poor association between the macrocyclic unit **M** and the guest binding site. These outcomes substantiate the fact that the binding strength must exceed a certain threshold value in order to allow efficient autocatalytic formation of the rotaxane structure. An obvious take home message here is that the efficiency of the crucial binding processes for the [**L•M**] complex, ultimately determined its potential to act as competent replicator. One way to overcome this problem is to optimize the binding

motif between the macrocycle and the guest component. Supplementary investigations of how different macrocycle frameworks incorporates a range of potential guests can dramatically effect the efficiency of the respective binding process can be found in **Chapter 4** of this thesis.

3.4.2 Replication model 2

Alternatively, we explored conceptually a second replication model in which one of the recognition site is located on the end of stopper reagent **S** and appending its complementary recognition site on to the macrocycle **M** (as depicted in **Figure 3.6**).

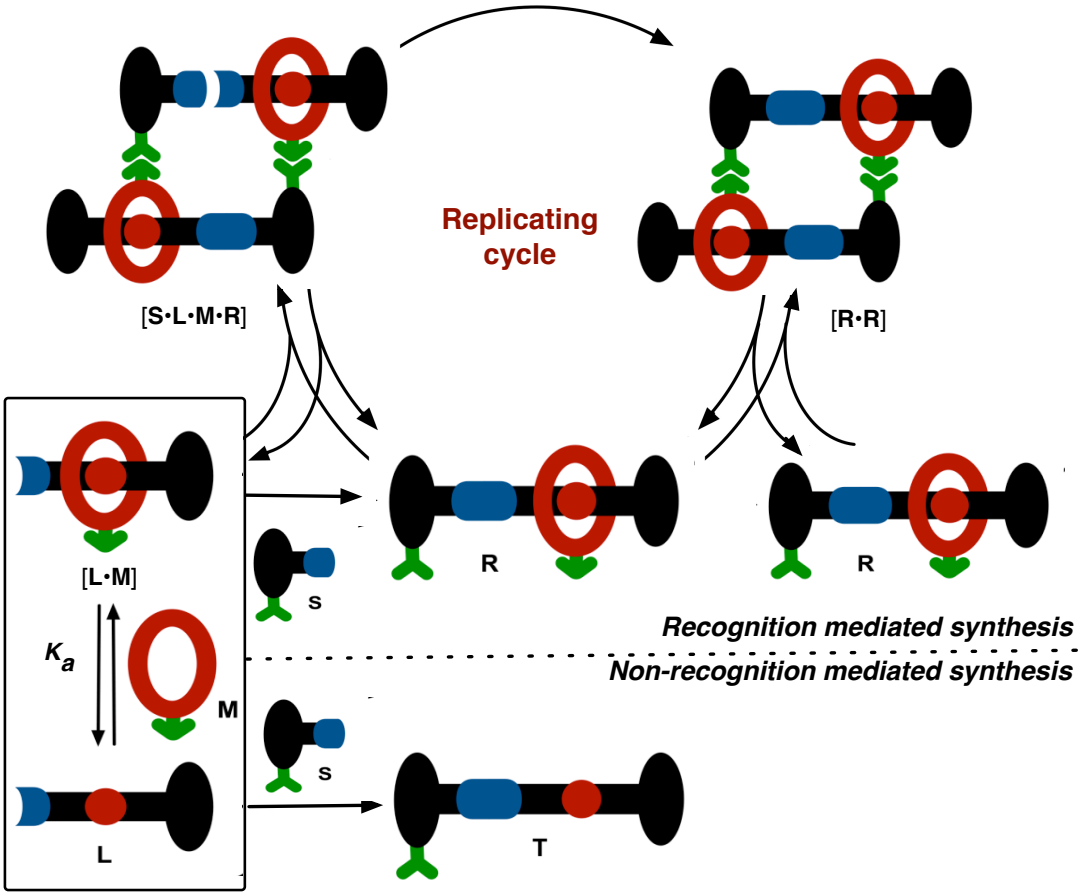

Figure 3.6. **Replication model 2** – based on the placement of one of the complementary recognition site on one of the stoppers end and appending its complementary recognition site on to the macrocycle itself. The unbound linear component **L** react with the stoppering reagent **S** to gives the thread **T**, in which unable to enter the replicating cycle as it only possessed one recognition site (***Non-recognition mediated synthesis***). Oppositely, the formation of [**L•M**] complex with complementary recognition site on the macrocycle **M** further react with stoppering reagent **S** to afford the rotaxane **R**. Rotaxane **R** capable to access the replicating cycle since both complementary recognition sites present in the structure and, hence catalyse the formation of a second molecule of rotaxane **R** (***Recognition mediated synthesis***). The blue cartoons represent the reactive sites, the green cartoons represent the recognition sites and the red cartoons represent the binding site.

This modification exclusively favoured the formation of rotaxane **R** structure by mean of recognition-mediated process, which in turn allow the rotaxane **R** to undergo the autocatalytic cycle and subsequently provide the second molecule of **R** to initiate the replicating cycle. On contrary, the thread **T** resulting from the reaction of the unbound **L** component with the stoppering reagent **S** are now incapable to gain access to the replicating cycle as a consequence of possessing only one recognition site. It is noteworthy that the binding process is now function as catalyst to ensure the exclusive formation of rotaxane **R** structure. Nevertheless, we have been struggling to control a number of factors in designing the suitable building blocks based on this replicating framework. The synthesis involving the recognition macrocycle is a significant synthetic challenge in itself and will be discussed in detailed in **Chapter 7**.

3.4.3 Replication model 3

The third replication model devised is shown in **Figure 3.7**. A fragment incorporating the binding site and one element stopper is attached to one of the buiding blocks constitutive of the template (either [**L•M**] or **L** component). The corresponding element stopper of the rotaxane **R** is formed by reaction with the stoppering reagent **S**. The complementary recognition sites are now located at only one stopper of the rotaxane **R**. As seen in previous minimal replication model, the reaction between [**L•M**] component and stoppering reagent **S** affords the rotaxane **R**. Stoppering reagent **S** and [**L•M**] complex can bind reversibly to the rotaxane **R** to form the catalytic quarternary complex [**S•L•M•R**]. Bond formation occurs between **S** and [**L•M**] to give the product duplex [**R•R**], which then dissociates to return two molecules of **R** to the start of the replicating cycle.

The essential advantage of this design is that we are capable of employing the known successful self-replicator design on the end of the stopper, which acts as sufficient end groups and efficiently accelerate the autocatalytic pathway to construct the rotaxane **R** structure. Nonetheless, the binding site itself did not behave as catalyst for the rotaxane formation. Consequently, there will be a competition in the rotaxane formation because the thread is also being formed simultaneously. Once more, a high association constant is the prime concern in the model devised. Additionally, there will be more binding sites available for the macrocycle. One of them being is the nitrone binding site as the nitrone will first bind to the macrocycle

before react with the maleimide compound. Moreover, there is a chance that crosscatalysis pathway operating in this replicating model.

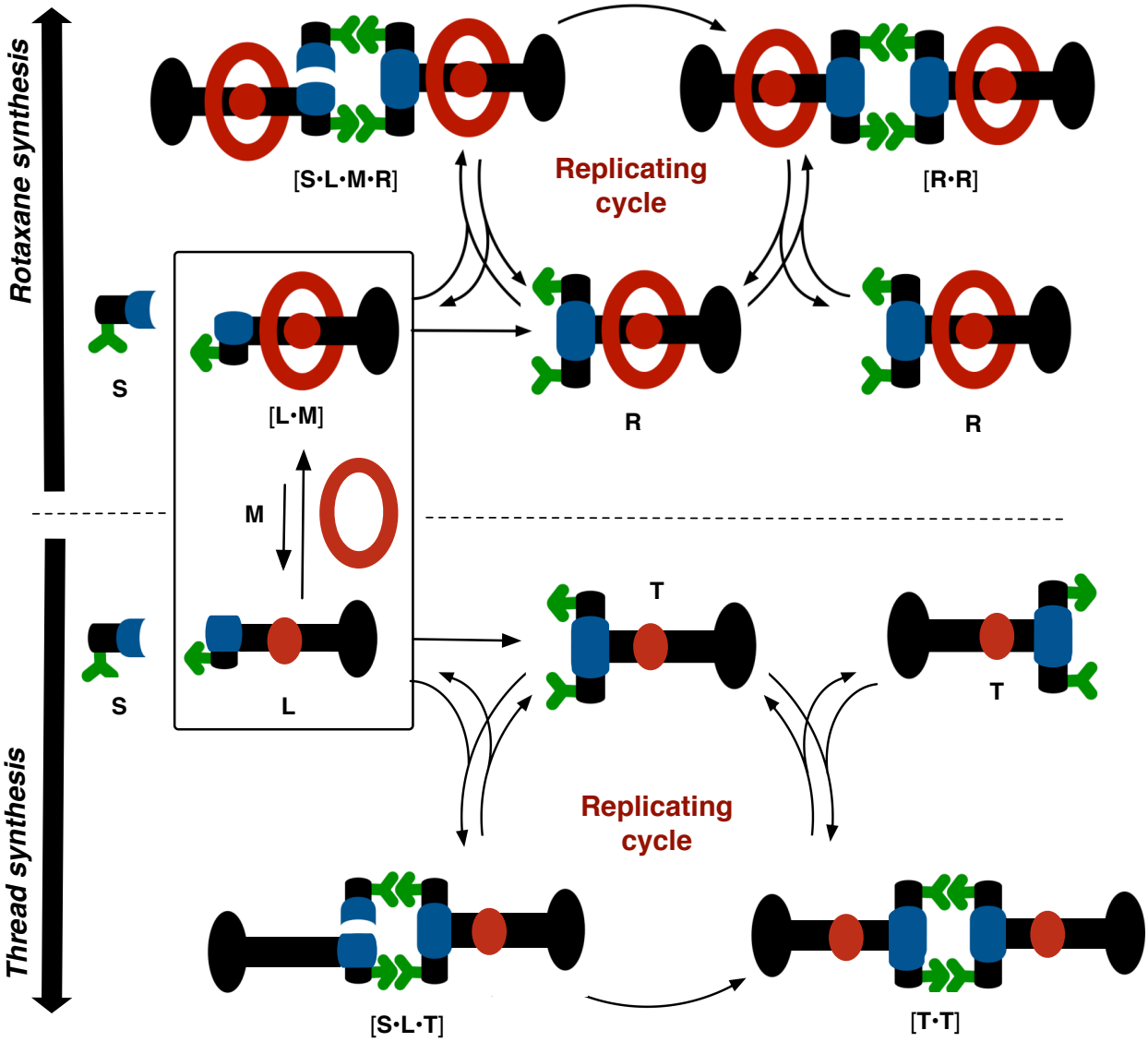

Figure 3.7. **Replication model 3** – based on the placement of the two recognition sites (green cartoons) on the same stoppers. Reaction between [2]-pseudorotaxane [**L•M**] and stoppering reagent **S** affords the rotaxane **R**. Stoppering reagent **S** and [**L•M**] complex can bind reversibly to the rotaxane **R** to form the catalytic quarternary complex [**S•L•M•R**]. Bond formation occurs between **S** and [**L•M**] to give the product duplex [**R•R**], and return two molecules of R to the start of the autocatalytic cycle. The blue cartoons represent the reactive sites, the green cartoons represent the recognition sites and the red cartoons represent the binding site.

3.5 Summary

In the course of these discussions, we have gained considerable information in the design and evaluation of minimal model of self-replicating rotaxanes. In this system, three critical design criteria are prescribed, namely the recognition event between the carboxylic acid and amidopyridine unit, the chemical reaction employed to form the template **T** (1,3-dipolar cycloaddition between nitrone and maleimide) and ultimately the binding site between macrocycle **M** and the guest. These essential aspects are explained in three independent replication models, designated as **Replication model 1**, **Replication model 2** and **Replication model 3**. In particular, **Replication model 1** was first described in the group but met with limited success. The poor association strength in the [**L**•**M**] complex lessened the yield of rotaxane **R** as exemplified in the simple kinetic of rotaxane formation. In order to arrive at a better and more solidly comprehension in our effort to integrate the replication process within the rotaxane structure, the remaining two models are further analysed. In essence, the specific advantages and disadvantages of individual minimal model implemented in this thesis were summarized below.

Replication model	Advantages	Disadvantages
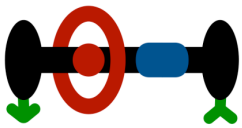 **Model 1**	A known self-replicating system. Easier to design the building blocks based on this framework .	The crucial binding processes in the assembly of pseudorotaxane complex (require a high association constant, K_a) determined the efficiency of rotaxane formation.
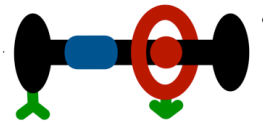 **Model 2**	The binding process now function as a catalyst to ensure the exclusive formation of rotaxane. Thread incapable of accessing the autocatalytic cycle since it posses only one recognition site.	An unknown replicating system. Synthetically challenging in designing the building blocks based on this model scheme.
 **Model 3**	Highly efficient replicator systems can be employed on the end of the stopper. Easier to design the building blocks based on this framework .	An unknown replicating system. Thread are being formed in parallel which allow the competition for rotaxane formation.

4

Design, synthesis and binding properties of macrocycles

4.1 Introduction

In the self-replicating rotaxanes framework, the paramount strategy involves the selection of an efficient macrocycle to accommodate the guest unit. A sufficient binding within the cavity of the macrocycle is crucial for the successful formation of pseudorotaxane in the threading processes. Previous study[200] employed the non-covalent interactions to assemble the rotaxane architecture. The macrocycle ranged from the crown ether to simple hydrogen bond donor and/or acceptor motif for both binding motif and macrocycle. These structures will adopt a coconformation that maximizes the donor and acceptor hydrogen bonding interactions.

4.2 First generation macrocycles

In the development of a synthetic route toward the formation of macrocycle, one of the most important and challenging tasks is the key macrocyclisation step. In the absence of a suitable template, the synthesis of macrocyclic component employs the high-dilution[208] conditions. The high-dilution approaches[209] have been used in a large number of macrocyclic syntheses. One rationale behind this strategy is that in dilute solution, the formation of the cyclic product by intramolecular reaction is more likely and thus faster than formation of a polymer, which requires a collision between two different starting reagents by means of intermolecular reaction. Furthermore, if the cyclisation reaction is intrinsically faster than the rate of addition of the starting reagents, then the concentration of the reactants will always be small and not increase during the course of the reaction[210]. These standard approaches have been taken to assemble the macrocycle skeleton in moderate yield and described in the following paragraphs. In addition to this methodology, many other approaches have

been described and engaged in the formation of wide variety of synthetic macrocyclic ligands.

4.2.1 Ethylene urea macrocycle (MEU)

A prototype amide-based macrocycles have been extensively[207,211-217] explored within our research laboratory and others. Prospective guests such as pyridone, urea and amide have been identified to probe as the binding components. Nevertheless, the binding affinity shown in previous work is moderate as a consequence of diminutive cavity and hence, decreasing the association constant, K_a in the pseudorotaxane complex. Therefore, a recent series of amide-based macrocycles are proposed to achieve a high K_a. The existing complementary motif between hydrogen bond donor and acceptor are maintained in the new macrocycle framework (**Figure 4.1**). For instance, the urea guest form primary hydrogen bond interaction between the oxygen and the two NHs of the macrocycle, whilst the second interaction occur between the hydrogen donor of the urea and the oxygen of the cyclic ethylene urea of the ring.

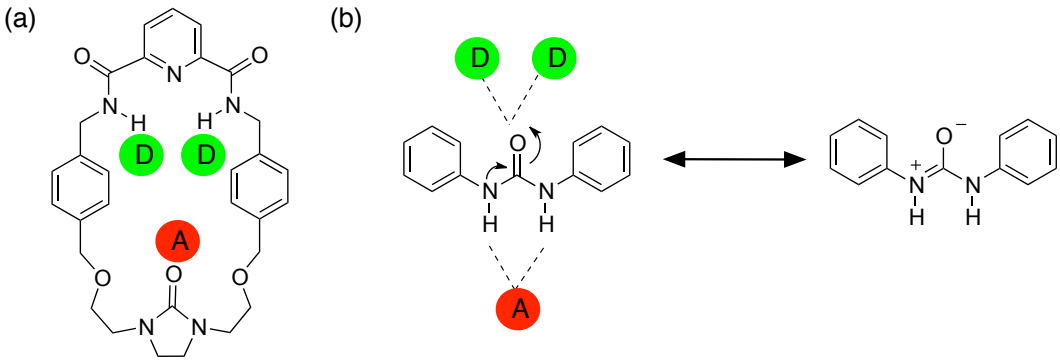

Figure 4.1. (a) Structural design of macrocycle ethylene urea (**MEU**) consists of two hydrogen donors and a single hydrogen bond acceptor. (b) Possible guest interaction with new design of macrocycle displayed by the urea derivatives. (D embedded in green circles denoted the hydrogen bond donors while A embedded in red circles denoted the hydrogen bond acceptors).

The synthesis of the ethylene urea macrocycle (**MEU**) was started by reacting 4-(bromomethyl) benzonitrile **78** with sodium in ethylene glycol to afford the alcohol **79** in excellent yield (**Scheme 4.1**). Subsequent tosylation leads to the formation of intermediate **80**. Two equivalents of the tosylate **80** activated the α–carbon, which undergo nucleophilic attack by the cyclic ethylene urea **81** in a suspension of sodium hydride in dry THF. The resulting nitrile **82** was further reduced to the corresponding amine derivative **83** using BH_3•THF complex in dry THF. The final ring closure takes

place by the formation of two amide bonds with 2,6-pyridine dicarbonyl dichloride affording macrocycle **MEU** in 26% yield.

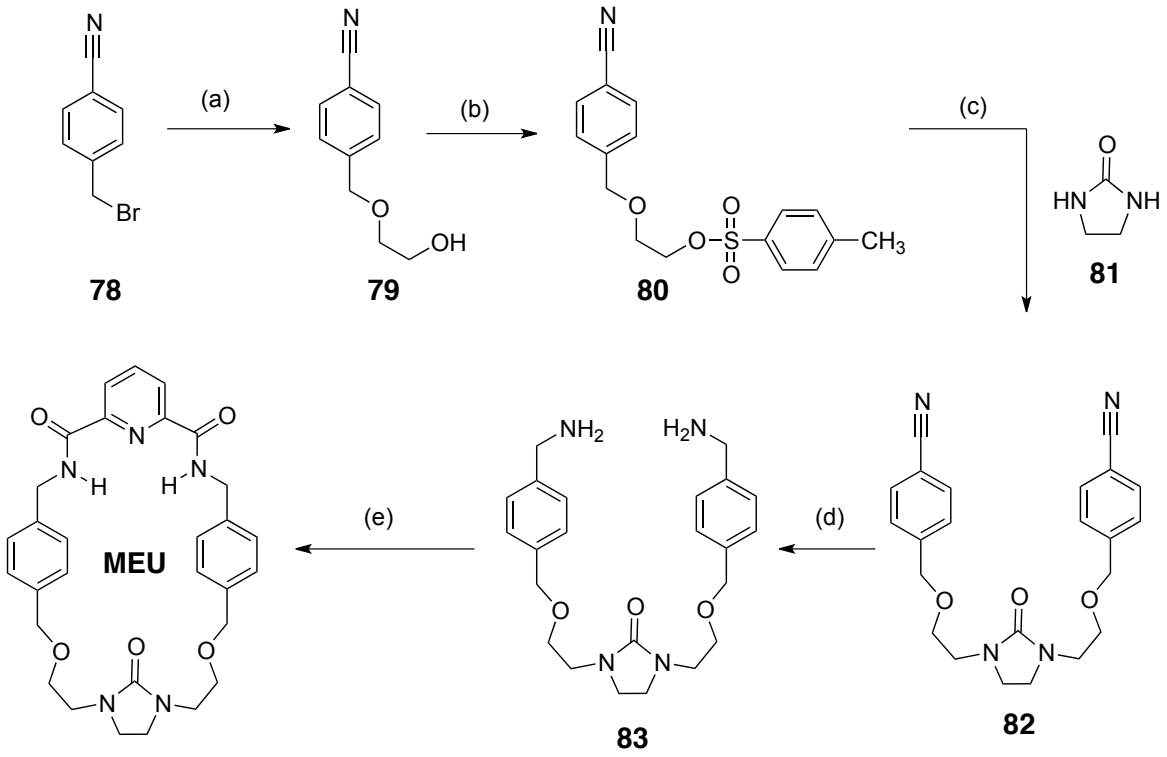

Scheme 4.1. Synthesis of macrocycle **MEU**. Reagents and yields: (a) Na, ethylene glycol, THF, reflux, 16 h, 90%; (b) TsCl, Et_3N, CH_2Cl_2, 0 ˚C to 1 h and reflux for 16 h, 77%; (c) NaH, THF, reflux, 16 h, 51%; (d) BH_3•THF, THF, 0 ˚C for 2 h and reflux for 16 h, 86%; (e) 2,6-pyridinedicarbonyl dichloride, Et_3N, CH_2Cl_2, rt, 3 days, 26%.

Crystals of macrocycle **MEU** were grown by vapor diffusion of hexane into a solution of macrocycle **MEU** in $CHCl_3$ at ambient temperature, and analysed by single crystal X-ray diffraction. A stick representation of the molecular structure is depicted in **Figure 4.2**. It came to our surprise, the two units of the macrocycle **MEU** were found to bind to each other through the proximity of the upper fragment of ring with a strong hydrogen bond from the carbonyl oxygen atoms to both of the amide NHs of the other ring. It is also important to note that the macrocycle crystallise with two molecules of chloroform used in the preparation of the crystals and, hence, reveal the inverted conformation of the ethylene urea carbonyl oxygen. This conformation is responsible for the hydrogen bonds contact with the solvent, which now acts as hydrogen bond acceptors. The O•••H distance is measured to be 2.03 Å. The subsequent binding studies were conducted with urea, amide and pyridone guests to

evaluate the capability of macrocycle **MEU** of hosting guest molecules, despite that inverted position of the carbonyl oxygen of the cyclic ethylene urea.

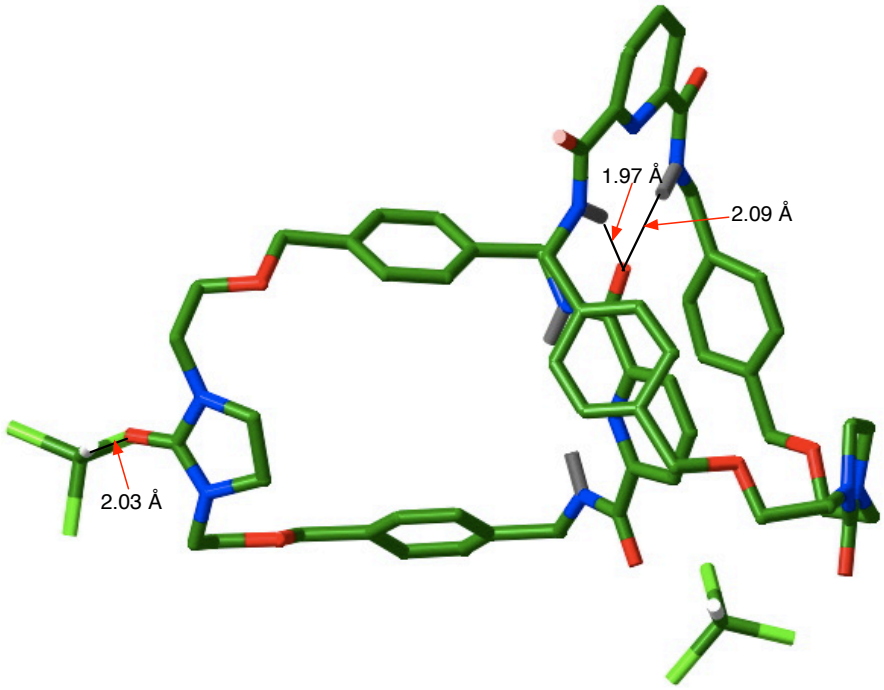

Figure 4.2. Stick representation of two units of macrocycle **MEU** in the solid state, which found to crystallise with each other and the solvent ($CHCl_3$) used in the preparation of the crystals is in the hydrogen bond contact with oxygen atom of the carbonyl group as determined by single crystal X-ray diffraction. Carbon atoms are coloured green, oxygen atoms in red, nitrogen atoms in blue and hydrogen atoms that are involved in hydrogen bonds (black lines) are coloured grey for the macrocycle and white for the chloroform.

4.2.2 Binding Studies – MEU

The 300.1 MHz ^{1}H NMR spectrum of an equimolar mixture of macrocycle **MEU** and guest **84** in $CDCl_3$ (**Figure 4.3b**) shows that the complex between macrocycle **MEU** and compound **84** is in fast exchange process on the ^{1}H NMR chemical shift timescale, which displays significant changes in the chemical shifts for the resonances of the complex relative to those of the free species (**Figure 4.3a** and **Figure 4.3c**). The resonance arising from the macrocycle NH proton, H^{11R} is shifted downfield (+0.76 ppm) as a result of the hydrogen bonds between these protons and the carbonyl group of urea **84**. The resonances of macrocycle methylene protons are shifted upfield (H^{10R}, H^{5R} and H^{4R}, –0.08, –0.04 and –0.17 ppm, respectively) and that of the diphenyl urea **84**, H^{9G} (–0.30 ppm). These chemical shift changes suggest that the urea **84** is located within the cavity of the macrocycle. The K_a was measured by ^{1}H NMR titration experiment and was estimated to be only 39 ± 4 M^{-1} in $CDCl_3$ at 25 ˚C.

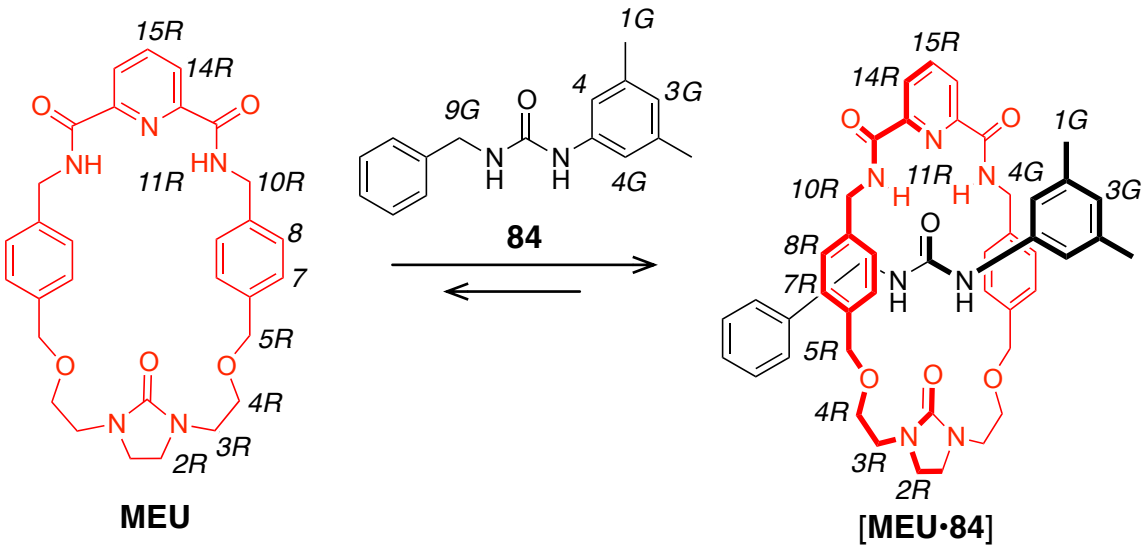

Proton resonances	$\delta_{unbound}$	δ_{bound}	$\Delta\delta$
NH^{11R}	8.04	8.83	+0.79
H^{10R}	4.69	4.62	–0.08
H^{5R}	4.48	4.44	–0.04
H^{4R}	3.60	3.43	–0.17
H^{4G}	6.88	7.00	+0.12
H^{1G}	2.25	2.30	+0.05

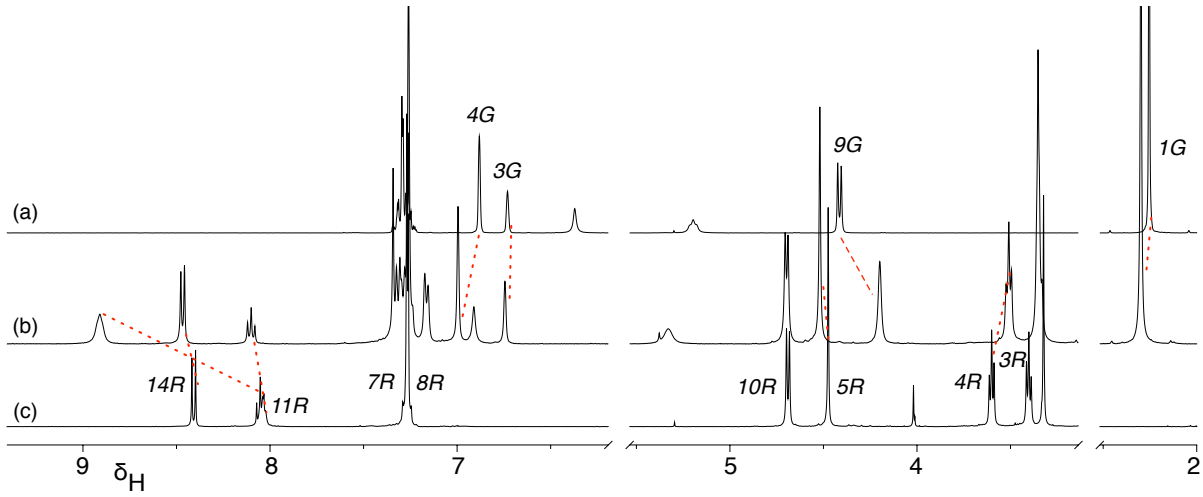

Figure 4.3. Partial ^{1}H NMR spectra (300.1 MHz, 25 ˚C, $CDCl_3$, 20 mM) of (a) urea **84** (b) an equimolar mixture of macrocycle **MEU** and urea **84** and (c) macrocycle **MEU**. Red dashed lines are shown to connect the resonances for specific protons in bound and unbound states. The saturation curve for the association of the macrocycle **MEU** and urea **84** gives an optimized K_a value of 39 ± 4 M^{-1} and ΔG = –2.17 kcal mol^{-1}. R corresponds to the ring (in this case, macrocycle **MEU**) and G denoted the guest (in this case, urea **84**). ($\Delta\delta = \delta_{unbound} - \delta_{bound}$).

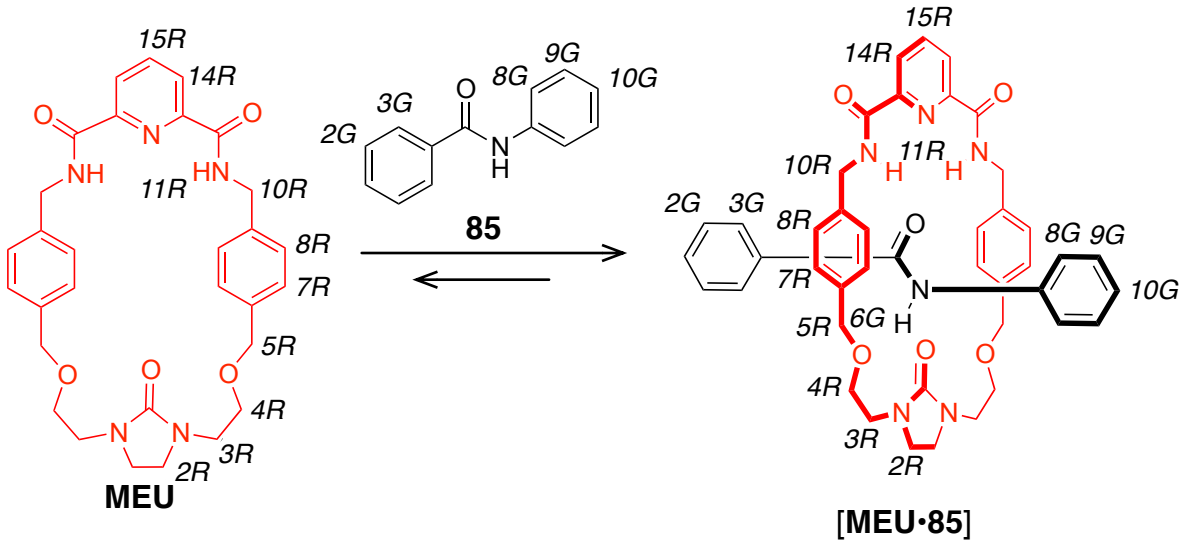

Proton resonances	$\delta_{unbound}$	δ_{bound}	$\Delta\delta$
NH^{11R}	8.04	8.53	+0.47
H^{8R}, H^{7R}	7.27	7.13	–0.14
H^{10R}	4.69	4.60	–0.09
H^{5R}	4.48	4.40	–0.08
H^{4R}	3.60	3.45	–0.15

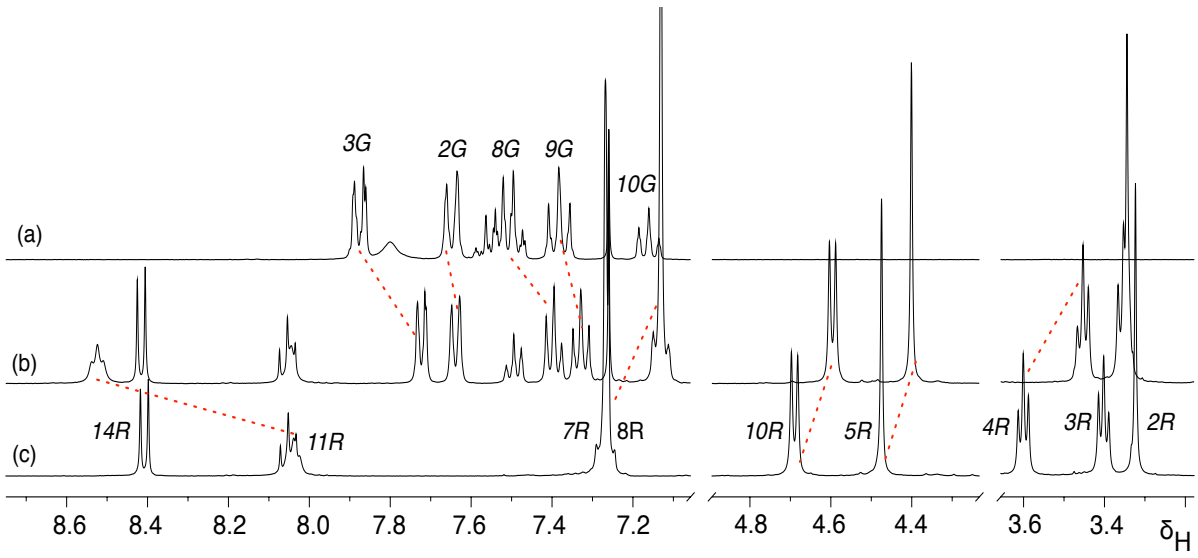

Figure 4.4. Partial ^{1}H NMR spectra (300.1 MHz, 25 ˚C, $CDCl_3$, 20mM) of (a) benzanilide **85** (b) an equimolar mixture of macrocycle **MEU** and guest **85** and (c) macrocycle **MEU**. Red dashed lines are shown to connect resonances for specific protons in bound and unbound states. The saturation curve for the association of the macrocycle **MEU** and benzanilide **85** gives an optimized K_a value of 41 ± 4 M^{-1} and ΔG = –2.20 kcal mol^{-1}. R corresponds to the ring component (in this case, macrocycle **MEU**) and G denoted the guest (in this case, benzanilide **85**). ($\Delta\delta = \delta_{unbound} - \delta_{bound}$).

The second binding experiment was conducted using benzanilide **85** under the same conditions. The 300.1 MHz ^{1}H NMR spectrum of an equimolar mixture of macrocycle **MEU** and benzanilide **85** exhibits (**Figure 4.4b**) a fast exchange process is taking place. The chemical shift changes observed in ^{1}H NMR spectrum are comparable to those observed for macrocycle **MEU** and diphenylurea **84**, for example the downfield shift for the resonances macrocycle NH protons H^{11R}, (+0.47 ppm), upfield shifts for the resonances of the macrocyle **MEU** phenylene protons H^{8R} and H^{7R} and that of the guest aromatic protons (H^{2G}, H^{3G}, H^{8G} and H^{9G}), and upfield shifts of the macrocycle **MEU** methylene protons H^{10R}, H^{5R} and H^{4R} (–0.09, –0.08 and –0.15 ppm, respectively). The strength of the complex formed between the macrocycle **MEU** and *N*-phenylbenzamide **85** was estimated by using ^{1}H NMR titration experiment and the K_a was found to be 41 ± 4 M^{-1} in $CDCl_3$ at 25 ˚C. A possible explanation for the low association constant obtained is that the crucial binding only occurred between the amide NHs proton of the macrocycle **MEU** and the carbonyl functional group from the guest. This evidence correlated with the molecular representation of macrocycle **MEU** in crystal structure as the carbonyl oxygen of the ethylene urea is in contact with the $CHCl_3$ solvent, which consequently incapable to participate as hydrogen bond donors with the guest.

We are aware that amide-based[220] macrocycles have been used to construct many elegant interlocked molecules. In most circumstances, the threading of the guest into these macrocycles required the cooperation of two or more suitably positioned carbonyl groups or anionic templates. On that account, the presence of the carbonyl group is essential for this binding behavior. Nevertheless, the poor association constant derived for both complexes in the ^{1}H NMR titration experiments was unanticipated and, hence, lead us in the quest for alternative binding site, such as thiourea. Additional binding experiment was performed under the same conditions using thiourea **86** (see **Table 4.1**) as guest. The ^{1}H NMR spectrum of an equimolar mixture of macrocycle **MEU** and thiourea **86** (not shown) reveals that this complex also display a fast exchange process and the chemical shift changes for the macrocycle resonances are similar to those observed in **Figure 4.3b** and **Figure 4.4b**, and thus, demonstrate that macrocycle **MEU** capable of binding a thiourea binding site.

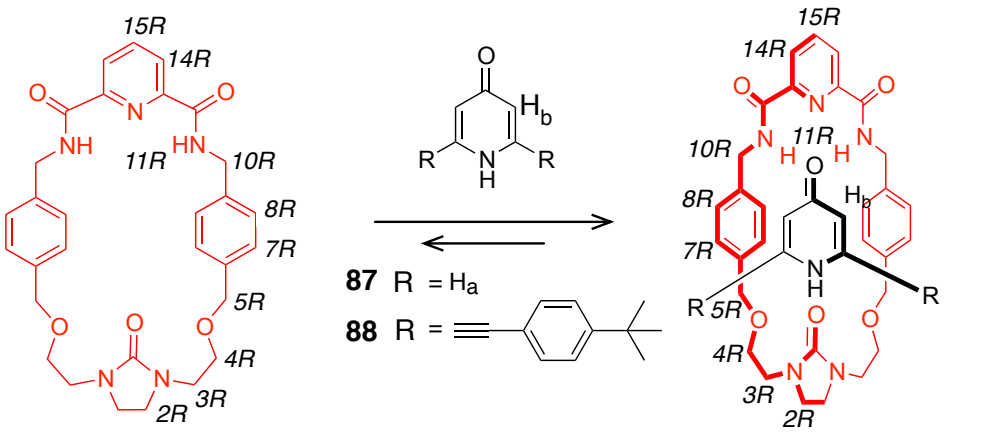

Chemical shift data for [**MEU·87**]

Proton resonances	$\delta_{unbound}$	δ_{bound}	$\Delta\delta$
NH^{11R}	10.04	8.06	+1.98
H^{8R}, H^{7R}	7.27	6.99	–0.28
H^{10R}	4.69	4.59	–0.10
H^{5R}	4.48	4.35	–0.13
$H_a{}^G$	7.64	6.91	–0.93
$H_b{}^G$	6.46	5.72	–0.74

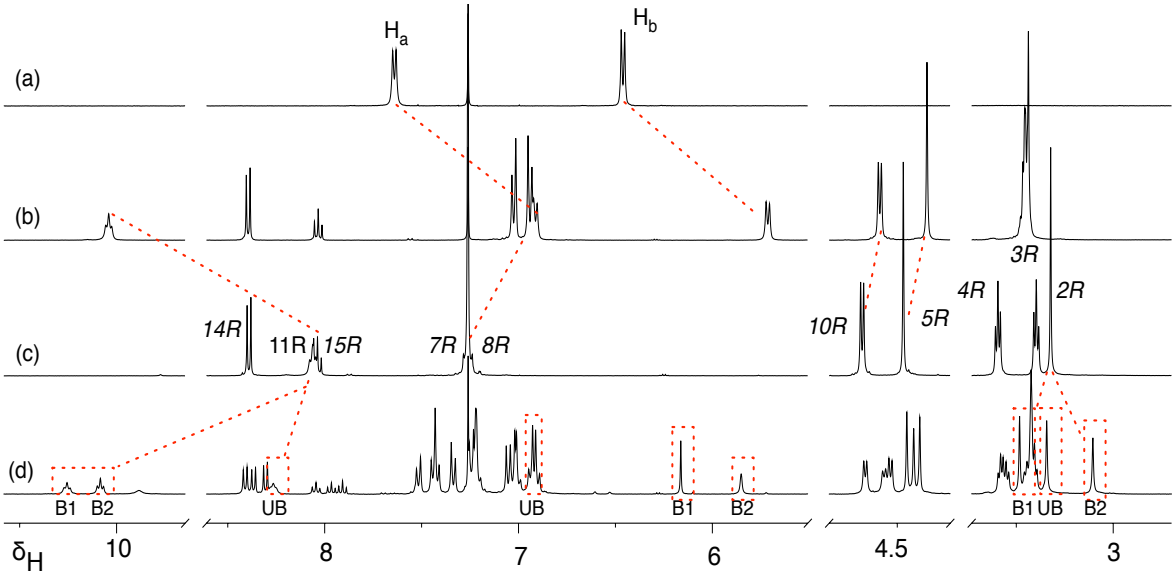

Figure 4.5. Partial ^{1}H NMR spectra (400.1 MHz, 25 ˚C, $CDCl_3$, 25 mM) of (a) 4-pyridone **87** (b) an equimolar mixture of macrocycle **MEU** and 4-pyridone **87** (c) macrocycle **MEU** and (d) an equimolar mixture of macrocycle **MEU** and extended pyridone **88**. Red dashed lines are shown to connect resonances for specific protons in bound and unbound states. **UB** stands for unbound species, and **B1** and **B2** corresponds to bound species 1 and bound species 2. R corresponds to the macrocycle **MEU** and G denoted the guest **87**. ($\Delta\delta = \delta_{unbound} - \delta_{bound}$).

Following this, we investigated the ability of macrocycle **MEU** to complex pyridone guests by performing the similar binding experiments. The 400.1 MHz ^{1}H NMR spectrum of an equimolar mixture of macrocycle **MEU** and 4-pyridone **87 (Figure 4.5b)** in $CDCl_3$ shows that the complex between macrocycle **MEU** and **87** is again in fast exchange process and displays remarkable changes in the chemical shifts for the complex's resonances relative to those of the free species (**Figure 4.5a** and **Figure 4.5c**). The resonance arising from the macrocycle NH protons, NH^{11R} is shifted downfield (+1.98 ppm) as a result of the hydrogen bonds between these protons and the carbonyl group of 4-pyridone **87**. The upfield shifts of both phenylene and methylene **MEU** protons indicate that **MEU** bind the guest very well.

An equimolar solution of macrocycle **MEU** and extended guest **88** was subsequently prepared in $CDCl_3$ by heating of this mixture to improve its solubility. The ^{1}H NMR spectrum (**Figure 4.5d**) exhibits four different sets of resonance, namely one for the free macrocycle **MEU** and a further three corresponding to (i) free pyridine guest **88** (ii) the first pseudorotaxane complex [**MEU·88**] – bound species 1 (**B1**) and (ii) the second pseudorotaxane complex [**MEU·88**]**'** – bound species 2 (**B2**). Both bound and unbound species equilibrated in a slow exchange process on the ^{1}H NMR chemical shift timescale.

Examining the 500.1 MHz 2D EXSY NMR spectrum recorded at 25 ˚C reveals a number of significant crosspeaks between the unbound, **UB** macrocycle **MEU (**NH^{11}) proton with the emergence of bound proton species, **B1** ($NH^{11'}$) and **B2** ($NH^{11''}$) (**Figure 4.6a**), unbound extended pyridone guest **88** phenylene proton, **UB** (H_b) and the two bound species, **B1** (H_b**'**) and **B2** (H_b**''**) (**Figure 4.6b**) and finally between the unbound macrocycle methylene proton, **UB** (H^2) and the corresponding bound species, **B1** ($H^{2'}$) and **B2** ($H^{2''}$) (**Figure 4.6c**). Fascinatingly, both bound species are shown to exchange with each other as well as exchanging with the unbound species. Important 2D NOESY crosspeaks can also be observed for both pseudorotaxane complexes. These duplicate resonances very likely originated from two alternative conformations that the macrocycle **MEU** accommodate during the complexation event. Efforts were pursued to investigate the possible lowest energy conformations of the two bound [2]-pseudorotaxane complexes (suggested by the calculated structure of **UB**, **B1** and **B2** as shown in **Figure 4.7**).

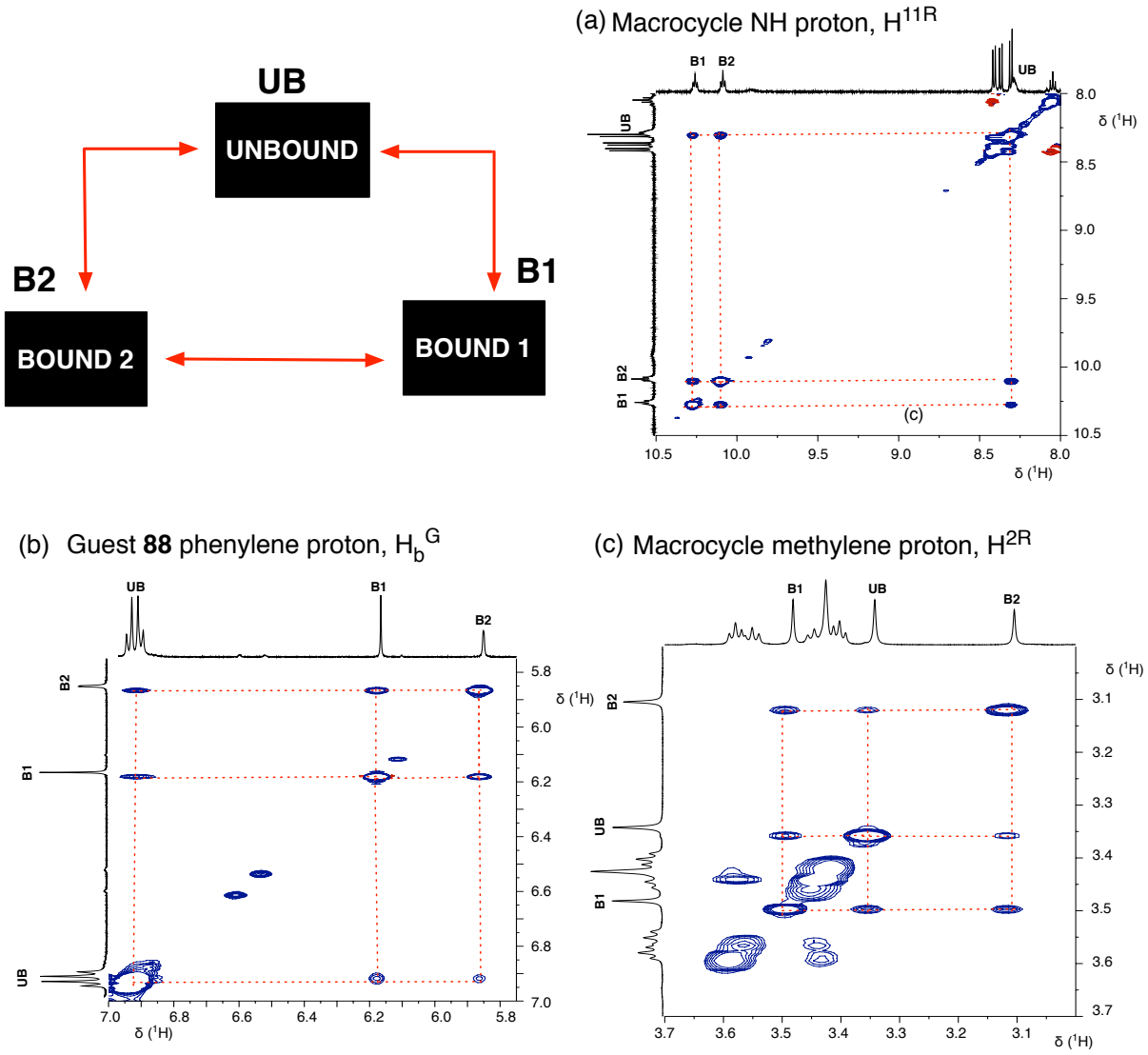

Figure 4.6. Partial 2D EXSY spectrum (500.1 MHz, 25 ˚C, $CDCl_3$, 25 mM) of an equimolar mixture of macrocycle **MEU** and extended pyridine guest **88**. Dashed boxes denotes the corresponding EXSY crosspeaks (blue points) between the two bound and unbound species. Red points represent the NOESY crosspeaks in the spectrum.

It is important to note the two separate orientations of the pyridine ring macrocycle **MEU** relative to the carbonyl group of the cyclic urea. In the case of **B1** complexes, the pyridine ring of the macrocycle is aligned almost parallel to the carbonyl group of the cyclic urea. However, gaining a strong hydrogen bond between the hydrogen bond acceptor of the cyclic urea and the NH proton of the pyridone guest is rather obscure. On the other hand, **B2** conformation reveal that the oxygen atom of the cyclic urea is pointing downward with respect to the pyridine ring which inevitably inhibited the preferred hydrogen bond contact with the NH of the guest **88**. These calculated structures are in agreement with the single crystal structure obtained for macrocycle **MEU** in which case the inverted location of the cyclic urea with respect to the pyridine ring in the upper fragment of the macrocycle is similarly observed. On

the whole, both bound species (**B1** and **B2**) represents 62% of the species in solution, compared to 38% of the unbound **UB** species in the mixture. Using the single-point method, the association constant, K_a derived for the bound species [**MEU·88**] was estimated to be 170 ± 20 M^{-1} in $CDCl_3$ at 25 ˚C and, hence, discriminated nearly 1:1 ratio between the two bound species. The following table (**Table 4.1**) summarizes all the binding experiments carried out at 25 ˚C between macrocycle **MEU** and different guests synthesised.

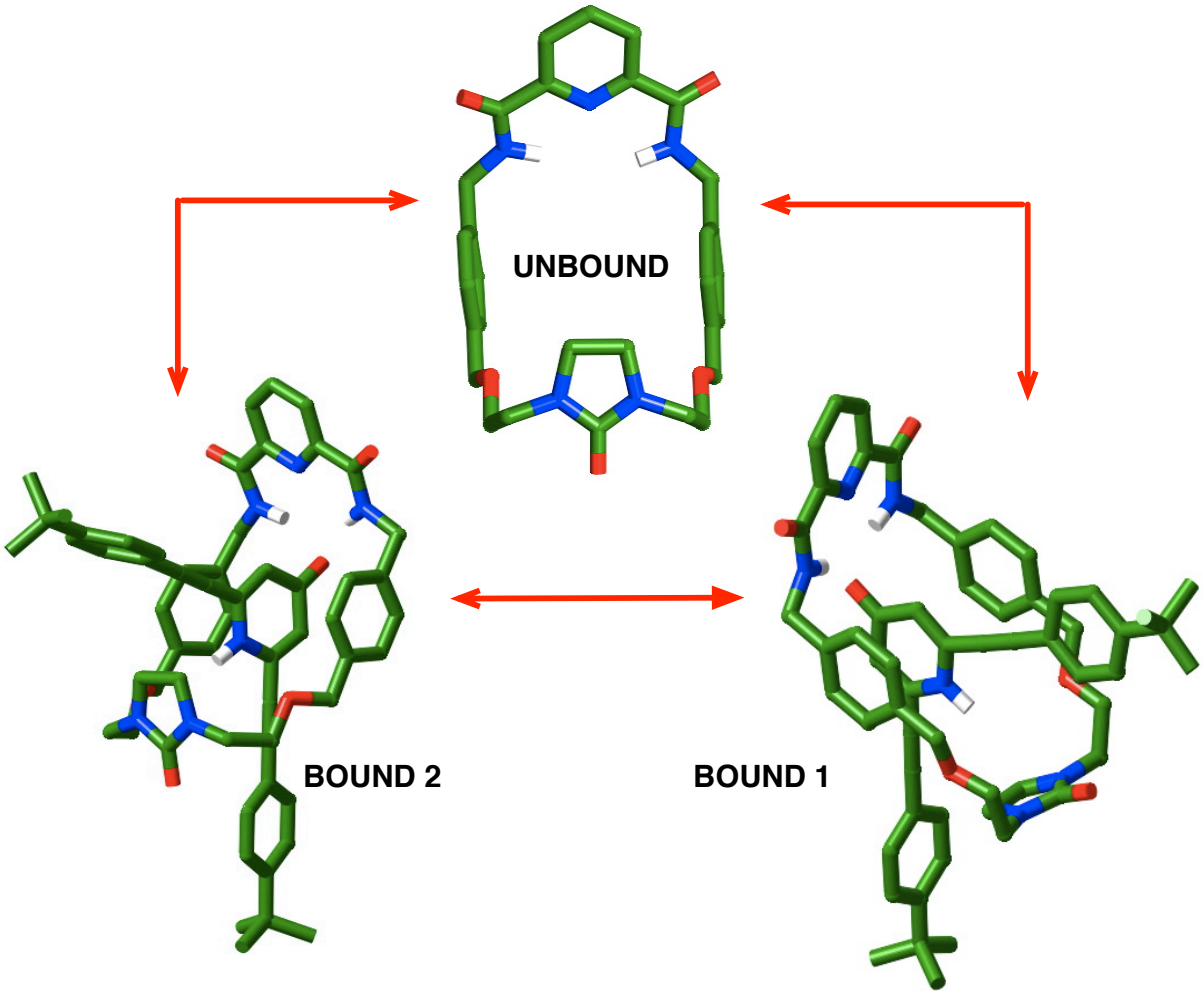

Figure 4.7. Stick representation of the calculated structure (OPLS2005, GB/SA $CHCl_3$) for **Unbound**, **Bound 1** and **Bound 2** species. The reversible exchange event shown as red arrows occurred between unbound species (**UB**) and bound species (**B1** and **B2**, respectively) in the reaction mixture.

Table 4.1. Binding experiments carried out with macrocycle **MEU**. The ^{1}H NMR spectra of the macrocycle **MEU** and guest showed complexes either in fast exchange (F), or in intermediate exchange (I), or in slow exchange (S) that can be attributed to significant binding process in comparison to the free species observed in isolation. The K_a usually determined by titration (*) technique in the case of fast exchange. In the case of slow exchange, the K_a was determined using the single-point method (#) by ^{1}H NMR resonance. Intermediate exchange normally leads to broad peaks and prevent the determination of K_a. The concentration used was 20 mM in $CDCl_3$ at room temperature unless otherwise stated.

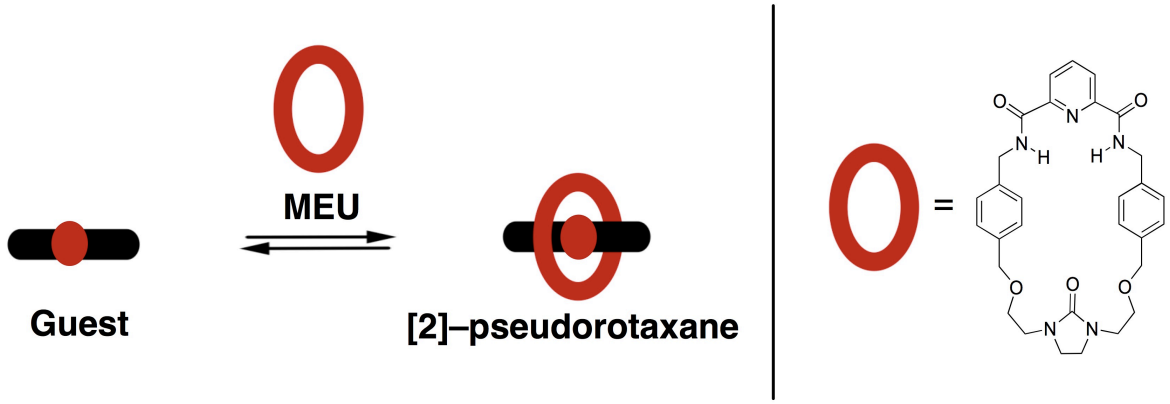

Guest	K_a / M^{-1}	Guest	K_a / M^{-1}
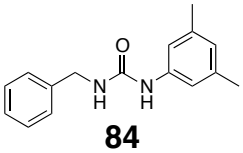 **84**	F * $K_a = 39 \pm 4$	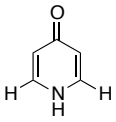 **87**	F
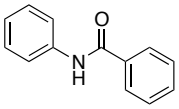 **85**	F * $K_a = 41 \pm 4$	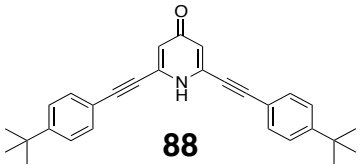 **88**	S # $K_a = 170 \pm 20$
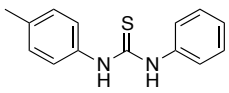 **86**	F	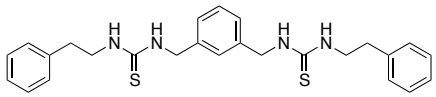 **89**	I

4.2.3 Acyclic urea macrocycle (MAU)

In order to improve the binding constant of pseduorotaxane complex, the framework of the macrocycle was subtly altered. The reasonable rationale behind the newly designed motif of host results from the weak binding displays between amide guest and macrocycle **MEU** previously. The structural design change is fabricated by creating an inclusive hydrogen bond donors pocket. Theoretically, the new adjustment will result in 'all hydrogen bond acceptors' pattern in designing the guest

candidates. In particular, an appropriate guest comprised an equal amount of hydrogen bond acceptor, namely the 2,5-substituted piperazine-2,5-dione **90** and benzoquinone **91** (**Scheme 4.2**). The proposed guest, piperazine-2,5-dione **90** contained two carbonyl groups acting as hydrogen bond acceptors. The oxygen atom have the ability to form two hydrogen bonds each, with only weak angle dependence[221] on the hydrogen bonds observed from the NH groups.

Thus, the macrocycle NH protons will provide exact complementarity. In addition, the 2,5-substitited benzoquinone **91** is an analogue of the piperazine-2,5-dione, in which case its two carbonyl groups can be chemically altered upon oxidation.The guest act as a hydrogen bond acceptor in the ground state to bind the macrocycle preferentially and the subsequent interconversion *via* reduction of the dione **91** to the diol **91a** would displace the bound macrocycle as a conflicting donor motifs. Since this is a reversible reaction, diol **91a** can be oxidized back to its conjugate dione **91** causing the macrocycle to shuttle back to its original position.

Therefore, molecular movement of this reversible nature means it is possible to control the position at which the macrocycle is bound. Ultimately, both of these suggested guest structures fundamentally increase the binding affinity between the guest and host. The synthesis of macrocycle **MAU** similarly begins with the alcohol substitution on addition of **78** to the sodium in the presence of ethylene glycol (**Scheme 4.3**).

The resultant alcohol **79** was tosylated in addition of *p*-toluenesulfonyl chloride to furnish a quantitative yield of intermediate **80**. The tosylated product **80** then becomes susceptible for nucleophilic attack by sodium azide, NaN_3. Selective hydrogenation of azide **92** using palladium on carbon as catalyst afforded the amine derivative **93**. Following that, triphosgene **94** was added neat to ensure that the conversion to the desired urea takes place.

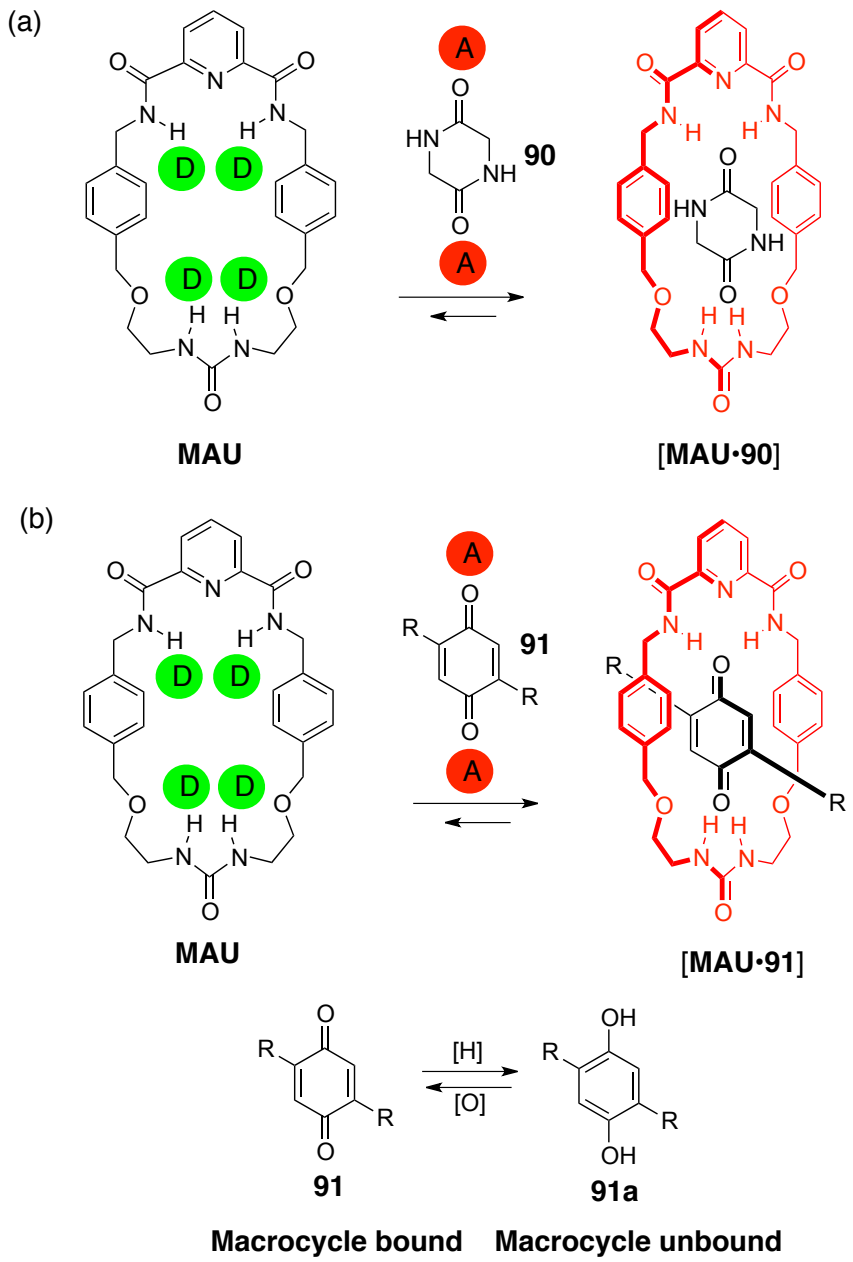

Scheme 4.2. (a) Schematic presentation of possible interactions between macrocycle **MAU** and piperazine-2,5-dione **90** derivative. (b) Schematic presentation of possible interactions between macrocycle **MAU** and 2,5-substituted benzoquinone **91**. It display reversible binding characteristic in response to external stimuli. In its ground state, benzoquinone **91** will preferentially bind the macrocycle **MAU** as a result of an increase in the number of hydrogen bond interactions. However, dione **91** can be reduced to the corresponding diol **91a**, thus transforming the acceptor motif to a donor motif and theoretically displace the macrocycle. (**D** embedded in green circles denoted the hydrogen bond donors while **A** embedded in red circles denoted the hydrogen bond acceptors).

Nonetheless, the reduction of the nitrile group **95** with BH_3•THF solution at 0 ˚C has found to be unsuccessful. The second approach was considered using stronger base, $LiAlH_4$ in dry THF, however the corresponding amine was not been able to synthesise. Later attempt on the hydrogenation in the presence of Raney-Nickel

catalysis was also inefficient. We reasoned that it is possible that with the presence of acidic hydrogen in compound **95** further assisted in the failure of the reaction to go to completion.

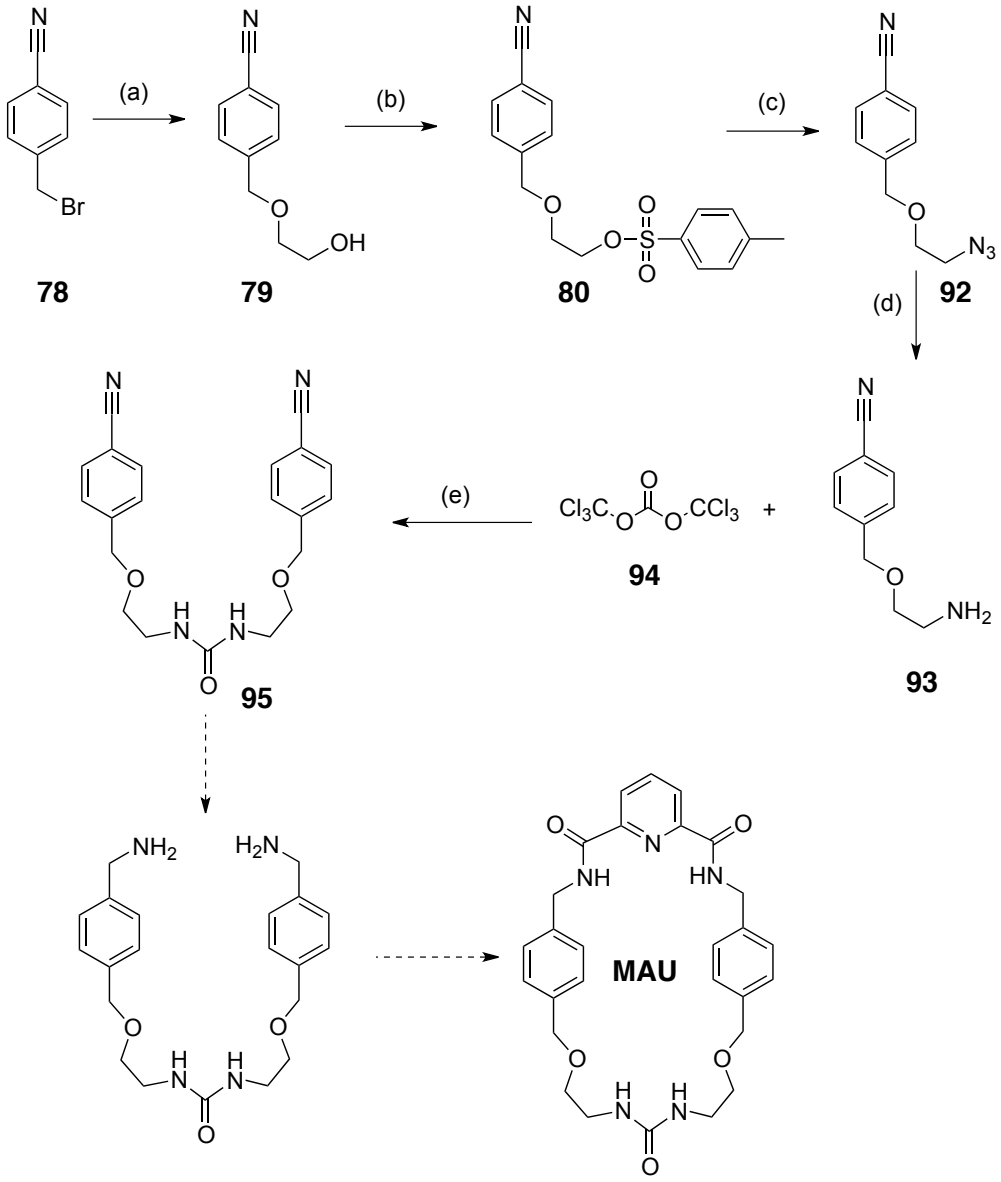

Scheme 4.3. Attempted synthesis of **MAU**. Reagents and yields: (a) Na, ethylene glycol, THF, reflux, 16 h, 90%; (b) TsCl, Et_3N, CH_2Cl_2, 0 ˚C to 1h and reflux for 16 h, 77%; (c) NaN_3, DMF, 80 ˚C, 16 h, 97%; (d) H_2, Pd/C, Pyridine, CH_3OH, rt, 8 h, 98%; (e) Et_2O, Et_3N, 0 ˚C followed by reflux, 6 h, 36%.

As a consequence, the synthesis of macrocycle **MAU** could not be completed to afford the hydrogen acceptors motif's host and its corresponding calculated structure is depicted in **Figure 4.8**.

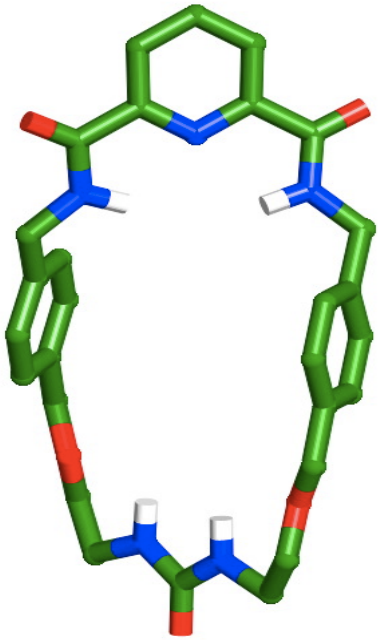

Figure 4.8. Stick representation of the calculated structure (OPLS2005, GB/SA $CHCl_3$) of macrocycle **MAU**. Carbon atoms are coloured green, oxygen atoms red, nitrogen atoms blue and hydrogen atoms white (most hydrogen atoms have been removed for clarity).

4.2.4 Symmetrical macrocycle (SM)

Preliminary synthetic effort[200] to construct the symmetrical macrocycle employed the alkyne dimeric coupling reaction to afford the hydrogen donors host, in which could similarly integrated the corresponding guests described in **Scheme 4.2**. Disappointedly, insufficient supply of the macrocycle hindered the performance of the essential binding study. On that account, it would be worth preparing the analogous symmetrical macrocycle, which include the two hydrogen bond acceptors site. An earlier attempt to synthesise the symmetrical macrocycle is described in **Scheme 4.4**. Addition of 2,6-pyridinedicarbonyl dichloride to propargyl alcohol in the presence of base, yielded compound **96** in a moderate yield.

The homocoupling reaction of **96** under standard and high dilution oxidative coupling conditions using copper diacetate as catalysts in the presence of *N*-ethyldiisopropylamine is however unsuccessful. We subsequently focused[222] on the standard conditions taken from the Sonogashira coupling of **96** with PPh_3, $PdCl_2(PPh_3)_2$, CuI in triethylamine/CH_3CN solvent mixture refluxed under a positive atmosphere of argon. Nonetheless, this attempt has also been inefficient in closing the ring. The lack of success is plausible to explain from the unusual conformation of

calculated structure of the macrocycle **SM** (shown in **Figure 4.9**), which reveals that the molecule is twisted by rotation of one pyridine ring unit relative to the other and hence, supported the unsuccessful attempts of the dimerisation reaction.

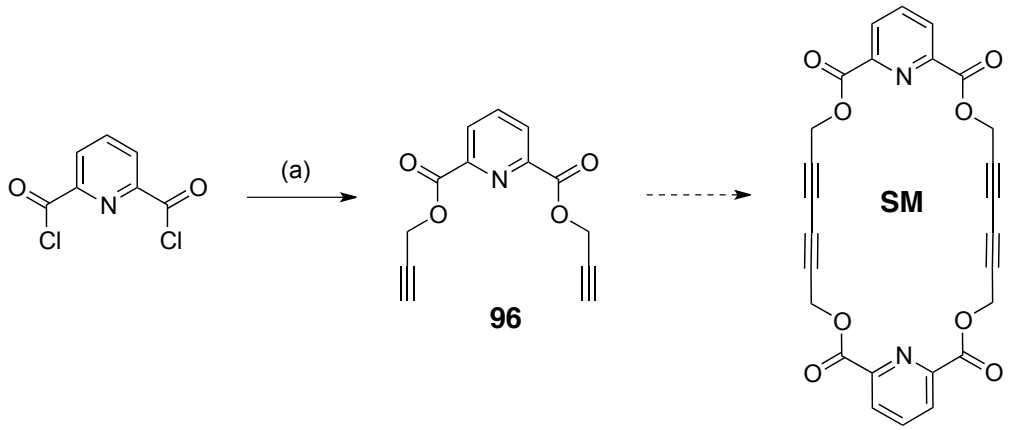

Scheme 4.4. Attempted synthesis of macrocycle **SM**. Reagents and yield: (a) 2,6-pyridinedicarbonyl dichloride, propargyl alcohol, Et_3N, $CHCl_3$, 0 ˚C to rt, 16 h, 50%.

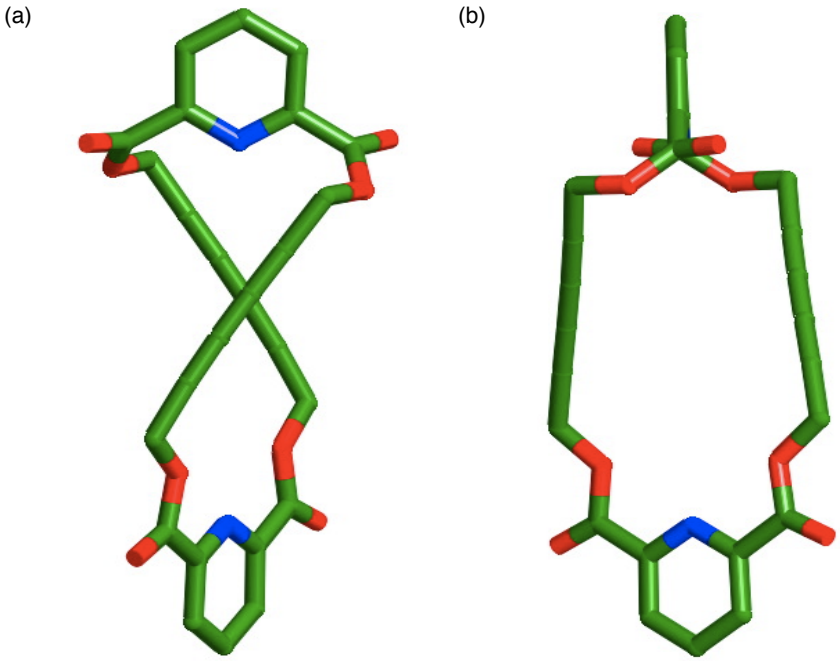

Figure 4.9. (a) Face and (b) side views of stick representations of the calculated structure (OPLS2005, GB/SA $CHCl_3$) of macrocycle **SM**. Carbon atoms are coloured green, oxygen atoms red, nitrogen atoms blue and hydrogen atoms white (most hydrogen atoms have been removed for clarity).

4.3 Second generation of macrocycles – Alternative synthesis

Further investigations were conducted to explore the binding properties of the preceeding macrocycles prepared in the group as well as to improve the yield by introducing an alternative synthetic route. This will allow us to deduce significant conclusions on the strength and potential between the first and second generation macrocycles.

4.3.1 Alkyne ethyleneurea macrocycle (MAEU)

We had found[200] evidence that macrocycle **MAEU** capable of bind 4-pyridone **87**, but we never tested with other different guests. Thus, a different approach is described to simplify the synthesis of **MAEU** (**Scheme 4.5**). The alkyne **98** was initially prepared in the group by the treatment of bis *N*-alkylation of cyclic ethylene urea **81** with propargyl benzenesulfonate **97**. 3-bromobenzonitrile **99** was employed as the starting material to couple the bis(alkyne) **98** under Sonogashira conditions to afford compound **100**. Despite that, an attempt to reduce the nitrile groups in **100** has been unsuccessful to furnish the corresponding amine compound and thus, no further binding experiment could be carried out with macrocycle **MAEU**.

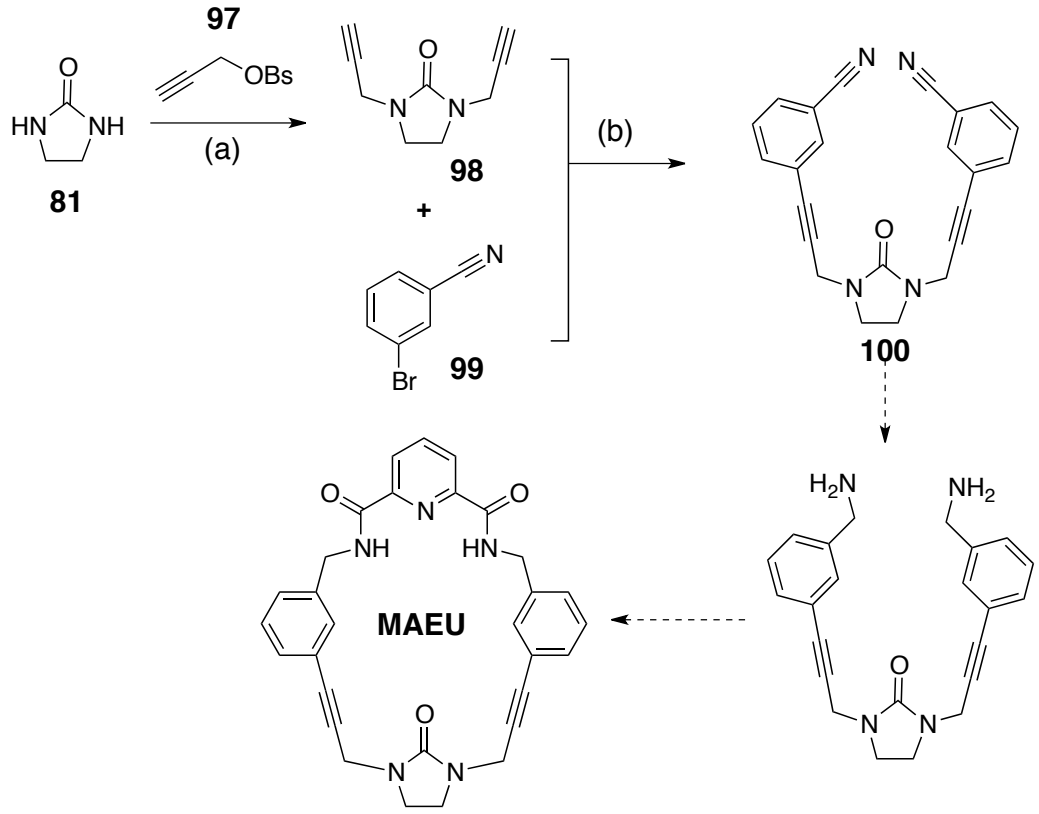

Scheme 4.5. Attempted synthesis of macrocycle **MAEU**. Reagents and yields: (a) Bu_4NBr, KOH, THF, 0 ˚C to rt for 1 h, followed by reflux, 2 days, 40%; (b) $PdCl_2(PPh_3)_2$, CuI, PPh_3, Et_3N, THF, 70 ˚C, 48 h, 36%.

The calculated conformation macrocycle **MAEU** (**Figure 4.10**) illustrated that the oxygen of the carbonyl group is pointing downward with respect to the pyridine ring unit.

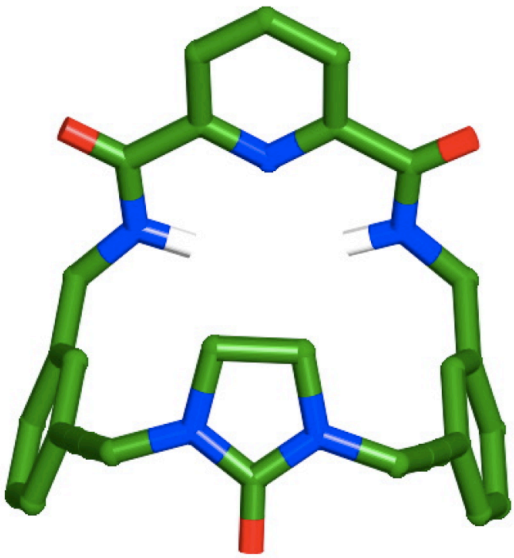

Figure 4.10. Stick representation of the calculated structure (OPLS2005, GB/SA $CHCl_3$) of macrocycle **MAEU**. Carbon atoms are coloured green, oxygen atoms are coloured red, nitrogen atoms blue and hydrogen atoms white (most hydrogen atoms have been removed for clarity).

4.3.2 Diethylene glycol macrocycle (MDG)

Earlier in **Section 4.2.2**, macrocycle **MEU** exhibited such ineffective binding with simple amide and urea guests. The pursuit to readdress these insufficiencies have forced us one step back to repeat the syntheses of known macrocycles in order to provide conclusive binding studies. The hydrogen bond donor and acceptor interactions displayed by macrocycle **MDG** on addition of amide and urea derivatives shown in **Figure 4.11**. The resulting [2]-pseudorotaxane complexes are stabilised through the cooperation effects of π stacking of the two xylyl rings and N–H•••O hydrogen bonding (between macrocycle NHs proton and the carbonyl oxygen atom of each simple amide and urea compounds and between the amide and urea proton(s) and the ether pocket of the ring).

The synthesis of macrocycle **MDG** was prepared[207] according to the literature. 4-(bromomethyl)benzonitrile **78** was reacted with diethylene glycol **101** under basic conditions to afford the dibenzonitrile **102**. BH_3•THF mediated reduction yielded the amine **103** followed by ring closure with 2,6-pyridinedicarbonyl dichloride in high dilutions with the aid of one equivalent of 4-pyridone **87**, which acted as template gave rise to 34% yield of the macrocycle **MDG** (**Scheme 4.6**).

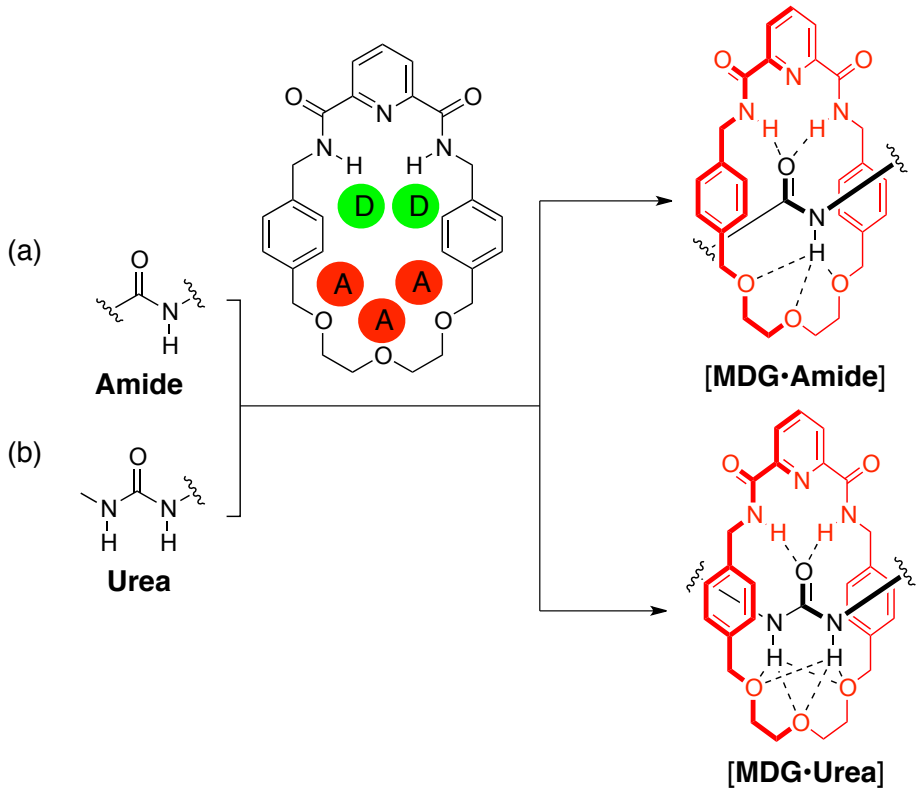

Figure 4.11. Structural design of macrocycle **MDG** comprised both hydrogen bond donors and acceptors motif with amide and urea guest interaction displayed by dashed lines. (D embedded in green circles denoted the hydrogen bond donors while A embedded in red circles denoted the hydrogen bond acceptors).

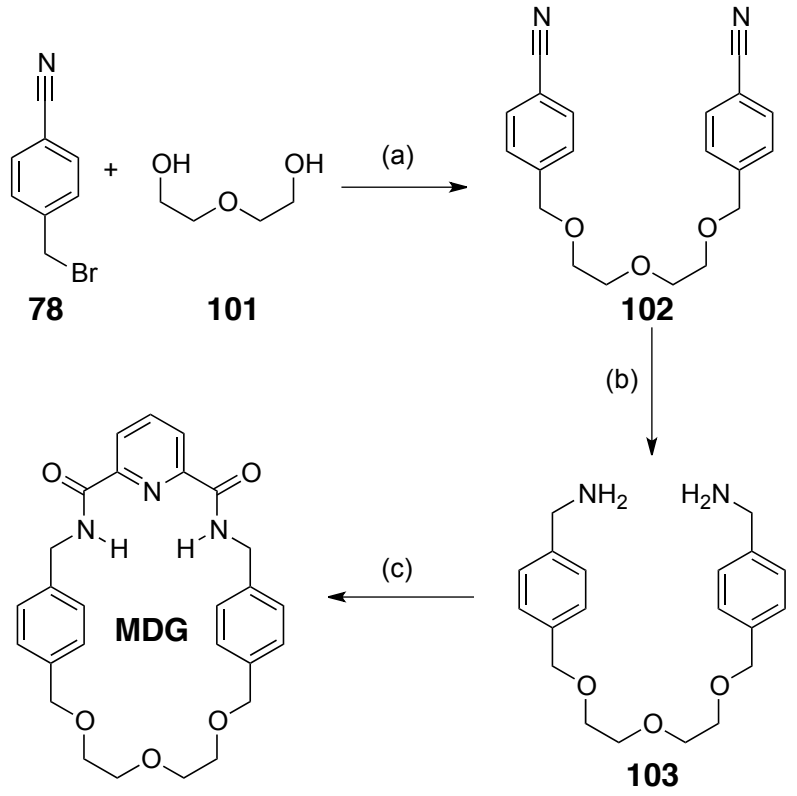

Scheme 4.6. Synthesis of macrocycle **MDG**. Reagents and yields: (a) NaH, THF, reflux, 16 h, 90%; (b) BH_3•THF, THF, 0 ˚C for 2 h to reflux for 24 h, 52%; (c) 2,6-pyridinedicarbonyl dichloride, 4-pyridone **87**, Et_3N, CH_2Cl_2, rt, 3 days, 34%.

4.3.3 Binding studies – MDG

In the past, we have established that macrocycle **MDG** can form [2]-pseudorotaxane complex, which stabilized through intermolecular hydrogen bonding with 4-pyridone derivatives **87a** (see **Table 4.2**) positioned within the cavity of the ring in low polarity solvent such as chloroform. From the ^{1}H NMR dilution experiment, the association constant was estimated around 1500 ± 150 M^{-1} from an equimolar mixture of macrocycle **MDG** and **87a**. It was also demonstrated that diarylamides **85** are capable of associating macrocycle **MDG** and the strength of the complex formed was approximated to be 160 ± 16 M^{-1} in $CDCl_3$ at 25 ˚C (see **Table 4.2**). Hence, it is evident that a great discrepancy in the binding strength when we changed the binding site from pyridone to an amide guest. On the basis of this result, simple urea and amide guest derivatives were produced (**Scheme 4.7**), which each compound now incorporate the electron-withdrawing 3,5-bis(trifluoromethyl) substituent. Model amide **105** is synthesised starting from 4-butyl aniline **104**, which was coupled to 3,5-bis(trifluoromethyl)benzoyl chloride **124**. Likewise, reaction of the same aniline with 3,5-bis(trifluoromethyl)phenyl isocyanate **127** yielded urea **106** in 80% yield.

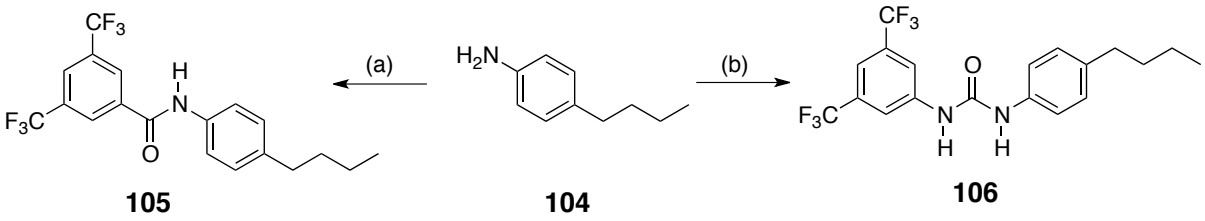

Scheme 4.7. Synthesis of model amide **105** and urea **106**. Reagents and yields: (a) 3,5-bis(trifluoromethyl)benzoyl chloride **124**, Et_3N, $CHCl_3$, –5 ˚C to rt, 16 h, 50%; (b) 3,5-bis(trifluoromethyl)phenyl isocyanate **127**, $CHCl_3$, –5 ˚C to rt, 16 h, 80%.

The binding experiment was initially carried out with an equimolar mixture of macrocycle **MDG** and model amide **105** in $CDCl_3$ at 25 ˚C at 20 mM concentration of the starting reagents. The resulting 400.1 MHz ^{1}H NMR spectrum of this association reveals a slow exchange process with significant chemical shifts changes for the bound and unbound guest **105** (see table in **Figure 4.12)**. Such elegant prove to demonstrate the formation of the pseudorotaxane species arise from the complex pattern in the macrocycle methylene regions (H^{8R}, H^{3R}, H^{2R} and H^{1R}) (red dashed boxes in **Figure 4.12b**) as a consequence of end-to-end asymmetry imposed by the amide **105**. We determined the binding constant using the ^{19}F NMR spectroscopy

using the single-point method (d_1 = 6 sec)[1] to be 900 ± 90 M^{-1}. The similar binding experiment was further conducted with model urea **106**, which also exhibited a slow exchange on the ^{1}H NMR chemical shift time scale (**Figure 4.13b**).

A careful analysis of the 400.1 MHz ^{1}H NMR spectrum display chemical shift changes (see table in **Figure 4.13**) similar to those observed for the pseudorotaxane assembly, such as typical downfield shift of NH macrocycle protons, NH^{9R}, upfield shifts for the resonances for the macrocycle phenylene protons H^{5R} and H^{6R}, and also upfield shifts of the guest **106** phenylene protons, H^{13G} and H^{14G}. Given the asymmetry nature of the urea compound **106**, apparently renders the resonances for proton H^{8R} and H^{3R} diastereotopic. Upon the interlocking of the guest and macrocycle **MDG**, H^{8R} appears as two set of doublet of doublet at δ_H 4.82 and δ_H 4.12 and the H^{3R}, which appear as singlet in the unbound state gave rise to an AB system. The strength of the association between macrocycle **MDG** and urea **106** was found to be broadly similar with K_a value of 980 ± 100 M^{-1} in $CDCl_3$ at 25 ˚C.

[1] After the first excitation, the sample returns to its equilibrium state at a rate $1/T_1$ where T_1 is the spin-lattice relaxation time-constant. In order to obtain the full signal intensity after the second excitation, a delay of approximately 5 × T_1 is thus required. A delay of this duration is necessary if accurate relative intensities and therefore signal integration are to be obtained in quantitative experiments. Hence, we determined the delay (d_1) of the sample by measuring the T_1 to be 6 sec between the two scans. See T.D.W. Claridge, in *Tetrahedron Organic Chemistry Series*, Volume 27, Elsevier **2009**, pp. 11-34.

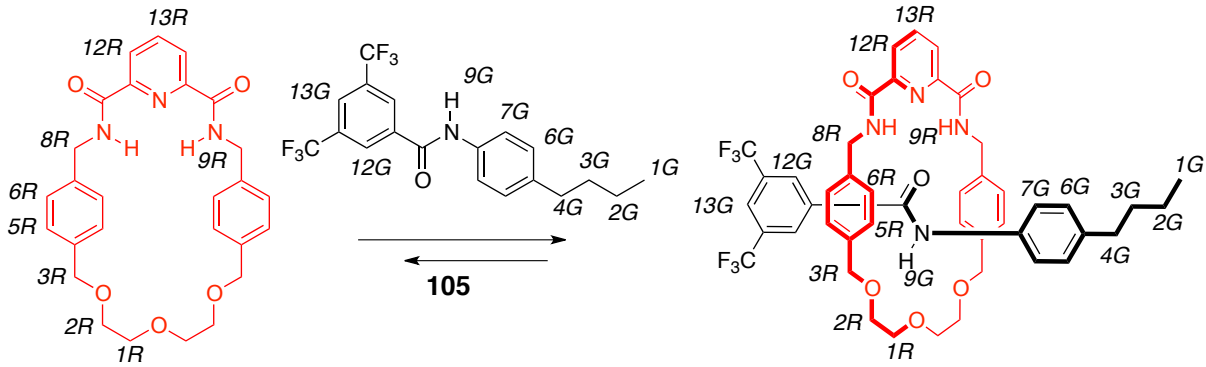

Proton resonances	$\delta_{unbound}$	δ_{bound}	$\Delta\delta$
NH^{9R}	7.98	9.00	+1.02
H^{5R}	7.32	6.68	–0.63
H^{6R}	7.23	6.53	–0.70
H^{12R}	8.30	8.49	+0.19
H^{13R}	8.03	8.12	+0.09
H^{13G}	8.05	7.85	–0.02
H^{12G}	8.31	7.94	–0.37
H^{6G}	7.98	7.42	–0.11
H^{7G}	7.98	7.02	–0.18

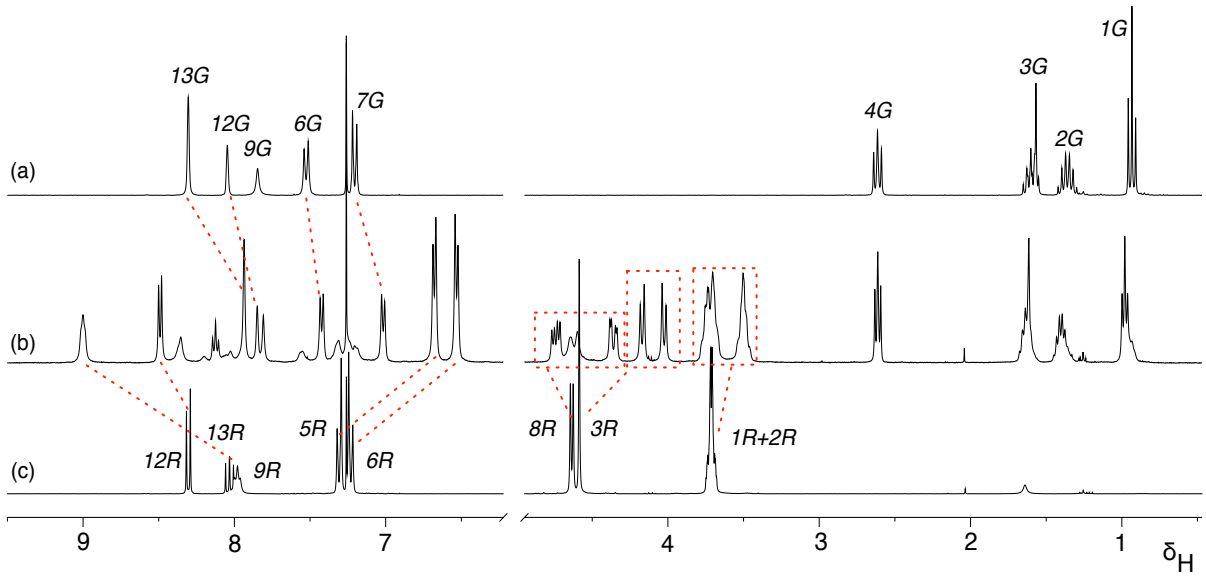

Figure 4.12. Partial ^{1}H NMR (400.1 MHz, 25 ˚C, $CDCl_3$, 20 m) of (a) amide **105**, (b) an equivalent molar mixture of macrocycle **MDG** and amide **105**; and (c) free macrocycle **MDG**. Red dashed lines are shown to connect resonances for specific protons in the bound and unbound states. The complex patterns the macrocycle methylene region (H^{8R}, H^{3R}, H^{2R} and H^{1R}) are shown in the red dashed boxes. R corresponds to macrocycle **MDG** and G denoted the guest **105**. ($\Delta\delta = \delta_{unbound} - \delta_{bound}$).

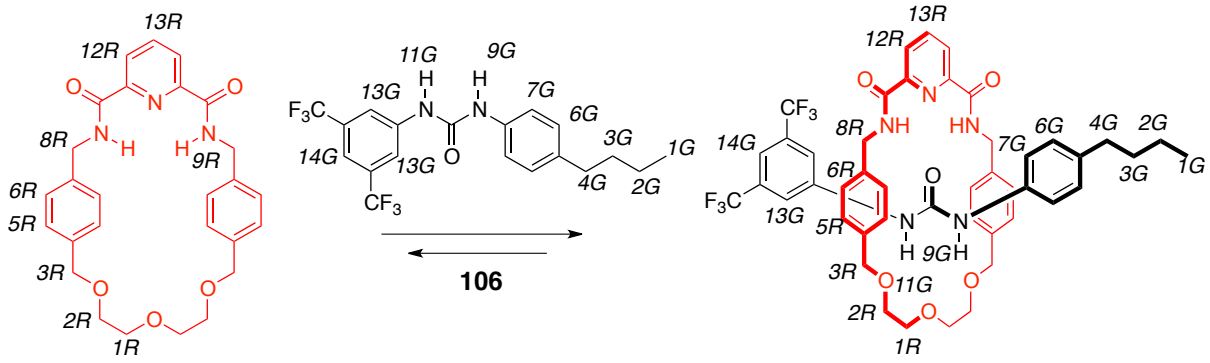

Proton resonances	$\delta_{unbound}$	δ_{bound}	$\Delta\delta$
NH^{9R}	7.98	9.35	+1.37
H^{12R}	8.30	8.47	+0.17
H^{13R}	8.03	8.11	+0.07
H^{5R}	7.31	6.78	–0.53
H^{6R}	7.23	6.78	–0.45
H^{13G}	7.80	7.46	–0.16
H^{14G}	7.49	7.33	–0.34

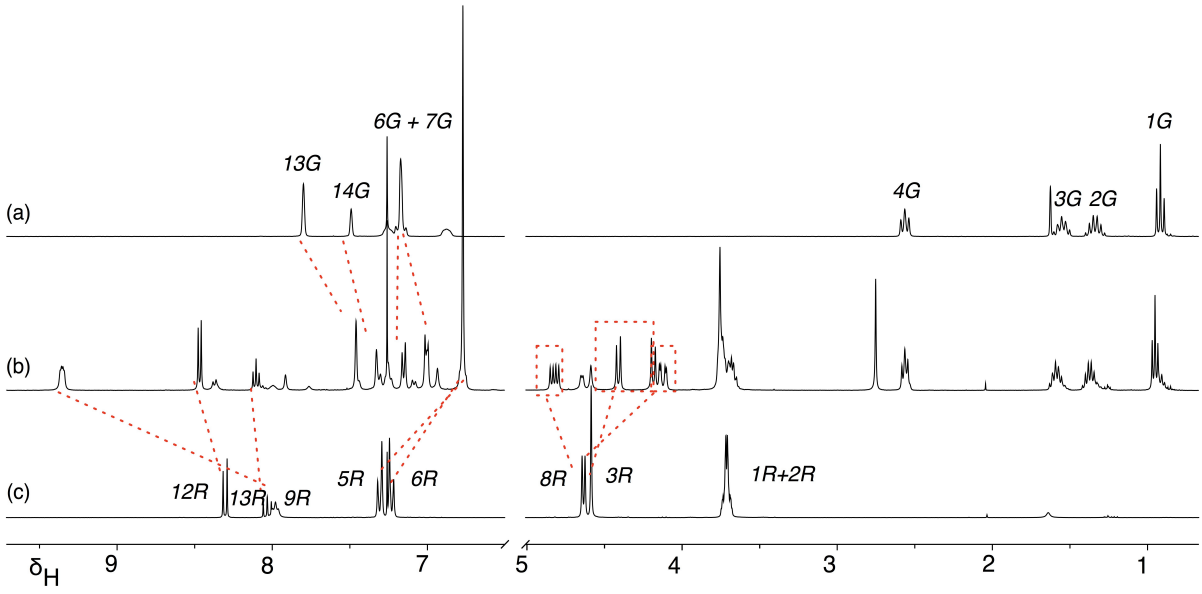

Figure 4.13. Partial ^{1}H NMR (400.1 MHz, 25 ˚C, $CDCl_3$, 20 mM) of (a) urea **106**, (b) an equivalent molar mixture of macrocycle **MDG** and urea **106**, and (c) free macrocycle **MDG**. Red dashed lines are shown to connect resonances for specific protons in the bound and unbound states. The complex pattern of macrocycle methylene region (H^{8R}, H^{3R}, H^{2R} and H^{1R}) are shown in the red dashed boxes. R corresponds to the macrocycle **MDG** and G denoted the guest **106**. ($\Delta\delta = \delta_{unbound} - \delta_{bound}$).

The slow exchange process on the ^{1}H NMR chemical shift timescale manifests that some of the complexation process is characterized by constrictive binding. The constrictive binding energy represents the magnitude of sterically imposed activation energy barrier to the CF_3 guest entry (both guest **105** and **106**) into the cavity of the macrocycle during the exchange process. This phenomena arise from the instability of the guest exchange transition state, which involves significant bond strain as the guest squeezes through the wall of macrocycle **MDG**. However, in the case of benzanilide guest **85** (smaller guest), the constrictive binding energy, which is generally much larger than the intrinsic binding energy (the complexation free energy for the guest binding reaction) decreases since the portal through which the guest must past gets larger. The constrictive and intrinsic nature of complexation between macrocycle **MDG** and urea compound 1**06** are further illustrated in **Figure 4.14**. Following this, **Table 4.2** summarizes the binding experiments carried out at 25 ˚C between macroycle **MDG** and different guests synthesised.

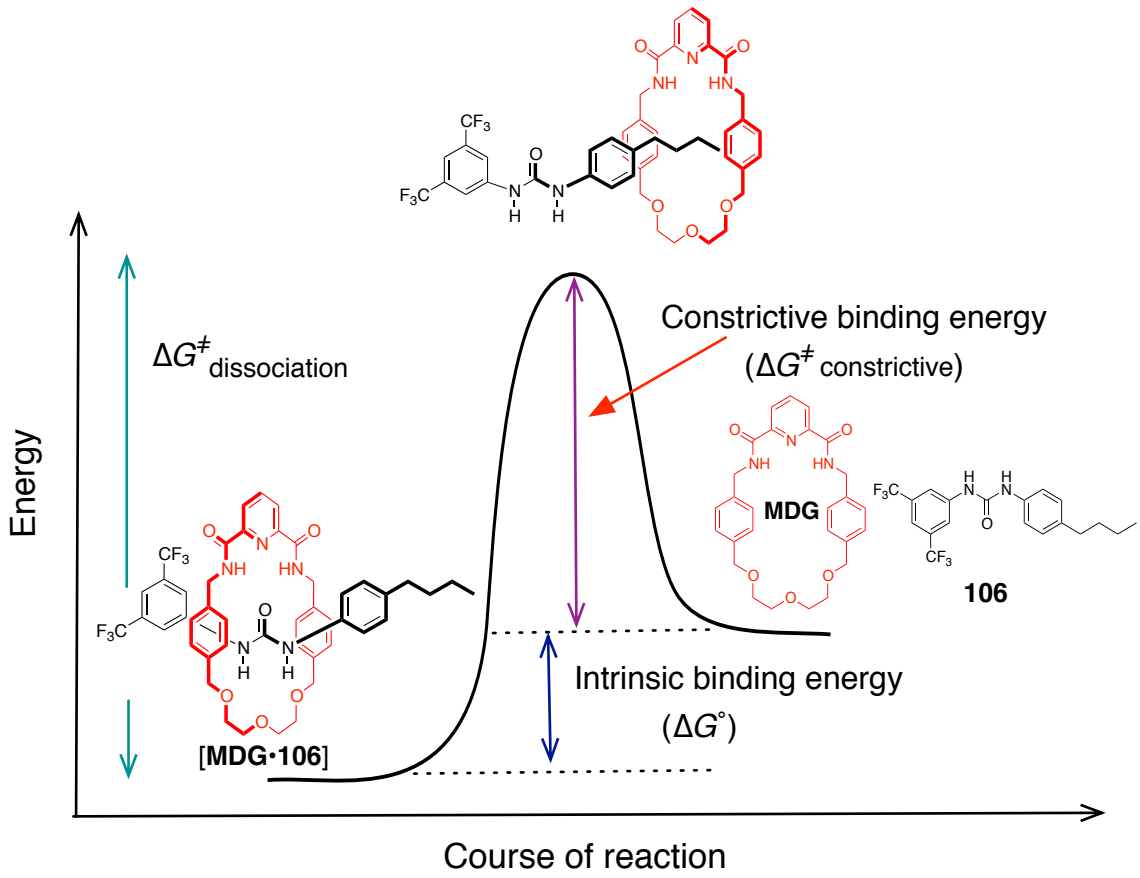

Figure 4.14. The activation energy depicted for urea **106** guest to enter the cavity of macrocycle **MDG** in a slow exchange process. ($\Delta G^{\ddagger}_{\text{constrictive}} = \Delta G^{\ddagger}_{\text{dissociation}} - (-\Delta G^{\circ})$).

Table 4.2. Binding experiments carried out with macrocycle **MDG**. The ^{1}H NMR spectrum of the macrocycle **MDG** and guest mixture showed complex either in fast exchange (F), or in slow exchange (S) that can be attributed to significant binding process in comparison to the free species observed in isolation. The K_a usually determined by titration (*) technique in the case of fast exchanges. In the case of slow exchanges, the K_a was determined using the single-point method (#) either by ^{1}H NMR resonance or ^{19}F NMR resonances (d_1 = 6 sec). The concentration used was 20 mM in $CDCl_3$ at room temperature unless otherwise stated.

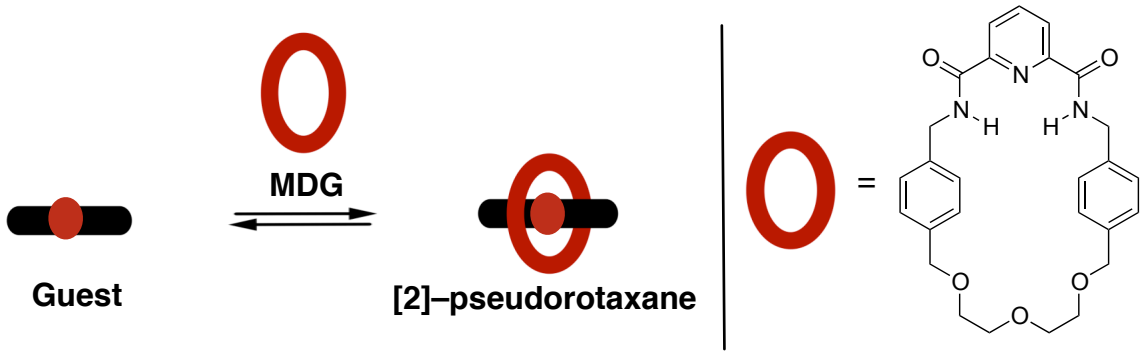

Guest	K_a / M^{-1}	Guest	K_a / M^{-1}
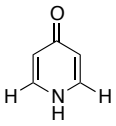 **87**	F * K_a = 450 ± 45	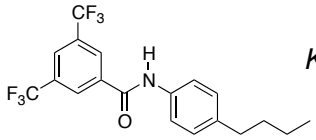 **105**	S # K_a = 900 ± 90
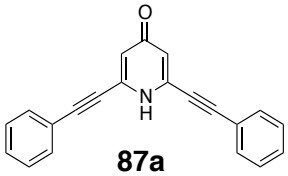 **87a**	F * K_a = 1500 ± 150	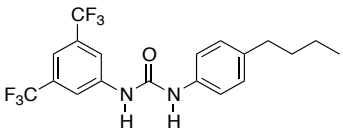 **106**	S # K_a = 980 ± 100
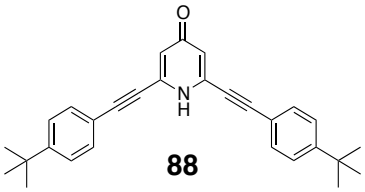 **88**	No binding	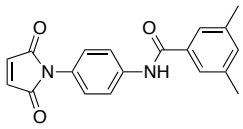 **108**	S # K_a = 70 ± 7
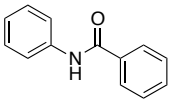 **85**	F * K_a = 160 ± 16	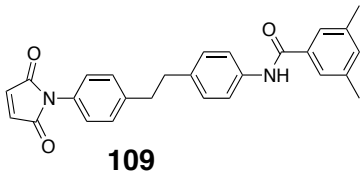 **109**	S # K_a = 50 ± 5
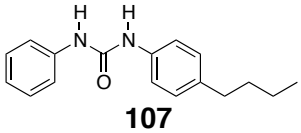 **107**	F * K_a = 370 ± 37	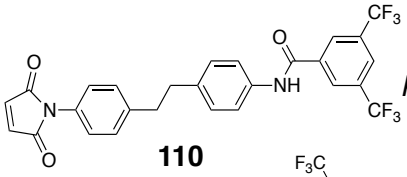 **110**	S # K_a = 1000 ± 100
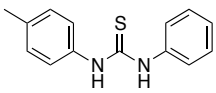 **86**	F	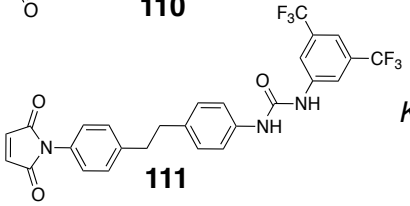 **111**	S # K_a = 350 ± 35

4.3.3 Pyridine macrocycle (MP)

The second macrocycle developed[200] in the group capable of complexing pyridone and acridone moiety in a [2]-pseudorotaxane type geometry. Nonetheless, limited studies have been carried out to examine the potential of this pyridine macrocycle, **MP** to bind urea and amide derivatives. The possible interactions of the guest compounds to associate with the hydrogen bond donors (D) and acceptors (A) of the macrocycle **MP** are illustrated in **Figure 4.15**.

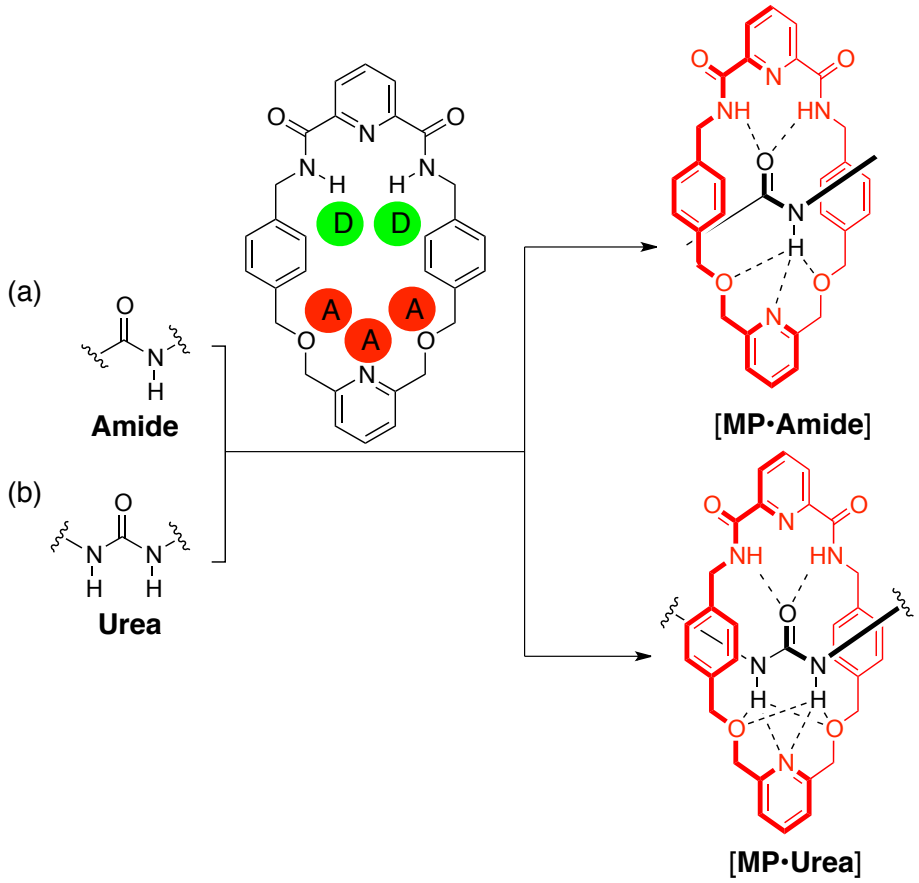

Figure 4.15. Structural design of macrocycle **MP** comprised both hydrogen bond donors and acceptors motif with amide and urea guest interaction displayed by dashed lines. (D embedded in green circles denoted the hydrogen bond donors while A embedded in red circles denoted the hydrogen bond acceptors).

In that case, macrocycle **MP** was produced in three step sequences (**Scheme 4.8**), starting from the 4-(bromomethyl)benzonitrile **78** with 2,6-pyridinedimethanol **112** in basic conditions, affording the dibenzonitrile **113**. The subsequent reduction provided the amine **114**, which was submitted to cyclization with 2,6-pyridinedicarbonyl dichloride in high dilution to obtain the macrocycle **MDG** in 22% yield.

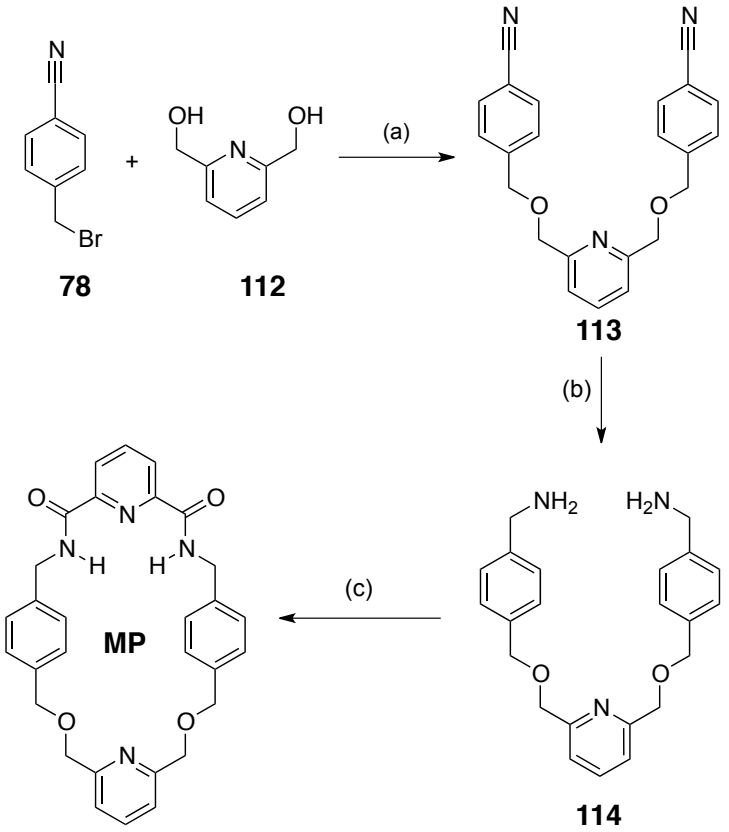

Scheme 4.8. Synthesis of macrocycle **MP**. Reagents and yields: (a) NaH, THF, reflux, 18 h, 88%; (b) BH_3•THF, THF, 0 ˚C to reflux, 18 h, 63%; (c) 2,6-pyridinedicarbonyl dichloride, Et_3N, CH_2Cl_2, rt, 3 days, 22%.

4.3.4 Binding Studies – MP

Binding studies were conducted with macrocycle **MP** in an equimolar mixture of model amide **105** compound in $CDCl_3$ at 20 mM reagent concentration at 25 ˚C. The 400.1 MHz ^{1}H NMR spectrum reveals that the association and dissociation rate between the ring component and the amide **105** is again slow on the ^{1}H NMR chemical shift timescale (see **Figure 4.16b**) relative to those unbound components (comparison with **Figure 4.16a** and **Figure 4.16c**). The macrocycle proton NHs resonances, NH^{11R} displays the typical downfield shifts (+1.25 ppm) as a consequence of the hydrogen bond contacts between these protons and the carbonyl group of amide **105**. An obvious upfield changes for the ring phenylene protons H^{7R} and H^{8R}, (–0.56 and –0.83 ppm, respectively) and that amide guest, H^{6G} and H^{7G} are valuable aspects to denote that upon the interlocking, these protons are now located in the shielding zone of the aromatic ring.

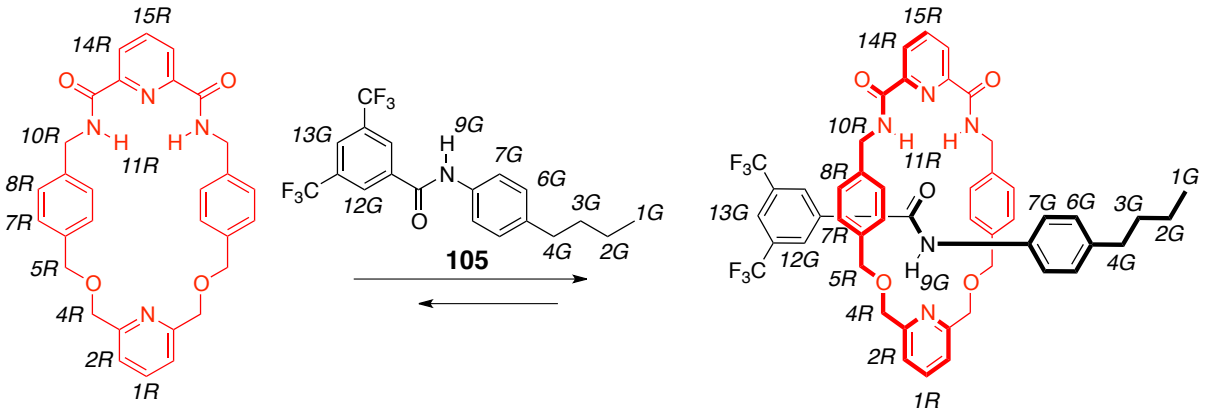

Proton resonances	$\delta_{unbound}$	δ_{bound}	$\Delta\delta$
NH^{11R}	7.98	9.23	+1.25
H^{14R}	8.36	8.51	+0.15
H^{15R}	8.03	8.14	+0.11
H^{7R}	7.31	6.75	–0.56
H^{8R}	7.25	6.67	–0.83
H^{1R}	7.70	7.79	+0.09
H^{12G}	8.30	8.12	–0.18
H^{13G}	8.05	7.76	–0.29
NH^{9G}	7.85	9.35	+1.50

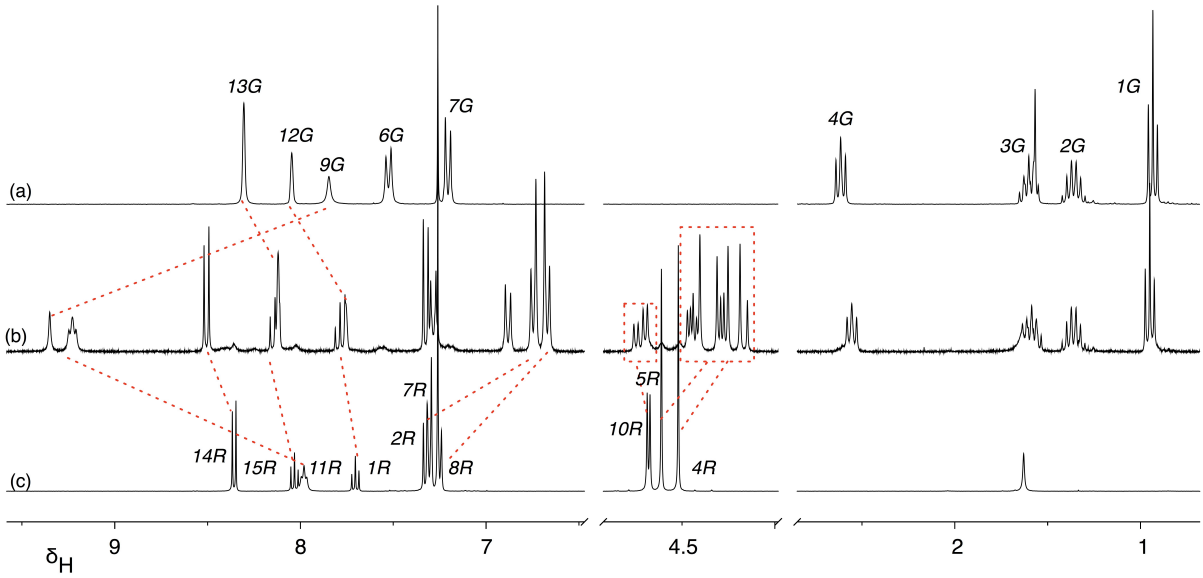

Figure 4.15. Partial ^{1}H NMR (400.1 MHz, 25 ˚C, $CDCl_3$, 20 mM) of (a) model amide **105**, (b) an equimolar mixture of macrocycle **MP** and amide **105** and (c) macrocycle **MP**. Red dashed lines are shown to connect resonances for specific protons in the bound and unbound states. The complex pattern of macrocycle methylene region (H^{10R}, H^{5R} and H^{4R}) are shown in the red dashed boxes. R corresponds to the macrocycle **MP** and G denoted the guest **105**. ($\Delta\delta = \delta_{unbound} - \delta_{bound}$).

In addition, the NH resonances of the guest, NH^{9G} moved (+1.50 ppm) to a higher field of δ_H 9.35 in contrast to δ_H 7.85 in its free state, in which case signify a strong interaction was achieved with the three hydrogen bond acceptors and, hence, suggested that the guest is preferentially located in the correct space in the macrocycle unit. The appearance of the diastereotopic protons of the macrocycle methylene region, namely H^{4R}, H^{5R} and H^{10R} (outlined as red dashed boxes in **Figure 4.16b**) have in fact corroborated these binding events and the association constant, K_a for the [**MP•105**] complex was determined to be 1440 ± 150 M^{-1} in $CDCl_3$ at 25 ˚C.

Likewise, the additional binding experiment was conducted with the model urea **106** compound. The 400.1 MHz ^1H NMR spectrum of an equimolar mixture of macrocycle **MP** and urea **106** in $CDCl_3$ (**Figure 4.17b**) also reveals the slow exchange process taking place with notable chemical shift changes in comparison with the free state of the starting components (**Figure 4.17a** and **Figure 4.17c**). The resulting resonance arising from the NHs macrocycle proton, NH^{11R} was deshielded to δ_H 9.05, which indicated the hydrogen bond contacts to the carbonyl group of urea **106**.

The following chemical shift changes are also noticed in the ^1H NMR spectrum: upfield shifts of macrocycle phenylene protons, H^{7R} and H^{8R}, upfield shift of the aromatic ring of the urea **106** guest, H^{13G} and H^{14G} and that complex pattern of the ring methylene protons, H^{10R}, H^{5R} and H^{4R} are characteristics of the emergence of the pseudorotaxane species in the solution. Accordingly, the strength of the complexation was evaluated using single-point method, giving a K_a value of 1920 ± 200 M^{-1}. On that account, both supplementary binding experiments investigated for macrocycle **MP** gave a comparable high association constant relative to macrocycle, which demonstrated that urea and amide are suitable candidates for macrocycle **MP**. The following table (**Table 4.3**) summarizes the binding experiments carried out at 25 ˚C between macrocycle **MP** and different guests.

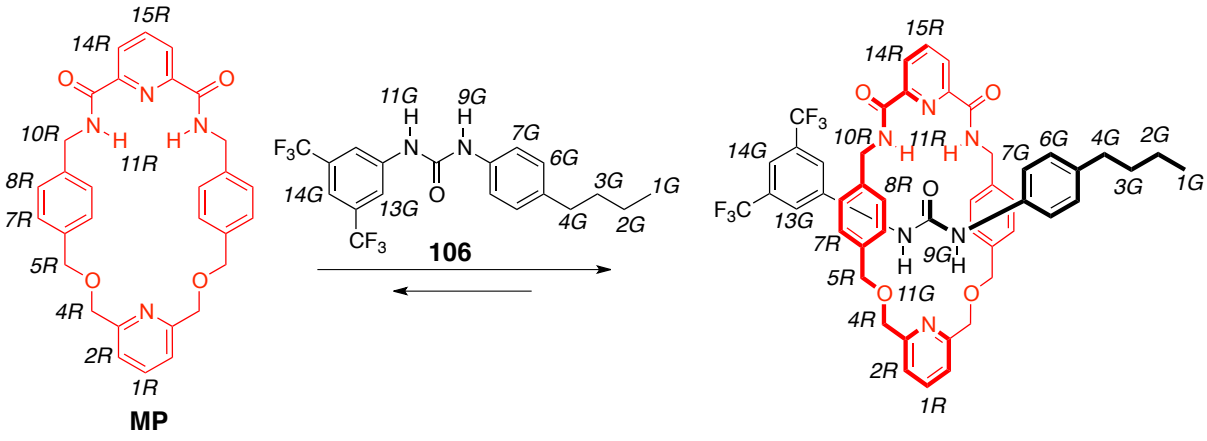

Proton resonances	$\delta_{unbound}$	δ_{bound}	$\Delta\delta$
NH^{11R}	7.98	9.05	+1.07
H^{14R}	8.36	8.48	+0.12
H^{15R}	8.03	8.11	+0.08
H^{1R}	7.70	7.84	+0.14
H^{10R}	4.68	Complex pattern	–
H^{4R}	4.61	Complex pattern	–
H^{5R}	4.52	Complex pattern	–
H^{14G}	7.49	7.34	–0.15

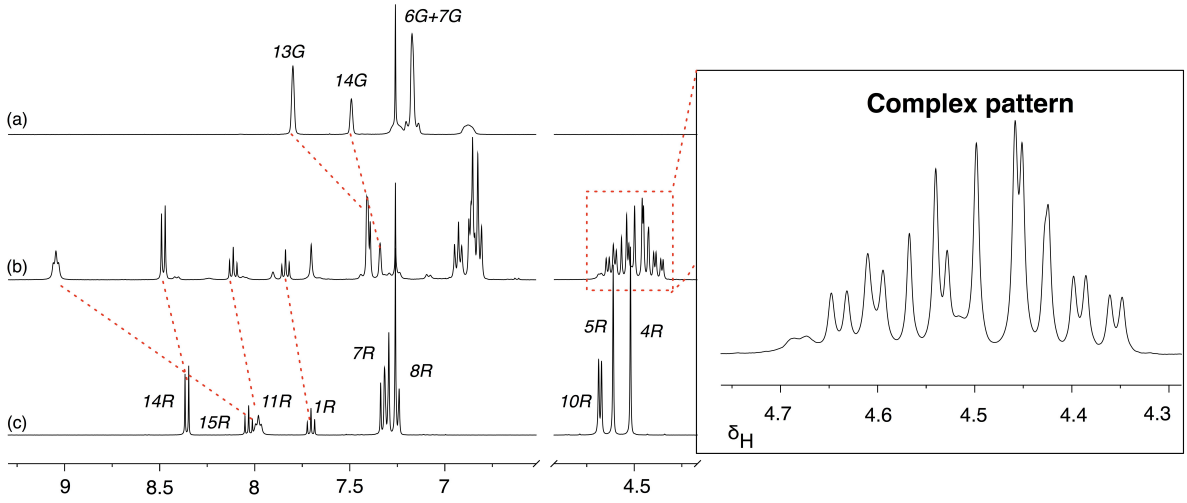

Figure 4.17. Partial ^{1}H NMR (400.1 MHz, 25˚C, $CDCl_3$, 20 mM) of (a) model urea **106**, (b) an equivalent molar mixture of macrocycle **MP** and urea **106** and (c) macrocycle **MP**. Red dashed lines are shown to connect resonances for specific protons in the bound and unbound states. The complex pattern of macrocycle methylene region (H^{10R}, H^{5R} and H^{4R}) are shown in the red dashed boxes. R corresponds to the macrocycle **MP** and G denoted the guest **106**. ($\Delta\delta = \delta_{unbound} - \delta_{bound}$).

Table 4.3. Binding experiments carried out with macrocycle **MP**. The ^{1}H NMR spectrum of the macrocycle **MP** and guest showed complexes either in fast exchange (F), or in slow exchange (S) that can be attributed to significant binding process in comparison to the species observed in isolation. The K_a usually determined by titration (*) technique in the case of fast exchanges. In the case of slow exchanges, the K_a was determined by the single-point method (#) either by ^{1}H NMR resonance or ^{19}F NMR resonances (d_1 = 6 sec). The concentration being used was 20 mM in $CDCl_3$ at room temperature unless otherwise stated.

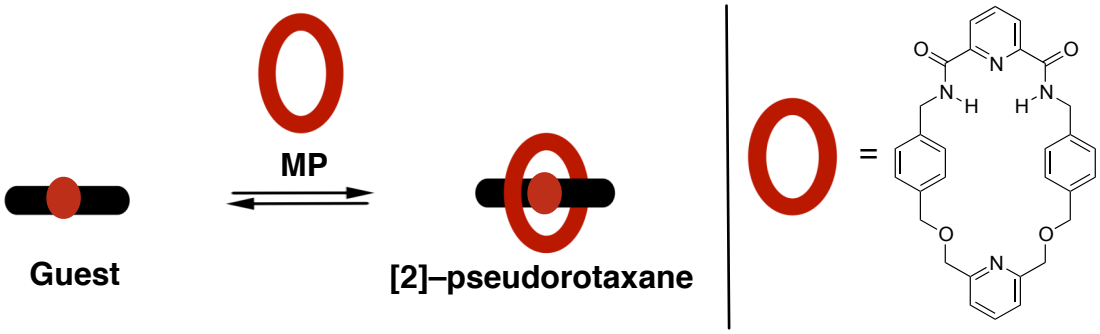

Guest	K_a / M^{-1}	Guest	K_a / M^{-1}
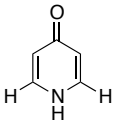 **87**	F	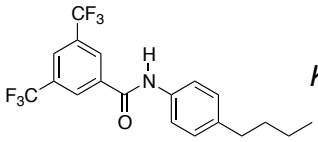 **105**	S # K_a = 1440 ± 150
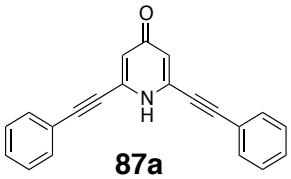 **87a**	S	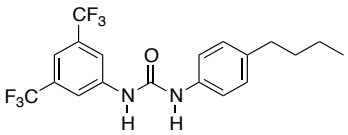 **106**	S # K_a = 1920 ± 200
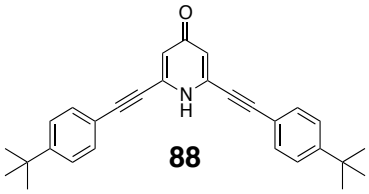 **88**	No binding	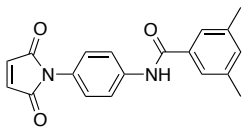 **108**	S # K_a = 280 ± 28
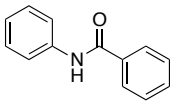 **85**	F * K_a = 210 ± 21	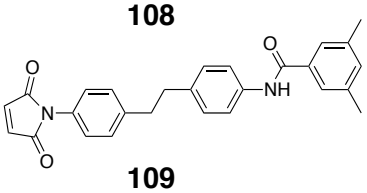 **109**	S # K_a = 170 ± 20
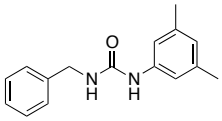 **84**	F* K_a = 260 ± 26	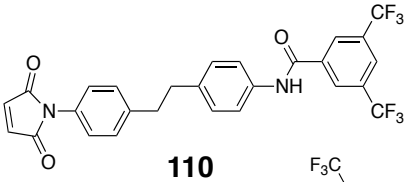 **110**	S # K_a = 4500 ± 450
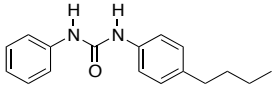 **107**	F	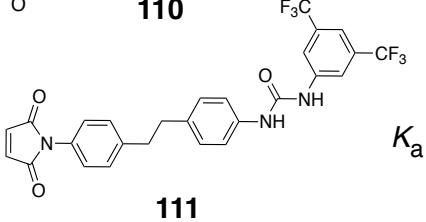 **111**	S # K_a = 1950 ± 200

4.4 Conclusion

The development of a series of macrocycles incorporating the hydrogen bond donors and/or hydrogen bond acceptors motif were reported and these macrocycles have been evaluated as suitable receptor for a variety of guest compounds ranging from pyridone, thiourea, benzoquinone, piperazine, acridone, amide and urea derivatives. In particular, the guests were designed and synthesised based on the mutual interactions with the macrocycle's framework and the binding experiment was described in details. The synthesis and the structure of novel macrocycle **MEU** containing a pyridine ring and cyclic ethylene urea demonstrated a deficient binding performances with both amide and urea compounds. The binding constant, K_a is improved moderately by the complexation with an elongated pyridone guest **88**, in which case demonstrated the dual mode of binding conformation of the macrocycle. The emergence of two pseudorotaxane species that exhibit an exchange event gave a justification that the threading and dethreading processes takes place simultaneously in the reaction mixture, as a consequence of the two preferential orientation of the ring associating the guest compound.

These outcomes shows that a limited interaction occurred during the binding event based on the single X-ray crystal structure of macrocycle **MEU**, which surprisingly crystallise the $CHCl_3$ solvent used to prepare the crystal and another unit of the ring component. Initial effort to increase the association strength between the host and the guest is carried out by optimizing the binding motif in the host framework. Nonetheless, it was found to be synthetically unsuccessful. On that account, we had produced the synthesis of second generati macrocycles to improve the preceding preparations as well as to provide a comprehensive binding investigation with a series of novel guest compounds. The incorporation of an electron-withdrawing substituent such as 3,5-bis(trifluromethyl) group in the amide **105** and urea **106** scaffolds significantly increased the binding strength of both macrocycle **MDG** (K_a was estimated between 900 to 1000 M^{-1}) and macrocycle **MP** (K_a was determined to be between 1400 to 2000 M^{-1}), respectively. Presumably, these guest compounds that integrate such substituent groups crucially assisted this binding process. The rationale behind this phenomenon is addressed through improved designs that exploit optimization using computational approaches, which are discussed in **Chapter 8**.

5

Replication model 1

5.1 Introduction

The initial performance of self-replicating rotaxanes revolves around **Replication model 1** which was simplified to two parallel autocatalytic pathways (**Figure 5.1**).

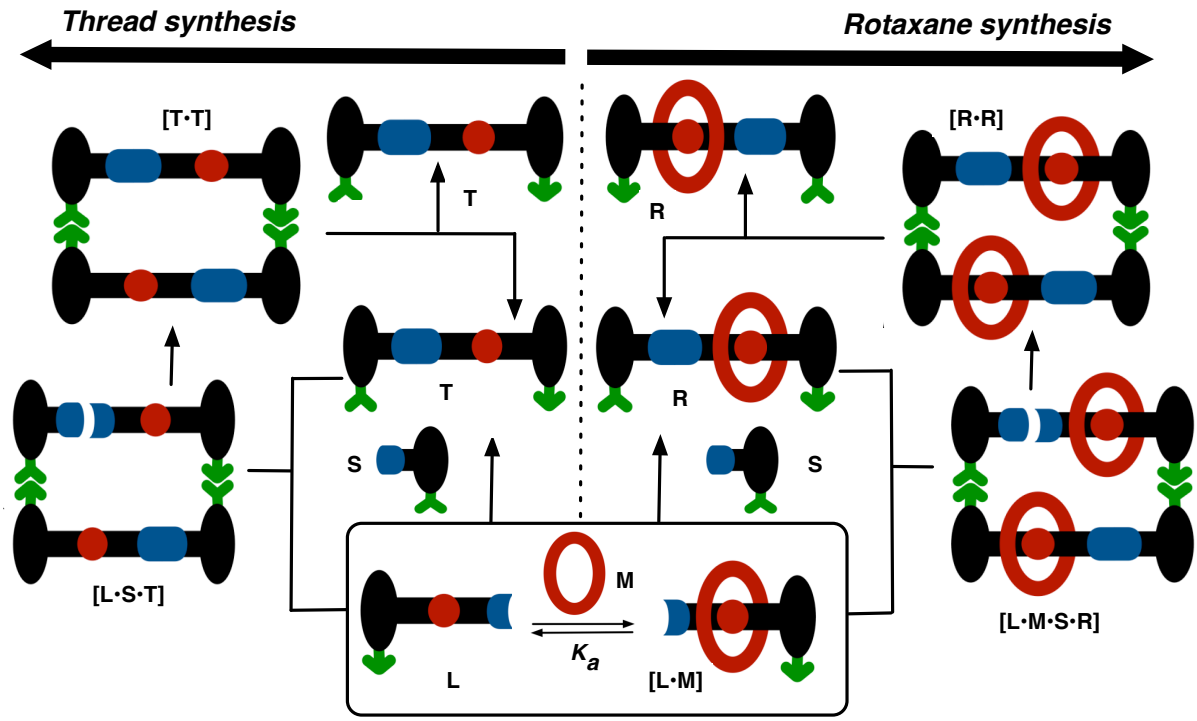

Figure 5.1. **Replication model 1** consists of two autocatalytic cycles, which emanates from the central binding event (boxed), the reversible formation of the [2]-pseudorotaxane [**L•M**] complex. The blue cartoons represent the reactive sites, the green cartoons represent the recognition sites and the red cartoons represent the binding unit.

In the rotaxane synthesis, the association between macrocycle **M** with the linear component **L** first afforded the [**L•M**] species. Reaction between [**L•M**] complex and stoppering reagent **S** gives the rotaxane **R**. [**L•M**] complex and **S** can bind reversibly to the rotaxane **R** to form a catalytically quarternary complex [**S•L•M•R**]. Following this, bond formation occurs between **S** and [**L•M**] to provide duplex [**R•R**], which then

withdraw two molecules of **R** to start a new replicating cycle. On the other hand, unbound linear component **L** react with the stoppering reagent **S** to form thread **T**. Similarly, thread **T** enter the autocatalytic cycle by collecting the unbound species **L** and **S** to catalyse the formation of a second molecule of thread **T**. In this model, the vital role of the association constant, K_a entailed an appropriate comprehension in preparation to implement this model. The reactivity of linear component, **L** and [**L**•**M**] complex to give the thread and rotaxane, respectively are preeminent in this case. On that account, we would like to further illustrate this effect within a set of real systems in conjunction with the kinetic investigation.

5.2 Structural invariances of thread component

It is essential to evaluate the reactivity influenced by thread component (reaction between linear component, **L** and stoppering reagent **S**) composed of 1,3-dipolar cycloaddition between maleimide and nitrone compound. The *trans* to *cis* ratio was determined directly from ^{1}H NMR spectrum as they exhibit markedly different resonances between δ_H 4.0 and δ_H 6.0 region, arising from the isoxazolidine protons (**Figure 5.2**). In the case of *cis* diasteroisomer protons ($H^{1'}$, $H^{2'}$ and $H^{3)'}$ are located on the same face of the fused ring system, which allowed them to couple to each other. The coupling constants are $^3J_{H1',H2'}$ 7.8 Hz and $^3J_{H2',H3'}$ 9.0 Hz.

In contrast, as a result of dihedral angle between H^2 and H^3 in the *trans* diastereoisomer, the coupling constant is close[223] to zero, and therefore H^3 exhibit as an apparent singlet resonance. In addition, the resonance of proton H^2 appears as a doublet, whereas $H^{2'}$ as a doublet of doublets. On the basis of the simple rotaxane formation, the nitrone structure **115** bearing an amidopicoline recognition unit has been selected. Both ends of nitrone **115**, the 4,6-dimethylpyridine and 4-*tert*-butylphenyl ring have exemplified its potential to act as the bulky blocking groups. The four maleimide compounds chosen for the synthesis of simple rotaxane were described in the absence of the carboxylic acid recognition site (**Figure 5.3**).

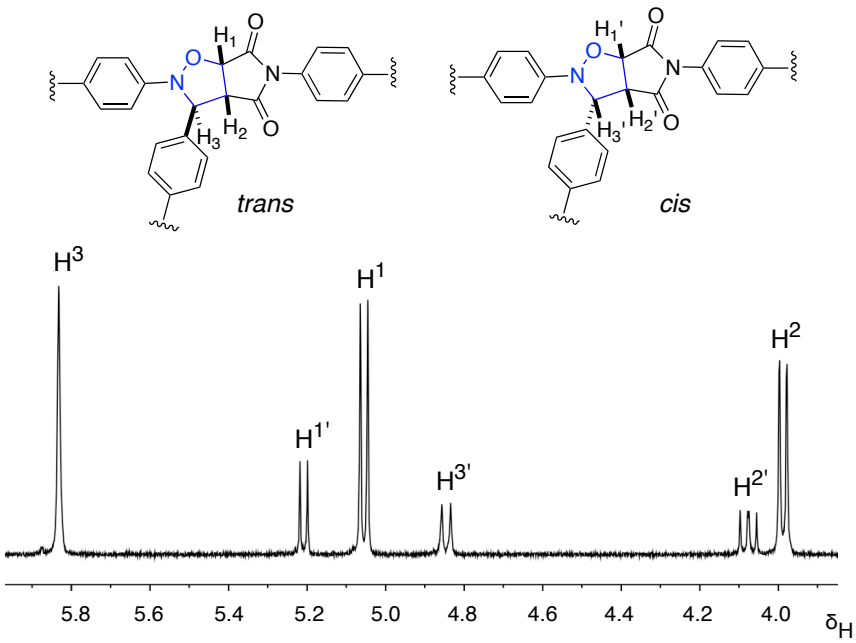

Figure 5.2. Partial ^{1}H NMR spectrum (400.1 MHz, $CDCl_3$, 25 ˚C) resulting from the reaction of nitrone and malemide derivatives. These particular resonances were used to characteristically identify the *trans* (H^1, H^2 and H^3) and *cis* ($H^{1'}$, $H^{2'}$ and $H^{3'}$) diastereoisomer of the reaction.

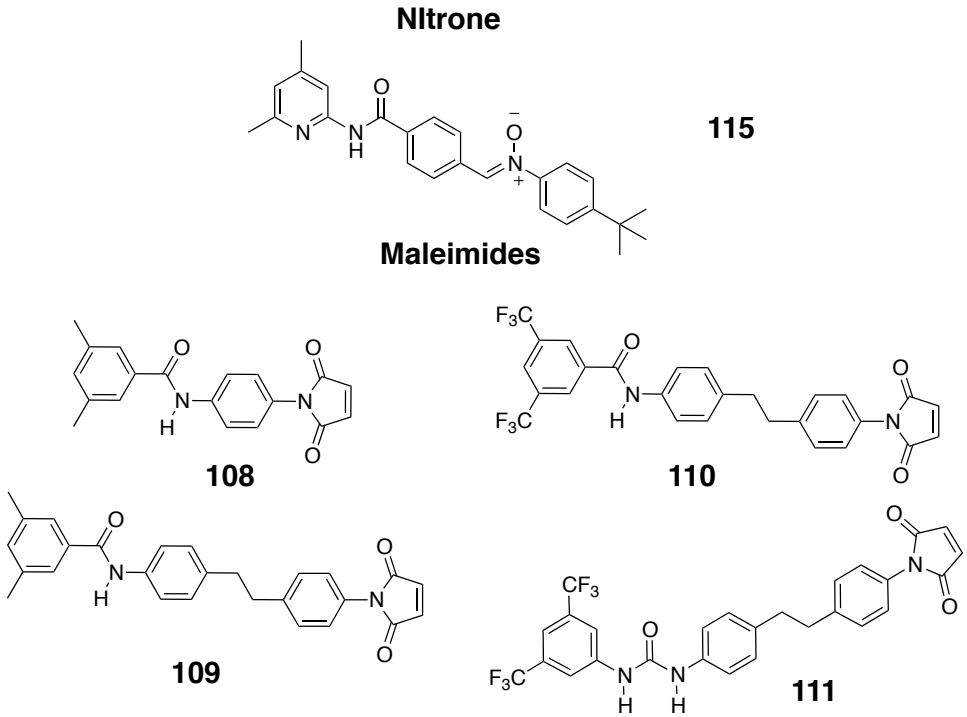

Figure 5.3. Nitrone and maleimide building blocks used in the screening of the structure dependent reactivity of the thread.

The alternative stopper group consists of 3,5-dimethylphenyl and 3,5-bis(trifluoromethyl)phenyl ring was selected. Furthermore, the introduction of fluorine tags into the maleimide compounds allowed a direct and facile observation of the reaction progress. In order to keep the reactive site far enough from the binding

site, the spacer must have a sufficient length. The spacer length was modified by the extension of aromatic ring and methylene groups to assure a certain degree of rigidity in the maleimide structures. The benzene ring (in structure **108**) was replaced with a diphenylethane spacer (in structure **109** – **111**) whereas maleimide **111** bearing the urea functionality has also been envisaged.

5.3 Improving the synthesis of the nitrone 115

The synthetic route of nitrone **115** was revised[224] starting from the formation of acid chloride derivative **116** from the 4-formylbenzoic acid **42** (**Scheme 5.1**). The nucleophilic attack of 2-amino-4,6-dimethylpyridine on aldehyde **116** afforded the amide **117**. In parallel, the resulting hydroxylamine **119** was prepared from commercially available 1-*tert*-butyl-4 nitrobenzene **118** in analogy to the previous conditions[225] in the synthesis of hydroxylamine and was reacted immediately with aldehyde **117** to give nitrone **115** in a good yield.

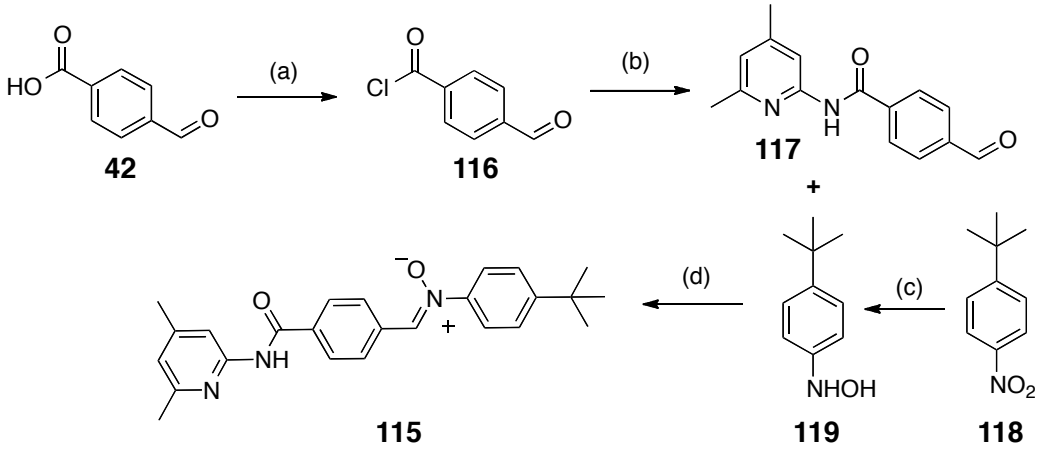

Scheme 5.1. Synthesis of nitrone **115**. Reagents and yields: (a) $SOCl_2$, toluene, 100 °C, 24 h, quant.; (b) 2-amino-4,6-dimethylpyridine, Et_3N, CH_2Cl_2, 0 °C to rt, 48 h, 72%; (c) Rh/C, $NH_2NH_2 \cdot H_2O$, THF, rt, 3 h, followed by (d) EtOH, rt, 3 days, 85% over 2 steps.

5.4 Synthesis of the model maleimides

The first model maleimide **108** that contain 1,4-phenylenediamine spacer was used directly[200] from previous preparation. Subsequently, the preparation of maleimide **109** was amended in four steps (**Scheme 5.2**) starting from 3,5-dimethylbenzoic acid **120**, which was converted to an acid chloride **121**. The activated intermediate **121** was coupled with an excess of 4,4'-ethylenedianiline to yield the amide **122**. The isolation of **122** was carried out by column chromatography from the disubstituted product and the excess of the 4,4'-ethylenedianiline. After treatment with maleic

anhydride in THF, compound **123** was converted to maleimide **109** in the presence of $ZnBr_2$ and HMDS in excellent yield.

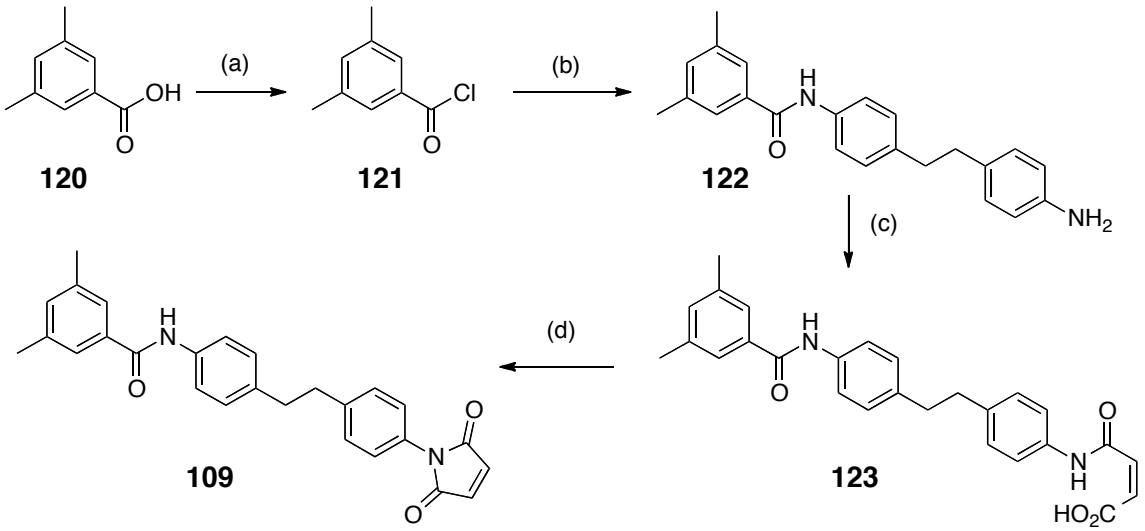

Scheme 5.2. Synthesis of malemide **109**. Reagents and yields: (a) $SOCl_2$, toluene, 80 ˚C, 16 h, quant.; (b) 4,4'-ethylenedianiline, Et_3N, CH_2Cl_2, rt, 16 h, 66%; (c) Maleic anhydride, THF, rt, 3 h, 66%; (d) $ZnBr_2$, HMDS, MeCN, reflux, 2 h, 96%.

Subsequently, maleimide **110** bearing a 3,5-bis(trifuloromethyl)phenyl ring was similarly constructed, starting from commercially-available 3,5-bis(trifluoromethyl) benzoyl chloride **124** as depicted in **Scheme 5.3**.

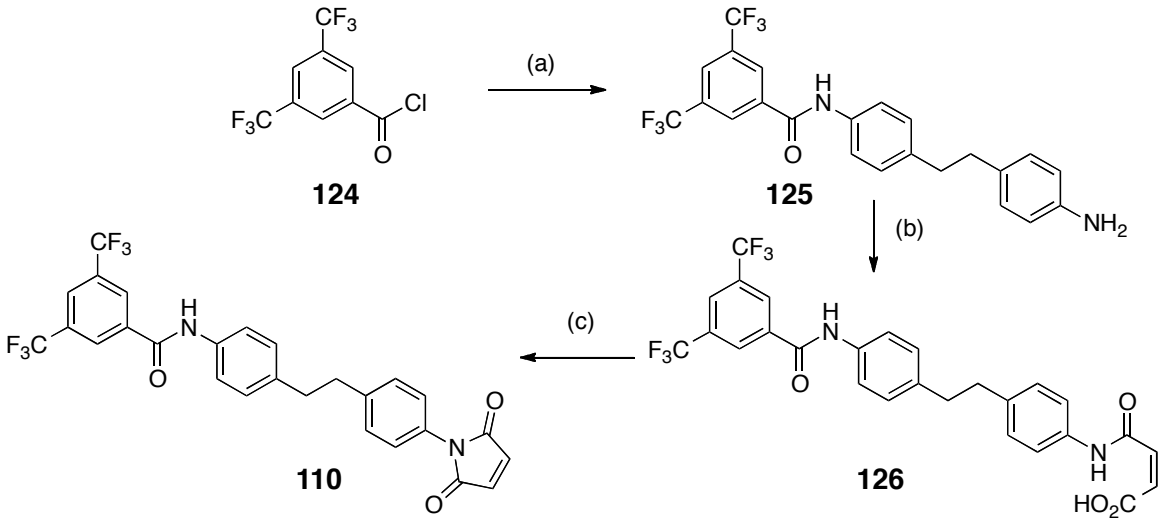

Scheme 5.3. Synthesis of CF_3 malemide **110**. Reagents and yields: (a) 4,4'-ethylenedianiline, Et_3N, CH_2Cl_2, –10 ˚C to rt, 16 h, 52%; (b) Maleic anhydride, THF, rt, 3 h, 98%; (c) $ZnBr_2$, HMDS, MeCN, reflux, 2 h, 44%.

The CF_3 urea maleimide **111** was prepared from 3,5-bis(trifluoromethyl)phenyl isocyanate **127** an converted to amine **128** in the presence of excess 4,4'ethylenedianiline. After treatment of **128** with maleic anhydride in THF, acid **129** compound afforded the maleimide **111** in 78% yield (**Scheme 5.4**). In the following sections, the kinetic analysis for each of the prepared model maleimides with nitrone **115** are discussed in detailed.

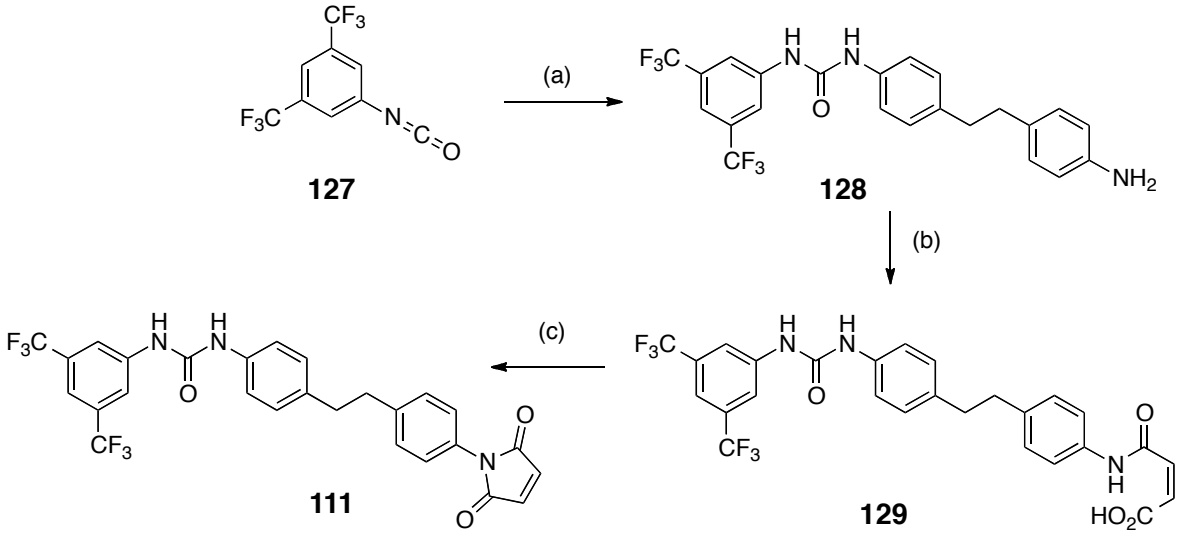

Scheme 5.4. Synthesis of CF_3 urea maleimide **111**. Reagents and yields: (a) 4,4'-ethylenedianiline, Et_3N, CH_2Cl_2, –5 ˚C to rt, 16 h, 63%; (b) Maleic anhydride, THF, rt, 3 h, 98%; (c) $ZnBr_2$, HMDS, MeCN, reflux, 1 h, 78%.

5.5 Kinetic analysis of thread

Satisfyingly, all nitrone and maleimide compounds synthesised were sufficiently soluble in $CDCl_3$, to permit the reactivity study of each pair of nitrone and maleimide by performing the kinetic experiments. Seeing that nitrone **115** is capable of reacting with one of the four maleimides to form a pair of diasteroisomeric products, a total of eight possible cycloadducts were further screened for their reactivities. The reaction between nitrone and maleimide is considered as bimolecular control, in which the recognition-mediated process is not feasible in the absence of complementary carboxylic acid recognition sites. Concentration *vs* time profile was then constructed by deconvolution of the resonances arising from the cycloadducts.

5.5.1 Reaction with short CH_3 maleimide 108

The kinetic analysis of the reaction between nitrone **115** and extra short maleimide **108** give rise to thread **130** was conducted in $CDCl_3$ at 25 ˚C with 20 mM

concentration of starting reagents for 16 hours. The time course of the reaction was recorded by 500 MHz ^{1}H NMR spectroscopic analysis, which monitored the disappearance of the resonance that arise from the maleimide reagent protons present in **108** at δ_H 6.84 and the simultaneous appearance of the resonances that emerge from the *trans* **130** at δ_H 5.85 and *cis* **130** δ_H 5.27. Reaction between nitrone **115** and maleimide **108** leads to 37% overall conversion and give a diasteroisomeric mixture of 2.8:1, in favour of the *trans* diasteroisomer (**Figure 5.4**).

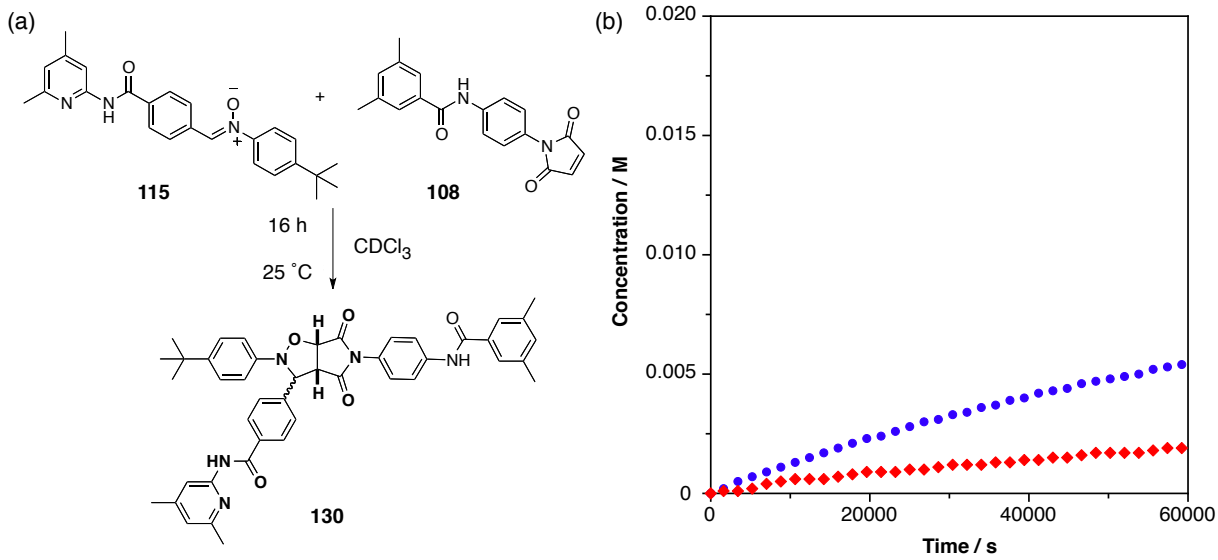

Figure 5.4. (a) 1,3-dipolar cycloaddition between nitrone **115** and maleimide **108** affording *trans* **130** and *cis* **130**; (b) Concentration *vs* time profile for the reaction between nitrone **115** and maleimide **108** with total thread conversion of 37%, affording *trans* **130** and *cis* **130** in 2.8:1 ratio. The formation of *trans* **130** is shown as blue filled circles and the formation of *cis* **130** as red filled diamonds. The reaction was performed at 25 ˚C in $CDCl_3$ at 20 mM reagent concentrations for 16 hours.

5.5.2 Reaction with long CH_3 maleimide 109

Kinetic analysis of the reaction between long maleimide **109** and nitrone was similarly conducted under similar conditions to afford thread **131**. The control experiments between both compounds give rise to the concentration *vs* time profile in **Figure 5.5b**. The situation is fundamentally similar to the one found for the extra short maleimide **108** with the selectivity was found to be 3:1 in favour of *trans* isomer. Overall conversion of the starting material increased nearly to 60%.

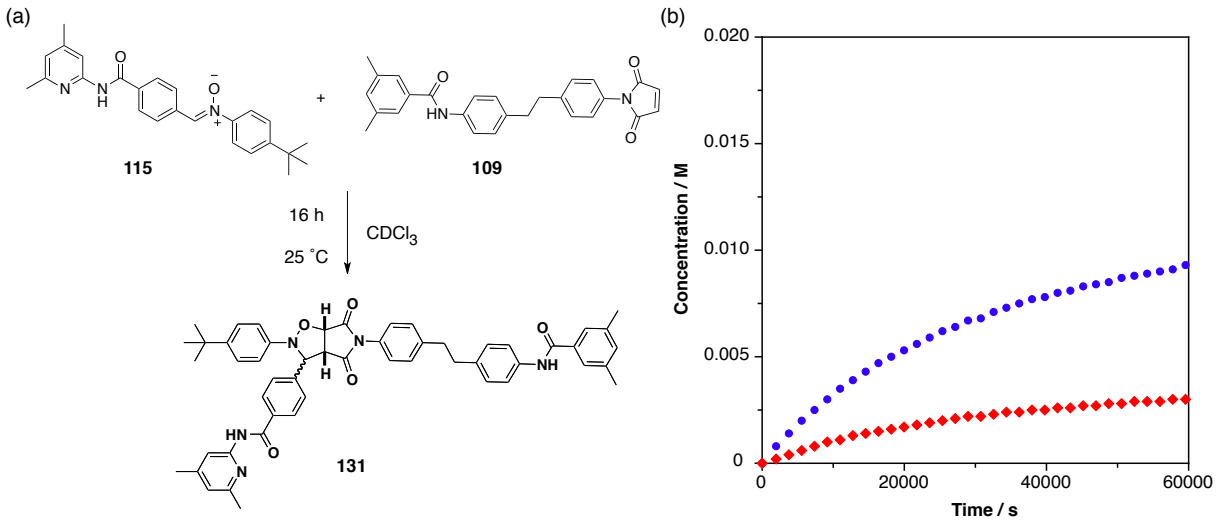

Figure 5.5. (a) 1,3-dipolar cycloaddition between nitrone **115** and maleimide **109** affording both *trans* **131** and *cis* **131**; (b) Concentration *vs* time profile for the reaction between nitrone **115** and maleimide **109** with total thread conversion of 60% affording *trans* **131** and *cis* **131** in 3.1:1 ratio. The formation of *trans* **131** is shown as blue filled circles and the formation of *cis* **131** as red filled diamonds. The reaction was performed at 25 ˚C in $CDCl_3$ at 20 mM reagent concentrations for 16 hours.

5.5.3 Reaction with CF_3 amide maleimide 110

Accordingly, the kinetic data between nitrone **115** and CF_3 maleimide **110** was recorded for 16 hours at 25 ˚C in $CDCl_3$ with 20 mM concentration of the starting materials. Deconvolution of the obtained 500 MHz ^{1}H NMR spectra allowed the construction of the concentration *vs* time profile as depicted in **Figure 5.6b**. The formation of thread **132** proceed with 24% conversion with a ratio of 2.7:1 *trans* isomer over *cis* isomer.

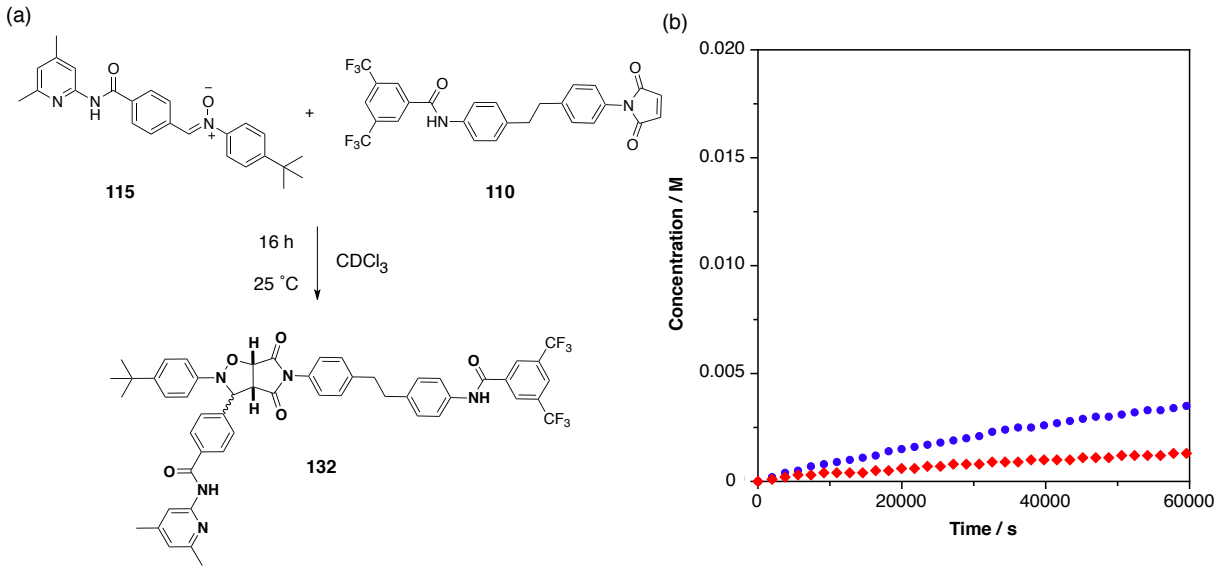

Figure 5.6. (a) 1,3-dipolar cycloaddition between nitrone **115** and maleimide **110** affording *trans* **132** and *cis* **132**; (b) Concentration *vs* time profile for the reaction between nitrone **115** and maleimide **110** with total thread conversion of 24% affording *trans* **132** and *cis* **132** in 2.7:1 ratio. The formation of *trans* **132** is shown as blue filled circles and the formation of *cis* **132** as red filled diamonds. The reaction was performed at 25 ˚C in $CDCl_3$ at 20 mM reagent concentrations for 16 hours.

5.5.4 Reaction with CF_3 urea maleimide 111

The final kinetic experiment to examine is the reaction between CF_3 urea maleimide **111** and nitrone **115** forming cycloadducts **133** (**Figure 5.7**), which was monitored using 500 MHz ^{1}H NMR spectroscopy.

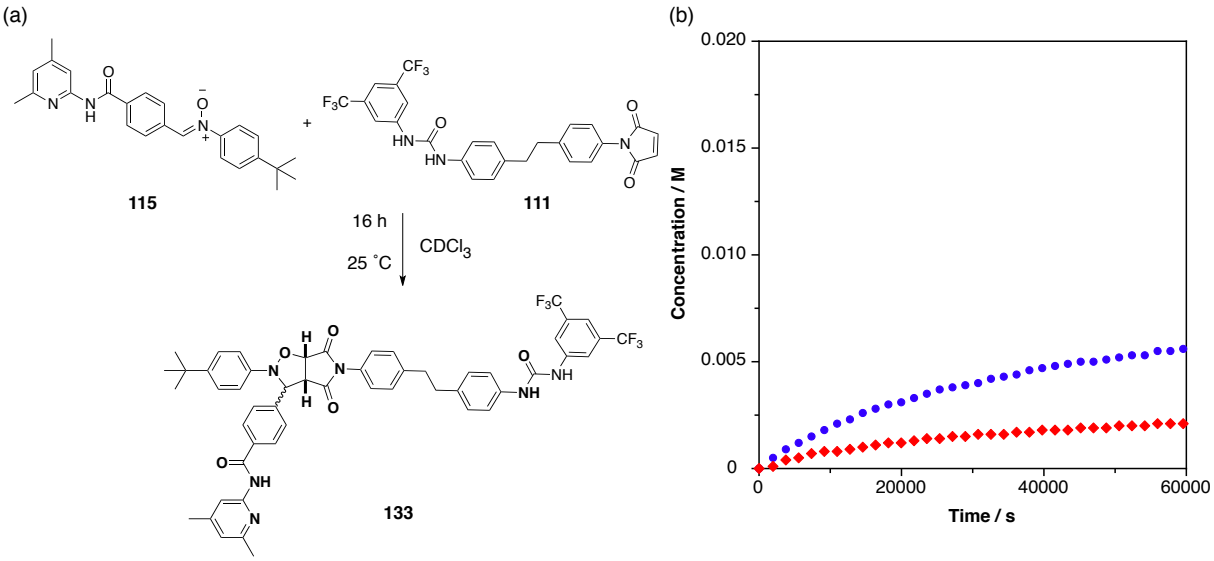

Figure 5.7. (a) 1,3-dipolar cycloaddition between nitrone **115** and maleimide **111** affording *trans* **133** and *cis* **33**; (b) Concentration *vs* time profile for the reaction between nitrone **115** and maleimide **111** with total thread conversion of 39% affording *trans* **133** and *cis* **133** in 2.6:1 ratio. The formation of *trans* **133** is shown as blue filled circles and the formation of *cis* **133** as red filled diamonds. The reaction was performed at 25 ˚C in $CDCl_3$ at 20 mM reagent concentrations for 16 hours.

The bimolecular reaction again give *trans* **133** in a ratio of 2.6:1 over its isomeric partner with 39% overall conversion. As a consequence of the change in spacer length, the overall conversion of the starting materials have significantly affected from 37% in the case of short maleimide **108** to 60% for longer maleimide **109**. However, in the case of CF_3 amide maleimide **110**, the overall conversion (24%) is less pronounced in comparison with CF_3 urea maleimide **111** (39%). It can be seen that the efficiency of the bimolecular reaction are least influenced by the introduction of the fluorine tag.

5.6 Synthesis of the control nitrone

In order to synthesise control nitrone **134** in two steps sequence, compound **118** was similarly reduced to the corresponding hydroxylamine **119** followed by the condensation with 4-*tert*-butylbenzaldehyde to furnish control nitrone **134** in **Scheme 5.5**.

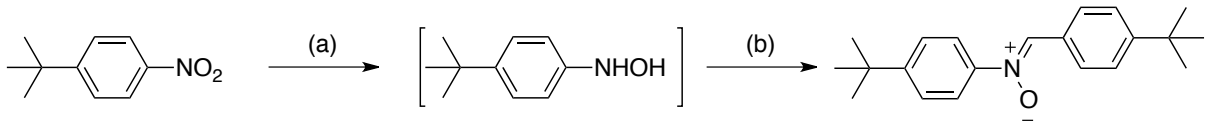

118 **119** **134**

Scheme 5.5. Synthesis of nitrone **134**. Reagents and yields: (a) Rh/C, $NH_2NH_2 \cdot H_2O$, THF, rt, 4 h; (b) 4-*tert*-butylbenzaldehyde, EtOH, rt, 16 h, 44% over 2 steps.

5.7 Kinetic analysis of simple rotaxane formation

We have realised that the ability of the system designed to self-replicate *via* **Replication model 1** is a big disadvantage, as a result of the low reactivity of the [**L•M**] pseudorotaxane. There will be a competition between thread and rotaxane formation, which dependent on the K_a values of [**L•M**] complex. In order to substantiate this fact, a thorough kinetic analysis of the formation of the non-replicating rotaxane was conducted. This investigation will only exploit short CH_3 maleimide **108** and long CH_3 malemide **109** in the presence of both macrocycles **MDG** and **MP**. All four experiments were followed using 500 MHz ^{1}H NMR spectroscopy in $CDCl_3$ for 16 hours at 25 ˚C with 20 mM concentration of the starting materials.

A kinetic model was developed for all plausible interactions between these three building blocks of nitrone, maleimide and macrocycle compounds. The obtained data were fitted using the SimFit program and the bimolecular rate constants were extracted for the formation of the free thread and rotaxane cycloadducts. The association constants between the model maleimide and the selected macrocycle were taken from **Chapter 4**, ranging from 50 M^{-1} to 280 M^{-1}. At least four different products are formed in the reaction mixture with elaborated structure of each potential diastereoisomers of thread and rotaxane component, rendering the spectra complex. The elucidation by ^{1}H NMR spectroscopy is however, not always straightforward. Hence, the total integration for both diastereosiomers of the thread and rotaxane were taken to provide useful information for the kinetic analysis of the system (see **Chapter 10** for details).

The reaction between nitrone **134** and maleimide **108** yielded almost 79% thread **135** in the absence of macrocycle **MDG** (**Figure 5.8a**). Under similar conditions, maleimide **108** and macrocycle **MDG** was pre-equilibrated for 1 hour to allow the formation of [2]-pseudorotaxane complex. The K_a of the [**MDG•108**] complex was determined to be 70 ± 7 M^{-1}. The [**MDG•108**] complex can then react with nitrone **134** to form rotaxane **136**. Alternately, free malemide **108** can react with the same nitrone **115** to form the thread **135**. The total conversion of rotaxane **136** is only 13% yield as a mixture of both *trans* **136** and *cis* **136** together with thread **135** in 60% yield. The thread to rotaxane ratio was calculated to be 4.6:1 in favour of *trans* diastereoisomers. The bimolecular rate contants were extracted from the fitting procedure giving k_{thread} = 3.30 × 10^{-3} M^{-1} s^{-1} and $k_{rotaxane}$ = 6.96 × 10^{-4} M^{-1} s^{-1}, respectively. Thus, the formation of the thread **135** was accelerated by a factor of 4.7 in comparison to the rotaxane **136** (**Figure 5.8b**).

Additionally, 500.1 MHz 2D ROESY NMR experiment was carried out at 295 K (**Figure 5.9**) to provide structural information of the isolated *trans* rotaxane **136**. Inspection of the 2D ROESY NMR spectrum revealed crosspeaks between the macrocycle NH protons NH^{33R} and the thread **135** protons, H^{4T} and H^{9T}. The analysis of the 2D ROESY experiment corroborated the predicted geometry of the rotaxane **136** as illustrated in **Figure 5.9a**.

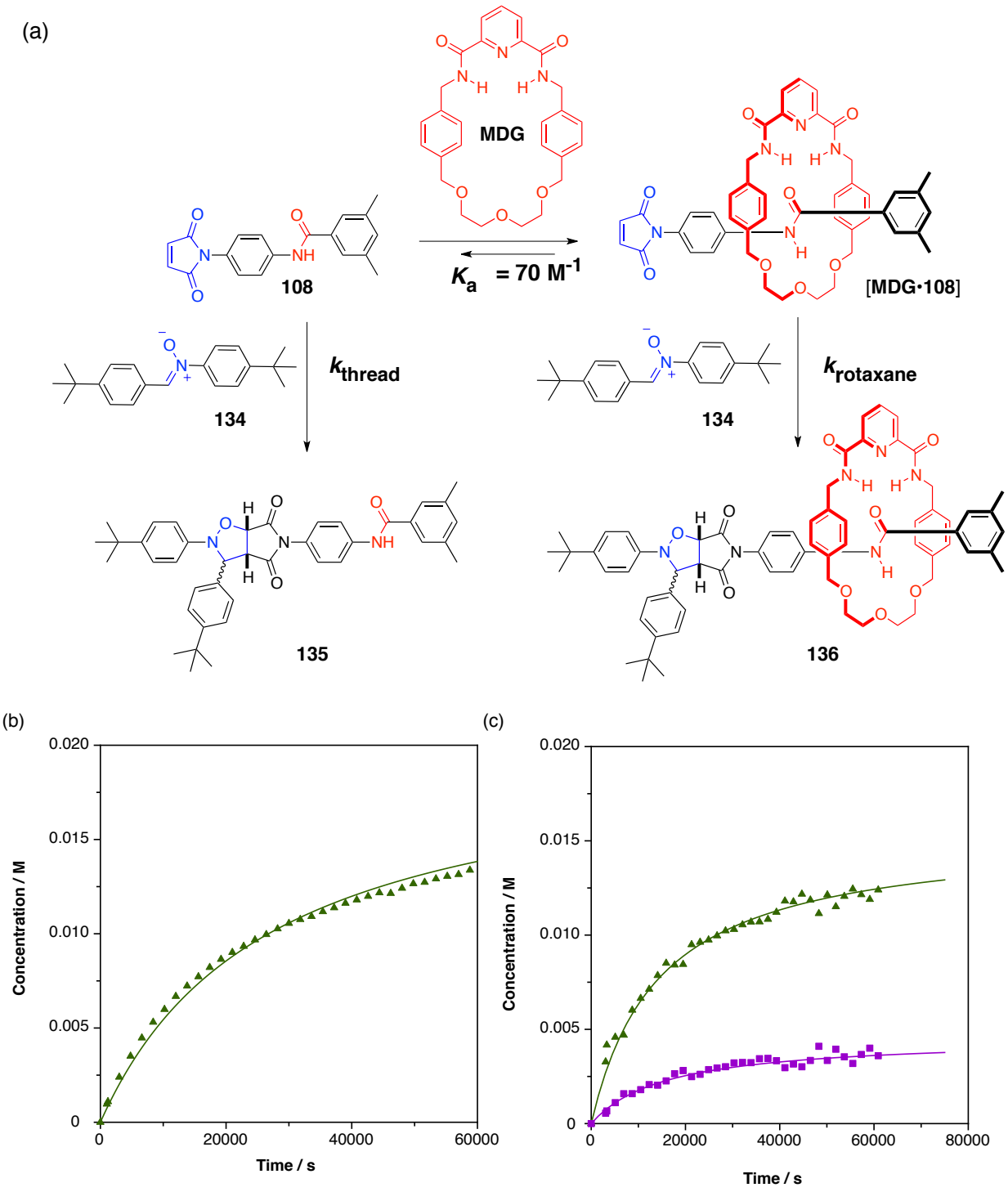

Figure 5.8. (a) The overall reaction scheme between maleimide **108**, macrocycle **MDG** and nitrone **134**. The reaction was performed at 25 ˚C in $CDCl_3$ at 20 mM reagent concentrations for 16 h; (b) Concentration *vs* time profile for the reaction of maleimide **108** and nitrone **134** to give thread **135**. In the absence of macrocycle **MDG**, thread **135** (79%) was isolated. (c) Concentration *vs* time profile for the reaction of maleimide **108**, macrocycle **MDG** and nitrone **134** to give rotaxane **136**. In the presence of **MDG**, thread conversion has drop to 60% alongside the formation of rotaxane of 13% yield. The formation of thread is shown as green filled triangles and the formation of rotaxane is shown as purple filled rectangulars. Solid lines represent the results for the fitting of the thread **135** (green line) and rotaxane **136** (purple line) product.

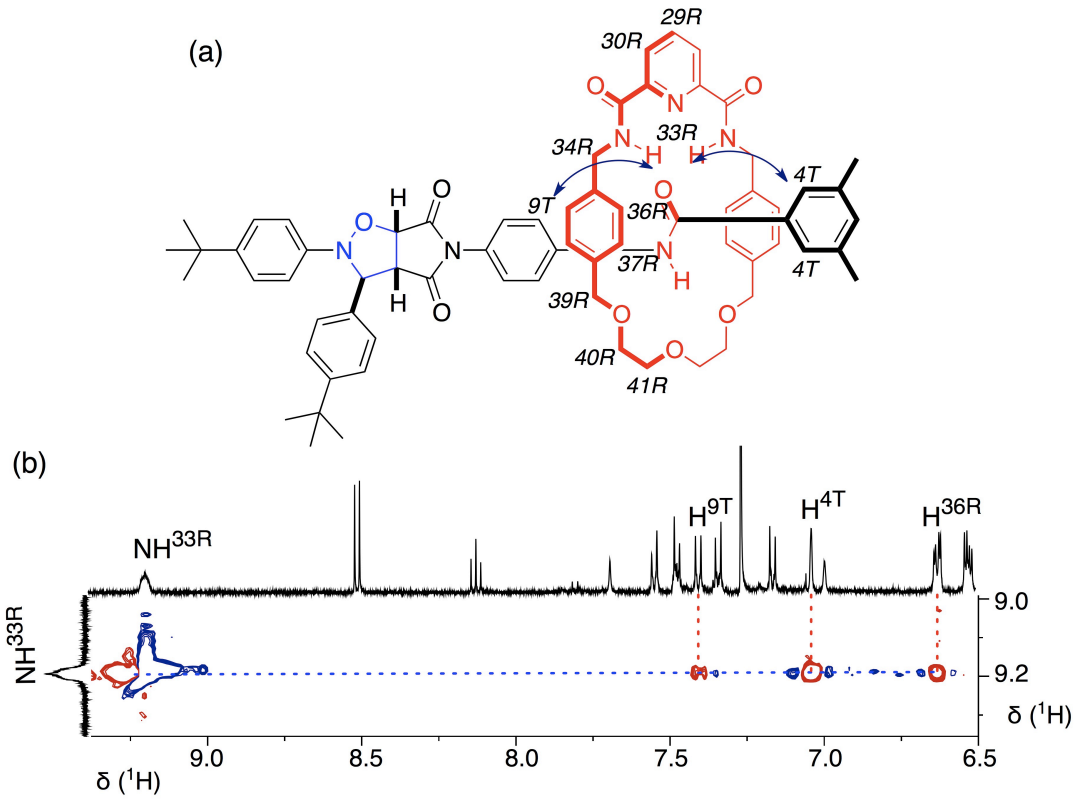

Figure 5.9. (a) ROESY contacts observed for the *trans* rotaxane **136** are shown as blue arrows. (b) Partial 2D ROESY (500.1 MHz, 295 K, $CDCl_3$) spectrum display crosspeaks (red points) between NH^{33R} of the macrocycle **MDG** (R) and H^{4T}, H^{9T} of thread **135** (T).

Accordingly, the macrocycle **MDG** was replaced with macrocycle **MP**. It was demonstrated that macrocycle **MP** can form a pseudorotaxane complex with short maleimide **108** and the K_a was estimated to be 280 ± 28 M^{-1}. The similar time course of the reaction was monitored by 500 MHz ^1H NMR spectroscopy. An equimolar solution of maleimide **108** and macrocycle **MP** in $CDCl_3$ was equilibrated at 25 ˚C for 1 hour, before nitrone **134** was added to the solution. The reaction gave after 16 hours rotaxane **137** in 31% yield and thread **135** in 44% yield as a mixture of its *trans* and *cis* diastereoisomers (**Figure 5.10b**).

However, the ratio of rotaxane to thread was low, due to the substantial amount of thread present over the rotaxane. The obtained data were fitted using the SimFit, to give the rate constants k_{thread} = 4.75 × 10^{-3} M^{-1} s^{-1} and $k_{rotaxane}$ =1.30 × 10^{-3} M^{-1} s^{-1}, respectively. Even though the ratio of rotaxane to thread has improved to 1.6:1 from previous experiment, the rate constant formation of thread **135** continue to be significantly higher than rotaxane **137** in a ratio of 3.7:1.0.

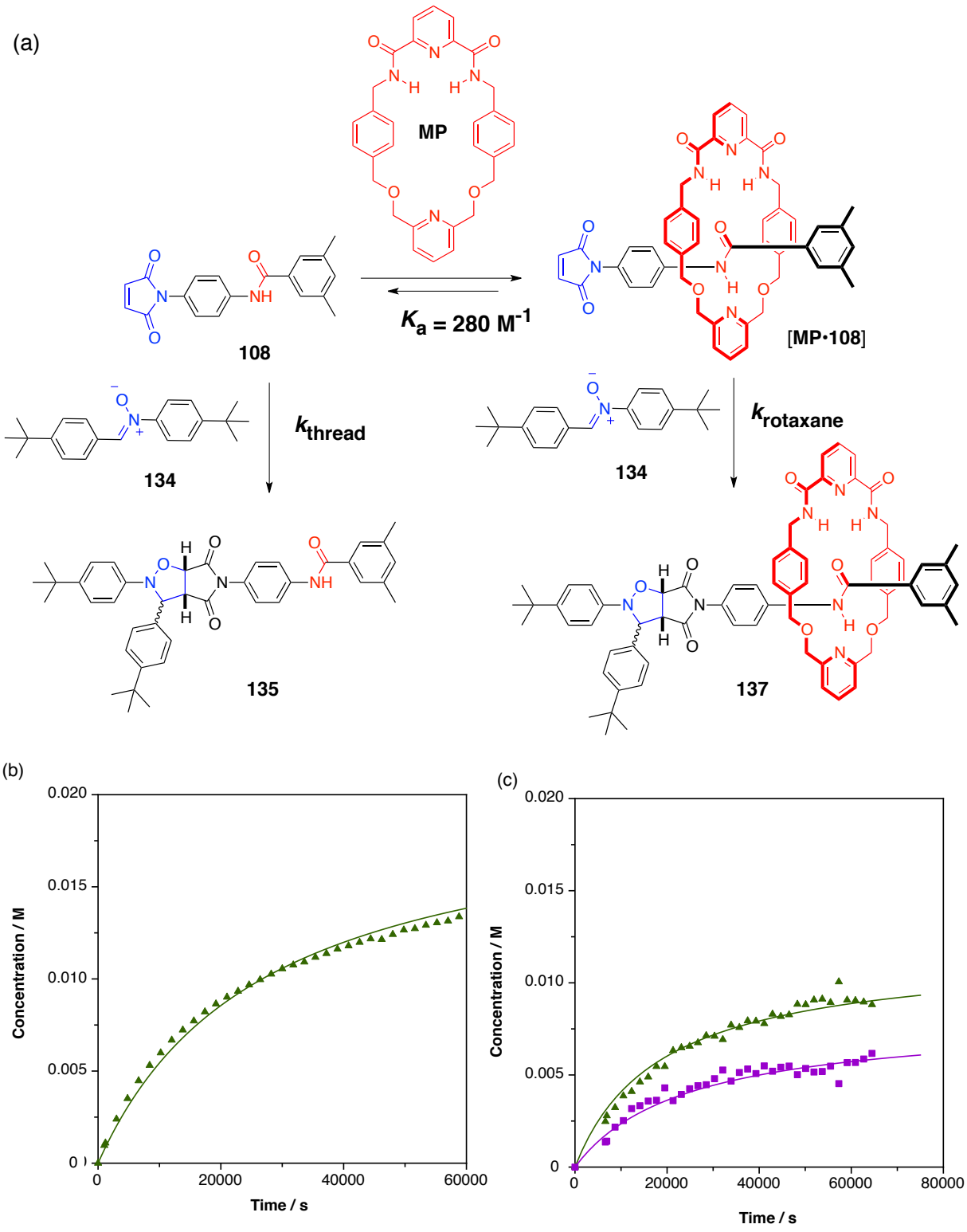

Figure 5.10. (a) The overall reaction scheme between maleimide **108**, macrocycle **MP** and nitrone **134**. The reaction was performed at 25 ˚C in $CDCl_3$ at 20 mM reagent concentration for 16 h; (b) Concentration *vs* time profile for the reaction of maleimide **108** and nitrone **134** to give thread **135**. In the absence of macrocycle **MP**, thread **135** (79%) was isolated. (c) Concentration *vs* time profile for the reaction of maleimide **108**, macrocycle **MP** and nitrone **134** to give rotaxane **137**. In the presence of macrocycle **MP**, thread conversion has drop to 44% with the increase formation of rotaxane in 31% yield. The formation of thread is shown as green filled triangles and the formation of rotaxane is shown as purple filled rectangulars. Solid lines represent the results for the fitting of the thread **135** (green line) and rotaxane **137** (purple line) product.

The 2D ROESY spectrum of *trans* rotaxane **137** displayed crosspeaks between the NH protons of the macrocycle, NH^{33R} with the aromatic proton H^{4T} and H^{9T} of the thread **135**. Additional crosspeaks were also observed between the proton resonance NH of the thread **135**, NH^{7T} and the macrocycle methylene protons, H^{40R}, and thus conformed the encircling of the macrocycle **MP** about the amide moiety of thread **135** (**Figure 5.11**).

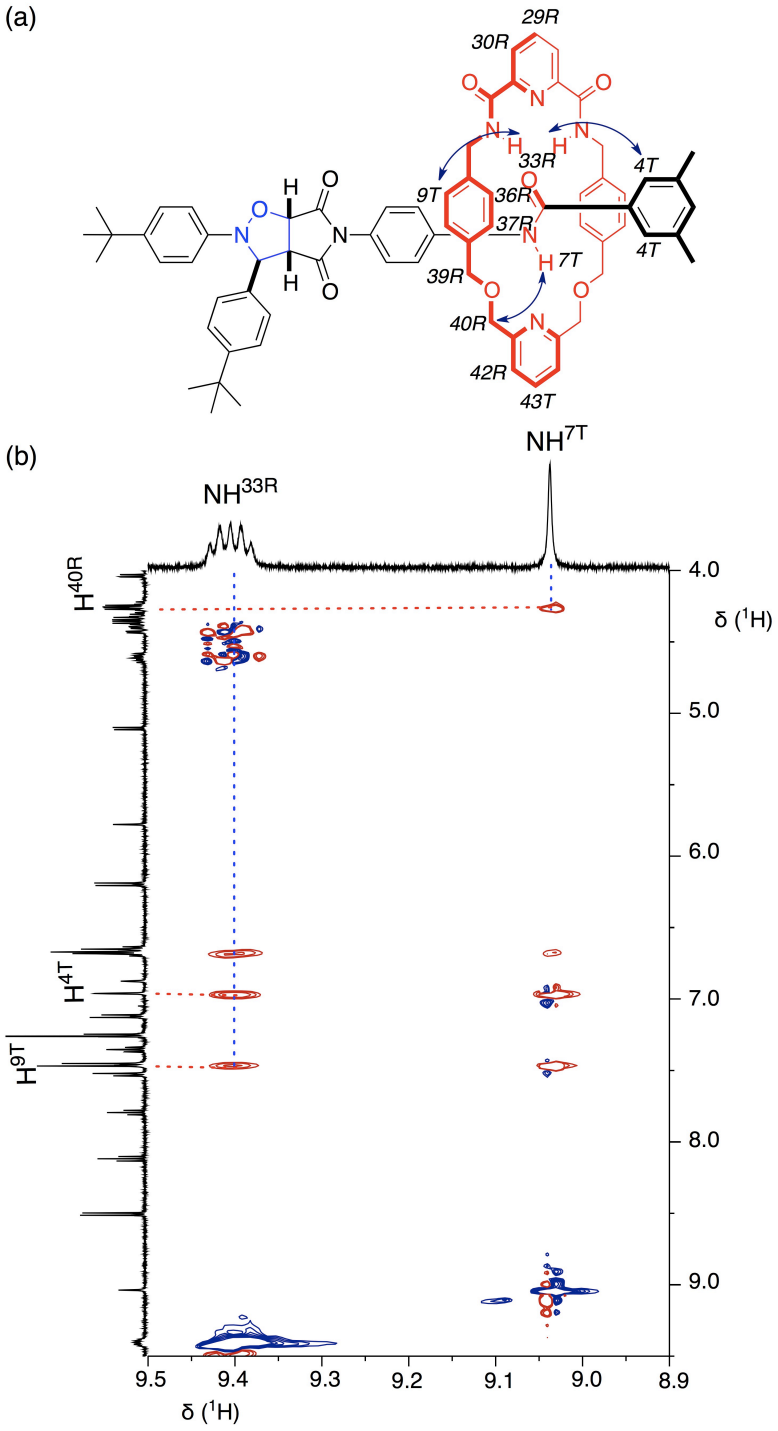

Figure 5.11. (a) ROESY contacts observed for the *trans* rotaxane **137** are shown as blue arrows. (b) Partial 2D ROESY (500.1 MHz, 294 K, $CDCl_3$) spectrum display crosspeaks (red points) between NH^{33R} of the ring (R) and H^{4T}, H^{9T} of thread (T) component. NH^{7T} of thread also display a crosspeak with H^{40R} of the ring.

Subsequently, the longer CH_3 maleimide **109** was reacted with nitrone **134** in the absence of macrocycle **MDG** (**Figure 5.12**). This reaction gave, after 16 hours in $CDCl_3$ at 25 ˚C with starting concentration of the reagents of 20 mM, the thread **138** in 67% yield ($k_{thread} = 4.19 \times 10^{-3}$ M^{-1} s^{-1}).

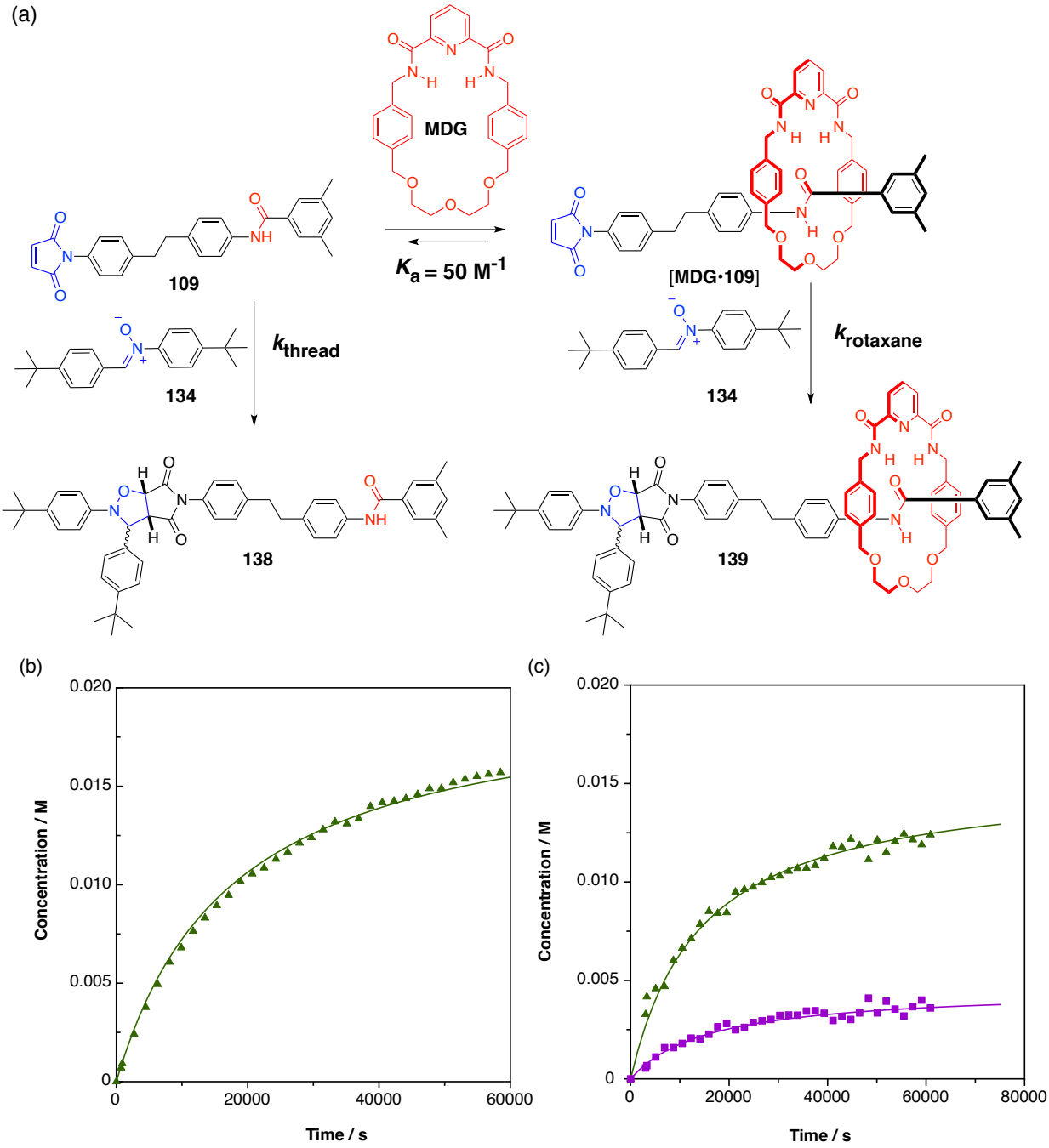

Figure 5.12. (a) The overall reaction scheme between maleimide **109**, **MDG** and nitrone **134**. The reaction was performed at 25 ˚C in $CDCl_3$ at 20 mM reagent concentration for 16 h; (b) Concentration *vs* time profile for the reaction of maleimide **109** and nitrone **134** to give thread **138**. In the absence of **MDG**, thread **138** (67%) was isolated. (c) Concentration *vs* time profile for the reaction of maleimide **138**, macrocycle **MDG** and nitrone **134** to give rotaxane **139**. In the presence of **MDG**, thread conversion has drop to 62% alongside the formation of rotaxane of 18% yield. The formation of thread is shown as green filled triangles and the formation of rotaxane is shown as purple filled rectangulars. Solid lines represent the results for the fitting of the thread **138** (green line) and rotaxane **139** (purple line) product.

Similarly, the reaction between the nitrone **134** and maleimide **109** was performed in the presence of macrocycle **MDG**. A mixture of maleimide **109** and macrocycle **MDG** was pre-equilibrated for 1 hour to allow the formation of [2]-pseudorotaxane [**MDG•109**]. The K_a for [**MDG•109**] complex was determined to be 50 ± 5 M^{-1}. The addition of nitrone **134** furnish the rotaxane **139** in 18% yield as a mixture of its *trans* and *cis* diastereoisomer and thread in 62% yield as a mixture of its *trans* and *cis* diasteroisomer (**Figure 5.12**). The overall conversion is 3.4:1 for thread to rotaxane, decrease from the one found with the extra short maleimide **108.** Furthermore, the bimolecular rate constant of k_{thread} is reduced to 4.42 × 10^{-3} M^{-1} s^{-1} as opposed to $k_{rotaxane}$ 1.89 × 10^{-3} M^{-1} s^{-1}. Nonetheless, the thread was formed 2.3 faster than the rotaxane.

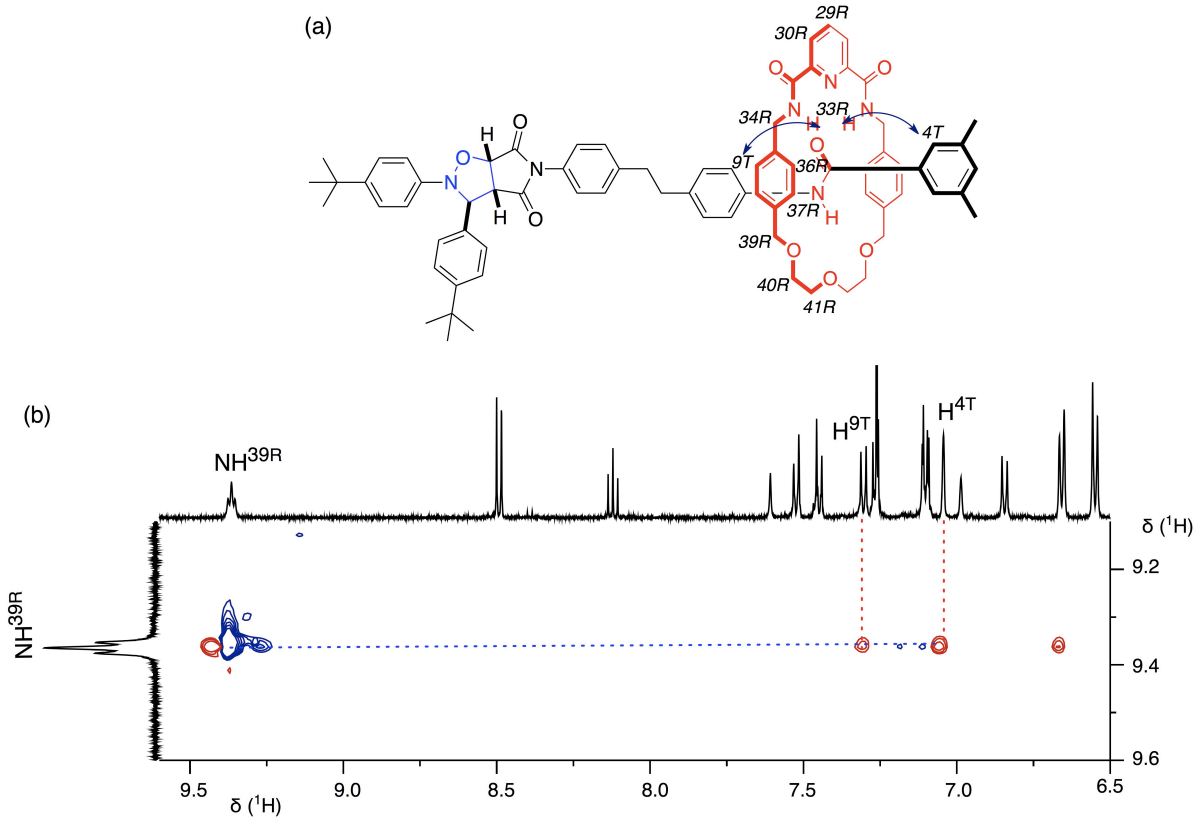

Figure 5.13. (a) ROESY contacts observed for the *trans* rotaxane **139** are shown as blue arrows. (b) Partial 2D ROESY (500.1 MHz, 294 K, $CDCl_3$) spectrum display crosspeaks (red points) between NH^{39R} of the ring (R) and H^{4T}, H^{9T} of thread (T) **138**.

Direct evidence of the proposed structure for *trans* rotaxane **139** was supported from the 2D ROESY NMR spectrum (**Figure 5.13**) in which two crosspeaks were revealed between the ring proton resonances, NH^{39R} with the two aromatic proton resonances, H^{4T} and H^{9T} of the thread components.

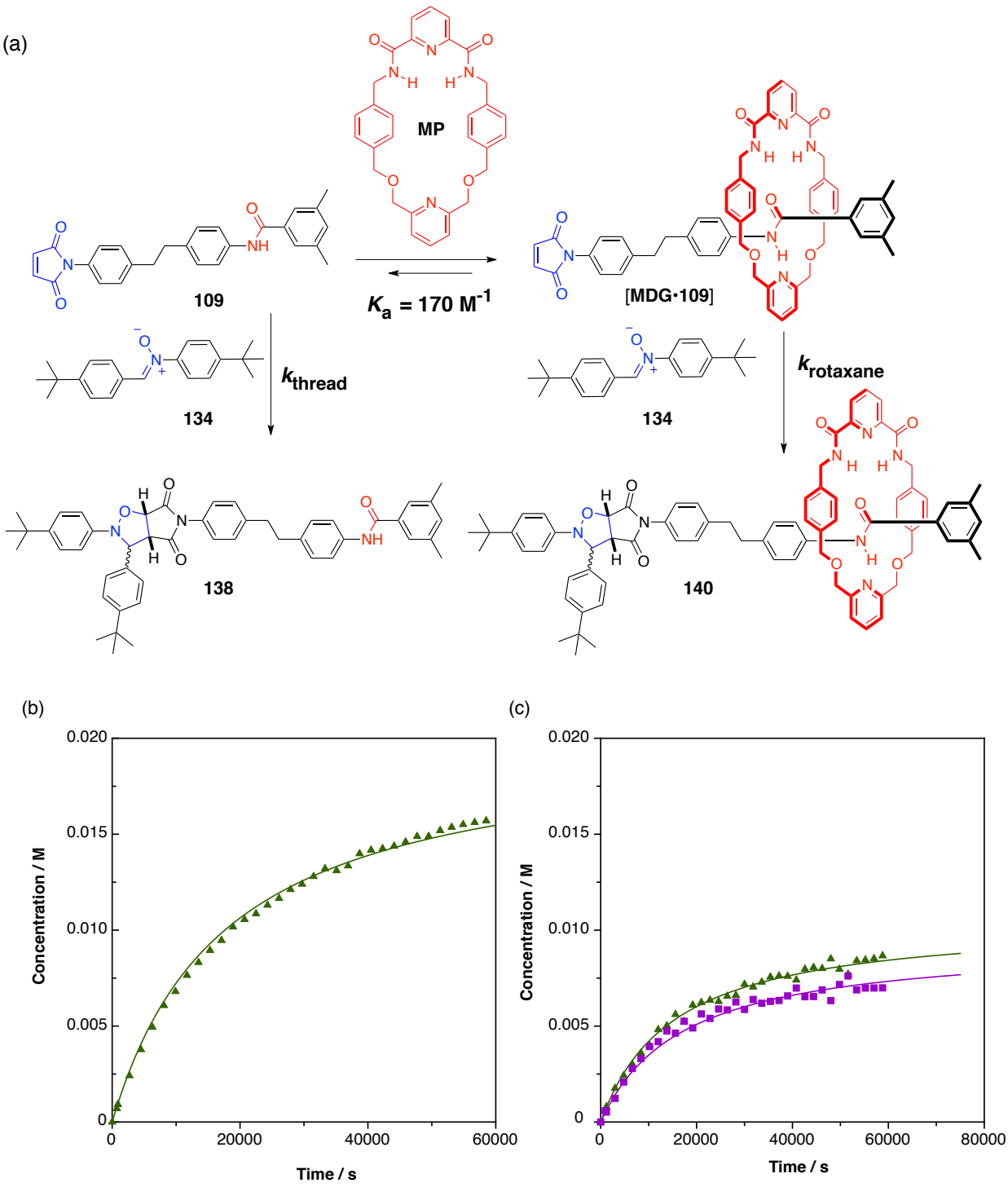

Figure 5.14. (a) The overall reaction scheme between maleimide **109**, **MP** and nitrone **134**. The reaction was performed at 25 ˚C in $CDCl_3$ at 20 mM reagent concentration for 16 h; (b) Concentration *vs* time profile for the reaction of maleimide **109** and nitrone **134** to give thread **138**. In the absence of **MP**, thread **138** (67%) was isolated. (c) Concentration *vs* time profile for the reaction of maleimide **138**, macrocycle **MP** and nitrone **134** to give rotaxane **140**. In the presence of **MP**, thread conversion has drop to 43% with the increase formation of rotaxane in 35% yield. The formation of thread is shown as green filled triangles and the formation of rotaxane is shown as purple filled rectangulars. Solid lines represent the results for the fitting of the thread **138** (green line) and rotaxane **140** (purple line) product.

The final utilization of macrocycle **MP** within the rotaxane framework was conducted subject to prior conditions for the same time course (**Figure 5.14**). The ability of macrocycle **MP** to associate with longer maleimide **109** was assessed and established the K_a value of 170 ± 20 M^{-1}. An equimolar solution of maleimide **109** and macrocycle **MP** in $CDCl_3$ was again pre-equilibrated for 1 hour before the addition of nitrone **134** to the solution. The overall conversion was found to be nearly 80% after 16 hours. In the case of rotaxane **140**, the total yield was about 35% yield for both cycloadducts while the thread **138** diastereosiomers was formed in 43% yield. It is important to note that the comparable yields between thread **138** and rotaxane **140** results from the exploitation of macrocycle **MP** and, therefore encouraging. On that account, the ratio of thread **138** to rotaxane **140** was lessened from 3.4:1 to 1.2:1 when the macrocycle **MP** was employed. Despite that, bimolecular rate constant for the formation of thread **138** (k_{thread} of 4.29 × 10^{-3} M^{-1} s^{-1}) was exhibited to be 1.8 faster than rotaxane **140** ($k_{rotaxane}$ of 2.41 × 10^{-3} M^{-1} s^{-1}).

The conformation of the synthesised *trans* rotaxane **140** was elucidated by 2D ROESY spectrum as shown in **Figure 5.15**. As predicted, the macrocycle **MP** was located around the amide moiety of thread **138**, which is apparent from the two set of crosspeaks in the ROESY spectrum between the NH proton of the ring, NH^{39R} and the thread aromatic protons, H^{4T} and H^{9T} and between the NH proton of the thread, H^{7T} and the methylene proton resonance of the ring, H^{46R}. As detailed above, the interaction between macrocycle **MP** and the thread **138** was through hydrogen bonding and, hence, corroborated the expected geometry shown in **Figure 5.15a**.

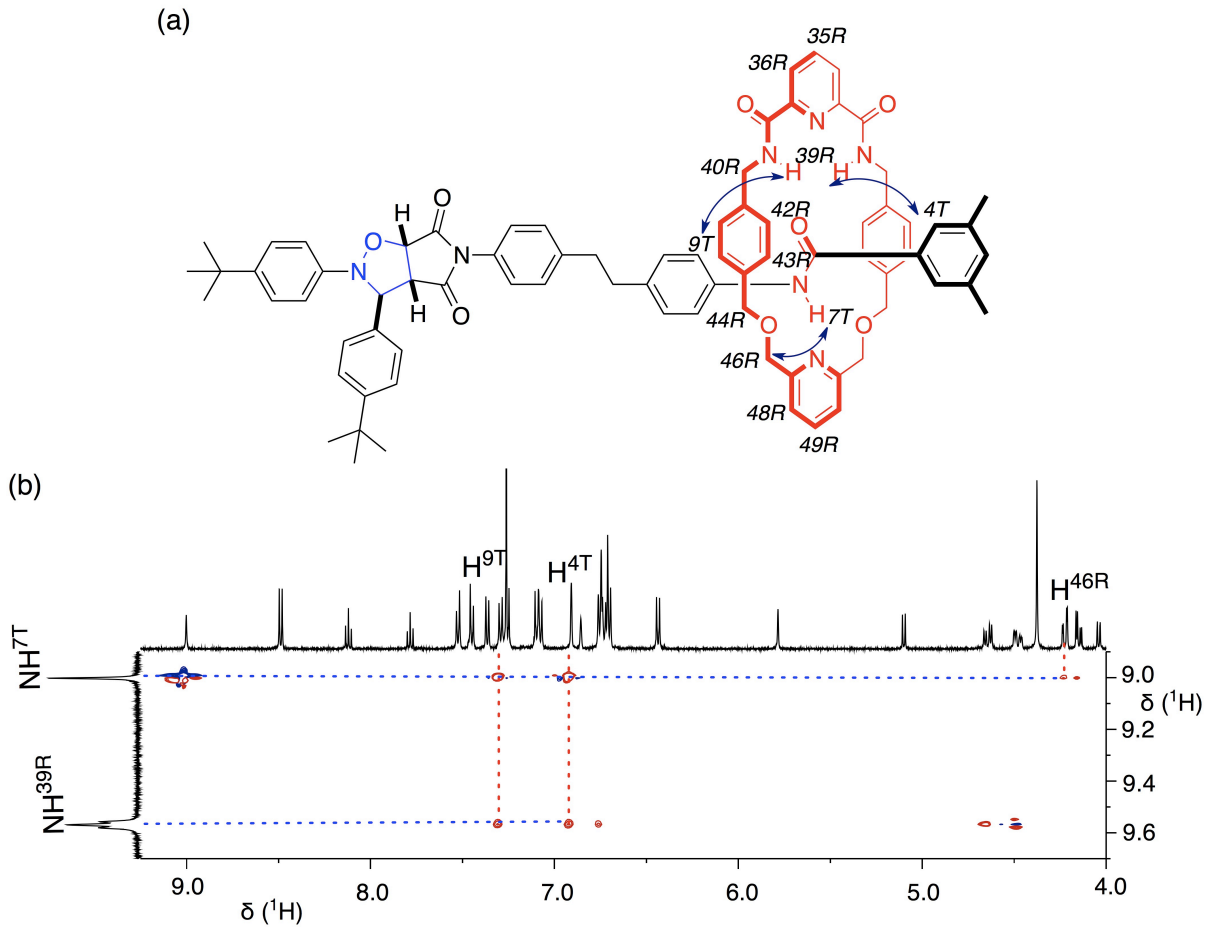

Figure 5.15. (a) ROESY contacts observed for the *trans* rotaxane **140** are shown as blue arrows. (b) Partial 2D ROESY (500.1 MHz, 294 K, $CDCl_3$) spectrum display crosspeaks (red points) between NH^{39R} of the ring (R) and H^{4T}, H^{9T} of thread (T) component. NH^{7T} of thread also display a crosspeak with H^{46R} of macrocycle **MP**.

5.7.1 Comparison of the analysed systems

It is noteworthy that the efficiency of bimolecular reaction increases with the spacer length of the maleimide compounds. For instance, the incorporation of a long spacer maleimide **109** influence the ratio of thread to rotaxane from 4.6:1 to 3.4:1 in the presence of macrocycle **MDG**. Additionally, more significant increase in the rotaxane formation was observed when macrocycle **MP** was involved in the reaction mixture, in which the ratio of rotaxane to thread has been largely improved to nearly 1:1.6 in the case of short maleimide **108** and 1:1.2 for longer maleimide **109**. Thus, the reduced reactivity of thread generated the formation of [2]-pseudorotaxane complex [**MP•108**] and [**MP•109**] more reactive towards the reaction with nitrone **134**.

It is apparent that there are two main obstacles to overcome. Fundamentally, this finding explain the critical role of high association constant, K_a to provide sufficient

amount of pseudorotaxane precursor in the rotaxane synthesis since the formation of this complex predominate the kinetic pathways that include the free maleimides, which eventually results in the formation of undesired thread. Thus, the diminution of free maleimides consequently shifts the central equilibrium to the right hand side, directing the rotaxane formation as presented in the simple kinetic model of rotaxane in **Chapter 3**. As an acceptable level of selectivity for rotaxane being at least 10:1, a K_a value greater than 5000 M^{-1} is desired. We have shown earlier in **Chapter 4** how these binding affinities between the macrocycle and the guest was varied to establish the stability of the pseudorotaxane complex to produce sufficient amount of rotaxanes.

However, the simple kinetic model is relevant only if we asumed that both the rate constants for the thread and rotaxane are the same ($k_{thread} = k_{rotaxane}$). In the current investigations, it is an obvious remark to make that the maleimide and pseudorotaxane complex in all cases did not have the same reactivity towards the stoppering reagent, the nitrone compound. Eventhough we managed to achieve a high association constant for the pseudorotaxane complex, the relative rate constant for rotaxane formation could still come behind and less reactive than the thread formation. As a consequence, the bimolecular reaction of the thread can start to operate much earlier than of the rotaxane. At this stage, it is important to emphasize the important consequence of this central equilibrium. It is evident from this evaluation that the position of the equilibrium between the free maleimide, **L** and macrocycle, **M** and the corresponding pseudorotaxane complex is central to the success of this enterprise.

Since our system is a second order reaction, the implementation of Curtin-Hammett principle is thus inappropriate. The reason is that the product ratio cannot only be determined on the basis of the relative heights of the activation energy barriers between the thread and the rotaxane cycloadducts because the reversible binding event between the free maleimide and the pseudorotaxane complex governs the final product composition. An overall summary of these kinetic observations was presented in **Table 5.1**.

Table 5.1. Overall conversion and bimolecular rate constants for the cycloadducts product of thread and rotaxane obtained from the (a) kinetic experiments of nitrone **134**, short maleimide **108**, macrocycle **MDG** or **MP** and (b) kinetic experiments of nitrone **134**, long maleimide **109**, macrocycle **MDG** or **MP**. These reactions were performed in $CDCl_3$ at 25 ˚C at 20 mM concentration of starting reagents for 16 hours.

(a) Short maleimide **108**

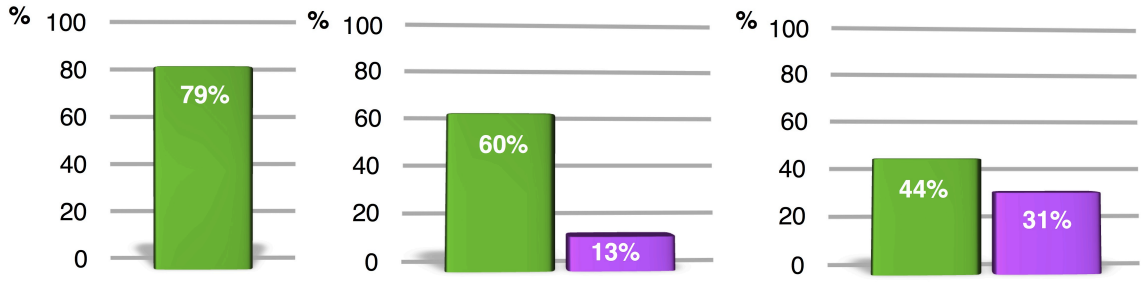

Macrocycle		**MDG**	**MP**
K_a	–	70 ± 7 M^{-1}	280 ± 28 M^{-1}
k_{thread}	3.47 × 10^{-3} M^{-1} s^{-1}	3.30 × 10^{-3} M^{-1} s^{-1}	4.75 × 10^{-3} M^{-1} s^{-1}
$k_{rotaxane}$	–	6.96 × 10^{-4} M^{-1} s^{-1}	1.30 × 10^{-3} M^{-1} s^{-1}

(b) Long maleimide **109**

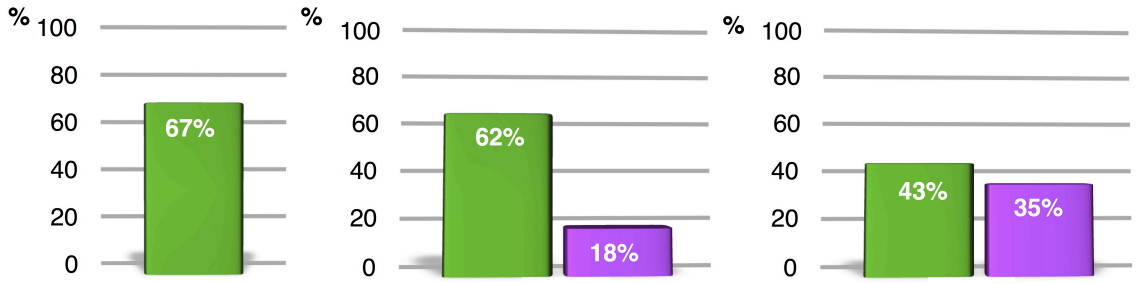

Macrocycle		**MDG**	**MP**
K_a	–	50 ± 5 M^{-1}	170 ± 20 M^{-1}
k_{thread}	4.19 × 10^{-3} M^{-1} s^{-1}	4.42 × 10^{-3} M^{-1} s^{-1}	4.29 × 10^{-3} M^{-1} s^{-1}
$k_{rotaxane}$	–	1.89 × 10^{-4} M^{-1} s^{-1}	2.41 × 10^{-3} M^{-1} s^{-1}

5.8 Kinetic analysis of simple rotaxane formation 2

As explained earlier, the ^{1}H NMR analysis of the previous kinetic experiments is not always straightforward as a consequence of the emergence of four different diastereoisomers with elaborated structures, rendering the spectra fairly crowded. In one occasion, the resonances for *trans* thread and *trans* rotaxane are partly coincide with each other in the first few hours of thse experiments. Additionally, the resonances arising from the *cis* diastereoisomers of thread and rotaxane overlap between each other throughout the experiment. On that account, the thread diastereoisomers were initially synthesised and isolated to simplify each kinetic analysis. The new approach was outlined which integrate the fluorine tags in the preparation of nitrone building blocks and the full kinetic analysis was conducted by monitoring the ^{19}F resonances (see **Chapter 10** for more detail). These resonances were further deconvoluted to construct the concentration *vs* time profile.

5.8.1 Synthesis of the control nitrone 2

1-*tert*-butyl-4-nitrobenzene **118** was converted to hydroxylamine intermediate as seen in **Scheme 5.5**. In order to substitute the *tert*-butyl group in the control nitrone **134**, 3,5-difluorobenzaldehyde and 3,5-bis(trifluoromethyl)benzaldehyde **148** were appropriately selected as the corresponding aldehyde in the condensation reaction to furnish F nitrone **141** and CF_3 nitrone **142** in a moderate yield.

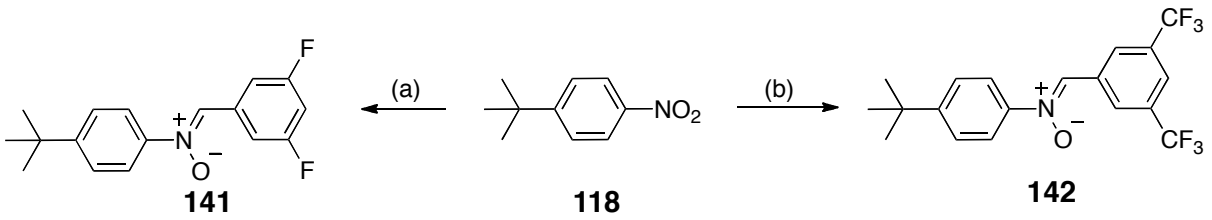

Scheme 5.6. Synthesis of F nitrone **141** and CF_3 nitrone **142**. Reagents and yields: (a) Rh/C, $NH_2NH_2{\bullet}H_2O$, THF, rt, 3 h; followed by 3,5-difluorobenzaldehyde, EtOH, rt, 16 h, 26% over 2 steps; (b) Rh/C, $NH_2NH_2{\bullet}H_2O$, THF, rt, 3 h; followed by 3,5-bis(trifluoromethyl)benzaldehyde **148**, EtOH, rt, 16 h, 49% over 2 steps.

The probability of macrocycle **MDG** to associate the synthesised control nitrone **141** and **142** prompted the investigation of additional binding experiments (**Figure 5.16**). An equimolar solution of macrocycle **MDG** and F nitrone **141** in $CDCl_3$ was prepared and analysed by ^{1}H NMR spectroscopy. The 300.1 MHz ^{1}H NMR spectrum of this mixture (**Figure 5.16d**) display an intermediate exchanges with broad peaks, and thus prevent the determination of K_a. In contrast, the binding study between CF_3

nitrone **142** and macrocycle **MDG** (**Figure 5.16b**) shows that the macrocyclic component does not form a pseudorotaxane with the nitrone guest, as such no noticeable changes on the ^{1}H NMR spectrum of macrocycle **MDG** upon addition of CF_3 nitrone **142**. On that account, CF_3 nitrone **142** was incorporated as alternative control nitrone compound in the second design of simple rotaxane formation.

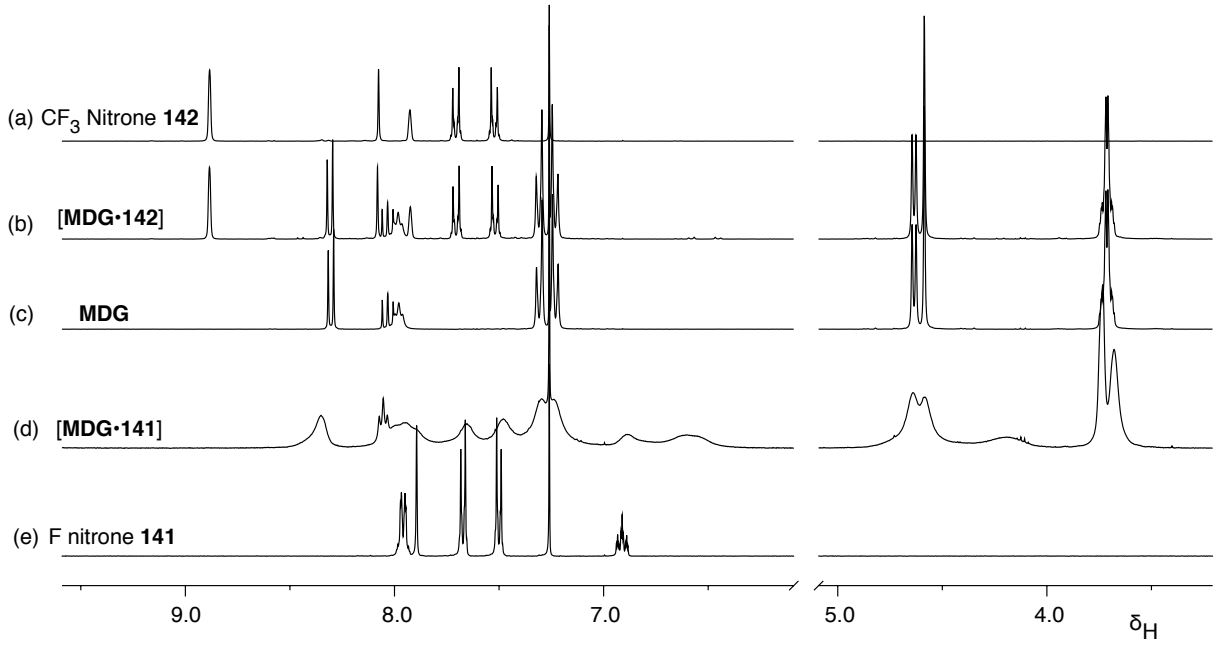

Figure 5.16. Partial ^{1}H NMR spectra (300.1 MHz, 25 ˚C, $CDCl_3$, 20 mM) of (a) CF_3 nitrone **142**; (b) an equimolar mixture of macrocycle **MDG** and CF_3 nitrone **142**,(c) macrocycle **MDG**, (d) an equimolar mixture of macrocycle **MDG** and F nitrone **141** and (e) F nitrone **141**.

The maleimide **108** was reacted with CF_3 nitrone **142** in the absence of macrocycle **MDG**. This reaction was monitored by ^{19}F NMR spectroscopy after 16 hours in $CDCl_3$ at 25 ˚C with starting concentration of 20 mM, give rise to thread **143** in 42% total conversion as a 6.2:1 mixture of its diastereoisomer, in favour of *trans* isomer. The bimolecular rate constant for thread **143** was extracted as 4.87×10^{-4} M^{-1} s^{-1}.

The reaction between maleimide **108** and CF_3 nitrone **142** was subsequently conducted in the presence of the macrocycle **MDG** (**Figure 5.17)**. A mixture of maleimide **108** and macrocycle **MDG** was pre-equilibrated for 1 hour to allow the substantial amount of pseudorotaxane complex [**MDG•108**]. Unfortunately, the addition of CF_3 nitrone **142** furnished rotaxane **144** in only 5% yield and thread **143** in 16% yield as a mixture of both diastereoisomers. The bimolecular rate constants for thread and rotaxane were extracted, giving $k_{thread} = 4.44 \times 10^{-4}$ M^{-1} s^{-1} and $k_{rotaxane} = 2.08 \times 10^{-4}$ M^{-1} s^{-1}, respectively.

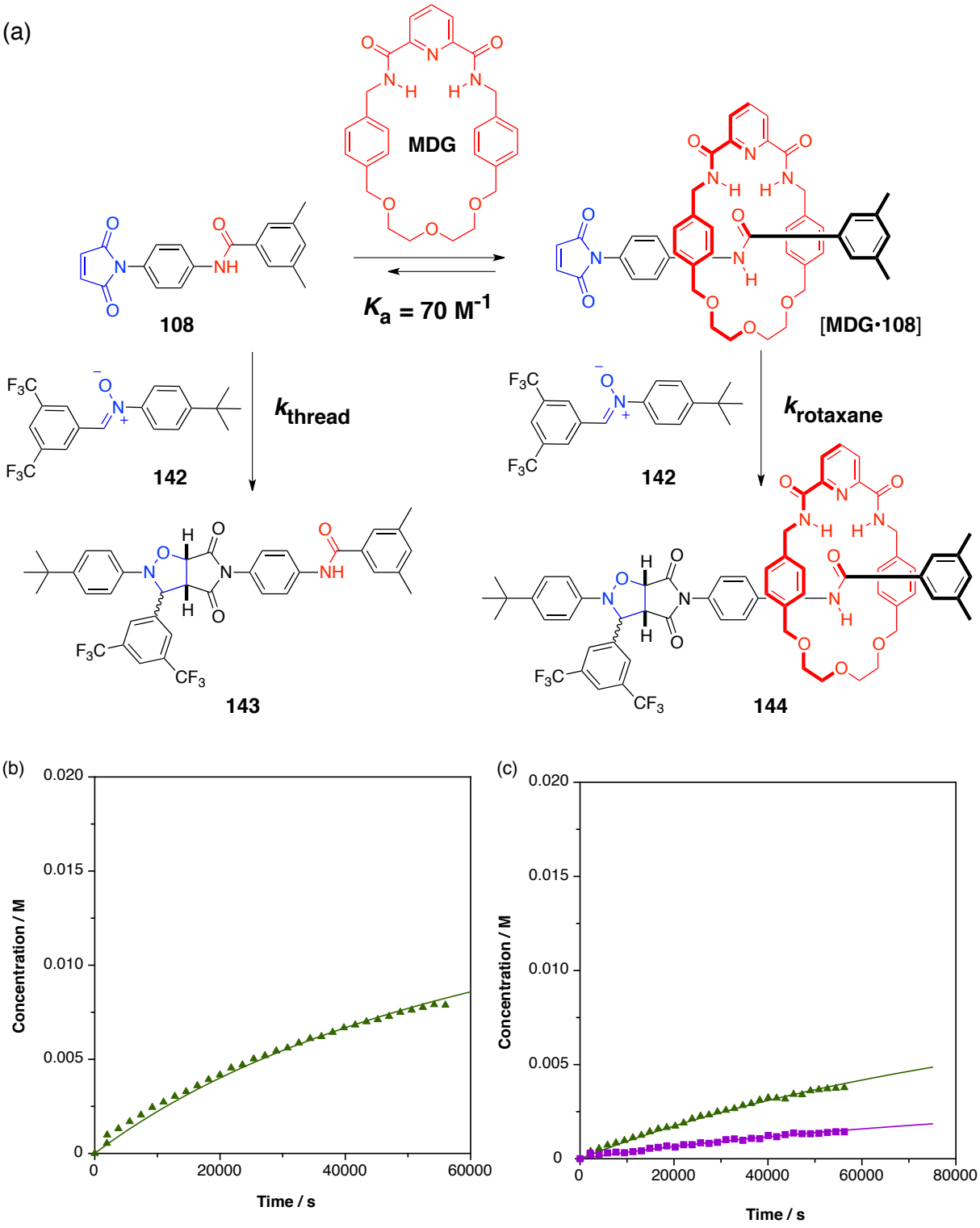

Figure 5.17. (a) The overall reaction scheme between maleimide **108**, macrocycle **MDG** and CF_3 nitrone **142**. The reaction was performed at 25 ˚C in $CDCl_3$ at 20 mM reagent concentration for 16 h; (b) Concentration *vs* time profile for the reaction of maleimide **108** and nitrone **142** to give thread **143**. In the absence of macrocycle **MDG**, thread **143** (42%) was isolated. (c) Concentration *vs* time profile for the reaction of maleimide **108**, macrocycle **MDG** and nitrone **142** to give rotaxane **144**. In the presence of macrocycle **MDG**, thread conversion has drop to 16% alongside the formation of rotaxane of 5% yield. The formation of thread is shown as green filled triangles and the formation of rotaxane is shown as purple filled rectangulars. Solid lines represent the results for the fitting of the thread (green line) and rotaxane (purple line) product.

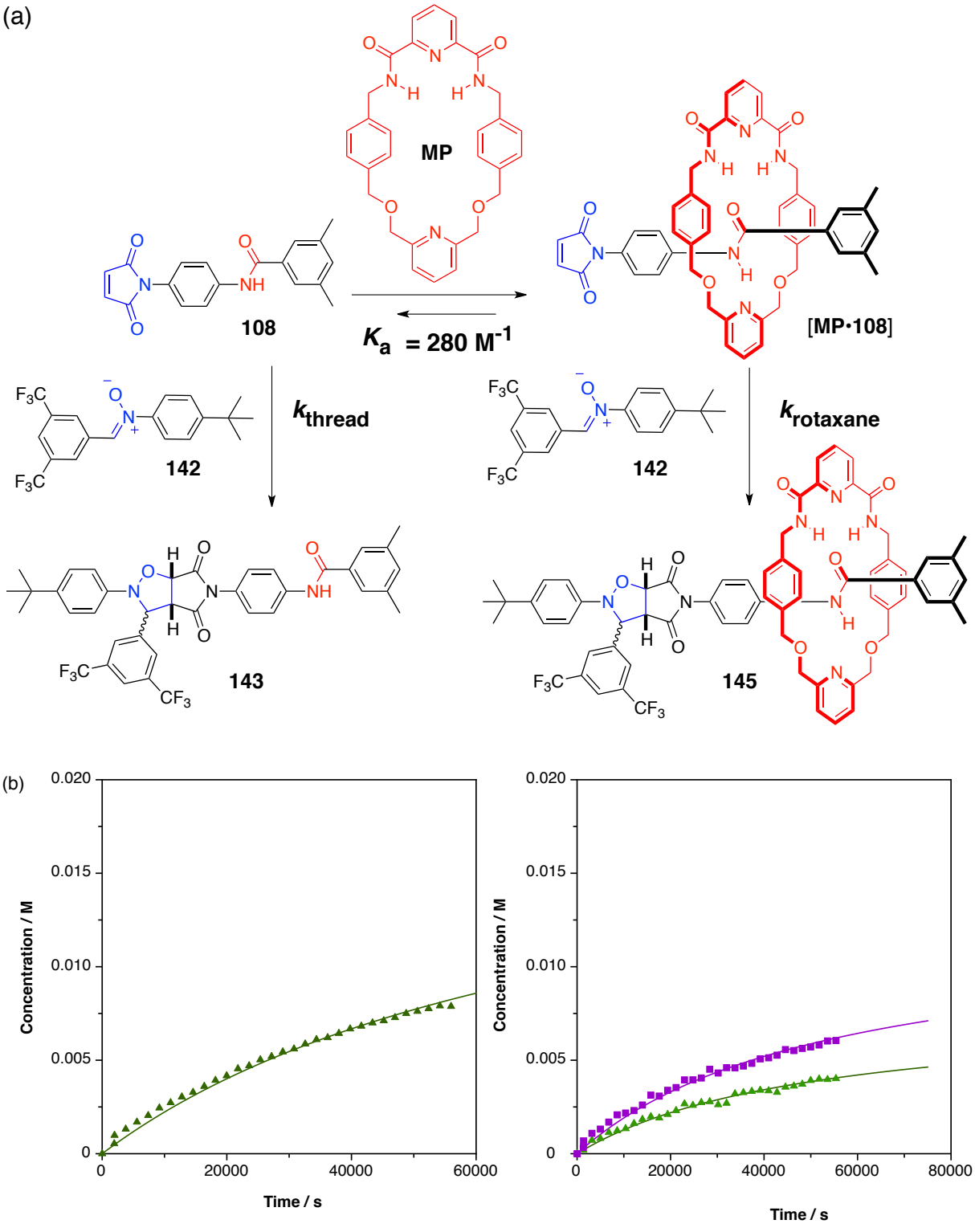

Figure 5.18. (a) The overall reaction scheme between maleimide **108**, macrocycle **MP** and nitrone **142**. The reaction was performed at 25 ˚C in $CDCl_3$ at 20 mM reagent concentrations for 16 h; (b) Concentration *vs* time profile for the reaction of maleimide **108** and nitrone **142** to give thread **143**. In the absence of macrocycle **MP**, thread **142** (42%) was isolated. (c) Concentration *vs* time profile for the reaction of maleimide **108**, macrocycle **MP** and nitrone **142** to give rotaxane **145**. In the presence of **MP**, thread conversion has drop to 20% with the increase formation of rotaxane in 30% yield. The formation of thread is shown as green filled triangles and the formation of rotaxane is shown as purple filled rectangulars. Solid lines represent the results for the fitting of the thread (green line) and rotaxane (purple line) product.

Accordingly, macrocycle **MP** and maleimide **108** was again pre-equilibrated in $CDCl_3$ for one hour to help with the formation of pseudorotaxane [**MP•108**] complex (**Figure 5.18**). The addition of CF_3 nitrone **142** gave, after 16 hours at 25 ˚C, rotaxane **145** in 30% yield and thread **143** in 20% yield as a mixture of *trans* and *cis* cycloadducts. The bimolecular rate constants were extracted and fitted using the SimFit protocol, to give k_{thread} of 1.12×10^{-3} M^{-1} s^{-1} and $k_{rotaxane}$ of 8.66×10^{-4} M^{1} s^{-1}, respectively. Likewise, the ratio of rotaxane to thread has improved compared to the previous system as a consequence of increase binding constant when macrocycle **MP** was employed. This is evident from the comparable rate formation of thread against the rotaxane formation with a ratio 1.3:1. Nevertheless, the overall conversion of the cycloadducts for both systems is not encouraging.

Comparing the concentration *vs* time profile between the rotaxane **136** and **137** from **Figure 5.8** shows that the introduction of the 3,5-bis(trifluoromethyl) substituent in the previous control nitrone compound **134** had an impact towards the outcome of the final cycloadducts. In the presence of macrocycle **MDG**, the fluorine tagged nitrone **142** yield only 5% yield of rotaxane **144** and further improved to 30% yield of rotaxane **145** in the presence of macrocycle **MP**. A brief summary of the two systems are presented in **Table 5.2**.

Table 5.2. Overall conversion and bimolecular rate constants for the thread and rotaxane obtained from the kinetic experiments of CF_3 nitrone **142**, short maleimide **108** in the presence of macrocycle **MDG** or macrocycle **MP**. The reactions were carried out in $CDCl_3$ at 25 ˚C with 20 mM concentration of starting reagents for 16 hours.

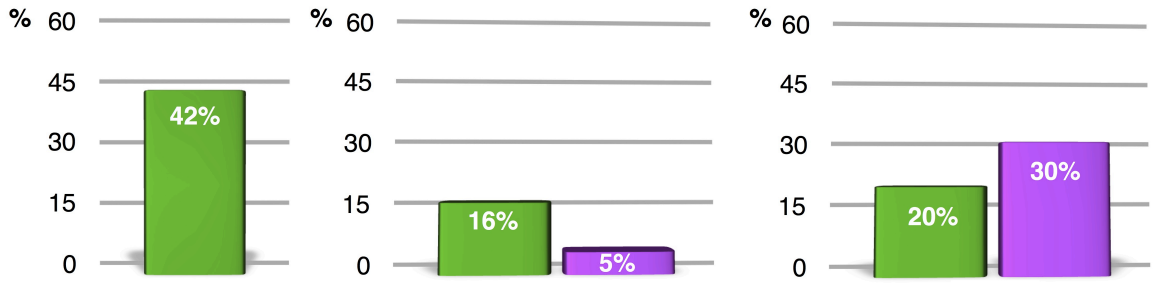

Macrocycle		MDG	MP
K_a	–	70 ± 7 M^{-1}	280 ± 28 M^{-1}
k_{thread}	4.87×10^{-4} M^{-1} s^{-1}	4.44×10^{-4} M^{-1} s^{-1}	1.12×10^{-3} M^{-1} s^{-1}
$k_{rotaxane}$	–	2.08×10^{-4} M^{-1} s^{-1}	8.66×10^{-4} M^{-1} s^{-1}

5.9 Computational study

In order to gain a comprehensive understanding on the reduced reactivity of the CF_3 nitrone **142**, the semi-empirical electronic structure calculations were employed to locate the transition state for the dipolar cycloaddition reaction in our systems. The transition state for a number of scenarios were located using a grid scanning method. The C–C and C–O bonds in the cycloadduct were gradually lengthened, in steps of 0.08 Å, and the RM1 energy computed at each point on the grid. These calculations allowed us to construct a contour plot (see **Figure 5.19**) for the transformation of nitrone and maleimide into the cycloadduct. The approximate location of the transition state determined in these grid calculations was then used as the basis for a further RM1 calculation[226] of the exact transition state structure. We have demonstrated previously that the RM1 semi-empirical method affords transition state structures in close agreement with higher level DFT calculations (for example, M06-2X or B3LYP) and are much more practical in terms of computation time given the large size of the structures under investigation here.

The reaction between the control nitrone **134** and short maleimide **108** was first computed using RM1 in the absence and the presence of macrocycle **MDG**. One of the feasible calculated transition state structure is illustrated in **Figure 5.19a** and **Figure 5.19c** for bis-*tert*-butyl thread and bis-*tert-butyl* rotaxane, respectively. It is visible from the calculated structure that the association of the macrocycle **MDG** to the amide binding site in maleimide compound exerted a remote steric effect on the transition state. The *tert*-butyl group of the nitrone is located close to the diethylene glycol region of the ring, issuing a pronounced van der Waals contacts. As a consequence, the transition state in the reaction between pseudorotaxane [**MDG•108**] and control nitrone **134** are certainly destabilized in comparison to the transition state obtained in the absence of macrocycle **MDG**.

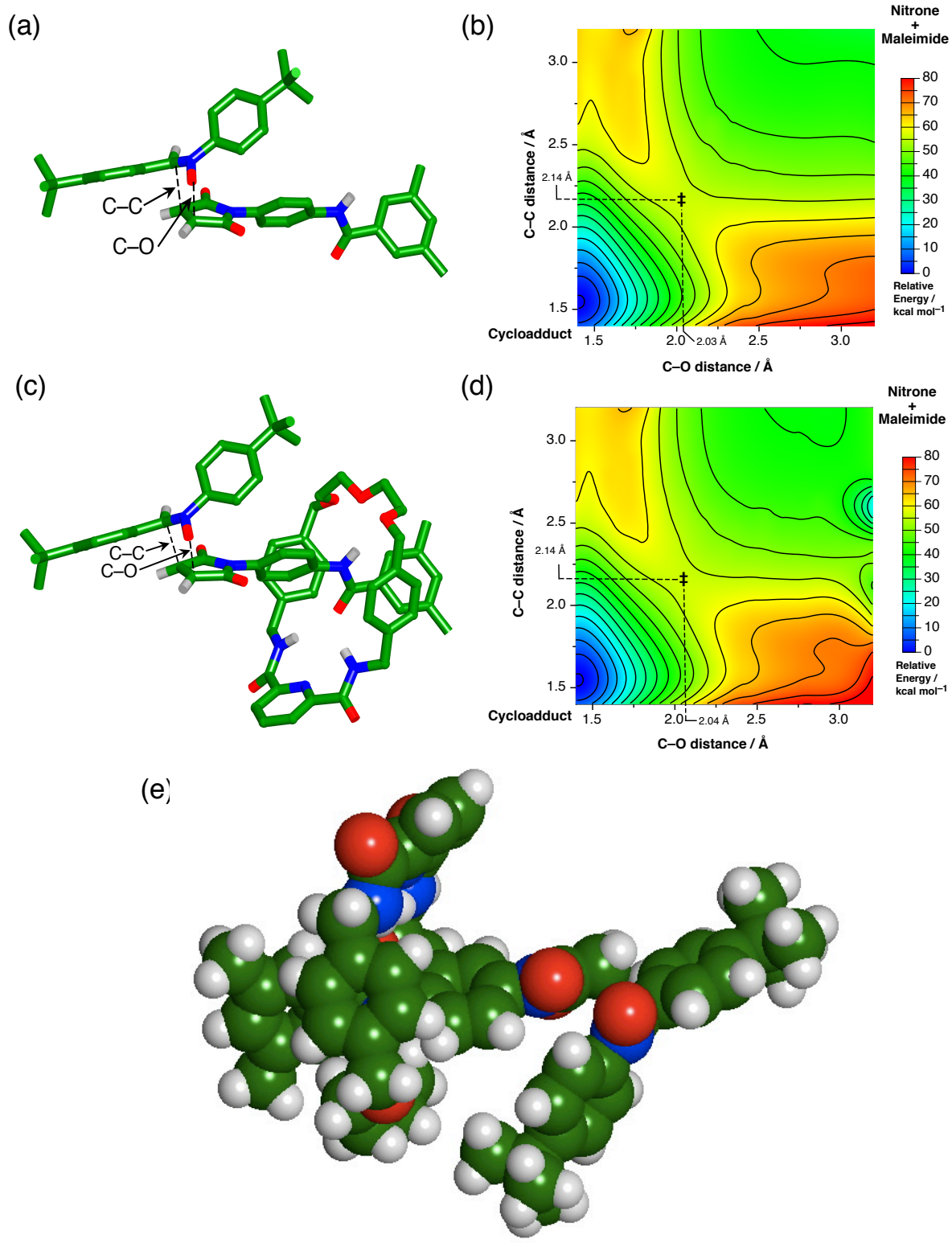

Figure 5.19. Stick representation of the calculated (RM1 semi-empirical method) transition state structures for (a) the reaction between control nitrone **134** and short maleimide **108** and (c) the reaction between the control nitrone **134** and the pseudorotaxane complex between short maleimide **108** and macrocycle **MDG**; (b) and (d) Contour plot of the potential energy surface for transition state obtained for reaction (a) and reaction (c) and; (e) space filling model of rotaxane formation revealed that the *tert*-butyl group of nitrone **134** is essentially in van der Waals contacts with the diethylene glycol unit of macrcycle **MDG.** Carbon atoms are coloured green, oxygen atoms in red, nitrogen atoms in blue and hydrogen atoms in white although most hydrogen atoms have been removed for clarity. Bond formations are shown as dotted line.

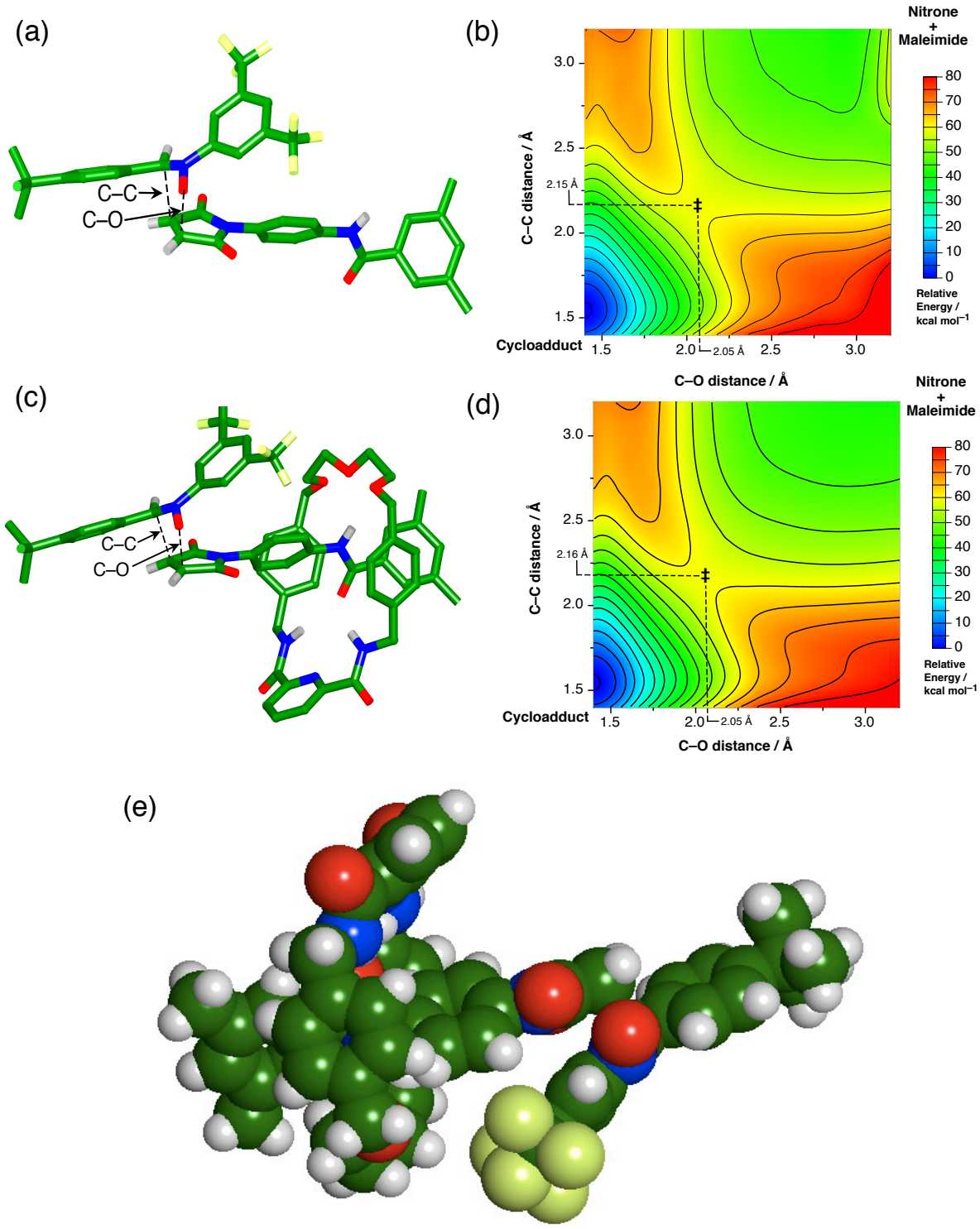

Figure 5.20. Stick representation of the calculated (RM1 semi-empirical method) transition state structures for (a) the reaction between nitrone **142** and short maleimide **108** and (c) the reaction between the nitrone **142** and the pseudorotaxane complex between short maleimide **108** and macrocycle **MDG**, (b) and (d) Contour plot of the potential energy surface for transition state obtained for reaction (a) and reaction (c) and; (e) space filling model of rotaxane formation revealed that a more severe steric impact imposed by the bis-CF_3 group of **142** in the transition state between [**MDG·108**] complex and nitrone **142** as a result of the closely packed location to the diethylene glycol loop of the macrocycle. Carbon atoms are coloured green, oxygen atoms in red, nitrogen atoms in blue and hydrogen atoms in white although most hydrogen atoms have been removed for clarity. Bond formations are shown as dotted line.

The drastic changes observed in the reduced reactivity of thread (**Figure 5.20a**) and rotaxane (**Figure 5.20c**) formation when we employed the control CF_3 nitrone **142**. This observation was similarly inspected by means of optimization of transition state calculated structure to provide a proper insight about the electronic structure and properties of CF_3 nitrone **142**. The space filling model (**Figure 5.20e**) reveals more severe steric impact opposed by the 3,5-bis(trifuloromethyl) substituent in the transition state between the complex of [**MDG•108**] and CF_3 nitrone **142** as a result of the closely packed location to the diethylene glycol loop of the macrocycle. The transition state of the rotaxane formation is undoubtedly deprived from the resulting steric barrier force, in which helps to justify the poor conversion in the rotaxane formation.

These calculations corroborated our recent investigations and once again suggests that an appropriate spacer length are vital to ensure that the reactive site on the thread component are sufficiently located away from the binding site of the macrocycle unit, rendering the introduction of the supramolecular steric effect and therefore help to improve the reactivity of the pseudorotaxane complex towards the stoppering reagent (the nitrone compound) to give a substantial amount of the desired rotaxane.

5.10 Conclusion

In the first part of the chapter, the analysis of the structural invariances of the thread component between nitrone **115** and the four maleimide compounds (**108** – **111**) were conducted. For all combinations, the reactivity of *trans* diastereoisomer of the cycloadducts is evident. The *trans* diastereoisomer dominated over the *cis* diastereoisomer by means of typical bimolecular reaction in 3:1 ratio. Overall, the four investigated systems demonstrated that the outcome of these control reactions can be predicted, even when a different maleimide compound was employed.

The second part of this chapter reveals the kinetic analysis for simple rotaxane formation. The relationship between a high association constant, K_a and the substantial amount of rotaxane, **R** over the thread, **T** is described. Although the binding constant for the pseudorotaxane [**L•M**] is considerably low, the notion of our simple kinetic model of rotaxane formation in **Chapter 3** are proved to be working as expected. In addition, the obtained bimolecular rate constants for the formation of thread and rotaxane compounds with two different maleimides, **108** and **109** issued two major importances. Bimolecular rate constant for rotaxane formation increase with the size of the spacer unit in the long CH_3 maleimide **109** in comparison with short CH_3 maleimide **108**. In general, a high bimolecular rate constant of the desired product in the self-replicating framework could shorten the lag period in the early stage of the reaction. On the basis of the thread:rotaxane ratio, the results presented in **Table 5.1** give an encouraging start as the yield of the thread:rotaxane ratio decrease from 4.6 to 3.4 when diphenylethane spacer was employed in the presence of macrocycle **MDG**. Hence, the incorporation[200] of the diphenylethane spacer in the maleimide component has considerably improved the productivity of the system.

We have learnt that the association constant, K_a can be manipulated by radical design of the binding site of the guest or the macrocycle. Therefore, the formation of rotaxanes are improved when employing alternative macrocycle **MP**, which leads to the thread: rotaxane ratio of 1.6:1 (in the case of short maleimide **108**) and 1.2:1 (in the case of long maleimide **109**), respectively. The introduction of the fluorine tagged compounds in one of the building blocks of non-replicating rotaxane is initially proposed to help with the deconvolution of the cycloadducts resonances arising from both thread and rotaxane. Nonetheless, the reaction between short maleimide **108**

and CF_3 nitrone **142** in the presence of macrocycle **MDG** or **MP** suffer severe steric effects in the transition state as a consequence of the clashing location of the *tert*-butyl or CF_3 groups that is closely orientated towards the lower fragment of the macrocycle component which destabilized the transitions states for the subsequent stoppering reaction.

As discussed earlier, the implementation of the simple kinetic model of rotaxane formation is appropiate if the bimolecular rate constants of k_{thread} and $k_{rotaxane}$ are equal. However, this is not what we found in our own systems. We observed different reactivity of thread and rotaxane, which emanates from the central reversible equilibrium of free maleimide compound and the pseudorotaxane complex. Thus, the position of this equilibrium is the primary concerns in the investigated systems. In conclusion, this finding reveal that the [**R**]/[**T**] ratio is sensitive to both the association constant, K_a for the pseudorotaxane complex [**L**•**M**] and to the ratio of $k_{rotaxane}/k_{thread}$.

6

Low temperature capture of pseudorotaxanes

6.1 Introduction

As explained earlier, our initial effort[207] to integrate replication processes with mechanically interlocked molecules in **Replication model 1** met with limited success. The reasons for our failure are again encapsulated in **Figure 6.1a**. A plausible kinetic model for rotaxane formation, in which we are trying to maximise the amount of rotaxane formed, involves two irreversible reactions coupled to a central equilibrium.

The linear component of the rotaxane **L** associates with macrocycle **M** to form the [**L**•**M**] complex. This complex is then captured irreversibly by reaction with **S** to form rotaxane **R**. If, however, the linear component **L** reacts directly with the capping reagent **S**, then product **T**, which does not contain the macrocycle, is formed. Therefore, a key marker for the efficiency of the rotaxane-forming protocol is the ratio of **R** to **T**. Kinetic simulation (**Figure 6.1b**) reveals that this [**R**]/[**T**] ratio is sensitive to both the association constant, K_a, for the [**L**•**M**] complex and to the ratio k_R/k_T. If we assume that the K_a for the [**L**•**M**] complex is 5000 M^{-1} and $k_T = k_R$, then the [**R**]/[**T**] ratio in the final reaction mixture is 10.8 (green line, **Figure 6.1b**).

However, if $k_T = 2\ k_R$, *i.e.* the [**L**•**M**] complex is less reactive than **L** itself, then a K_a for the [**L**•**M**] complex of 5000 M^{-1} results in a [**R**]/[**T**] ratio of 6.1 (orange line, **Figure 6.1b**). Such situations are relatively common in rotaxane synthesis as there are frequently remote steric effects[227-230] arising from the close proximity of the three species **L**, **M** and **S** at the transition state leading to **R**. The situation deteriorates as the k_R/k_T ratio diminishes – when $k_T = 4\ k_R$ the [**R**]/[**T**] ratio in the final reaction mixture is only 3.4 (red line, **Figure 6.1b**).

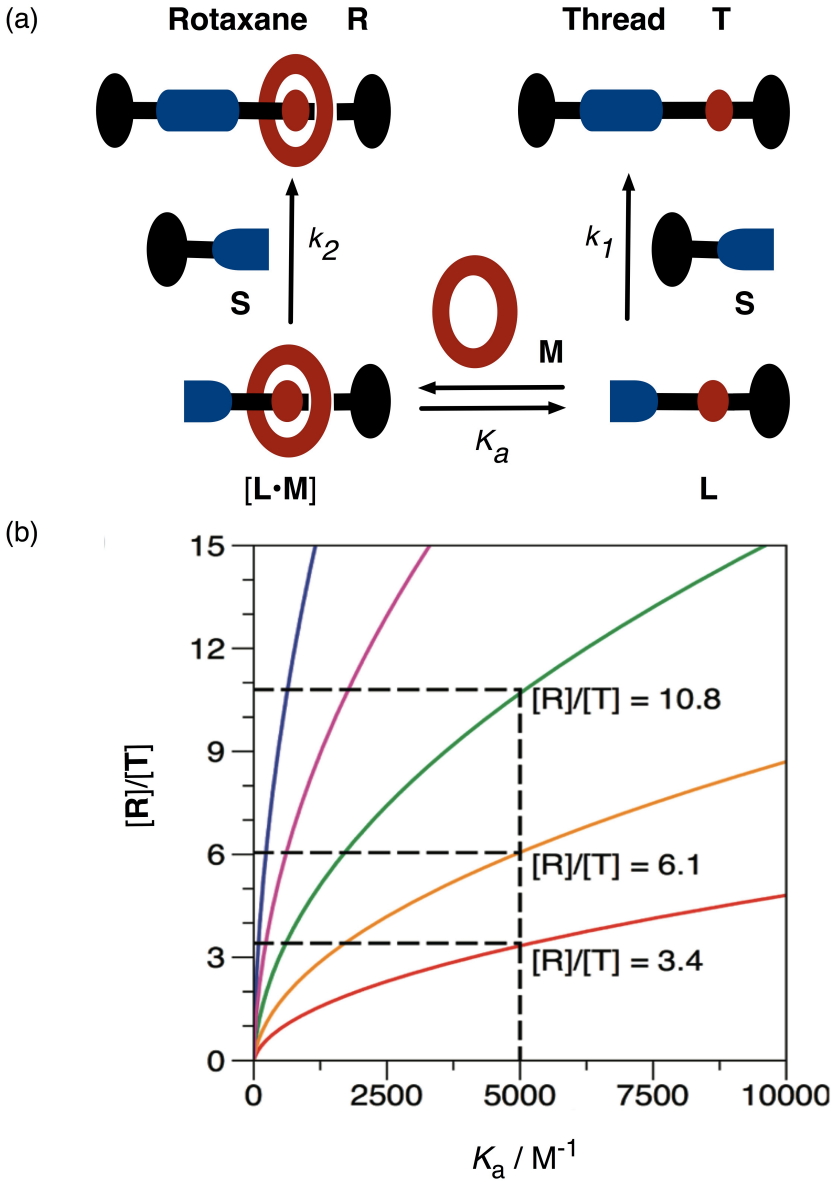

Figure 6.1. (a) The linear component of the rotaxane **L** associates with macrocycle **M** to form the [**L•M**] complex. This complex is then captured irreversibly by reaction with **S** to form rotaxane, **R**. The linear component **L** can also react directly with the capping reagent **S**, forming **T**, which does not contain the macrocycle. (b) Plot of [**R**]/[**T**] against K_a for the kinetic scheme described in part (a). In the simulation, the starting concentrations of **L**, **M** and S are 25 mM. Rate constant k_T is 1×10^{-3} $M^{-1}s^{-1}$ and k_R was varied from 4×10^{-3} $M^{-1}s^{-1}$ (blue line) to 2.5×10^{-4} $M^{-1}s^{-1}$ (red line) – the value of k_R being halved in each step.

In our original work (see example in **Chapter 5**), the K_a for the [**L•M**] complex was around 100 M^{-1} and $k_T = 3\ k_R$. This set of parameters led to unacceptably small [**R**]/[**T**] ratios. Clearly, this situation could be addressed by a radical redesign of the recognition event that creates the [**L•M**] complex in order to increase the strength of this association. However, in some situations, this strategy may be difficult to implement and synthetically challenging.

6.2 An alternative stoppering reaction

As an alternative strategy, we reasoned that it should be possible to manipulate the K_a for the [**L•M**] complex by means of a change in temperature. By lowering the temperature, the K_a should increase and leading, therefore increase the population of [**L•M**] species. Manipulating the population of [**L•M**] will, ultimately, lead to an increase in the [**R**]/[**T**] ratio. However, as the temperature decreases, the efficiency of the capping reactions between either **L** or [**L•M**] and **S** also decreases (**Figure 6.2**). It is unlikely that capping chemistry that is rapid at room temperature scenario would also be fast enough at lower temperatures. Nevertheless, a limited number of stoppering reactions that could possibly occur at low temperature was proving quite a challenge.

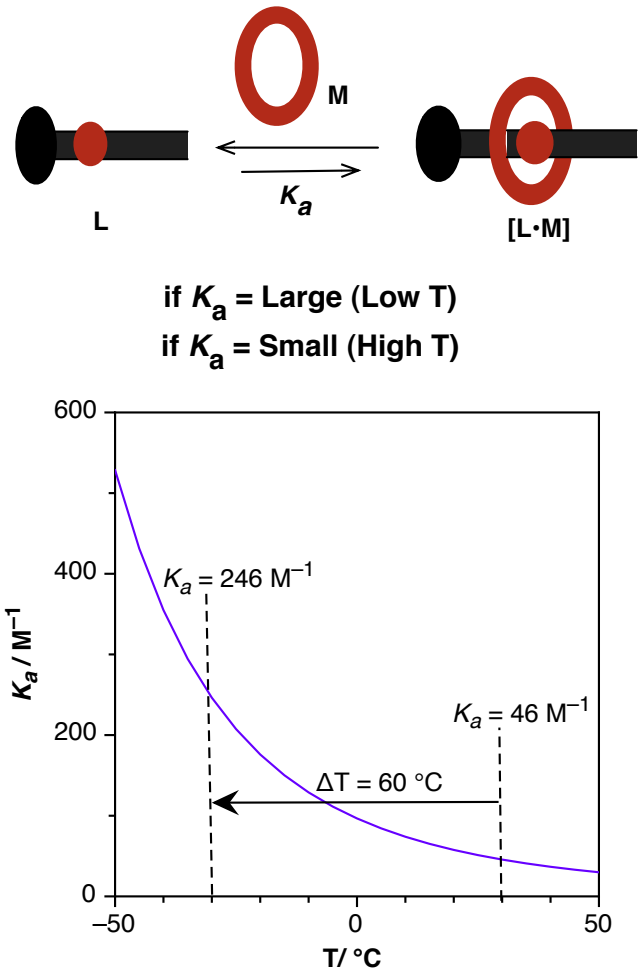

Figure 6.2. Cartoon representation of the effect of temperature on K_a. In order to establish a larger K_a, either the macrocycle, **M** or guest, **L** can be altered to increase the binding (*chemical modification*). Alternately, a lower temperature (*condition modification*) can be employed to encourage pseudorotaxane formation by increasing the K_a.

Herein, we describe the rapid reaction between phosphines and organic azide at low temperature as an intermediate capping step by means of Staudinger reaction

(**Figure 6.3a**). The iminophosphorane formed in this process can then be captured permanently through reaction with an aldehyde in an aza-Wittig reaction as depicted in **Figure 6.3b**.

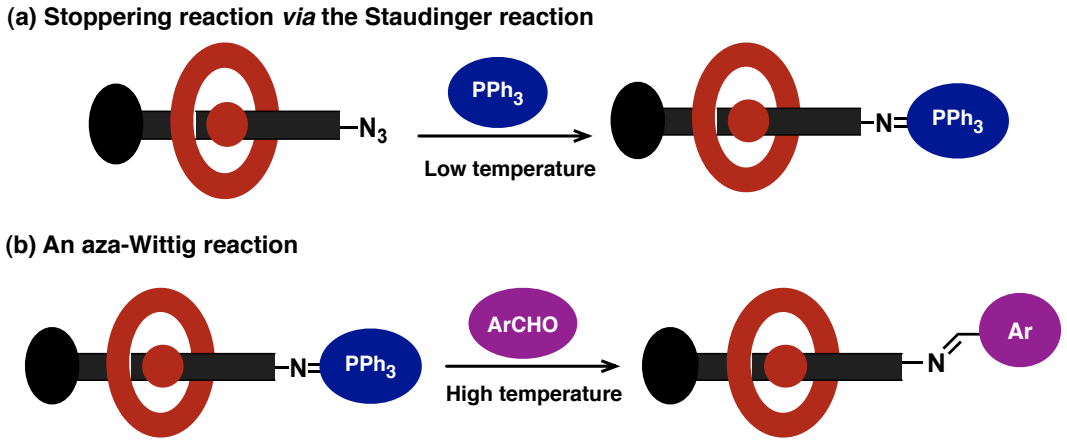

Figure 6.3. Cartoon representation of the stoppering process which involves:- (a) Stoppering by a Staudinger reaction, using a reactive stopper at low temperature to maximize the yield. Azide being placed at the terminus of the thread while phosphine group acted as a large capping molecule, respectively. Once the reactive stopper is bound to the guest at low temperature, a [2]-rotaxane will be formed. However, the newly formed bond (P=N) between the stopper and guest is labile and consequently the isolation of the rotaxane is unlikely. (b) An alternative route, additional synthetic conversion of functionality by way of an aza-Wittig reaction will form a stable bond, imine (C=N) in which isolation and characterization is feasible *via* an aza-Wittig reaction.

Thus far, this novel stoppering strategy of converting a pseudorotaxane to a rotaxane at low temperature ought to effectively trapped as much [2]-pseudorotaxane species as possible before sequential conversion to a stable [2]-rotaxane can takes place. It is vital for the successful formation of rotaxane that sufficient binding was achieved between both the macrocycle and guest or otherwise formation of the important pseudorotaxane precursor will be limited.

As a consequence, this stoppering method relies on a large binding constant between both the macrocycle and guest to form a substantial amount of rotaxane. However, if the K_a value is small, a large percentage of unbound to bound species will be present thus lowering the overall yield of the rotaxane. In order to counteract this undesirable reduction in reactivity at lower temperature, we have identified a new strategy[231] as depicted in **Scheme 6.1**. Accordingly, we designed azide **146** as a suitable linear component for incorporation within a rotaxane framework.

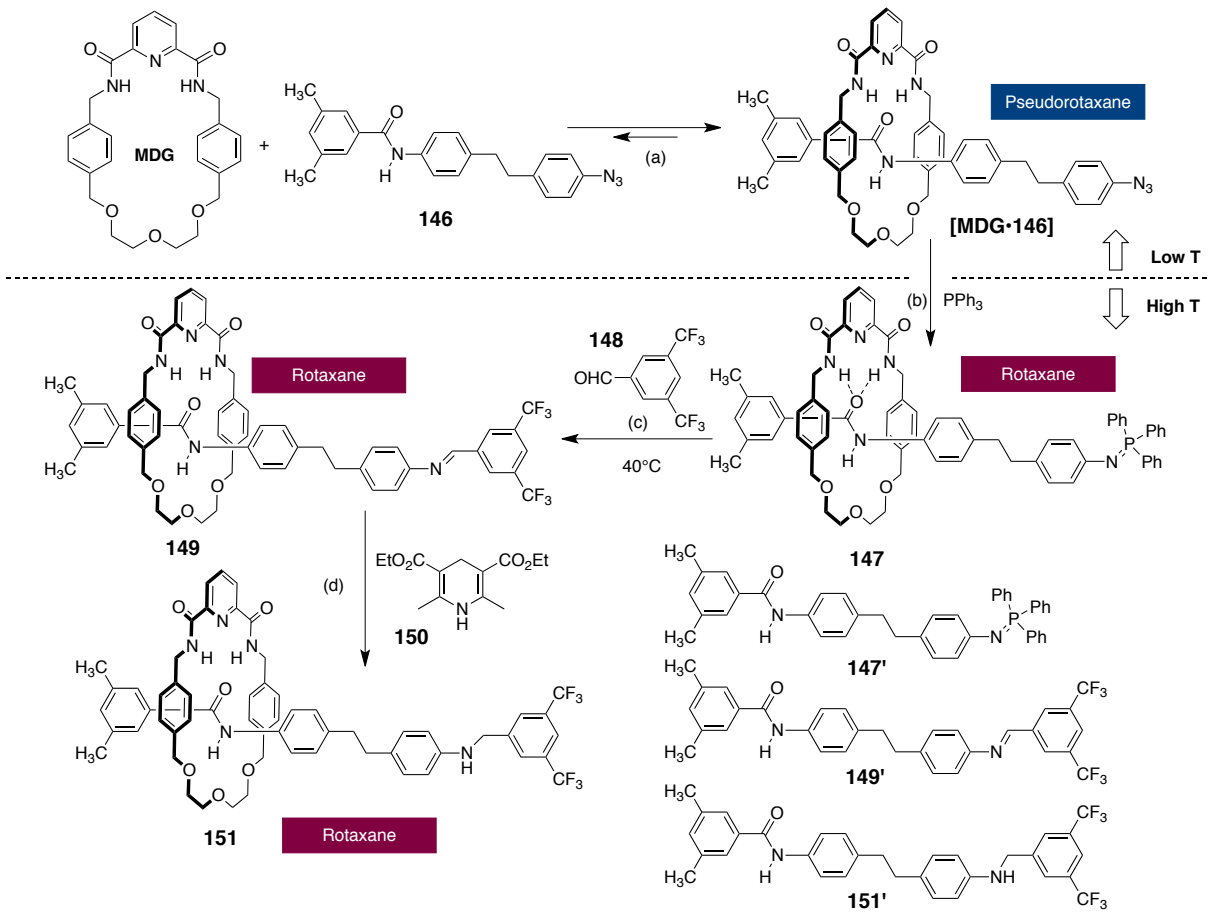

Scheme 6.1. Synthesis of rotaxane **151** *via* novel stoppering strategy. Reagents and conditions: (a) Macrocycle **MDG**, $CDCl_3$, rt to −10 ˚C, 1 h; (b) PPh_3, $CDCl_3$, 10 ˚C, 48 h; (c) 3,5-bis(trifluoromethyl)benzaldehyde **148**, $CDCl_3$, 40 ˚C, 48 h; (d) diethyl 1,4-dihydro-2,6-dimethyl-3,5-pyridinedicarboxylate **150**, $CDCl_3$, 40 ˚C, 48 h, 28% over 4 steps.

Previously, we and others[207,211,214,232-234] have demonstrated that diaryl amide, such as **146**, can be recognised and bound by macrocycle **MDG**, forming a complex, in this case [**MDG·146**] with a pseudorotaxane geometry. The dimethyl substituted aromatic ring is of the correct size and presents suitable steric hindrance to prevent slipping of the macrocycle, and thus, acting as an inert stopper. The synthesis of azide formation of **146** is accomplished in **Scheme 6.2**.

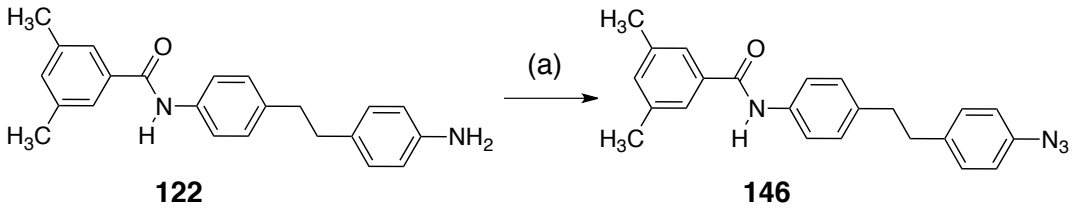

Scheme 6.2. Synthesis of azide compound **146**. Reagents and conditions: (a) HCl (conc.), $NaNO_2$ (aq.), −10 ˚C, 1 h; followed by NaN_3 (aq.), −10 ˚C, rt, 2 h, 97%.

Aniline derivative **122** is treated with nitrous acid, which is generated in situ from sodium nitrite and hydrochloric acid at –10 ˚C to give the diazonium salts and subsequently reacted with sodium azide in aqueous solution to afford azide **146** in excellent yield. The small cavity size present in macrocycle **MDG** introduces a constrictive[235] element to the binding of diaryl amide in solvents such as $CDCl_3$. As a result, the 500 MHz ^{1}H NMR spectrum of the [**MDG•146**] complex in $CDCl_3$, recorded at 10 °C exhibits separate resonances for free **146** and bound **146**, indicating that azide **146**, macrocycle **MDG** and [**MDG•146**] complex and are in slow exchange process on the ^{1}H NMR chemical shift timescale. Therefore, it is possible to assay the K_a for the [**MDG•146**] complex in $CDCl_3$ using the integrals of the CH_3 resonances. Hence, the ^{1}H NMR data were recorded at five temperatures between +10 °C and –10 °C (**Figure 6.4**).

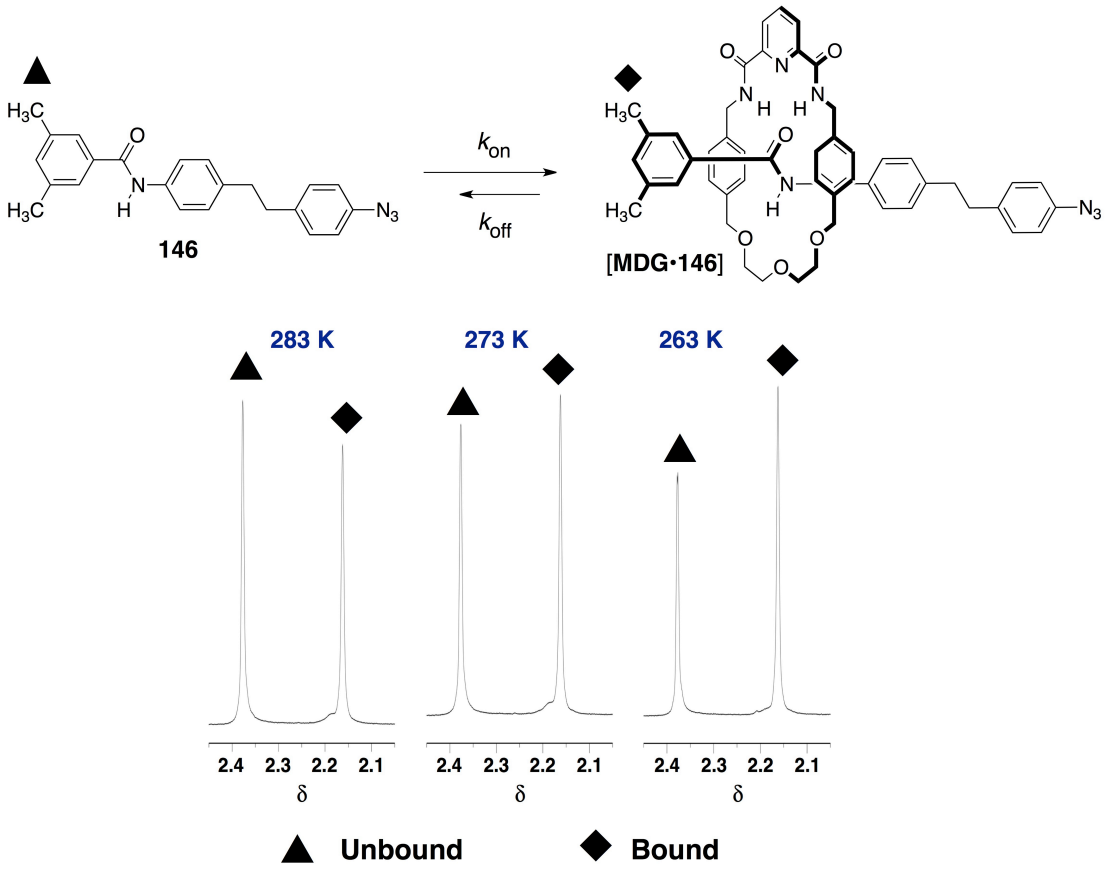

Figure 6.4. Partial ^{1}H NMR (500 MHz, $CDCl_3$) spectra either at 283 K, 273 K or 263 K, exhibited separate resonance for free azide **146** and bound azide **146**, indicating that **146**, macrocycle **MDG** and [**MDG•146**] are in slow exchange process on the ^{1}H NMR chemical shift timescale with corresponding δ_H 2.37 arising from free azide **146** and the pseudorotaxane [**MDG•146**] complex at δ_H 2.16 and further show that pseudorotaxane formation is favoured at low temperature. In particular, the resonances arising from the CH_3 groups on the terminal aromatic ring of compound **146** are very well resolved.

As expected, the association constant is temperature dependent. At +10 °C, the K_a for [**MDG•146**] complex is 67 ± 5 M^{-1} in $CDCl_3$, rising to 118 ± 6 M^{-1} at –10 °C. Fitting of the experimental binding data to the van't Hoff equation gives an excellent fit (**Figure 6.5**) and affords values of ΔH and ΔS of binding for pseudorotaxane [**MDG•146**] of –17.2 kJ mol^{-1} and –25.7 J mol^{-1} K^{-1}, respectively.

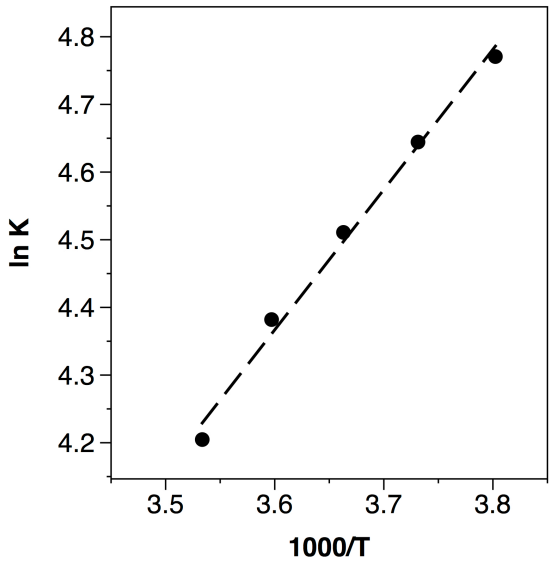

Figure 6.5. Plot of ln K_a for the [**MDG•146**] complex against 1000/T. Linear regression affords the line of best fit (dashed line). The gradient of this line is 10^3 ΔH/R and the intercept is ΔS/R.

Having established the relationship between temperature and the stability of the [**MDG•146**] complex, we next sought to trap this pseudorotaxane by capping. To this end, we reacted a solution of azide **146** and macrocycle **MDG**, each at 20 mM concentration, with PPh_3 at a series of temperatures from +10 °C to –10 °C. The result was rapid conversion of the pseudorotaxane [**MDG•146**] into rotaxane **147** *via* the Staudinger mechanism as illustrated in **Scheme 6.3**.

The progress of this reaction was monitored readily by ^{31}P NMR spectroscopy analysis – namely, the formation of the iminophosphorane results from the emergence of a new broad resonance at around δ_P +5.5. Gratifyingly, the ratio of rotaxane **147** to capped linear component **147'** mirrored the ratio of **146** and **MDG** to [**MDG•146**] complex before the addition of PPh_3 to the solution. Furthermore, this ratio did not change upon heating the solution, indicating that **147** was, indeed, a rotaxane and that iminophosphorane capping group was robust (**Figure 6.6**).

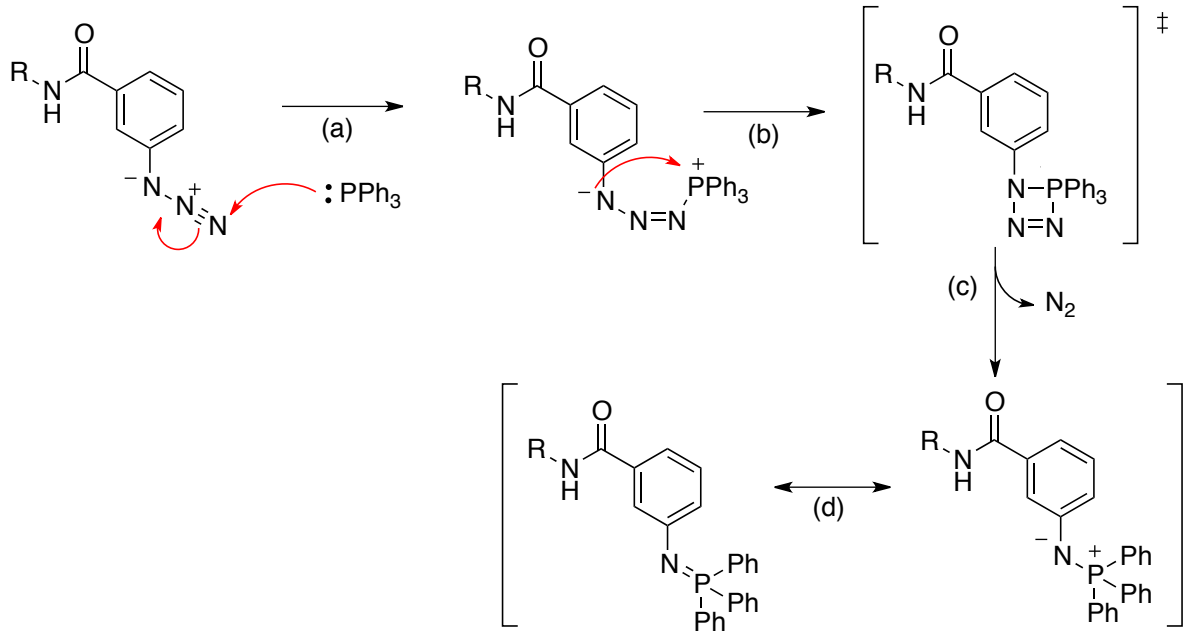

Scheme 6.3. The Staudinger mechanism. (a) Triphenylphosphine (PPh_3) reacts with azide derivative to generate a phosphoazide; (b) The mechanism then proceeds *via* a four membered cyclic transition state; (c) Loss of N_2 (g) forms an iminophosphorane; (d) The resonance form of the charged species equates to the P=N bond.

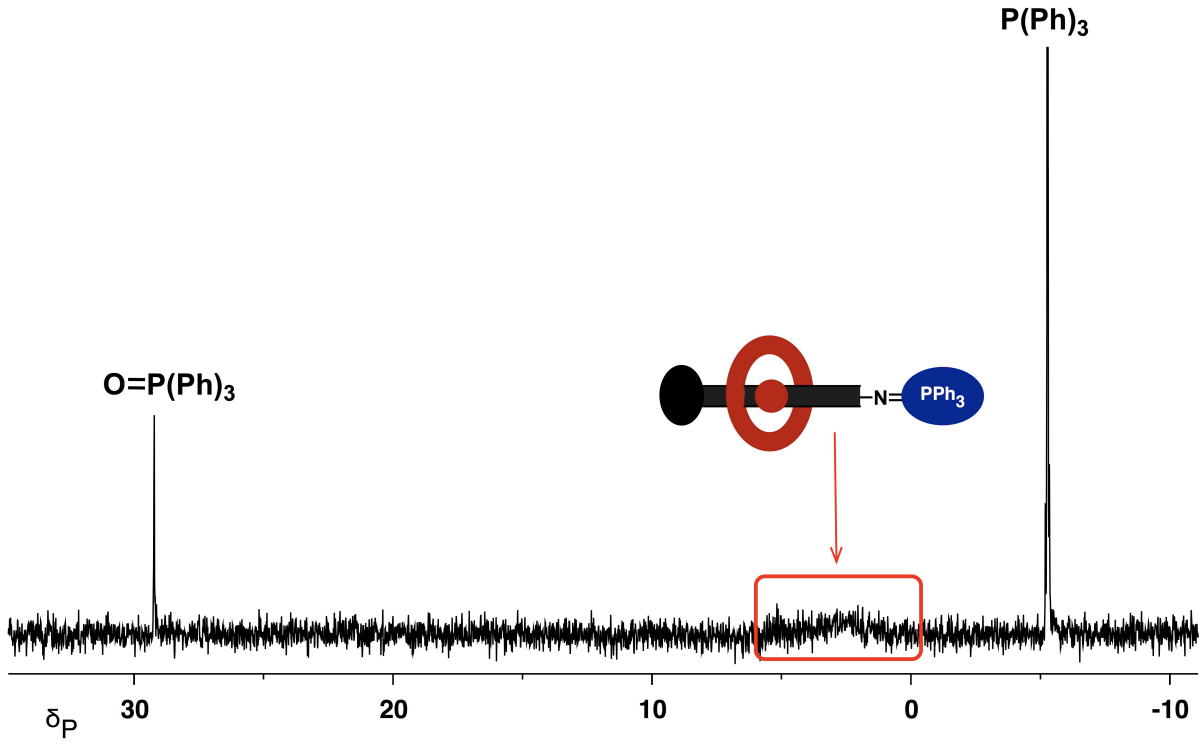

Figure 6.6. Partial ^{31}P NMR (121.5 MHz, $CDCl_3$) spectrum of P=N rotaxane **147** formation. The final stoppering process involves the addition of PPh_3 at –10 °C to maximize rotaxane formation. The P=N rotaxane gives a very broad signal. An excess of PPh_3 and triphenylphosphine oxide as side product has also been clearly identified in the same spectrum.

Thus, P=N rotaxane display a very broad resonance in the 121.5 MHz ^{31}P spectra together with triphenylphosphine oxide as a side product. In order to maximize the total conversion of pseudorotaxane [**MDG•146**] to rotaxane **147**, this novel stoppering method required an excess of PPh_3, which was clearly identifiable by ^{31}P NMR. Once macrocycle **MDG** is part of the rotaxane **147**, we are able to manipulate this rotaxane structure synthetically by virtue of its reactive iminophosphorane capping group. Hence, the addition of aldehyde **148** and one equivalent[236] of 4-bromophenylacetic acid to the mixture of iminophosphoranes **147** and **147'** in $CDCl_3$, followed by heating at 40 °C for another 48 hours effected an aza-Wittig reaction; and thus affording a mixture of imines **149** and **149'**. These imines could be reduced readily by treament with dihydropyridine **150** in $CDCl_3$ for 48 hours at room temperature; giving rise to a mixture of the rotaxane **151** and thread **151'**, which could be separated readily by column chromatography. The 400.1 MHz ^{1}H NMR spectrum of rotaxane **151**, recorded in $CDCl_3$ at room temperature, (**Figure 6.7 middle**) shows the characteristic pattern of chemical shift changes associated with the coconformation of the macrocycle and linear component within the rotaxane.

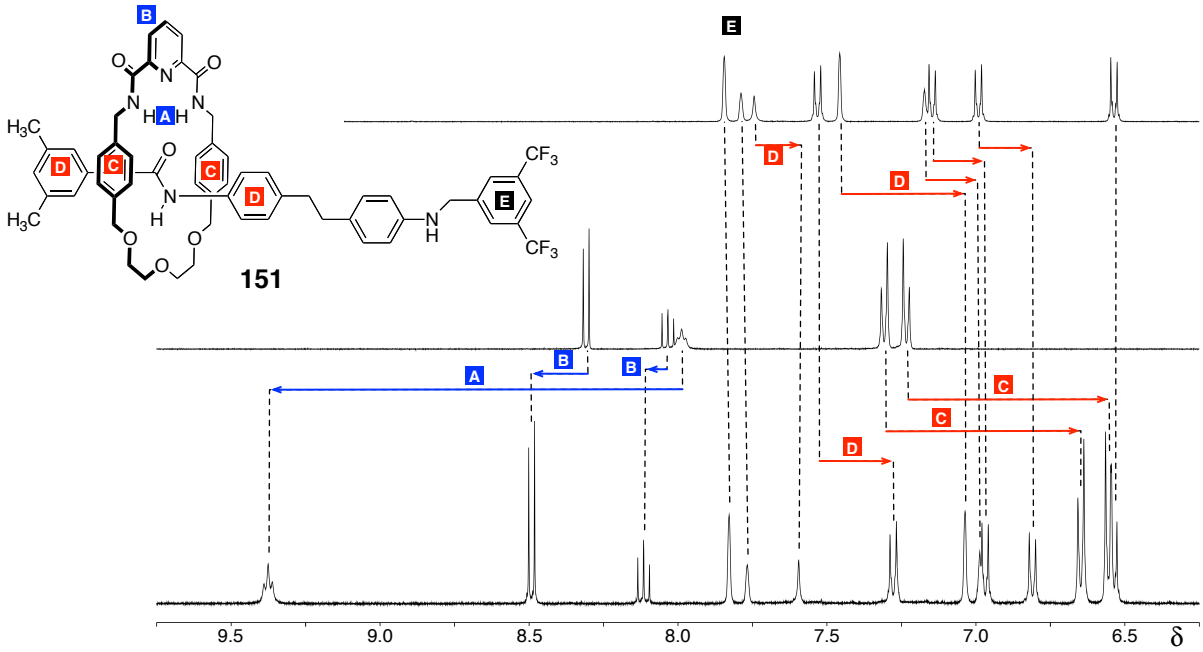

Figure 6.7. Partial 400.1 MHz ^{1}H NMR spectrum of rotaxane **151** (bottom) recorded in $CDCl_3$ at room temperature. The same chemical shift region is also shown for free macrocycle **MDG** (middle) and secondary amine **151'** for comparison. Downfield chemical shift changes on rotaxane formation are marked with blue arrows and upfield chemical shift changes on rotaxane formation are marked with red arrows.

In particular, the amide NH resonance (**A**, **Figure 6.7**) exhibits a downfield shift of more than 1.3 ppm, consistent with its participation in a hydrogen bond with the carbonyl oxygen atom of the diarylamide unit. The resonances associated with the pyridine ring (**B**, **Figure 6.7**) in the macrocyclic component of **MDG** experience strong downfield shifts of up to 0.4 ppm as a result of their location within the deshielding region of the aromatic rings associated with the diarylamide in the linear component of **151 (D**, **Figure 6.7)**. The resonances arising from the diarylamide **(D**, **Figure 6.7)** are themselves shielded significantly by their proximity to the *para*-disubstituted aromatic rings (**C**, **Figure 6.7**). The location of the macrocycle at the diarylamide end of the structure is supported by the fact that the aromatic proton resonances associated with the CF_3-containing ring show no chemical shift changes on rotaxane formation (**E**, **Figure 6.7**).

Satisfyingly, there is an excellent fit (**Figure 6.8**) of the experimental yield of rotaxane **151**, synthesised through the process shown in **Scheme 6.1**, to the behaviour expected from the kinetic model (**Figure 6.1**) on which the process is based. Thus, transiently raising the K_a for pseudorotaxane formation by lowering the temperature results in an increased yield of rotaxane after conversion of the temporary iminophosphorane capping group to a secondary amine through the combination of an aza-Wittig reaction followed by reduction.

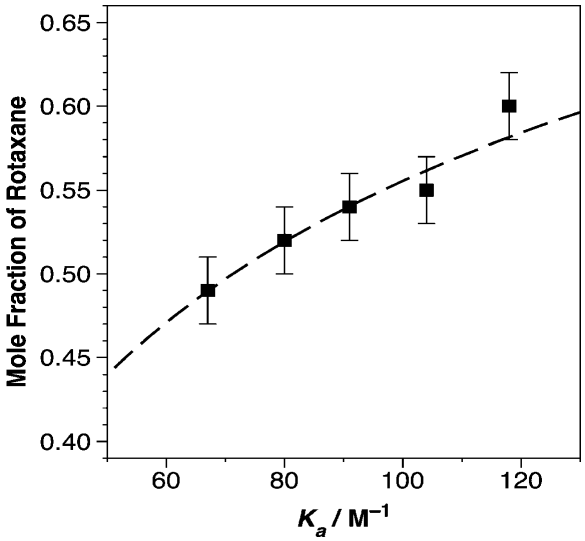

Figure 6.8. Yield of rotaxane **151** as a function of the K_a for [**MDG·146**] complex. Filled squares represents experimental data and the dashed line represents the relationship expected based on the kinetic model shown in **Figure 6.1** with $k_T = 1.7\ k_R$.

6.3 Conclusion

The main principles of the simple kinetic model of rotaxane formation have been established previously in **Chapter 5**, which highlighted the importance of the association of the macrocycle to the binding site. When considering this in more detail, the reversible formation of pseudorotaxane complex, which emanate from the central equilibrium (**Figure 6.1a**) plays a crucial role. As a matter of fact, the efficiency of the pseudorotaxane formation relies in a high association constant, K_a. It was evident that as a consequence of low K_a, a substantial amount of thread is present over rotaxane. Kinetic simulation revealed that for rotaxane to be present in at least 10 times the thread, an association constant, K_a of 5000 M^{-1} is required. We have also demonstrated that we can manipulate this by the modification of the macrocycle and/or the guest used. This approach has been found to be such a laborious job if we need to change it each time we wish to alter our rotaxane system.

Therefore, one possibility to circumvent this scenario is to manipulate the K_a for the pseudorotaxane complex by means of temperature. By lowering the temperature, we will increase the K_a and lead to an increase in the population of pseudorotaxanes and ultimately lead to an increase in the rotaxane to thread ratio. However, as the temperature decreases, the efficiency of the stoppering reactions will also subsequently decreases. Therefore, we identified a new strategy to counteract these issues by employing a rapid reaction between a phosphine and organic azide at low temperature as an intermediate capping step. The iminophosphorane formed can then be captured permanently with aldehyde in an aza-Wittig reaction. Following this, these imines could be reduced readily by the treatment with Hanstzh ester **150** to afford the secondary amine rotaxane **151** and thread **151'** that later separated by column chromatography.

The partial ^{1}H NMR spectra (**Figure 6.4**) of pseudorotaxane complex [**MDG•146**] is recorded at variable temperature from 10 ˚C, 0 ˚C to –10 ˚C. At 10 ˚C, the K_a is almost 70 M^{-1} rising to 120 M^{-1} at –10 ˚C, which demonstrated that the K_a is temperature dependent. The van't Hoff analysis (**Figure 6.5**) gives an excellent fit and affords value of enthalpy of –17.2 kJ mol^{-1} and entropy of –25.7 J mol^{-1} K^{-1}, which clearly manifested the enthalpically driven processes which is typical in the formation of the two hydrogen bonds.

7

Replication model 2

7.1 Introduction

Replication model 2 has been proposed in **Chapter 3** as an alternative replication framework to integrate replication processes within the mechanically interlocked architecture of our interest. Some minor modifications were made, in which one of the complementary recognition site (carboxylic acid in this case) is being positioned on to the macrocyclic component and the thread backbone carries the corresponding amidopyridine recognition unit on its end group (**Figure 7.1**).

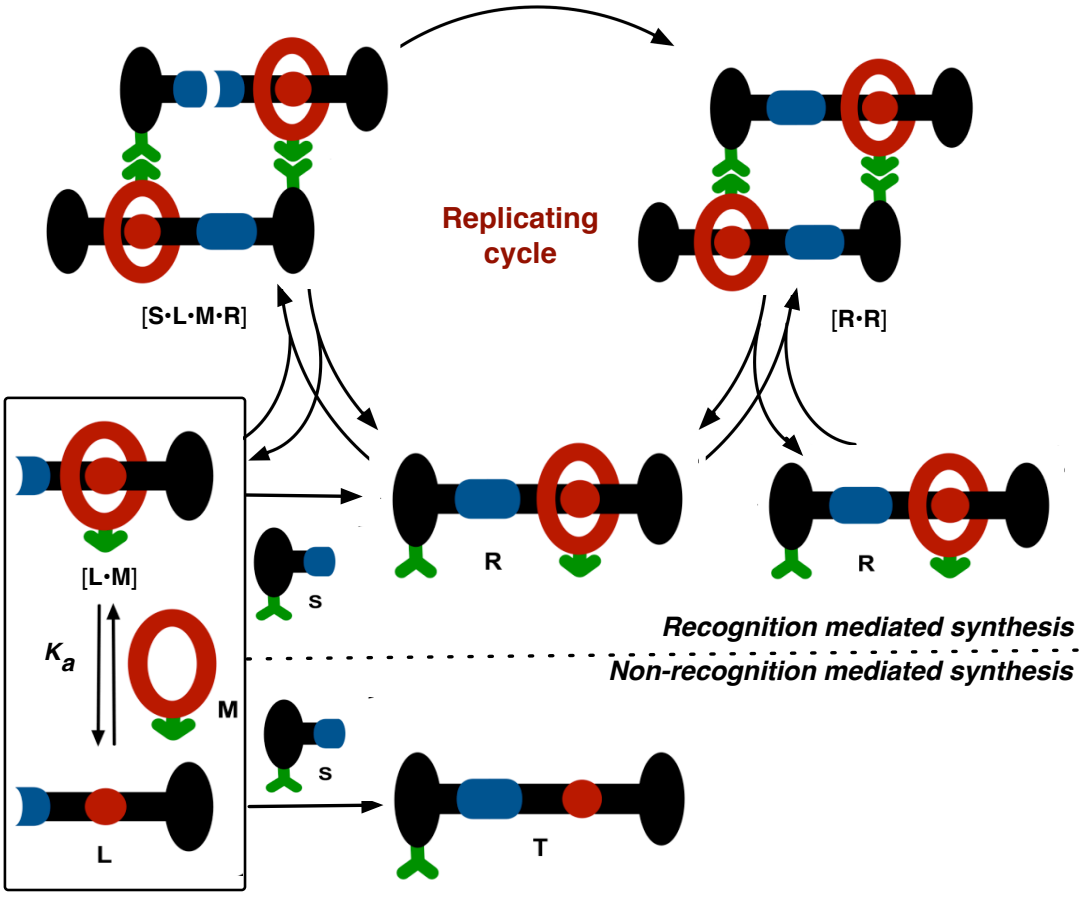

Figure 7.1. **Replication model 2** for self-replicating rotaxanes based on the placement of one recognition site (green cartoons) on one of the stoppers and the other recognition site on to the macrocycle.

The model realised a significant advantage over **Replication model 1**. As a consequence of the thread possessing one recognition unit, the thread instantly become incompetent in the autocatalytic cycle, which hinges on recognition-mediated processes between the carboxylic acid and an amidopyridine unit. In other words, the linear molecule **L** is only capable of reacting with the stoppering reagent **S** at the bimolecular reaction rate. Only the pseudorotaxane species [**L•M**] that contains the recognition site will participate in the replicating cycle. Therefore, under no circumstances will there be a reactivity conflict between k_{thread} and $k_{rotaxane}$. In fact, a substantial formation of [**L•M**] complex will ensure explicit opportunities to react with the stoppering reagent, **S** to assemble the rotaxane **R**, without the competition from the free thread **T** species. This design element allows the rotaxane, **R** to take part in the autocatalytic pathway exclusively and further aid the formation of the second rotaxane, **R**. In the present discussion, we will describe and summarize some of our recent experiments, which were directed toward establishing the design and synthetic approaches of potential self-replicating rotaxane in the case of **Replication model 2**.

7.2 Synthesis of control macrocycles

Our own work included the synthesis of several types of ring components in the first and second generation of macrocycles. The ability of both macrocycle **MDG** and **MP** to complex with a number of different guests through non-covalent interaction has been previously tested. Therefore, we concluded that both cyclic components are capable to interacte and locate the guest within their cavities. Therefore, we are keen to preserve the important fragment of their building blocks before appending the recognition site on to their framework (**Figure 7.2**).

On that account, we began with the synthesis of preliminary control macrocycles to probe the binding performances with previous synthesised guests in comparison to the parent macrocycle **MDG** and **MP**. The first control macrocycle devised is based on the substructure of macrocycle **MDG**. The pyridine unit was substituted with the *tert*-butyl isophthaloyl building block. The control macrocycle based on **MDG** was constructed starting from 5-*tert*-butylisophthalic acid **152** which was activated to acid chloride derivative **153** using thionyl chloride in toluene as outlined[237] in literature.

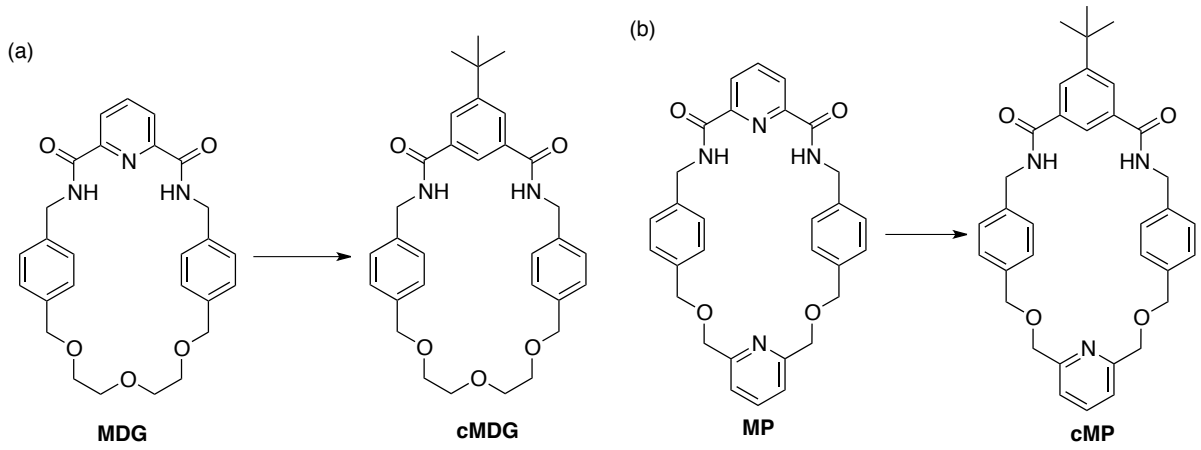

Figure 7.2. Structure of control macrocycles relative to their parent macrocycle **MDG** and **MP**; namely (a) **cMDG** and (b) **cMP**, respectively with minimal adjustment in the upper fragment of the structure consists of *tert*-butyl isophthaloyl building block. Notice that nitrogen atom has been removed in the new design for some synthetic reason.

The intermediate **153** was subsequently coupled to the bis amine compound **103** to give the macrocycle **cMDG** (11% yield) *via* high dilution synthesis. All the reactions described here are carried out as outlined in **Scheme 7.1**. The synthesis of the analogous framework of the control macrocycles has been reported in other works[215,233,238-242]. An attempt was made to grow crystals of **cMDG** using several types of solvents, by growing them using slow diffusion, layering or slow evaporation. Unfortunately, all of these attempts failed to generate suitable crystals for single crystal structure analysis.

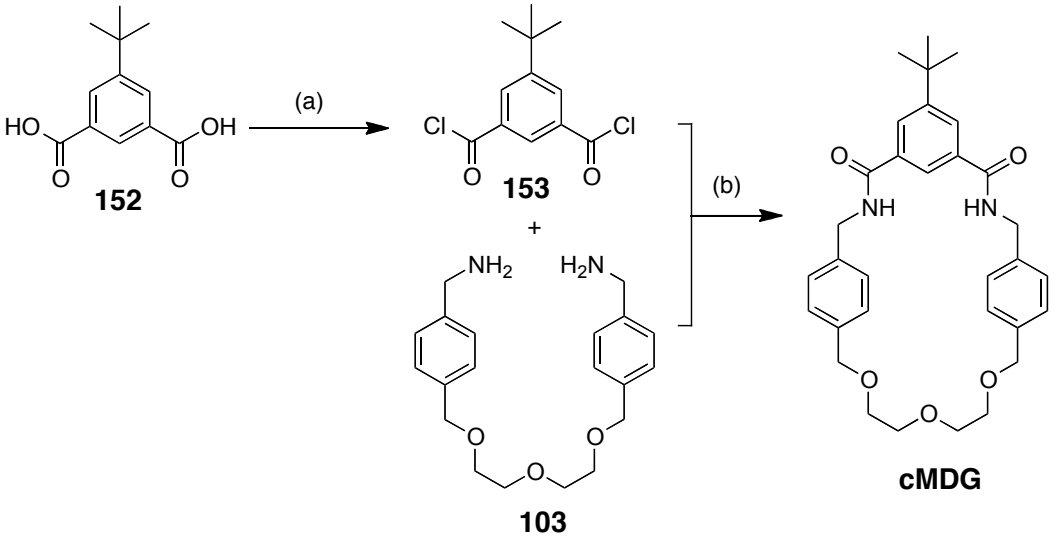

Scheme 7.1. Synthesis of macrocycle **cMDG**. Reagents and yields: (a) $SOCl_2$, toluene, 80 ˚C, 18 h, 98%; (b) Et_3N, THF, rt, 3 days, 11%.

Following this, we examined its calculated structure (**Figure 7.2**) to model the behaviour of its structure. There are obvious differences when comparing with the parent macrocycle **MDG**; such that the opposite orientation of one of the carbonyl group in the upper fragment and the position of the diethylene glycol unit give rise to a bigger cavity in this new macrocycle.

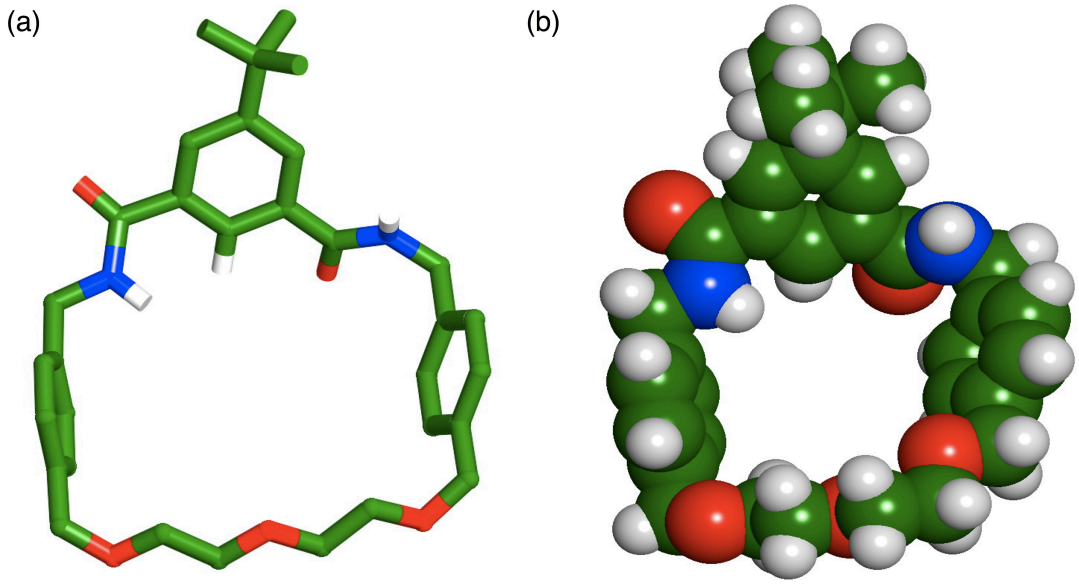

Figure 7.2. (a) Stick representation and (b) space filling model of the calculated structure (OPLS2005, GB/SA $CHCl_3$) of two preferable conformations for macrocycle **cMDG**. Carbon atoms are coloured green, oxygen atoms in red, nitrogen atoms in blue and hydrogen atoms in white (most hydrogen atoms has been removed for clarity).

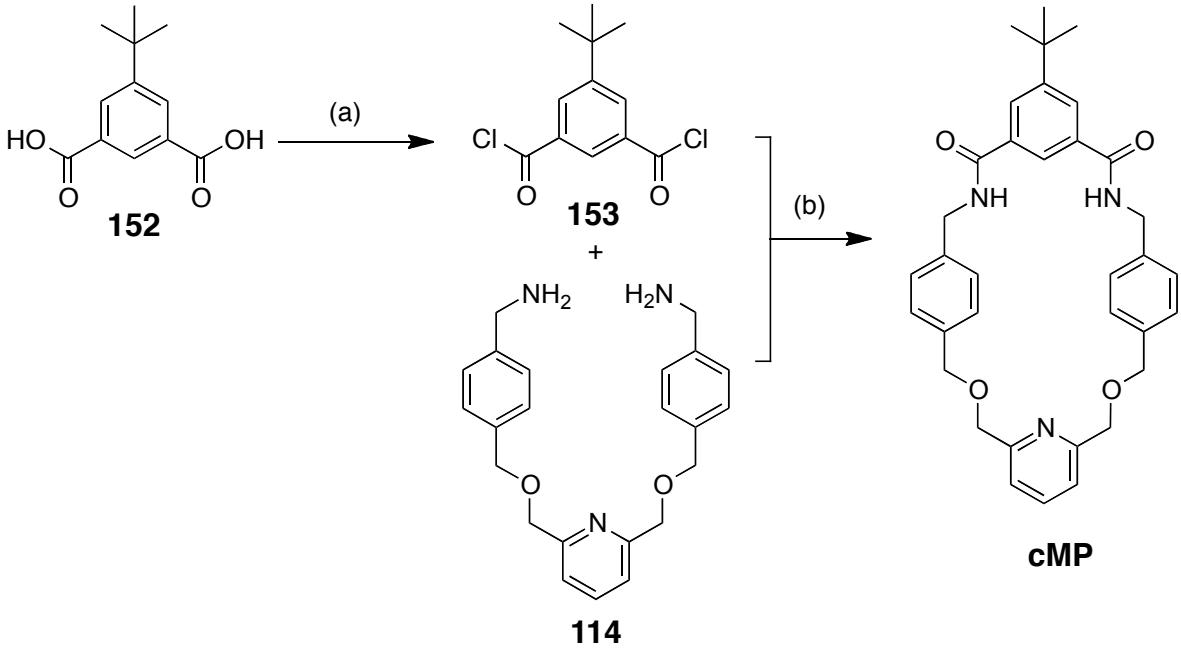

Scheme 7.2. Synthesis of control macrocycle **cMP**. Reagents and yields: (a) $SOCl_2$, toluene, 80 ˚C, 18 h, 98%; (b) Et_3N, THF, rt, 3 days, 11%.

Further, the synthesis of the second control macrocycle based on macrocycle **MP** is encapsulated in **Scheme 7.2**. In similar way, treatment of the diacid **152** with thionyl chloride under dry conditions led to the formation of diacid dichloride **153**, which then coupled to the previous diamine derivative **114**, affording the macrocycle **cMP** in only 11% yield. Thus, using simple molecular mechanics calculations, which are convenient for our purpose, we model the compound structure for macrocycle **cMP** (**Figure 7.3**).

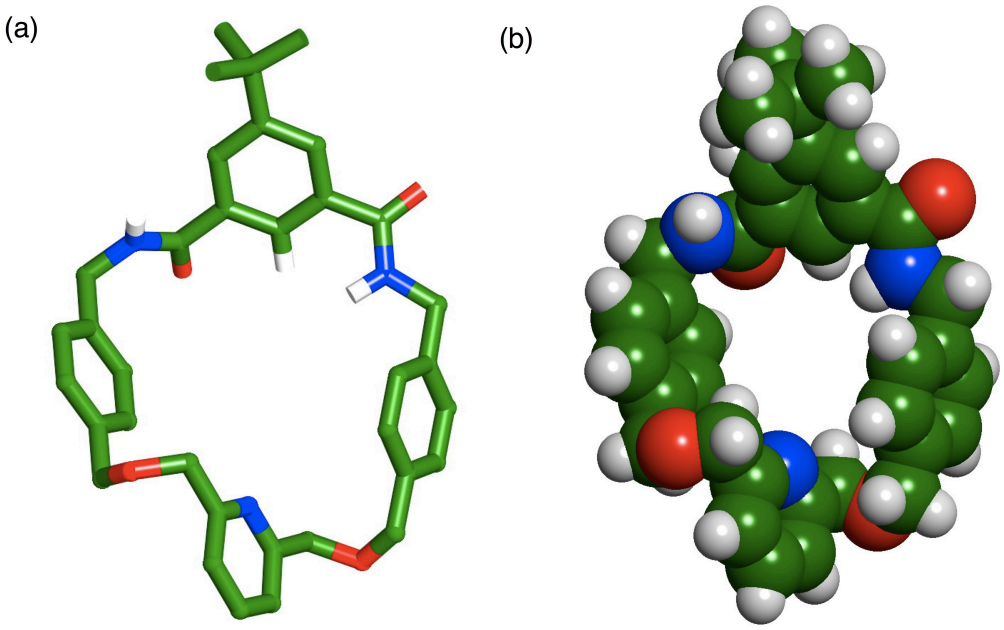

Figure 7.3. (a) Stick representation and (b) space filling model of the calculated structure (OPLS2005, GB/SA $CHCl_3$) of two preferable conformation of macrocycle **cMP**. Carbon atoms are coloured green, oxygen atoms red, nitrogen atoms are coloured blue and hydrogen atoms are coloured white (most hydrogen atoms has been removed for clarity).

It is important to note that the yield of both cyclization step for macrocycle **cMDG** and **cMP** is significantly lower than their parent macrocycles, **MDG** (34%) and **MP** (22%), when the reactions were carried out in dichloromethane (4% yield). As might be expected, the possibility of the nucleophilic attack in the amide bond formation step is relatively minimal in high dilution synthesis, but the use of the isophthalolyl building block further diminishes the efficiency of the ring closure step. The question arose, however as to whether the coordination of the pyridine nitrogen in the upper fragment was necessary for pseudorotaxane formation to occur.

Our preceding report[200] on the formation of **MDG** and **MP** reveals the two hydrogen atoms of the amides and the electron pair of the pyridine nitrogen of the upper fragment of the macrocycle point into the interior of the macrocycle. In contrast to benzene, the electron density of the pyridine ring is not evenly distributed over the ring, reflecting the negative inductive effect of the nitrogen atom. For this reason, pyridine has a large dipole moment, which importantly influences the formation of the amide bond between the acid chloride and the amine. After the formation of the first amide bond, the other set of the acid chloride is in ideal position to aid the following nucleophilic attack and close the ring. The possible mechanism of the ring closure is depicted in **Figure 7.4**.

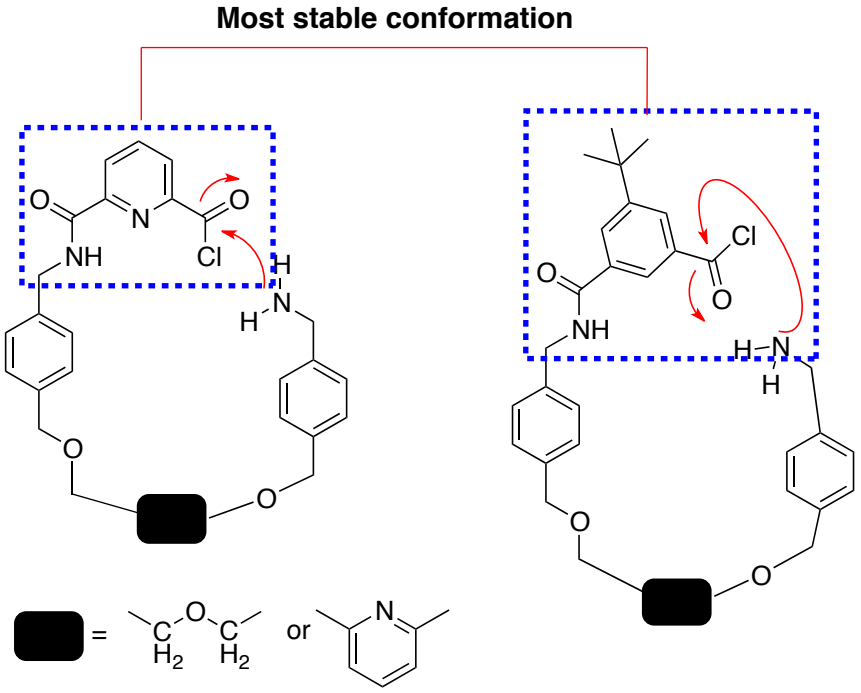

Figure 7.4. Possible mechasim of the ring closure forming macrocycle, in comparison for (a) macrocycle **MDG** or **MP** and (b) macrocycle **cMDG** or **cMP.**

On that account, we considered another option, in which we carried out the ring closure step in THF. This approach is inspired from our observation from the single crystals[200] structure solution of macrocycle **MP** in THF and cyclohexane, which reveals that the molecular structure crystallise with a molecule of THF located within its cavity, whereas the THF oxygen is now acting as hydrogen bond acceptor with N•••O distances calculated as 3.06 Å and 3.10 Å (**Figure 7.5**).

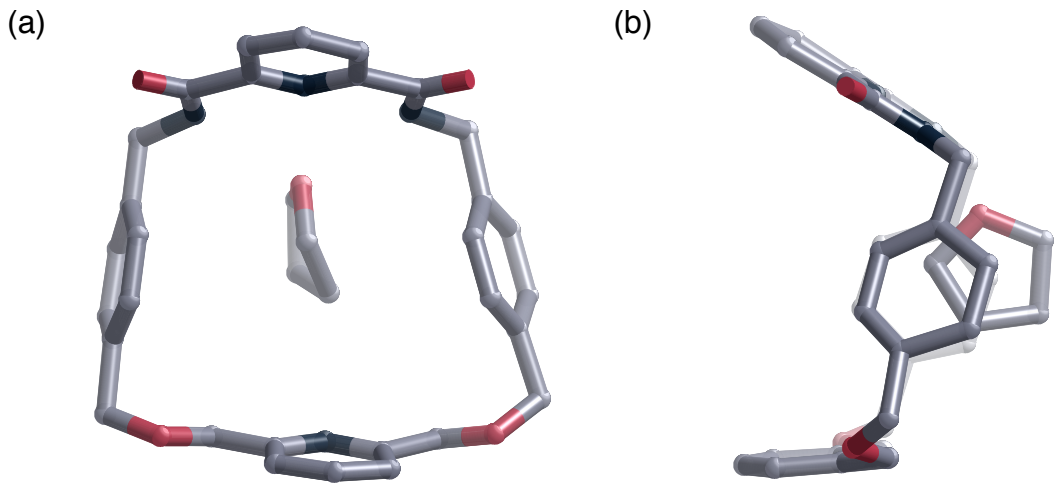

Figure 7.5. Stick representation of macrocycle **MP** molecular structure (a) face and (b) side views in the solid state as determined by single crystal X-ray diffraction. A molecule of solvent (THF) is present within the cavity of the macrocycle. Carbon atoms are coloured grey, oxygen atoms red and nitrogen atoms blue. Figure taken from reference 200.

This evidence supported the idea that in the presence of THF, it can act as template as well as the solvent in the high dilution synthesis and hence, a ring closure for both macrocycles is at least possible, albeit in the poor yield. Additionally, the representation of the molecular structure for macrocycle **cMDG** (**Figure 7.2a**) and **cMP** (**Figure 7.3a**) reveals that their cavities are substantially larger than the parent macrocycles as a result of the absence of nitrogen atom in the upper fragment of their frameworks. On that account, the necessity to provide a larger stopper groups in order to accommodate the formation of stable interlocked products is crucial and has later proven to be strenuous. Besides that, the ability of these control macrocycles to complex with the potential guests is quantitatively tested in the following section.

7.3 Binding studies – cMDG and cMP

Additional investigations must be conducted to evaluate the influence of the benzene ring in the framework of both control macrocycles in order to test its ability to complex the guests. In order to address this possibility, the following binding experiments were carried out with long maleimide **109** and CF_3 maleimide **110**. An equimolar mixture of macrocycle **cMDG** and maleimide **109** in $CDCl_3$ was initially prepared and analysed by ^{1}H NMR spectroscopy. Some of the resonances in the 300.1 MHz ^{1}H NMR spectrum of [**cMDG·109**] (see **Figure 7.6a**) are rather broad at 25 ˚C, yet we

observed notable chemical shift changes, which corresponds to the pseudorotaxane formation.

The typical downfield shift (+1.15 ppm) of the macrocycle NH protons H^{8R}, the upfield shift for the macrocycle phenylene protons, H^{11R} and H^{12R} (–0.57 ppm and –0.68 ppm) and the upfield shift for the macrocycle methylene protons H^{14R} (–0.36 ppm) are noted. In addition, we recognized that the CH_3 resonance of maleimide **109** is separated into two sharp resonances, which corresponds to the unbound and bound state of maleimide **109**.

This separation allows us to measure the association constant using the single-point method and we concluded that **cMDG** are capable of binding the maleimide **109** with a K_a value of 190 ± 20 M^{-1} at 25 ˚C in $CDCl_3$. An equimolar mixture of macrocycle **cMDG** and maleimide **110** in $CDCl_3$ was subsequently prepared. The 400.1 MHz ^1H NMR spectrum (**Figure 7.6c**) shows that the exchange resulting from the complexation and decomplexation rate of maleimide **110** is slow on the ^1H NMR chemical shift timescale and exhibits significant changes in chemical shifts upon the pseudorotaxane formation.

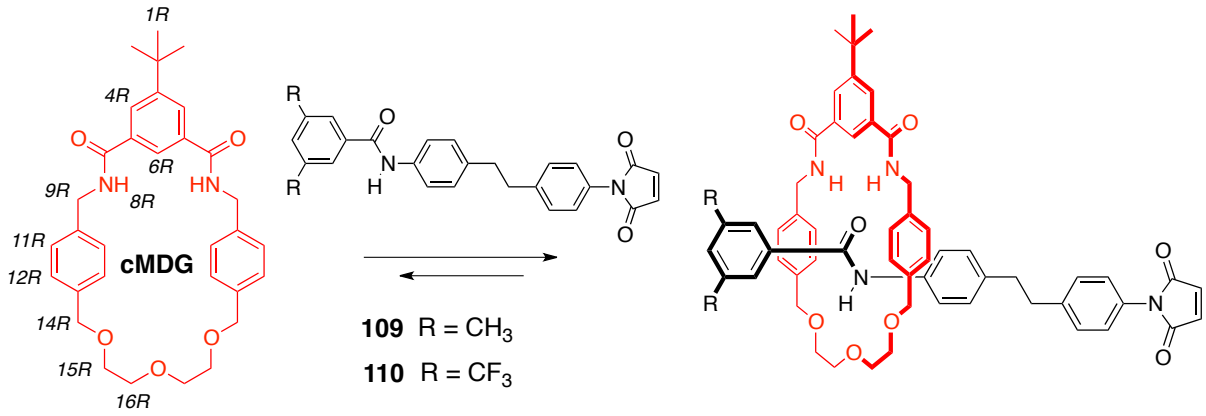

i. Chemical shift data for (a) [**cMDG·109**]

Proton resonances	$\delta_{unbound}$	δ_{bound}	$\Delta\delta$
NH^{8R}	6.39	7.54	+1.15
$H^{11R}+H^{12R}$	7.30	6.73	−0.57
		6.62	−0.68
H^{14R}	4.51	4.15	−0.36
H^{4R}	8.08	8.36	+0.34

ii. Chemical shift data for (c) [**cMDG·110**]

Proton resonances	$\delta_{unbound}$	δ_{bound}	$\Delta\delta$
NH^{8R}	6.39	7.17	+0.78
$H^{11R}+H^{12R}$	7.30	6.77	−0.53
		6.61	−0.69
H^{14R}	4.51	4.12	−0.39
H^{4R}	8.08	8.36	+0.28

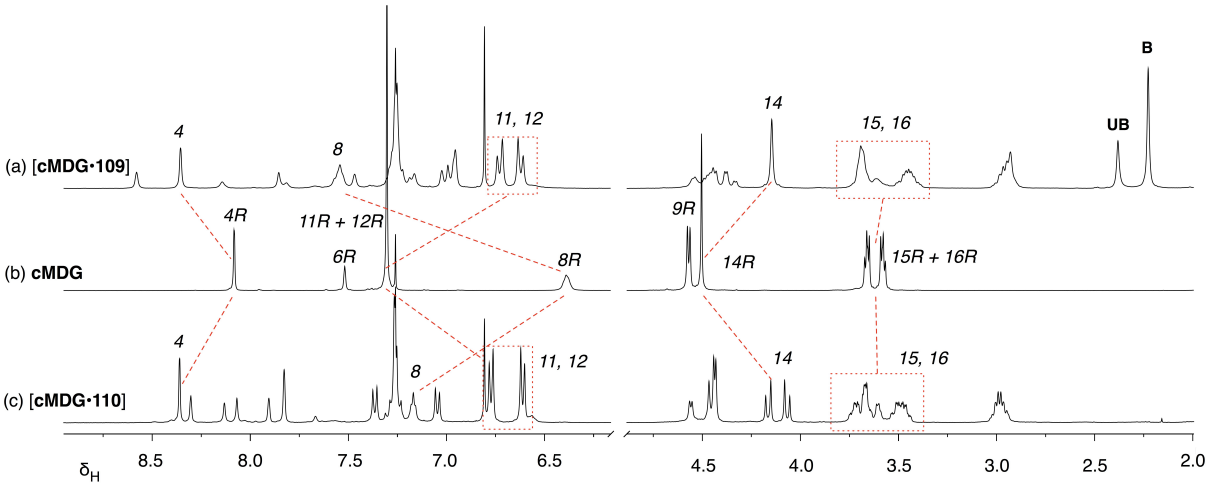

Figure 7.6. Partial ^{1}H NMR spectra (300.1 MHz, 25 ˚C, $CDCl_3$, 20 mM) of (a) an equimolar mixture of macrocycle **cMDG** and maleimide **109** (b) macrocycle **cMDG** and (c) an equimolar mixture of macrocycle **cMDG** and maleimide **110**. R stands for ring component and in this case the macrocycle **cMDG**. Red dashed lines are shown to connect resonances for specific protons in bound and unbound states. **UB** stands for unbound species and **B** corresponds to bound species. ($\Delta\delta = \delta_{unbound} - \delta_{bound}$).

The resonance arising from the macrocycle NH protons, H^{8R}, is again moved downfield (+0.78 ppm) as a result of the hydrogen bonding between these protons and the carbonyl group of the maleimide **110** and the characteristic upfield shifts of the macrocycle phenylene protons, H^{11R} and H^{12R} (–0.53 ppm and –0.69 ppm) residing in the shielding zone of an aromatic ring. Moreover, the macrocycle methylene protons H^{14R} (singlet at δ_H 4.51 in the free macrocycle) give rise to an AB system at δ_H 4.12. From the ^{19}F NMR spectroscopy (376.5 MHz), the association constant for [**cMDG•110**] complex was estimated to be 1000 ± 100 M^{-1} at 25 ˚C in $CDCl_3$.

The next step is to conduct the similar binding experiment in the presence of macrocycle **cMP**. An equimolar mixture of macrocycle **cMP** and maleimide **109** was prepared and analysed by ^1H NMR spectroscopy. The 300.1 MHz ^1H NMR spectrum, (see, **Figure 7.7a**) shows that the [**cMP•109**] complex is near to a slow exchange process and we also observed the corresponding downfield shift of the macrocycle NH protons, H^{8R} (+1.29 ppm) and the upfield shifts of the macrocycle phenylene protons, H^{11R} and H^{12R} (–0.41 and –0.56 ppm, respectively). The association constant for the complexation of [**cMDG•109**] are determined similarly using the ^1H NMR single-point method and obtained a K_a value of 160 ± 20 M^{-1}.

Binding experiment was performed next with maleimide **110**. The 400.1 MHz ^1H NMR spectrum of an equimolar mixture of macrocycle **cMP** and guest **110** in $CDCl_3$ (**Figure 7.7c**) again displays a slow exchange process on the ^1H NMR chemical shift timescale. The resonances arising from NH^{8R} is shifted downfield (+0.95 ppm), and the upfield shifts for both H^{11R} and H^{12R} (–0.49 and –0.56 ppm) are comparable with earlier observation in the presence of macrocycle **cMDG**. The macrocycle methylene protons resonances H^{9R}, H^{14R} and H^{15R} are rendered magnetically inequivalent as a consequence of the unsymmetrical nature of maleimide **110**, leading to distinct complex patterns. The association constant for [**cMP•110**] complex was estimated to be 460 ± 50 M^{-1} by ^{19}F NMR spectroscopy (376.5 MHz) at 25 ˚C in $CDCl_3$.

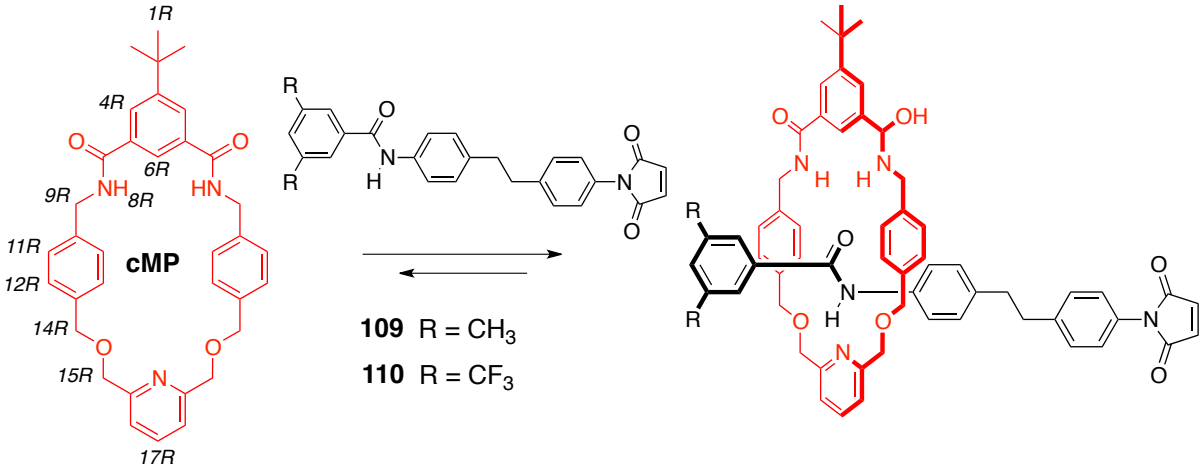

i. Chemical shift data for (a) [**cMP•109**]

Proton resonances	$\delta_{unbound}$	δ_{bound}	$\Delta\delta$
NH^{8R}	6.41	7.70	+1.29
$H^{11R}+H^{12R}$	7.30	6.89	–0.41
		6.74	–0.56
H^{4R}	8.07	8.37	+0.30

ii. Chemical shift data for (c) [**cMP•110**]

Proton resonances	$\delta_{unbound}$	δ_{bound}	$\Delta\delta$
NH^{8R}	6.41	7.36	+0.95
$H^{11R}+H^{12R}$	7.30	6.81	–0.49
		6.74	–0.56
H^{4R}	8.07	8.38	+0.31

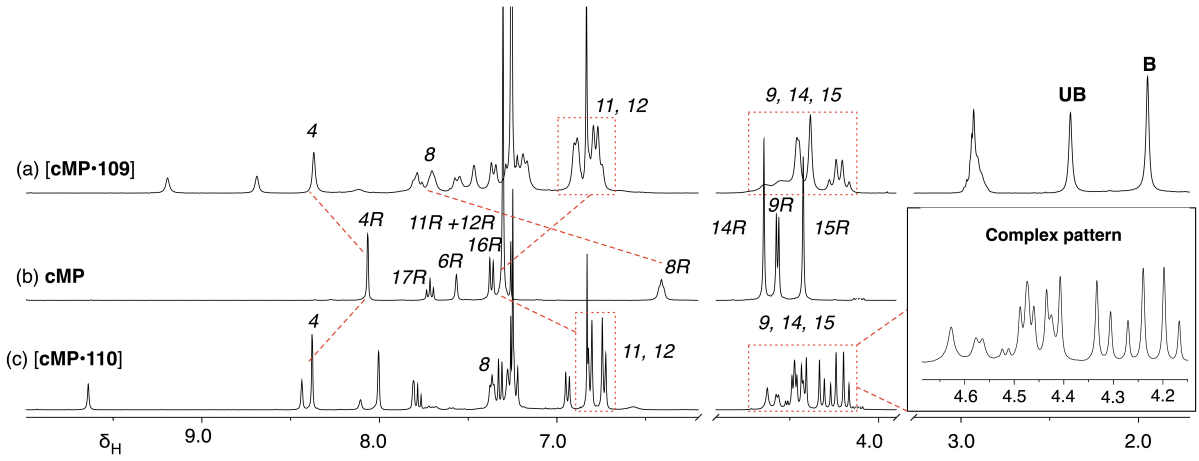

Figure 7.7. Partial ^{1}H NMR spectra (300.1 MHz, 25 °C, $CDCl_3$, 20 mM) of (a) an equimolar mixture of macrocycle **cMP** and maleimide **109** (b) macrocycle **cMP** and (c) an equimolar mixture of macrocycle **cMP** and maleimide **110**. R stands for the ring component and in this case, the macrocycle **cMP**. Red dashed lines are shown to connect resonances for specific protons in bound and unbound states. **UB** stands for unbound species and **B** corresponds to bound species. ($\Delta\delta = \delta_{unbound} - \delta_{bound}$).

We realised that the association constant, K_a for [**cMDG•110**] complex is identical to its parent pseudorotaxane [**MDG•110**] (see **Table 4.2**). However, in the presence of **cMP**, the value deteriorated to 460 M^{-1} ± 50 M^{-1} when compared to macrocycle **MP** (see **Table 4.3**), which attributed to only lower fragments of the macrocycle participating in the binding event. We reasoned that the new cavity of **cMP** is responsible for the insufficient preorganisation of maleimide **110** as a result of the loss of rigidity of the parent macrocycle **MP**. The outcomes for the binding experiments are summarized in **Table 7.1**.

Table 7.1. Binding assessments conducted with control macrocycle **cMDG** and **cMP**. The ^{1}H NMR spectrum of the macrocycle and guest showed complex is in slow exchange (**S**) that can be attributed to significant binding events, compared to the free species observed in isolation. In the case of slow exchange, the K_a was determined using the single-point method (#) either by ^{1}H NMR or ^{19}F NMR resonance (Relaxation time, d_1 is 6 sec). The concentration used was 20 mM in $CDCl_3$ at 25 ˚C unless otherwise stated.

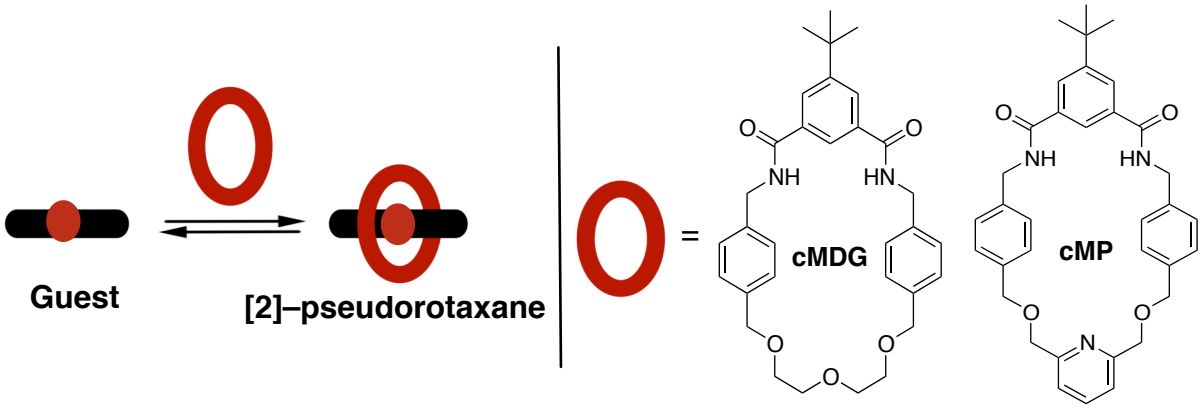

Maleimide guest	K_a / M^{-1} (cMDG)	K_a / M^{-1} (cMP)
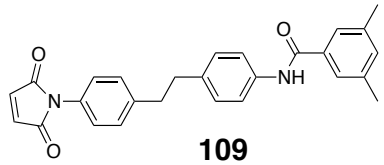 **109**	S # K_a = 190 ± 20	S # K_a = 160 ± 20
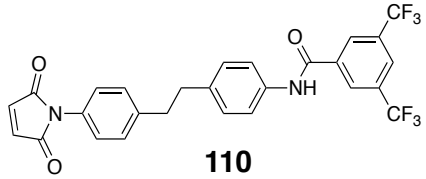 **110**	S # K_a = 1000 ± 100	S # K_a = 460 ± 50

7.4 Synthesis of a potential self-replicating rotaxane

Accordingly, a new scheme of a potential self-replicating rotaxane is envisaged utilizing both macrocycle **cMDG** and **cMP** (**Scheme 7.3**). Given that previous experimental results obtained, the initial design involved the use of CF_3 maleimide **110** and nitrone **115**, which incorporates 4,6-dimethyl substituted and *tert*-butyl ring acted as a blocking group that are sufficiently large to prevent the complexation of these macrocycles with two possible binding sites in nitrone building blocks as well as prohibiting the ring from slipping over the thread backbone.

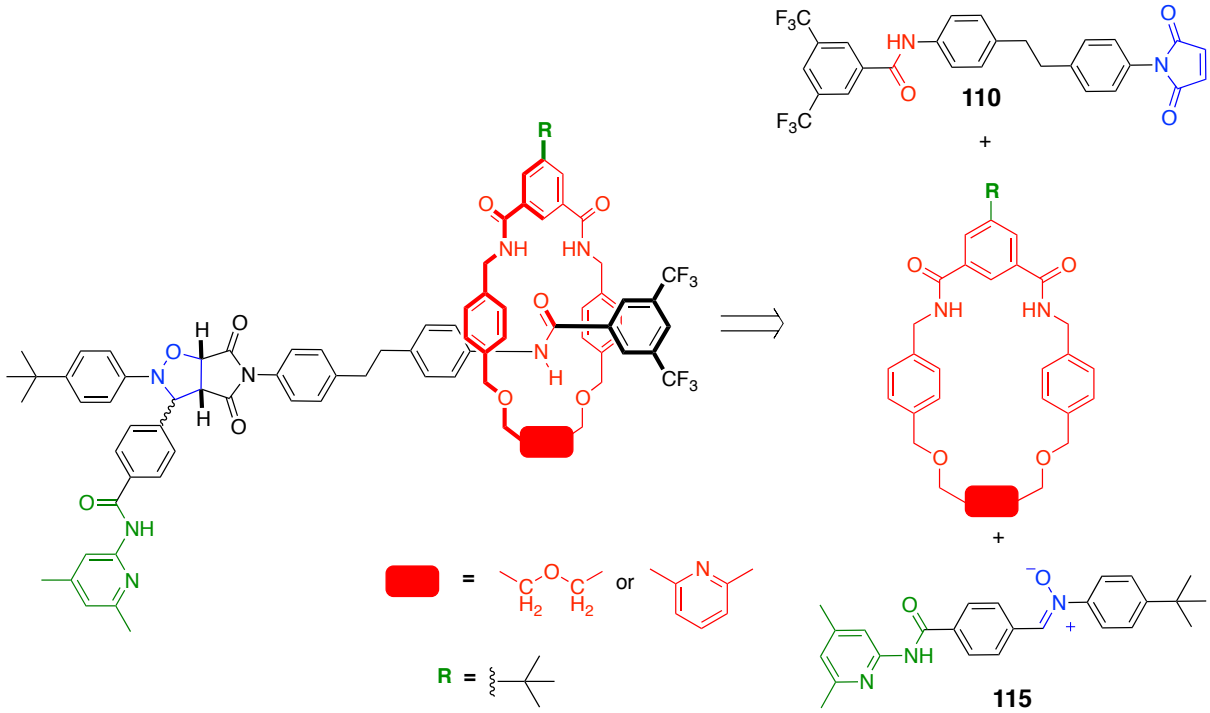

Scheme 7.3. Retrosynthesis of a potential self-replicating rotaxane consists of control macrocycle (**cMDG** or **cMP**), CF_3 maleimide **110** and nitrone **115**.

7.5 Synthesis of acid recognition macrocycles

The third generation of macrocycles consists of carboxylic acid recognition site appended on variable length spacer are shown in **Figure 7.8**, from having no spacer to alkyne spacer and further integrate either the phenyl ring or an alkyne to maximise the length of the spacer. Despite that, due to synthetic difficulties, we managed to explore two variable spacer lengths, namely the alkynyl phenyl and phenyl ring. The key intermediate in this synthesis is the formation of iodophenyl and bromophenyl macrocycles, which helps to facilitate the Suzuki and Sonogashira coupling, respectively in later stage.

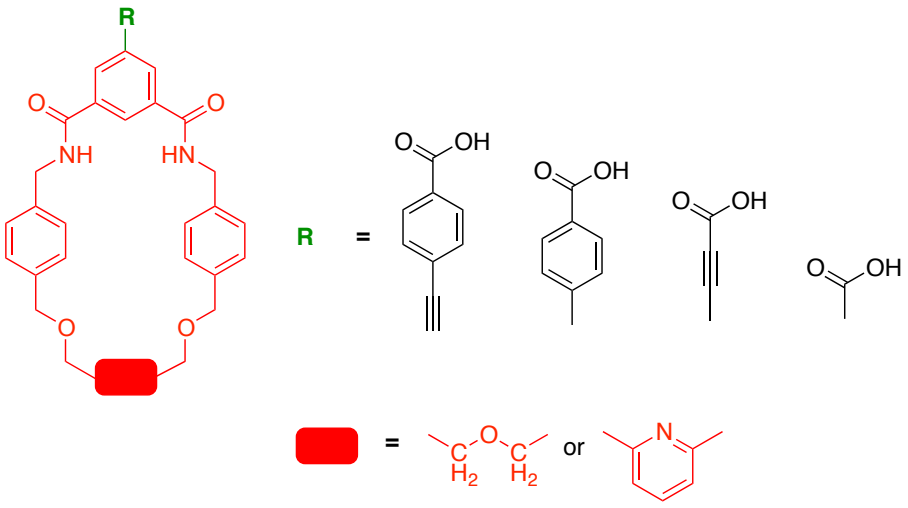

Figure 7.8. Spacer of different lengths that replaced the *tert*-butyl group on the macrocycle.

In order to prepare compound **157** (**Scheme 7.4**), amino diacid **154** was treated with sodium nitrate in concentrated HCl at 0 ˚C for an hour before the addition of potassium iodide to afford compound **155** in a yield of 44%.

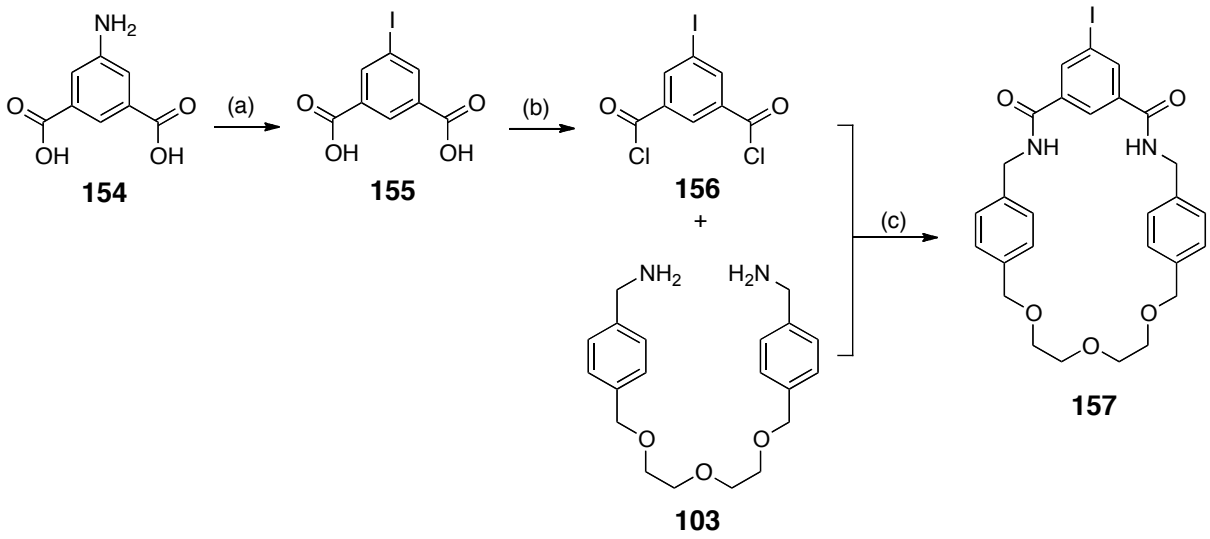

Scheme 7.4. Synthesis of iodophenyl glycol macrocycle **157**. Reagents and yields: (a) $NaNO_2$ (aq.), HCl (conc.), 0 ˚C, 1 h followed by KI neat, rt, 18 h, 44%; (b) $SOCl_2$, DMF, 100 ˚C, 48 h, 98%; (c) Et_3N, THF, rt, 3 days, 21%.

Compound **155** was subsequently treated[243] with thionyl chloride to give the corresponding acid dichloride derivative **156** and further reacted with the prepared intermediate diamine **103** in high dilution synthesis. The condensation between diamine compound **103** and acid dichloride **156** leads to the formation of iodophenyl glycol macrocycle **157**, which contain identical internal cavity as control macrocycle **cMDG**. Purification by flash column chromatography led to the isolation of iodophenyl

glycol macrocycle **157** in 21%. Following that, we prepared the iodophenyl pyridine macrocycle **158** in 18% yield after the purification (**Scheme 7.5**).

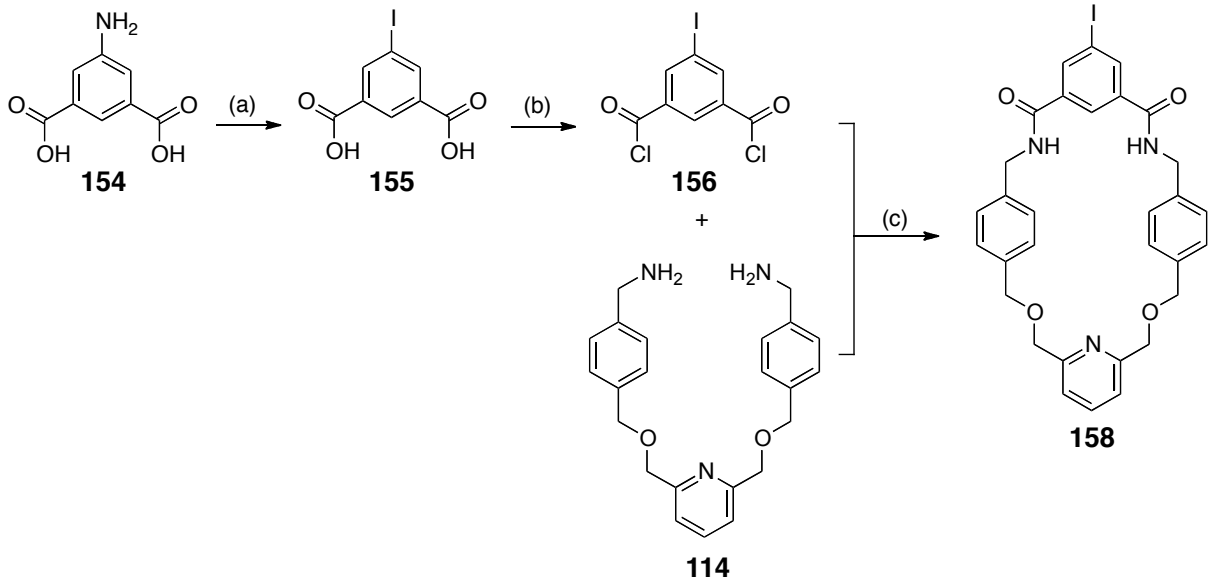

Scheme 7.5. Synthesis of iodophenyl pyridine macrocycle **158**. Reagents and yields: (a) $NaNO_2$ (aq.), HCl (conc.), 0 ˚C, 1 h followed by KI neat, rt, 18 h, 44%; (b) $SOCl_2$, DMF, 100 ˚C, 48 h, 98%; (c) Et_3N, THF, rt, 3 days, 18%.

In order to replace the inefficient Sandmeyer reaction in preparing compound **155**, we become interested in assembling analogous bromophenyl macrocycle in two consecutive steps by using the commercially available bromoacid **159**.

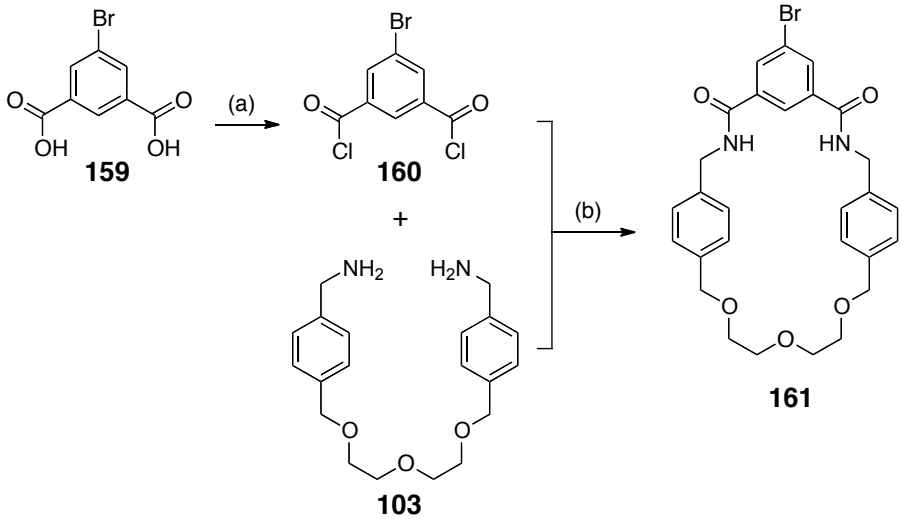

Scheme 7.6. Synthesis of bromophenyl glycol macrocycle **161**. Reagents and yields: (a) $SOCl_2$, DMF, 100 ˚C, 6 h, 98%; (b) Et_3N, THF, rt, 3 days, 8%.

In the first step, we prepared the diacid dichloride **160** and coupled with the diamine intermediate **103** to give 8% yield of bromophenyl glycol macrocycle **161** under the

same conditions. Despite the fact that the yield is very poor, this route supplied a sufficient amount of material to conduct the following experiments (**Scheme 7.6**). In common with the cyclisation of **156**, treatment of dichloride **160** with amine **114** afforded limited amount of macrocycle **162** and significant quantities of other acyclic oligomeric and polymeric products (**Scheme 7.7**).

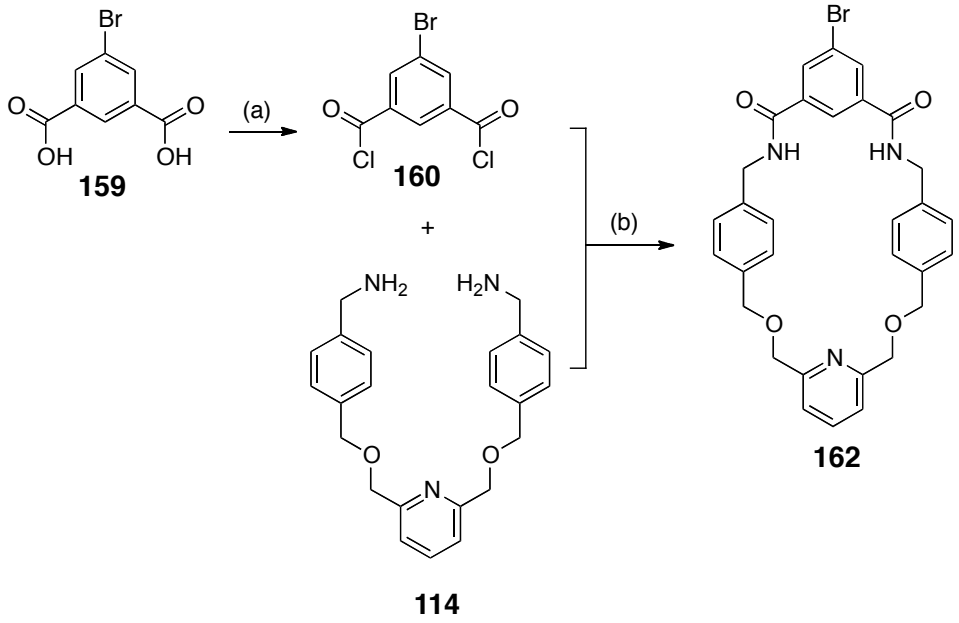

Scheme 7.7. Synthesis of bromophenyl pyridine macrocycle **162**. Reagents and yields: (a) $SOCl_2$, DMF, 100 ˚C, 6 h, 98%; (b) Et_3N, THF, rt, 3 days, 8%.

The advantageous of using the commercial 5-bromoisophthaloyl acid **159** to assist the cyclization of the corresponding bromophenyl macrocycles **161** and **162** was hampered by the poor conversion and, hence, the overall yield to furnish both iodophenyl and bromophenyl macrocycles are only 8% yield. Therefore, these poor yields again corroborated our postulation on the possible mechanism of the ring closure for analogous isophthaloyl macrocycles (**Figure 7.4**). It seems that the folding of the uncyclized oligomeric precursors of macrocycle into an ideal position to influence the formation of the second amide bonds, were enforced by highly unfavourable intramolecular interaction. Thus, the presence of a nitrogen atom in the upper fragment of the ring vitally influenced the efficiency of the cyclization processes.

7.5.1 Synthesis of acid recognition macrocycles with ethynylbenzene spacer

The synthesis of macrocycle **AEMDG** was achieved in five steps. The following procedure for the synthesis of terminal alkyne **166** was prepared as described in prior

report[200] in three sequences starting from 4-bromobenzoyl chloride **163**. Reaction with *tert*-butyl alcohol afford[244] the ester **164**. Subsequent Sonogashira coupling reaction with 2,2-dimethyl propargyl alcohol yielded compound **165**. Final removal of the propan-2-ol group with sodium hydroxide in toluene provided the terminal alkyne **166**. The remainder of the synthesis of macrocycle **AEMDG** is outlined in **Scheme 7.8**. A comparable design of macrocycles was also evident in other research groups[245-250].

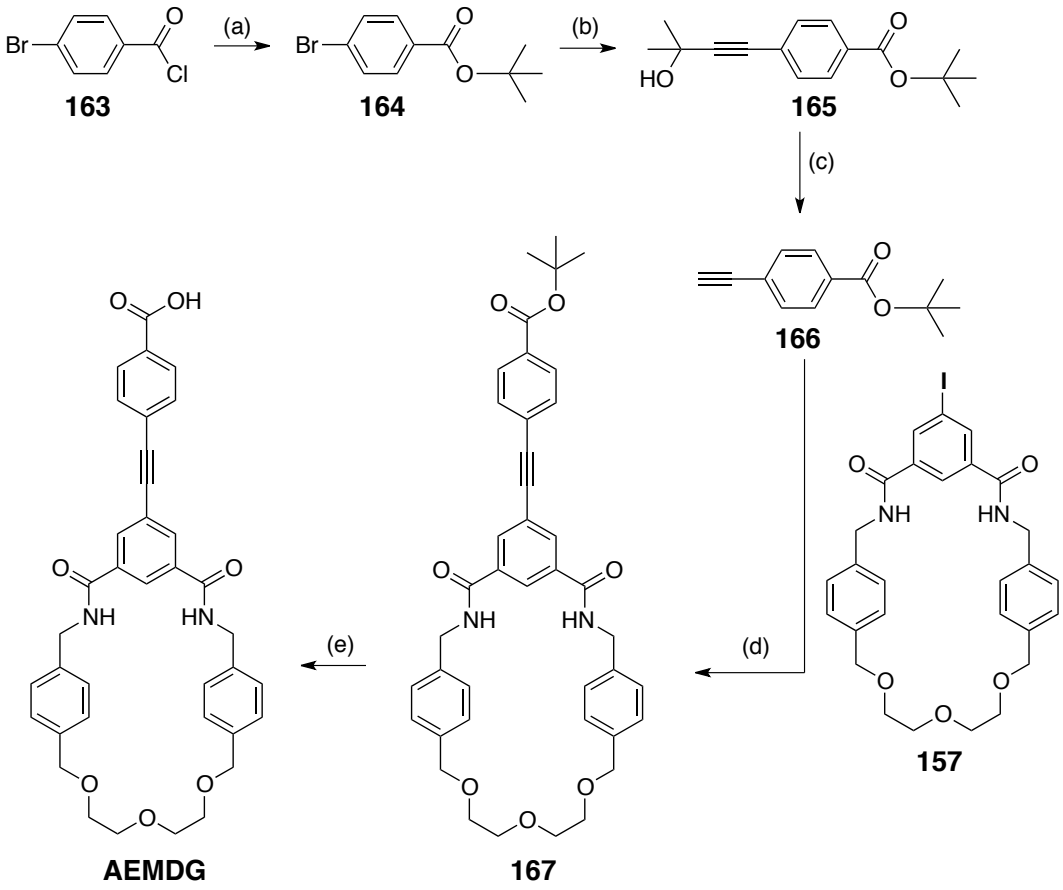

Scheme 7.8. Synthesis of acid macrocycle **AEMDG**. Reagents and yields: (a) *tert*-butyl alcohol, pyridine, CH_2Cl_2, rt, 48 h, 91%; (b) 2,2-dimethylpropargyl alcohol, $PdCl_2(PPh_3)_2$, CuI, PPh_3, Et_3N, THF, 70 ˚C, 48 h, 87%; (c) NaOH, toluene, 120 ˚C, 3 h, 69%; (d) $PdCl_2(PPh_3)_2$, CuI, PPh_3, Et_3N, THF, 60 ˚C, 42 h, 90%; (e) Et_3SiH, TFA/CH_2Cl_2, 0 ˚C to rt, 16 h, 51%.

Iodophenyl glycol macrocycle **157** was coupled to alkyne **166** under standard Sonogashira conditions to give **167**. The ester macrocycle **167** was prepared to allow the study of the non-recognition mediated reaction when one of the recognition sites was blocked. The macrocycle ester **167** was next hydrolysed under the acidic conditions to afford the macrocycle **AEMDG** in 51% yield. Likewise, acid recognition with ethynylbenzene spacer based on pyridine macrocycle, macrocycle **AEMP** was

prepared next. The iodophenyl pyridine macrocycle **158** was coupled with alkyne **166** to afford the ester macrocycle **168** in 72% yield. Treatment of the ester macrocycle **168** with triethylsilane in a mixture of trifluoroacetic acid and dichloromethane afforded the acid recognition macrocycle **AEMP**.

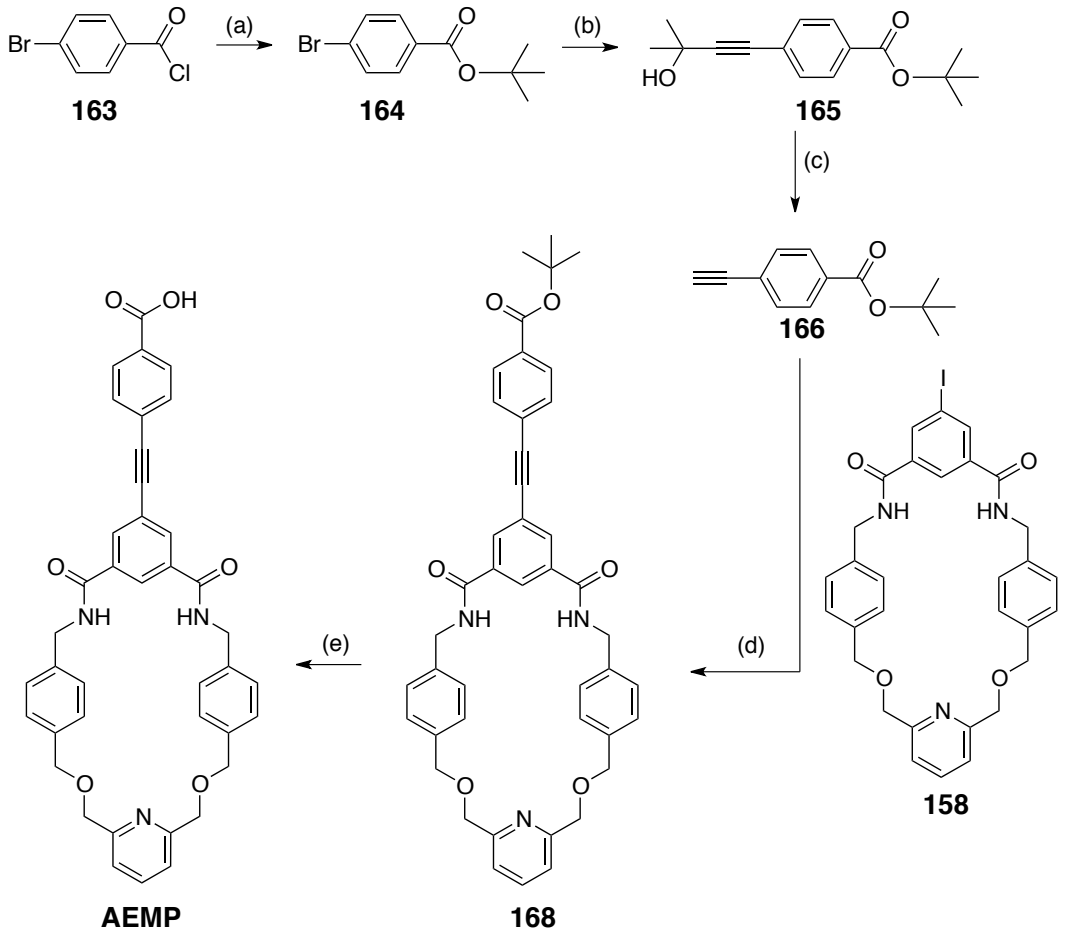

Scheme 7.9. Synthesis of acid macrocycle **AEMP**. Reagents and yields: (a) pyridine, CH_2Cl_2, rt, 48 h, 91%; (b) 2,2-dimethylpropargyl alcohol, $PdCl_2(PPh_3)_2$, CuI, PPh_3, Et_3N, THF, 70 ˚C, 48 h, 87%; (c) NaOH, toluene, 120 ˚C, 3 h, 69%; (d) $PdCl_2(PPh_3)_2$, CuI, PPh_3, Et_3N, THF, 65 ˚C, 48 h, 56%; (e) Et_3SiH, TFA/CH_2Cl_2, 0 ˚C to rt, 16 h, 63%.

7.5.2 Synthesis of acid recognition macrocycles with phenyl spacer

In order to synthesise the acid recognition macrocycle with phenyl spacer, the bromophenyl glycol macrocycle **161** prepared earlier was coupled with 4-(methoxycarbonyl)phenylboronic acid under Suzuki coupling reaction resulting in the intermediate macrocycle **169**. In accordance with the preparation in the literature[251], ester macrocycle **169** was dissolved in THF with potassium trimethyl silanolate. The nucleophilic attack of the trimethylsilanolate anion on the carbon atom of methyl group with carboxylate anion as the leaving group yielded desired acid macrocycle **APMDG** (**Scheme 7.10**).

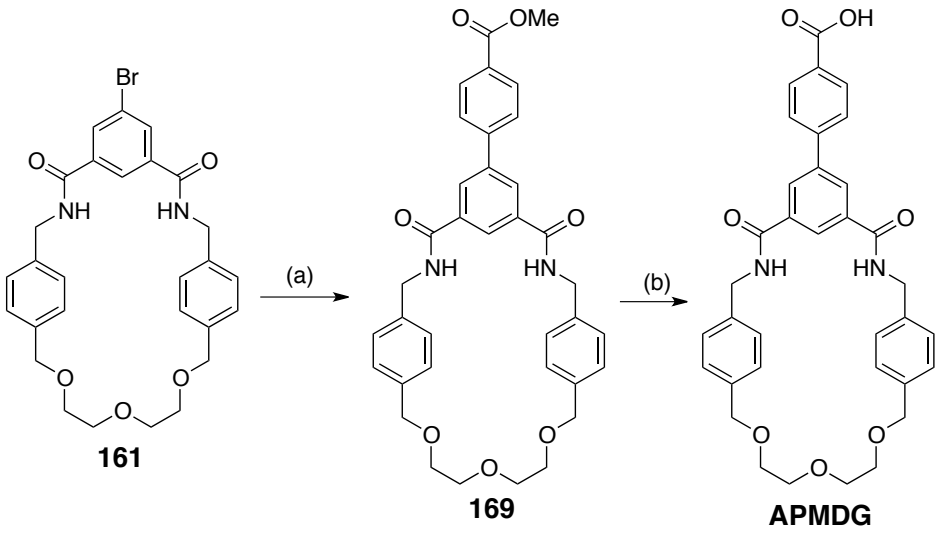

Scheme 7.10. Synthesis of acid macrocycle **APMDG**. Reagents and yields; (a) 4-(methoxycarbonyl)phenylboronic acid, K_2CO_3, $PdCl_2(PPh_3)_2$, THF/H_2O, rt, 16 h, 87%; (b) Me_3SiOK, THF, 75 ˚C, 16 h, 70%.

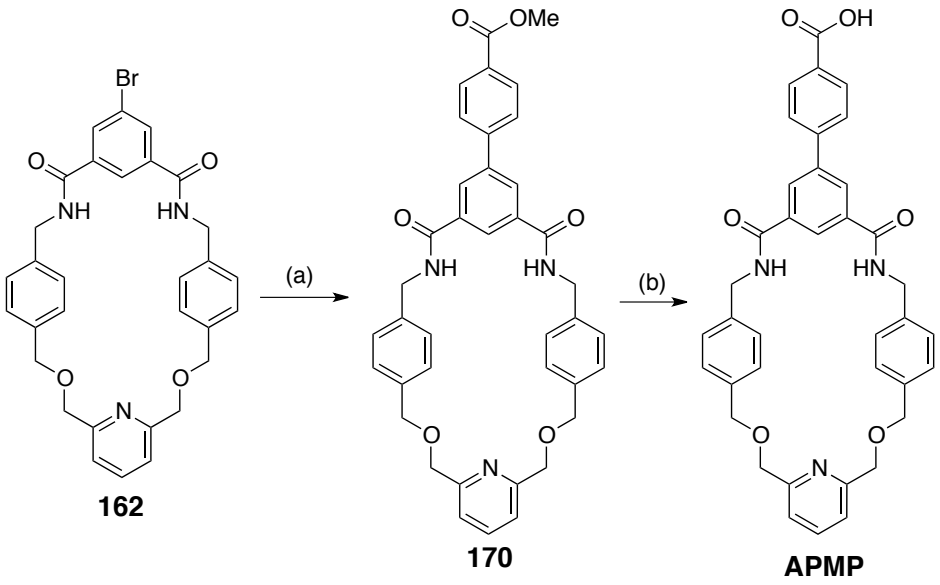

Scheme 7.11. Synthesis of acid macrocycle **APMP**. Reagents and yields; (a) 4-(methoxycarbonyl)phenylboronic acid, K_2CO_3, $PdCl_2(PPh_3)_2$, THF/H_2O, rt, 16 h, 78%; (b) Me_3SiOK, THF, 75 ˚C, 16 h, 76%.

The phenyl spacer analogue based on pyridine macrocycle was similarly constructed. Treatment of the bromophenyl pyridine macrocycle **162** in a Pd-catalysed Suzuki coupling to attach the phenyl spacer on to the ester control macrocycle **170** met with 78% conversion. The methyl ester group was further hydrolysed[251] to furnish acid macrocycle **APMP** in a moderate yield of 63%.

7.6 Binding studies with maleimides

It is clear that we must learn to thread the linear component before we can learn to perform more intricate actions with interlocked molecules in the replication processes (see **Figure 7.9**).

The general structure of the thread molecule has a single blocking group so that when threading is achieved, the particular kind of pseudorotaxane species requires an addition of only one end group to become a rotaxane. In the [2]-pseudorotaxane assembly, the influence of rapid threading and dethreading process is evident and can be discerned from the ^{1}H NMR spectrum. If the exchange between these processes are slow on the ^{1}H NMR chemical shift timescale, the spectrum will contain two populated resonances, v_A and v_B as the intensities of these resonances represents the relative amounts of each species (see **Figure 7.9a**). The linear component now incorporates a maleimide group at one side along with bulky stopper group (green circles) being appended at the other end.

For system in which exchange process is appreciably faster than the ^{1}H NMR chemical shift timescale, the chemical shift is the average, v_M of the individual species chemical shift, that give rise to single populated resonance as a consequence of small end groups on the linear component (denoted by purple circles in **Figure 7.9c)**. However, if both A and B species is in equal concentration, there will be an intermediate exchange, where the separate lines for the two species are no longer distinguishable and give rise to a coalescence resonance as depicted in **Figure 7.9b**.

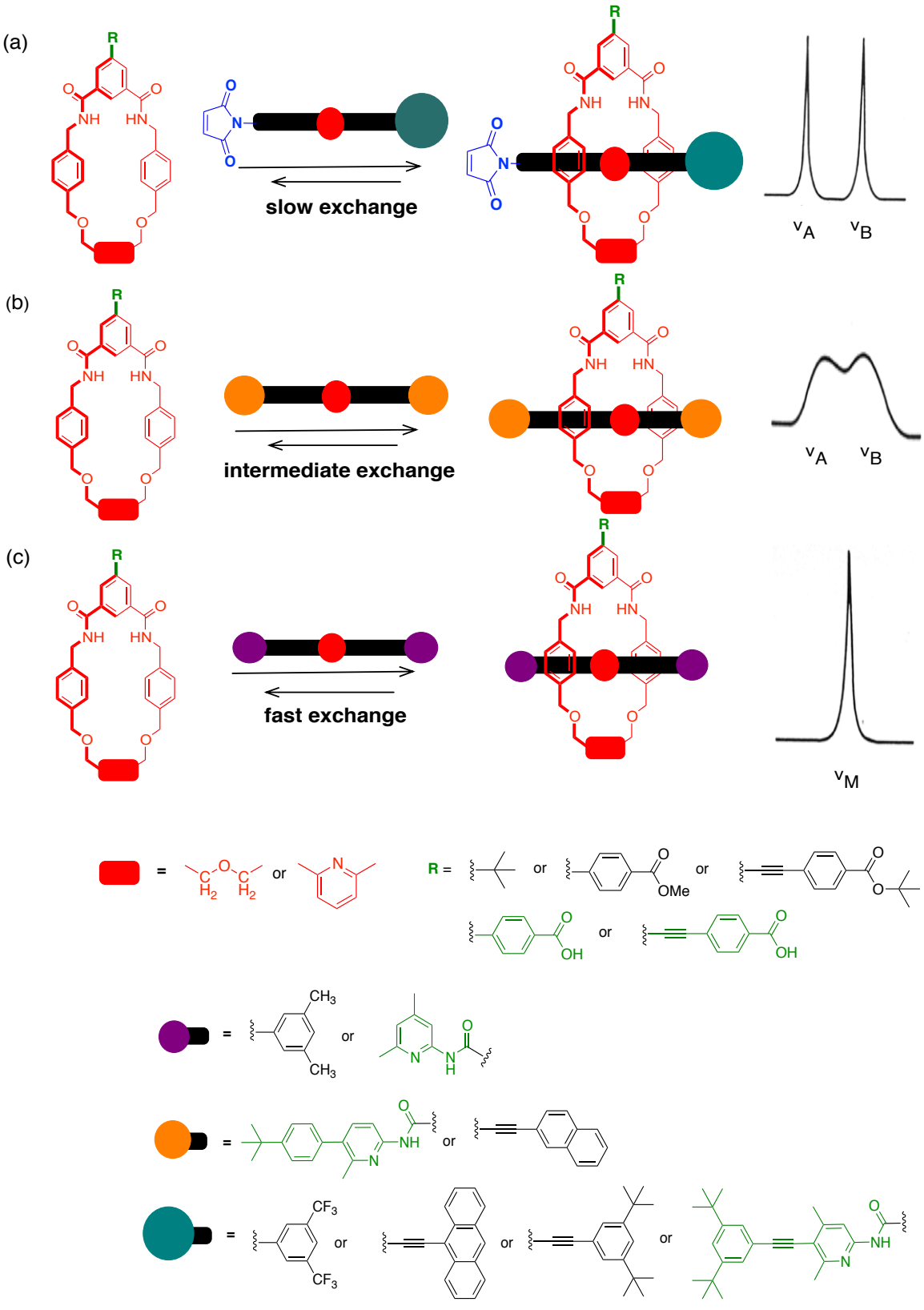

Figure 7.9. Influence of threading and dethreading process in the [2]-pseudorotaxane assembly on ^{1}H NMR spectrum give (a) slow exchange, (b) intermediate exchange or (c) fast exchange. Two resonances (ν_A and ν_B) denoted the single atom signal corresponding to A and B species, respectively. Population of the species corresponds to the relative concentration in the reaction mixture. In the intermediate exchange, the signals observed begin to coalescence. Additionally, for a rapidly exchanging system, the average frequency ν_M, observed is $\nu_M = (\nu_A + \nu_B)/2$.

In more detail, the slow exchange process depicted in **Figure 7.10** highlight the effect of the unsymmetrical nature of the maleimide component. In the free ring, the protons are regarded as chemically and magnetically equivalent, reflecting the existence plane of symmetry in the ring. Nonetheless, in the formation of pseudorotaxane complex, the plane of symmetry in the ring is broken. Consequently, the protons located on the opposite faces of the ring are rendered magnetically inequivalent, giving rise to an AB spin system. The proton α on one face of the macrocycle is directed toward the maleimide, whereas the protons β on the opposing face of the ring is orientated toward the bulky end group. Additional end-to-end asymmetry imposed by the axle component could subsequently leads to complex signal patterns and example of this behaviour was found earlier in **Chapter 4** and also evident in this chapter.

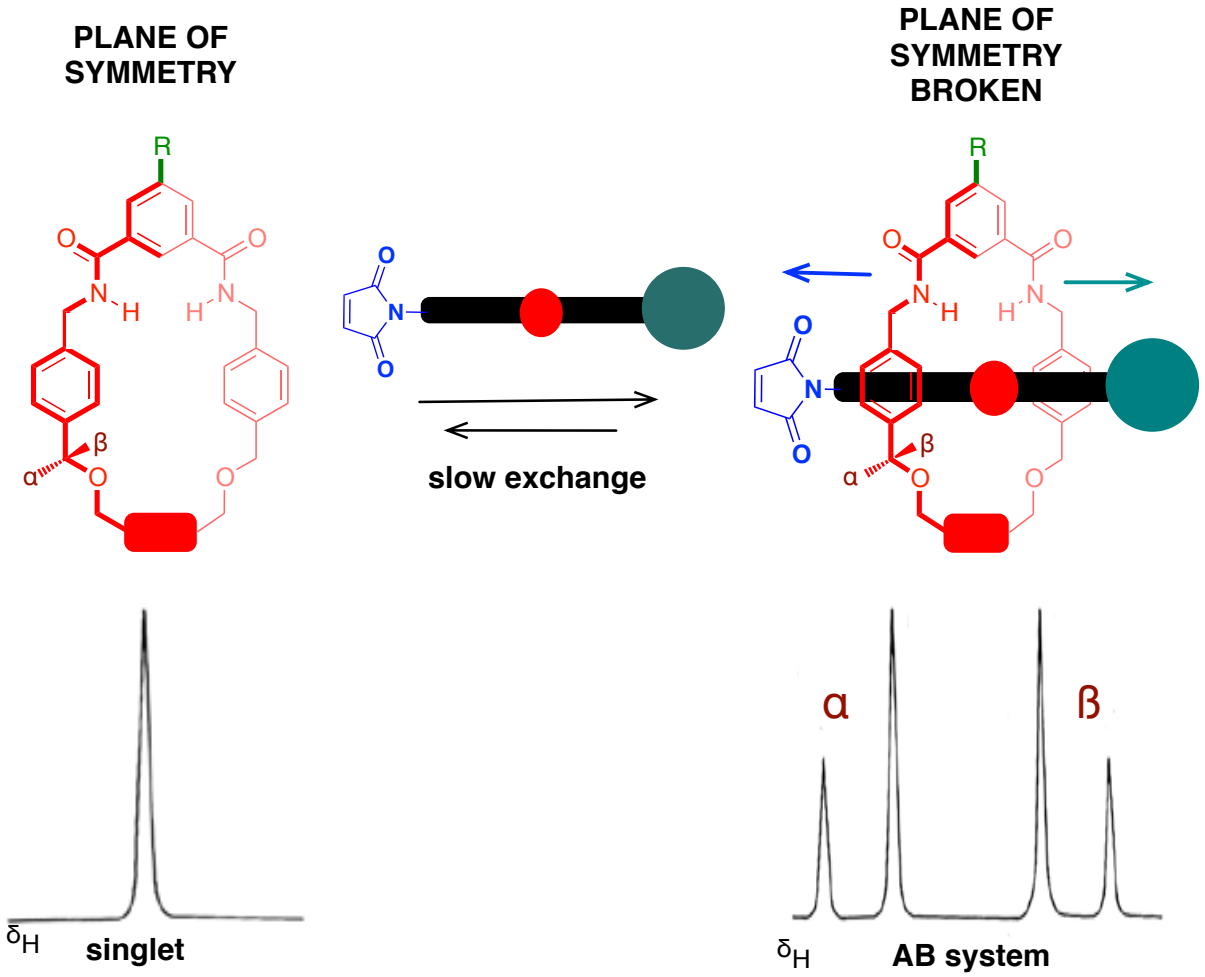

Figure 7.10. The effect of the unsymmetrical nature of the maleimide component as depicted earlier in **Figure 7.9a** upon the assembly of [2]-pseudorotaxane rendered the H_α and H_β of the free ring to be diasterotopic, which results in AB spin system. In the free ring, H_α and H_β are regarded as chemically and magnetically equivalent, giving rise to a singlet resonance.

Various examples[217,252,253] of amide backbones, or side chains threaded through macrocycles have been published. Our own pseudorotaxane based on amide systems have been studied in **Chapter 4** and substantiate the fact that a complementary hydrogen bonding[254,255] between the amide-based macrocycle and the linear amide threading group is a requirement for high yield of the rotaxane and, hence, established the pseudorotaxane as the intermediate of prime importance. Measurement of the effect of substitution on the phenyl ring of the thread component on pseudorotaxane formation[256] reveals the inhibiting effect of electron-donating substituents, which reduced the hydrogen bond donating ability of the threading group. Steric effects due to substitution in other systems[124,257] have also been examined and show that even small changes in steric bulk imposed deleterious effects on pseudorotaxane formation.

Here, we attempt to add answers to simple questions that provide a more complete evaluation of the effects of certain basic structural relationships on the abilities of linear molecules to thread through the cavity of our macrocycles. As in the previous example, the isophthalyl control macrocycles **cMDG** and **cMP**, binds both the CH_3 maleimide **109** and CF_3 maleimide **110**. These promising preliminary results encouraged the subsequent investigation into the assembly of a range of [2]-pseudorotaxanes with newly prepared acid macrocycles.

Based on this knowledge, we reason that the structural analogue acid macrocycles should also afford [2]-pseudorotaxane assemblies using the same maleimide compound. The preparation of new pseudorotaxane was demonstrated by employing the ester macrocycle, namely macrocycle **168** and **169** for solubility reasons and we limit our attention to CF_3 maleimide **110**. Discussion of these results and their significance follows.

Mixing an equimolar solution of ester macrocycle **168** and maleimide **110** in $CDCl_3$ at 25 ˚C reveals approximately 90% threaded species in the solution. The 400.1 MHz ^{1}H NMR spectrum of this mixture indicated that the bound and unbound species equilibrated slowly with respect to one another on the ^{1}H NMR chemical shift timescale. This phenomena allow the determination of the association constant, K_a using the single-point method. However, the overlapping signal hampered these

assignments. ^{19}F NMR spectroscopy (376.5 MHz, $CDCl_3$) was utilized and the concentration of the products were calculated by deconvolution of each of the characteristic resonances, which corresponds to unbound and bound species. The binding constant that quantify the threading of maleimide **110** through macrocycle **168** was determined to be 1270 ± 130 M^{-1} at 298 K.

The chemical shift changes observed are representative of pseudorotaxane formation (**Figure 7.11b**) – a typical downfield shift of the macrocycle NH protons H^{14R} (+0.76 ppm) and upfield shifts of the macrocycle phenylene protons (H^{17R}, H^{18R}) (–0.50 ppm). In addition, the high chemical shift of the NH proton of maleimide **110**, H^{7T} (+1.87 ppm) indicates that the amide group is participating in hydrogen bonding interactions. The binding affinity of the ring for the amide binding site was manifested from the intricate pattern of the proton resonances in the methylene regions (H^{15R}, H^{20R} and H^{21R}) due to the magnetically inequivalent environments. However, these proton resonances are not very well resolved with extra broader peak beneath the H^{15R}, even when the temperature was lowered to 263 K.

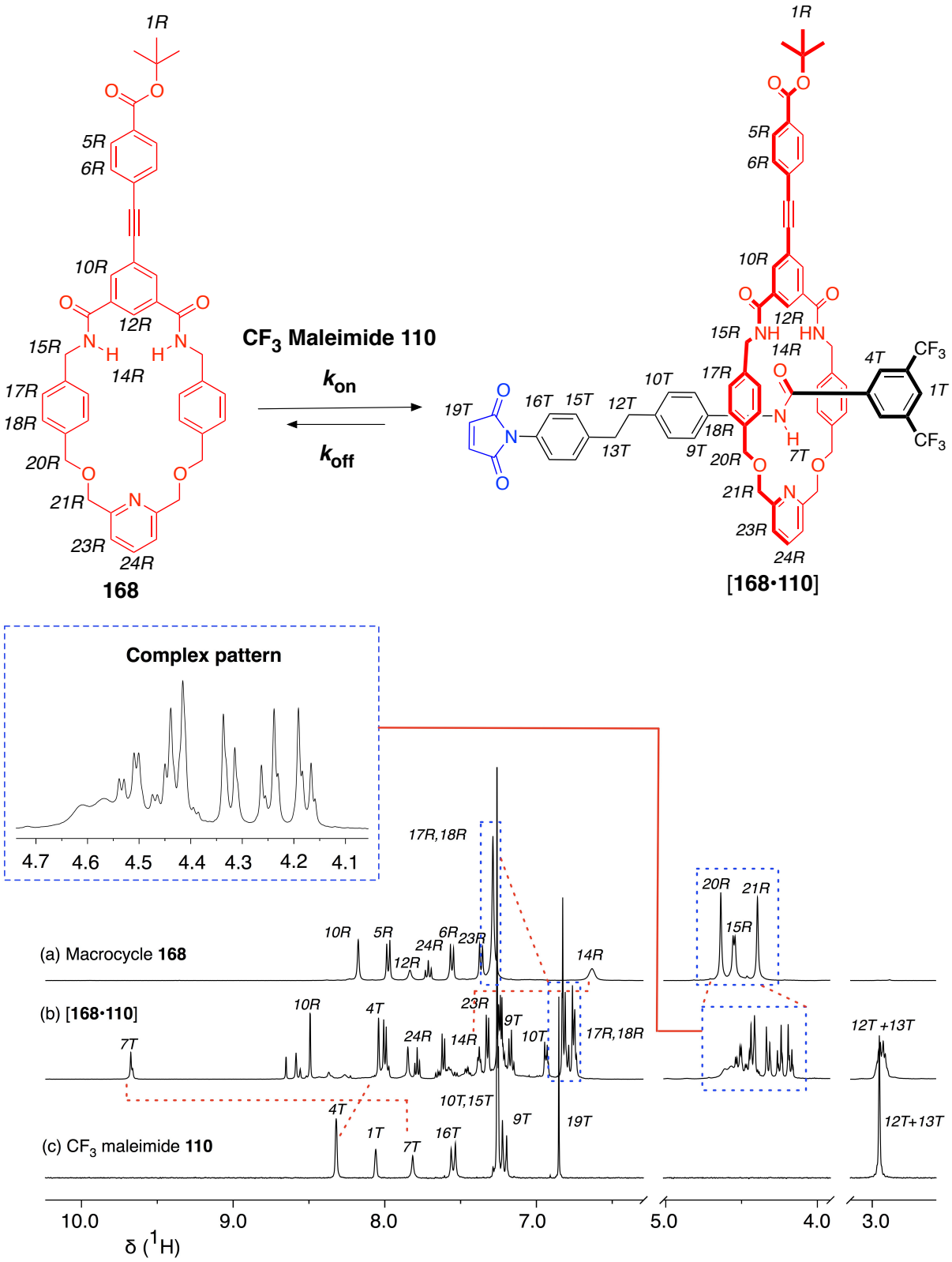

Figure 7.11. Self-assembly of an equimolar mixture of CF_3 maleimide **110** with macrocycle **168** to form the pseudorotaxane complexes [**168•110**]. Partial ^1H NMR spectra (400.1 MHz, $CDCl_3$, 20 mM, 298 K) of (a) Macrocycle **168**, (b) an equimolar mixture of **168** and CF_3 maleimide compound **110** (R corresponds to ring, in this case macrocycle **168** and T denoted as thread, in this case maleimide **110**) and (c) CF_3 maleimide compound **110**. Red dashed lines and blue dashed boxes are shown to connect resonances for specific protons in bound and unbound states.

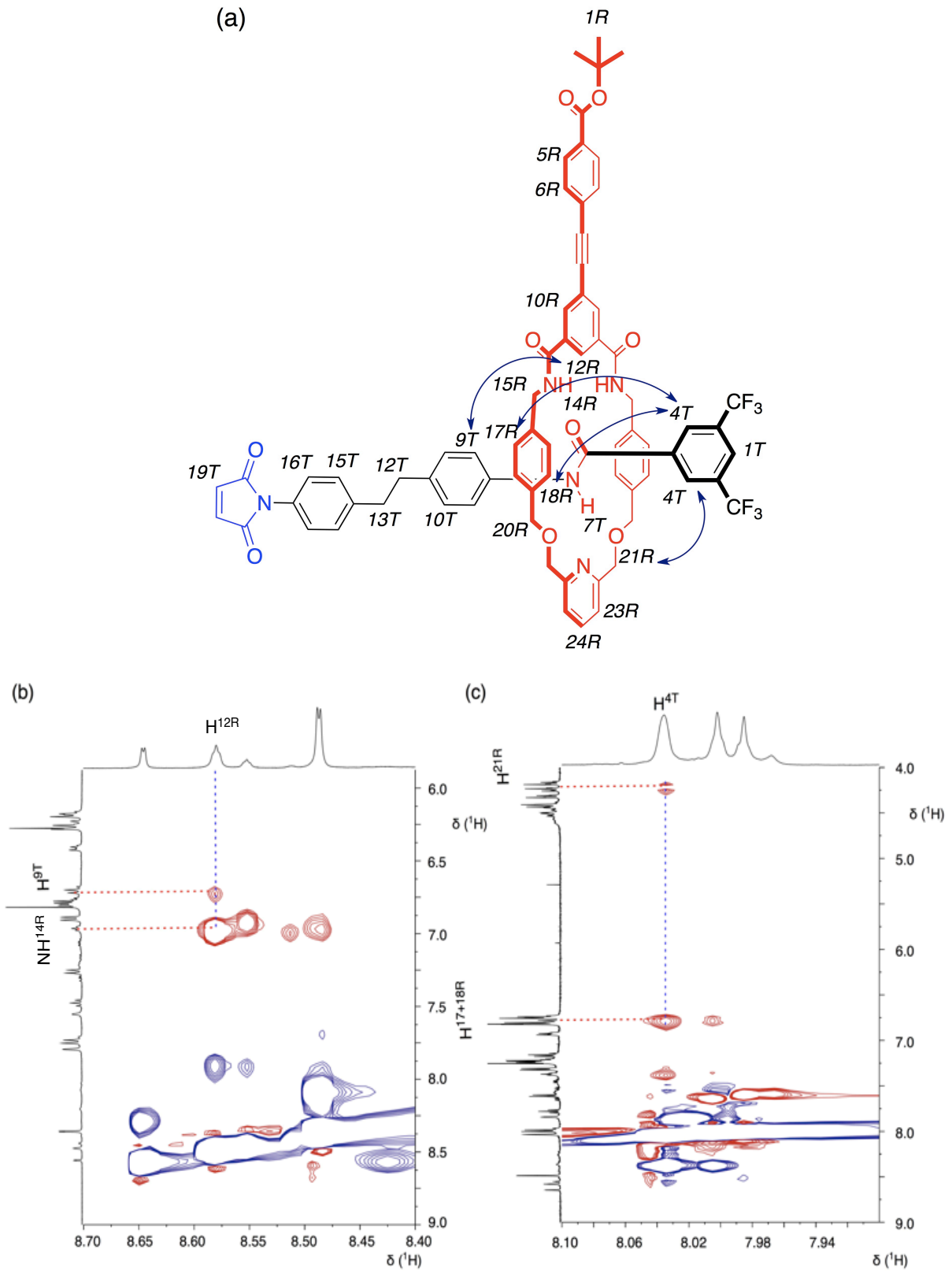

Figure 7.12. (a) The ROESY contacts observed for the complex between macrocycle **168** and maleimide **110** are shown as blue arrows; (b) and (c) Partial 2D ROESY NMR spectra (500.1 MHz, 263 K, $CDCl_3$, 20 mM) display crosspeaks (red points) between macrocycle **168** and maleimide compound **110**.

This broadening resonance resulted from k_{on} and k_{off} being at the same order as the ^{1}H NMR chemical shift timescale. Similar behaviour was noticed for maleimide phenylene protons with concomitant downfield changes, H^{4T} (+0.28 ppm). The structural conformation of the pseudorotaxane complex [**168•110**] was elucidated using the 2D ROESY NMR study at 295 K as shown in **Figure 7.12**. Inspection of the 500.1 MHz 2D ROESY spectra revealed meaningful crosspeaks between the aromatic protons, H^{4T} with macrocycle methylene protons, H^{21R} and subsequently phenylene protons, H^{17R} and H^{18R} (see **Figure 7.12c**). Additionally, the macrocycle isophthaloyl bridge proton H^{12R} also displayed a crosspeak with alternative phenylene proton of maleimide, H^{9T} (see **Figure 7.12b**) confirming the encircling of the macrocyclic component about the amide moiety and therefore the pseudorotaxane has the expected geometry shown in **Figure 7.12a**. However, no apparent crosspeaks were observed with two NH protons of the macrocycle with maleimide **110**.

The subsequent binding experiment utilized macrocycle **169** (**Figure 7.13a**). Upon addition of maleimide **110**, the 400.1 MHz ^{1}H NMR spectrum displays the existence of nearly 80% pseudorotaxane species in the solution at room temperature (not shown). Likewise, the exchange process between bound and unbound state are relatively slow on the ^{1}H NMR chemical shift timescale. The exchange rate between bound and unbound state was sufficiently slow at 263 K (see **Figure 7.13b**) to obtain different sets of resonances for free macrocycle **169**, unbound maleimide **110** and pseudorotaxane complex [**169•110**].

The K_a value for [**169•110**] complex was estimated to be 5500 ± 550 M^{-1} in $CDCl_3$. The formation of the [2]-pseudorotaxane [**169•110**] complex at 263 K give rise to similar spectral result as previously observed with [**168•110**] complex, that exhibited classic downfield shift of NH macrocycle, H^{12R} (δ_H 7.29) and lead to substantial upfield changes in the macrocycle phenylene protons, namely H^{15R} and H^{16R}, which become more resolved and desymmetrized. Additionally, the macrocycle **169** shift upfield towards the 3,5-bis triflurомethyl group of maleimide 110, which is apparent from the shifts of the phenylene proton of maleimide **110**, H^{4T} (–0.53 ppm) and H^{1T} (–0.15 pm), respectively.

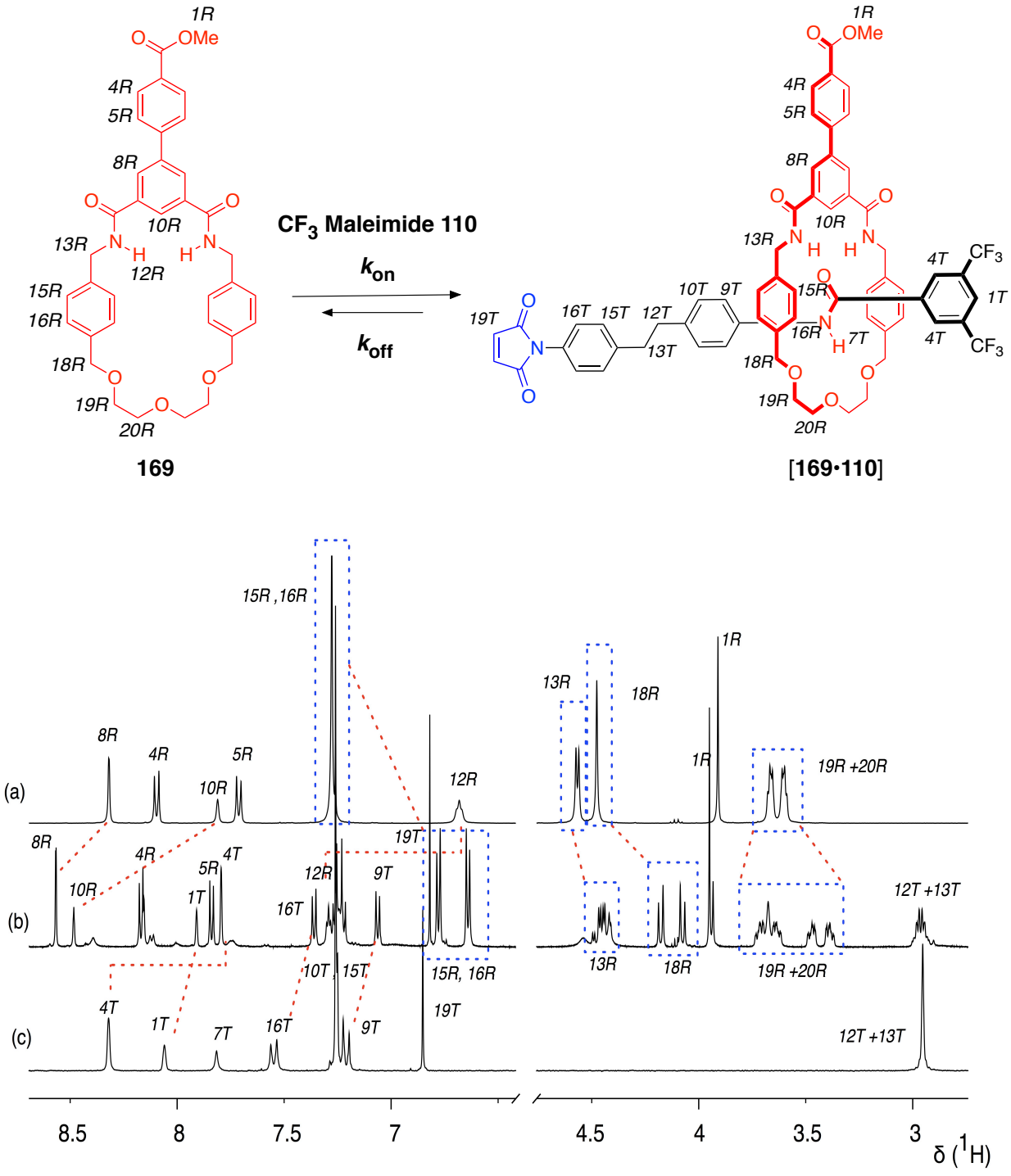

Figure 7.13. Self-assembly of CF_3 maleimide **110** with macrocycle **169** to form the pseudorotaxane [**169•110**] complex. Partial ^{1}H NMR spectra (400.1 MHz, $CDCl_3$, 20 mM) of (a) Macrocycle **169**, (b) an equimolar mixture of macrocycle **169** and CF_3 maleimide compound **110.** (R corresponds to ring, in this case macrocycle **169** and T denoted as thread, in this case maleimide **110**) at 263 K and (c) CF_3 maleimide compound **110**. Red dashed lines and blue dashed boxes are shown to connect resonances for specific protons in bound and unbound states.

The observed changes constituted evidences from the effect of shielding in the core of the aromatic regions of the phenlyene protons, H^{15R} and H^{16R}, which demonstrated that they are participating in the parallel π – π stacking. Furtermore, the visible EXSY crosspeaks within the region of δ_H 7.45 – 7.65 suggests the existence of unbound and bound species in accordance with the exchange process. Protons labelled 13 and 18 on the macrocycle (**Figure 7.13a**) are rendered anisochronous by end-to-end asymmetry inherent in the pseudorotaxane [**169•110**] complex. Consequently, the resonances for these protons appear as AB pattern at 4.45 and 4.25 ppm, respectively (see **Figure 7.13b**). In addition, the previous overlapping signals for the methylene protons of macrocycle **169** H^{19R} and H^{20R} are now dispersed. These observations are consistent with the prior findings in the binding studies of macrocycle **MDG** in **Chapter 4** and **5**.

A section of 500.1 MHz 2D ROESY NMR spectra of the [2]-pseudorotaxane recorded in $CDCl_3$ at 263 K reveals important crosspeaks between the phenylene protons of the ring, H^{15R} and H^{16R} with the maleimide proton, H^{4T} (**Figure 7.14b**). Such interaction could only possibly occur through the vacant amide moiety in a manner shown in **Figure 7.14a**, and thus give rise to the proposed geometry.

With the aim of investigating both the modes of the maleimide binding and its effect have on the solid state packing of these receptors, an attempt was made to grow the crystals for the two pseudorotaxane complexes, [**168•110**] and [**169•110**], using several types of solvents, by growing these complexes using slow diffusion or slow evaporation. Unfortunately, all of these failed to generate suitable crystals for single crystal structure analysis.

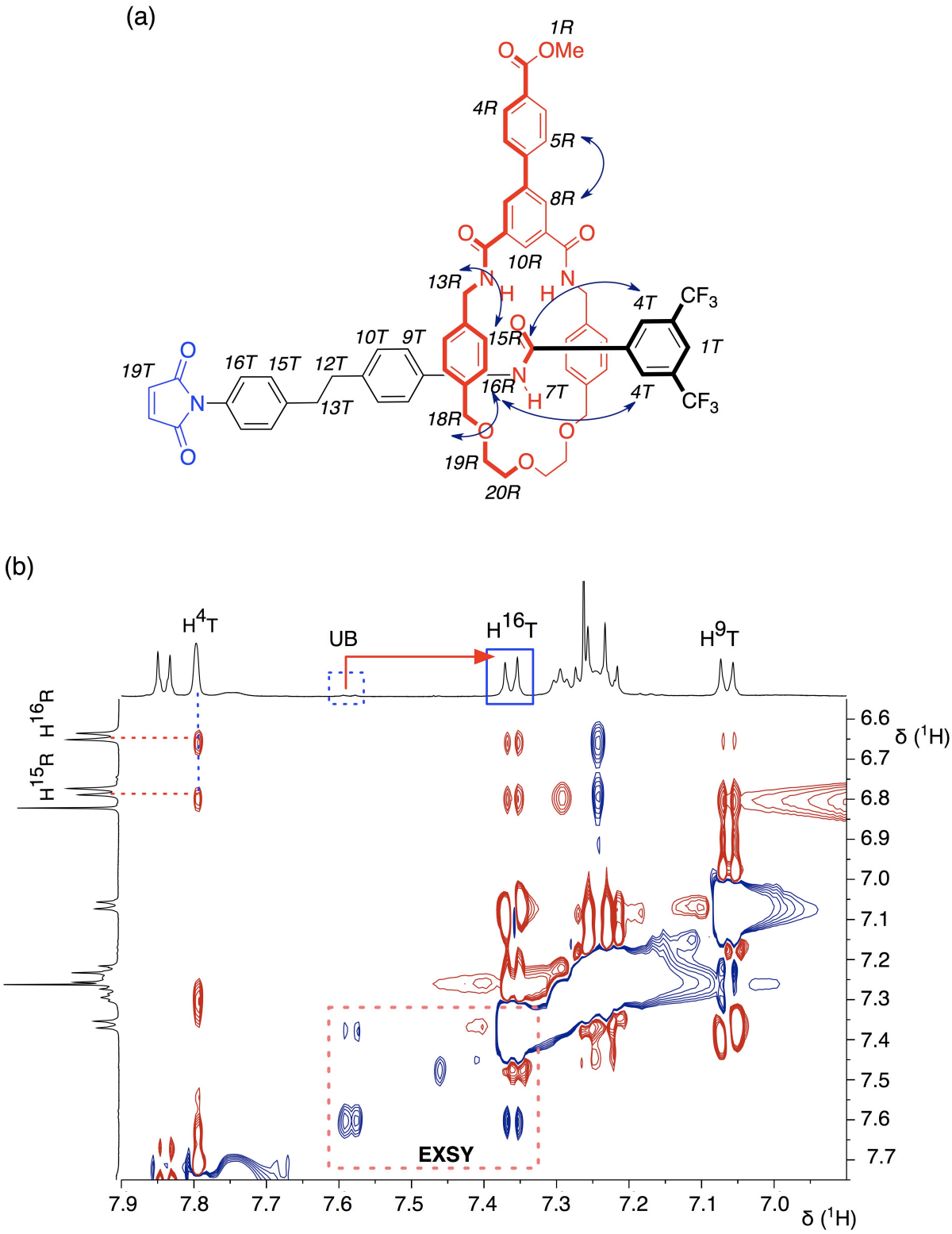

Figure 7.14. (a) ROESY contacts observed for the complex between macrocycle **169** and maleimide **110** are shown as blue arrows. (b) Partial 2D ROESY NMR spectrum (500.1 MHz, 263 K, $CDCl_3$, 20 mM) display crosspeaks (red points) between macrocycle **169** and CF_3 maleimide compound **110**. **UB** stands for unbound species in the blue dashed boxes. EXSY crosspeaks (blue points) are shown within the region δ_H 7.45 – 7.65 in the red dashed boxes between the unbound species and H^{16T}.

7.7 Design of a potential self-replicating rotaxane

A potential self-replicating rotaxane was designed accordingly to accommodate the prepared acid macrocycles and nitrone **115** compound. It has been demonstrated[200] that 4,6-dimethylpyridine ring and 4-*tert*-butylphenyl ring in nitrone **115** incapable of threading the cavity of both macrocycles **MDG** and **MP**, which are the structural analogues of the acid macrocycles (**Scheme 7.12**).

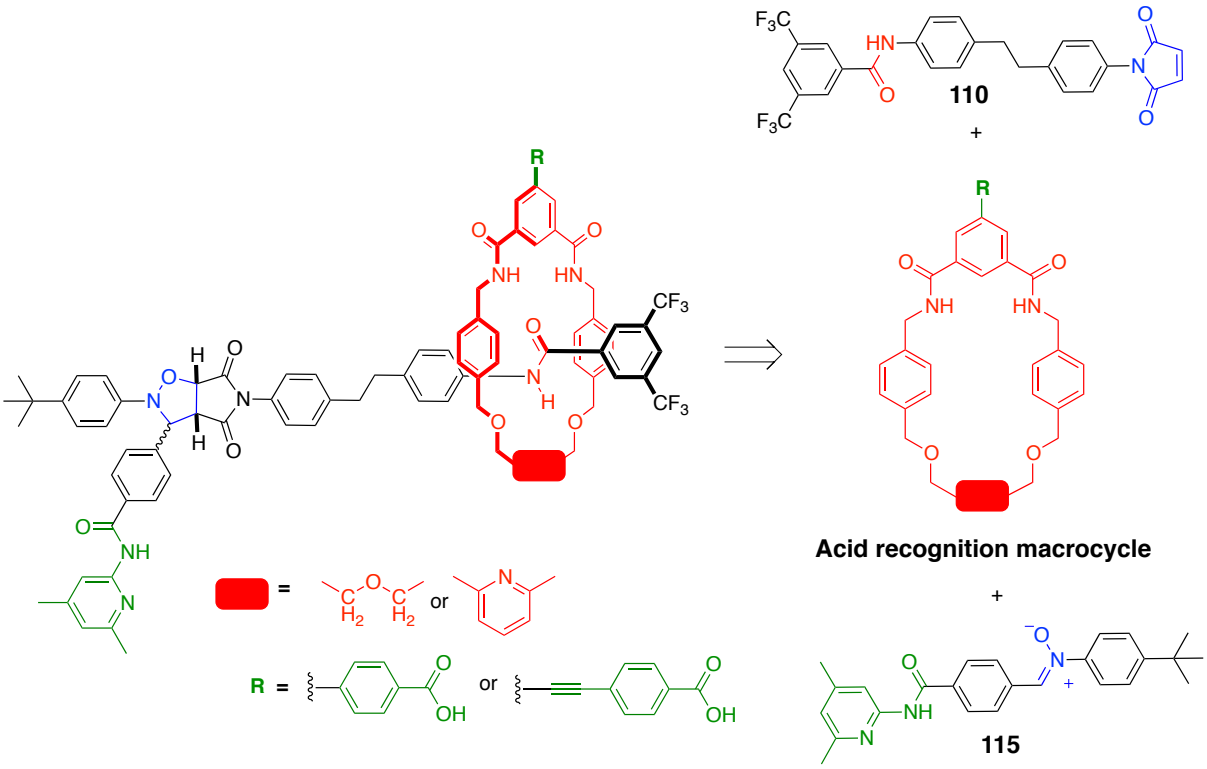

Scheme 7.12. Retrosynthesis of potential self-replicating rotaxanes consists of acid recognition macrocycles, nitrone **115** and CF_3 maleimide **110** compound.

7.7.1 Synthesis of first generation nitrones

We changed the *tert*-butylphenyl ring by employing different blocking group in the nitrone structure while maintaining the 4,6-dimethylpyridine ring on the other end, to provide the first generation nitrones **176** and **182** as depicted in **Figure 7.15**.

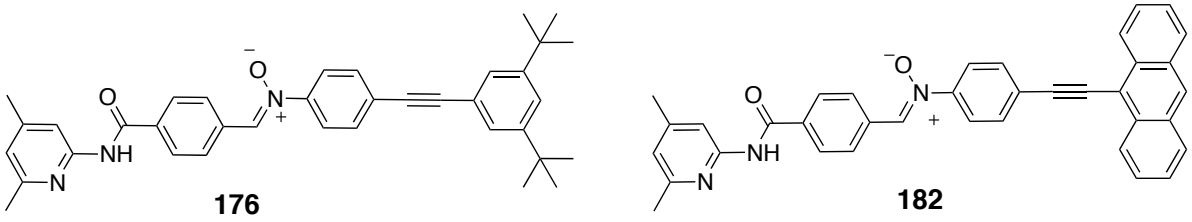

Figure 7.15. The first generation nitrone compounds with the introduction of di-*tert*-butylphenyl and anthracene ring as an alternative blocking groups, affording compound **176** and **182**.

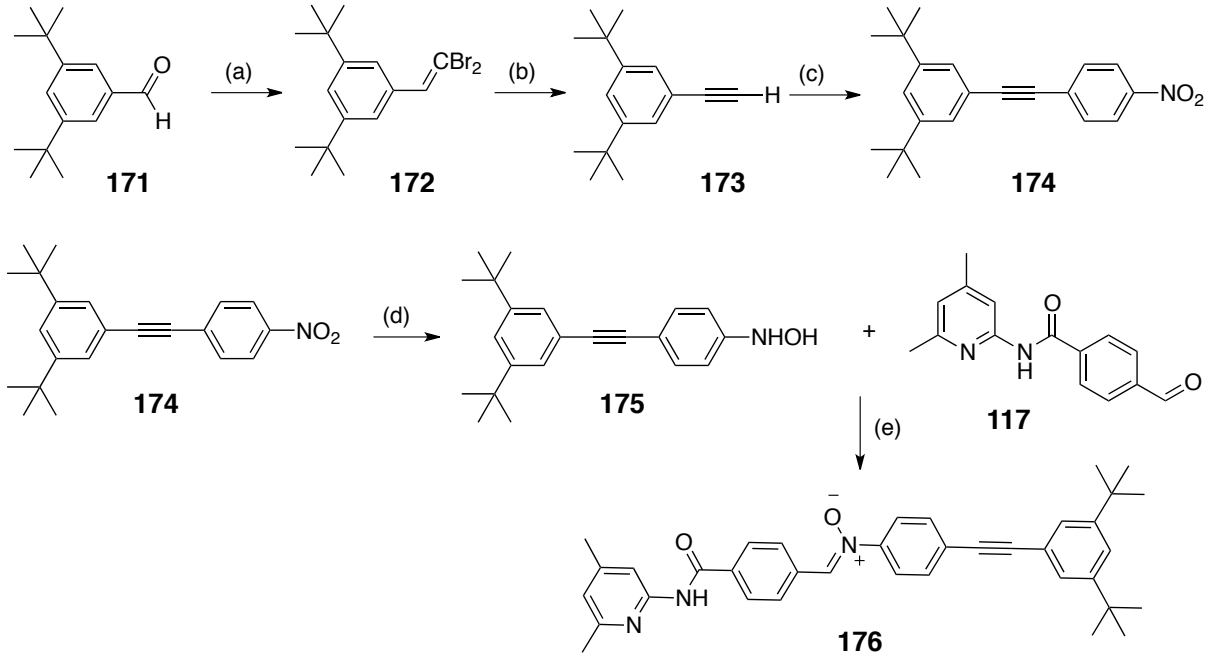

Scheme 7.14. Synthesis of di-*tert*-butylphenyl nitrone **176**. Reagents and yields: (a) CBr_4, PPh_3, Zn, CH_2Cl_2, 0 ˚C to rt, 4 h, 81%; (b) *N*-butyllithium, THF, –78 ˚C to rt, 16 h, 58%; (c) 1-iodo-4-nitrobenzene, $PdCl_2(PPh_3)_2$, CuI, PPh_3, Et_3N, 50 ˚C, 16 h, 81%; (d) Rh/C, $NH_2NH_2{\bullet}H_2O$, THF, rt, 3 h; (e) Aldehyde **117**, EtOH, rt, 3 days, 39% over 2 steps.

The synthesis of di-*tert*-butylphenyl nitrone **176** is included in **Scheme 7.14** to illustrate the synthetic route used for this new compound. Treatment of aldehyde **171** with tetrabromomethane in the presence of triphenylphosphine and zinc afforded the intermediate **172** in good yield. Reaction of intermediate **172** with two equivalents of *N*-butyllithium in dry THF at –78 ˚C for two hours before vigorously stirring at room temperature give the terminal alkyne **173** in 52% yield. Nitro compound **174** was subsequently obtained in 81% yield, utilizing Sonogashira coupling between alkyne **173** with 1-iodo-4-nitrobenzene. The di-*tert*-butylphenyl nitrone **176** was successfully synthesised in 39% yield by carrying out the partial reduction of nitro group **174** followed by condensation reaction between the resultant hydroxylamine **175** with the synthesised aldehyde **117**.

Recently, the research conducted by Philp group[258] utilized a fluorescent material, namely an anthracene ring located at *para* position of the benzene ring of the nitrone, which works as a fluorescent tag in the development of novel self-replicating structure. This feature provides the possibility of following the reaction by the naked eyes. As a consequence of the extended π conjugated system, the nitrone compound emits fluorescence in the yellow region of visible light. However, when the reaction

takes place, the conjugation was interrupted by the engagement of the -C=NO- double bond in the formation of the cycloadducts, giving the product a blue fluorescent colour. The dramatic colour changes visually aids our observation when the thread and/or rotaxane are formed in the solution. Therefore, the integration of anthracene scaffold in one of our building blocks is exceptionally important. Hence, it was decided that a new antharacene nitrone compound should be synthesised to incorporate into our design of potential self-replicating rotaxanes. The following synthetic scheme was described to produce the anthracene compound **182** as shown in **Scheme 7.15**.

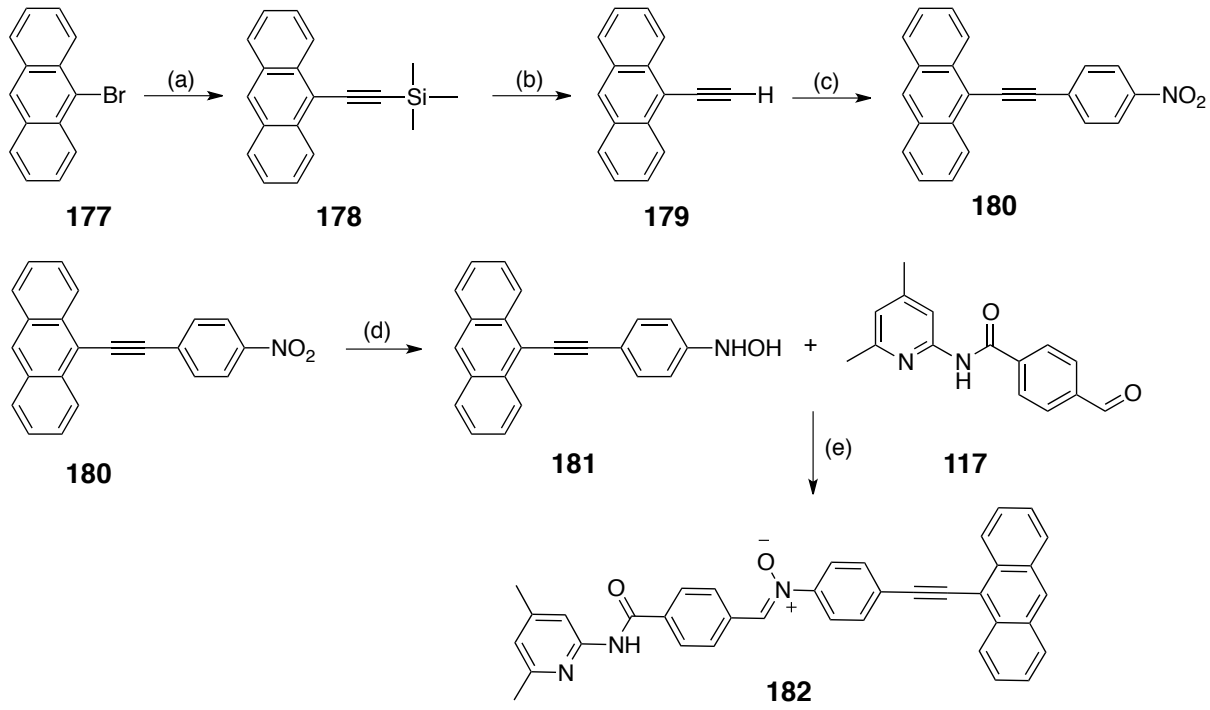

Scheme 7.15. Synthesis of antharacene nitrone **182**. Reagents and yields: (a) (trimethylsilyl)acetylene, $PdCl_2(PPh_3)_2$, CuI, PPh_3, Et_3N, 80 ˚C, 24 h, 87%; (b) K_2CO_3, MeOH, THF, rt, 4 h, followed by (c) 1-iodo-4-nitrobenzene, $PdCl_2(PPh_3)_2$, CuI, PPh_3, Et_3N, 50 ˚C, 24 h, 67%; (d) Rh/C, $NH_2NH_2{\cdot}H_2O$, THF, rt, 3 h; (e) Aldehyde **117**, EtOH, rt, 3 days, 81% over 2 steps.

There are at least five synthetic steps to yield anthracene nitrone **182**, commencing from the Sonagashira coupling of 9-bromoanthracene **177** with an excess amount of (trimethylsilyl)acetylene to yield[259] intermediate **178** in excellent yield. The acetylene **178** was deprotected under basic conditions to give the terminal alkyne **179** before the second Sonogashira coupling with 1-iodo-4-nitrobenzene to install the nitro group in compound **180**. Compound **180** was further reduced with two equivalents of hydrazine monohydrate to yield hydroxylamine **181** before reacted with aldehyde **117**

to produce anthracene nitrone **182** in 81% yield of. Satisfyingly, this nitrone shows fluorescence in the yellow region of visible light.

7.7.2 Binding studies with first generation nitrones

There are various binding possibilities for macrocycle originated from the additional binding sites present in the nitrone structure or the amide moiety from the amidopyridine fragment of the thread. Therefore, the crucial thing is to prevent the association of the macrocycle with these competitive binding sites, which could be problematic in the construction of rotaxane since the macrocycle not only bind the maleimide but also the nitrone. Unfortunately, the binding experiment between nitrone **176** and control macrocycle, **cMDG** shows that the macrocycle form the undesired pseudorotaxane complex, [**cMDG•176**]. The chemical shift changes similar to those observed for the pseudorotaxane formation (not shown) - upfield shifts for the resonances for the macrocycle phenylene protons H^{11R} and H^{12R}, macrocycle methylene protons H^{9R} and H^{14R} and complex pattern for H^{15R} and H^{16R} (refer **Figure 7.6b**). The supplementary binding experiment with anthracene nitrone **182** was also carried out, which give the similar outcomes (**Table 7.2**).

Table 7.2. Chemical shift changes, Δδ (in ppm) for selected protons of macrocycle **cMDG** complexing the first generation nitrone compounds **176** and **182**. (Note : **S** denoted a slow exchange process occuring on the ^{1}H NMR chemical shift timescale).

Macrocycle **cMDG**	Δδ (H^{11}, H^{12})	Δδ H^{9}	Δδ H^{14}	Δδ (H^{15}, H^{16})
i. Nitrone **176** (**S**)	–0.62, –0.74	–0.19	–0.35	complex pattern
ii. Nitrone **182** (**S**)	–0.55, –0.67	–0.14	–0.30	complex pattern

Thus, these results are surprising, demonstrating that both nitrones **176** and **182** are capable of penetrating the cavity of the macrocycle **cMDG**. It could be reason that the macrocyclic unit passed through the fragment of 4,6-dimethylpyridine ring. In that case, we require a larger end group to hamper the formation of this disadvantageous pseudorotaxane species. We are hoping to address this issue by replacing the 4,6-dimethylpyridine ring end with the 4-*tert*-butylphenyl ring in the new design.

7.7.3 Improving the design for second generation nitrones

The second strategy involves the 4-*tert*-butylphenyl ring as the end group in the new nitrone structure. In order to alter the other end of the blocking groups, we employed three distinct groups from naphthalene, di-*tert*butylphenyl ring to anthracene ring (**Figure 7.16**).

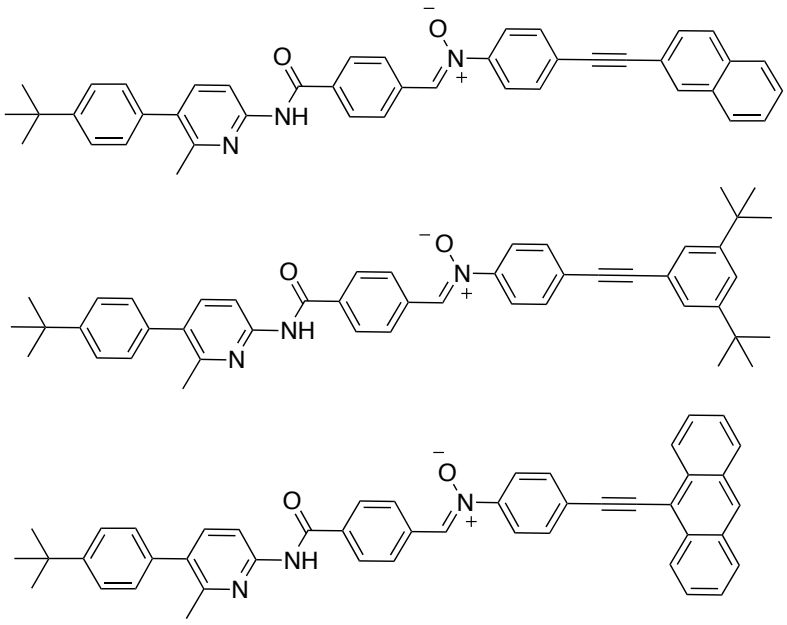

Figure 7.16. The second generation nitrone compounds incorporates the 4-*tert*butylphenyl ring on the amidopyridine recognition site and three different bulky groups at the other ends, giving rise to three new nitrone compounds (nitrone **192**, **193** and **194**).

Herein, we described the synthesis of nitrone compounds **(192**, **193** and **194**) in the following paragraphs. In the preceding communications[260], the iodination of 2-amino-6-methylpyridine, **183** was achieved in the presence of periodic acid in concentrated sulfuric acid and acetic acid to yield iodoaniline derivative **184** in a good yield (**Scheme 7.16**). Subsequently, an amide coupling was performed with the 4-formylbenzoyl chloride **116** under standard conditions to furnish the iodo-aldehyde **185** in a fair yield. Furthermore, Suzuki coupling inserted the 4-*tert*-butylphenyl ring on aldehyde **186** under mild conditions in an excellent yield of 98%. Concurrently, the terminal alkyne **189** was synthesised by the oxidation and decarboxylation strategies as illustrated in earlier report[261] in the group. The palladium-catalysed crosscoupling of **187** with propargyl alcohol gave the prop-2-yn-1-ol **188**, which successively oxidised and decarboxylated using activated manganese (IV) oxide to afford alkyne **189** in a good yield of 82%. The subsequent Sonogashira coupling under standard conditions with 2-bromonaphthelene installed the naphthalene fragment on to the

compound **190**. This nitro derivative **190** compound was used directly from the work in the group and the subsequent partial reduction with hydrazine monohydrate in the presence of Rh/C catalyst allows the formation of the hydroxylamine **191**.

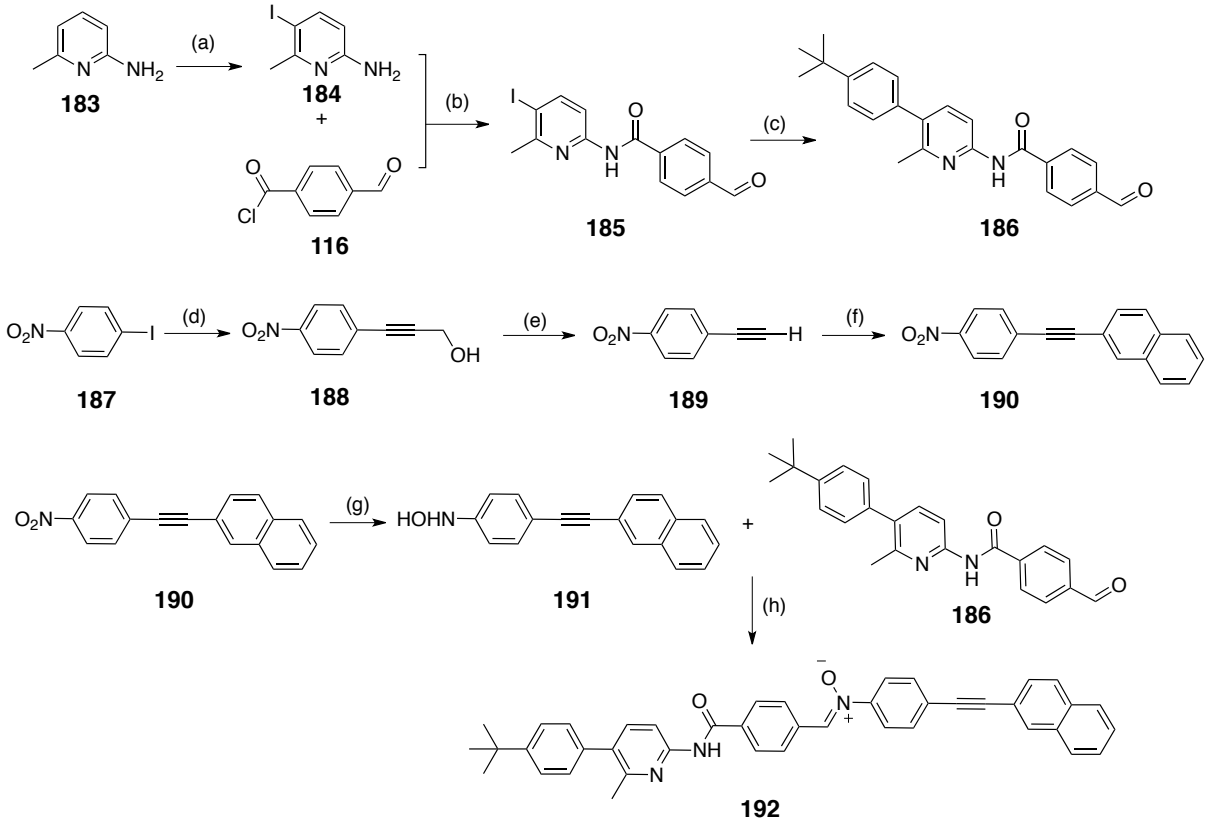

Scheme 7.16. Synthesis of naphthalene nitrone **192**. Reagents and yields: (a) CH_3COOH, H_2SO_4, HIO_4, I_2, 60 ˚C, 20 h, 85%; (b) Et_3N, CH_2Cl_2, 0 ˚C to rt, 48 h, 93%; (c) *tert*-butylboronic acid, K_2CO_3, $PdCl_2(PPh_3)_2$, THF/H_2O, 70 ˚C, 16 h, 98%; (d) propargyl alcohol, $PdCl_2(PPh_3)_2$, PPh_3, Cu(II)acetate, Et_3N; (e) MnO_2, KOH, CH_2Cl_2, rt, 2 h, 81%; (f) 2-bromonaphthalene, $PdCl_2(PPh_3)_2$, PPh_3, CuI, Et_3N, 80 ˚C, 16 h, 35%; (g) Rh/C, $NH_2NH_2{\bullet}H_2O$, rt, 3 h, (h) EtOH, rt, 3 days, 44% over 2 steps.

Previous works shows that the synthetic approaches using palladium or rhodium on activated carbon with an equimolar amount of hydrazine monohydrate in THF solved the problem for the formation of highly substituted hydroxylamine derivatives. However, in some cases, we observed over reduction to an amine or an exclusive formation of the azoxy compound by the condensation of hydroxylamine and *in situ* formed nitroso compound. Therefore, the obtained hydroxylamine **191** was usually left to dry on the high vacuum for overnight to get rid of the excess hydrazine before reacted with aldehyde **186** to afford the corresponding nitrone **192** in 45% yield. Simultaneously, the prepared aldehyde **186** was reacted in two sequences starting from the same nitro compound **174** bearing the di-*tert*-butylphenyl ring to afford the

intermediate hydroxylamine **175**. The resulting nitrone **193** was assembled *via* the condensation reaction between hydroxylamine **175** and aldehyde **186** (**Scheme 7.17**).

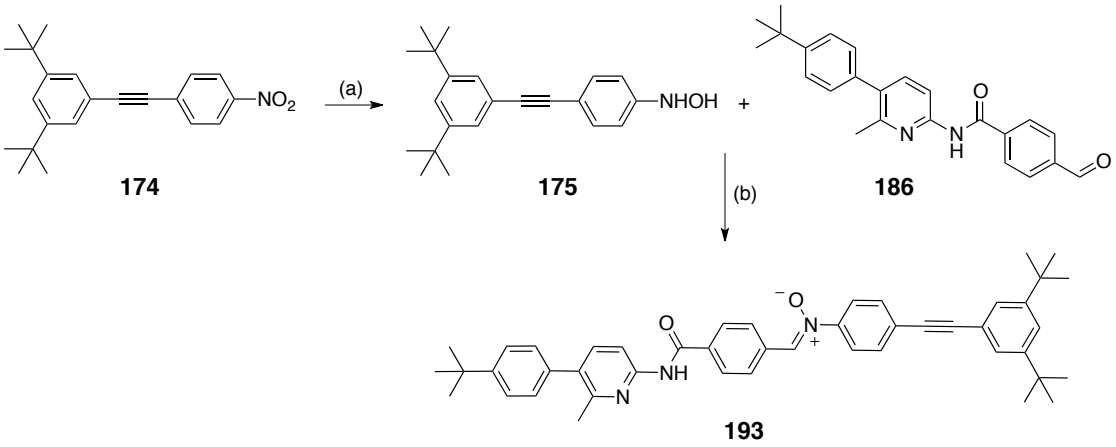

Scheme 7.17. Synthesis of nitrone **193**. Reagents and yields: (a) Rh/C, $NH_2NH_2 \cdot H_2O$, rt, 3 h; (b) EtOH, THF, rt, 3 days, 40% over 2 steps.

Scheme 7.18 depicted the synthesis of the analogous antharacene nitrone compound **194**. Preparation of anthracene hydroxylamine **181** through the reduction pathway described in the preceding procedure (**Scheme 7.15d**) was similarly reacted with aldehyde **186** to give the second anthracene nitrone **194** in 94% yield.

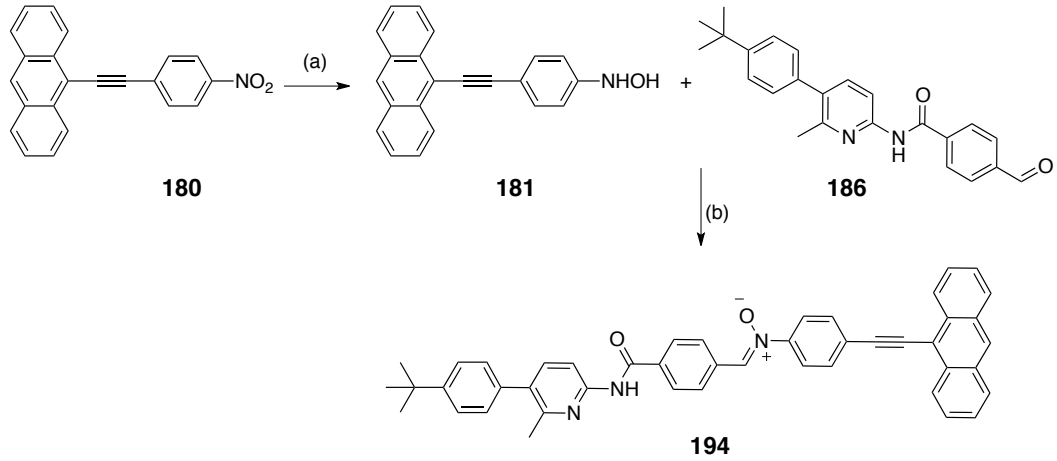

Scheme 7.18. Synthesis of nitrone **194**. Reagents and yields: (a) Rh/C, $NH_2NH_2 \cdot H_2O$, rt, 3 h, followed by (b) EtOH, rt, 3 days, 94% over 2 steps.

7.7.4 Binding studies with second generation nitrones

As mentioned earlier, the binding studies with the second generation nitrones **192** and **194** were first carried out with macrocycle **cMDG** to examine the possibilities of pseudorotaxane formation. An equimolar mixture of the macrocycle and nitrone was monitored by ^{1}H NMR spectroscopy at room temperature in $CDCl_3$.

Nonetheless, the naphthalene nitrone **192** afforded pseudorotaxane assemblies with control macrocycle, **cMDG**. From the ^{1}H NMR spectrum (not shown), the bound and unbound species equilibrate slowly with respect to the threading and dethreading process on the ^{1}H NMR chemical shift timescale. Further evidence of pseudorotaxane formation was obtained from the significant downfield shift (+1.57 ppm) of the macrocycle NH protons (refer **Figure 7.6b**), upfield shifts for the resonances of macrocycle phenylene protons H^{11R} and H^{12R} (–0.58 and –0.70 ppm), upfield shifts for the resonance of macrocycle methylene protons, H^{9R} (–0.16 ppm) and H^{14R} (–0.31 ppm) and the emergence of the complex patterns, which corresponds to the diastereotopic methylene protons of H^{15R} and H^{16R} (**Table 7.3i**).

In the case of anthracene nitrone **194**, the spectrum (not shown) suggests that the complex is however in fast exchange on the ^{1}H NMR chemical shift timescale. Unexpectedly, thus also yielded a pseudorotaxane assembly, in which was inferred from the upfield shift of macrocycle NH protons (+1.14 ppm), downfield shifts of the macrocycle phenylene protons, H^{11R} and H^{12R} (–0.10 ppm), H^{9R} (–0.02 ppm) and H^{14R} (–0.05 ppm) (**Table 7.3ii**) together with similar complex pattern for H^{15R} and H^{16R}.

Table 7.3. Chemical shift changes, Δδ (in ppm) for selected protons of macrocycle **cMDG** upon complexation with nitrone compound **192** and **194**. (Note : **S** and **F** denoted a slow and fast exhange process occuring on the ^{1}H NMR chemical shift timescale).

Macrocycle **cMDG**	Δδ (H^{11}, H^{12})	Δδ H^9	Δδ H^{14}	Δδ (H^{15}, H^{16})
i. Nitrone **192** (**S**)	–0.58, –0.70	–0.16	–0.31	complex pattern
ii. Nitrone **194** (**F**)	–0.10	–0.02	–0.05	complex pattern

These observations demonstrated that macrocycle **cMDG** was capable of forming the interlocked species with naphthalene nitrone **194**, which bring us to the final binding experiment with nitrone **193** (**Table 7.4**). Likewise, the formation of undesired pseudorotaxane is again favoured with significant upfield shifts from the resonance of the macrocycle **169** (refer **Figure 7.13a**) phenylene protons, H^{15R} and H^{16R}, that give a singlet at δ_H 7.30 when the macrocycle is free in the $CDCl_3$ solution but upon pseudorotaxane formation, each of these protons dispersed as a pair of doublet at 6.73 and 6.61 ppm. The ring methylene protons H^{13R} and H^{18R} are rendered diastereotopic when the nitrone **193** was encircled by the ester macrocycle **169** and

give rise to another set of resonances. Furthermore, the overlapping methylene protons H^{19R} and H^{20R} also led to the same complex patterns, and thus confirmed the pseudorotaxane complex formation. Altogether, these observations unambiguously indicated that the *tert*-butylphenyl ring is not sufficiently large to prevent the formation of undesired pseudorotaxane complexes.

Table 7.4. Chemical shift changes, Δδ (in ppm) for selected protons of ester macrocycle **169** upon complexation with the nitrone **193**. (Note : S denoted a slow exchange process occuring on the ^{1}H NMR chemical shit timescale).

Macrocycle **169**	Δδ (H^{15}, H^{16})	Δδ H^{13}	Δδ H^{18}	Δδ (H^{19}, H^{20})
Nitrone **193** (**S**)	–0.57, –0.68	–0.17	–0.31	complex pattern

7.7.5 Synthesis and binding study with third generation nitrone

Having demonstrated that all nitrones prepared to date assembled into undesired pseudorotaxanes with macrocycle **cMDG**, we realized that 4-*tert*-butylphenyl stopper was responsible for this threading. Attention now focused on probing the appropriate size for alternative end groups, so it is incapable of passing through the cavity of macrocycle **cMDG**. In order to test this proposition, a new strategy was employed to prepare the bulky nitrone compound **197** as shown in **Scheme 7.19**.

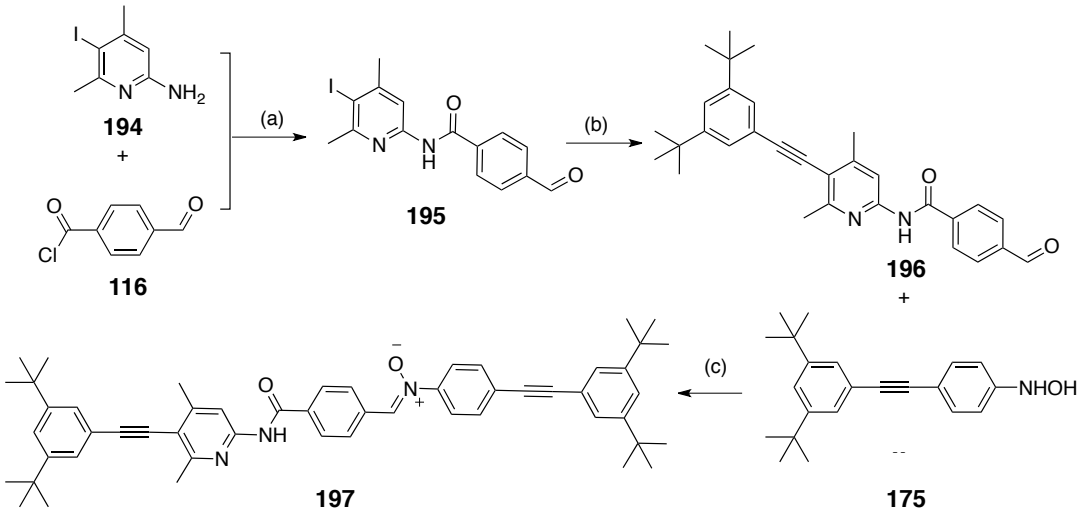

Scheme 7.19. Synthesis of bulky nitrone **197**. Reagents and yields: (a) Et_3N, CH_2Cl_2, 0 ˚C to rt, 48 h, 38%; (b) Alkyne **173**, $PdCl_2(PPh_3)_2$, CuI, PPh_3, Et_3N, 60 ˚C, 24 h, 25%, (c) EtOH, rt, 48 h, 24% over 2 steps.

The iodo-aniline **194** was used directly from the work in the group and reacted with the acid chloride **116** to give the iodo-aldehyde **195**, which was subsequently

functionalized with the terminal alkyne **173** *via* Sonogashira coupling under standard conditions affording the aldehyde **196** in a yield of 25%. The sterically di-*tert*-butylphenyl ring terminus from the hydroxylamine **175** was appended to produce the bulky nitrone **197**. Following the replacement of the 4-*tert*-butylphenyl ring with the 3,5-di-*tert*-butylphenyl ring, subsequent binding experiment (not shown) with ester macrocycle **169** confirmed that no pseudorotaxane complexes were obtained. Pleasingly, both of terminal groups, 3,5-di-*tert*-butylphenyl were able to function as an effective stoppering group.

The overall outcome of the binding experiments carried out between macrocycle **cMDG** or ester macrocycle **169** with the first, second and third generation of nitrone compounds are presented and summarized in **Table 7.5**. Therefore, only the bulky nitrone compound **197** did not give the pseudorotaxane complex with the macrocyclic component (in this case, ester macrocycle **169**) and will be further employed in our second design of potential self-replicating rotaxanes.

Table 7.5. Binding experiments carried out between macrocycle **cMDG** or ester macrocycle **169** with the first, second and third generation nitrone compounds, giving the undesired [2]-pseudorotaxane complex are listed below.

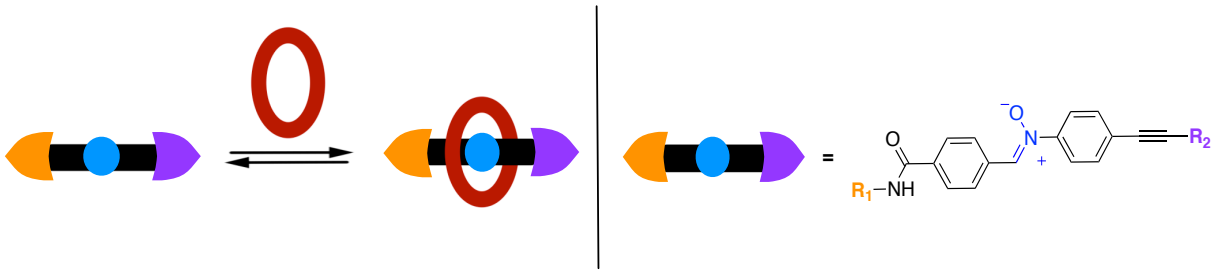

R_1	R_2	Compounds	[2]-pseudorotaxane
i. First generation nitrone			
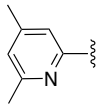	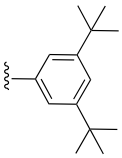	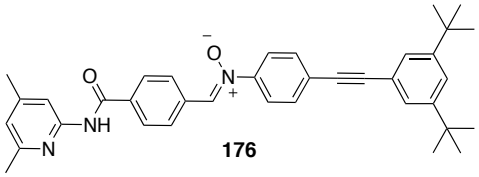 **176**	✓
	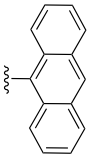	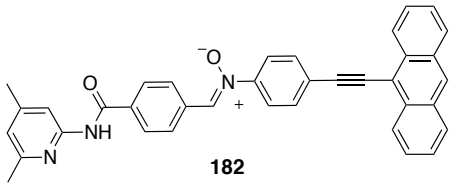 **182**	✓
ii. Second generation nitrone			
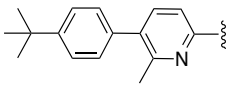	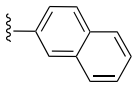	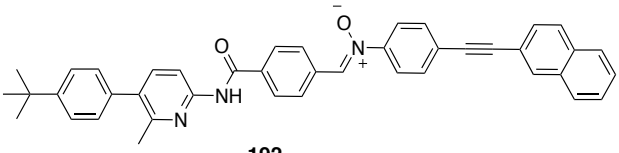 **192**	✓
	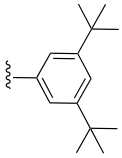	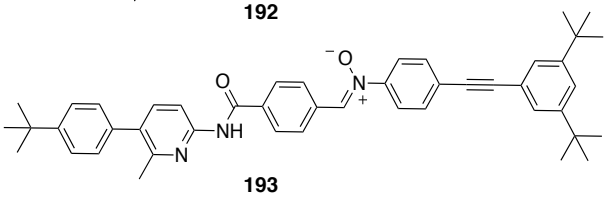 **193**	✓
	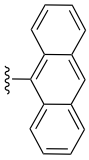	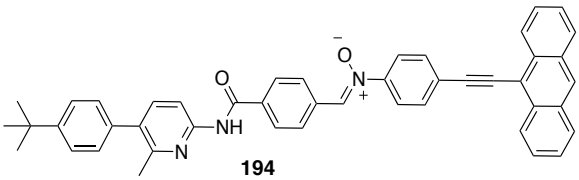 **194**	✓
iii. Third generation nitrone			
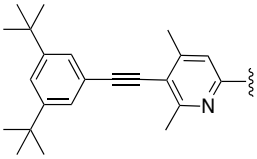	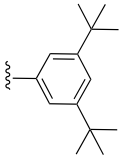	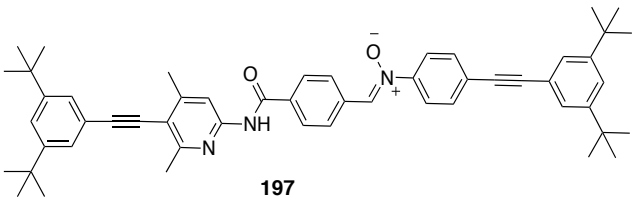 **197**	✗

7.8 Design of a potential self-replicating rotaxane 2

Building on this work, we prepared the second design of a potential self-replicating rotaxane (**Scheme 7.20**), which features the acid recognition macrocycle, CF_3 maleimide **110**, and the bulky nitrone compound **197**.

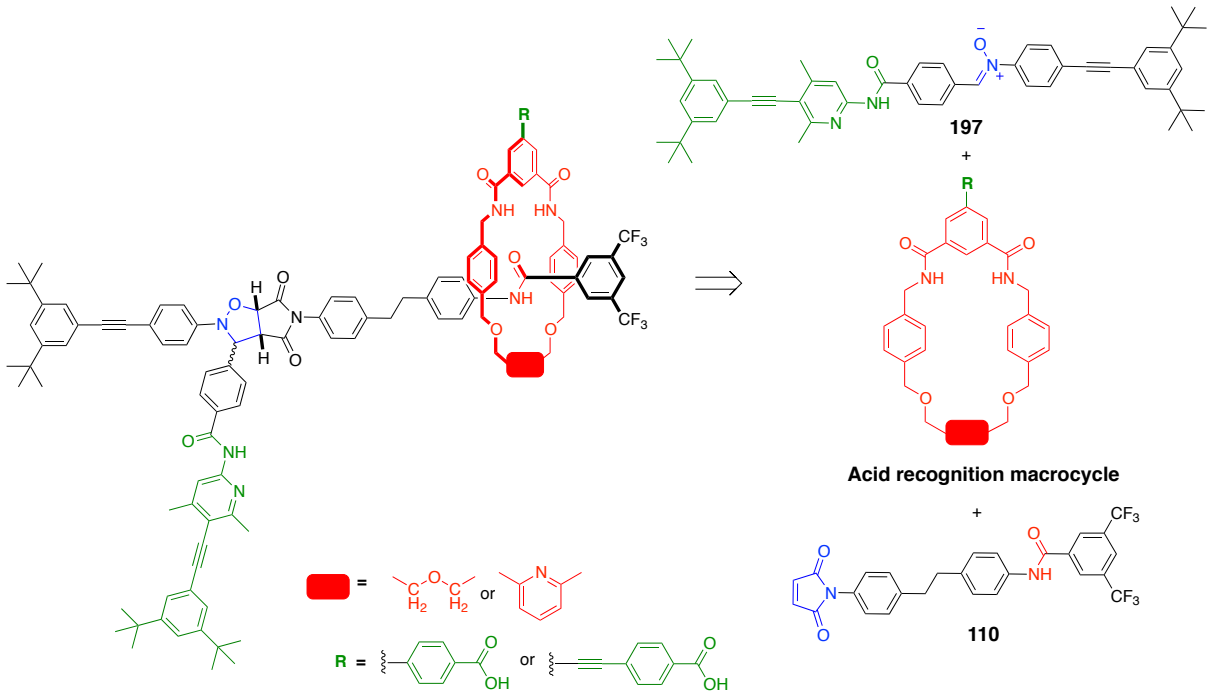

Scheme 7.20. Retrosynthetic of potential self-replicating rotaxanes 2 containing bulky nitrone **197**, acid recognition macrocycle and CF_3 maleimide **110**.

However, the development of this self-replicating rotaxane was discontinued because the CF_3 maleimide **110** is insoluble in less polar solvent ($CDCl_3$) upon addition of the acid recognition macrocycle.

7.9 Design of a potential self-replicating rotaxane 3

In the pursuit of self-replicating rotaxanes, we refined the alternative synthetic strategies to replace the CF_3 maleimide **110**. The final scheme comprises bulky nitrone compound **197**, acid recognition macrocycle and maleimide **198** (**Scheme 7.21**). Maleimide component **198** has been successfully[200] utilized to prepare a number of simple rotaxane structure, and involved particularly in the complexation of macrocycle **MDG**. It has been demonstrated that maleimide **198** capable of threading and the stoppers are proven to big enough to prevent dethreading. We were therefore interested to conduct a binding experiment between acid recognition macrocycle and maleimide **198**.

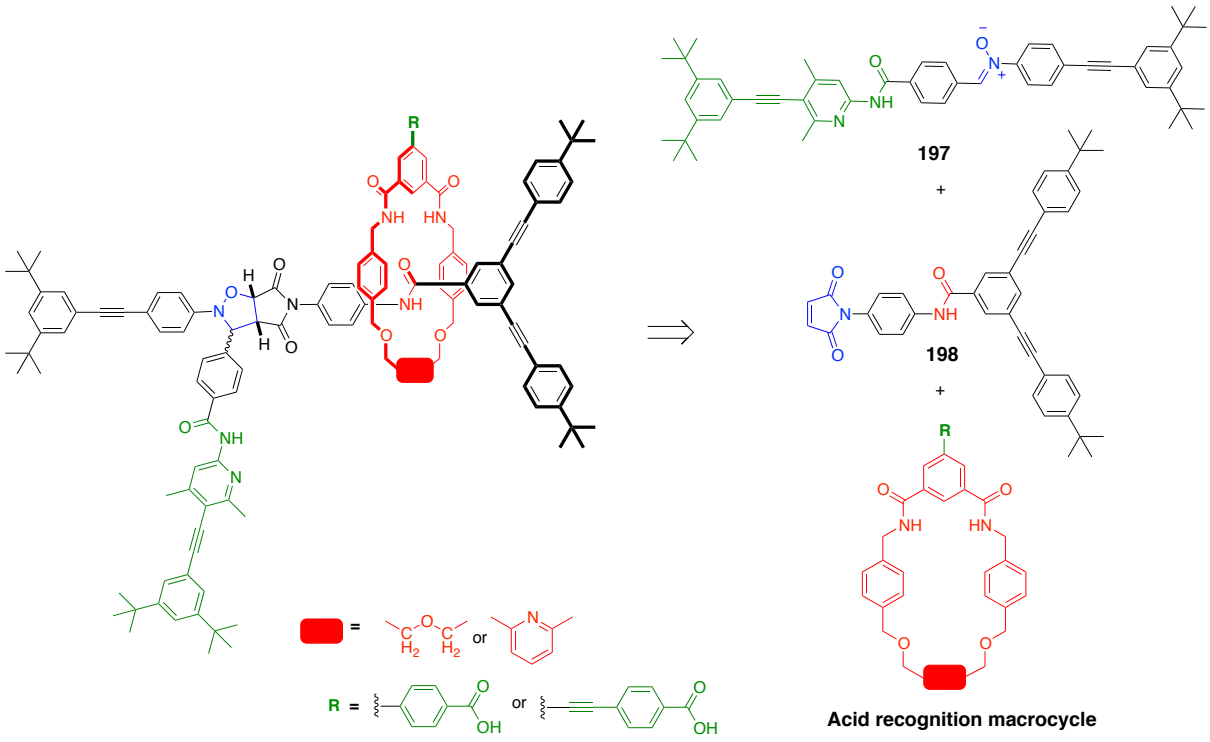

Scheme 7.21. Retrosynthetic of potential self-replicating rotaxanes 3 comprises big bulky nitrone **197**, Maleimide **198** and acid recognition macrocycle.

7.9.1 Binding study with maleimide 198

Binding experiment with acid macrocycle **AEMDG** was carried out with maleimide **198**. The solubility of macrocycle **AEMDG** in chloroform was poor, but improved with the addition of the maleimide compound **198**. This solubility change is an indication of the interaction between the macrocycle and maleimide guest as such the supramolecular species often being more soluble than the two separate entities. The reaction was monitored by ^{1}H NMR spectroscopy, which revealed that the free and bound species equilibrate slowly with one another relative to the threading and dethreading process on the ^{1}H NMR chemical shift timescale.

The 400.1 MHz ^{1}H NMR spectrum of the macrocycle methylene regions is shown in **Figure 7.17**. These protons are all rendered magnetically inequivalent upon pseudorotaxane formation as a results of end-to-end asymmetry imposed by maleimide **110**. Furthermore, using the single-point method, the binding constant was estimated to be 260 ± 30 M^{-1} in $CDCl_3$ at 25 ˚C.

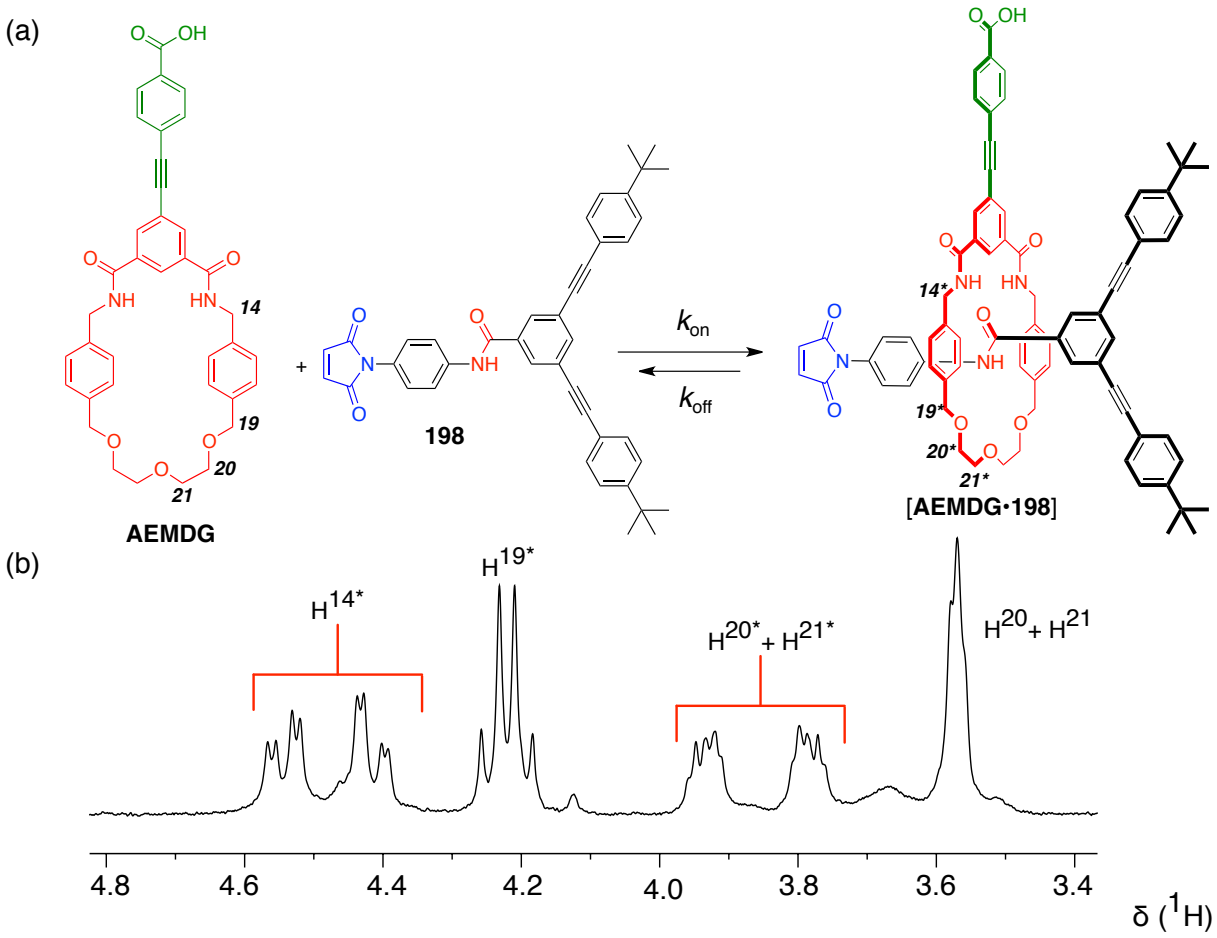

Figure 7.17. (a) Self-assembly of macrocycle **AEMDG** with maleimide **198** forming pseudorotaxane complex; (b) Macrocycle methylene resonances region of ^{1}H NMR spectrum (400.1 MHz, 25 ˚C, $CDCl_3$, 10 mM) of an equimolar mixture of macrocycle **AEMDG** and maleimide **198**, exhibited signals that can be attribute to the intermolecular hydrogen bonding. Star symbols coincide with the diastereotopic proton in the pseudorotaxane complex.

Subsequently, we performed the kinetic simulation to assess the ratio of rotaxane to thread. As shown in **Figure 7.18**, the simulation reveals that [**R**]/[**T**] ratio in 1:1 stoichiometry is dependent on the ratio of k_{rot}/k_{thread}. If we take the K_a for the [**AEMDG·198**] complex as 260 ± 30 M^{-1} and $k_{thread} = k_{rotaxane}$, then the [**R**]/[**T**] ratio in the reaction mixture should be slightly more than 1 (dashed line).

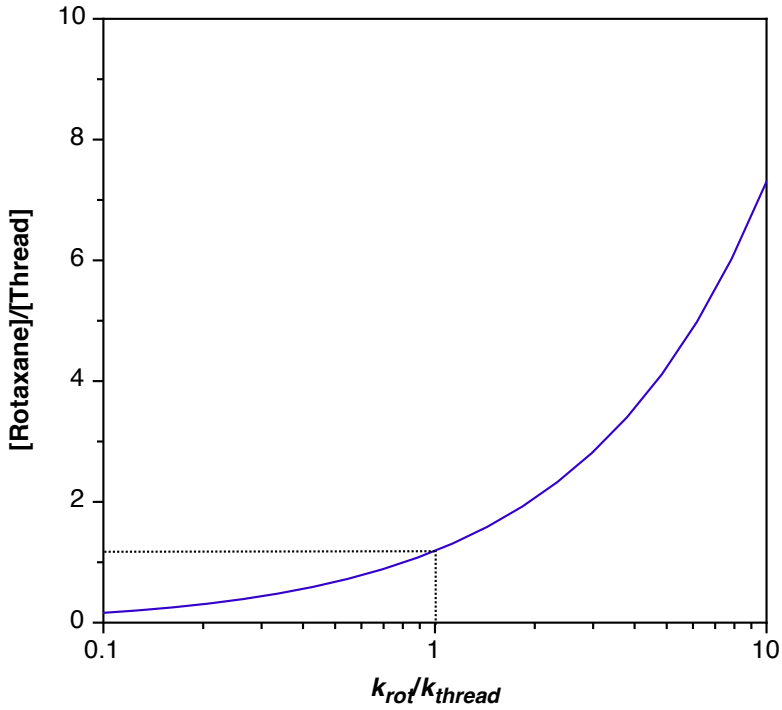

Figure 7.18. Plot of [**R**]/[**T**] against k_{rot}/k_{thread}. Noted that in the simulation, the starting concentrations of maleimide **198**, nitrone **197** and macrocycle **AEMDG** are 10 mM and plotted in the logarithmic scales.

We must now determine the reaction rate for the formation of both thread and rotaxane cycloadducts in our real system, and which diastereoisomers are favoured in the reaction mixture. Therefore, the kinetic analysis for the thread and rotaxane formation in isolation must be conducted.

7.9.2 Kinetic study of the thread

The kinetic of maleimide **198** and nitrone **197** in the absence of macrocycle **AEMDG** was performed to investigate the rate of bimolecular reaction of resulting thread **199** (**Scheme 7.22**). A solution containing the nitrone **197** and maleimide **198**, with starting concentrations of 10 mM each were prepared in $CDCl_3$.

The reaction progress was followed at 298 K over 24 hours by ^{1}H NMR spectroscopy, which monitored the disappearance of the resonance that arises from the maleimide **198** present at δ_H 6.85 and the concomitant emergence of the resonances that result from the *trans* diastereoisomer at δ_H 5.13 – 5.80 and that from the *cis* diastereoisomer at δ_H 4.14 – 5.30 (**Figure 7.19**). The profile of concentration *vs* time for the formation of both cycloadducts was additionally constructed by

deconvolution of these resonances. Reaction between nitrone **197** and maleimide **198** proceed slowly at 298 K leading to 54% overall conversion after 24 hours, which accompanied by typical diastereoisomeric ratio of 2:1 in favour of *trans* **199**, and thus establishing the importance of recognition process in the bimolecular reaction.

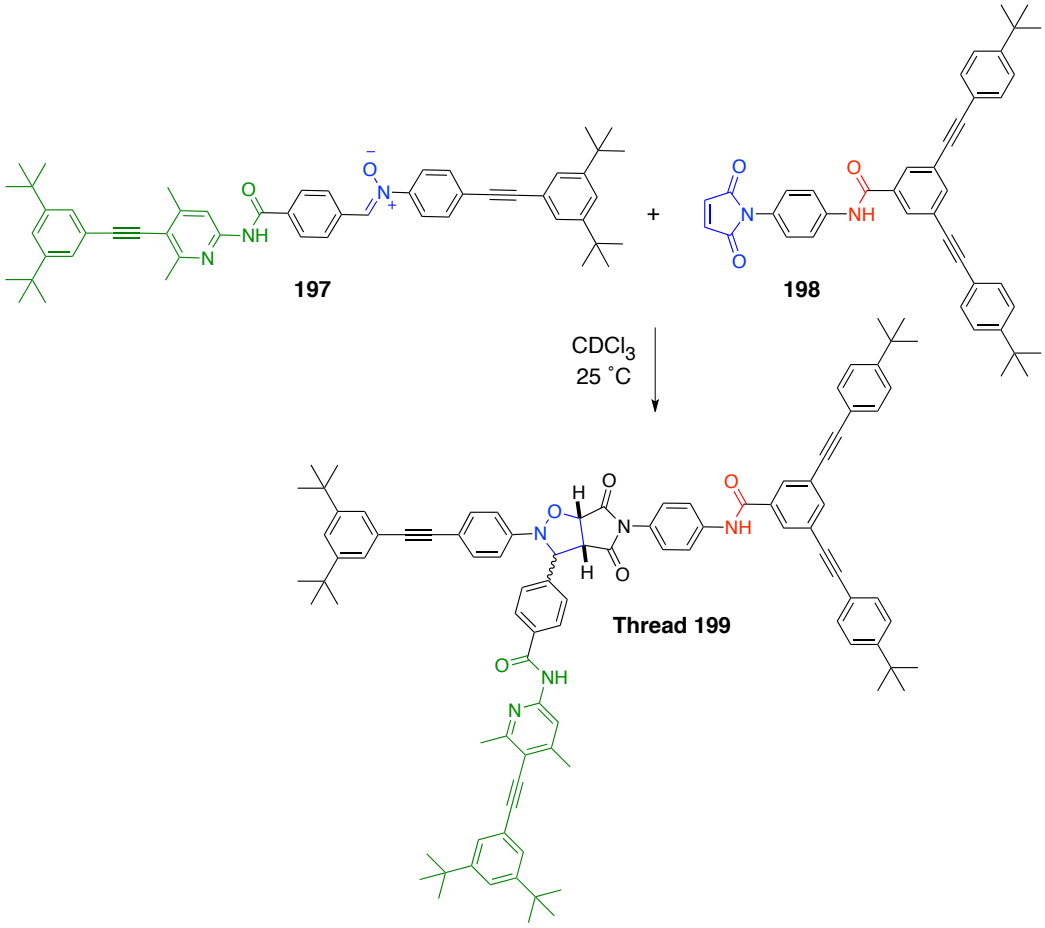

Scheme 7.22. 1,3-dipolar cycloaddition between nitrone **197** and maleimide **198** to give thread **199** in $CDCl_3$ at 298 K.

The kinetic data of the non-recognition mediated reaction were extracted and employed in the fitting protocol using the SimFit package (**Figure 7.20**). The quality of the fit was reflected by the solid line derived from the kinetic model compared with the experimental data points. Bimolecular rates extracted from the control experiment were determined to be 9.04×10^{-4} M^{-1} s^{-1} for *trans* thread **199** and 4.45×10^{-4} M^{-1} s^{-1} for *cis* thread **199**. In addition, the formation of thread **199** cycloadducts were corroborated by MALDI mass spectrometry from the crude reaction mixture (**Figure 7.21**).

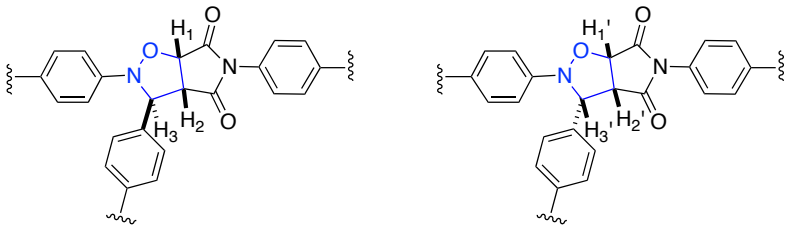

trans thread **199** *cis* thread **199**

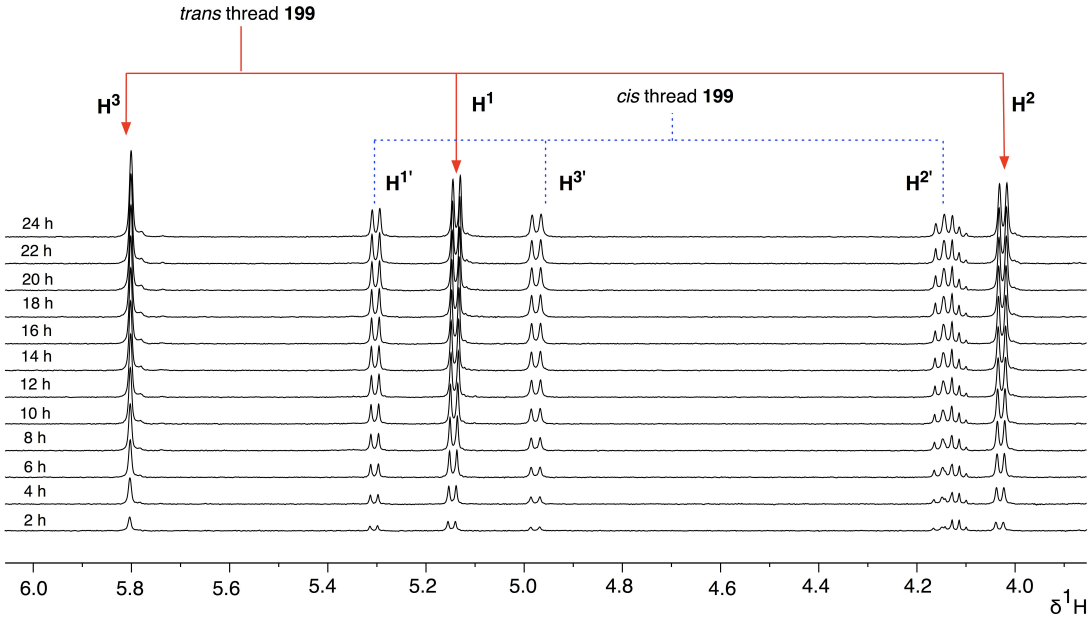

Figure 7.19. Partial ^{1}H NMR spectra (500.1 MHz, 25 ˚C, $CDCl_3$, 24 h) of the cycloaddition reaction between maleimide **198** and bulky nitrone **197**, illustrating spectral region associated with the resonances of the *trans* thread **199** and *cis* thread**199** protons, respectively.

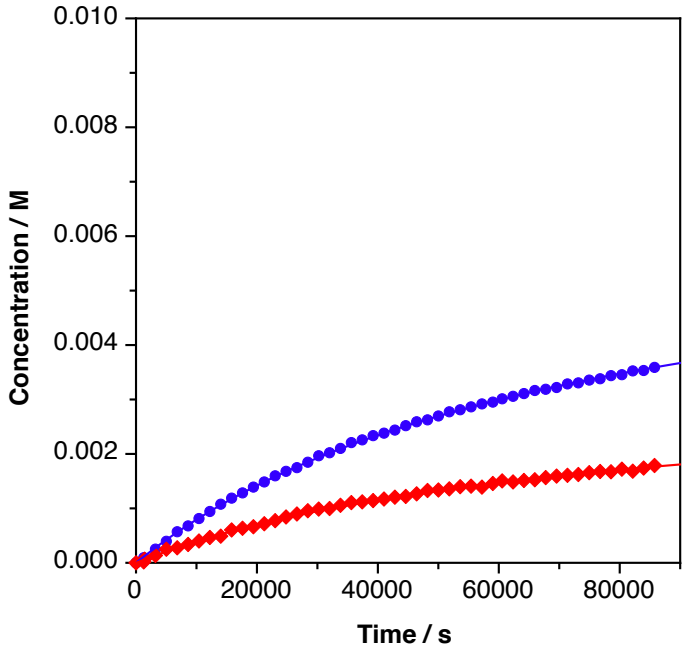

Figure 7.20. Concentration *vs* time profile for the reaction (500 MHz, $CDCl_3$, 10 mM, 298 K, 24 h) between nitrone **197** and maleimide **198**. The formation of *trans* thread **199** is shown as blue filled circles and the formation of *cis* thread **199** as red filled diamonds. Solid lines represent the results for the fitting of the *trans* thread **199** (blue line) and *cis* thread **199** (red line) product.

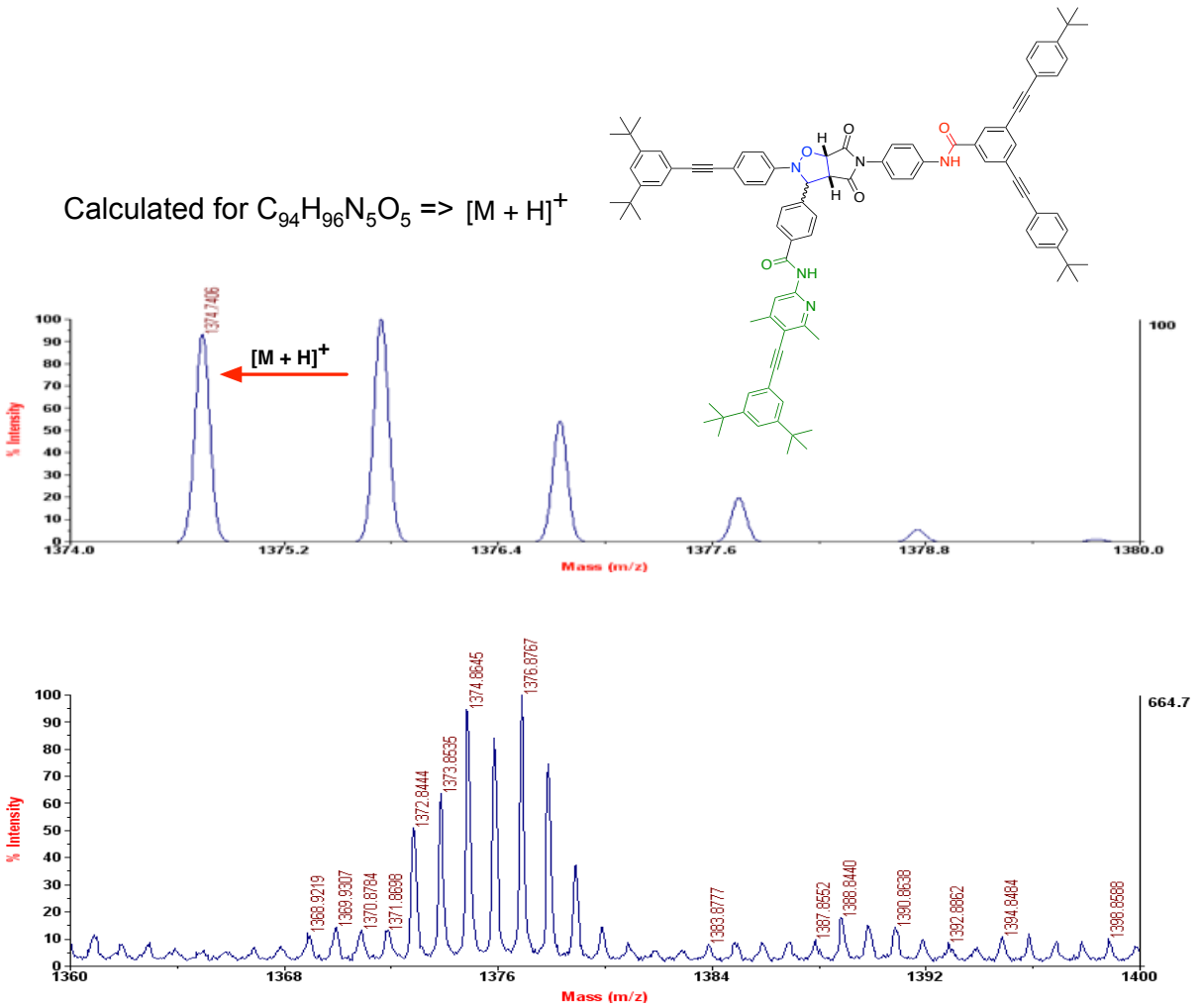

Figure 7.21. MALDI mass-spectra of thread component **199.** Mass spectrometry (MALDI) *m/z* 1374.86 (95%, $[M+H]^+$), calculated for $C_{94}H_{96}N_5O_5$.

7.9.3 Kinetic study of the rotaxane

The kinetic analysis of the full system in the presence of macrocycle **AEMDG** was investigated to determine the behaviour of rotaxane **200** as potential replicator (**Scheme 7.23**). At least, four possible products can be formed in this system, which emanates from the reversible binding interaction of pseudorotaxane [**AEMDG·198**]. The [**AEMDG·198**] complex reacted with nitrone **197** to form *trans* and *cis* rotaxane **200** and alternately the nitrone **197** reacted with the free maleimide **198**, giving *trans* and *cis* thread **199**.

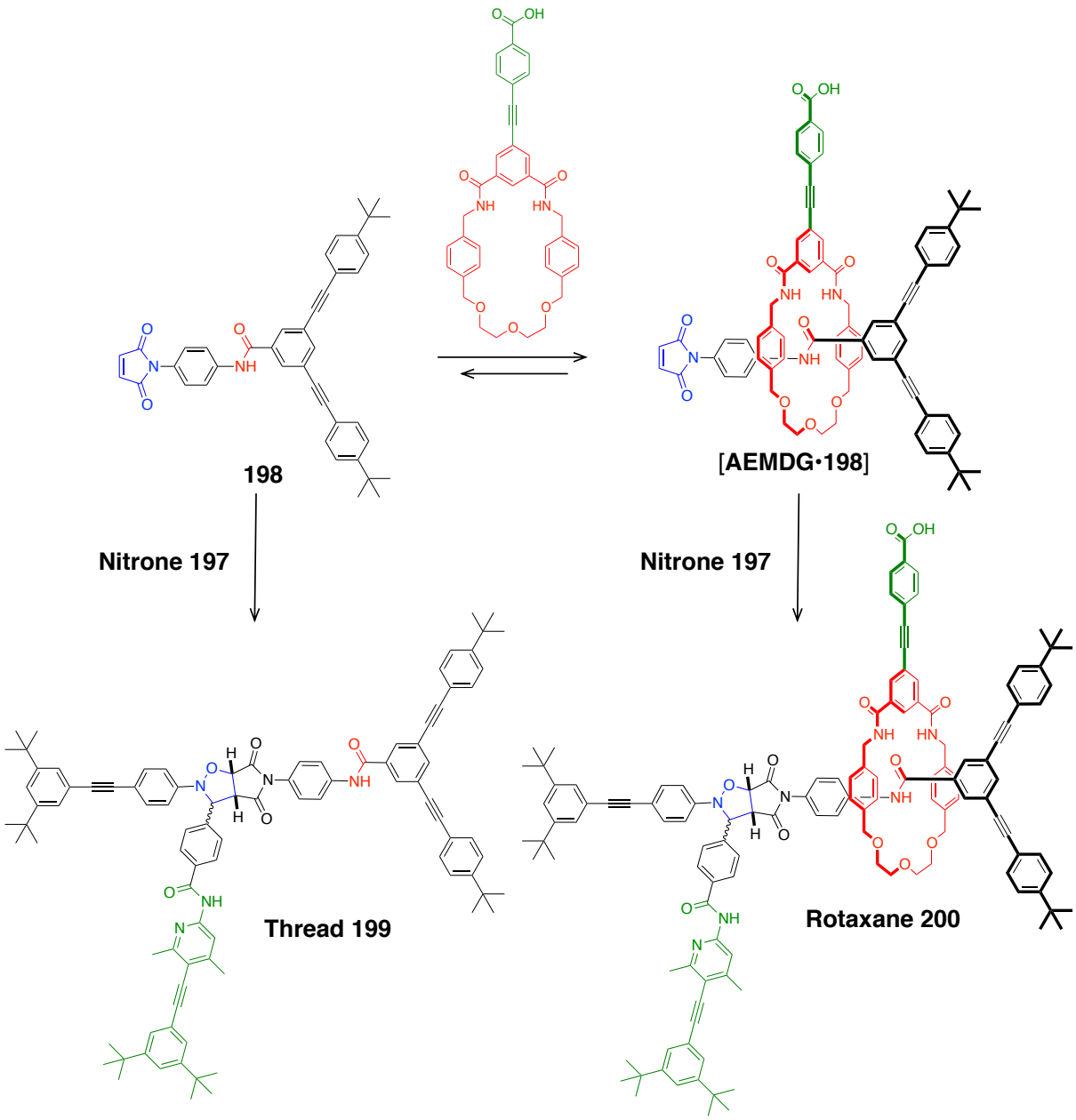

Scheme 7.23. Possible reaction pathways during the formation of potential self-replicating rotaxane **200**. Nitrone **197** can either react with unbound maleimide **198** to afford *trans* thread **199** and *cis* thread **199** or with pseudorotaxane [**AEMDG·198**] to afford *trans* rotaxane **200** and *cis* rotaxane **200**.

The experimental results presented in **Figure 7.20** clearly prove that the bimolecular reaction rate between maleimide **198** and nitrone **197** is relatively low in the absence of recognition. With the experimental data in hand, we turned to simulation to provide an insight how far the behaviour of the recognition-mediated process can be predicted from the behaviour in simple system. Based on the K_a for [**AEMDG·198**] complex and assuming both this complex and maleimide **198** have the same rate of reaction with nitrone **197**, we can predict the outcome of the recognition-mediated reaction. Assuming starting concentrations of the reagents of 10 mM, using the

ISOSIM mode of SimFit provides the predicted product distributions shown in **Figure 7.22**. The results of this simulation indicate that we should expect to see significantly more thread than rotaxane in the distribution of products. Indeed, the major product should be the *trans* thread.

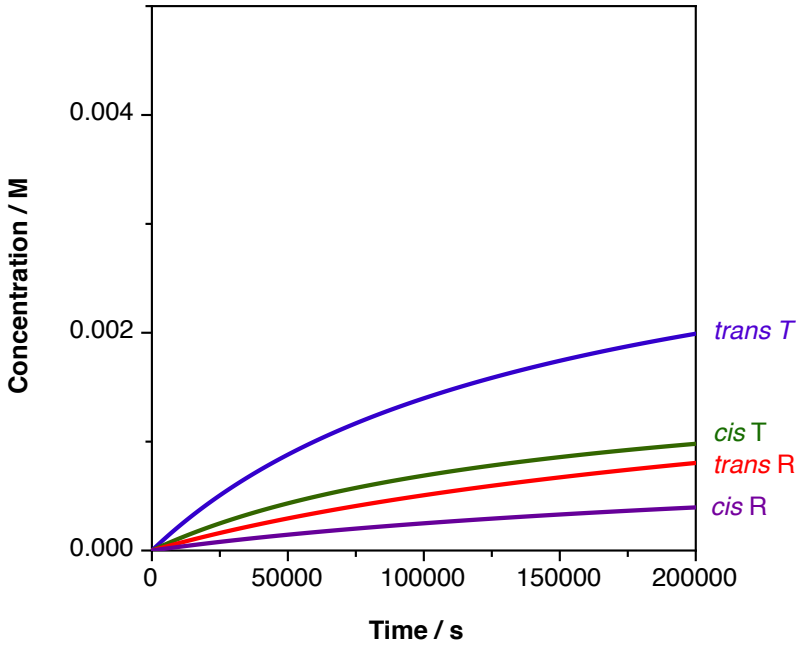

Figure 7.22. Simulation of the rotaxane and thread formation between maleimide **198**, nitrone **197** and macrocycle **AEMDG** at 10 mM starting concentrations, giving accordingly the *trans* thread **199** (blue line), *cis* thread **199** (green line), *trans* rotaxane **200** (red line), and *cis* rotaxane **200** (purple line). (T and R represents the thread and rotaxane, respectively).

In order to test whether these simulations of the thread and rotaxane formation reflect the real behaviour of the system, therefore we must explore the real scenario in the laboratory. An equimolar solution of maleimide **198** and macrocycle **AEMDG** in $CDCl_3$ was pre-equilibrated at 25 ˚C for one hour, before the addition of nitrone **197** to the mixture and the starting concentrations each of the three reagents thus set at 10 mM.

The course of reaction was assayed by ^{1}H NMR spectroscopy at 298 K for 48 hours. The 500 MHz ^{1}H NMR spectra of the reaction mixture are crowded, however the resonances arising from the formation of the cycloadducts can be monitored (**Figure 7.23**) – kinetic data for the formation of *trans* rotaxane **200**, *cis* rotaxane **200**, *trans* thread **199** and *cis* thread **199** can all be obtained. It is noteworthy that the appearance of the resonances for the *cis* diastereoisomers for both rotaxane and thread cannot be assayed accurately until four hours of the experiment.

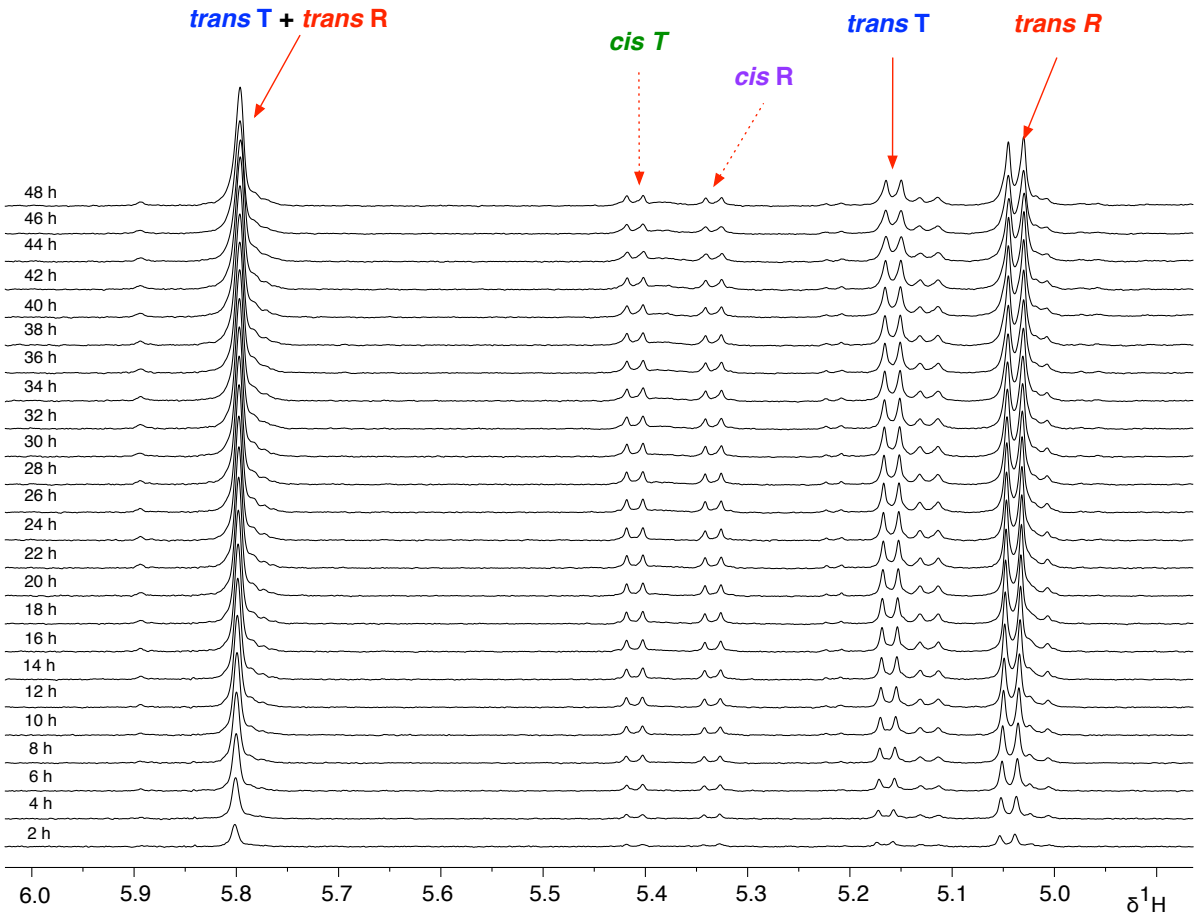

Figure 7.23. Partial ^{1}H NMR spectra (500 MHz, 298 K, $CDCl_3$, 10 mM) of the reaction between maleimide **198**, nitrone **197** and macrocycle **AEMDG** over 48 hours, illustrating spectral region associated with the resonances of the *trans* thread **199**, *cis* thread **199**, *cis* rotaxane **200** and *trans* rotaxane **200**.

Deconvolution of the obtained spectra resulted in the concentration *vs* time profile for this experimental data and fitted using SimFit in **Figure 7.24** by varying the rate of pseudorotaxane [**AEMDG·198**] and nitrone compound **197**.

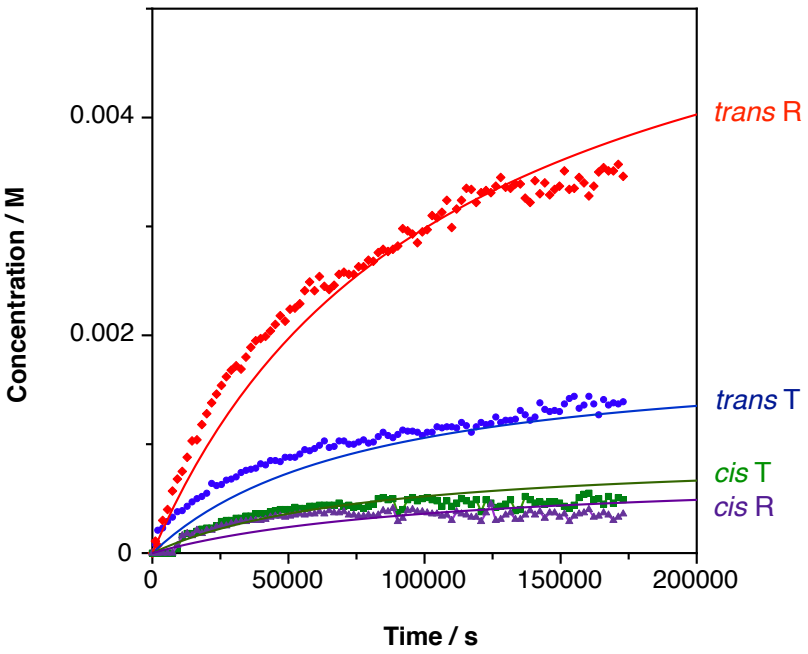

Figure 7.24. Concentration *vs* time profile for the reaction (500 MHz, $CDCl_3$, 298 K, 48 h) between nitrone **197**, maleimide **198** and macrocycle **AEMDG** at 10 mM reagent concentrations. The formation of *trans* rotaxane **200** is shown as red filled diamonds, *trans* thread **199** as blue filled circles, *cis* thread **199** as green filled squares and *cis* rotaxane **200** is plotted as purple triangles filled. Solid lines represent the results for the fitting of *trans* rotaxane **200** (red line), *trans* thread **199** (blue line), *cis* thread **199** (green line) and *cis* rotaxane **200** (purple line), respectively.

The reaction resulted in 57% conversion of maleimide, macrocycle **AEMDG** and nitrone to cycloadducts, with the ratio of rotaxane to thread being approximately 2:1. From the beginning of the reaction, the rate constant of formation of *trans* rotaxane **200**, 4×10^{-3} M^{-1} s^{-1} is higher than t*rans* thread **199**, 9×10^{-4} M^{-1} s^{-1}. As a consequence of this reactivity, *trans* rotaxane **200** present in 4 mM after 48 hours to compare of only 1.5 mM concentration of *trans* thread **199**. The ratio of *trans* rotaxane **200** to *trans* thread **199** was 2.5:1, *i.e.* there was more rotaxane present than thread. Following this, the diastereomeric ratio of the *cis* cycloadducts (*cis* thread **199** and *cis* rotaxane **200**) were estimated to be close to 1.3:1 ratio, respectively. Hence, the *trans* diastereoisomers were favoured nearly about 6:1 over the *cis* diastereoisomers.

On average, the simulation (solid line, **Figure 7.24**) matches reasonably well with the experimental results for the reaction in the presence of macrocycle **AEMDG** even though the progression for *trans* rotaxane and *trans* thread does not correspond correctly to the simulation. The concentrations for *trans* diastereoisomers of rotaxane **200** is about 2.7 mM higher than that from the earlier calculated concentration from

the simulation whereas the experimental value for *trans* thread is 0.61 mM short of the one found in calculated concentrations. Concomitantly, the experimental data provided satisfactorily values of *cis* diastereoisomers for thread and rotaxane in the calculation, which were formed to minor extent, between 0.4 to 0.5 mM. All data presented clearly suggests that the formation of *trans* rotaxane **200** is significantly faster than the formation of *trans* thread **199**, which can be attributed to the existence of one or more complexes that consequently enable it to facilitate its own formation. This finding is supported by space filling model of *trans* rotaxane **200** (**Figure 7.25**).

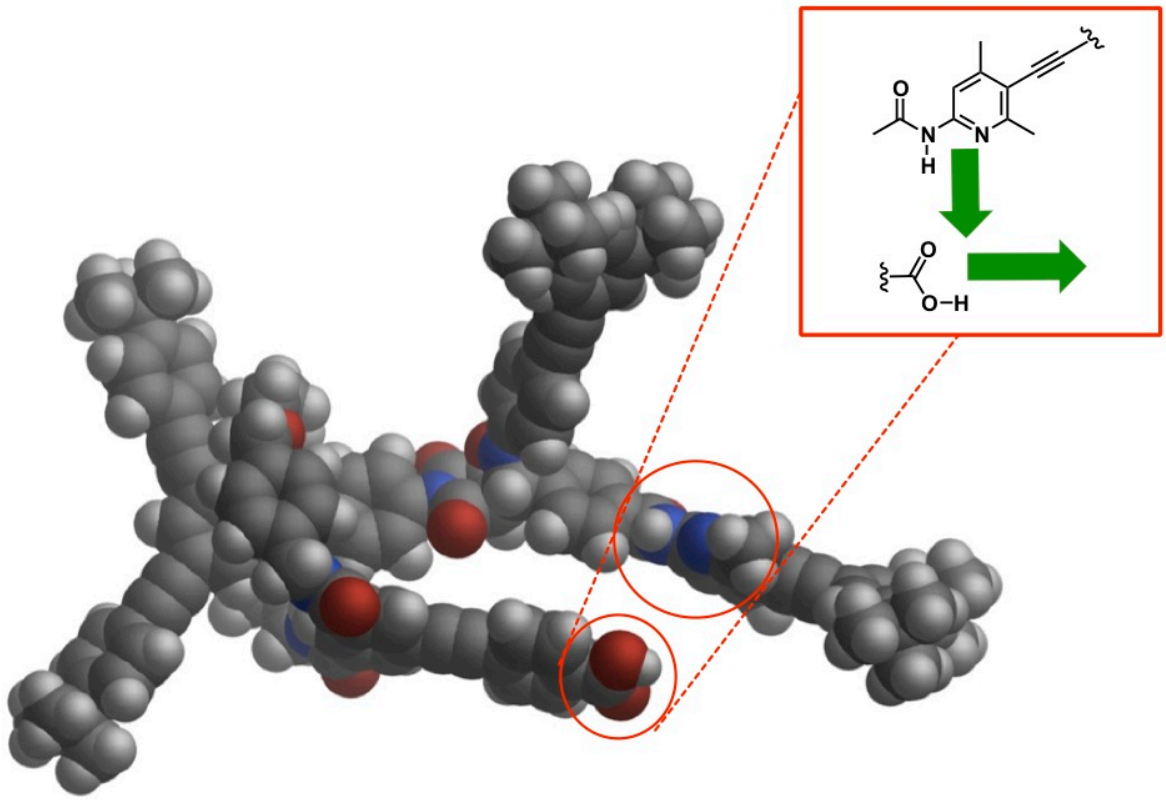

Figure 7.25. Space filling model of *trans* rotaxane **200**. Carbon atoms are shown in dark grey, nitrogen atoms in blue, oxygen atoms in red and hydrogen atoms are coloured white. The clashing orientation of hydrogen donor from the amidopyridine and carboxylic acid recognition motif are shown in inset.

The corresponding rotaxane is predicted computationally to provide the correct geometry to support replication. As a consequence of the length mismatch between the acid building blocks on macrocycle **AEMDG** and the amidopyridine site of nitrone **197**, the formation of a productive binary complex between the nitrone **197** and macrocycle **AEMDG** through the [**A•B**] pathway can be ruled out. Furthermore, it is hard to imagine the rigid structure of the acetylene fragment from the upper ring component is capable of bending to the contrasting orientation of hydrogen donor of

the amidopyridine recognition motif (inset, **Figure 7.25**). Although, an explanation for the selectivity of *trans* rotaxane **200** enhancement is yet unknown, the feasibility of the product duplex of *trans* rotaxane **200** is highlighted in the calculated structure, in which the self-complementary of the duplex structure is visible (**Figure 7.26**).

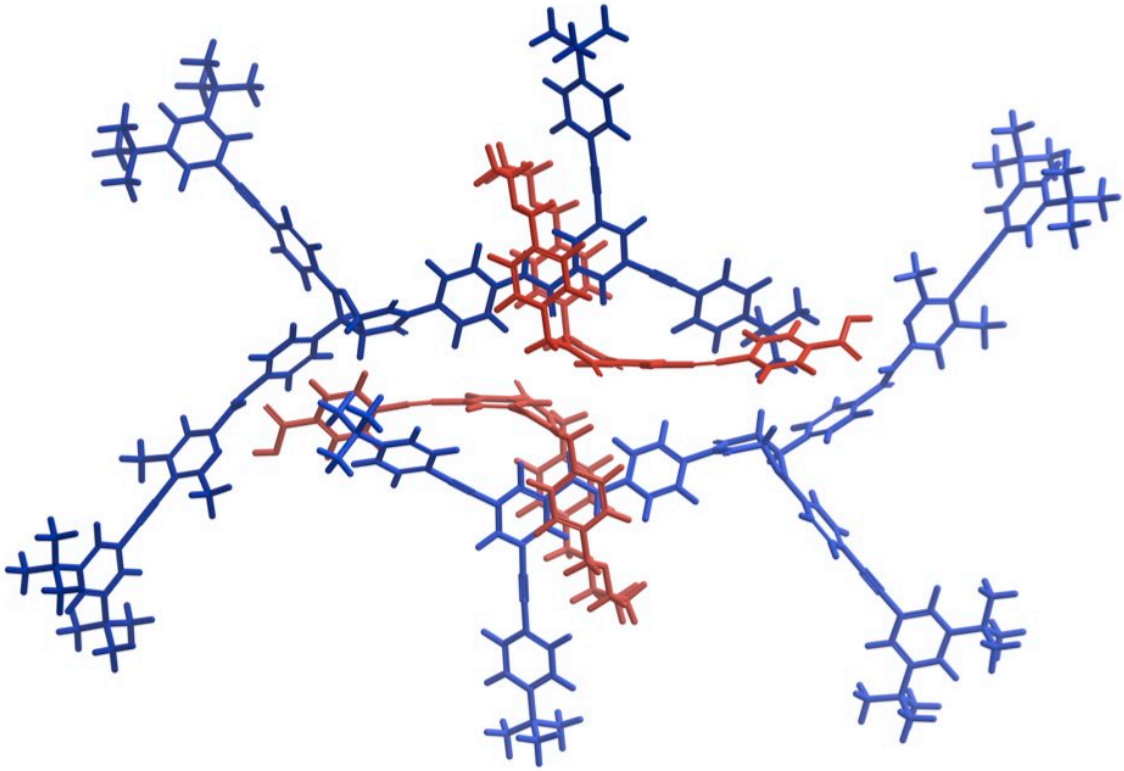

Figure 7.26. Molecular model (OPLS2005, GB/SA $CHCl_3$) of the *trans* rotaxane **200** duplex. The thread component are shown in dark and light blue whereas the macrocycle **AEMDG** are shown in dark and light red colour. Most of the hydrogen atoms were omitted for clarity.

Its rigid structure allows for the formation of a duplex structure, in which the recognition sites on both ends of the template possess the right orientation to associate through hydrogen bonding. As a consequence, template-directed synthesis of *trans* rotaxane **200** through a ternary complex with both reagents seems feasible. In addition, the formation of rotaxane **200** cycloadducts were corroborated by MALDI mass spectrometry from the crude ^{1}H NMR kinetic reaction (**Figure 7.27**).

Principally, in order to prove unambiguously replicating behaviour of this system, supplementary doping experiment with the product itself should be carried out. In addition of the pre-synthesised *trans* rotaxane **200** at the beginning of the reaction between nitrone **197**, maleimide **198** and macrocycle **AEMDG** should resulted in an

increase in the initial rate of formation of *trans* rotaxane **200**. The envisaged control experiment provide evidences of that *trans* rotaxane **200** templating and accelerating its own emergence. Moreover, in order to address the reliance of the system on molecular recognition, the remainder of the full kinetic analysis could be demonstrated by performing the inhibitor control experiment. In the presence of 4-bromophenylacetic acid, a decrease on the rate of the reaction as a consequence of the interference of the competitive inhibitor with the recognition process should be observed. Nonetheless, given small quantity of nitrone **197** available, the exhaustive kinetic investigation of the rotaxane system could not be conducted.

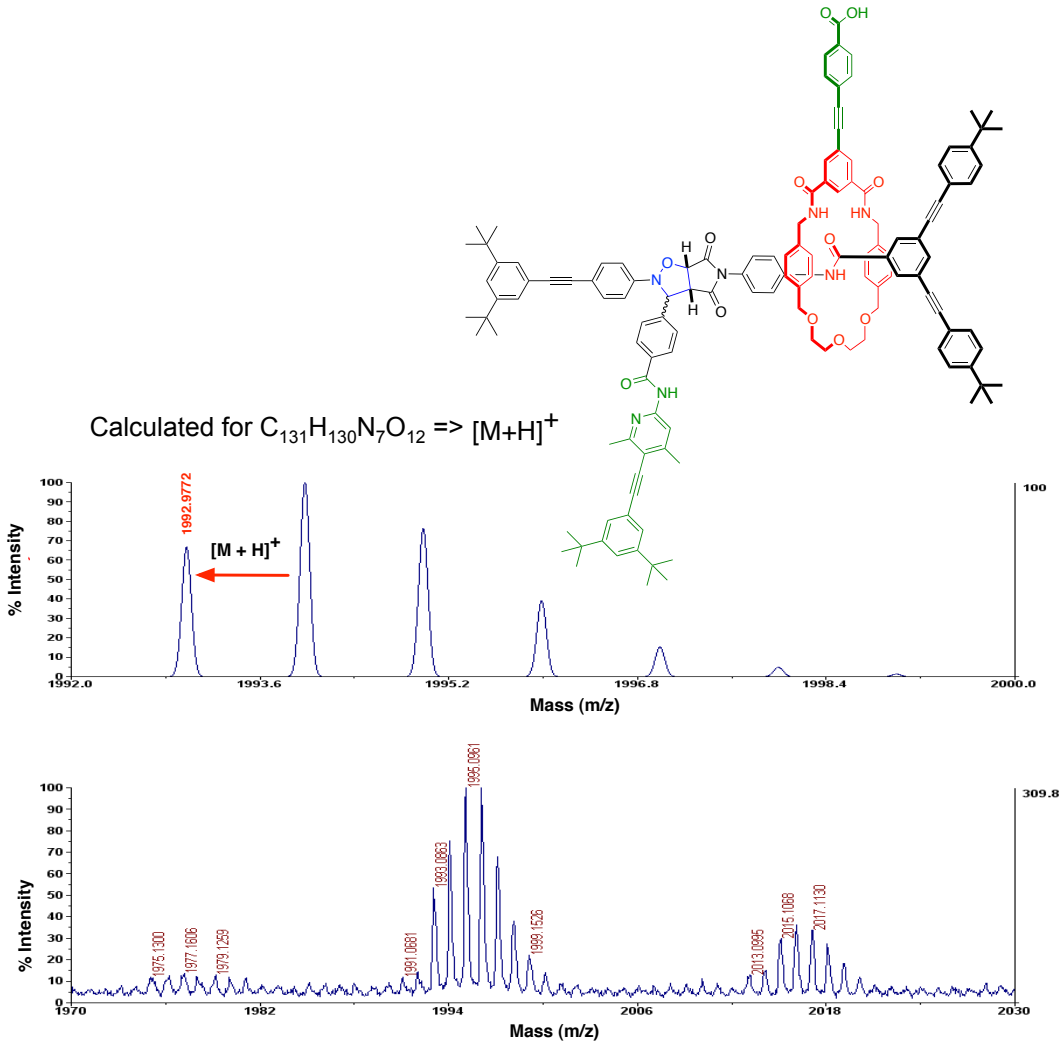

Figure 7.27. MALDI mass-spectra of rotaxane compound **200**. Mass spectrometry (MALDI) *m/z* 1992.9772 (60%, $[M+H]^+$), calculated for $C_{131}H_{130}N_7O_{12}$.

7.10 Conclusion

This chapter describe a potential approach to the assembly of self-replicating rotaxanes by employing the alternative **Replication model 2**. The formation of the replicating structure of rotaxanes relies heavily on the stronger complexation of the acid-substituted macrocycle with the desired maleimide component, in which enable them to adjust themselves to participate in the recognition-mediated pathway of the autocatalytic cycle with nitrone compound in the rotaxane formation. The pseudorotaxane complex is central element within a self-replicating framework.

A number of design potential of self-replicating rotaxanes have been devised in order to integrate self-replication with the formation of [2]-rotaxane. It is important to recognize the unanticipated larger cavity of the third generation macrocycles as a result of the insertion of acid recognition motif on the isophthaloyl building blocks of the ring component. These changes force us to modify our current nitrone compounds in order to protect the larger cavities of the newly prepared acid macrocycles. The quest for a reliable nitrone structure has intensified to integrate a bulky end group on the amidopyridine recognition site to impede the unfavourable pseudorotaxane formation species between the acid macrocycle and the nitrone compound. Satisfyingly, some of the macrocycle and guest pairs presented here have been successfully exploited to construct rotaxanes.

Nevertheless, as a consequence of solubility and synthetic difficulty, we had to compromise the macrocycle binding site, which eventually affected in a low association constant for the pseudorotaxane complex. In the system ultimately designed, pleasingly, a substantial amount of rotaxane was present, mostly as *trans* diastereoisomer. The initial kinetic behaviour of this system suggests that the resulting rotaxane structures are self-replicating through the recognition-mediated pathways.

8

Replication model 3

8.1 Introduction

Ultimately, we envisaged the final replication scheme of replicating rotaxanes based on the placement of the two recognition sites (green cartoons in **Figure 8.1**) on the same stopper.

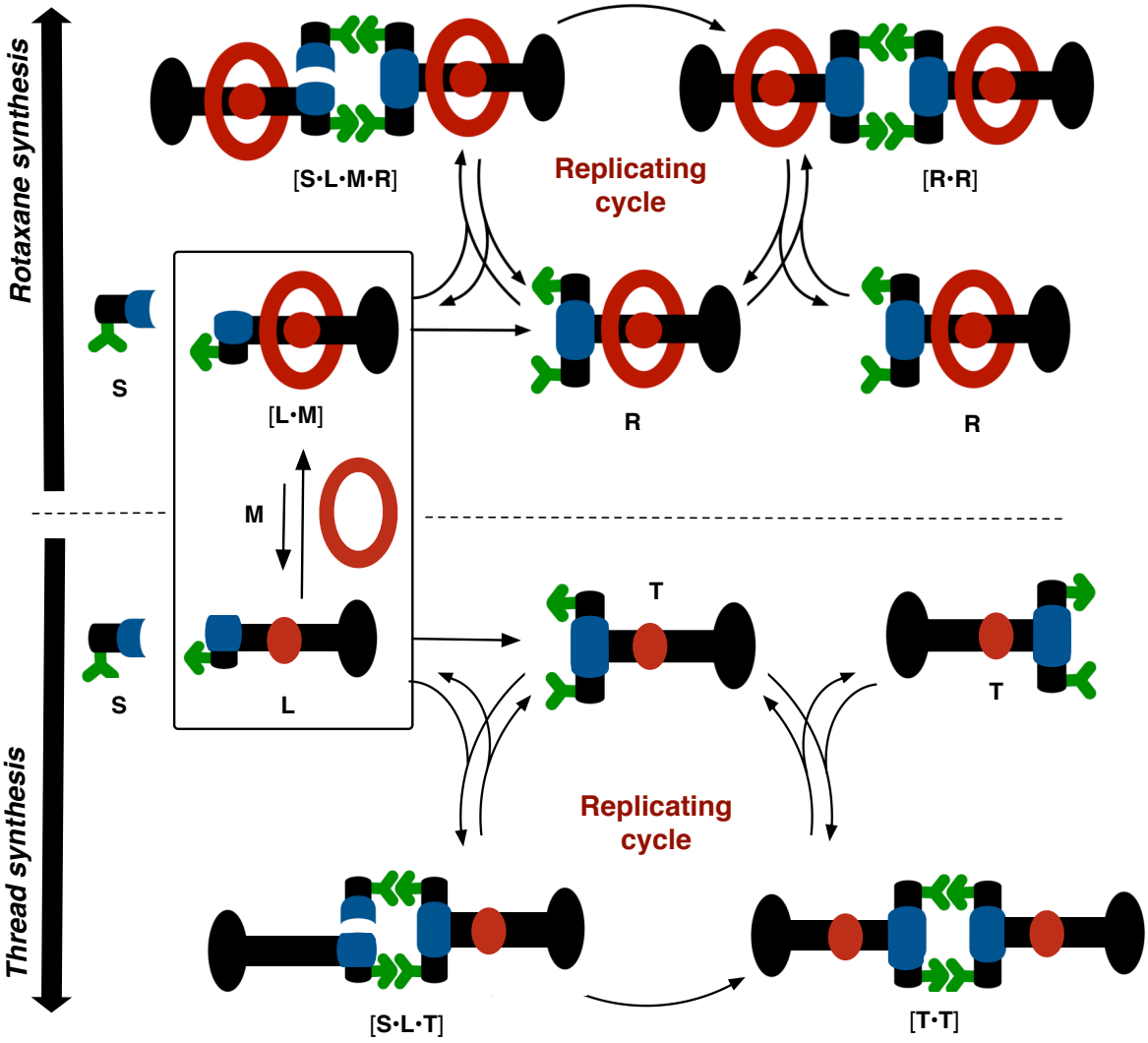

Figure 8.1. **Replication model 3** of self-replicating rotaxanes based on the placement of two recognition sites (green cartoons) on the same stopper. The blue cartoons represent the reactive sites, and the red cartoons represent the binding site.

The linear component simultaneously incorporates the binding site (red cartoons) and the recognition site (green cartoons) appended on the reactive sites stopper (blue cartoons) to allow the formation of the [**L•M**] complex. The subsequent reaction with the second element of the stoppering reagent **S**, which comprise complementary recognition site provide the rotaxane **R** molecule. Stoppering reagent **S** and pseudorotaxane [**L•M**] can bind reversibly to the **R** molecule to form the catalytic quarternary complex [**S•L•M•R**]. Additional bond formation takes place between reagent **S** and [**L•M**] complex to give the product duplex [**R•R**], which then the two molecules of **R** disassociates to reinstall the autocatalytic cycle. The obvious drawback from **Replication model 1** yet remain – the optimisation of the binding constant between the ring component and the guest is the prime importance in order to facilitate the maximal formation of [**L•M**] complexes. Despite this setback, it is possible to exploit the developed replicator molecules in the group. The chosen replicator is suitable to incorporate in the self-replicating rotaxanes system such that, it proceeds readily at room temperature in maximum rate and high diastereoselectivity, and will be described in the following paragraphs.

8.2. Design of a potential self-replicating rotaxane

The parent macrocycles **MDG** and **MP** (first described in **Chapter 4**) were designed to incorporate the amide binding site. The pseudorotaxane assembly are thus expected, resulting from the mutual association of the macrocycle with the amide guest. The initial step in the construction of potential self-replicating rotaxane presented in **Scheme 8.1** comprised either macrocycle **MDG** or **MP** as the ring component. The nitrone compound **201** consist of the carboxylic acid recognition site and di-*tert*-butylphenyl ring as the blocking group to furnish the pseudorotaxane complex between macrocycle **MDG** and nitrone compound **201** in solution.

The second stopper was attached to this complex by employing the 4,6-dimethylpyridine ring maleimide compound **202**, to yield the [2]-rotaxane. It has been established so far that 4,6-dimethylpyridine and 4-*tert*-butylphenyl ring (as discussed in **Chapter 4**) are adequately large end groups to prevent macrocycle **MDG** from deslipping of the thread component. Both maleimide **202** and acid nitrone compound **201** have been previously developed[262] in our laboratory for the construction of small molecule replicator.

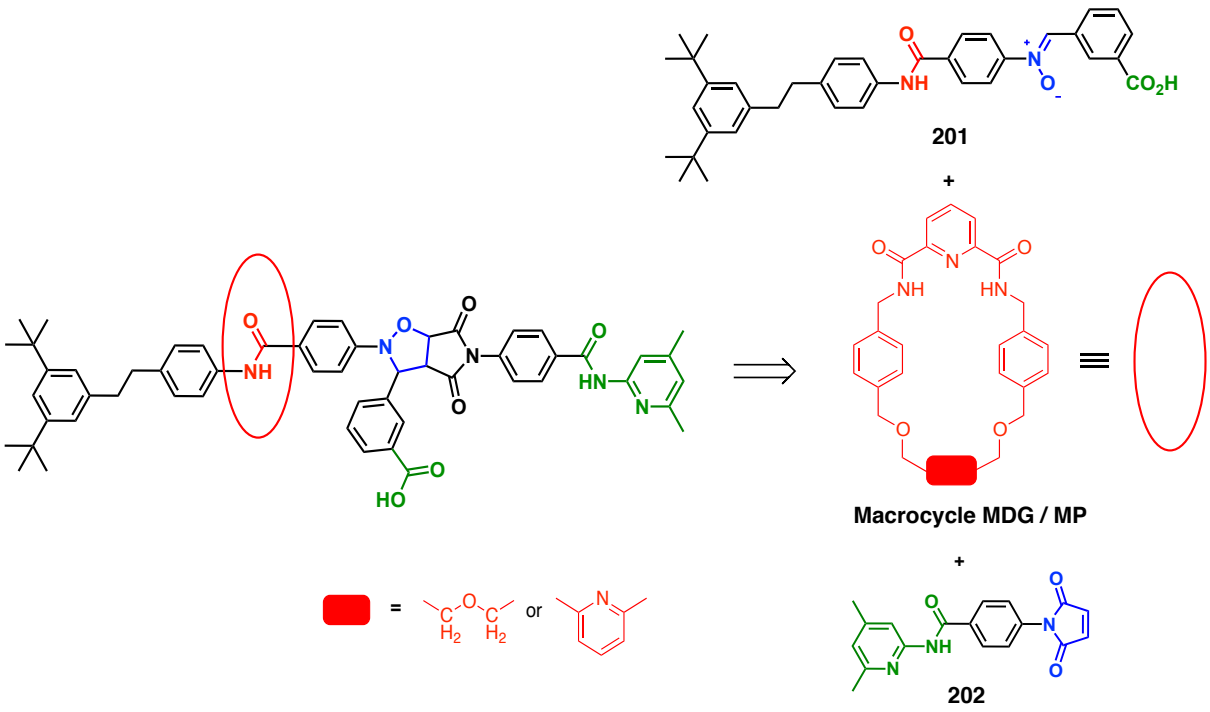

Scheme 8.1. Retrosynthesis of potential self-replicating rotaxanes consists of an acid nitrone **201**, macrocycle **MDG** or **MP** and 4,6-dimethylpyridine maleimide **202**.

8.2.1 Binding study

As a result of limited solubility of nitrone compound **201** in non-polar solvents, no binding experiments were carried out between both macrocycles and the acid nitrone **201**. Although nitrone **201** has greater solubility in polar solvent such as methanol and dimethylsulfoxide, such solvent can not be utilized as additive in a chloroform solution to increase its solubility since they acts as competitive inhibitors for the binding events to occur by disrupting the association of the macrocycle with the amide binding site and the recognition between the complementary recognition sites. Satisfactorily, the solubility was improved in the presence of the maleimide compound **202**.

8.2.2 Kinetic study of the thread

The kinetic study was first carried out in the absence of macrocycle, in order to analyse the performance of the thread in isolation (**Scheme 8.2**). The course of the reaction was assayed by ^{1}H NMR spectroscopy in $CDCl_3$ at 298 K for 24 hours with the initial concentration of 10 mM for both starting materials. 1,3-dipolar cycloaddition reaction between the acid nitrone **201** and maleimide **202** was proved to afford thread **203** by closely monitored the disappearance of the resonance that arises from

the maleimide protons at δ_H 6.89 and the concomitant appearance of the resonances that arise from the *trans* **203** at δ_H 5.82.

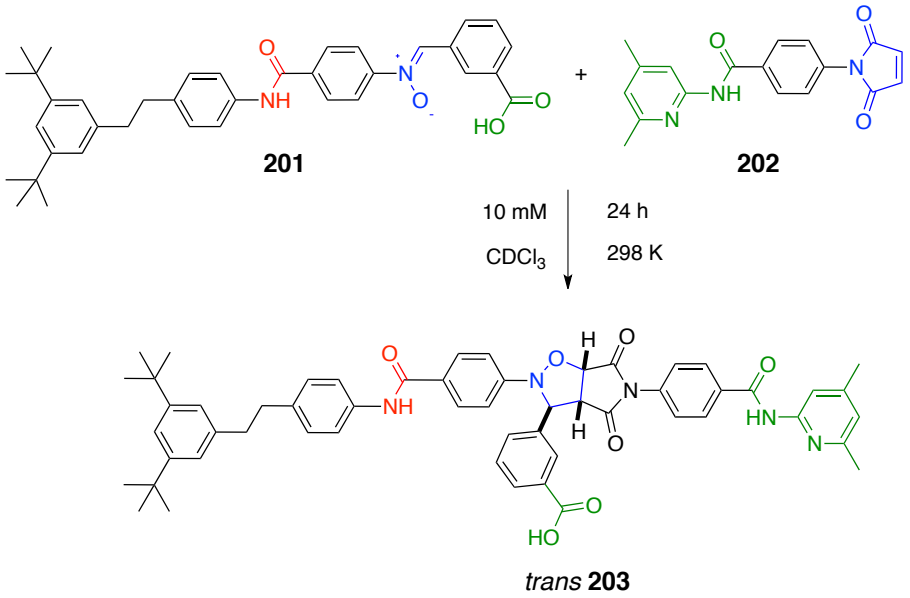

Scheme 8.2. 1,3-dipolar cycloaddition between acid nitrone **201** and maleimide **202** affording the highly selective *trans* **203** isoxazolidines.

Accordingly, the concentration *vs* time profile for *trans* **203** was plotted from the deconvolution of these resonances (**Figure 8.2**).

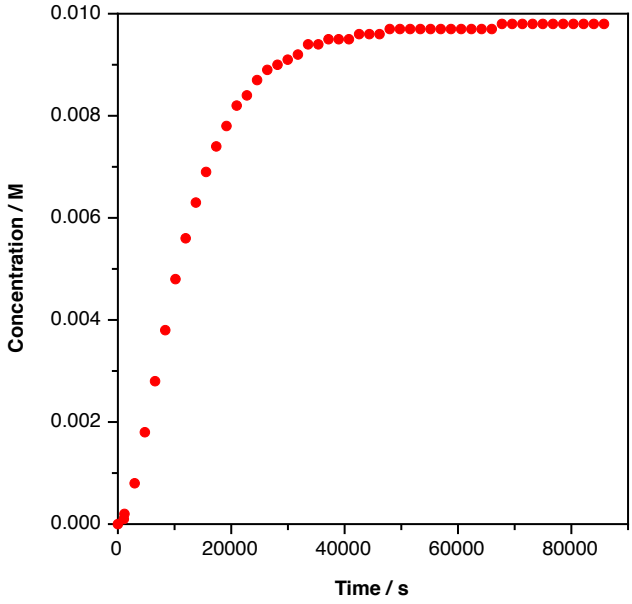

Figure 8.2. Concentration *vs* time profile for the reaction (500 MHz, $CDCl_3$, 10 mM) between acid nitrone **201** and maleimide **202** affording *trans* **203** at 298 K over 24 hours.

Reaction between acid nitrone **201** and maleimide compound **202** at 298 K result in 98% overall conversion over 24 hours, giving exclusively the *trans* **203**

diastereoisomer. The formation of the *trans* **203** denoted an efficient self-replicating behaviour with obvious sigmoidal rate profile, whereas the *cis* **203** revealed no recognition-mediated behaviour. The finding was supported from the molecular modelling of the monomer *trans* **203** (**Figure 8.3**).

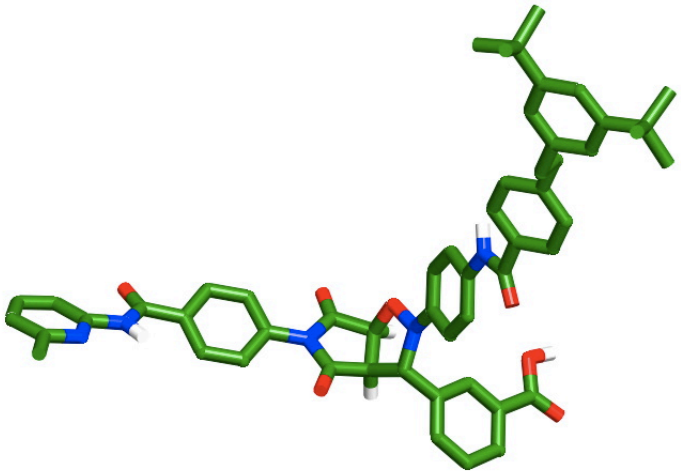

Figure 8.3. Stick representation of the calculated structure (OPLS2005.GB/SA $CHCl_3$) of the major *trans* **203** diastereoisomer. Carbon atoms are coloured green, oxygen atoms red, nitrogen atoms blue and hydrogen atoms white (most hydrogen atoms have been removed for clarity).

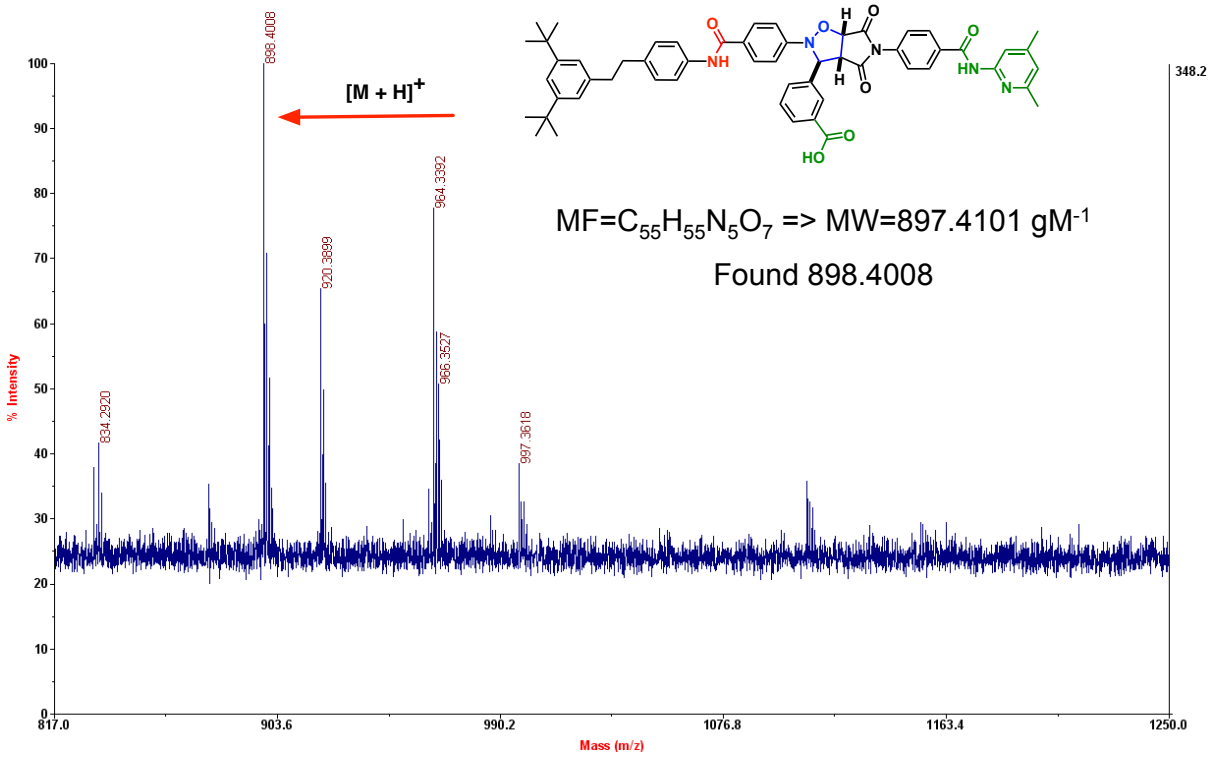

Figure 8.4. MALDI mass-spectra of *trans* **203** diastereoisomer correspond to molecular weight ions of $[M+H]^+$.

The feasible geometry of *trans* **203** permit the self-complementary duplex to slightly wrap each other in order to position the recognition units correctly, in which hydrogen

bonding between the recognition units at both ends of the template molecule can take place and self-replicating activity of *trans* **203** is established. It is also noteworthy that the ^{1}H NMR spectrum and MALDI mass spectrometry also reveals the formation of *trans* **203** diastereoisomer.

8.2.3 Kinetic study of the rotaxane

The analogous kinetic experiment was conducted in the presence of macrocycle **MDG**, afforded simultaneously the [2]-rotaxane and thread component. In this experiment, the reversible formation of [**MDG•201**] complex reacted with acid nitrone compound **201** to yield rotaxane **204**. Alternatively, thread **203** was obtained from the reaction between free maleimide **202** and acid nitrone **201** (**Scheme 8.3**).

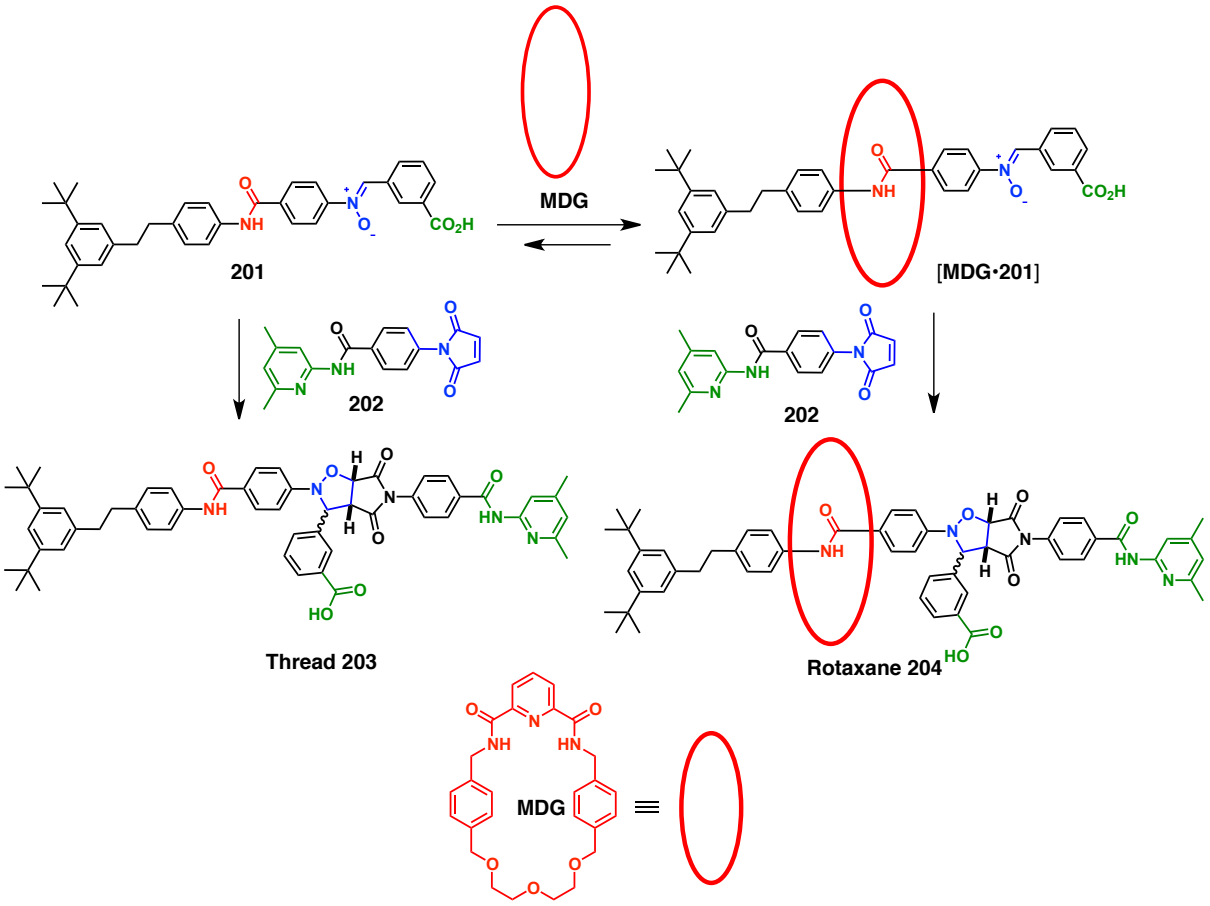

Scheme 8.3. Possible reaction pathways during the formation of potential self-replicating rotaxane **204**. Maleimide **202** can react either with unbound acid nitrone **201** to afford thread **203** or with pseudorotaxane [**MDG•201**] to afford rotaxane **204**, respectively.

An equimolar solution of acid nitrone **201** and macrocycle **MDG** in $CDCl_3$ was bring into equilibrium at 298 K for one hour followed with the addition of maleimide **202** to the mixture. As noted in the kinetic study of thread **203**, the initial concentration of the

starting materials was 10 mM. The resulting product was monitored using 500 MHz ^{1}H NMR spectroscopic analysis, which observed the development of the resonances (**Figure 8.5**) of proton H^{3T} that arise from the *trans* thread **203** at δ_H 5.81 and of proton H^{3R} originated from the *trans* rotaxane **204** at δ_H 5.56. It is noteworthy that no *cis* diastereoisomer was identified from the reaction mixture.

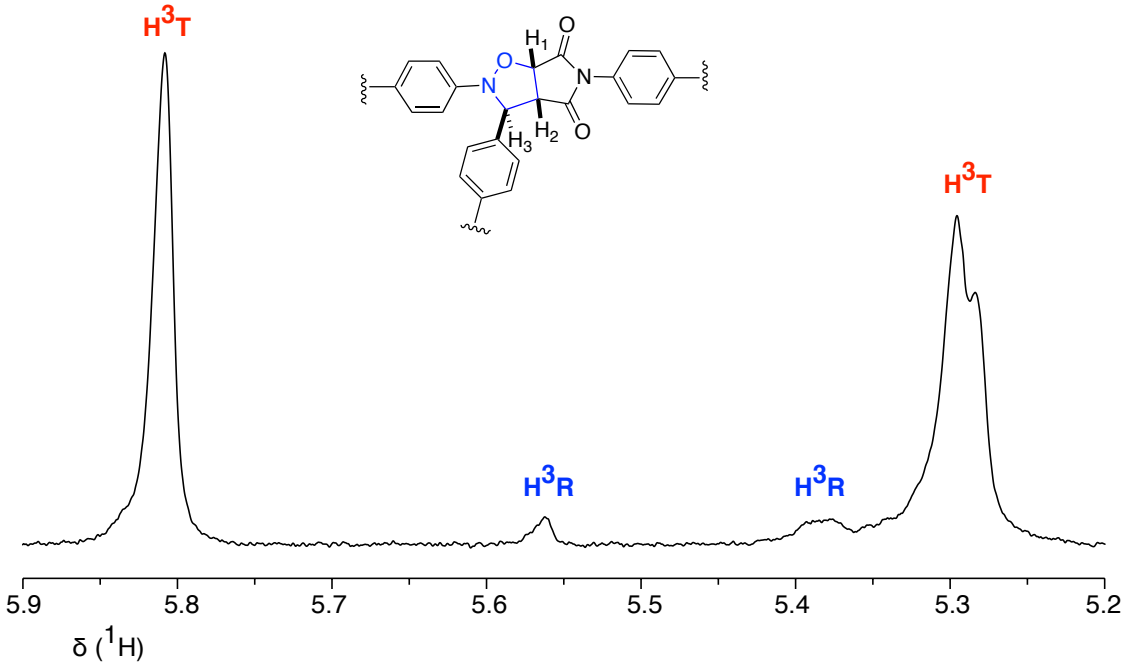

Figure 8.5. Partial ^{1}H NMR spectrum (500 MHz, 298 K, $CDCl_3$, 10 mM) of the reaction between macrocycle **MDG**, acid nitrone **201** and maleimide **202** over 48 hours. **T** and **R** represents thread and rotaxane respectively.

Analysis of the rate profile for this new system revealed that the thread conversion dropped to 33% over 48 hours in the presence of macrocycle **MDG**. Unexpectedly, the reaction yielded the corresponding rotaxane **204** in reduced yield of 2% in the presence of one equivalent of macrocycle **MDG** (**Figure 8.6**).

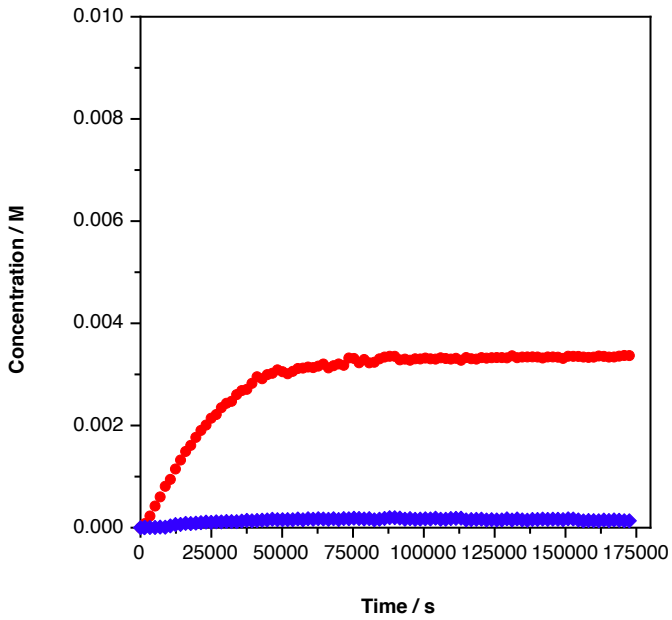

Figure 8.6. Concentration *vs* time profile for the reaction (500 MHz, $CDCl_3$, 10 mM) between acid nitrone **201** and maleimide **202** in the presence of one equivalent of macrocycle **MDG** at 298 K over 48 hours. The formation of *trans* thread **203** is shown as red filled circles and *trans* rotaxane **204** as blue filled diamonds.

As a consequence, the ratio of thread to rotaxane was found to be at least 25:1 in favour of *trans* cycloadducts for each thread and rotaxane. Despite the fact that the formation of thread appear to be highly selective for the *trans* diastereoisomer, this selectivity was lessened in the existence of macrocycle **MDG** in the system. As explained in **Replication model 1**, the formation of the [2]-rotaxane again critically dependent on the pseudorotaxane precursor, which unambiguously demonstrated the critical binding event between the macrocycle **MDG** and the amide moiety of the maleimide **202**.

Whilst it is presumed that macrocycle **MDG** bind preferably the amide moiety on the acid nitrone **201** *via* the formation of hydrogen bonds, the formation of pseudorotaxane complex nonetheless results in the reduced reactivity. In order to investigate the reduced reactivity of these complexes, the electronic structure calculation was subsequently applied (**Figure 8.7**).

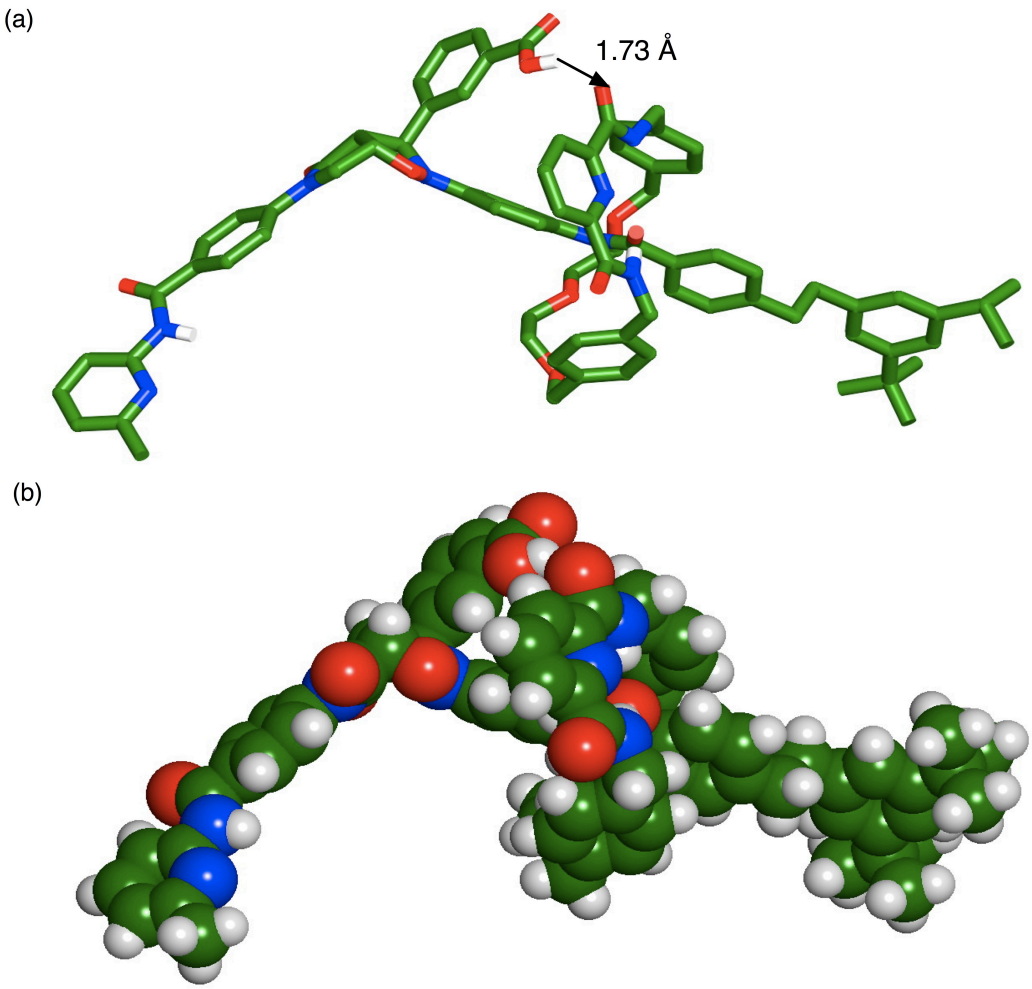

Figure 8.7. Stick representations of the calculated structures (OPLS2005, GB/SA $CHCl_3$) of (a) [2]-rotaxane formation [**MDG·201·202**] displays that the carbonyl group of the macrocycle **MDG** and the hydroxyl group of the acid nitrone **201** are extensively hydrogen bonded (1.73 Å) and (b) The carboxylic acid of thread **203** exerts marked steric effect on the ring component as illustrated in the close-packed space filling model. Carbon atoms are coloured green, oxygen atoms red, nitrogen atoms blue and hydrogen atoms white (most hydrogen atoms have been removed for clarity).

In prior investigations, we became aware[207] that the reactive site on the **L** component must be placed sufficiently far away from the binding site to prevent the introduction of a supramolecular steric effect through the proximity of the macrocyclic component **M**. These examples should also serve to illustrate the cause for the low reactivity of pseudorotaxane in this case.

Additionally, the carboxylic acid group from thread **203** was positioned in the vicinity of the approaching ring component, consequently exerts marked steric effect results in the unfavourable formation of the mechanically interlocked molecules. It is also visible from the calculated structure that the oxygen atom from the carbonyl group (H-acceptor) of the macrocycle **MDG** and the hydroxyl group (H-donor) of the acid

nitrone **201** are extensively hydrogen bonded (1.73 Å). The result of this calculation again suggests[200] that in the framework of the self-replicating rotaxane, the reactive site on the **L** component must be located far from the complexation site of the macrocycle to prevent the pronounced supramolecular steric effect. Satisfyingly, Matrix Assisted Laser Desorption Ionization (MALDI) mass spectrometry confirms the formation of rotaxane **204** in the reaction mixture (**Figure 8.8**).

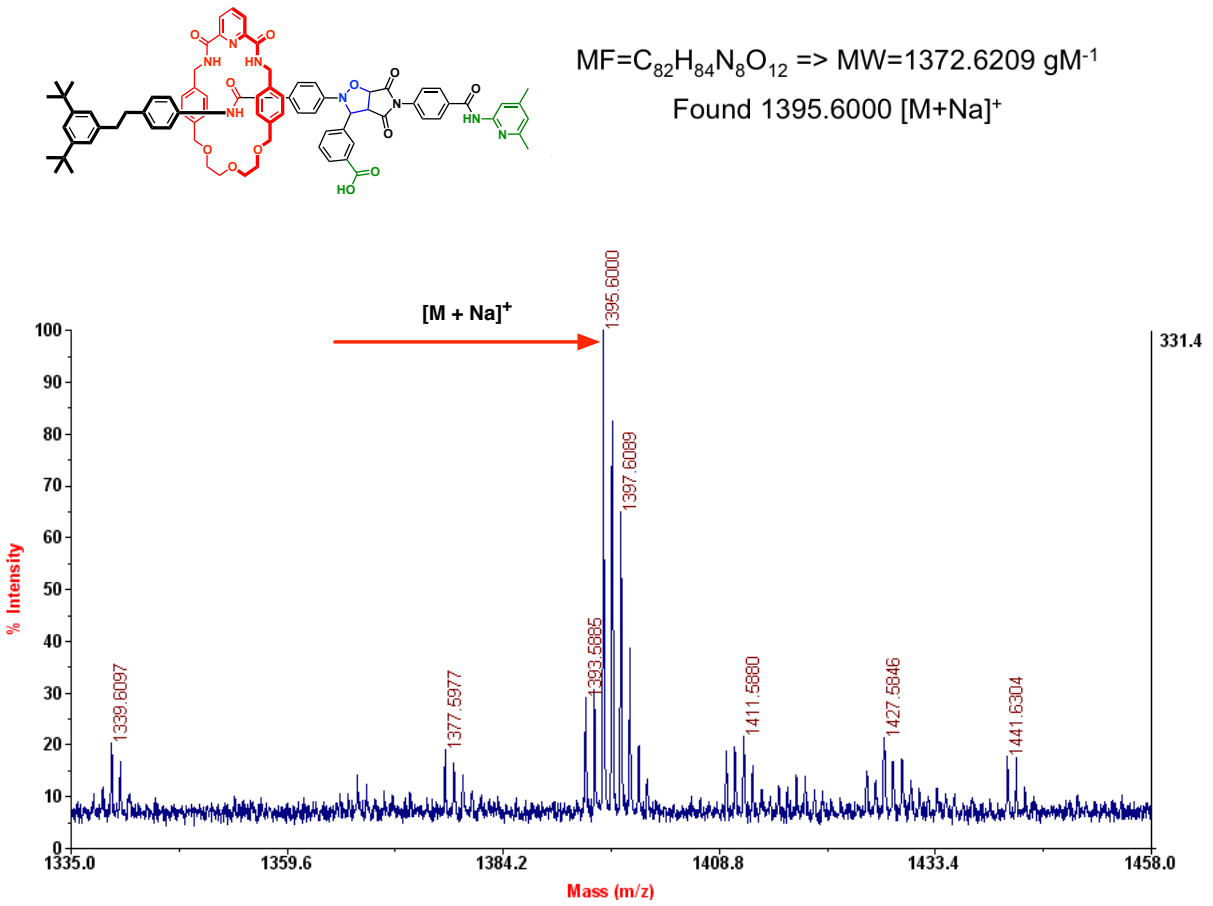

Figure 8.8. MALDI mass-spectra of rotaxane **204** compound which corresponds to molecular weight ions of $[M+Na]^+$.

8.3 Modified design of a potential self-replicating rotaxane

On the basis of designing recognition-mediated reactions, we have managed to resolve the solubility issues by reversing[207] the location of recognition sites on both the **L** and **S** components of the rotaxane design. Accordingly, a new system was envisaged in which the amidopyridine recognition site is now situated on the stopper of nitrone compound (for example nitrone **C**) while the carboxylic acid recognition site is appended on the stopper of maleimide **205** (stoppering reagent **S**) as depicted in **Scheme 8.4**.

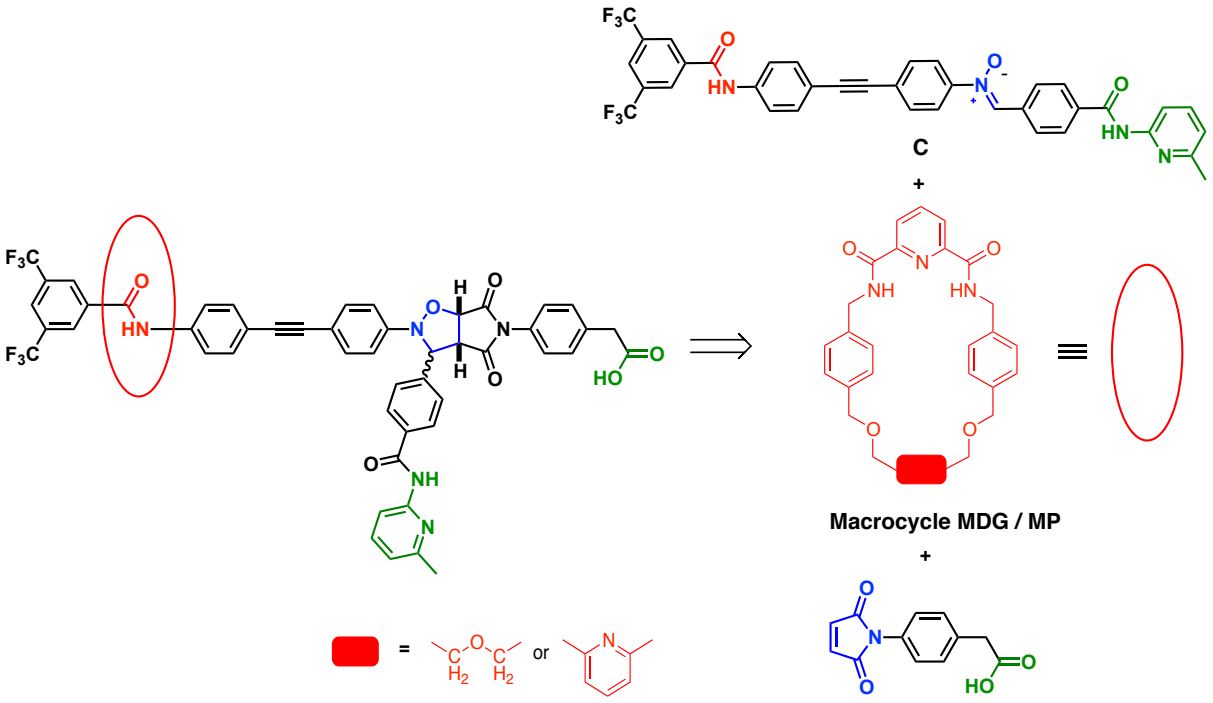

Scheme 8.4. Retrosynthesis of a potential self-replicating rotaxane 2. Amidopyridine recognition site (green colours) is positioned on the stopper of nitrone compound **C** (**L** component) containing the diarylamide binding site (red colour) and the carboxylic acid recognition site (green colour) on the stopper of maleimide compound **205** (**S** component). Both macrocycles **MDG** and **MP** are utilized in the modified design of self-replicating rotaxanes.

As noted earlier, length segregation must be established between the reactive site and the binding site to forbid any degree of supramolecular steric effect. Following this, the nitrone reactive site was placed markedly apart from the 3,5-bis(trifluoromethyl) amide binding moiety. According to preliminary binding experiments, 4,6-dimethylpyridine ring has been evaluated as sufficiently large end group for macrocycle **MDG**. On that account, an alternative 6-methylpyridine ring are exploited to allow the ring component to associate the diarylamide moiety of the linear component. A considerable attention was made to ensure that the ring has a higher affinity of binding the diarylamide moiety than the competitive binding sites, namely the nitrone itself and alternative amide site on the amidopyridine ring.

The selection of 3,5-bis(trifluoromethyl) substituent in the revised scheme of potential self-replicating rotaxanes (**Scheme 8.4**) is in accordance with prior K_a values found in **Chapter 4**. The association strength for [**MDG·110**] complex was estimated to be 1000 ± 100 M^{-1} and 4500 ± 500 M^{-1} [**MP·110**] complex, respectively. This observation was accompanied with significant chemical shift changes upon the formation of both

[2]-pseudorotaxane complexes. In our initial attempt to influence the positioning of the ring on the thread component, we have analysed the potential of a set of 3,5-disubstituted aryl amide end groups. Additionally, the correlation between the structure and the reactivity are revealed and used as a delicate probe into the effects of which electronic perturbation produces upon interlocking process.

8.4 Synthesis of the nitrone

In order to rationalize the binding affinity of the macrocycle to the targeted amide moiety, the following set of 3,5-disubstitited phenyl ring are devised. The substituent groups are introduced from $–OC_5H_{11}$, –Cl and $–CF_3$ in which the electron-withdrawing effects brought about by this substitution were referred to a reference substituent –H, that are considered to be neutral (neither electron-donating or -withdrawing).

Hammett parameters, σ_m for a set of substituent groups (nitrone compound **A** – **C**) and the obtained association constants are summarized below in **Figure 8.9**. On the whole, the differences in structure produce proportional changes in the K_a values. The reason[263] is that the changes in K_a (ΔG°) brought by the *m*-substituents are effectively change ΔH° since substitution does not greatly affect ΔS°. The K_a values are evidently increased to 2000 M^{-1} by substituent on the *m*–OC_5H_{11}.

Additionally, relative to hydrogen in the series, the substituents of *m*-Cl and *m*-CF_3 are increasingly electron withdrawing, and consequently ordered by increasing K_a of about 4600 M^{-1} and 5500 M^{-1}, respectively. In fact, the plot of log K_a for these substituents relative to that hydrogen is reasonably linear and evidence of the known linear free energy relationship. Thus, as you go through the series, only the substituent matter, which subsequently correlate with higher K_a values.

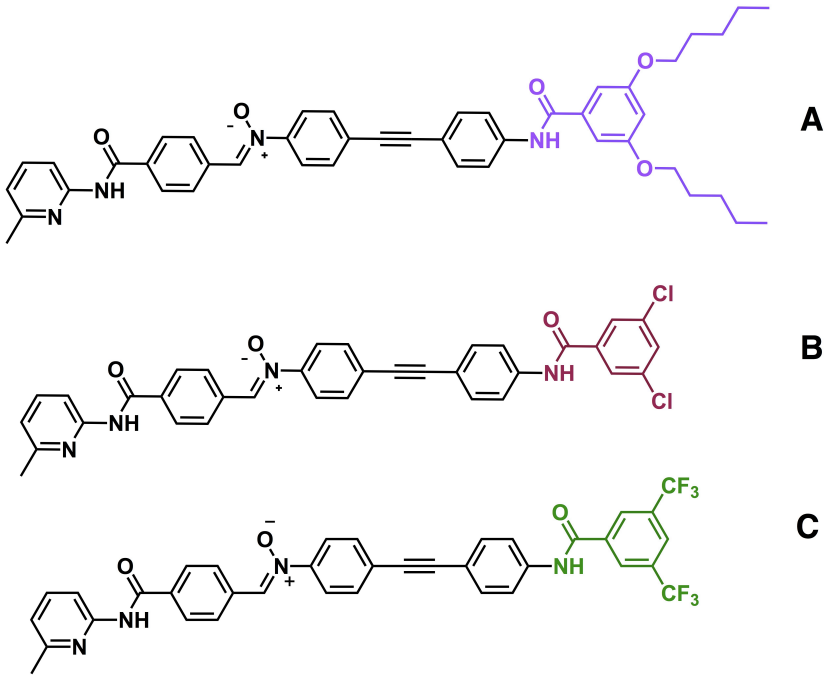

X	σ_m	K_a/M^{-1}
A	+0.12	2000
B	+0.37	4600
C	+0.46	5500

$$\log \frac{K_a(X)}{K_a(H)} = 1.325\sigma + 0.8473$$

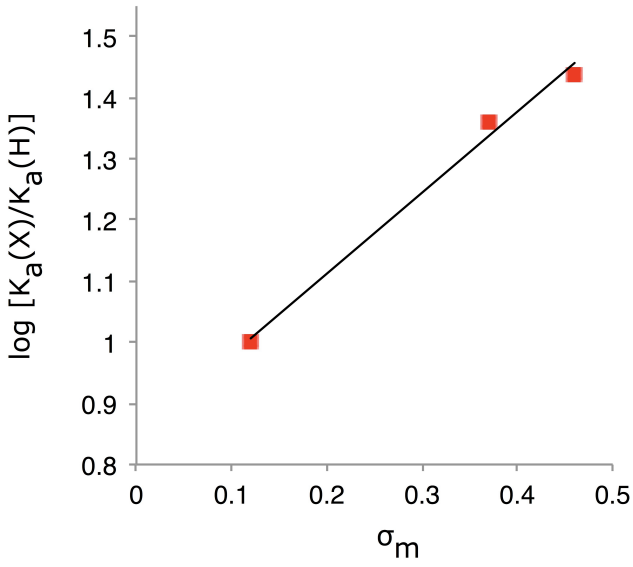

Figure 8.9. The effect of reactivities of electron-withdrawing substituents appended on the amide moiety of the nitrone component (structures **A**, **B** and **C**) relative to hydrogen with respect to the association constant, K_a (M^{-1}). Electron-withdrawing substituents are characterized by positive values of σ and hydrogen as reference point has σ = 0.0. Plot of log [K_a(X)/K_a(H)] against the σ_m value.

The best way to convey this observation is by visually represent it as in an electronic potential energy maps, comparing the two model compounds incorporating *m*–CH_3 and *m*-CF_3 (**Figure 8.10**). Electrostatic potential energy maps are useful when illustrating the charge distributions of molecules and changes in reactive site when molecules acquire or lose different functional groups. The electrostatic potential energies for both 3,5-dimethyl and 3,5-bis(trifluoromethyl) groups of the amide model

compounds were calculated. Noted that the three dimensional model of the electrostatic potential map is very similar to the fundamental structure of the two dimensional molecular structure. Area of low energy potential, red is characterize by the oxygen atom from the carbonyl group, whilst the blue region that emerge from the bottom of the molecule corresponds to the location of the hydrogen atom of the amide. However, there is a great deal of intermediary potential energy (yellow and green colour spectrum), which indicates the smaller electronegativity difference in both samples.

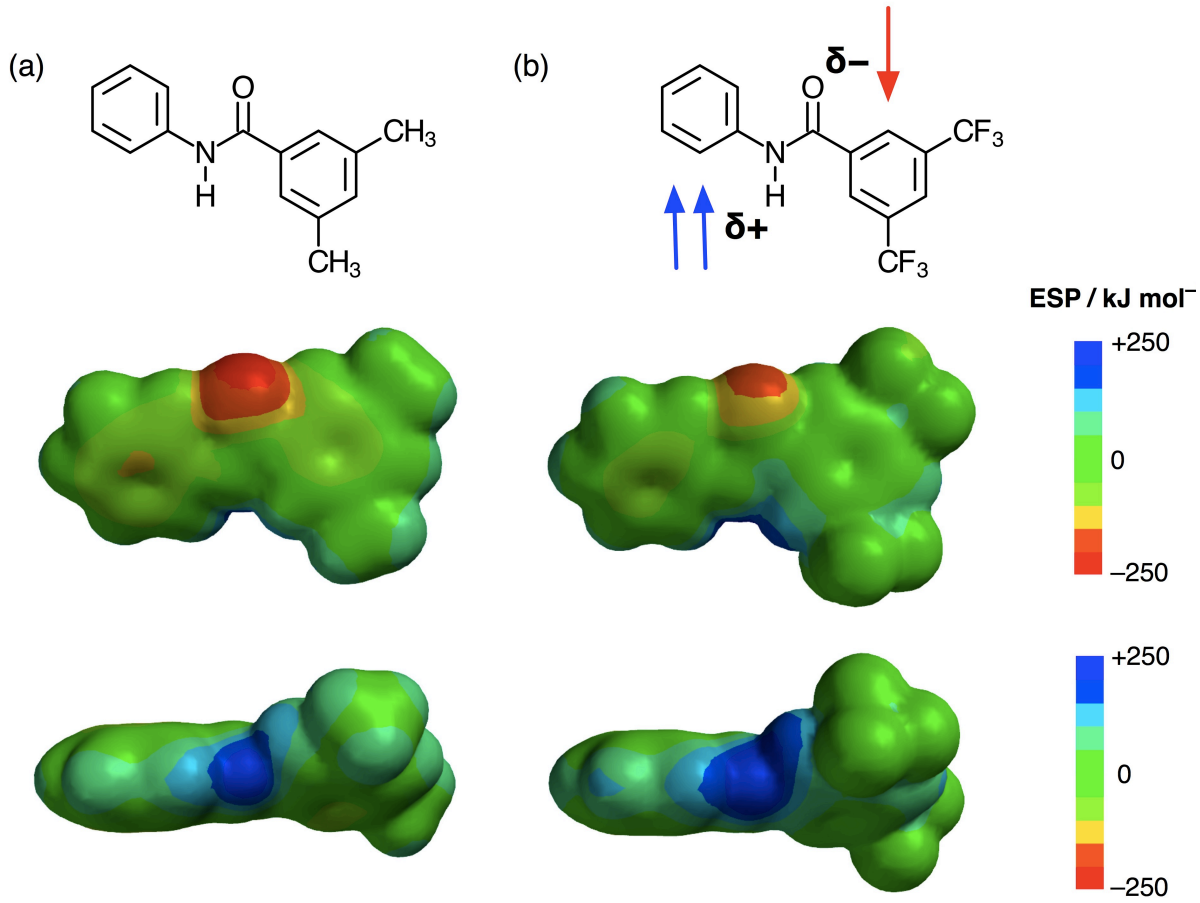

Figure 8.10. The illustrated electrostatic potential energy for (a) 3,5-dimethylaryl benzanilide and (b) 3,5-bis(trifluoromethyl)benzyl amide, plotted on the same scale in kJ mol^{-1} for comparison. The varying intensities of the electrostatic potential energy values can be conveyed with blue colour as the highest electrostatic potential energy value, red colour as the lowest and intermediary colour represent intermediary electrostatic potentials. Thus, a high electrostatic potential indicates the relative absence of electrons and a low electrostatic potential indicates an abundance of electrons.

One of the conspicuous differences is that the negative region in dimethyl substituent is considerably larger than bis(trifluoromethyl) substituent as a consequence of the electronegativity redistribution imposed by the CF_3 groups. These relative

distributions of electrons introduced intense positive charges on the hydrogen atom of the amide in latter group, and results in prominent feature of hydrogen donor. Therefore, the association constant is at the highest when 3,5-bis(trifluoromethyl) substituent was employed. In the pursuit of achieving high association constant in the formation of [2]-pseudorotaxane species, 3,5-di-Cl and 3,5-bis-CF_3–nitrone **B** and **C** were initially synthesised. The strategy employed to prepare 3,5-di-Cl–nitrone **B** was first illustrated in **Scheme 8.5**.

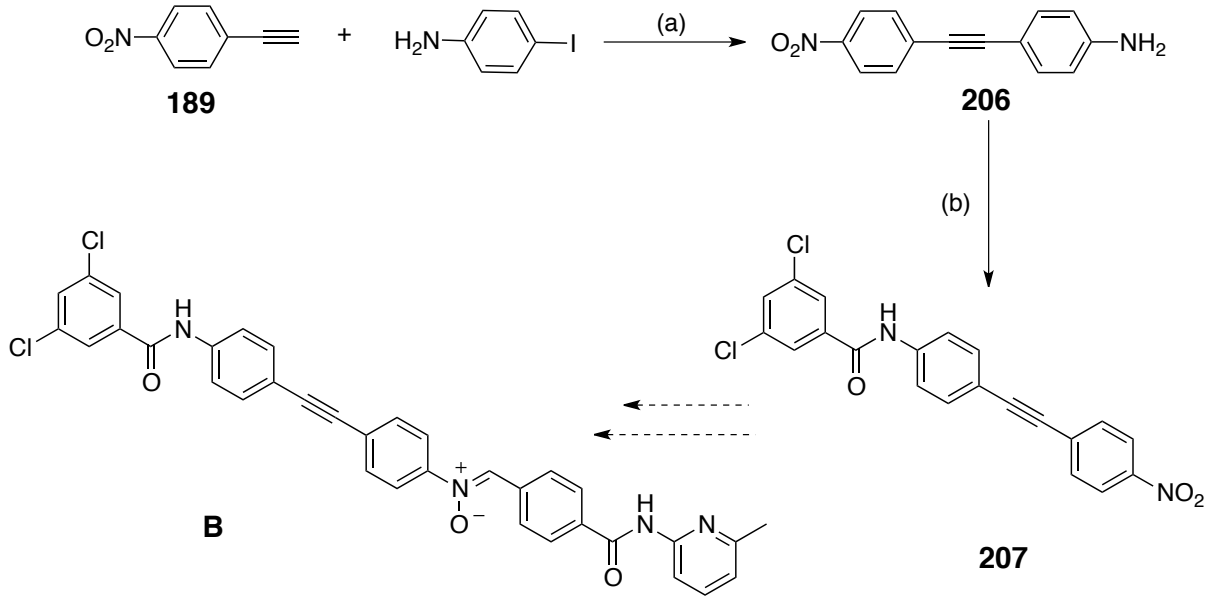

Scheme 8.5. Attempted synthesis of 3,5-di-Cl nitrone **B**. Reagents and yields: (a) 4-iodoaniline, $PdCl_2(PPh_3)_2$, PPh_3, CuI, Et_3N/THF, 65 ˚C, 16 h, 28%; (b) 3,5-dichlorobenzoyl chloride, Et_3N, CH_2Cl_2, 0 ˚C to rt, 16 h, 56%.

The nitro alkyne **189** was coupled with 4-iodoaniline under Sonogashira conditions to give 27% yield of amine **206** after purification. The nucleophilic attack of **206** on the readily obtained 3,5-dichlorobenzoyl chlorides afforded the corresponding nitro compound **207** in a yield of 56%. Nevertheless, the subsequent partial reduction to afford the hydroxylamine has been unsuccessful. Besides that, we are aware that the solubility of nitrone **B** in non-polar solvents is likely to be limited. Therefore, we are more interested in assembling second model nitrone **C**, consists of 3,5-bis(trifuoromethyl) phenyl ring as its two sterically end groups in the new scheme of potential self-replicating rotaxanes. An attempt to synthesise the analogous 3,5-bis-CF_3 nitrone **C** has been undertaken as depicted in **Scheme 8.6**. Compound **208** was obtained in a yield of 38% after precipitation and washed with cool dichloromethane. The following Sonogashira reaction of compound **208** with

synthesized terminal alkyne **189** give the corresponding nitro derivative compound **209**, in a yield of 75%. Unfortunately, all efforts to reduce the nitro compound to the desired hydroxylamine has been unsuccessful and proven to be fairly troublesome.

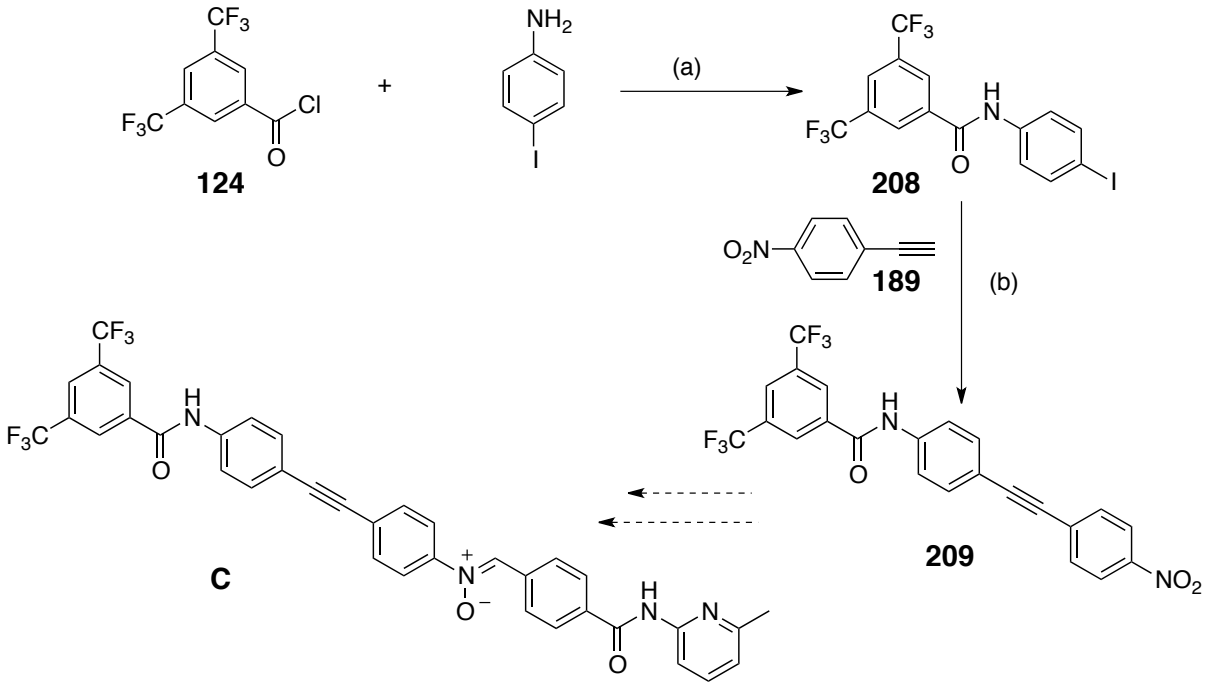

Scheme 8.6. Attempted synthesis of 3,5-bis-(CF_3) nitrone **C**. Reagents and yields: (a) 4-iodoaniline, Et_3N, CH_2Cl_2, 0 ˚C to rt, 1 h, 38%; (b) Alkyne **189**, $PdCl_2(PPh_3)_2$, PPh_3, CuI, Et_3N/THF, 65 ˚C, 16 h, 75%.

The failure to obtain 3,5-bis-CF_3 nitrone **C** is more likely due to the formation of the azoxy compound. Furthermore, MALDI spectrometry revealed the signal that correspond to the stable azoxy compound. An attempt to circumvent the solubility limitation in the case of 3,5-di-Cl nitrone **B** brought us to the formation of 3,5-di-OC_8H_{17} nitrone **A**. The alternative strategy in synthesising nitrone **A** was outlined in **Scheme 8.7**. In the alkylation of 3,5-dihydroxybenzoic acid **210**, its esterification occurred concomitantly as described[264] in the work of Tamiaki *et al*. The corresponding benzoate was hydrolysed to give the corresponding carboxylic acid **211** and quantitatively transformed to acid chloride **212** by the treatment of thionyl chloride in toluene. Subsequently, the condensation of amine **206** and acid chloride **212** resulted in the formation of nitro derivative compound **213**. However, the synthetic approach to obtain the desired nitrone **A** was impeded by the similar reasoning, which has proven to become an unfortunate start in our early work.

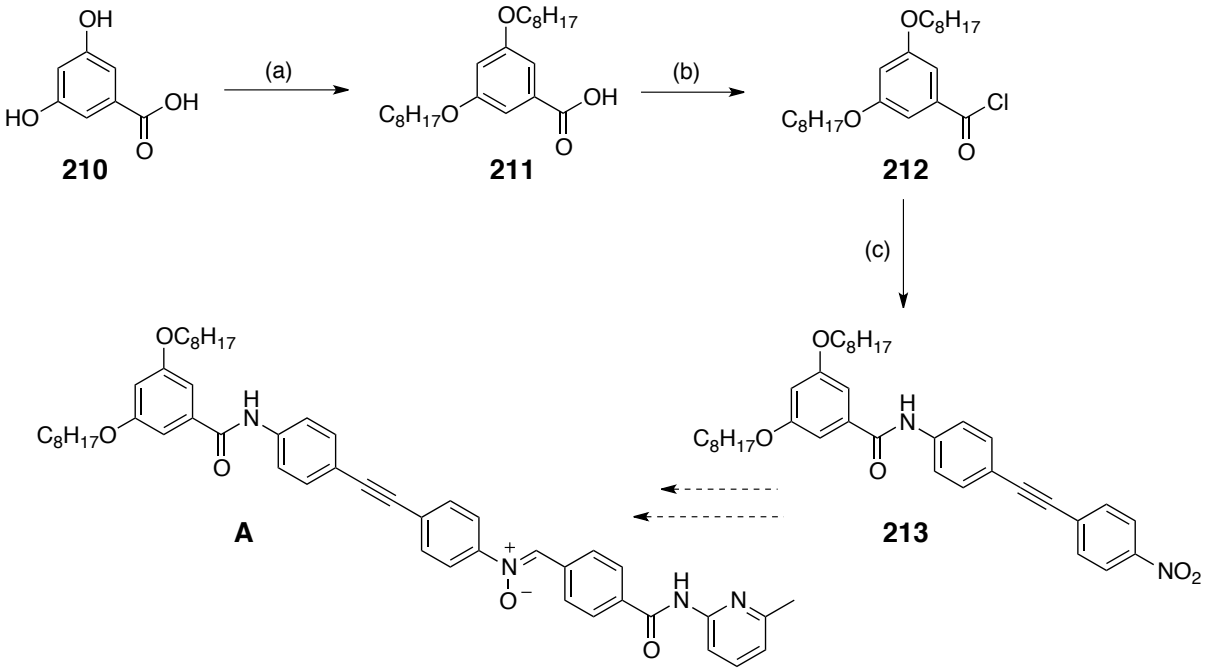

Scheme 8.7. Attempted synthesis of 3,5-di-OC_8H_{17} nitrone **A**. Reagents and yields: (a) i. $CH_3(CH_2)_6CH_2Br$, K_2CO_3, dry DMF, 65 ˚C, 16 h; ii. KOH/EtOH/H_2O, 88 ˚C, 16 h, 40% over 2 steps; (b) $SOCl_2$, toluene, 110 ˚C, 16 h, 98%; (c) Compound **206**, Et_3N, $CHCl_3$, reflux, 10 h, 60%.

8.5 Binding study with CF_3 nitro 209

Herein, we described the formation of pseudorotaxane complex between macrocycle **MDG** or **MP** with CF_3 nitro compound **209** and monitored by ^{1}H NMR spectroscopy as described in the previous binding experiments. The first 400.1 MHz ^{1}H NMR spectrum of an equimolar mixture of macrocycle **MDG** and nitro compound **209** in $CDCl_3$ at room temperature undergo a slow exchange process on the ^{1}H NMR chemical shift timescale (**Figure 8.11b).** It is noteworthy that some significant changes in the chemical shifts of the protons of the complex (**Figure 8.11b**) are relative to those of its free components (**Figure 8.11a** and **Figure 8.11c**). The typical downfield shift of the macrocycle proton NH^{9R} (+0.88 ppm), the upfield shift of macrocycle **MDG** phenylene protons H^{5R} and H^{6R} and the appearance of broad complex pattern resonances for macrocycle methylene protons (H^{8R}, H^{3R}, H^{2R} and H^{1R}) suggests the assembly of [**MDG•209**] complex.

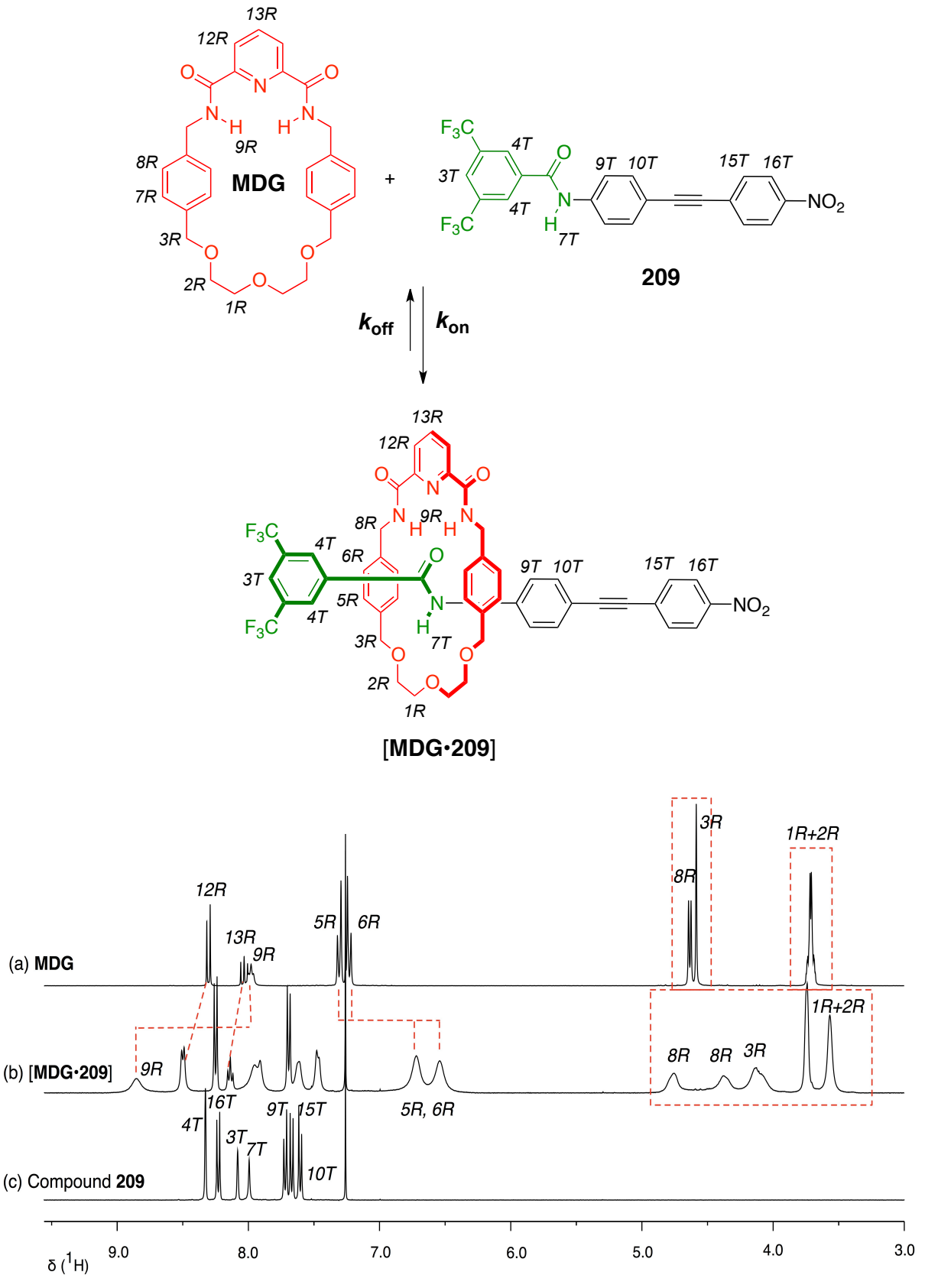

Figure 8.11. Partial ^{1}H NMR spectra (400.1 MHz, 298 K, $CDCl_3$, 20 mM) of: (a) Macrocycle **MDG**; (b) an equimolar mixture of macrocycle **MDG** and compound **209** (c) Compound **209**. Red dashed lines are shown to connect resonances for specific protons in the free and complex states. Red dashed boxes shows the broad resonances of methylene protons (H^{8R}, H^{3R}, H^{2R} and H^{1R}) upon pseudorotaxane complex [**MDG·209**] formation. R stands for ring (in this case macrocycle **MDG**) and T for thread (in this case nitro compound **209**).

These observations are consistent with the appearance of new fluorine resonance from ^{19}F NMR spectrum at δ_F –63.1 (not shown), which corresponds to the formation [**MDG•209**] complex, compared to the free species of nitro **209** in solution δ_F –63.4. We suspect that this result is partly due to the electron withdrawing of CF_3 substituents of compound **209**, which essentially increase[265] the hydrogen donor's ability of the NH bond.

The second binding experiment was conducted in the presence of macrocycle **MP** (**Figure 8.12**) under similar condition. In contrast to the above spectra, the spectral changes were more resolved and desymmetrized, due to the fact that the face of the ring is no longer symmetrically planar. For instance, the macrocycle NH protons, H^{11R} are typically shifted downfield (+1.11 ppm) upon hydrogen bonding to the oxygen of the carbonyl group of nitro compound **209**. Such large downfield change was also evidenced for the NH proton resonance of nitro compound **209**, H^{7T} (+1.50 ppm), (**Figure 8.12c**) which signify the association strength between the two components in the pseudorotaxane assembly as illustrated in **Figure 8.12b**.

Furthermore, the changes in the methylene protons (H^{10R}, H^{5R} and H^{4R}) of the free macrocycle **MP** (**Figure 8.12a**) are most affected – these proton resonances lead to a complex pattern between the region of δ_H 4.53 – 4.17 because they are now rendered magnetically inequivalent as a results of the end-to-end asymmetry imposed by compound **209**. The binding constant for the pseudorotaxane [**MP•209**] complex was determined to be 3100 ± 300 M^{-1} by ^{19}F NMR spectroscopy (376.5 MHz, $CDCl_3$) using the single-point method. On the whole, we have demonstrated that both macrocycles **MDG** and **MP** are capable of forming the [2]-pseudorotaxane type geometry with nitro compound **209**, which consequently stabilized *via* intermolecular hydrogen bonding in the low polarity solvents.

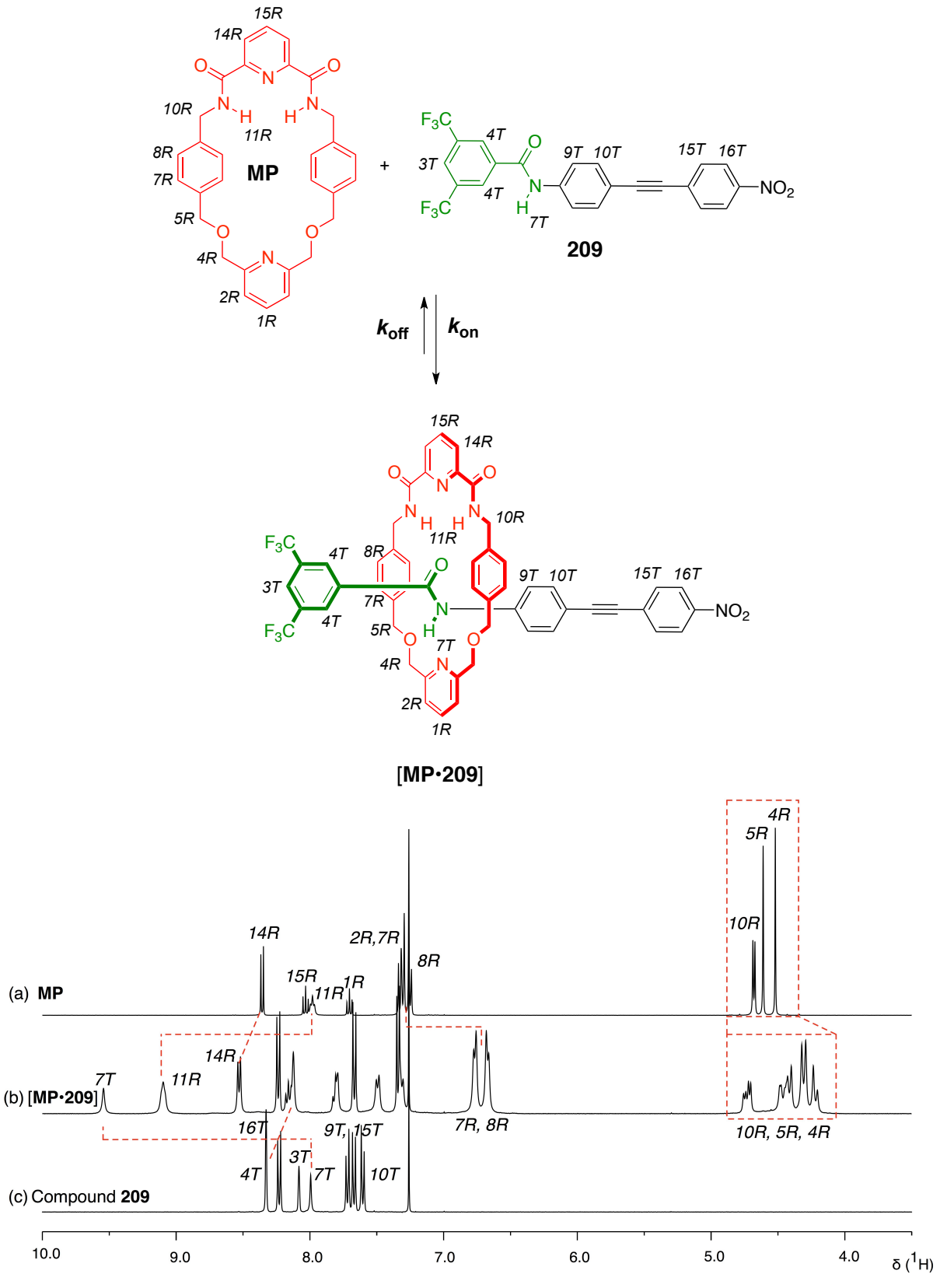

Figure 8.12. Partial ^{1}H NMR spectra (400.1 MHz, 298 K, $CDCl_3$, 20 mM) of (a) Macrocycle **MP**; (b) an equimolar mixture of macrocycle **MP** and nitro compound **209** (c) 3,5-bis CF_3 nitro compound **209**. Red dashed lines are shown to connect resonances for specific protons in the free and bound states. Red dashed boxes shows the complex pattern resonances for methylene protons (H^{10R}, H^{5R} and H^{4R}) upon pseudorotaxane [**MP•209**] complex formation. R stands for ring (in this case the macrocycle **MP**) and T stands for thread (in this case compound **209**).

8.6 Binding study of OC_8H_{17} nitro 213

Similar binding behaviour was observed for nitro compound **213** as such the pseudorotaxane formation of [**MDG•213**] complex also encountered a slow exchange process on the ^{1}H NMR chemical shift timescale. The variable temperature study for the pseudorotaxane [**MDG•213**] assembly was carried out to evaluate the binding interaction.

The stack plots of the 500.1 MHz ^{1}H NMR spectra of the corresponding pseudorotaxane complex were recorded from 297 K to 250 K (**Figure 8.13a** to **Figure 8.13e**) and displays slow exchange process between the free and bound species and on all occasions, a small contribution from the intermediate species was observed from the new broad peak. Thus, this [2]-pseudorotaxane [**MDG•213**] was stabilized predominantly through hydrogen bonding interactions between the two components.

The conformation of the [2]-pseudorotaxane [**MDG•213**] was confirmed from 2D ROESY NMR spectrum as shown in **Figure 8.14**. As predicted, macrocycle **MDG** was predominantly located around the amide moiety of nitro compound **213** and the resonance of macrocycle NH^{9R} proton shift toward the terminus of the compound **213** is apparent from the significant upfield shifts (up to δ_H 9.33). In addition, the spectra revealed crosspeaks between the NH proton of macrocycle MDG, H^{9R} and the nitro aromatic protons H^{11T} and H^{16T}. As detailed above, the interaction between macrocycle **MDG** and nitro compound **213** *via* hydrogen bonding and, hence, confirmed the geometry shown in **Figure 8.14**.

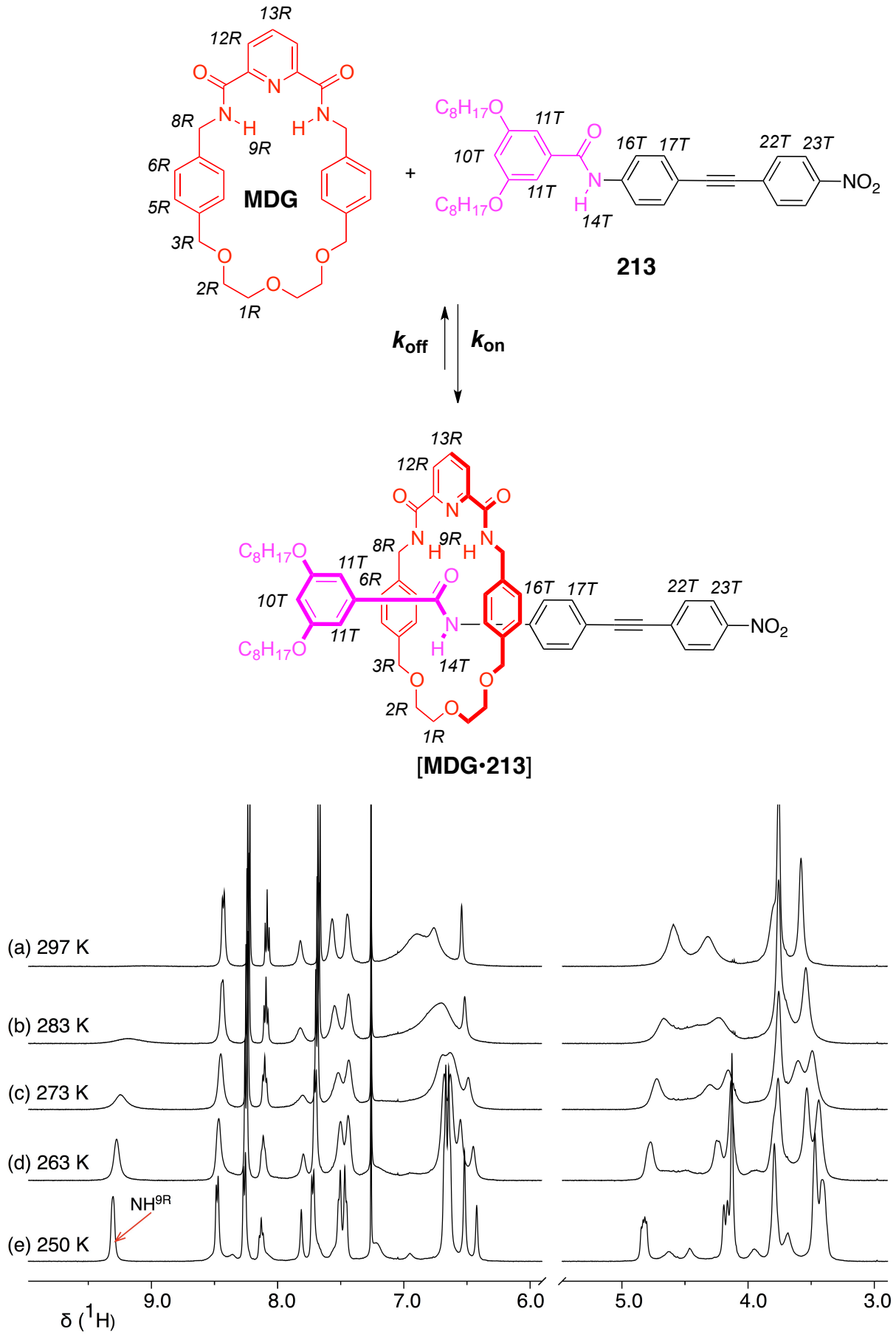

Figure 8.13. Variable temperature ^{1}H NMR (500.1 MHz, $CDCl_3$, 20 mM) binding study of an equimolar mixture of macrocycle **MDG** and nitro compound **213**.

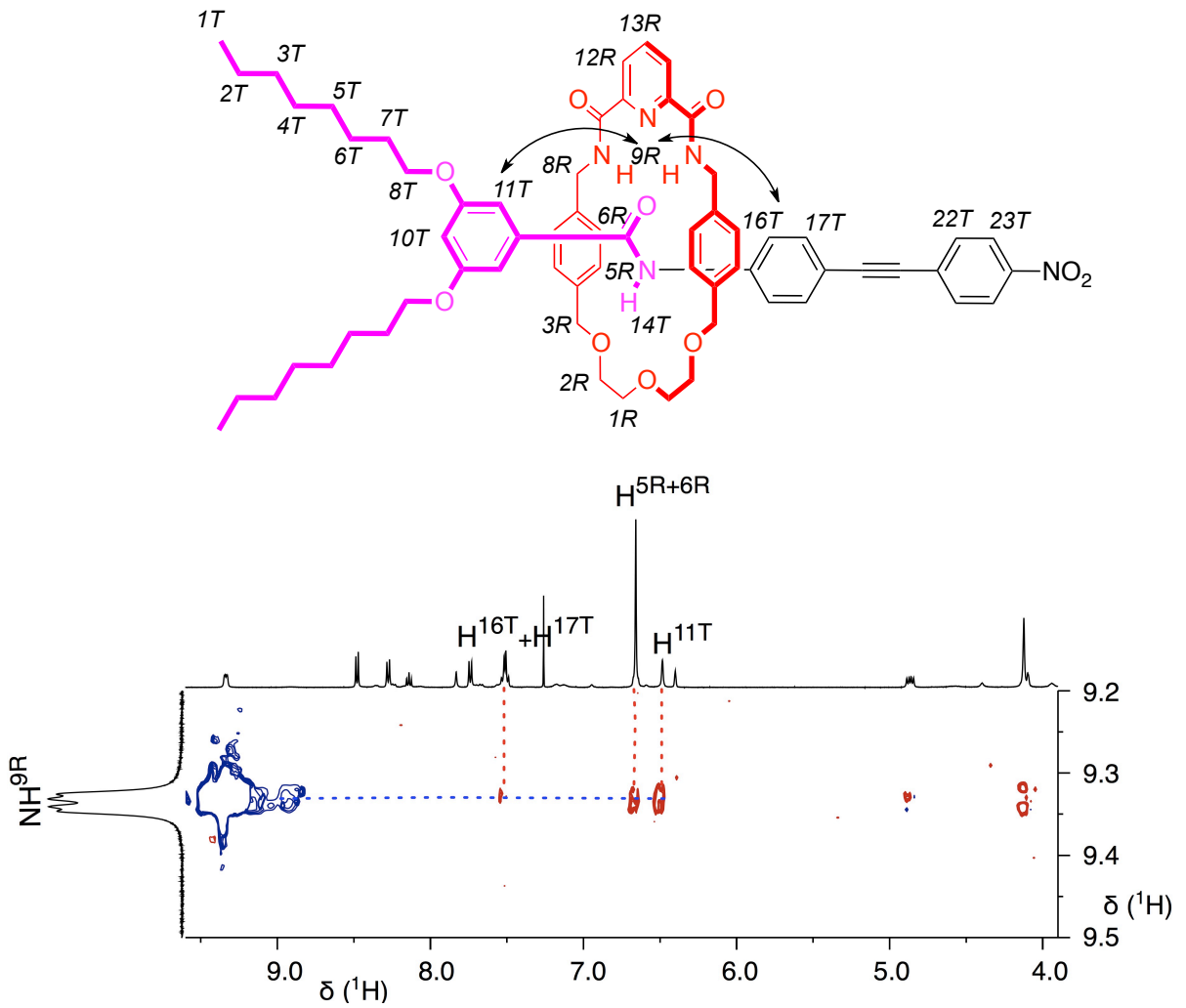

Figure 8.14. Partial 2D ROESY spectrum (500.1 MHz, 20 mM, –40 ˚C, $CDCl_3$) of an equimolar of macrocycle **MDG** and nitro compound **213**. ROESY crosspeaks (red points) are observed for the complex between macrocycle **MDG** and nitro compound **213** are shown as black arrows.

When the binding experiment was repeated using macrocycle **MP**, nitro compound **213** and macrocycle **MP** exhibited a similar binding trend at room temperature for 1:1 binding stoichiometry. 500.1 MHz ^{1}H NMR spectra of the complex when recorded at variable temperature in $CDCl_3$ are shown in **Figure 8.15**. As depicted from **Figure 8.15**, the 500.1 MHz ^{1}H NMR spectra are more resolved at 248 K, which allows us to observe the dominant species of pseudorotaxane [**MP•213**] complex with a slow exchange process on the ^{1}H NMR chemical shift timescale.

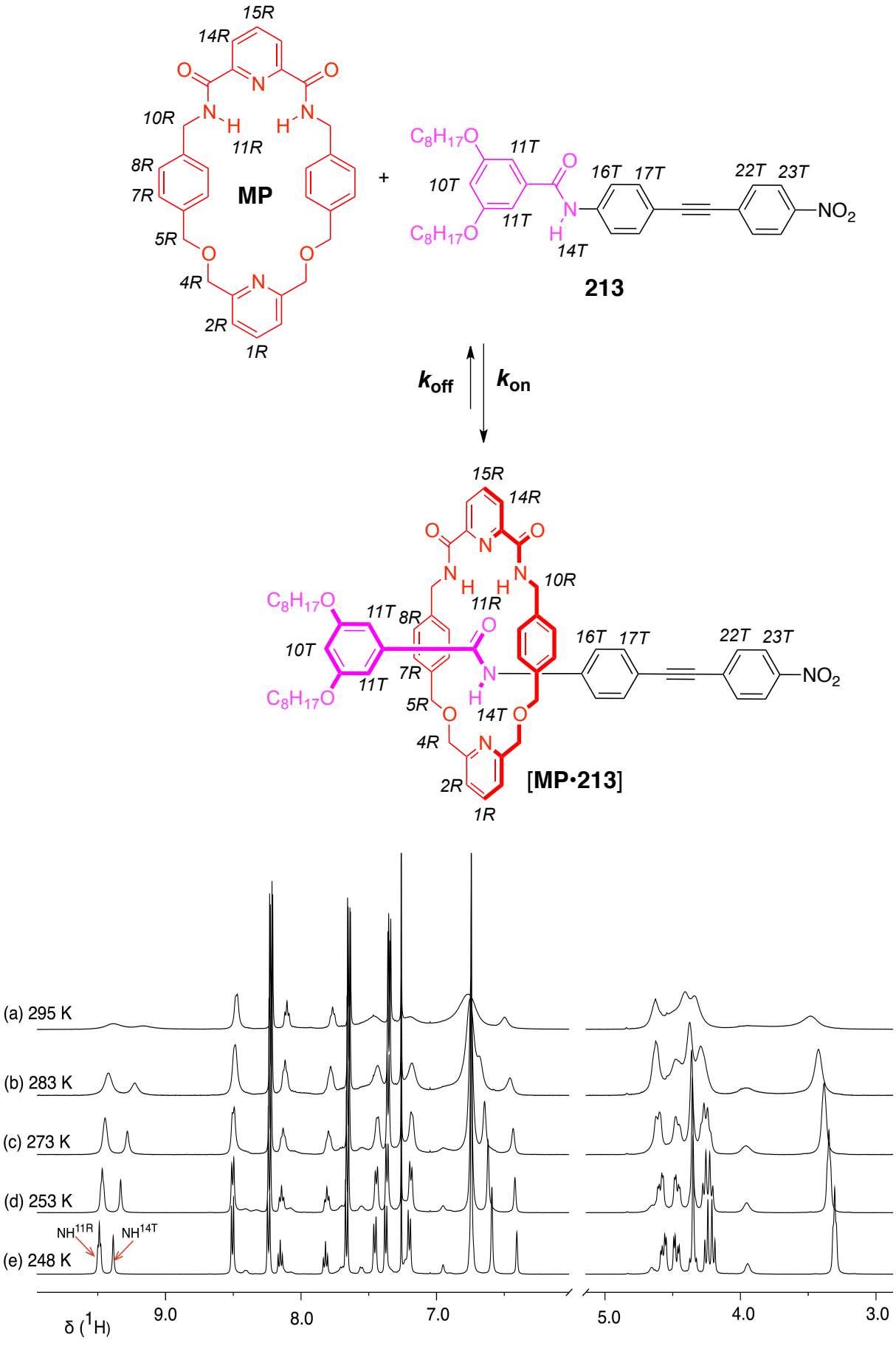

Figure 8.15. Variable temperature of ^{1}H NMR spectra (500.1 MHz, $CDCl_3$, 20 mM) of an equimolar mixture of macrocycle **MP** and nitro compound **213**.

We observed significant chemical changes in the ^{1}H NMR spectra of the corresponding [2]-pseudorotaxane [**MP•213**] as such the NH protons of the macrocycle **MP**, NH^{11R} are significantly shifted downfield upon binding to nitro compound **213**. Furthermore, the amide proton of nitro compound **213** NH^{14T} was also largely affected and display pronounced downfield shift, which suggests that this proton is hydrogen bonded to the lower cavity of macrocycle **MP**. The slow exchange process does not only yield sharp separate resonance but also yield exchange peaks in the 2D EXSY experiment. **Figure 8.16** show the 500.1 MHz 2D EXSY spectrum of the pseudorotaxane [**MP•213**] complex.

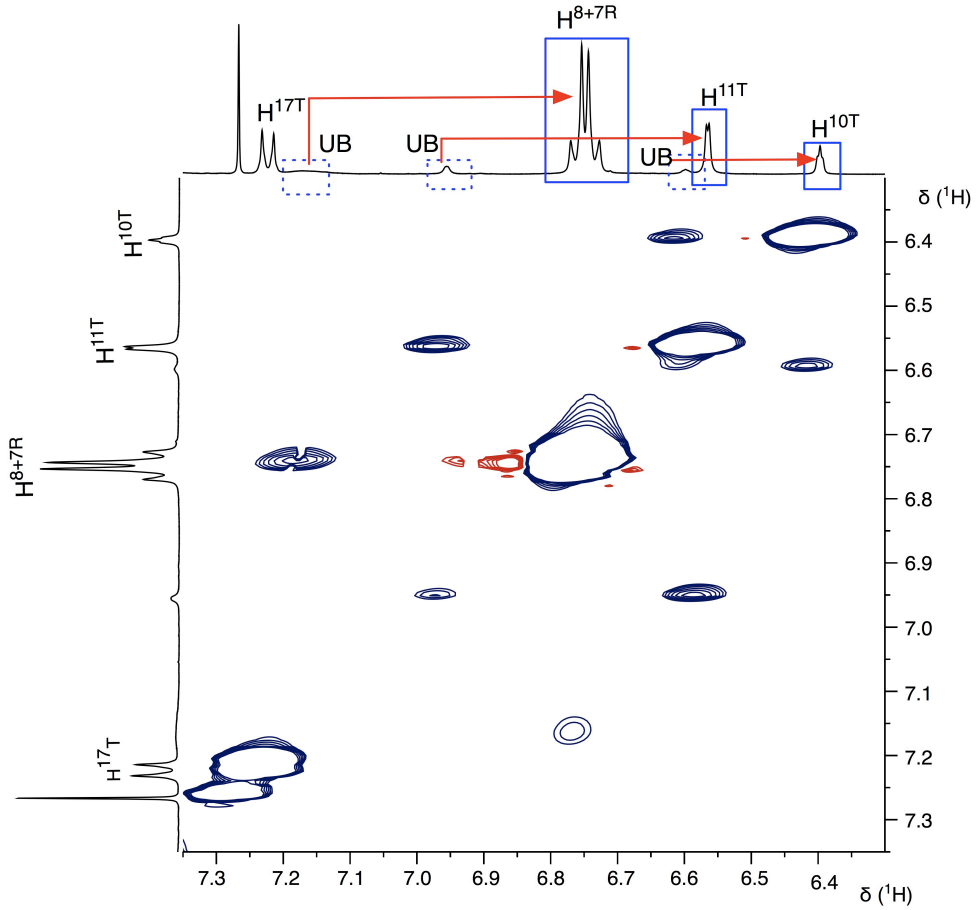

Figure 8.16. Partial 2D EXSY spectrum (500.1 MHz, 20 mM, 233 K, $CDCl_3$) display crosspeaks (blue points) between macrocycle **MP** and nitro compound **213**. T and R represents thread and rotaxane compound, respectively. **UB** (blue dashed boxes) represents the unbound species in the reaction mixture.

It is apparent that the bound and the unbound species exchange slowly with one another from the 2D EXSY spectrum. This is evident by the three crosspeaks in the spectrum from the pseudorotaxane [**MP•213**] complex – H^{7R} and H^{8R} of the macrocycle **MP** and H^{10T} and H^{11T} of the nitro compound **213** (solid blue boxes) and that from the unbound species (dashed blue boxes). Hence, the association constant,

K_a for the pseudorotaxane assembly was estimated to be 5560 ± 560 M^{-1}. The 2D ROESY spectra of the pseudorotaxane complex (**Figure 8.17**) exhibit distinct crosspeaks between the proton resonance of the macrocycle **MP** NH^{11R} and aromatic proton of nitro compound **213**, namely H^{11T} and H^{16T}. In a similar manner, the NH proton resonance of compound **213**, H^{14T} exhibit a crosspeak with the methylene proton of macrocycle **MP**, H^{4R} and thus confirmed the encircling of the macrocyclic component about the amide moiety of compound **213** with the anticipated geometry.

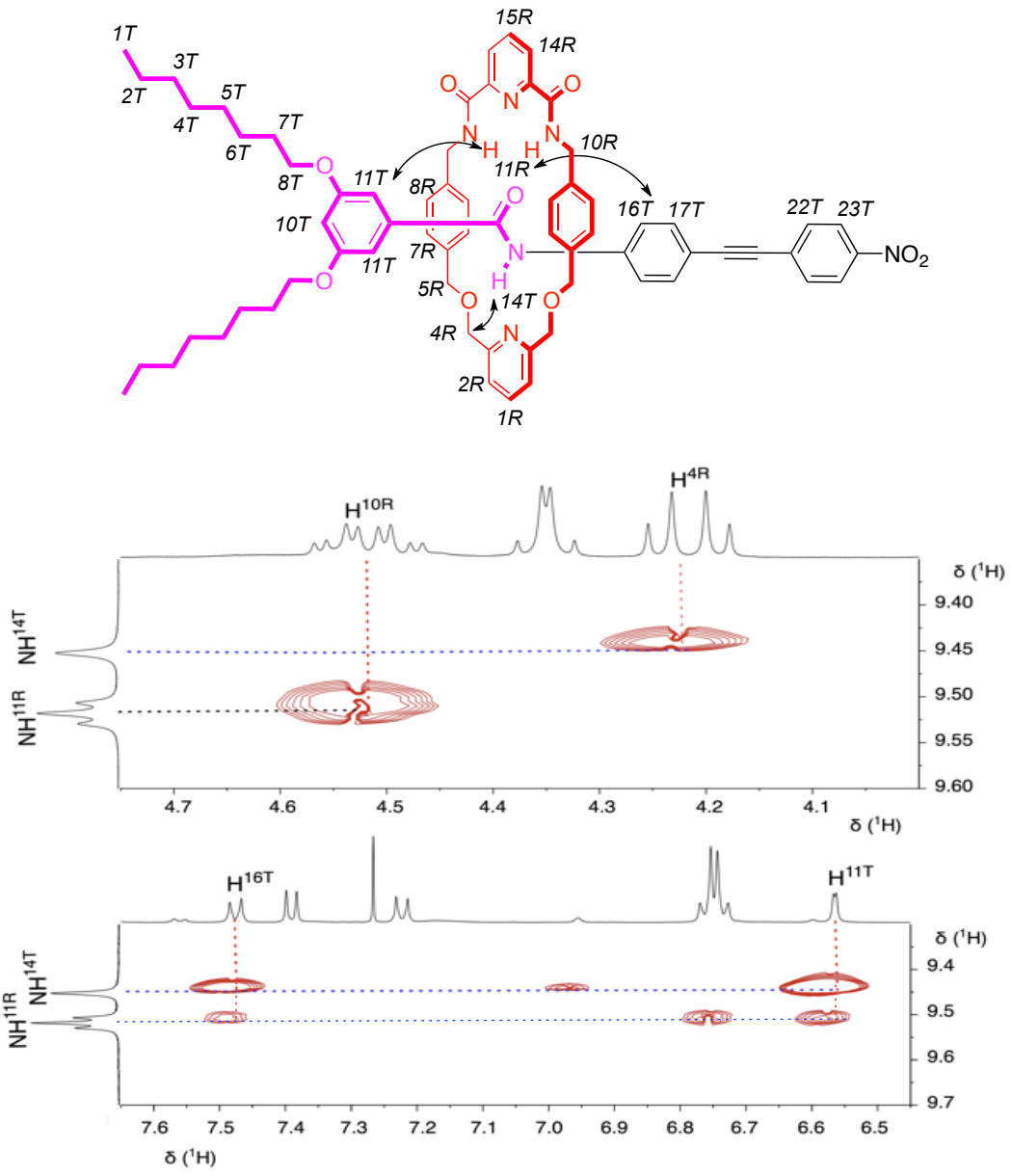

Figure 8.17. Partial 2D ROESY spectra (500.1 MHz, 20 mM, –40 ˚C, $CDCl_3$) of an equimolar of macrocycle **MP** and nitro compound **213**. ROESY crosspeaks (red points) observed for the complex between macrocycle **MP** and nitro compound **213** are shown as black arrows.

8.7 Conclusion

The first and unsuccessful attempt to integrate the developed replicator molecules in **Replication model 3** originated from the reduced reactivity of [2]-pseudorotaxane species. There is a close connection between this reduced circumstances and the relative position of the reactive site with the binding site. It is concluded that the reactive site must be placed sufficiently far away from the binding site to prevent the introduction of a supramolecular steric effect through the proximity of the macrocyclic component.

On that account, we improved the initial scheme of self-replicating rotaxanes, which introduced length segregation between the reactive site and binding site. In addition, we have demonstrated that we are able to influence the position of the ring component to the targeted binding site by means of high association constant. Our effort to demonstrate the fundamental idea behind the third minimal model has been properly illustrated, as such we have successfully ensured that the ring component encircled the preferable binding site of the guest compound and achieved a high association constant in the formation of the pseudorotaxane complex. All is good, except for the fact that the unsuccessful procedure to obtain the key hydroxylamine compound prevented us to explore the potential behaviour of self-replicating rotaxanes, and hence, it is necessary to consider the current synthetic approaches of the nitrone compound.

9

General conclusion

The concepts of artificial self-replicating system have become scientifically acknowledged over the past twenty-five years with significant number of replicator structures based on simple organic molecules have been published. In the self-replicating process, the product molecule acts as a template for its own formation by generating a catalytically active complex and exploiting the association with its building blocks *via* non-covalent interactions. In this context, the development of model for studying self-replication also demonstrated that the chemical information can be transmitted and amplified. These objectives required a comprehensive understanding of the recognition-mediated process that allow the product molecules to template their own formation.

The work presented here, revolves around the minimal model of replication and its incorporation into the design of mechanically interlocked molecules namely rotaxanes. Having established the fundamental properties in designing [2]-rotaxane (**Chapter 3**), three discrete minimal model of replication were designed. Theoretical discussions of each replication model at the start of the investigation help us to visualize both good and bad points in each framework. Initial investigations on the first replication model showed that the binding between the self-replicating thread and the macrocycle must exceed a certain threshold value in order to allow efficient autocatalytic formation of the rotaxane structure (**Chapter 4, 5** and **6**). Alternatively, we explored the second replication model (**Chapter 7**) in which one of the recognition unit was moved from the thread on to the macrocycle. This modification ensures that only the rotaxane structure undergoes the autocatalytic reaction. Ultimately, we devised conceptually the third replication model (**Chapter 8**), which incorporate the binding site and one element of the stopper group appended to one of the building blocks constitutive of the template, either the pseudorotaxane precursor or the linear

component. Nonetheless, we do not anticipate any significant problems beyond the prior context until the implementation of these replication models were carried out. Current approaches towards important achievements and disappointments to reach this target are summarized together in **Table 9.1** within each minimal model designed. We are also investigating the underlying factors in greater details.

Table 9.1. Important achievements and disappointments within each minimal model of replicating [2]-rotaxanes.

Observations	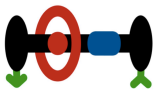 Model 1	 Model 2	 Model 3
1. High association constant, K_a is necessary to attain substantial amount of the pseudorotaxane precursor and, hence, increased the overall yield of rotaxanes.	A high K_a is attainable and greatly improved with the modification of the guest design and by lowering the temperature. Revolves around the simple kinetic model of rotaxane formation.	Potential improvements in K_a hampered by guest solubility.	Greatly improved with the modification of the guest design.
2. The feasible design of the building blocks (macrocycle, maleimide and nitrone compounds).	Limited challenge.	Very challenging.	Challenging.
3. Synthetic approaches towards the implementation of the replication model.	Generally straight forward and effective.	Generally straight forward but less effective.	Generally straight forward but less effective.
4. Reduced reactivity of pseudorotaxane complex as a consequence of pronounced supramolecular steric effect.	Less reactive than thread. Can be modified by guest design.	Pseudorotaxane apparently more reactive than thread.	Less reactive than thread. Can be modified by guest design.
5. Effect of recognition on thread and/or pseudorotaxane reactivity.	Thread and pseudorotaxane rates affected.	Pseudorotaxane only.	Thread and pseudorotaxane rates affected.
6. Solubility problems.	Limited.	Very significant.	Limited.

10

Experimental and synthetic procedures

10.1 General experimental procedures

Chemicals were purchased from ABCR GmbH & Co, Alfa-Aesar, Apollo Scientific Ltd., Avocado Research Chemicals Ltd Fisher Scientific UK Ltd., Sigma-Aldrich Company Ltd. or VWR International Ltd. and were used as received or otherwise purified[266] by standard techniques where required. Most of the non-aqueous reactions were carried out under an inert Ar or N_2 atmosphere with the inert gas passing through a bed of 4 Å molecular sieves and self-indicating silica gel. Brine refers to a saturated aqueous solution of sodium chloride.

Anhydrous solvents were obtained under the following conditions, such as dry MeCN was distilled from calcium hydride in a recycling still, dry CH_2Cl_2 was obtained using a MBRAUN GmbH MB SPS-800 solvent purification system, which the solvent was dried by passage through filter columns and dispensed under an atmosphere of Ar or N_2 gas, $CDCl_3$ was neutralised over $CaCl_2$ filtered and stored over 4 Å activated molecular sieves and dry THF was distilled from sodium in a recycling still using benzophenone kethyl as indicator.

Analytical Thin Layer Chromatography (TLC) analysis was performed on MACHEREY-NAGEL GmbH & Co, POLYGRAM® SIL G/UV_{254} plates, plastic backed 0.2 mm silica gel plates with fluorescent indicator. Developed plates were air-dried and visualized under UV lamp (λ_{max} 254 or 366 nm) or incubating with iodine on sand. Where necessary, thermal development after dipping in: methanolic DNP and sulfuric acid solution and ninhydrin in *n*-butanol or a solution of aqueous potassium permanganate, was used to aid visualization.

Flash Column chromatography and silica plugs were carried out on Apollo Scientific Ltd. silica gel 40-63 micron or Silicycle SiliaFash® P60 silica gel (230-400 mesh) eluting with solvents as supplied under a positive pressure of compressed air.

Melting points were measured in open capillary tubes using an Electrothermal 9200 melting point apparatus and are uncorrected.

Mass spectra were recorded on a Micromass GCT spectrometer for electron impact (EI) operating at 70 eV or chemical ionization (CI) using isobutane as the ionising gas. Electrospray ionisation spectra (ES) were performed on a Micromass LCT spectrometer operating in positive or negative mode from solutions of methanol, acetonitrile or water. *m/z* values are reported in Daltons and followed by their percentage abundance in parentheses. 4800 MALDI TOF/TOF^{TM} Analyzer is capable of operating in either linear or reflectron mode allowing either high sensitivity detection over a large mass range or improved signal resolution with the associated increase mass accuracy.

10.2 General NMR spectroscopy procedures

^{1}H NMR spectra were recorded on a Bruker Avance 300 (300.1 MHz), a Bruker Avance II 400 (400.1 MHz), a Bruker Avance 500 (499.9 MHz) or a Varian UNITYplus 500 (500.1 MHz) spectrometer using the deuterated solvent as the lock and the residual spectra as the internal reference in all cases. The chemical shift information (δ_H) for each resonance signal is given in units of parts per million (ppm) relative to trimethylsilane (TMS) where δ_H TMS = 0.00. The number of protons (n) for a reported resonances signal are indicated from their integral value and their multiplicity are represented by the symbols s, d, t, q, m and br which denote singlet, doublet, triplet, quartet, multiplet and broad singlet, respectively. Their coupling constant (*J*) are determined by analysis using iNMR© (Version 3.6.3, Mestrelab Research, 2010) and quoted to the nearest 0.1 Hz. Identical coupling constants are averaged in each spectrum and also reported to the nearest 0.1 Hz.

^{13}C NMR spectra were recorded on a Bruker Avance 300 (75.5 MHz), a Bruker Avance II 400 (100.6 MHz) or a Bruker Avance 500 (125.7 MHz) spectrometer utilizing the DEPTQ pulse sequences with broadband proton decoupling using the

deuterated solvents as the lock and the residual solvent as the internal reference in all cases. In the assignment of ^{13}C NMR spectra, the chemical shift information (δ_C) for each resonance signal are given in units of parts per million (ppm) relative to trimethylsilane (TMS) where δ_C TMS = 0.00. Mainly, the signals are singlets or unless stated, which their multiplicity is represented by the symbol d for doublet.

^{19}F NMR spectra were recorded using a Bruker Avance 300 (282.4 MHz), a Bruker Avance II 400 (376.5 MHz) or a Bruker Avance 500 (470.3 MHz) spectrometer using a broadband proton decoupling pulse sequence with the deuterated solvent as the internal lock. The chemical shift information (δ_F) for each resonance signal are given in units of parts per million (ppm) relative to CCl_3F where δ_F CCl_3F = 0.00. The analysis of ^1H, ^{13}C and ^{19}F spectra were carried out using iNMR© software (Version 3.6.3, Mestrelab Research, 2010).

10.3 ^1H NMR spectroscopy : Preparation, kinetic measurements and deconvolution data

Masses of reagents were measured using a Sartorius BP 211D balance (± 0.01 mg) and reagent solutions were prepared by dissolving three starting materials in 0.7 mL volume of dry $CDCl_3$ at 20 mM reaction concentration. Of particular note, the maleimide and macrocycle compound were pre-equilibrated at 273 K for 1 h prior to mixing with nitrone compound. By using Hamilton gas-tight syringes, the reaction solution was transferred immediatedly to a 5 mM NMR tube (Wilmad 528PP) and was then fitted with a polyethylene pressure cap to minimise solvent evaporation. The tube was transferred promptly to a 500 MHz NMR spectrometer (Varian UNITYplus) regulated at reaction temperature.

The ^1H NMR spectra were acquired automatically at a set time interval (every 1800 s) over a period of 16 h. Analysis and deconvolution of the arrayed ^1H NMR spectra recorded in the course of the reaction was performed using iNMR© software (Version 3.6.3, Mestrelab Research, 2010). We monitored the chemical reaction of 1,3-dipolar cyclcoaddition between a maleimide and a nitrone, which give rise to two cycloadduct protons. These diasteroisomeric products, namely *trans* and *cis* are distinguishable in

the ^{1}H NMR spectrum with different splitting pattern for each as a consequence of their different dihedral angles of H^2 to H^3 as illustrated in **Figure 10.1**.

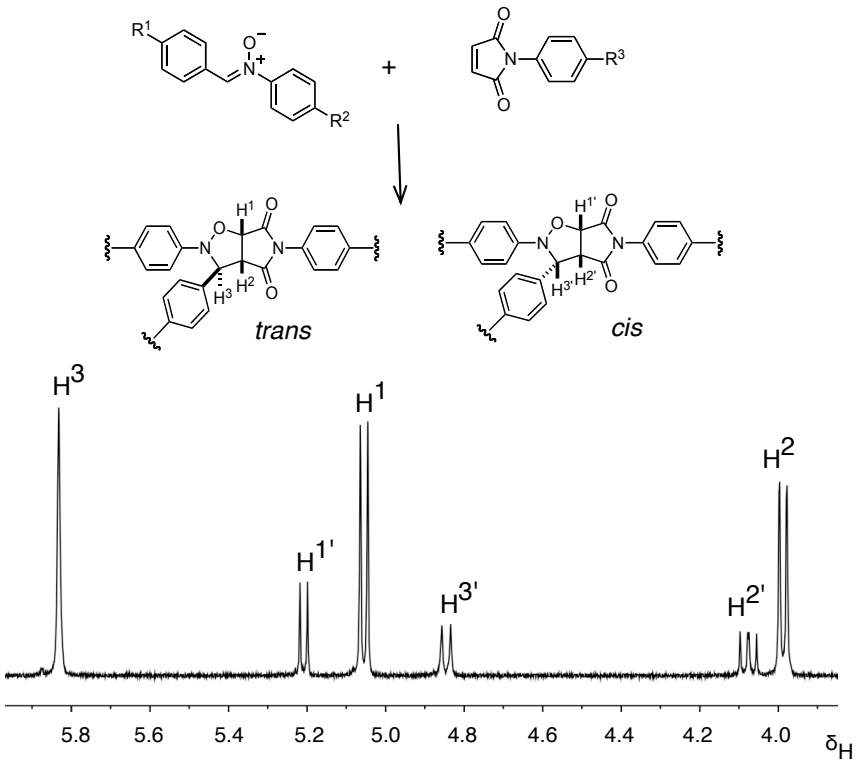

Figure 10.1. Partial 500.1 MHz ^{1}H NMR spectrum featuring the characteristic splitting patterns for the proton resonances arising from the isoxazolidine ring for the *trans* and *cis* diasteroisomer in the reaction between nitrone and maleimide derivative compound. In the case of *trans* cycloadduct, the signal for proton H^3 is singlet and doublet for H^1 and H^2. On the other hand, the *cis* cycloadduct give doublets for $H^{3'}$ and $H^{1'}$ and doublet of doublet for $H^{2'}$.

The concentration of reactants and products at each time point was determined by monitoring the consumption of either maleimide or nitrone proton resonances and the appearance of cycyloadduct proton resonances. For instance, the area of the maleimide proton resonances and either one of the cyclcoadduct proton resonances were calculated through deconvolution of the spectrum. The area of maleimide protons resonances was initially divided by two and added to the area of the cycloadduct proton resonances. The resulting number indicates the area of a proton resonance of a species at fixed reaction concentration and was further employed as a reference to calculate the concentration of other detectable species in the ^{1}H NMR spectra. This procedure was repeated for remaining spectra recorded at later time points. The time at which each spectrum was recorded was extracted from the log file alongside the NMR spectroscopy data. Having established the concentration of

products at each time point, the reaction profiles were plotted using the ProFit program (version 6.2.4, Quantum Soft, Switzerland). This is particularly straightforward to be employed in the kinetic analysis of thread formation as described in **Section 5.5** (**Chapter 5**).

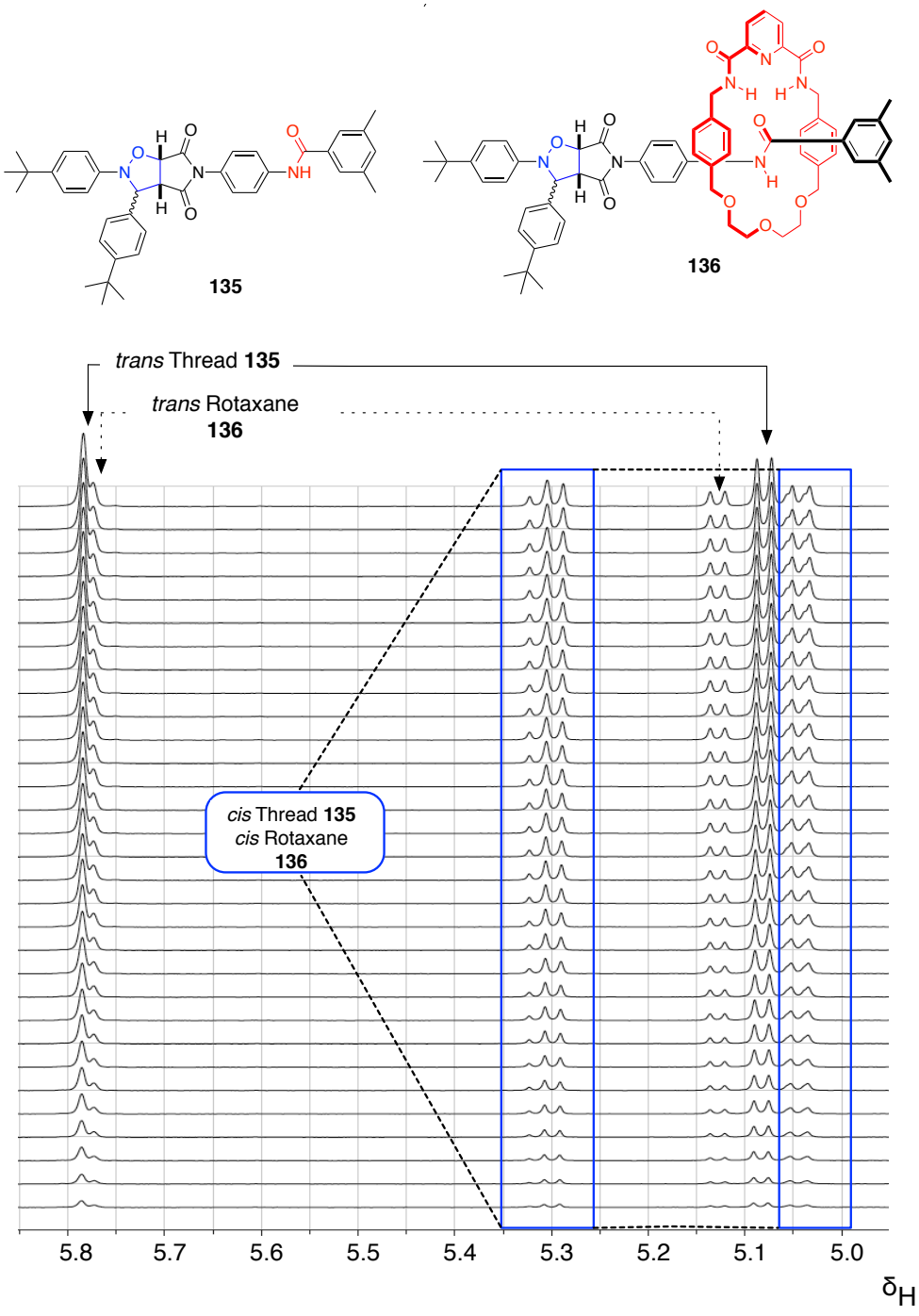

Figure 10.2. Partial ^{1}H NMR spectra (500.1 MHz, 25 ˚C, $CDCl_3$, 16 h) of the reaction between nitrone **134**, maleimide **108** and macrocycle **MDG**, illustrating spectral region associated with the resonances of the isoxazolidines proton for thread **135** and rotaxane **136** at 20 mM concentration.

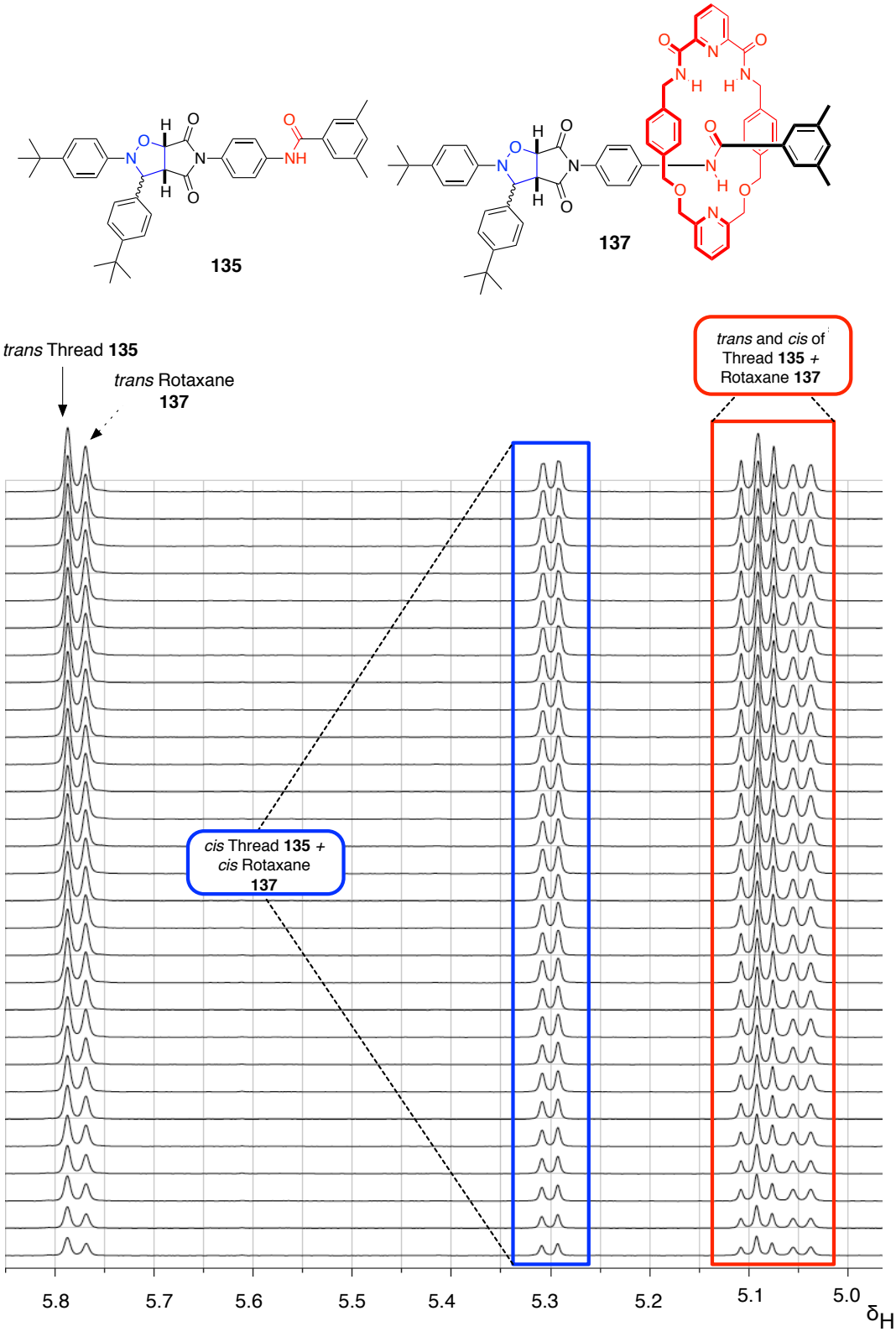

Figure 10.3. Partial ^{1}H NMR spectra (500.1 MHz, 25 ˚C, 16 h, $CDCl_3$) of the reaction between nitrone **134**, maleimide **108** and macrocycle **MP**, illustrating spectral region associated with the resonances of the isoxazolidines proton at 20 mM concentration.

Nonetheless, the elucidation by ^{1}H NMR spectroscopy is however not always straightforward. For instance, in the formation of simple rotaxane formation utilizing macrocycle **MDG**, nitrone **134** and maleimide **108** (as described in **Figure 5.8a, Chapter 5**), a total integration for both diastereoisomers for each thread and rotaxane was taken to provide useful information for the kinetic analysis of the system are shown in **Figure 10.2**.

The partial ^{1}H NMR showed that the resonances arising from the *trans* rotaxane **137** and of the *trans* thread **135** are no longer overlap between each other when we replaced the macrocycle with macrocycle **MP** (as illustrated in **Figure 5.10a**, **Chapter 5**). Despite that, the resonances arising from the *cis* cycloadducts of thread and rotaxane remains overlap over 16 hours of the experiment. Likewise, the reaction profile for the reaction was similarly constructed from the total integration of potential diastereoisomers related to thread and rotaxane, respectively and shown in **Figure 10.3**.

10.3 ^{19}F NMR spectroscopy : Preparation, kinetic measurements and deconvolution data

The NMR sample was similarly prepared as described previously. The tube was transferred immediatedly to a 470.4 MHz Bruker Avance 500 NMR spectrometer regulated at reaction temperature. ^{19}F{^{1}H} were acquired automatically at a set time interval (every 1800 s) over a period of 16 h. Analysis and deconvolution of the arrayed ^{19}F NMR spectra recorded in the course of the reaction was performed using iNMR© software (Version 3.6.3, Mestrelab Research, 2010). For instance, the ^{19}F NMR spectrum shown in **Figure 10.4** for the reaction between CF_3 nitrone **142**, maleimide **108** and macrocycle **MDG** (as described in **Figure 5.12a**) provide much improved signal dispersion signals for the formation of all potential cycloadducts in comparison when analysed using ^{1}H NMR spectroscopy (inset).

The area of the CF_3 nitrone **142** and the area of potential cycloadducts were summed up and the given number was used as reference to calculate the concentration of other species in the ^{19}F NMR spectra. This procedure was repeated for remaining spectra recorded at later time points. The time at which each spectrum was recorded

was extracted from the log file alongside the NMR spectroscopy data. Having established the concentration of products at each time point, the reaction profiles were plotted using the ProFit program (version 6.2.4, Quantum Soft, Switzerland).

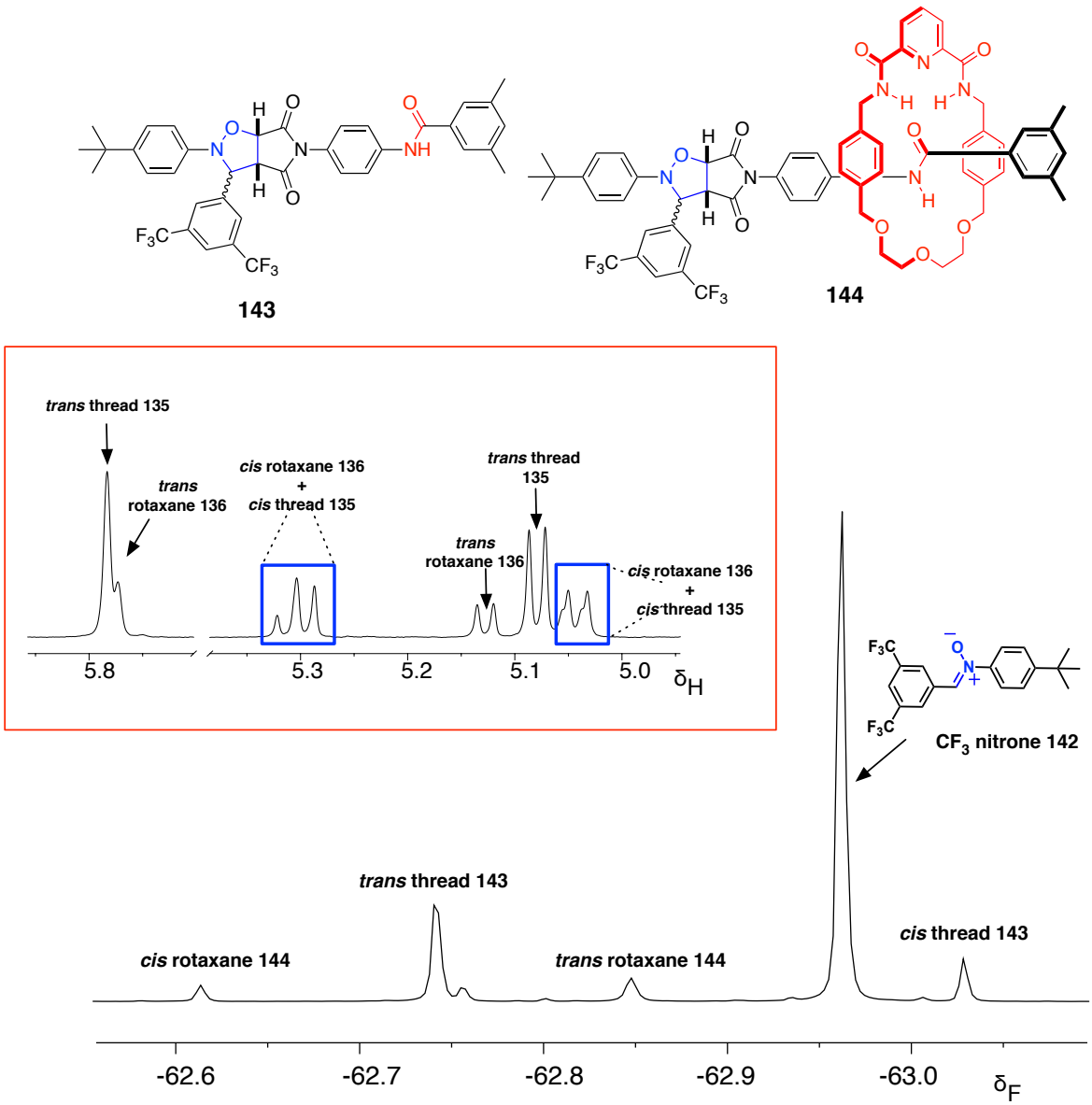

Figure 10.4. Partial ^{19}F NMR spectrum (470.4 MHz, 25 ˚C, $CDCl_3$) for the reaction between CF_3 nitrone **142**, maleimide **108** and macrocycle **MDG**, illustrating distinct signals associated with the formation of cycloadducts from the thread and rotaxane at 20 mM concentration. The inset show the overlapping ^{1}H NMR resonances in **Figure 10.2** for comparison.

10.4 Determination of binding constants

In the case of fast exchange (F) on the NMR chemical shift timescale between the complexed and uncomplexed species, the change in the observed chemical shift for discrete resonance is a weighted average between the bound and unbound species. The association constant, K_a was determined by NMR titration method using ^{1}H NMR spectroscopy at 298 K. The stock solutions and samples were made up in dry $CDCl_3$ using volumetric flask (accuracy ± 0.02 mL). In a typical ^{1}H NMR titration experiment, small aliquots of guest are added to a solution of host of known concentration and the NMR spectrum of the sample monitored as a function of guest concentration. Various atomic nuclei are often reported for their changes in chemical shift. The binding constant is extracted from the titration curve, which is the plot of changes in chemical shift against added guest concentration by fitting the curve using a non-linear curve-fitting program. However, if the exchange of bound and unbound species is slow (S) on the NMR chemical shift timescale, then the association constant is estimated by simple integration of the ^{1}H and ^{19}F NMR resonances for bound and unbound host or guest, so called the single-point method.

10.5 Computational methods

All molecular mechanics calculations were performed on a Linux workstation using the OPLS2005 forcefield together with the GB/SA solvation model for chloroform as implemented in Macromodel (Version 9.8, Schrödinger Inc., **2010**). Electronic structure calculations were carried out[267,268] using MOPAC2009 running on a Linux cluster. Transition states were successfully located using the semi empirical RM1 methods[226] as implemented in MOPAC2009. Version 11.038L was used in all calculations.

10.6 Kinetic simulation and fitting

All kinetic fitting and simulations were performed using the software SimFit (von Kiedrowski, 2003) and the ISOSIM package incorporated within the SimFit package. The kinetic model of all possible interactions involved in the investigated system was constructed. This model was converted into a series of rate equations whose solution determine the concentration of reactant and product species as a function of time. The program is allowed to vary the kinetic values to optimize the calculation to our experimental data. The ISOSIM procedure allowed the usage of data obtained from

the fitting to simulate scenarios under a series of different conditions, which were not experimentally available.

10.7 Synthetic procedures

The structure and the number of the compound were arranged with the description of the procedure and spectroscopic data.

4-((2-Hydroxyethoxy)methyl)benzonitrile 79

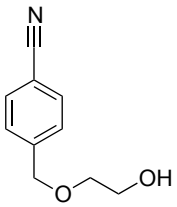

A solution of 4-(bromomethyl) benzonitrile **78** (7.50 g, 38.0 mmol) in dry THF (40 mL) was added to a solution of sodium (1.77 g, 77.0 mmol) in ethylene glycol (45 mL). The resultant mixture was heated to 60 ˚C for 16 h and followed by quenching with sat. solution of NH_4Cl. The product was extracted into CH_2Cl_2 and dried with $MgSO_4$. The solution was filtered, and concentrated *in vacuo* to yield **79** as a yellow oil (6.07 g, 90%). ^{1}H NMR (300.1 MHz, $CDCl_3$): δ_H 7.64 (2H, d, $^3J_{HH}$ 8.1 Hz; 2×Ar*H*), 7.45 (2H, d, $^3J_{HH}$ 8.6 Hz; 2×Ar*H*), 4.67 (2H, s; C*H*$_2$), 3.79 (2H, t, $^3J_{HH}$ 4.5 Hz; C*H*$_2$), 3.63 (2H, t, $^3J_{HH}$ 4.5 Hz; C*H*$_2$), 2.00 (1H, br s; O*H*); ^{13}C NMR (75.5 MHz, $CDCl_3$): δ_C 143.7 (Ar*C*), 132.3 (Ar*C*), 127.8 (Ar*C*H), 118.8 (*C*≡N), 111.4 (Ar*C*H), 72.3 (*C*H$_2$), 72.0 (*C*H$_2$), 61.8 (*C*H$_2$). MS (ES$^+$) *m/z* 200.1 ([M+Na]$^+$, 100); HRMS (ES$^+$) *m/z* calculated for $C_{10}H_{11}NO_2Na$ [M+Na]$^+$ 200.0687, found 200.0690.

2-((4-Cyanobenzyl)oxy)ethyl 4-methylbenzenesulfonate 80

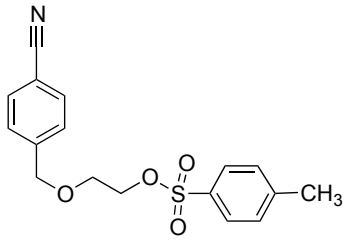

The corresponding alcohol **79** (3.0 g, 17.0 mmol) was dissolved in dry CH_2Cl_2 (34 mL) and Et_3N (2.84 mL, 20.4 mmol) was added dropwise into the solution. *p*-toluene sulphonyl chloride (3.57 g, 18.7 mmol) was added next to the resulting mixture at 0 ˚C for 1 h. The reaction mixture refluxed for 16 h. The resulting solution was quenched with distilled H_2O and washed sequentially with sat. solution of NH_4Cl and extracted into CH_2Cl_2. The organic layers were combined, dried over anhydrous $MgSO_4$. The solution was filtered, concentrated and the crude product was subjected to the silica gel chromatography (Cyclohexane:EtOAc, 3:1). Fractions containing the product were concentrated *in vacuo* to give the title compound **80** as colourless solid (4.3 g, 77%); M.p. 54.3 – 56.2

˚C; ^{1}H NMR (300.1 MHz, $CDCl_3$): δ_H 7.79 (2H, d, $^{3}J_{HH}$ 8.4 Hz; 2×Ar*H*), 7.61 (2H, d, $^{3}J_{HH}$ 8.3 Hz; 2×Ar*H*), 7.38 – 7.31 (4H, m; 4×Ar*H*), 4.55 (2H, s; CH_2), 4.22 (2H, t, $^{3}J_{HH}$ 4.6 Hz; CH_2), 3.72 (2H, t, $^{3}J_{HH}$ 4.6 Hz; CH_2), 2.44 (3H, s; CH_3); ^{13}C NMR (75.5 MHz, $CDCl_3$): δ_C 148.2 (Ar*C*), 145.4 (Ar*C*), 143.6 (Ar*C*), 132.6 (Ar*C*H), 130.3 (Ar*C*H), 128.4 (Ar*C*H), 128.0 (Ar*C*H), 119.1 (*C*≡N), 111.4 (Ar*C*), 72.6 (*C*H_2), 69.5 (*C*H_2), 68.6 (*C*H_2), 22.1 (*C*H_3). MS (ES^+) *m/z* 354.9 $[M+Na]^+$ (100); HRMS (ES^+) *m/z* calculated for $C_{17}H_{17}NO_4NaS$ $[M+Na]^+$ 354.0776, found 354.0775.

4,4'-((((2-Oxoimidazolidine-1,3-diyl)bis(ethane-2,1-diyl))bis(oxy))bis(methylene))dibenzonitrile 82

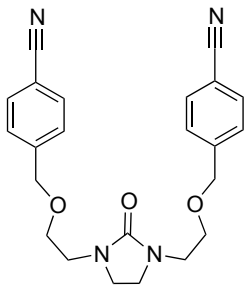

NaH (0.68 g, 28.5 mmol) was added to a solution of 2-imidazoline **81** (0.25 g, 2.9 mmol) in dry THF (15 mL). The suspension was left to reflux for 1.5 h under the N_2 atmosphere. While it was allowed to cool at ambient temperature, a solution of **80** (2.0 g, 6.0 mmol) in dry THF (15 mL) was reacted slowly into the resulting solution. The reaction mixture was refluxed at 75 ˚C for 16 h. The resulting solution was diluted with CH_2Cl_2 and washed with distilled H_2O followed by the sat. solution of NH_4Cl. The organic layer was dried with $MgSO_4$, concentrated and the crude was subjected to silica gel chromatography (EtOAc:Hexane, 5:1). Fractions containing the product were concentrated *in vacuo* to give compound **82** as a yellow oil (0.6 g, 51%). ^{1}H NMR (400.1 MHz, $CDCl_3$): δ_H 7.62 (4H, d, $^{3}J_{HH}$ 8.1 Hz; 4×Ar*H*), 7.42 (4H, d, $^{3}J_{HH}$ 8.5 Hz; 4×Ar*H*), 4.57 (4H, s; 2×CH_2), 3.65 (4H, t, $^{3}J_{HH}$ 5.3 Hz; 2×CH_2), 3.44 (4H, t, $^{3}J_{HH}$ 5.4 Hz; 2×CH_2), 3.43 (4H, s; 2×CH_2); ^{13}C NMR (75.5 MHz, $CDCl_3$): δ_C 161.3 (*C*=O), 143.8 (Ar*C*), 132.3 (Ar*C*H), 127.6 (Ar*C*H), 118.8 (*C*≡N), 111.3 (Ar*C*), 71.9 (*C*H_2), 69.7 (*C*H_2), 44.4 (*C*H_2), 44.2 (*C*H_2); MS (CI^+) *m/z* 405.2 ($[M+H]^+$, 100); HRMS (CI^+) *m/z* calculated for $C_{23}H_{25}N_4O_3$ $[M+H]^+$ 405.1927, found 405.1929.

1,3-Bis(2-((4-(aminomethyl)benzyl)oxy)ethyl)imidazolidin-2-one 83

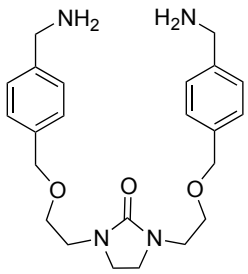

BH_3•THF complex (1M solution in THF, 11 mL, 11 mmol) was slowly added to a stirred solution of **82** (1.0 g, 2.47 mmol) in dry THF (15 mL) at 0 ˚C under N_2 atmosphere and stirred at ambient temperature for 2 h. Following this, the reaction mixture was heated to reflux for 16 h. The reaction mixture was quenched with 1M HCl, concentrated *in vacuo* and extracted once with CH_2Cl_2. The aqueous layer was then adjusted to pH 12 with 5M KOH and extracted into CH_2Cl_2. The combined organic layers were dried with $MgSO_4$ and the solvent was removed by evaporation *in vacuo*. The residue was purified by silica gel chromatography (CH_2Cl_2:CH_3OH:Et_3N, 98:1:1 to 90:5:5) to furnish **83** (0.86 g, 86%) as colourless oil. ^{1}H NMR (400.1 MHz, $CDCl_3$): δ_H 7.31 – 7.27 (8H, m; 8×Ar*H*), 4.50 (4H, s; 2×CH_2), 3.85 (4H, s; 2×CH_2), 3.60 (4H, t, $^3J_{HH}$ 5.2 Hz; 2×CH_2), 3.41 (4H, t, $^3J_{HH}$ 5.2 Hz; 2×CH_2), 3.41 (4H, s; 2×CH_2); ^{13}C NMR (100.6 MHz, $CDCl_3$): δ_C = 161.4 (*C*=O), 142.5 (Ar*C*), 136.9 (Ar*C*H), 128.0 (Ar*C*H), 127.3 (Ar*C*), 73.4 (*C*H_2), 72.8 (*C*H_2), 69.4 (*C*H_2), 46.2 (*C*H_2), 44.3 (*C*H_2); MS (Cl^+) *m/z* 413.26 ([M+H]$^+$, 100); HRMS (Cl^+) *m/z* calculated for $C_{23}H_{33}N_4O_3$ [M+H]$^+$ 413.2553, found 413.2551.

Ethylene Urea Macrocycle (MEU)

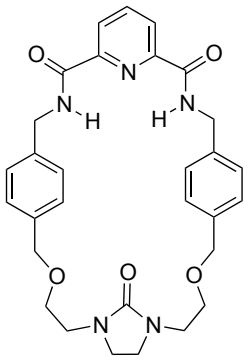

Compound **83** (0.28 g, 0.68 mmol) in dry CH_2Cl_2 (10 mL) and a solution of 2,6-pyridinedicarbonyl dichloride (0.14 g, 0.68 mmol) in dry CH_2Cl_2 (10 mL) were added simultaneously over 50 min to a solution of Et_3N (0.38 mL, 2.72 mmol) in dry CH_2Cl_2 (48 mL) at ambient temperature under a N_2 atmosphere. The reaction mixture was left stirred for 3 days. The reaction mixture was then washed successively with 1M HCl and 1M KOH. The organic layer was dried with $MgSO_4$ and concentrated by evaporation under reduced pressure. The residue was purified by column chromatography (EtOAc:Cyclohexane, 3:1) and yielded macrocycle **MEU** (96 mg, 26%) as a colourless powder. M.p. = 125.5 – 127.5 ˚C; ^{1}H NMR (400.1 MHz, $CDCl_3$): δ_H 8.41 (2H, d, $^3J_{HH}$ 7.8 Hz; 2xAr*H*), 8.05 (1H, t, $^3J_{HH}$ 7.8 Hz; Ar*H*), 8.04 (2H, br s; 2×N*H*), 7.27 (8H, s; 8×Ar*H*), 4.69 (4H, d, $^3J_{HH}$ 6.2 Hz; 2×CH_2), 4.47 (4H, s; 2×CH_2), 3.60 (4H, t, $^3J_{HH}$ 5.1 Hz; 2×CH_2), 3.40

(4H, t, $^{3}J_{HH}$ 5.1 Hz; 2×CH_2), 3.32 (4H, s; 2×CH_2); ^{13}C NMR (100.6 MHz, $CDCl_3$): δ_C 163.3 (*C*=O), 161.3 (*C*=O), 148.8 (Ar*C*), 139.1 (Ar*C*H), 137.9 (Ar*C*), 137.4 (Ar*C*), 128.2 (Ar*C*H), 127.9 (Ar*C*H), 125.5 (Ar*C*H), 72.6 (*C*H_2), 69.4 (*C*H_2), 44.3 (*C*H_2), 44.0 (*C*H_2), 43.3 (*C*H_2); MS (ES$^+$) *m/z* 566.17 ([M+Na]$^+$, 100); HRMS (ES$^+$) *m/z* calculated for $C_{30}H_{33}N_5O_5Na$ [M+Na]$^+$ 566.2379, found 566.2372. Crystals suitable for analysis by single crystal X-ray diffraction were grown by vapour diffusion of hexane into a solution of macrocycle **MEU** in $CHCl_3$ at ambient temperature.

4-((2-Azidoethoxy)methyl)benzonitrile 92

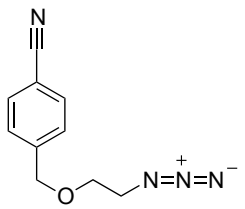

NaN_3 (3.9 g, 60.0 mmol) was added to a solution of **80** (6.6 g, 20.0 mmol) in DMF (100 mL). The resulting mixture was then refluxed at 80 ˚C for 16 h. The formation of azide was checked to be completed *via* TLC. DMF was removed *in vacuo* and the reaction mixture was diluted with CH_2Cl_2 and washed several times with 0.1M HCl and H_2O to dilute the acid. The organic extracts were dried over $MgSO_4$, filtered and concentrated under reduced pressure to obtain the desired product **92** as brown oil (3.9 g, 97%). ^{1}H NMR (300.1 MHz, $CDCl_3$): δ_H 7.62 (2H, d, $^{3}J_{HH}$ 8.5 Hz; 2×Ar*H*), 7.43 (2H, d, $^{3}J_{HH}$ 7.9 Hz; 2×Ar*H*), 4.60 (2H, s; CH_2), 3.68 (2H, t, $^{3}J_{HH}$ 4.8 Hz; CH_2), 3.41 (2H, t, $^{3}J_{HH}$ 4.8 H; CH_2); ^{13}C NMR (75.5 MHz, $CDCl_3$): δ_C 143.9 (Ar*C*), 132.5 (Ar*C*H), 128.1 (Ar*C*H), 119.2 (*C*≡N), 111.6 (Ar*C*), 72.5 (*C*H_2), 69.8 (*C*H_2), 51.1 (*C*H_2); MS (CI$^+$) *m/z* 203.09 ([M+H]$^+$, 100); HRMS (CI$^+$) *m/z* calculated for $C_{10}H_{11}N_4O$ [M+H]$^+$ 203.0933, found 203.0936.

4-((2-Aminoethoxy)methyl)benzonitrile 93

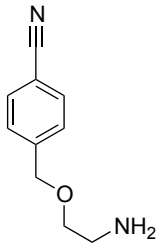

Pyridine (0.2 mL, 2.47 mmol) was added to azide compound **92** (1.0 g, 4.95 mmol) in CH_3OH (20 mL) followed by Pd/C (50 mg, 0.04 mmol). The reaction mixture was hydrogenated at ambient temperature and stirred for 8 h. The resultant suspension was filtered through a pad of Celite and washed with minimum amount of CH_3OH. The resulting compound **93** was formed *in situ* and carried out to the next step without further purification. ^{1}H NMR (300.1 MHz, $CDCl_3$): δ_H 7.74 (2H, d, $^{3}J_{HH}$ 8.3 Hz; 2×Ar*H*), 7.43

(2H, d, $^3J_{HH}$ 8.5 Hz; 2×Ar*H*), 4.63 (2H, s; CH_2), 3.70 (2H, t, $^3J_{HH}$ 4.7 Hz; CH_2), 3.44 (2H, t, $^3J_{HH}$ 4.7 Hz, CH_2); ^{13}C NMR (75.5 MHz, $CDCl_3$): δ_C 143.9 (Ar*C*), 132.2 (Ar*C*H), 127.7 (Ar*C*H), 112.4 (Ar*C*), 118.1 (*C*≡N), 72.1 (*C*H_2), 70.3 (*C*H_2), 49.3 (*C*H_2); MS (ES^+) *m/z* 177.06 ($[M+H]^+$, 100).

1,3-Bis(2-(4-cyanobenzyloxy)ethyl)urea 95

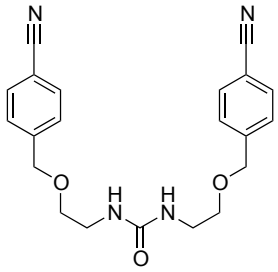

A solution of Et_3N (1.4 mL, 9.90 mmol) in Et_2O (25 mL) was added to the solution of compound **93** (1.0 g, 4.95 mmol) in minimal amount of dry CH_2Cl_2. The resulting solution was cooled at 0 ˚C. Triphosgene **94** (0.25 g, 0.83 mmol) was added neat under N_2 atmosphere and stirred for 6 h. The suspension was diluted with $CHCl_3$, acidified with 1M HCl up to pH 1 followed by H_2O. The resulting solution was extracted with $CHCl_3$ and the organic layers were dried over $MgSO_4$, filtered and evaporated *in vacuo*. The residue was further purified by recrystallisation from $CHCl_3$:Hexane to give product **95** as a yellow solid (0.34 g, 36%). M.p. = 156.5 – 158.5 ˚C; ^{1}H NMR (300.1 MHz, $CDCl_3$): δ_H 7.62 (4H, d, $^3J_{HH}$ 8.4 Hz; 4×Ar*H*), 7.41 (4H, d, $^3J_{HH}$ 8.6 Hz; 4×Ar*H*), 4.83 (2H, br s; 2×N*H*), 4.55 (4H, s; 2×CH_2), 3.58 (4H, t, $^3J_{HH}$ 5.1 Hz; 2×CH_2), 3.43 (4H, t, $^3J_{HH}$ 5.0 Hz; 2×CH_2); ^{13}C NMR (75.5 MHz, $CDCl_3$): δ_C 158.7 (*C*=O), 143.9 (Ar*C*), 132.7 (Ar*C*H), 128.2 (Ar*C*H), 111.9 (Ar*C*), 111.8 (*C*≡N), 72.5 (*C*H_2), 70.9 (*C*H_2), 40.8 (*C*H_2); MS (ES^+) *m/z* 401.2 ($[M+Na]^+$, 100); HRMS (ES^+) *m/z* calculated for $C_{21}H_{22}N_4O_3Na$ $[M+Na]^+$ 401.1590, found 401.1580.

Diprop-2-ynyl pyridine-2,6-dicarboxylate[269] 96

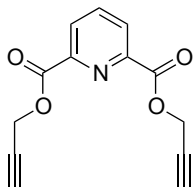

A solution of 2,6-pyridinedicarbonyl dichloride (1.0 g, 4.90 mmol) and propargyl alcohol (470 µL, 8.03 mmol) were added simultaneously in $CHCl_3$ (25 mL) together with Et_3N (2.1 mL, 14.7 mmol) at 0 ˚C and left stirred for 10 min. The resulting mixtures were left stirred at ambient temperature for 16 h. Next, the reaction mixture was diluted in $CHCl_3$ and the resulting residue was purified by recrystallisation from $CHCl_3$:Hexane to give compound **96** as a beige solid (0.6 g, 50%). M.p. 116.4 –

118.5 ˚C (lit[269]. 124 ˚C); ^{1}H NMR (300.1 MHz, $CDCl_3$): δ_H 8.34 (2H, d, $^{3}J_{HH}$ 7.9 Hz; 2×Ar*H*), 8.04 (1H, dd, $^{3}J_{HH}$ 7.6 and $^{3}J_{HH}$ 8.1 Hz; Ar*H*), 5.02 (4H, d, $^{4}J_{HH}$ 2.5 Hz; 2×CH_2), 2.53 (2H, t, $^{4}J_{HH}$ 2.5 Hz, 2×C*H*); ^{13}C NMR (75.5 MHz, $CDCl_3$): δ_C 163.7 (*C*=O), 147.9 (Ar*C*), 138.6 (Ar*C*H), 128.6 (Ar*C*H), 75.8 (*C*H), 75.6 (q*C*), 53.6 (*C*H_2); MS (ES$^+$) *m/z* 265.98 ([M+Na]$^+$, 100); HRMS (ES$^+$) *m/z* calculated for $C_{13}H_9NO_4Na$ [M+Na]$^+$ 266.0429, found 266.0439.

3,3'-(3,3'-(2-Oxoimidazolidine-1,3-diyl)bis(prop-1-yne-3,1-diyl))dibenzonitrile 100

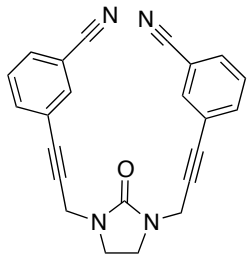

A degassed (by bubbling Ar) solution of 3-bromobenzonitrile **99** (1.45 g, 7.7 mmol) in Et_3N (15 mL) was cannulated into a degassed (by bubbling Ar) suspension of 1,3-di(prop-2-yn-1-yl)imidazolidin-2-one **98** (0.6 g, 3.70 mmol), PPh_3 (97 mg, 370 µmol), CuI (35 mg, 185 µmol), $PdCl_2(PPh_3)_2$ (130 mg, 185 µmol) and Et_3N (10 mL) in dry THF (45 mL). The reaction mixture was heated at 70 ˚C under an Ar atmosphere for 48 h, and then filtered through a pad of Celite. The filtrate was concentrated under reduced pressure. The residue was dissolved in $CHCl_3$. The organic layer was washed with water, dried ($MgSO_4$) and concentrated by evaporation *in vacuo*. The residue was purified by column chromatography (Cyclohexane:EtOAc, 2:1) to give compound **100** as a yellow solid (490 mg, 36%). M.p. = 121.9 – 124.9 ˚C; ^{1}H NMR (300.1 MHz, $CDCl_3$) : δ_H 7.67 (2H, td, $^{4}J_{HH}$ 1.6 and $^{4}J_{HH}$ 0.5 Hz; 2×Ar*H*), 7.62 (2H, dt, $^{3}J_{HH}$ 7.8 and $^{4}J_{HH}$ 1.5 Hz; 2×Ar*H*), 7.58 (2H, dt, $^{3}J_{HH}$ 7.9 and $^{4}J_{HH}$ 1.4 Hz; 2×Ar*H*), 7.41 (2H, td, $^{3}J_{HH}$ 7.8 and $^{4}J_{HH}$ 0.4 Hz; 2×Ar*H*), 4.28 (4H, s; 2×CH_2), 3.52 (4H, s; 2×CH_2); ^{13}C NMR (100.6 MHz, $CDCl_3$): δ_C 159.2 (*C*=O), 135.9 (Ar*C*H), 135.2 (Ar*C*H), 131.7 (Ar*C*H), 129.4 (Ar*C*H), 124.2 (Ar*C*), 118.0 (*C*≡N), 112.9 (Ar*C*), 86.2 (q*C*), 82.1 (q*C*), 42.2 (*C*H_2), 34.8 (*C*H_2); MS (ES$^+$) *m/z* 387 ([M+Na]$^+$, 100); HRMS (ES$^+$) *m/z* calculated for $C_{23}H_{16}N_4ONa$ [M+Na]$^+$ 387.1222, found 387.1211

4,4'-(2,2'-Oxybis(ethane-2,1-diyl)bis(oxy))bis(methylene)dibenzonitrile[207] 102

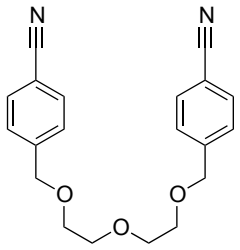

4-(bromomethyl)benzonitrile **78** (3.01 g, 15.4 mmol) was slowly added to a suspension of NaH (0.76 g, 19.0 mmol) in dry THF (60 mL) and diethylene glycol (730 µL, 7.30 mmol). The resulting mixture was refluxed at 70 ˚C for 16 h. The resultant solution was quenched with ethanol followed by H_2O and extracted into EtOAc. The organic extracts were dried over $MgSO_4$, filtered and concentrated under reduced pressure. The residue was further purified *via* column chromatography (Cyclohexane:EtOAc, 1:1) to obtain the desired compound **102** as yellow oil (2.34 g, 90%). ^{1}H NMR (300.1 MHz, $CDCl_3$): δ_H 7.61 (4H, d, $^3J_{HH}$ 8.4 Hz; 4×Ar*H*), 7.44 (4H, d, $^3J_{HH}$ 8.6 Hz; 4×Ar*H*), 4.62 (4H, s; 2×CH_2), 3.65 – 3.73 (8H, m; 4×CH_2); ^{13}C NMR (75.5 MHz, $CDCl_3$): δ_C 144.0 (Ar*C*), 132.3 (Ar*C*H), 127.8 (Ar*C*H), 118.9 (*C*≡N), 111.3 (Ar*C*), 72.3 (*C*H_2), 70.7 (*C*H_2), 70.2 (*C*H_2); MS (CI$^+$) *m/z* 337 ([M+H]$^+$, 100); HRMS (CI$^+$) *m/z* calculated for $C_{20}H_{21}N_2O_3$ [M+H]$^+$ 337.1552, found 337.1556.

(4,4'-(2,2'-Oxybis(ethane-2,1-diyl)bis(oxy))bis(methylene)bis(4,1-phenylene))di methanamine[207] 103

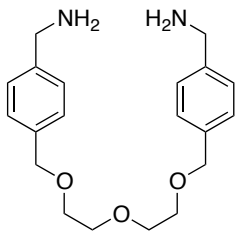

A solution of BH_3•THF complex (1M solution in THF, 35 mL, 35.0 mmol) was added dropwise to a solution of compound **102** (2.6 g, 7.7 mmol) in dry THF (33 mL) at 0 ˚C under N_2 atmosphere. The reaction mixture was stirred at ambient temperature for 2 h followed by refluxing the solution for 24 h. The reaction mixture was quenched with 1M HCl and extracted once with CH_2Cl_2. The separated aqueous layer was adjusted to pH 12 using 5M KOH and extracted further into CH_2Cl_2. The collected organic layers were dried over $MgSO_4$, filtered and concentrated *in vacuo*. The compound **103** (1.37 g, 52%) was isolated as a yellow oil. ^{1}H NMR (300.1 MHz, $CDCl_3$): δ_H 7.31 (4H, d, $^3J_{HH}$ 8.2 Hz; 4×Ar*H*), 7.26 (4H, d, $^3J_{HH}$ 8.2 Hz; 4×Ar*H*), 4.55 (4H, s; 2×CH_2), 3.85 (4H, s; 2×CH_2), 3.70 – 3.61 (8H, m; 4×CH_2), 1.60 (4H, br s; 2×NH_2); ^{13}C NMR (75.5 MHz, $CDCl_3$): δ_C 142.8 (Ar*C*), 136.9 (Ar*C*H), 128.2 (Ar*C*H), 127.2 (Ar*C*), 73.1 (*C*H_2), 70.8 (*C*H_2), 69.5 (*C*H_2), 46.4 (*C*H_2); MS (CI$^+$) *m/z* 105 (22), 119 (46), 120 (100), 328 (20), 345 ([M+H]$^+$, 12); HRMS (CI$^+$) *m/z* calculated for

$C_{20}H_{29}N_2O_3$ $[M+H]^+$ 345.2178, found 345.2177.

Diethylene Glycol Macrocycle (MDG)[207]

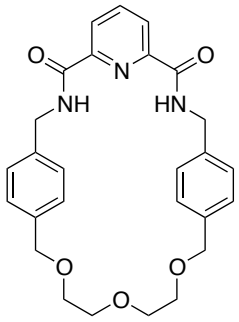

A solution of **103** (1.21 g, 3.51 mmol) in dry CH_2Cl_2 (70 mL) and 2,6-pyridinedicarbonyl dichloride (0.72 g, 3.51 mmol) in dry CH_2Cl_2 (70 mL) were added simultaneously over a period of 1 h to the solution containing 4-pyridone **87** (0.33 g, 3.51 mmol) and Et_3N (1.96 mL, 14.1 mmol) in dry CH_2Cl_2 (80 mL) at ambient temperature under N_2 atmosphere. The reaction mixture was left stirred for 3 days. The resulting solution was once washed with 1M HCl followed by 1M KOH. The organic extracts was dried over $MgSO_4$, filtered and concentrated *in vacuo*. The residue was purified by column chromatography (EtOAc:$CHCl_3$, 9:1) to give macrocycle **MDG** as a colourless solid (0.54 g, 34%). M.p. = 230.6 – 232.5 ˚C; ^{1}H NMR (300.1 MHz, $CDCl_3$): δ_H 8.25 (2H, d, $^3J_{HH}$ 7.8 Hz; 2×Ar*H*), 8.10 (2H, br s; 2×N*H*), 8.03 (1H, t, $^3J_{HH}$ 7.8 Hz; Ar*H*), 7.28 (4H, d, $^3J_{HH}$ 8.0 Hz; 4×Ar*H*), 7.21 (4H, d, $^3J_{HH}$ 8.0 Hz; 4×Ar*H*), 4.63 (4H, d, $^3J_{HH}$ 5.7 Hz; 2×CH_2), 4.56 (4H, s; 2×CH_2), 3.74 – 3.68 (8H, m; 4×CH_2); ^{13}C NMR (75.5 MHz, $CDCl_3$): δ_C 163.4 (*C*=O), 148.6 (Ar*C*), 139.6 (Ar*C*H), 138.1 (Ar*C*), 137.0 (Ar*C*), 128.3 (Ar*C*H), 127.5 (Ar*C*H), 125.2 (Ar*C*H), 72.9 (*C*H_2), 71.0 (*C*H_2), 69.8 (*C*H_2), 43.3 (*C*H_2); MS (ES^+) *m/z* 498.03 ($[M+Na]^+$, 100); HRMS (ES^+) *m/z* calculated for $C_{27}H_{29}N_3O_5Na$ $[M+Na]^+$ 498.2005, found 498.2008.

***N*-(4-Butylphenyl)-3,5-bis(trifluoromethyl)benzamide 105**

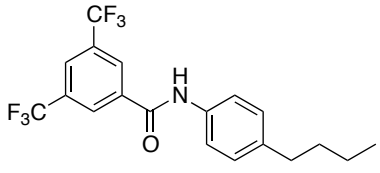

3,5-bis(trifluoromethyl)benzoyl chloride **124** (500 µL, 2.76 mmol) was added dropwise at –5 ˚C to the resulting solution of 4-butylaniline **104** (270 mg, 1.81 mmol) in $CHCl_3$ (10 mL) and Et_3N (500 µL, 3.62 mmol). The resulting solution was left stirred for 16 h at rt. The reaction mixture was diluted with $CHCl_3$, washed once with 1M HCl and followed by H_2O. The organic layers were dried over $MgSO_4$, filtered and concentrated *in vacuo* to furnish the compound **105** as colourless solid (350 mg, 50%). M.p. = 100.5 – 103.2 ˚C; ^{1}H NMR (300.1 MHz, $CDCl_3$) : δ_H 8.30 (2H, s; 2×Ar*H*), 8.03 (1H, s; Ar*H*), 7.97 (1H, br s; N*H*), 7.51 (2H, d, $^3J_{HH}$ 8.4 Hz; 2×Ar*H*), 7.18 (2H, d, $^3J_{HH}$ 8.5 Hz; 2×Ar*H*), 2.62 (2H, t, $^3J_{HH}$ 7.7 Hz; CH_2), 1.65 – 1.55 (2H, m; CH_2), 1.42 – 1.30 (2H, m; CH_2), 0.91 (3H, t, $^3J_{HH}$

7.3 Hz; C*H*$_3$); ^{13}C NMR (75.5 MHz, $CDCl_3$) : δ_C 163.2 (*C*=O), 140.8 (Ar*C*), 137.5 (Ar*C*), 134.9 (Ar*C*), 132.5 (q, $^2J_{CF}$ 32.6 Hz; Ar*C*), 129.5 (Ar*C*H), 127.6 (m; ArC*H*), 125.6 (m; Ar*C*H), 123.1 (q, $^1J_{CF}$ 275.0 Hz; CF_3), 121.0 (Ar*C*H), 35.5 (*C*H$_2$), 34.0 (*C*H$_2$), 22.7 (*C*H$_2$), 14.4 (*C*H$_3$); ^{19}F NMR (376.5 MHz, $CDCl_3$): δ_F –62.9 (ArC*F*$_3$); MS (ES$^+$) *m/z* 412.0 ([M+Na]$^+$, 100); HRMS (ES$^+$) *m/z* calculated for $C_{19}H_{17}NONaF_6$ [M+Na]$^+$ 412.1112, found 412.1119.

1-(3,5-Bis(trifluoromethyl)phenyl)-3-(4-butylphenyl)urea 106

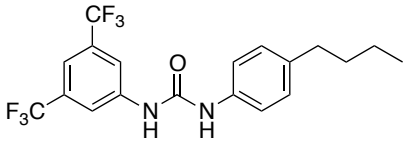

3,5-bis(trifluoromethyl)phenyl isocyanate **127** (0.50 g, 1.96 mmol), was added dropwise at –5 ˚C to a solution of 4-butylaniline **104** (0.29 g, 1.96 mmol) in $CHCl_3$ (10 mL) and left to stir at ambient temperature for 16 h. The resulting precipitate was filtered and further purified by recrystallisation from $CHCl_3$:Petroluem ether. The desired product **10**6 was isolated as a colourless solid (630 mg, 80%). M.p. = 165.3 – 168.5 ˚C; ^{1}H NMR (300.1 MHz, $CDCl_3$) : δ_H 8.69 (1H, br s; N*H*), 7.92 (1H, br s; N*H*), 7.89 (2H, s; 2×Ar*H*), 7.36 (1H, s; Ar*H*), 7.28 – 7.24 (2H, m; 2×Ar*H*), 7.07 – 7.02 (2H, m; 2×Ar*H*), 2.59 (2H, t, $^3J_{HH}$ 7.7 Hz; C*H*$_2$), 1.63 – 1.52 (2H, m; C*H*$_2$), 1.41 – 1.29 (2H, m; C*H*$_2$), 0.85 (3H, t, $^3J_{HH}$ 7.3 Hz; C*H*$_3$); ^{13}C NMR (75.5 MHz, $CDCl_3$) : δ_C 153.2 (*C*=O), 141.9 (Ar*C*), 138.1 (Ar*C*), 136.6 (Ar*C*), 132.3 (q, $^2J_{CF}$ 32.9 Hz, Ar*C*), 123.0 (q, $^1J_{CF}$ 273.0 Hz, CF_3), 129.2 (Ar*C*H), 124.9 (Ar*C*), 119.7 (Ar*C*H), 118.2 (m; Ar*C*H), 115.1 (m; Ar*C*H), 35.3 (*C*H$_2$), 34.1 (*C*H$_2$), 22.6 (*C*H$_2$), 13.7 (*C*H$_3$); ^{19}F NMR (376.5 MHz, $CDCl_3$) : δ_F –63.1 (ArC*F*$_3$); MS (ES$^+$) *m/z* 427.03 ([M+Na]$^+$, 100); HRMS (ES$^+$) *m/z* calculated for $C_{19}H_{18}N_2OF_6Na$ [M+Na]$^+$ 427.1221, found 427.1220.

***N*-(4-(4-(2,5-Dioxo-2,5-dihydro-1*H*-pyrrol-1-yl)phenethyl)phenyl)-3,5-dimethylbenzamide 109**

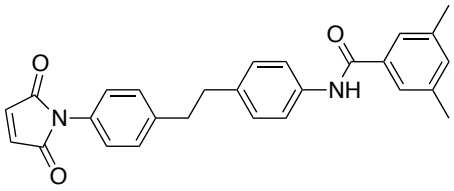

The acid derivative **123** (0.34 g, 0.78 mmol) was dissolved in dry CH_3CN (20 mL) and refluxed for 2 h after the subsequent addition of $ZnBr_2$ (0.18 g, 10.78 mmol) and hexamethyldisilazone (0.83 mL, 3.91 mmol). The reaction mixture was filtered and the filtrate was reduced to 10%. The solution was acidified with 0.5M HCl until pH 1 and extracted into CH_2Cl_2. The

organic layers were combined and dried over $MgSO_4$. The solvent was evaporated to give the desired product as yellow crystalline solid (0.32 g, 96%); M.p. = 229.3 – 231.4 ˚C; ^{1}H NMR (400.1 MHz, $CDCl_3$): δ_H 7.81 (1H, s; N*H*), 7.57 – 7.54 (2H, m; 2×Ar*H*), 7.46 (2H, s; 2×Ar*H*), 7.29 – 7.27 (2H, m; 2×Ar*H*), 7.25 – 7.22 (2H, m; 2×Ar*H*), 7.19 – 7.17 (3H, m; 3×Ar*H*), 6.84 (2H, s; 2×C*H*), 2.97 – 2.89 (4H, m; 2×CH_2), 2.38 (6H, s; 2×CH_3); ^{13}C NMR (100.6 MHz, $CDCl_3$): δ_C 169.8 (*C*=O), 166.1 (*C*=O), 141.8 (Ar*C*), 138.6 (Ar*C*), 137.7 (Ar*C*), 136.2 (Ar*C*), 135.2 (Ar*C*), 134.3 (*C*H), 133.5 (Ar*C*H), 129.4 (Ar*C*H), 129.2 (Ar*C*), 129.1 (Ar*C*H), 126.1 (Ar*C*H), 124.9 (Ar*C*H), 120.4 (Ar*C*H), 37.7 (*C*H_2), 37.3 (*C*H_2), 21.4 (*C*H_3); MS (ES^+) *m/z* 447 ([M+Na]$^+$, 75), 479 (100); HRMS (ES^+) *m/z* calculated for $C_{27}H_{24}N_2O_3Na$ [M+Na]$^+$ 447.1685, found 447.1674.

N-(4-(4-(2,5-Dioxo-2,5-dihydro-1*H*-pyrrol-1-yl)phenethyl)phenyl)-3,5-bis(trifluoromethyl)benzamide 110

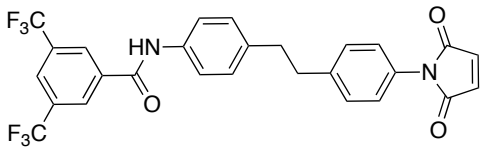

The acid derivative **126** (0.60 g, 1.09 mmol) was dissolved in dry CH_3CN (20 mL) and refluxed for 2 h after the subsequent addition of $ZnBr_2$ (0.25 g, 1.09 mmol) and hexamethyldisilazone (0.88 g, 1.2 mL, 5.45 mmol). The reaction mixture was filtered and the filtrate was reduced to 10%. The solution was acidified with 0.5M HCl until pH 1 and extracted into CH_2Cl_2. The organic layers were combined and dried over $MgSO_4$. The solvent was evaporated to give the desired product as yellow crystalline solid (0.25 g, 44%). M.p. = 249.5 – 251.3 ˚C; ^{1}H NMR (300.1 MHz, d_6-DMSO): δ_H 10.6 (1H, s; N*H*), 8.61 (2H, s; 2×Ar*H*), 8.36 (1H, s; Ar*H*), 7.68 (2H, d, $^3J_{HH}$ 8.6 Hz; 2×Ar*H*), 7.34 (2H, d, $^3J_{HH}$ 8.5 Hz; 2×Ar*H*), 7.27 (2H, d, $^3J_{HH}$ 8.6 Hz; 2×Ar*H*), 7.22 (2H, d, $^3J_{HH}$ 8.5 Hz; 2×Ar*H*), 7.17 (2H, s; 2×C*H*), 2.98 – 2.87 (4H, m; 2×CH_2); ^{13}C NMR (100.6 MHz, d_6-DMSO) : δ_C 170.4 (*C*=O), 162.7 (*C*=O), 141.5 (Ar*C*), 137.8 (Ar*C*), 137.5 (Ar*C*), 136.7 (Ar*C*), 135.0 (*C*H), 130.8 (q, $^2J_{CF}$ 33.2 Hz, Ar*C*), 129.3 (Ar*C*), 128.7 (Ar*C*H), 128.2 (Ar*C*H), 128.1 (m; Ar*C*H), 126.4 (Ar*C*H), 124.7 (m; Ar*C*H), 123.5 (q, $^1J_{CF}$ 276.6 Hz; CF_3), 120.2 (Ar*C*H), 36.9 (*C*H_2), 36.7 (*C*H_2); ^{19}F NMR (376.5 MHz, d_6-DMSO) : δ_F –61.7 (ArC*F*$_3$); MS (ES^-) *m/z* 531.1 ([M–H]$^-$, 100); HRMS (ES^-) *m/z* calculated for $C_{27}H_{17}N_2O_3F_6$ [M–H]$^-$ 531.1143, found 531.1140.

1-(3,5-Bis(trifluoromethyl)phenyl)-3-(4-(4-(2,5-dioxo-2,5-dihydro-1*H*-pyrrol-1-yl)phenethyl)phenyl)urea 111

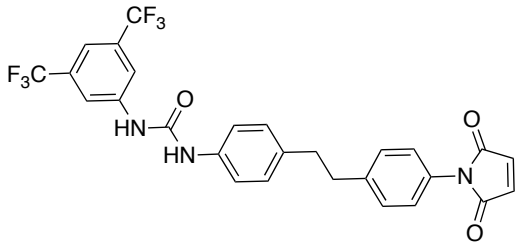

The acid derivative **129** (0.20 g, 0.35 mmol) was dissolved in dry CH_3CN (10 mL) and refluxed for 1 h after the subsequent addition of $ZnBr_2$ (80 mg, 0.35 mmol) and hexamethyldisilazone (0.38 mL, 1.77 mmol). The reaction mixture was filtered and the filtrate was reduced to 10%. The solution was acidified with 0.5M HCl until pH 1 and extracted into CH_2Cl_2. The organic layer were combined and dried over $MgSO_4$. The solvent was evaporated *in vacuo* to give the maleimide **111** as yellow solid (152 mg, 78%). M.p. = 205.3 – 208.3 ˚C; ^{1}H NMR (300.1 MHz, d_6-DMSO) : δ_H 9.36 (1H, s; N*H*), 8.89 (1H, s, N*H*), 8.13 (2H, s; 2×Ar*H*), 7.61 (1H, s; Ar*H*), 7.39 (2H, d, $^3J_{HH}$ 8.4 Hz; 2×Ar*H*), 7.33 (2H, d, $^3J_{HH}$ 8.4 Hz; 2×Ar*H*), 7.22 (2H, d, $^3J_{HH}$ 8.4 Hz; 2×Ar*H*), 7.18 (2H, d, $^3J_{HH}$ 8.4 Hz; 2×Ar*H*), 7.16 (2H, s; 2×C*H*), 2.94 – 2.82 (4H, m; 2×CH_2); ^{13}C NMR (75.5 MHz, d_6-DMSO): δ_C 170.0 (*C*=O), 152.4 (*C*=O), 142.0 (Ar*C*), 141.3 (Ar*C*), 136.8 (Ar*C*), 135.5 (Ar*C*), 134.6 (Ar*C*H), 130.7 (q, $^2J_{CF}$ 32.7 Hz, Ar*C*), 129.3 (Ar*C*), 128.8 (Ar*C*H), 128.7 (Ar*C*H), 126.6 (*C*H), 123.3 (q, $^1J_{CF}$ 272.3 Hz, CF_3), 119.0 (Ar*C*H), 117.8 (m; Ar*C*H), 114.2 (m, Ar*C*H), 36.7 (*C*H_2), 36.3 (*C*H_2) ; ^{19}F NMR (376.5 MHz, d_6-DMSO) : δ_F –62.2 (ArCF_3); MS (ES^-) *m/z* 546 ([M–H]$^-$, 100); HRMS (ES^-) *m/z* calculated for $C_{27}H_{18}N_3O_3F_6$ [M–H]$^-$ 546.1252, found 546.1257.

4,4'-(Pyridine-2,6-diylbis(methylene))bis(oxy)bis(methylene)dibenzonitrile 113

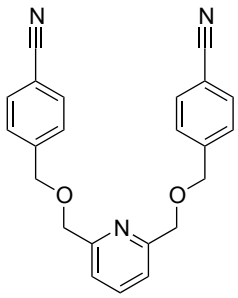

NaH (1.44 g, 36.0 mmol) was carefully added to a solution of 2,6-pyridine dimethanol **112** (2.0 g, 14.4 mmol) in dry THF (70 mL). The resulting mixture was refluxed for 1.5 h and allowed to cool to room temperature. Next, 4-bromomethyl benzonitrile **78** (5.93 g, 30.2 mmol) was added and continue to reflux for 18 h at 75 ˚C. H_2O was slowly added to quench the reaction. The organic layers were extracted into EtOAc. The combined organic layers were dried over $MgSO_4$, filtered and concentrated under reduced pressure. The resulting residue

was purified by recrystallisation from Petroleum ether:$CHCl_3$ to furnish a yellow solid (4.70 g, 88%). M.p. 105.8 – 107.1 ˚C; ^{1}H NMR (300.1 MHz, $CDCl_3$): δ_H 7.75 (1H, t, $^3J_{HH}$ 7.7 Hz; Ar*H*), 7.65 (4H, d, $^3J_{HH}$ 8.4 Hz; 4×Ar*H*), 7.49 (4H, d, $^3J_{HH}$ 8.6 Hz; 4×Ar*H*), 7.40 (2H, d, $^3J_{HH}$ 7.8 Hz; 2×Ar*H*), 4.71 (4H, s; 2×CH_2), 4.70 (4H, s; 2×CH_2); ^{13}C NMR (75.5 MHz, $CDCl_3$): δ_C 157.6 (Ar*C*), 143.6 (Ar*C*), 137.6 (Ar*C*H), 132.4 (Ar*C*H), 127.9 (Ar*C*H), 120.4 (Ar*C*H), 118.9 (*C*≡N), 111.6 (Ar*C*), 73.7 (*C*H_2), 72.1 (*C*H_2); MS (Cl^+) *m/z* 239.0 (27), 370.2 ([M+H]$^+$, 100); HRMS (Cl^+) *m/z* calculated for $C_{23}H_{20}N_3O_2$ [M+H]$^+$ 370.1556, found 370.1563.

(4,4'-Pyridine-2,6-diylbis(methylene))bis(oxy)bis(methylene)bis(4,1-phenylene))dimethanamine 114

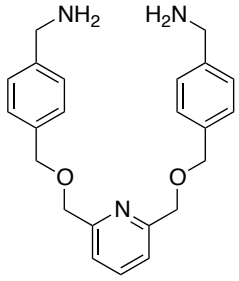

A solution of BH_3•THF complex (1M solution in THF, 57 mL, 57.2 mmol) was added dropwise to a solution of **113** (4.70 g, 12.7 mmol) in dry THF (64 mL) at 0 ˚C under N_2 atmosphere. The reaction mixture was stirred at ambient temperature for 2 h and heated to reflux for 18 h. The reaction was slowly quenched with 1M HCl and extracted once into CH_2Cl_2. The aqueous layers were collected and adjusted to pH 1 using 1M KOH and continue to extract into CH_2Cl_2. The organic layers were dried over $MgSO_4$, filtered and concentrated *in vacuo* to yield the title compound **114** as a yellow oil (3.0 g, 63%). ^{1}H NMR (300.1 MHz, $CDCl_3$) : δ_H 7.71 (1H, t, $^3J_{HH}$ 7.7 Hz; Ar*H*), 7.39 (2H, d, $^3J_{HH}$ 7.8 Hz; 2×Ar*H*), 7.36 (4H, d, $^3J_{HH}$ 8.2 Hz; 4×Ar*H*), 7.30 (4H, d, $^3J_{HH}$ 8.2 Hz; 4×Ar*H*), 4.66 (4H, s; 2×CH_2), 4.63 (4H, s; 2×CH_2), 3.87 (4H, s; 2×CH_2), 1.46 (4H, br s; 2×NH_2); ^{13}C NMR (75.5 MHz, $CDCl_3$) : δ_C 158.1 (Ar*C*), 143.1 (Ar*C*), 137.4 (Ar*C*H), 136.5 (Ar*C*), 128.3 (Ar*C*H), 127.3 (Ar*C*H), 120.1 (Ar*C*H), 73.2 (*C*H_2), 72.9 (*C*H_2), 46.5 (*C*H_2); MS (ES^+) *m/z* 374 (50), 378 ([M+H]$^+$, 100), 400 (47); HRMS (ES^+) *m/z* calculated for $C_{23}H_{27}N_3O_2Na$ [M+Na]$^+$ 400.2001. found 400.2005.

Pyridine Macrocycle (MP)

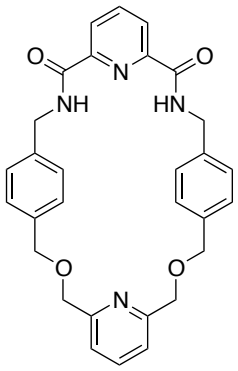

A solution of **114** (1.0 g, 2.65 mmol) in CH_2Cl_2 (50 mL) and a solution of 2,6-pyridinedicarbonyl dichloride (540 mg, 2.65 mmol) in CH_2Cl_2 (50 mL) was added simultaneously to a solution of Et_3N (1.50 mL, 10.6 mmol) in dry CH_2Cl_2 (133 mL) over 1 h and the resulting solution was left stirred for 3 days. The reaction mixture was diluted with CH_2Cl_2 and washed once with 1M HCl followed by sat. solution of $NaHCO_3$. The organic layers were further extracted into CH_2Cl_2. The combined organic layers were dried over $MgSO_4$ and concentrated *in vacuo*. The resulting residue was purified by column chromatography (EtOAc:Hexane, 2:1) to furnish the macrocycle **MP** as colorless solid (0.3 g, 22%). M.p. = 209.2 – 210.5 ˚C; ^{1}H NMR (300.1 MHz, $CDCl_3$) : δ_H 8.40 (2H, d, $^3J_{HH}$ 7.8 Hz; 2×Ar*H*), 8.06 (1H, dd, $^3J_{HH}$ 7.6 and $^3J_{HH}$ 8.0 Hz; Ar*H*), 7.98 (2H, t, $^3J_{HH}$ 5.8 Hz; 2×N*H*), 7.70 (1H, t, $^3J_{HH}$ 7.7 Hz; Ar*H*), 7.34 – 7.31 (6H, m; 6×Ar*H*), 7.28 – 7.26 (4H, m; 4×Ar*H*), 4.70 (4H, d, $^3J_{HH}$ 6.1 Hz; 2×CH_2), 4.62 (4H, s; 2×CH_2), 4.52 (4H, s; 2×CH_2); ^{13}C NMR (75.5 MHz, $CDCl_3$) : δ_C 163.4 (*C*=O), 157.6 (Ar*C*), 148.9 (Ar*C*), 139.3 (Ar*C*H), 137.5 (Ar*C*), 137.4 (Ar*C*), 137.3 (Ar*C*H), 129.1 (Ar*C*H), 127.9 (Ar*C*H), 125.5 (Ar*C*H), 121.2 (Ar*C*H), 72.0 (*C*H_2), 71.8 (*C*H_2), 43.3 (*C*H_2); MS (ES^+) *m/z* 531.11 ([M+Na]$^+$, 100); HRMS (ES^+) *m/z* calculated for $C_{30}H_{28}N_4O_4Na$ [M+Na]$^+$ 531.2008, found 531.2009.

(*Z*)-4-(*tert*-Butyl)-*N*-(4-((4,6-dimethylpyridin-2-yl)carbamoyl)benzylidene)aniline oxide 115

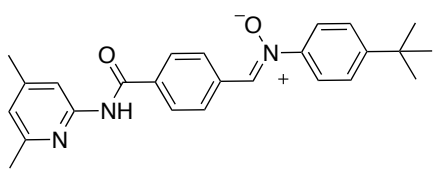

4-*tert*-butylnitrobenzene **118** (0.56 g, 3.12 mmol) was dissolved in THF (15 mL). Rh/C (0.2 g, 30 wt. %) was added and stirred for about 15 min before the addition of hydrazine monohydrate (0.19 mL, 3.74 mmol). The reaction progress was monitored by TLC until the disappearance of the starting material. The solution was then filtered through a pad of Celite and concentrated *in vacuo* to give the intermediate compound. The 4-*tert*-butyl-*N*-hydroxyaniline **119** (3.12 mmol) was carried out to the next step without further

purification. Hydroxylamine **119** was dissolved in EtOH (15 mL), and aldehyde **117** (0.79 g, 3.12 mmol) was added neat. The reaction mixture was left stirred at ambient temperature in the dark for 3 days. The solvent was removed by evaporation under reduced pressure. The crude product was additionally crystallised from EtOH to give a yellow solid (1.06 g, 85% over 2 steps). M.p. = 185.1 – 187.6 °C; ^{1}H NMR (400.1 MHz, $CDCl_3$): δ_H 8.55 (1H, br s; N*H*), 8.51 – 8.48 (2H, m; 2×Ar*H*), 8.05 (1H, s; Ar*H*), 8.04 – 8.01 (2H, m; 2×Ar*H*), 7.99 (1H, s; C*H*), 7.73 – 7.69 (2H, m; 2×Ar*H*), 7.52 – 7.49 (2H, m; 2×Ar*H*), 6.79 (1H, s; Ar*H*), 2.44 (3H, s; CH_3), 2.37 (3H, s; CH_3), 1.36 (9H, s, 3×CH_3); ^{13}C NMR (100.6 MHz, $CDCl_3$): δ_C 164.8 (*C*=O), 156.6 (Ar*C*), 153.9 (Ar*C*), 150.8 (Ar*C*), 150.3 (Ar*C*), 146.7 (Ar*C*), 135.6 (Ar*C*), 134.1 (Ar*C*), 133.1 (*C*H), 129.1 (Ar*C*H), 127.6 (Ar*C*H), 126.3 (Ar*C*H), 121.4 (Ar*C*H), 120.9 (Ar*C*H), 111.8 (Ar*C*H), 35.0 (q*C*), 31.3 (*C*H_3), 23.9 (*C*H_3), 21.4 (*C*H_3); MS (Cl^+) *m/z* 424 ($[M+Na]^+$, 100); HRMS (ES^+) *m/z* calculated for $C_{25}H_{28}N_3O_2$ $[M+H]^+$ 402.2182, found 402.2188.

4-Formylbenzoyl chloride 116[270]

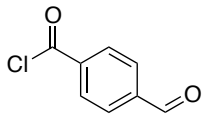

4-formylbenzoic acid **42** (5.0 g, 33.3 mmol) in a mixture of thionyl chloride and toluene (60 mL) was refluxed at 100 °C for 24 h. A clear solution was obtained and reduced in vacuum to yield a quantitative yield of yellow solid of compound **116**, which was used in the next step without further purification. ^{1}H NMR (300.1 MHz, $CDCl_3$): δ_H 10.1 (1H, s; C*H*O), 8.26 (2H, d, $^{3}J_{HH}$ 8.4 Hz; 2×Ar*H*), 8.00 (2H, d, $^{3}J_{HH}$ 8.4 Hz; 2×Ar*H*); ^{13}C NMR (75.5 MHz, $CDCl_3$) : δ_C 191.0 (*C*HO), 167.8 (*C*OCl), 140.5 (Ar*C*), 137.6 (Ar*C*), 131.8 (Ar*C*H), 129.8 (Ar*C*H).

***N*-(4,6-Dimethylpyridin-2-yl)-4-formylbenzamide 117**[207]

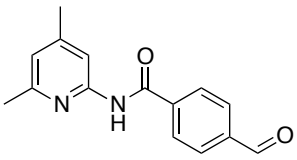

4-formylbenzoyl chloride **116** (5.61 g, 33.3 mmol) in dry CH_2Cl_2 (30 mL) was slowly reacted with a solution of 4,6-dimethylpyridin-2-amine (4.07 g, 33.3 mmol) and Et_3N (5.1 mL, 36.6 mmol) in dry CH_2Cl_2 (50 mL) at 0 °C under Ar atmosphere. The reaction was left stirred for 48 h at ambient temperature before quenched with water (50 mL). The organic layer was washed with 1M HCl (50 mL) and sat. solution of $NaHCO_3$ (50 mL) and extracted into CH_2Cl_2. The combined organic layers were dried over $MgSO_4$,

filtered and concentrated *in vacuo*. The crude was purified by column chromatography (Hexane:EtOAc, 4:1) to afford a colourless solid (6.0 g, 72%). M.p. = 130.8 – 133.2 ˚C; ^{1}H NMR (300.1 MHz, $CDCl_3$): δ_H 10.1 (1H, s; C*H*O), 8.50 (1H, br s; N*H*), 8.09 – 8.06 (2H, m; 2×Ar*H*), 8.03 (1H, s; Ar*H*), 8.02 – 7.99 (2H, m; 2×Ar*H*), 6.81 (1H, s; Ar*H*), 2.43 (3H, s; CH_3), 2.38 (3H, s; CH_3); ^{13}C NMR (100.6 MHz, $CDCl_3$) : δ_C 191.5 (*C*HO), 164.6 (*C*=O), 156.7 (Ar*C*), 150.6 (Ar*C*), 150.5 (Ar*C*), 139.7 (Ar*C*), 138.7 (Ar*C*), 130.1 (Ar*C*H), 128.0 (Ar*C*H), 121.2 (Ar*C*H), 111.9 (Ar*C*H), 23.9 (*C*H_3), 21.5 (*C*H_3); MS (ES^-) *m/z* 253 ([M–H]$^-$, 100); HRMS (ES^-) *m/z* calculated for $C_{15}H_{13}N_2O_2$ [M–H]$^-$ 253.0977, found 253.0982.

3,5-Dimethylbenzoyl chloride 121

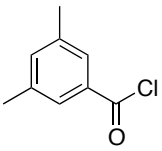

A solution of 3,5-dimethylbenzoic acid **120** (2.0 g, 13.3 mmol) in toluene (50 mL) and thionyl chloride (1.1 mL, 14.6 mmol) was heated to reflux at 80 ˚C for 16 h. The excess thionyl chloride was distilled off by the azeotropic distillation with toluene under reduced pressure, affording **121** as brownish oil quantitatively. The product was used in the next step without further purification. ^{1}H NMR (400.1 MHz, $CDCl_3$) : δ_H 7.70 (2H, s; 2×Ar*H*), 7.29 (1H, s; Ar*H*), 2.38 (6H, s; 2×CH_3); ^{13}C NMR (100.6 MHz, $CDCl_3$) : δ_C 168.5 (*C*=O), 138.8 (Ar*C*), 137.1 (Ar*C*H), 133.1 (Ar*C*), 129.2 (Ar*C*H), 21.1 (*C*H_3).

***N*-(4-(4-Aminophenethyl)phenyl)-3,5-dimethylbenzamide 122**

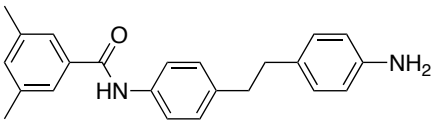

3,5-dimethylbenzoyl chloride **121** (2.24 g, 13.3 mmol) in dry CH_2Cl_2 (20 mL) was added dropwise over 1.5 h to a solution of 4,4'-ethylenedianiline (6.20 g, 29.2 mmol) and Et_3N (3.7 mL, 26.6 mmol) in dry CH_2Cl_2 (50 mL) at ambient temperature under a N_2 atmosphere. The reaction mixture was stirred at ambient temperature for 16 h. The organic phase was washed successively with sat. solution of $NaHCO_3$ and brine, dried over $MgSO_4$ and concentrated by evaporation under reduced pressure. The residue was purified by column chromatography (Hexane:EtOAc, 2:1), affording **122** as a yellow solid (3.0 g, 66%). M.p. = 139.8 – 142.7 ˚C; ^{1}H NMR (300.1 MHz, $CDCl_3$): δ_H 7.72 (1H, s; CON*H*), 7.56 – 7.51 (2H, m; 2×Ar*H*), 7.46 (2H, s; 2×Ar*H*), 7.18 – 7.14 (3H, m; 3×Ar*H*), 6.99 – 6.94 (2H, m;

2×Ar*H*), 6.65 – 6.60 (2H, m; 2×Ar*H*), 3.62 (2H, br s, NH_2), 2.89 – 2.75 (4H, m; 2×CH_2), 2.39 (6H, d, $^4J_{HH}$ 0.6 Hz; 2×CH_3); ^{13}C NMR (100.6 MHz, $CDCl_3$): δ_C 166.1 (CON*H*), 144.4 (Ar*C*), 138.7 (Ar*C*), 138.4 (Ar*C*), 136.0 (Ar*C*), 135.3 (Ar*C*), 133.5 (Ar*C*H), 131.9 (Ar*C*), 129.4 (Ar*C*H), 129.2 (Ar*C*H), 124.7 (Ar*C*H), 120.2 (Ar*C*H), 115.4 (Ar*C*H), 37.9 (*C*H_2), 37.3 (*C*H_2), 21.4 (*C*H_3); MS (ES^+) *m/z* 367 ([M+Na]$^+$, 100); HRMS (ES^+) *m/z* calculated for $C_{23}H_{24}N_2ONa$ [M+Na]$^+$ 367.1786, found 367.1787.

(*Z*)-4-((4-(4-(3,5-Dimethylbenzamido)phenethyl)phenyl)amino)-4-oxobut-2-enoic acid 123

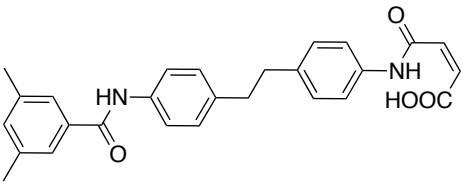

Maleic anhydride (0.14 g, 1.45 mmol) was added to a solution of **122** (0.5 g, 1.45 mmol) in THF (15 mL). The reaction mixture was stirred at ambient temperature under a N_2 atmosphere for 3 h. The yellow precipitate (420 mg, 66%) was filtered and carried out to the next step without further purification. ^{1}H NMR (500.1 MHz, $CDCl_3$ + 3 drops of d_6-DMSO) : δ_H 10.63 (1H, br s; N*H*), 9.12 (1H, br s; N*H*), 7.43 (2H, d, $^3J_{HH}$ 8.3 Hz; 2×Ar*H*), 7.32 (4H, m; 4×Ar*H*), 6.94 (2H, s; 2×Ar*H*), 6.93 (1H, s; Ar*H*), 6.90 (2H, d, $^3J_{HH}$ 8.3 Hz; 2×Ar*H*), 6.42 (1H, d, $^3J_{HH}$ 12.9 Hz; C*H*), 6.11 (1H, d, $^3J_{HH}$ 12.9 Hz; C*H*), 2.68 (4H, s; 2×CH_2), 2.17 (6H, s; 2×CH_3); ^{13}C NMR (125.7 MHz, $CDCl_3$ + 3 drops of d_6-DMSO) : δ_C 166.7 (*C*=O), 166.0 (*C*=O), 164.7 (*C*=O), 138.5 (*C*H), 138.4 (Ar*C*), 137.7 (Ar*C*), 137.5 (Ar*C*), 136.2 (*C*H), 135.1 (Ar*C*), 134.8 (Ar*C*), 134.3 (Ar*C*H), 134.0 (Ar*C*), 128.4 (Ar*C*H), 127.9 (Ar*C*H), 127.5 (Ar*C*H), 121.5 (Ar*C*H), 120.6 (Ar*C*H), 37.4 (*C*H_2), 37.0 (*C*H_2), 21.2 (*C*H_3).

***N*-(4-(4-Aminophenethyl)phenyl)-3,5-bis(trifluoromethyl)benzamide 125**

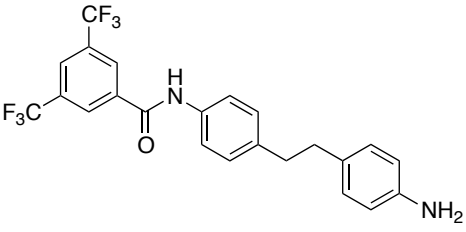

3,5-bis(trifluoromethyl)benzoyl chloride **124** (0.5 g, 1.81 mmol) diluted in CH_2Cl_2 (3.0 mL) was slowly added at –10 ˚C to the resulting mixture of 4,4'-ethylene dianiline (0.58 g, 2.72 mmol) in CH_2Cl_2 (15 mL) and Et_3N (5 mL, 3.62 mmol). The resulting mixture was allowed to warm to ambient temperature and left stirred for 16 h. Following this, the reaction mixture was diluted with CH_2Cl_2, washed once with sat.

solution of $NaHCO_3$,dried over $MgSO_4$ and the solvent was removed *in vacuo*. The residue was purified on silica gel column (Hexane:EtOAc, 7:3) to obtain the product as yellow solid (0.43 g, 52%). M.p. = 146.7 – 148.2 ˚C; ^{1}H NMR (300.1 MHz, $CDCl_3$) : δ_H 8.31 (2H, s; 2×Ar*H*), 8.05 (1H, s; Ar*H*), 7.89 (1H, s; N*H*), 7.52 (2H, d, $^3J_{HH}$ 8.4 Hz; 2×Ar*H*), 7.18 (2H, d, $^3J_{HH}$ 8.5 Hz; 2×Ar*H*), 6.95 (2H, d, $^3J_{HH}$ 8.4 Hz; 2×Ar*H*), 6.62 (2H, d, $^3J_{HH}$ 8.4 Hz; 2×Ar*H*), 3.57 (2H, br s; NH_2), 2.90 – 2.77 (4H, m; 2×CH_2); ^{13}C NMR (100.6 MHz, $CDCl_3$) : δ_C 163.0 (*C*=O), 144.4 (Ar*C*), 139.6 (Ar*C*), 137.2 (Ar*C*), 134.8 (Ar*C*), 132.4 (q, $^2J_{CF}$ 34.1 Hz; Ar*C*), 131.7 (Ar*C*), 129.4 (Ar*C*H), 129.3 (Ar*C*H), 127.5 (m; Ar*C*H), 125.3 (m; Ar*C*H), 123.1 (q, $^1J_{CF}$ 273.1 Hz; CF_3), 121.0 (Ar*C*H), 115.4 (Ar*C*H), 37.8 (*C*H_2), 37.1 (*C*H_2); ^{19}F NMR (376.5 MHz, $CDCl_3$) : δ_F –63.4 (Ar*C*F_3); MS (CI^+) *m/z* 453.14 ([M+H]$^+$, 100); HRMS (CI^+) *m/z* calculated for $C_{23}H_{19}N_2OF_6$ [M+H]$^+$ 453.1402, found 453.1412.

(*Z*)-4-(4-(4-(3,5-Bis(trifluoromethyl)benzamido)phenethyl)phenylamino)-4-oxobut-2-enoic acid 126

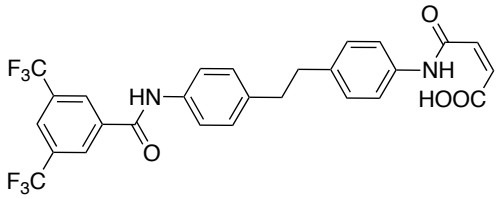

Compound **125** (0.5 g, 1.11 mmol) was dissolved in THF (15 mL). Maleic anhydride (0.11 g, 1.11 mmol) was added neat to the solution. The mixture was left stirred at ambient temperature for 3 h under positive atmosphere of Ar. The precipitate (0.59 g, 98%) was then filtered and carried out to the next step without further purification. M.p. = 207.4 – 209.3 ˚C; ^{1}H NMR (300.1 MHz, $CDCl_3$ + 3 drops of d_6-DMSO) : δ_H 11.7 (1H, s; N*H*), 11.4 (1H, s; N*H*), 9.66 (2H, s; 2×Ar*H*), 9.43 (1H, s; Ar*H*), 8.72 (2H, d, $^3J_{HH}$ 8.6 Hz; 2×Ar*H*), 8.58 (2H, d, $^3J_{HH}$ 8.6 Hz; 2×Ar*H*), 8.29 (2H, d, $^3J_{HH}$ 8.6 Hz; 2×Ar*H*), 8.24 (2H, d, $^3J_{HH}$ 8.6 Hz; 2×Ar*H*), 7.53 (1H, d, $^3J_{HH}$ 12.1 Hz; C*H*), 7.37 (1H, d, $^3J_{HH}$ 12.1 Hz; C*H*), 6.82 (1H, s, O*H*), 3.92 (4H, s; 2×CH_2); ^{13}C NMR (75.5 MHz, $CDCl_3$ + 3 drops of d_6-DMSO) : δ_C 165.5 (*C*=O), 164.1 (*C*=O), 162.9 (*C*=O), 139.2 (Ar*C*), 137.6 (Ar*C*), 137.1 (Ar*C*), 136.1 (Ar*C*), 134.7 (*C*H), 133.0 (*C*H), 132.8 (Ar*C*), 131.5 (q, $^2J_{CF}$ 34.3 Hz, ArC), 129.0 (Ar*C*H), 128.7 (Ar*C*H), 128.4 (m, Ar*C*H), 124.5 (m, Ar*C*H), 121.0 (Ar*C*H), 120.8 (Ar*C*H), 37.2 (*C*H_2), 37.1 (*C*H_2); ^{19}F NMR (376.5 MHz, $CDCl_3$) : δ_F –63.2 (ArC*F*$_3$); MS (ES^-) *m/z* 549 ([M–H]$^-$, 100); HRMS (ES^+) *m/z* calculated for $C_{27}H_{20}N_2O_4F_6Na$ [M+Na]$^+$ 573.1225, found 573.1216.

1-(4-(4-Aminophenethyl)phenyl)-3-(3,5-dimethylphenyl)urea 128

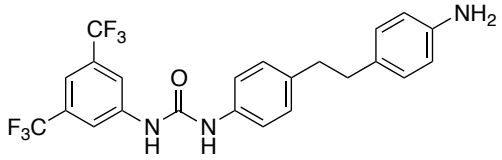

4,4'-ethylene dianiline (1.08 g, 5.1 mmol) was dissolved in dry CH_2Cl_2 (20 mL) followed by the slow addition of 3,5-dimethyl phenylisocyanate **127** (0.5 g, 3.4 mmol) at –5 ˚C and allowed to stir at ambient temperature for 16 h. The solvent was removed under reduced pressure. The residue was then purified by column chromatography (CH_2Cl_2:EtOAc, 8:1). The product **128** was obtained as yellow solid (0.58 g, 63%). M.p. = 165.7 – 168.3 ˚C; ^{1}H NMR (400.1 MHz, d_6-DMSO) : δ_H 9.37 (1H, s; N*H*,), 8.89 (1H, s; N*H*), 8.12 (2H, s; 2×Ar*H*), 7.62 (1H, s; Ar*H*), 7.37 – 7.34 (2H, m; 2×Ar*H*), 7.13 – 7.10 (2H, m; 2×Ar*H*), 6.86 – 6.83 (2H, m; 2×Ar*H*), 6.48 – 6.45 (2H, m; 2×Ar*H*), 4.80 (2H, br s; NH_2), 2.75 – 2.63 (4H, m; 2×CH_2); ^{13}C NMR (100.6 MHz, d_6-DMSO) : δ_C 152.5 (*C*=O), 146.5 (Ar*C*), 142.0 (Ar*C*), 136.7 (Ar*C*), 136.2 (Ar*C*), 130.8 (q, $^2J_{CF}$ 32.3 Hz; Ar*C*), 128.93 (Ar*C*H), 128.91 (Ar*C*H), 128.6 (Ar*C*), 123.4 (q, $^1J_{CF}$ 277.6 Hz; CF_3), 119.1 (Ar*C*H), 118.0 (m, Ar*C*H), 114.5 (m, Ar*C*H), 114.1 (Ar*C*H), 36.6 (*C*H_2), 37.1 (*C*H_2); ^{19}F NMR (376.5 MHz, $CDCl_3$ + 3 drops of d_6-DMSO) : δ_F –63.0 (ArC*F*$_3$); MS (ES$^+$) *m/z* 490 ([M+Na]$^+$, 100); HRMS (ES$^+$) *m/z* calculated for $C_{23}H_{20}N_3OF_6$ [M+H]$^+$ 468.1511, found 468.1505.

(*Z*)-4-(4-(4-(3-(3,5-Bis(trifluoromethyl)phenyl)ureido)phenethyl)phenylamino)-4-oxobut-2-enoic acid 129

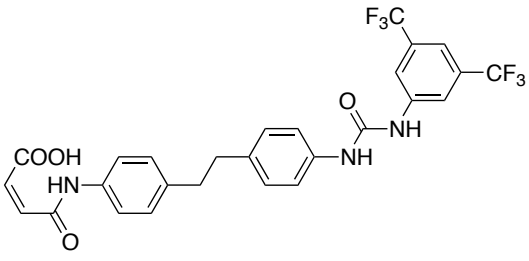

Maleic anhydride (82 mg, 0.84 mmol) was added to solution of **128** (0.3 g, 0.84 mmol) in THF (10 mL). The reaction mixture was stirred at ambient temperature under a Ar atmosphere for 3 h. The precipitate was filtered and the acid compound **129** (460 mg, 98%) was carried out to the next step without further purification. M.p. = 219.2 ˚C (decomposed); ^{1}H NMR (300.1 MHz, $CDCl_3$ + 3 drops of d_6-DMSO) : δ_H 10.7 (1H, s; N*H*), 8.77 (1H, s; N*H*), 7.82 (2H, s; 2×Ar*H*), 7.39 – 7.35 (2H, m; 2×Ar*H*), 7.26 (1H, br s; Ar*H*), 7.19 – 7.15 (2H, m; 2×Ar*H*), 6.99 – 6.95 (2H, m; 2×Ar*H*), 6.92 – 6.88 (2H, m; 2×Ar*H*), 6.47 (1H, d, $^3J_{HH}$

12.9 Hz; C*H*), 6.16 (1H, d, $^{3}J_{HH}$ 12.9 Hz; C*H*), 2.74 – 2.65 (4H, m; 2×CH_2); ^{13}C NMR (75.5 MHz, $CDCl_3$ + 3 drops of d_6-DMSO): δ_C 165.2 (*C*=O), 163.8 (*C*=O), 152.4 (*C*=O), 141.2 (Ar*C*), 138.9 (Ar*C*), 136.3 (Ar*C*), 135.6 (Ar*C*), 134.5 (Ar*C*), 134.3 (*C*H), 132.9 (*C*H), 131.4 (q, $^{2}J_{CF}$ 32.9 Hz, Ar*C*), 128.7 (Ar*C*H), 128.6 (Ar*C*H), 120.5 (Ar*C*H), 118.8 (Ar*C*H), 117.5 (m, Ar*C*H), 114.3 (m, Ar*C*H), 37.0 (*C*H_2), 36.6 (*C*H_2); ^{19}F NMR (376.5 MHz, $CDCl_3$) : δ_F –58.6 (ArC*F*$_3$); MS (ES^-) *m/z* 564 ([M-H]$^-$, 10), 228 (100); HRMS (ES^-) *m/z* calculated for $C_{27}H_{20}N_3O_4F_6$ $[M-H]^-$ 564.1358, found 564.1367.

(*Z*)-4-*tert*-Butyl-*N*-(4-*tert*-butylbenzylidene)aniline oxide 134

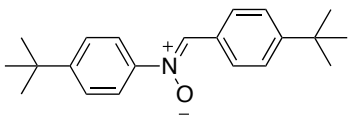

4-*tert*-butylnitrobenzene **118** (0.56 g, 3.12 mmol) was dissolved in THF (15 mL). Rhodium (20 mg, 30 wt.% on carbon, wet) and hydrazine monohydrate (0.19 mL, 3.75 mmol) and the reaction was followed by TLC (Hex:EtOAc, 3:1). After completion, the solution was filtered through Celite and concentrated *in vacuo* to obtain the desired intermediate product **119** as a dark brown liquid, which was directly used in the next step without further purification. The obtained hydroxylamine **119** (3.12 mmol) was dissolved in EtOH (15 mL) and 4-*tert*-butylbenzaldehyde (0.51 mL, 3.12 mmol) was added dropwise to the solution. The reaction mixture was left stirred in the dark for 16 h at ambient temperature. The solvent was concentrated by evaporation under reduced pressure and the resulting residue was purified by column chromatography (Cyclohexane:EtOAc:Et_3N, gradient from 99.5:0:0.5 to 94.5:5.0:0.5) to give **134** as yellow solid (0.42 g, 44% over 2 steps). M.p. = 152.5 – 154.4 ˚C; ^{1}H NMR (300.1 MHz, $CDCl_3$) : δ_H 8.35 – 8.30 (2H, m; 2×Ar*H*), 7.88 (1H, s; C*H*), 7.72 – 7.67 (2H, m; 2×Ar*H*), 7.52 – 7.46 (4H, m; 4×Ar*H*), 1.35 (18H, s; 6×CH_3); ^{13}C NMR (75.5 MHz, $CDCl_3$) : δ_C 154.5 (Ar*C*), 153.3 (Ar*C*), 146.8 (Ar*C*), 134.2 (*C*H), 129.1 (Ar*C*H), 128.3 (Ar*C*), 126.1 (Ar*C*H), 125.7 (Ar*C*H), 121.4 (Ar*C*H), 35.2 (q*C*), 35.0 (q*C*), 31.4 (*C*H_3), 31.3 (*C*H_3); MS (ES^+) *m/z* 332.0 ($[M+Na]^+$, 95), 641.0 (100); HRMS (ES^+) *m/z* calculated for $C_{21}H_{27}NONa$ 332.1990 $[M+Na]^+$, found 332.1994.

***N*-(4-((3*S*,3a*R*,6a*S*)-2,3-Bis(4-*tert*-butylphenyl)-4,6-dioxodihydro-2*H*-pyrrolo[3,4-*d*]isoxazol-5(3*H*,6*H*,6a*H*)-yl)phenyl)-3,5-dimethylbenzamide**

***trans* Thread 135**

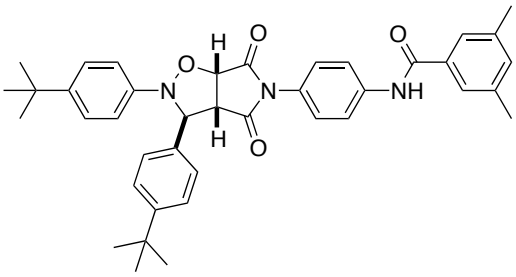

Maleimide **108** (50.0 mg, 0.16 mmol) was dissolved in $CHCl_3$ (8 mL) followed by the addition of nitrone **134** (48.3 mg, 0.16 mmol). The reaction mixture was stirred at ambient temperature under Ar atmosphere in the dark for 6 days. The solvent was removed by evaporation under reduced pressure. The residue was purified by column chromatography (Cyclohexane:EtOAc; 9:1), to enable the isolation of the *trans* **135** as yellow solid (53 mg, 56%). Representative data for *trans* thread **135** : M.p. = 148.7 – 149.3 ˚C; ^{1}H NMR (300.1 MHz, $CDCl_3$) : δ_H 7.82 (1H, s; N*H*), 7.39 – 7.32 (4H, m; 4×Ar*H*), 7.29 – 7.26 (4H, m; 4×Ar*H*), 7.09 – 7.04 (2H, m; 2×Ar*H*), 6.98 (1H, s; Ar*H*), 6.92 – 6.87 (2H, m; 2×Ar*H*), 6.24 (2H, d, $^3J_{HH}$ 8.8 Hz; 2×Ar*H*), 5.58 (1H, s, C*H*), 4.86 (1H, d, $^3J_{HH}$ 7.7 Hz, C*H*), 3.82 (1H, dd, $^4J_{HH}$ 0.8 and $^3J_{HH}$ 7.5 Hz, C*H*), 2.17 (6H, s; 2×CH_3), 1.17 (9H, s; 3×CH_3), 1.10 (9H, s; 3×CH_3); ^{13}C NMR (75.5 MHz, $CDCl_3$) : δ_C 174.5 (*C*=O), 173.1 (*C*=O), 166.2 (*C*=O), 151.3 (Ar*C*), 146.8 (Ar*C*), 146.0 (Ar*C*), 138.8 (Ar*C*), 138.6 (Ar*C*), 136.0 (Ar*C*), 134.7 (Ar*C*), 133.8 (Ar*C*H), 127.0 (Ar*C*H), 126.6 (Ar*C*), 126.3 (Ar*C*H), 126.2 (Ar*C*H), 126.0 (Ar*C*H), 125.0 (Ar*C*H), 120.3 (Ar*C*H), 114.0 (Ar*C*H), 77.1 (*C*H), 69.5 (*C*H), 57.4 (*C*H), 34.7 (q*C*), 34.3 (q*C*), 31.6 (*C*H_3), 31.4 (*C*H_3), 21.2 (*C*H_3, C_1); MS (ES^+) *m/z* 652.1 ([M+Na]$^+$, 100); HRMS (ES^+) *m/z* calculated for $C_{40}H_{43}N_3O_4Na$ [M+Na]$^+$ 652.3151, found 652.3135.

***trans* Rotaxane 136**

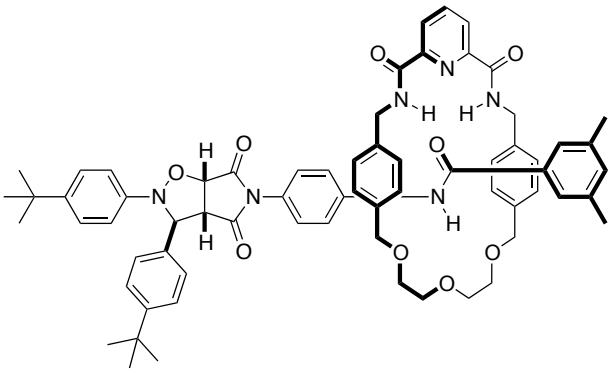

A mixture of macrocycle **MDG** (30 mg, 0.06 mmol) and maleimide **108** (20 mg, 0.06 mmol) in $CHCl_3$ (3 mL) were stirred at ambient temperature for 2 h. Nitrone **134** (20 mg, 0.06 mmol) was then added to the resulting solution. This reaction mixture was stirred under Ar atmosphere at ambient temperature in the dark for 5 days. The solvent was removed by evaporation *in vacuo*. The residue was purified by column chromatrography (Cyclohexane:EtOAc, gradient from 95:5 to 80:20) to yield the *trans* rotaxane **136** as yellow solid (20 mg, 29%). Representative data for *trans* rotaxane **136**: M.p. = 136.0 – 139.8 ˚C; ^{1}H NMR (400.1 MHz, $CDCl_3$) : δ_H 9.19 (2H, br s; 2×N*H*), 8.50 (2H, d, $^3J_{HH}$ 7.9 Hz; 2×Ar*H*), 8.12 (1H, t, $^3J_{HH}$ 7.7 Hz; Ar*H*), 7.69 (1H, s; N*H*), 7.54 (2H, d, $^3J_{HH}$ 8.3 Hz; 2×Ar*H*), 7.47 (2H, d, $^3J_{HH}$ 8.6 Hz; 2×Ar*H*), 7.40 (2H, d, $^3J_{HH}$ 8.8 Hz; 2×Ar*H*), 7.32 (2H, d, $^3J_{HH}$ 8.9 Hz; 2×Ar*H*), 7.16 (2H, d, $^3J_{HH}$ 8.9 Hz; 2×Ar*H*), 7.03 (2H, s; 2×Ar*H*), 6.99 (1H, s; Ar*H*), 6.64 – 6.61 (4H, m; 4×Ar*H*), 6.54 – 6.51 (4H, m; 4×Ar*H*), 6.35 (2H, d, $^3J_{HH}$ 8.9 Hz; 2×Ar*H*), 5.78 (1H, s; C*H*), 5.13 (1H, d, $^3J_{HH}$ 7.5 Hz; C*H*), 4.77 – 4.70 (2H, m; CH_2), 4.31 – 4.24 (2H, m; CH_2), 4.10 – 4.09 (4H, m; 2×CH_2), 4.07 – 4.05 (1H, m; C*H*), 3.72 – 3.69 (4H, m; 2×CH_2), 3.50 – 3.48 (4H, m; 2×CH_2), 2.13 (6H, s; 2×CH_3), 1.35 (9H, s; 3×CH_3), 1.31 (9H, s; 3×CH_3); ^{13}C NMR (100.6 MHz, $CDCl_3$): δ_C 174.5 (*C*=O), 173.0 (*C*=O), 165.4 (*C*=O), 164.1 (*C*=O), 151.3 (Ar*C*), 149.6 (Ar*C*), 146.9 (Ar*C*), 145.8 (Ar*C*), 139.5 (Ar*C*), 138.7 (Ar*C*H), 136.9 (Ar*C*), 136.8 (Ar*C*), 136.1 (Ar*C*), 135.4 (Ar*C*), 133.5 (Ar*C*), 132.9 (Ar*C*H), 128.8 (Ar*C*H), 127.8 (Ar*C*H), 126.4 (Ar*C*H), 126.2 (Ar*C*H), 126.1 (Ar*C*), 126.1 (Ar*C*H), 126.0 (Ar*C*H), 125.8 (Ar*C*), 125.5 (Ar*C*H), 124.7 (Ar*C*H), 119.8 (Ar*C*H), 114.3 (Ar*C*H), 77.6 (*C*H), 73.7 (*C*H_2), 71.1 (*C*H_2), 69.7 (*C*H), 69.1 (*C*H_2), 57.5 (*C*H), 43.7 (*C*H_2), 34.7 (q*C*), 34.4 (q*C*), 31.7 (*C*H_3), 31.5 (*C*H_3), 21.2 (*C*H_3); MS (MALDI) *m/z* 1106 ($[M+H]^+$, 100); HRMS (MALDI) *m/z* calculated for $C_{67}H_{72}N_6O_9Na$ $[M+Na]^+$ 1127.5258, found 1127.5209.

***trans* Rotaxane 137**

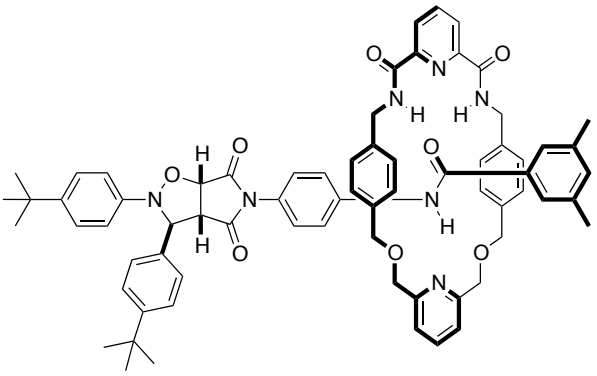

A mixture of macrocycle **MP** (30 mg, 0.06 mmol) and maleimide **108** (19 mg, 0.06 mmol) in $CHCl_3$ (3 mL) were stirred at ambient temperature for 2 h. Nitrone **134** (18.3 mg, 0.06 mmol) was then added to the resulting solution. This reaction mixture was stirred under Ar atmosphere at ambient temperature in the dark for 5 days. The solvent was removed by evaporation *in vacuo*. The residue was purified by column chromatrography (Cyclohexane:EtOAc, gradient from 95:5 to 80:20) to yield the *trans* rotaxane **137** as yellow solid (20 mg, 30%). Representative data for *trans* rotaxane **137** : M.p. = 145.8 – 148.3 ˚C; ^{1}H NMR (300.1 MHz, $CDCl_3$) δ_H = 9.43 – 9.37 (2H, m; 2×N*H*), 9.03 (1H, s; N*H*), 8.51 (2H, d, $^3J_{HH}$ 7.8 Hz; 2×Ar*H*), 8.12 (1H, t, $^3J_{HH}$ 7.8 Hz; Ar*H*), 7.79 (1H, t, $^3J_{HH}$ 7.7 Hz; Ar*H*), 7.55 – 7.51 (2H, m; 2×Ar*H*), 7.49 – 7.44 (4H, m; 4×Ar*H*), 7.37 – 7.34 (2H, m; 2×Ar*H*), 7.27 – 7.24 (3H, m; 3×Ar*H*), 7.15 – 7.10 (2H, m; 2×Ar*H*), 6.96 (2H, s; 2×Ar*H*), 6.87 (1H, s; Ar*H*), 6.74 – 6.62 (7H, m; 7×Ar*H*), 6.22 – 6.19 (2H, m; 2×Ar*H*), 5.78 (1H, s; Ar*H*), 5.11 (1H, d, $^3J_{HH}$ 7.9 Hz; Ar*H*), 4.65 – 4.58 (2H, m; 2×Ar*H*), 4.43 (2H, d, $^3J_{HH}$ 4.9 Hz; CH_2), 4.42 – 4.21 (8H, m; 4×CH_2), 4.04 (1H, dd, $^4J_{HH}$ 0.9 and $^3J_{HH}$ 7.5 Hz; C*H*), 1.85 (6H, s; 2×CH_3), 1.35 (9H, s; 3×CH_3), 1.12 (9H, s; 3×CH_3); ^{13}C NMR (100.6 MHz, $CDCl_3$): δ_C 174.6 (*C*=O), 173.1 (*C*=O), 166.2 (*C*=O), 164.3 (*C*=O), 164.3 (C=O), 157.3 (Ar*C*), 157.2 (Ar*C*), 151.3 (Ar*C*), 149.6 (Ar*C*), 149.5 (Ar*C*), 146.9 (Ar*C*), 145.7 (Ar*C*), 139.7 (Ar*C*), 138.7 (Ar*C*H), 137.8 (Ar*C*H), 137.4 (Ar*C*), 137.3 (Ar*C*), 136.7 (Ar*C*), 136.1 (Ar*C*), 135.2 (Ar*C*), 135.1 (Ar*C*), 133.4 (Ar*C*), 132.7 (Ar*C*H), 129.1 (Ar*C*H), 129.1 (Ar*C*H), 127.8 (Ar*C*H), 126.3 (Ar*C*H), 126.2 (Ar*C*H), 126.1 (Ar*C*H), 126.0 (Ar*C*H), 125.9 (Ar*C*H), 125.9 (Ar*C*), 125.5 (Ar*C*H), 121.6 (Ar*C*H), 121.5 (Ar*C*H), 120.1 (Ar*C*H), 114.0 (Ar*C*H), 77.7 (*C*H), 73.3 (*C*H_2), 73.3 (*C*H_2), 71.4 (*C*H_2), 71.3 (*C*H_2), 69.6 (*C*H), 57.4 (*C*H), 43.6 (*C*H), 34.8 (q*C*), 34.2 (q*C*), 31.5 (*C*H_3), 31.4 (*C*H_3), 29.8 (q*C*), 20.7 (*C*H_3); MS (MALDI) *m/z* 1138.5 ([M+H]$^+$, 100); HRMS (MALDI) *m/z* calculated for $C_{70}H_{71}N_7O_8Na$ [M+H]$^+$ 1138.5442, found 1138.5371.

***trans* Thread 138**

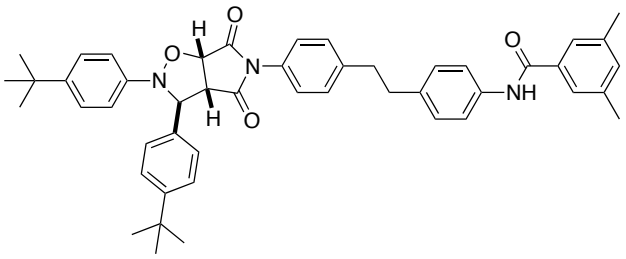

Maleimide **109** (30 mg, 0.07 mmol) was dissolved in $CHCl_3$ (3 mL) followed by the addition of nitrone **134** (22 mg, 0.07 mmol). The reaction mixture was stirred at ambient temperature under Ar atmosphere in the dark for 6 days. The solvent was removed by evaporation under reduced pressure. The residue was purified by column chromatography (Cyclohexane:EtOAc, gradient from 95:5 to 75:25), which enabled the isolation of the major *trans* compound **138** as yellow solid (16 mg, 31%). Representative data for *trans* thread **138**: M.p. = 174.8 – 177.6 ˚C; ^{1}H NMR (300.1 MHz, $CDCl_3$) : δ_H 7.78 (1H, s; N*H*), 7.59 – 7.43 (8H, m; 8×Ar*H*), 7.30 – 7.25 (2H, m; 2×Ar*H*), 7.18 (1H, s; Ar*H*), 7.17 – 7.13 (2H, m; 2×Ar*H*), 7.14 – 7.07 (4H, m; 4×Ar*H*), 6.43 – 6.39 (2H, m; 2×Ar*H*), 5.79 (1H, s; Ar*H*), 5.08 (1H, d, $^3J_{HH}$ 7.8 Hz; Ar*H*), 4.03 (1H, dd, $^4J_{HH}$ 0.9 and $^3J_{HH}$ 7.5 Hz; Ar*H*), 2.92 – 2.81 (4H, m; 2×CH_2), 2.39 (6H, s; 2×CH_3), 1.35 (9H, s; 3×CH_3), 1.29 (9H, s; 3×CH_3); ^{13}C NMR (75.5 MHz, $CDCl_3$): δ_C 174.6 (*C*=O), 173.9 (*C*=O), 166.2 (*C*=O), 151.3 (Ar*C*), 146.9 (Ar*C*), 145.9 (Ar*C*), 142.9 (Ar*C*), 138.6 (Ar*C*), 137.6 (Ar*C*), 136.2 (Ar*C*), 136.1 (Ar*C*), 135.2 (Ar*C*), 133.5 (Ar*C*H), 129.1 (Ar*C*H), 129.1 (Ar*C*H), 128.9 (Ar*C*H), 128.9 (Ar*C*) 126.5 (Ar*C*H), 126.2 (Ar*C*H), 126.0 (Ar*C*H), 124.8 (Ar*C*H), 120.4 (Ar*C*H), 113.1 (Ar*C*H), 77.5 (*C*H), 69.6 (*C*H), 57.5 (*C*H), 37.6 (*C*H_2), 37.1 (*C*H_2), 34.7 (q*C*), 34.3 (q*C*), 31.6 (*C*H_3), 31.5 (*C*H_3), 21.4 (*C*H_3); MS (ES$^+$) *m/z* 756.2 ([M+Na]$^+$, 100); HRMS (ES$^+$) *m/z* calculated for $C_{48}H_{51}N_3O_4Na$ [M+Na]$^+$ 756.3777, found 756.3782.

***trans* Rotaxane 139**

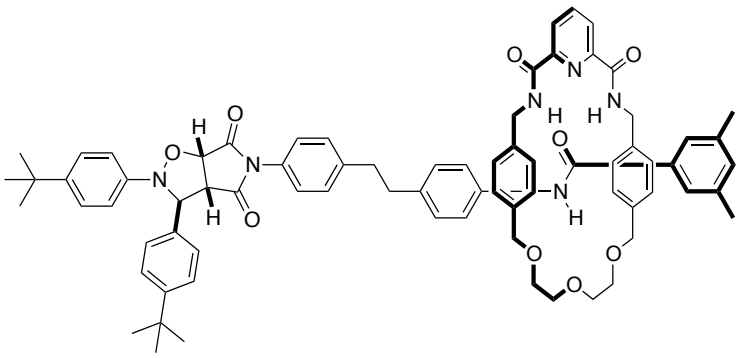

A mixture of macrocycle **MDG** (30 mg, 0.06 mmol) and maleimide **109** (27 mg, 0.06 mmol) in $CHCl_3$ (3 mL) were stirred at ambient temperature for 2 h. Nitrone **134** (20 mg, 0.06 mmol) was then added to the resulting solution. This reaction mixture was stirred under Ar atmosphere at ambient temperature in the dark for 5 days. The solvent was removed by evaporation under reduced pressure. The residue was purified by column chromatrography (Cyclohexane:EtOAc, gradient from 95:5 to 80:20) to yield the *trans* rotaxane **139** as pale yellow solid (20 mg, 26%). M.p. = 136.2 – 139.9 ˚C, ^{1}H NMR (300.1 MHz, $CDCl_3$) : δ_H 9.36 (2H, t, $^3J_{HH}$ 5.7 Hz; 2×Ar*H*), 8.49 (2H, d, $^3J_{HH}$ 7.9 Hz; 2×Ar*H*), 8.12 (1H, t, $^3J_{HH}$ 7.9 Hz; Ar*H*), 7.61 (1H, s; Ar*H*), 7.54 – 7.50 (2H, m; 2×Ar*H*), 7.47 – 7.43 (2H, m; 2×Ar*H*), 7.30 (2H, d, $^3J_{HH}$ 8.5 Hz; 2×Ar*H*), 7.26 (2H, d, $^3J_{HH}$ 8.9 Hz; 2×Ar*H*), 7.13 – 7.07 (4H, m; 4×Ar*H*), 7.05 (2H, s; 2×Ar*H*), 6.99 (1H, s; Ar*H*), 6.85 (2H, d, $^3J_{HH}$ 8.5 Hz; 2×Ar*H*), 6.66 (4H, d, $^3J_{HH}$ 7.8 Hz; 4×Ar*H*), 6.55 (4H, d, $^3J_{HH}$ 7.9 Hz; 4×Ar*H*), 6.45 (2H, d, $^3J_{HH}$ 8.27 Hz; 2×Ar*H*), 5.78 (1H, s; C*H*), 5.10 (1H, d, $^3J_{HH}$ 7.6 Hz; C*H*), 4.58 (2H, dd, $^3J_{HH}$ 5.90 and $^2J_{HH}$ 14.7 Hz; CH_2), 4.48 (2H, dd, $^3J_{HH}$ 5.30 and $^2J_{HH}$ 14.7 Hz; CH_2'), 4.13 (4H, ABq, J_{AB} 14.7 Hz; 2×CH_2), 4.04 (1H, d, $^3J_{HH}$ 7.44 Hz; C*H*), 3.75 – 3.66 (4H, m; 2×CH_2), 3.50 – 3.39 (4H, m; 2×CH_2), 2.91 – 2.78 (4H, m; 2×CH_2), 2.17 (6H, s; 2×CH_3), 1.34 (9H, s; 3×CH_3), 1.30 (9H, s; 3×CH_3); ^{13}C NMR (100.6 MHz, $CDCl_3$): δ_C 175.4 (*C*=O),173.0 (*C*=O), 165.8 (*C*=O), 164.1 (*C*=O), 156.8 (Ar*C*), 150.4 (Ar*C*), 149.5 (Ar*C*), 146.9 (Ar*C*), 145.9 (Ar*C*), 142.9 (Ar*C*), 138.7 (Ar*C*H), 137.8 (Ar*C*H), 137.7 (Ar*C*), 137.1 (Ar*C*), 136.6 (Ar*C*), 136.1 (Ar*C*), 135.5 (Ar*C*), 134.0 (Ar*C*), 132.4 (Ar*C*H), 130.3 (Ar*C*H), 129.2 (Ar*C*H), 128.9 (Ar*C*H), 128.0 (Ar*C*H), 127.9 (Ar*C*H), 126.4 (Ar*C*H), 126.3 (Ar*C*H), 126.2 (Ar*C*H), 126.0 (Ar*C*H), 125.4 (Ar*C*H), 122.4 (Ar*C*H), 119.7 (Ar*C*H), 114.0 (Ar*C*H), 77.7 (*C*H), 73.6 (*C*H_2), 71.1 (*C*H_2), 69.7 (*C*H), 68.8 (*C*H), 43.7 (*C*H_2), 37.7 (*C*H_2), 37.6 (*C*H_2), 34.7 (q*C*), 34.3 (q*C*), 31.6 (*C*H_3), 31.5 (*C*H_3), 21.2 (*C*H_3); MS (MALDI) *m/z* 1210 ([M+H]$^+$, 100); HRMS (MALDI) *m/z* calculated for $C_{75}H_{80}N_6O_9Na$ [M+Na]$^+$ 1231.5884, found 1231.5194.

***trans* Rotaxane 140**

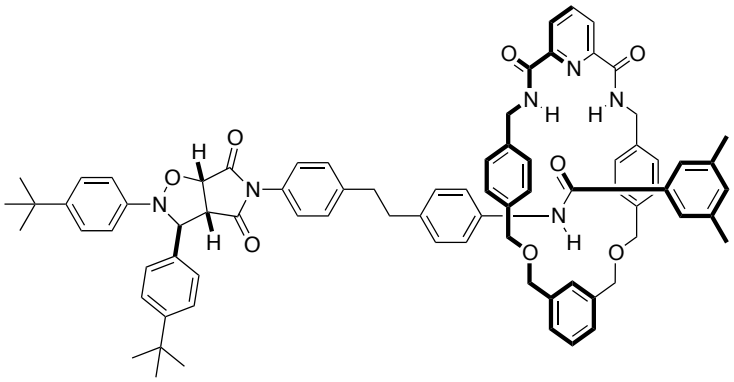

A mixture of macrocycle **MP** (30 mg, 0.06 mmol) and maleimide **109** (25 mg, 0.06 mmol) in $CHCl_3$ (3 mL) were stirred at ambient temperature for 2 h. Nitrone **134** (18.3 mg, 0.06 mmol) was then added to the resulting solution. The reaction mixture was stirred under Ar atmosphere at ambient temperature in the dark for 5 days. The solvent was removed by evaporation under reduced pressure. The residue was purified by column chromatrography (Cyclohexane:EtOAc, gradient from 95:5 to 80:20) to yield the *trans* rotaxane **140** as pale yellow solid (15 mg, 20%). M.p. = 172.4 – 178.5 ˚C, ^{1}H NMR (400.1 MHz, $CDCl_3$) : δ_H 9.56 (2H, t, $^3J_{HH}$ 5.7 Hz; 2×N*H*), 8.99 (1H, s; N*H*), 8.49 (2H, d, $^3J_{HH}$ 7.8 Hz; 2×Ar*H*), 8.12 (1H, t, $^3J_{HH}$ 7.8 Hz; Ar*H*), 7.78 (1H, t, $^3J_{HH}$ 7.7 Hz; Ar*H*), 7.53 (2H, d, $^3J_{HH}$ 8.4 Hz; 2×Ar*H*), 7.45 (2H, d, $^3J_{HH}$ 8.4 Hz; 2×Ar*H*), 7.36 (2H, d, $^3J_{HH}$ 7.7 Hz; 2×Ar*H*), 7.29 (2H, d, $^3J_{HH}$ 8.5 Hz; 2×Ar*H*), 7.25 (2H, d, $^3J_{HH}$ 8.7 Hz; 2×Ar*H*), 7.11 – 7.07 (4H, m; 4×Ar*H*), 6.91 (2H, s; 2×Ar*H*), 6.86 (1H, s; Ar*H*), 6.76 – 6.69 (10H, m; 10×Ar*H*), 6.44 (2H, d, $^3J_{HH}$ 8.3 Hz; 2×Ar*H*), 5.78 (1H, s; C*H*), 5.10 (1H, d, $^3J_{HH}$ 7.6 Hz; C*H*), 4.64 (2H, dd, $^3J_{HH}$ 6.0 and $^2J_{HH}$ 14.8 Hz; CH_2), 4.48 (2H, dd, $^3J_{HH}$ 5.1 and $^2J_{HH}$ 20.0 Hz; CH_2), 4.38 (4H, s; 2×CH_2), 4.23 (2H, dd, $^4J_{HH}$ 1.4 and $^2J_{HH}$ 11.3 Hz; CH_2), 4.15 (2H, dd, $^4J_{HH}$ 3.1 and $^2J_{HH}$ 14.4 Hz; CH_2'), 4.04 (1H, d, $^3J_{HH}$ 7.5 Hz; C*H*), 2.91 – 2.66 (4H, m; 2×CH_2), 1.89 (6H, s; 2×CH_3), 1.34 (9H, s; 3×CH_3), 1.29 (9H, s; 3×CH_3); ^{13}C NMR (100.6 MHz, $CDCl_3$): δ_C 174.5 (*C*=O), 173.2 (*C*=O), 166.2 (*C*=O), 164.3 (*C*=O), 157.3 (Ar*C*), 151.3 (Ar*C*), 149.5 (Ar*C*), 146.9 (Ar*C*), 145.9 (Ar*C*), 142.9 (Ar*C*), 138.7 (Ar*C*H), 137.8 (Ar*C*H), 137.7 (Ar*C*), 137.1 (Ar*C*), 136.6 (Ar*C*), 136.2 (Ar*C*), 136.1 (Ar*C*), 135.3 (Ar*C*), 134.0 (Ar*C*), 132.4 (Ar*C*H), 129.1 (Ar*C*H), 129.0 (Ar*C*H), 128.9 (Ar*C*), 128.0 (Ar*C*H), 127.9 (Ar*C*H), 126.4 (Ar*C*H), 126.3 (Ar*C*H), 126.2 (Ar*C*H), 126.0 (Ar*C*H), 125.9 (Ar*C*H), 125.3 (Ar*C*H), 122.0 (Ar*C*H), 120.1 (Ar*C*H), 114.0 (Ar*C*H), 77.7 (*C*H), 73.2 (*C*H_2), 71.2 (*C*H_2), 69.7 (*C*H), 57.4 (*C*H), 43.5 (*C*H_2), 37.6 (*C*H_2), 37.1 (*C*H_2), 34.7 (q*C*), 34.3 (q*C*), 31.6 (*C*H_3), 31.5 (*C*H_3), 20.7 (*C*H_3); MS (MALDI) *m/z* 1243 ([M+H]$^+$, 100); HRMS (MALDI) *m/z* calculated for $C_{78}H_{79}N_7O_8Na$

[M+Na]$^+$ 1264.5888, found 1264.5853.

(*Z*)-4-*tert*-Butyl-*N*-(3,5-difluorobenzylidene)aniline oxide 141

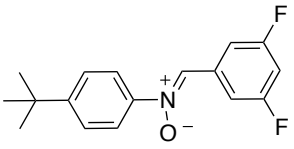

4-*tert*-butylnitrobenzene **118** (0.56 g, 3.12 mmol) was dissolved in THF (15 mL). Rh/C (0.2 g, 30 wt. %) was then added and continued to stir for another 15 min before the following addition of the hydrazine monohydrate (0.19 mL, 3.75 mmol). The reaction progress was monitored by TLC (Hexane:EtOAc; 3:1)and the solution was filtered through a pad of Celite. The solvent was removed to give the intermediate product and used for the next step without further purification. The hydroxylamine **119** (3.12 mmol) was dissolved in EtOH (15 mL) and 3,5-difluorobenzaldehyde (0.44 g, 3.12 mmol) was added. The reaction mixture was stirred for another 16 h at ambient temperature in the dark. The solvent was concentrated by evaporation under reduced pressure. The residue was purified by column chromatography (Cyclohexane:EtOAc:Et_3N; gradient from 99.5:0:0.5 to 94.5:5.0:0.5) to give **141** as yellow solid (0.23 g, 26% over 2 steps). M.p. = 68.8 – 70.5 ˚C; ^{1}H NMR (400.1 MHz, $CDCl_3$) : δ_H 7.99 – 7.93 (2H, m; 2×Ar*H*), 7.89 (1H, s; C*H*), 7.69 – 7.65 (2H, m; 2×Ar*H*), 7.51 – 7.47 (2H, m; 2×Ar*H*), 6.90 (1H, tt, $^4J_{HH}$ 2.4 and $^3J_{HF}$ 8.6 Hz, Ar*H*), 1.35 (9H, s, 3×CH_3); ^{13}C NMR (100.6 MHz, $CDCl_3$) : δ_C 163.0 (dd, $^1J_{CF}$ 247.7 and $^3J_{CF}$ 12.7 Hz; Ar*C*-F), 154.2 (Ar*C*), 146.1 (Ar*C*), 133.3 (t, $^3J_{CF}$ 10.7 Hz; Ar*C*), 132.2 (m; *C*H), 126.3 (Ar*C*H), 121.4 (Ar*C*H), 111.4 (dd, $^3J_{CF}$ 7.7 and $^2J_{CF}$ 18.3 Hz, Ar*C*H), 106.2 (t, $^2J_{CF}$ 25.7 Hz; Ar*C*H), 35.1 (q*C*), 31.4 (3×CH_3); ^{19}F NMR (376.5 MHz, $CDCl_3$) : δ_F –109.5 (Ar*F*); MS (ES$^+$) *m/z* 312.0 ([M+Na]$^+$, 100), 601.1 (12); HRMS (ES$^+$) *m/z* calculated for $C_{17}H_{17}NOF_2Na$ [M+Na]$^+$ 312.1176, found 312.1178.

(*Z*)-*N*-(3,5-Bis(trifluoromethyl)benzylidene)-4-*tert*-butylaniline oxide 142

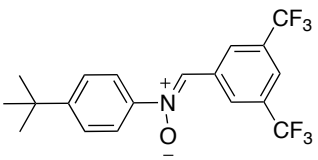

4-*tert*-butylnitrobenzene **118** (0.56 g, 3.12 mmol) was dissolved in THF (15 mL). Rh/C (0.2 g, 30 wt. %) was then added and continued to stir for another 15 min before the following addition of the hydrazine monohydrate (0.19 mL, 3.75 mmol). The reaction progress was monitored by TLC (Hexane:EtOAc; 3:1) and the solution was filtered through a pad of Celite. The solvent was then removed to

give the intermediate product. The hydroxylamine **119** (3.12 mmol) was dissolved in EtOH (15 mL) and 3,5-bis(trifluoromethyl)benzaldehyde (0.52 mL, 3.12 mmol) was added. The reaction mixture was stirred for another 16 h at ambient temperature in the dark. The solvent was concentrated *in vacuo* and the residue was purified by column chromatography (Cyclohexane:EtOAc:Et_3N gradient from 99.5:0:0.5 to 94.5:5.0:0.5) to give **142** as yellow solid (0.59 g, 49% over 2 steps). M.p = 123.8 – 126.4 ˚C; ^{1}H NMR (300.1 MHz, $CDCl_3$): δ_H 8.89 (2H, s; 2×Ar*H*), 8.08 (1H, s; Ar*H*), 7.92 (1H, s; C*H*), 7.72 – 7.69 (2H, m; 2×Ar*H*), 7.53 – 7.51 (2H, m; 2×Ar*H*), 1.37 (9H, s; 3×CH_3); ^{13}C NMR (75.5 MHz, $CDCl_3$): δ_C 154.5 (Ar*C*), 146.3 (Ar*C*), 132.6 (Ar*C*), 132.2 (q, $^2J_{CF}$ 33.4 Hz; Ar*C*), 131.2 (*C*H), 128.3 (m; Ar*C*H), 126.5 (Ar*C*H), 123.6 (m, Ar*C*H), 123.4 (q, $^1J_{CF}$ 275.0 Hz, CF_3), 121.3 (Ar*C*H), 35.1 (q*C*), 31.3 (3×*C*H_3); ^{19}F NMR (376.5 MHz, $CDCl_3$) : δ_F –63.5 (ArC*F*$_3$); MS (ES^+) *m/z* 412.0 ([M+Na]$^+$, 100); HRMS (ES^+) *m/z* calculated for $C_{19}H_{17}NOF_6Na$ [M+Na]$^+$ 412.1112, found 412.1108.

_N_-(4-((3_S_,3a_R_,6a_S_)-3-(3,5-Bis(trifluoromethyl)phenyl)-2-(4-*tert*-butylphenyl)-4,6-dioxodihydro-2_H_-pyrrolo[3,4-*d*]isoxazol-5(3_H_,6_H_,6a_H_)-yl)phenyl)-3,5-dimethylbenzamide *trans* Thread 143

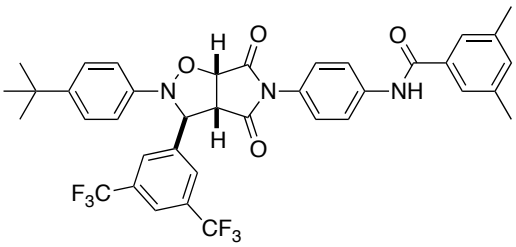

Maleimide **108** (50 mg, 0.16 mmol) was dissolved in $CHCl_3$ (12 mL) followed by the addition of CF_3 nitrone **142** (60.7 mg, 0.16 mmol). The reaction mixture was stirred at ambient temperature under Ar atmosphere in the dark for 6 days. The solvent was removed by evaporation *in vacuo*. The residue was purified by column chromatography (Hexane:EtOAc; 9:1), which enabled the isolation of the *trans* thread **143** as pale yellow solid in (72 mg, 65%). Representative data for *trans* thread **143** : M.p. = 192.7 – 195.3 ˚C; ^{1}H NMR (400.1 MHz, $CDCl_3$): δ_H 8.08 (2H, s; 2×Ar*H*), 7.89 (1H, s; N*H*), 7.89 (1H, s; Ar*H*), 7.59 – 7.55 (2H, m; 2×Ar*H*), 7.43 (2H, s; 2×Ar*H*), 7.32 – 7.29 (2H, m, 2×Ar*H*), 7.17 (1H, s, Ar*H*), 7.12 – 7.08 (2H, m; 2×Ar*H*), 6.46 – 6.43 (2H, m; 2×Ar*H*), 5.91 (1H, s; C*H*), 5.07 (1H, d, $^3J_{HH}$ 7.8 Hz; C*H*), 4.02 (1H, dd, $^4J_{HH}$ 0.8 Hz and $^3J_{HH}$ 7.5 Hz; C*H*), 2.37 (6H, s; 2×CH_3), 1.30 (9H, s; 3×CH_3); ^{13}C NMR (100.6 MHz, $CDCl_3$): δ_C 173.7 (*C*=O), 173.1 (*C*=O), 166.3 (*C*=O), 147.1 (Ar*C*), 145.8 (Ar*C*), 141.8 (Ar*C*), 139.1 (Ar*C*), 138.9 (Ar*C*), 134.6 (Ar*C*), 133.9 (Ar*C*H), 132.6 (q, J_{CF} 35.4 Hz, Ar*C*), 127.1 (m, Ar*C*H), 127.0 (Ar*C*H), 126.6

(Ar*C*H), 126.4 (Ar*C*), 125.0 (Ar*C*H), 123.3 (q, $^{1}J_{CF}$ 276.1 Hz, Ar*C*-CF_3), 122.4 (m, Ar*C*H), 120.4 (Ar*C*H), 114.1 (Ar*C*H), 77.6 (*C*H), 68.8 (*C*H), 57.3 (*C*H), 34.7 (q*C*), 31.6 (CH_3), 21.3 (CH_3); ^{19}F NMR (376.5 MHz, $CDCl_3$) : δ_F –63.2 (ArCF_3); MS (ES^+) *m/z* 731.9 ($[M+Na]^+$, 100); HRMS (ES^+) *m/z* calculated for $C_{38}H_{33}N_3O_4F_6Na$ $[M+Na]^+$ 732.2273, found 732.2279.

_N_-(4-(4-Azidophenethyl)phenyl)-3,5-dimethylbenzamide 146

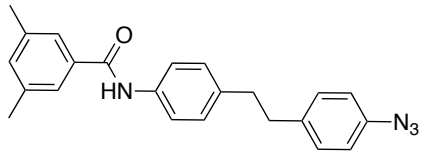

Aniline derivative **122** (0.2 g, 0.58 mmol) was suspended in conc. HCl (2 ml) and cooled down to –10 ˚C. Sodium nitrite solution (44 mg in 2 ml H_2O, 0.64 mmol) was added dropwise at –10 ˚C. Reaction mixture was stirred for 1 h. Sodium azide solution (46 mg in 2 ml H_2O, 0.70 mmol) was then added at –10˚C. The reaction mixture was allowed to get to ambient temperature and stirred for 2 h. The resulting precipitate was filtered off and dried. The product **146** was obtained as yellow solid (207 mg, 97%). M.p. = 166.3 –169.2 ˚C; ^{1}H NMR (400.1 MHz, $CDCl_3$) : δ_H 7.74 (1H, s; C(O)N*H*), 7.54 (2H, d, $^{3}J_{HH}$ 8.5 Hz; 2×Ar*H*), 7.46 (2H, s; 2×Ar*H*), 7.18 (1H, s; Ar*H*), 7.13 (2H, d, $^{3}J_{HH}$ 8.5 Hz; 2×Ar*H*), 7.12 (2H, d, $^{3}J_{HH}$ 8.5 Hz; 2×Ar*H*), 6.93 (2H, d, $^{3}J_{HH}$ 8.5 Hz; 2×Ar*H*), 2.89 (4H, s; 2×CH_2), 2.39 (6H, s; 2×CH_3); ^{13}C NMR (100.6 MHz, $CDCl_3$): δ_C 166.1 (Ar*C*), 138.7 (Ar*C*), 138.5 (Ar*C*), 137.8 (Ar*C*), 137.7 (Ar*C*), 136.2 (Ar*C*), 135.2 (Ar*C*), 133.6 (Ar*C*H), 130.0 (Ar*C*H), 129.2 (Ar*C*H), 124.9 (Ar*C*H), 120.3 (Ar*C*H), 119.1 (Ar*C*H), 37.5 (CH_2), 37.4 (CH_2), 21.4 (CH_3); MS (ES^+) *m/z* 393.06 ($[M+Na]^+$, 100); HRMS (CI^+) *m/z* calculated for $C_{23}H_{23}N_4$ $[M+H]^+$ 371.187, found 371.188.

Rotaxane 151[231]

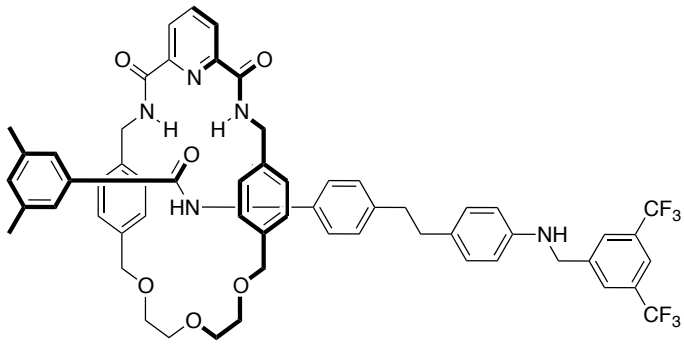

Azide derivative **146** (0.1 g, 0.27 mmol,) and macrocycle **MDG** (0.13 g, 0.27 mmol) were pre-equilibrated at –10 ˚C for 1 h in dry $CDCl_3$ (10 mL) before PPh_3 (142 mg, 0.54 mmol) in dry $CDCl_3$ (0.8 mL) was added to the reaction mixture and left to stir for 48 h under positive Ar atmosphere at 10 ˚C. The resulting mixture was warmed up to the ambient temperature. Subsequently, 3,5-trifluoromethylbenzaldehyde **148** (72 mg, 0.30 mmol) and 2-(4-bromophenyl)acetic acid (58 mg, 0.27 mmol), dissolved in dry $CDCl_3$ (0.85 mL) were added and stirred for 48 h at ambient temperature. Eventually, Hanztsch ester (0.21 g, 0.81 mmol) was added neat to the reaction mixture and allowed to heat at 40 ˚C. The reaction mixture was left stirred for another 48 h, before to remove the solvent by evaporation in *vacuo*. The residue was purified by careful column chromatography (Cyclohexane:EtOAc, 2:1), which enabled the isolation of the rotaxane **151** as yellow solid (75 mg, 28%). M.p. = 115.5 – 117.3 ˚C; ^{1}H NMR (400.1 MHz, $CDCl_3$) : δ_H 9.38 (2H, t, $^3J_{HH}$ 5.45 Hz; 2×N*H*), 8.49 (2H, d, $^3J_{HH}$ 7.8 Hz; 2×Ar*H*), 8.12 (1H, t, $^3J_{HH}$ 7.8 Hz; Ar*H*), 7.83 (2H, s; 2×Ar*H*), 7.77 (1H, s; Ar*H*), 7.60 (1H, s; N*H*), 7.27 (2H, d, $^3J_{HH}$ 8.5 Hz; 2×Ar*H*), 7.03 (2H, s; 2×Ar*H*), 7.00 (2H, d, $^3J_{HH}$ 8.4 Hz; 2×Ar*H*), 6.99 (1H, s; Ar*H*), 6.81 (2H, d, $^3J_{HH}$ 8.3 Hz; 2×Ar*H*), 6.65 (4H, d, $^3J_{HH}$ 7.9 Hz; 4×Ar*H*), 6.56 (4H, d, $^3J_{HH}$ 8.4 Hz; 4×Ar*H*), 6.54 (2H, d, $^3J_{HH}$ 7.4 Hz; 2×Ar*H*), 4.52 (4H, d, $^3J_{HH}$ 3.6 Hz; 2×CH_2), 4.43 (2H, s; CH_2), 4.13 (4H, ABq, J_{AB} 10.4 Hz; 2×CH_2), 3.75 – 3.66 (4H, m; 2×CH_2), 3.60 (1H, s; N*H*), 3.48 – 3.37 (4H, m; 2×CH_2), 2.81 (4H, s; 2×CH_2), 2.18 (6H, s; 2×CH_3); ^{13}C NMR (100.6 MHz, $CDCl_3$): δ_C 165.1 (*C*(O)NH), 164.2 (*C*(O)NH), 149.6 (Ar*C*), 145.7 (Ar*C*), 142.9 (Ar*C*), 138.7 (Ar*C*H), 137.1 (Ar*C*), 137.0 (Ar*C*), 136.8 (Ar*C*), 136.7 (Ar*C*), 136.6 (Ar*C*), 135.4 (Ar*C*), 134.1 (Ar*C*), 132.5 (Ar*C*H), 131.8 (Ar*C*), 131.7 (Ar*C*), 129.6 (Ar*C*H), 129.3 (Ar*C*H), 128.9 (Ar*C*H), 128.1 (Ar*C*H), 127.9 (Ar*C*H), 126.0 (Ar*C*H), 125.4 (Ar*C*H), 124.4 (Ar*C*H), 119.6 (Ar*C*H), 113.2 (Ar*C*H), 73.6 (*C*H_2), 71.1 (*C*H_2), 68.7 (*C*H_2), 48.1 (*C*H_2), 43.7 (*C*H_2), 37.5 (*C*H_2), 37.0 (*C*H_2), 21.2 (*C*H_3); ^{19}F NMR (376.5 MHz, $CDCl_3$): δ_F –63.3 (ArC*F*$_3$).

N-(4-(4-(3,5-Bis(trifluoromethyl)benzylamino)phenethyl)phenyl)-3,5-dimethylbenzamide Thread 151'[231]

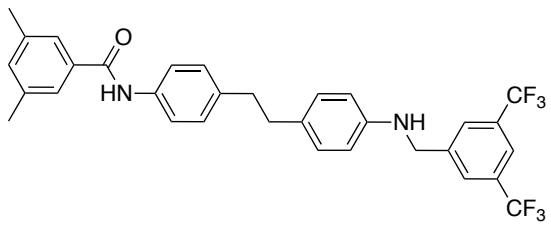

Compound **122** (0.2 g, 0.58 mmol) and 3,5-bis(trifluoromethyl)benzaldehyde **148** (0.14 g, 0.53 mmol) were suspended in dry MeCN (10 mL) together with 2 drops of formic acid. The mixture was heated for 3 h at 45 ˚C before it was allowed to cool at room temperature. $NaBH_4$ (40 mg, 1.06 mmol) was added neat and the reaction mixture was vigorously stirred for 12 h under positive Ar atmosphere before it was quenched with 5 mL of sat. solution of NH_4Cl. The organic material was extracted into CH_2Cl_2 and washed with deionised water, dried ($MgSO_4$) and the solvent and volatiles evacuated under reduced pressure to afford the crude. Column chromatography (Cyclohexane:EtOAc, 1:1) was used to purify the product as colorless solid (65 mg, 20%). M.p. = 153.4 – 156.2 ˚C; ^{1}H NMR (400.1 MHz, $CDCl_3$) : δ_H 7.85 (2H, s; 2×Ar*H*), 7.79 (1H, s; Ar*H*), 7.75 (1H, s; N*H*), 7.53 (2H, d, $^3J_{HH}$ 8.5 Hz; 2×Ar*H*), 7.46 (2H, s; 2×Ar*H*), 7.18 (1H, s; Ar*H*), 7.15 (2H, d, $^3J_{HH}$ 8.5 Hz; 2×Ar*H*), 6.99 (2H, d, $^3J_{HH}$ 8.5 Hz; 2×Ar*H*), 6.54 (2H, d, $^3J_{HH}$ 8.5 Hz; 2×Ar*H*), 4.46 (2H, s; CH_2), 4.13 (1H, br s; N*H*), 2.84 – 2.83 (4H, m; 2×CH_2), 2.39 (6H, s; 2×CH_3); ^{13}C NMR (100.6 MHz, $CDCl_3$): δ_C 166.1 (Ar*C*), 145.6 (Ar*C*), 142.9 (Ar*C*), 138.6 (Ar*C*), 138.3 (Ar*C*), 136.0 (Ar*C*), 135.2 (Ar*C*), 133.5 (Ar*C*H), 132.1 (Ar*C*), 131.8 (Ar*C*), 129.5 (Ar*C*H), 129.2 (Ar*C*H), 127.4 (Ar*C*H), 124.9 (Ar*C*H), 122.1(Ar*C*), 121.4 (Ar*C*H), 120.2 (Ar*C*H), 113.2 (Ar*C*H), 48.1 (*C*H_2), 37.8 (*C*H_2), 37.2 (*C*H_2), 21.4 (*C*H_3); ^{19}F NMR (376.5 MHz, $CDCl_3$): δ_F –63.3 (ArC*F*$_3$); MS (ES$^+$) *m/z* 592.81 ([M+Na]$^+$, 100); HRMS (ES$^+$) *m/z* calculated for $C_{32}H_{28}N_2ONaF_6$ [M+Na]$^+$ 593.200, found 593.199.

5-*tert*-Butylisophthaloyl dichloride[237] **153**

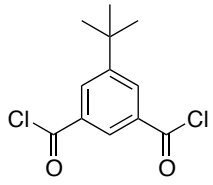

5-*tert*-butylisophtalic acid **152** (2.0 g, 9.0 mmol) was suspended in toluene (45 mL) together with thionyl chloride (0.72 mL, 18.0 mmol) and refluxed at 80˚C for 18 h. An excess of thionyl chloride was

distilled off by the azeotropic distillation with toluene to furnish dark yellow oil (2.28 g, 98%) as desired product. This product was used in the next step without further purification. ^{1}H NMR (300.1 MHz, $CDCl_3$) : δ_H 8.69 (1H, t, $^{4}J_{HH}$ 1.6 Hz; Ar*H*), 8.40 (2H, d, $^{4}J_{HH}$ 1.7 Hz; 2×Ar*H*), 1.41 (9H, s; 3×CH_3); ^{13}C NMR (75.5 MHz, $CDCl_3$) : δ_C 167.8 (*C*OCl), 154.1 (Ar*C*), 134.4 (Ar*C*), 134.2 (Ar*C*H), 131.8 (Ar*C*H), 35.5 (q*C*), 31.1 (*C*H_3); MS (ES^+) *m/z* 273.1 ([M+H]$^+$, 100), 477 (20).

Macrocycle cMDG

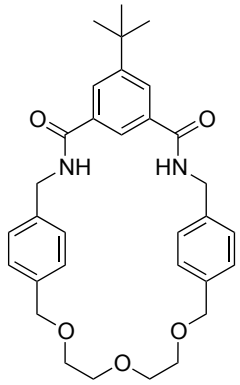

A solution of amine derivative **103** (0.5 g, 1.45 mmol) and 5-*tert*-butylisophthaloyl dichloride **153** (0.38 g, 1.45 mmol) in dry THF (100 mL) were added simultaneously over 1 h to a solution of Et_3N (1.25 mL, 8.71 mmol) in dry THF (82 mL) and left stirred at ambient temperature under N_2 atmosphere for 3 days. The reaction mixture was concentrated by evaporation under reduced pressure and diluted with CH_2Cl_2. The solution was then washed successively with 1M HCl and 1M KOH. The organic layers were dried with $MgSO_4$ and concentrated *in vacuo*. The residue was purified by column chromatography (Hexane:EtOAc, 1:1) to yield macrocycle **cMDG** as a colorless solid (81 mg, 11%). M.p. = 247.8 – 250.4 ˚C; ^{1}H NMR (400.1 MHz, $CDCl_3$) : δ_H 8.10 (2H, d, $^{3}J_{HH}$ 1.5 Hz; 2×N*H*), 7.53 (1H, br s; Ar*H*), 7.30 (8H, s; 8×Ar*H*), 6.43 (2H, br s; 2×Ar*H*), 4.57 (4H, d, $^{3}J_{HH}$ 5.4 Hz; 2×CH_2), 4.50 (4H, s; 2×CH_2), 3.58 – 3.68 (8H, m; 4×CH_2), 1.37 (9H, s; 3×CH_3); ^{13}C NMR (75.5 MHz, $CDCl_3$) : δ_C 167.3 (*C*=O), 153.2 (Ar*C*), 137.8 (Ar*C*), 137.4 (Ar*C*), 134.7 (Ar*C*), 128.8 (Ar*C*H), 128.5 (Ar*C*H), 128.4 (Ar*C*H), 120.6 (Ar*C*H), 73.1 (*C*H_2), 70.7 (*C*H_2), 69.6 (*C*H_2), 44.3 (*C*H_2), 35.3 (q*C*), 31.3 (*C*H_3); MS (ES^+) *m/z* 553.1 ([M+Na]$^+$, 100) 554.2 (30); HRMS (ES^+) *m/z* calculated for $C_{32}H_{38}N_2O_5Na$ [M+Na]$^+$ 553.2678, found 553.2664.

Macrocycle cMP

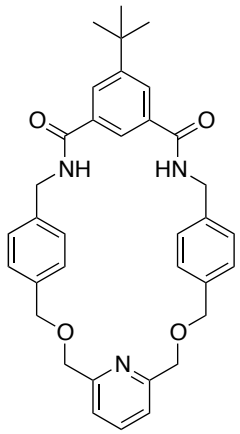

A solution of amine derivative **114** (0.6 g, 1.59 mmol) and 5-*tert*-butylisophthaloyl dichloride **153** (0.42 g, 1.59 mmol) in dry THF (100 mL) were added simultaneously over 2 h to a solution of Et_3N (1.3 mL, 9.36 mmol) in dry THF (95 mL) and left stirred at ambient temperature under N_2 atmosphere for 3 days. The reaction mixture was concentrated *in vacuo* and diluted with CH_2Cl_2. The solution was then washed successively with 1M HCl and 1M KOH. The organic layers were dried with $MgSO_4$ and concentrated *in vacuo*. The residue was purified by column chromatography (Hexane:EtOAc, 1:1) to yield macrocycle **cMP** as a colorless solid (100 mg, 11%). M.p. = 256.3 – 258.9 ˚C; ^{1}H NMR (500.1 MHz, $CDCl_3$) : δ_H 8.07 (2H, d, $^3J_{HH}$ 1.4 Hz; 2×N*H*), 7.71 (1H, t, $^3J_{HH}$ 7.8 Hz; Ar*H*), 7.57 (1H, s; Ar*H*), 7.36 (2H, d, $^3J_{HH}$ 7.8 Hz; 2×Ar*H*), 7.31 (8H, s; 8×Ar*H*), 6.39 (2H, br s; 2×Ar*H*), 4.65 (4H, s; 2×CH_2), 4.58 (4H, d, $^3J_{HH}$ 5.5 Hz; 2×CH_2), 4.42 (4H, s; 2×CH_2), 1.37 (9H, s; 3×CH_3); ^{13}C NMR (100.6 MHz, $CDCl_3$) : δ_C 167.3 (*C*=O), 157.4 (Ar*C*), 152.9 (Ar*C*), 137.6 (Ar*C*), 137.3 (Ar*C*H), 137.2 (Ar*C*), 134.6 (Ar*C*), 129.0 (Ar*C*H), 128.7 (Ar*C*H), 128.1 (Ar*C*H), 120.8 (Ar*C*H), 120.3 (Ar*C*H), 72.2 (*C*H_2), 71.5 (*C*H_2), 44.3 (*C*H_2), 35.3 (q), 31.2 (*C*H_3); MS (ES^+) *m/z* 586.1 ([M+Na]$^+$, 100) ; HRMS (ES^+) *m/z* calculated for $C_{35}H_{37}N_3O_4Na$ [M+Na]$^+$ 586.2682, found 586.2684.

5-Iodoisophthalic acid[271] **155**

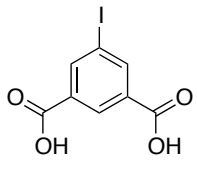

5-aminoisophthalic acid **154** (3.50 g, 19.3 mmol) was suspended in 20 mL of H_2O. The suspension was cooled down to 0 ˚C. HCl conc. (18 mL) was added dropwise followed with the solution of $NaNO_2$ (1.40 g, 20.3 mmol). The resulting solution was stirred for 1 h at 0 ˚C. Potassium iodide (12.74 g, 77.2 mmol) was added neat in small portions. The reaction mixture was allowed to warm to ambient temperature and stirred for 18 h. The resulting precipitate was collected by filtration and washed with H_2O. Solid was tritrated with CH_3OH:Hexane to give the desired product as pale orange solid (2.37 g,

44%). M.p. = 274.8˚C (decomposed); ^{1}H NMR (300.1 MHz, $CDCl_3$ + 3 drops of d_6-DMSO) : δ_H 8.44 (1H, t, $^{4}J_{HH}$ 1.5 Hz; Ar*H*), 8.32 (2H, d, $^{4}J_{HH}$ 1.5 Hz; 2×Ar*H*); ^{13}C NMR (75.5 MHz, d_6-DMSO) : δ_C 169.3 (*C*OOH), 144.0 (Ar*C*), 131.7 (Ar*C*), 129.5 (Ar*C*H), 94.5 (Ar*C*-I).

5-Iodoisophthaloyl dichloride[243] 156

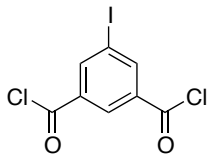

A solution of 5-iodoisophthalic acid **155** (0.40 g, 1.37 mmol) in thionyl chloride (8 mL, 17.0 mmol) and DMF (3-5 drops) was refluxed at 100 ˚C for 48 h under dry condition with subsequent removal of the excess of thionyl chloride *in vacuo* to yield red brownish oil (0.44 g, 98%). This compound was used in the next step without further purification. ^{1}H NMR (300.1 MHz, $CDCl_3$) : δ_H 8.79 (1H, t, $^{4}J_{HH}$ 1.8 Hz; Ar*H*), 8.69 (2H, dd, $^{4}J_{HH}$ 0.2 and $^{4}J_{HH}$ 1.70 Hz; 2×Ar*H*); ^{13}C NMR (100.6 MHz, $CDCl_3$) : δ_C 166.1 (*C*OCl), 145.4 (Ar*C*H), 135.7 (Ar*C*), 132.7 (Ar*C*H), 94.5 (Ar*C*-I).

Iodophenyl glycol macrocycle 157

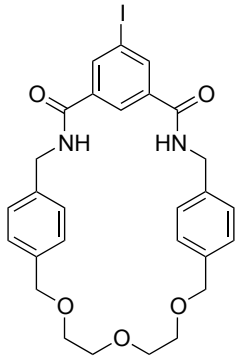

A solution of amine derivatives **103** (0.9 g, 2.58 mmol) and 5-iodoisophthaloyl dichloride **156** (0.85 g, 2.58 mmol) in dry THF (200 mL) were added simultaneously over 1.5 h to a solution of Et_3N (2.2 mL, 16.0 mmol) in dry THF (82 mL) and stirred at ambient temperature under N_2 atmosphere for 3 days. The reaction mixture was concentrated by evaporation under reduced pressure and diluted with CH_2Cl_2. The solution was then washed successively with 1M HCl and 1M KOH solution. The organic layers were dried with $MgSO_4$ and concentrated *in vacuo*. The residue was purified by column chromatography ($CHCl_3$:EtOAc, 1:1) to yield macrocycle **157** as a pale yellow solid (110 mg, 21%). M.p. = 269.7 – 271.7˚C; ^{1}H NMR (300.1 MHz, $CDCl_3$) : δ_H 8.25 (2H, s; 2×N*H*), 7.67 (1H, s; Ar*H*), 7.30 (8H, s; 8×Ar*H*), 6.57 (2H, t, $^{3}J_{HH}$ 3.7 Hz; 2×Ar*H*), 4.55 (4H, d, $^{3}J_{HH}$ 5.3 Hz; 2×CH_2), 4.49 (4H, s; 2×CH_2), 3.56 – 3.67 (8H, m; 4×CH_2); ^{13}C NMR (75.5 MHz, $CDCl_3$) : δ_C 165.2 (*C*=O), 140.2 (Ar*C*H), 137.2 (Ar*C*), 136.9 (Ar*C*), 135.7 (Ar*C*), 128.8 (Ar*C*H), 128.7 (Ar*C*H), 122.8 (Ar*C*H), 95.0 (Ar*C*-I), 73.5 (*C*H_2), 70.4 (*C*H_2), 70.1 (*C*H_2), 44.5 (*C*H_2); MS (ES$^+$) *m/z* 622.9 ([M+Na]$^+$, 100);

HRMS (ES$^+$) *m/z* calculated for $C_{28}H_{29}N_2O_5NaI$ [M+Na]$^+$ 623.1019, found 623.1013.

Iodophenyl pyridine macrocycle 158

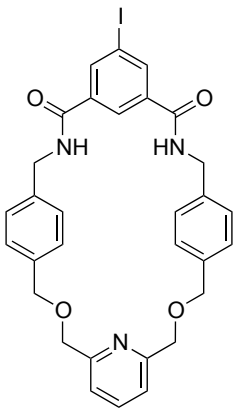

A solution of amine derivative **114** (0.7 g, 1.85 mmol) and 5-iodoisophthaloyl dichloride **156** (0.61 g, 1.85 mmol) in dry THF (100 mL) were added simultaneously over 2 h to a solution of Et_3N (1.6 mL, 11.1 mmol) in dry THF (82 mL) and left stirred at ambient temperature under N_2 atmosphere for 3 days. The reaction mixture was concentrated *in vacuo* and diluted with CH_2Cl_2. The solution was then washed successively with 1M HCl and sat. solution of $NaHCO_3$. The organic layers were dried with $MgSO_4$ and concentrated under reduced pressure. The residue was purified by column chromatography ($CHCl_3$:EtOAc, 1:1) to yield macrocycle **158** as a colorless solid (210 mg, 18%). M.p. = 248.7 – 250.5 ˚C; ^{1}H NMR (300.1 MHz, $CDCl_3$ + 3 drops of d_6-DMSO) : δ_H 8.44 (2H, d, $^3J_{HH}$ 1.4 Hz; 2×Ar*H*), 8.24 (1H, s; Ar*H*), 7.94 (2H, t, $^3J_{HH}$ 5.4 Hz; 2×N*H*), 7.65 (1H, t, $^3J_{HH}$ 7.6 Hz; Ar*H*), 7.27 (2H, d, $^3J_{HH}$ 6.0 Hz; 2×Ar*H*), 7.23 (8H, s; 8×Ar*H*), 4.59 (4H, d, $^3J_{HH}$ 5.3 Hz; 2×CH_2), 4.52 (4H, s; 2×CH_2), 4.30 (4H, s; 2×CH_2); ^{13}C NMR (100.6 MHz, $CDCl_3$ + 3 drops of d_6-DMSO) : δ_C 164.7 (*C*=O), 139.9 (Ar*C*H), 138.1 (Ar*C*), 136.7 (Ar*C*), 135.2 (Ar*C*), 130.1 (Ar*C*H), 129.2 (Ar*C*H), 128.5 (Ar*C*H), 126.7 (Ar*C*H), 123.4 (Ar*C*H), 120.8 (Ar*C*H), 94.2 (Ar*C*-I), 72.4 (*C*H_2), 71.4 (*C*H_2), 43.7 (*C*H_2); MS (ES$^+$) *m/z* 656 ([M+Na]$^+$, 100); HRMS (ES$^+$) *m/z* calculated for $C_{31}H_{28}N_3O_4NaI$ [M+Na]$^+$ 656.1022, found 656.1027.

5-Bromoisophthaloyl dichloride 160

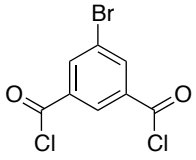

A solution of 5-bromoisophthalic acid **159** (0.5 g, 2.04 mmol) in thionyl chloride (10 mL, 20.0 mmol) and DMF (3-5 drops) was refluxed at 100 ˚C for 6 h with subsequent removal of the excess of thionyl chloride in *vacuo*. The residue was dried under high vacuum to furnish a brownish oil (0.56 g, 98%). The acid chloride **160** was used in the next step without further purification. ^{1}H NMR (400.1 MHz, $CDCl_3$) : δ_H 8.76 (1H, t, $^4J_{HH}$ 1.6 Hz; Ar*H*), 8.52 (2H, d, $^4J_{HH}$ 1.6 Hz; 2×Ar*H*); ^{13}C NMR (100.6 MHz, $CDCl_3$) : δ_C 166.2 (*C*OCl), 139.6 (Ar*C*H), 135.8 (Ar*C*), 132.0 (Ar*C*H), 124.0 (Ar*C*-Br).

Bromophenyl glycol macrocycle 161

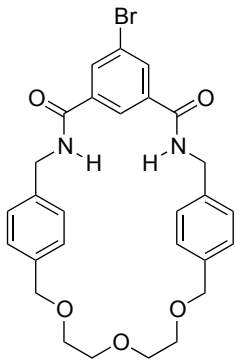

A solution of 5-bromoisophthaloyl dichloride **160** (0.5 g, 1.77 mmol) in dry THF (60 mL) was added simultaneously with a solution of amine derivatives **103** (0.61 g, 1.77 mmol) in dry THF (60 mL) to a solution of Et_3N (1.5 mL, 11.0 mmol) in dry THF (130 mL) over 1 h under a N_2 atmosphere. The reaction mixture was stirred at ambient temperature for 3 days and washed successively with 1M HCl and sat. solution of $NaHCO_3$. The organic layers were dried ($MgSO_4$) and the solvent was removed by evaporation in *vacuo*. The residue redissolved minimally in CH_2Cl_2 and purified by column chromatography ($CHCl_3$:EtOAc, 1:1) to afford macrocycle **161** (70 mg, 8%) as a colourless solid. M.p. = 219.5 – 223.7 ˚C; ^{1}H NMR (400.1 MHz, $CDCl_3$): δ_H 8.18 (2H, d, $^4J_{HH}$ 1.4 Hz; 2×Ar*H*), 8.12 (1H, t, $^4J_{HH}$ 1.4 Hz; Ar*H*), 7.87 (2H, br s; 2×N*H*), 7.22 – 7.16 (8H, m; 8×Ar*H*), 4.48 (4H, d, $^3J_{HH}$ 4.8 Hz; 2×CH_2), 4.29 (4H, s; 2×CH_2), 3.42 – 3.43 (8H, m; 4×CH_2); ^{13}C NMR (100.6 MHz, $CDCl_3$): δ_C 164.9 (*C*=O), 137.5 (Ar*C*), 137.2 (Ar*C*), 135.5 (Ar*C*), 134.2 (Ar*C*H), 129.3 (Ar*C*H), 128.9 (Ar*C*H), 123.1 (Ar*C*), 122.6 (Ar*C*H), 73.1 (*C*H_2), 70.2 (*C*H_2), 69.1 (*C*H_2), 44.1 (*C*H_2); MS (ES^+) *m/z* 577 ([M+Na]$^+$, 100); HRMS (ES^+) *m/z* calculated for $C_{28}H_{29}N_2O_5Na^{79}Br$ [M+Na]$^+$ 575.1158, found 575.1163.

Bromophenyl pyridine macrocycle 162

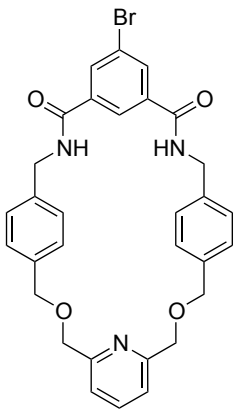

A solution of 5-bromoisophthaloyl dichloride **160** (1.15 g, 4.09 mmol) in dry THF (100 mL) was added simultaneously with a solution of amine derivative **114** (1.55 g, 4.09 mmol) in dry THF (100 mL) to a solution of Et_3N (1.72 mL, 25.0 mmol) in dry THF (140 mL) over 1 h under a N_2 atmosphere. The reaction mixture was left stirred at ambient temperature for 3 days, and then washed successively with 1M HCl and sat. solution of $NaHCO_3$. The organic layers were dried ($MgSO_4$) and the solvent was removed by evaporation under reduced pressure. The residue was redissolved

minimally in CH_2Cl_2 and purified by column chromatography ($CHCl_3$:EtOAc, 1:1) to afford macrocycle **162** (190 mg, 8%) as a colourless solid. M.p. = 219.5 – 223.7 ˚C; ^{1}H NMR (300.1 MHz, $CDCl_3$): δ_H 8.23 (2H, s; 2×Ar*H*), 8.18 (1H, s; Ar*H*), 7.94 (2H, br t; 2×N*H*), 7.63 (1H, t, $^3J_{HH}$ 7.7 Hz; Ar*H*), 7.25 (2H, d, $^3J_{HH}$ 7.8 Hz; 2×Ar*H*), 7.22 (8H, s; 8×Ar*H*), 4.53 (4H, d, $^3J_{HH}$ 5.1 Hz; 2×CH_2), 4.51 (4H, s; 2×CH_2), 4.28 (4H, s; 2×CH_2); ^{13}C NMR (75.5 MHz, $CDCl_3$): δ_C 165.0 (*C*=O), 156.9 (Ar*C*), 138.2 (Ar*C*), 137.0 (Ar*C*), 135.5 (Ar*C*), 134.4 (Ar*C*H), 129.9 (Ar*C*H), 129.4 (Ar*C*H), 128.7 (Ar*C*H), 123.1 (Ar*C*-Br), 122.7 (Ar*C*H), 120.9 (Ar*C*H), 72.6 (*C*H_2), 71.7 (*C*H_2), 43.9 (*C*H_2); MS (ES^+) *m/z* 609 ([M+Na]$^+$, 75), 607 (100); HRMS (ES^+) *m/z* calculated for $C_{31}H_{28}N_3O_4Na^{79}Br$ [M+Na]$^+$ 608.1161, found 608.1154 and $C_{31}H_{28}N_3O_4Na^{81}Br$ [M+Na]$^+$ 610.1140, found 610.1155.

tert-Butyl 4-bromobenzoate 164[244]

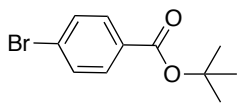

A solution of 4-bromobenzoyl chloride **163** (4.68 g, 21.3 mmol) in dry CH_2Cl_2 (25 mL) was added dropwise to a stirred mixture of *tert*-butyl alcohol (3.49 g, 47.1 mmol) and dry pyridine (3.5 mL) in dry CH_2Cl_2 (15 mL). The reaction mixture was stirred at ambient temperature under a N_2 atmosphere for 48 h and then diluted with CH_2Cl_2. The organic phase was washed successively with 1M HCl, water and sat. solution of NaCl, dried ($MgSO_4$) and concentrated by evaporation under reduced pressure. The residue was taken up in cyclohexane and filtered off. The filtrate was concentrated by evaporation under reduced pressure to afford **164** (5.0 g, 91%) as a pale yellow oil and was used without further purification. ^{1}H NMR (400.1 MHz, $CDCl_3$): δ_H 7.85 – 7.82 (2H, m; 2×Ar*H*), 7.56 – 7.52 (2H, m; 2×Ar*H*), 1.58 (9H, s; 3×CH_3); ^{13}C NMR (100.6 MHz, $CDCl_3$): δ_C 165.1 (*C*=O), 131.6 (Ar*C*H), 131.1 (Ar*C*H), 131.0 (Ar*C*), 127.5 (Ar*C*), 81.6 (q*C*), 28.3 (*C*H_3).

tert-Butyl 4-(3-hydroxy-3-methylbut-1-yn-1-yl)benzoate 165

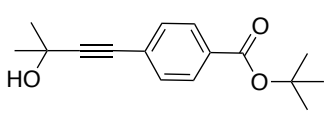

A degassed (by bubbling Ar for 45 min) solution of 2,2-dimethylpropargyl alcohol (2.90 mL, 29.2 mmol) in Et_3N (50 mL) was cannulated into a degassed (by bubbling Ar for 45 min) suspension of compound **164** (5.0 g, 19.4 mmol), PPh_3 (0.51

g, 1.94 mmol), CuI (180 mg, 0.97 mmol), $PdCl_2(PPh_3)_2$ (68 mg, 0.97 mmol), Et_3N (50 mL) and dry THF (20 mL). The reaction mixture was heated at 70 ˚C under an Ar atmosphere for 48 h, and then concentrated by evaporation *in vacuo*. The residue was taken up in CH_2Cl_2. The organic phase was washed with water, dried ($MgSO_4$) and concentrated by evaporation in *vacuo*. The residue was purified by column chromatography (Cyclohexane:EtOAc, 7:3) to give compound **165** as brown solid (4.40 g, 87%). M.p. = 66.8 – 68.6 ˚C; ^{1}H NMR (400.1 MHz, $CDCl_3$): δ_H 7.93 – 7.90 (2H, m; 2×Ar*H*), 7.45 – 7.42 (2H, m; 2×Ar*H*), 2.20 (1H, br s, O*H*), 1.63 (6H, s; 2×CH_3), 1.59 (9H, s; 3×CH_3); ^{13}C NMR (100.6 MHz, $CDCl_3$): δ_C 165.3 (*C*=O), 131.6 (Ar*C*), 131.5 (Ar*C*), 129.4 (Ar*C*H), 127.0 (Ar*C*), 96.5 (q*C*), 81.7 (q*C*), 81.5 (q*C*), 65.8 (q*C*), 31.5 (*C*H_3), 28.3 (*C*H_3); MS (ES^+) *m/z* 283 ($[M+Na]^+$, 100); HRMS (ES^+) *m/z* calculated for $C_{16}H_{20}O_3Na$ $[M+Na]^+$ 283.1310, found 283.1307.

tert-Butyl 4-ethynylbenzoate 166[244,272]

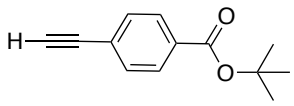

A solution of compound **165** (2.0 g, 7.68 mmol) in toluene (70 mL) was treated with with powdered NaOH (0.61 g, 15.0 mmol). The reaction mixture was heated to reflux for 3 h under a N_2 atmosphere, and then concentrated by evaporation under reduced pressure. The residue was taken up in $CHCl_3$. The organic phase was washed with water, dried ($MgSO_4$) and concentrated by evaporation under reduced pressure. The residue was purified by column chromatography (Cyclohexane:EtOAc, 19:1) to give terminal alkyne **166** (1.07 g, 69%) as a yellow oil. ^{1}H NMR (400.1 MHz, $CDCl_3$): δ_H 7.95 – 7.92 (2H, m; 2×Ar*H*), 7.54 – 7.51 (2H, m; 2×Ar*H*), 3.14 (1H, s; C*H*), 1.52 (9H, s; 3×CH_3); ^{13}C NMR (100.6 MHz, $CDCl_3$): δ_C 165.2 (*C*=O), 132.2 (Ar*C*), 132.0 (Ar*C*H), 129.4 (Ar*C*H), 126.3 (Ar*C*), 83.1 (q*C*), 81.5 (q*C*), 79.8 (q*C*), 28.3 (*C*H_3); MS (ES^+) *m/z* 225 ($[M+Na]^+$, 100); HRMS (ES^+) *m/z* calculated for $C_{13}H_{14}O_2Na$ $[M+Na]^+$ 225.0891, found 225.0892.

Macrocycle 167

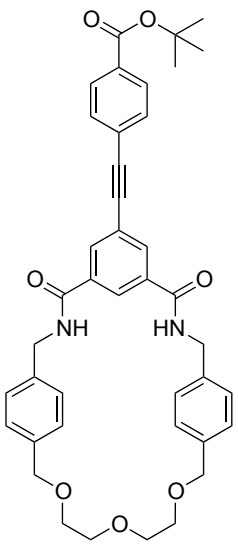

A degassed (by bubbling Ar) solution of **166** (62 mg, 0.30 mmol) in Et_3N (5 mL) was cannulated into a degassed (by bubbling Ar) suspension of macrocycle **157** (122 mg, 0.23 mmol), PPh_3 (53 mg, 0.02 mmol), CuI (27 mg, 0.014 mmol), $PdCl_2(PPh_3)_2$ (10 mg, 0.014 mmol) and Et_3N (5 mL) in dry THF (10 mL). The reaction mixture was heated at 60 ˚C under an Ar atmosphere for 42 h, and then filtered through a pad of Celite. The filtrate was concentrated by evaporation *in vacuo*. The residue was dissolved in $CHCl_3$. The organic layers were washed with water, dried ($MgSO_4$) and concentrated by evaporation *in vacuo*. The residue was purified by column chromatography ($CHCl_3$:EtOAc, 1:1) to give macrocycle **167** as a yellow solid (140 mg, 90%). M.p. = 197.0 – 200.5 ˚C; ^{1}H NMR (400.1 MHz, $CDCl_3$) : δ_H 8.19 (2H, d, $^4J_{HH}$ 1.5 Hz; 2×Ar*H*), 7.97 (2H, d, $^3J_{HH}$ 8.6 Hz; 2×Ar*H*), 7.75 (1H, br s, Ar*H*), 7.56 (2H, d, $^3J_{HH}$ 8.6 Hz; 2×Ar*H*), 7.31 – 7.27 (8H, m; 8×Ar*H*), 6.71 (2H, br s; 2×N*H*), 4.54 (4H, d, $^3J_{HH}$ 5.3 Hz; 2×CH_2), 4.48 (4H, s; 2×CH_2), 3.66 – 3.59 (8H, m; 4×CH_2), 1.60 (9H, s; 3×CH_3); ^{13}C NMR (75.5 MHz, $CDCl_3$) : δ_C 166.0 (*C*=O), 165.2 (*C*=O), 137.6 (Ar*C*), 137.2 (Ar*C*), 135.2 (Ar*C*), 133.9 (Ar*C*H), 132.0 (Ar*C*), 131.7 (Ar*C*H), , 129.6 (Ar*C*H), 128.8 (Ar*C*H), 128.7 (Ar*C*H), 126.8 (Ar*C*), 124.7 (Ar*C*), 123.6 (Ar*C*H), 90.9 (q*C*), 90.2 (q*C*), 81.5 (q*C*), 73.1 (*C*H_2), 70.5 (*C*H_2), 69.8 (*C*H_2), 44.5 (*C*H_2), 28.3 (*C*H_3); MS (ES$^+$) *m/z* 697 ([M+Na]$^+$, 100); HRMS (ES$^+$) *m/z* calculated for $C_{41}H_{42}N_2O_7Na$ [M+Na]$^+$ 697.2890, found 697.2897.

Macrocycle AEMDG

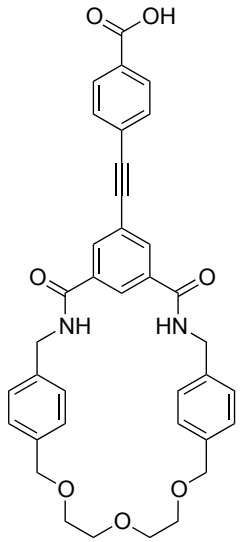

To a solution of ester macrocycle **167** (0.27 g, 0.40 mmol), in CH_2Cl_2 (15 mL) was added at 0 ˚C trifluoroacetic acid in excess. Triethylsilane (0.13 mL, 0.80 mmol) was added dropwise into the resulting solution. The reaction mixture was left stirred at ambient temperature for 16 h. The solvent was reduced in *vacuo*, diluted with CH_2Cl_2 and washed with deionised H_2O. The aqueous layer was made acidic to pH 1 and extracted into CH_2Cl_2. The organic layers were dried over $MgSO_4$ and evaporated. The crude product was additionally purified by flash chromatography (EtOAc:Cyclohexane, 2:1) to yield the desired compound as yellow solid (100 mg, 51%). M.p. = 320.8 ˚C (decomposed); ^{1}H NMR (500.1 MHz, $CDCl_3$ + 3 drops of d_6-DMSO): δ_H 8.23 (2H, s; 2×Ar*H*), 8.18 (1H, br s; Ar*H*), 7.94 (2H, d, $^3J_{HH}$ 8.3 Hz; 2×Ar*H*), 7.91 (2H, t, $^3J_{HH}$ 4.7 Hz; 2×N*H*), 7.49 (2H, d, $^3J_{HH}$ 8.3 Hz; 2×Ar*H*), 7.22 (8H, m; 8×Ar*H*), 4.52 (4H, d, $^3J_{HH}$ 4.8 Hz; 2×CH_2), 4.32 (4H, s; 2×CH_2), 3.46 (8H, s; 4×CH_2); ^{13}C NMR (100.6 MHz, $CDCl_3$ + 3 drops of d_6-DMSO): δ_C 167.6 (*C*=O), 165.6 (*C*=O), 137.8 (Ar*C*), 137.2 (Ar*C*), 134.4 (Ar*C*H), 134.1 (Ar*C*), 131.4 (Ar*C*H), 130.5 (Ar*C*), 129.8 (Ar*C*H), 129.4 (Ar*C*H), 128.8 (Ar*C*H), 126.9 (Ar*C*), 124.2 (Ar*C*H), 123.7 (Ar*C*), 90.6 (q*C*), 89.8 (q*C*), 73.3 (*C*H_2), 70.6 (*C*H_2), 69.2 (*C*H_2), 44.2 (*C*H_2); MS (ES$^+$) *m/z* 641.0 ([M+Na]$^+$, 100); HRMS (ES$^+$) *m/z* calculated for $C_{37}H_{34}N_2O_7Na$ [M+Na]$^+$ 641.2264, found 641.2247.

Macrocycle 168

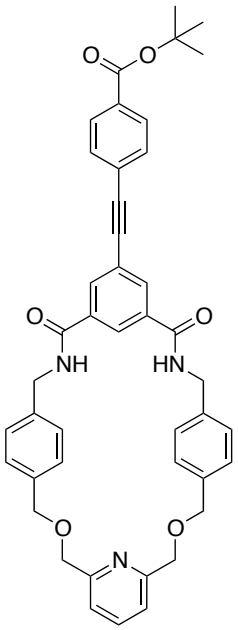

A degassed (by bubbling Ar) solution of alkyne **166** (0.11 g, 0.55 mmol) in Et_3N (35 mL) was cannulated into a degassed (by bubbling Ar) suspension of macrocycle **158** (0.32 g, 0.50 mmol), PPh_3 (24 mg, 0.09 mmol), CuI (13 mg, 0.07 mmol), $PdCl_2(PPh_3)_2$ (35 mg, 0.05 mmol) and Et_3N (3 mL) in dry THF (6 mL). The reaction mixture was heated to 65 ˚C under an Ar atmosphere for 48 h, and then filtered through a pad of Celite. The filtrate was concentrated by evaporation in *vacuo*. The residue was dissolved in $CHCl_3$. The organic layer was washed with water, dried ($MgSO_4$) and concentrated by evaporation in *vacuo*. The residue was purified by column chromatography ($CHCl_3$:EtOAc, 1:1) to give a colorless solid (0.20 g, 56%). M.p. = 255.2 ˚C (decomposed); ^{1}H NMR (400.1 MHz, $CDCl_3$) : δ_H 8.19 (2H, br s; 2×Ar*H*), 7.99 (2H, d, $^3J_{HH}$ 8.6 Hz; 2×Ar*H*), 7.85 (1H, br s; Ar*H*), 7.74 (1H, t, $^3J_{HH}$ 7.5 Hz; Ar*H*), 7.58 (2H, d, $^3J_{HH}$ 8.4 Hz; 2×Ar*H*), 7.39 (2H, d, $^3J_{HH}$ 7.6 Hz; 2×Ar*H*), 7.30 (8H, s; 8×Ar*H*), 6.53 (2H, br s; 2×N*H*), 4.64 (4H, s; 2×CH_2), 4.57 (4H, d, $^3J_{HH}$ 5.8 Hz; 2×CH_2), 4.40 (4H, s; 2×CH_2), 1.61 (9H, s; 3×CH_3); ^{13}C NMR (100.6 MHz, $CDCl_3$) : δ_C 165.9 (*C*=O), 165.2 (*C*=O), 157.5 (Ar*C*), 137.6 (Ar*C*), 137.4 (Ar*C*H), 137.3 (Ar*C*), 135.3 (Ar*C*), 133.6 (Ar*C*H), 132.0 (Ar*C*), 131.6 (Ar*C*H), 129.5 (Ar*C*H), 129.0 (Ar*C*H), 128.8 (Ar*C*H), 126.7 (Ar*C*), 124.4 (Ar*C*), 124.1 (Ar*C*), 120.2 (Ar*C*H), 90.8 (q*C*), 90.2 (q*C*), 81.6 (q*C*), 72.4 (*C*H_2), 71.6 (*C*H_2), 44.4 (*C*H_2), 28.3 (*C*H_3); MS (ES$^+$) *m/z* 730 ([M+Na]$^+$, 100); HRMS (ES$^+$) *m/z* calculated for $C_{44}H_{41}N_3O_6Na$ [M+Na]$^+$ 730.2893, found 730.2877.

Macrocycle AEMP

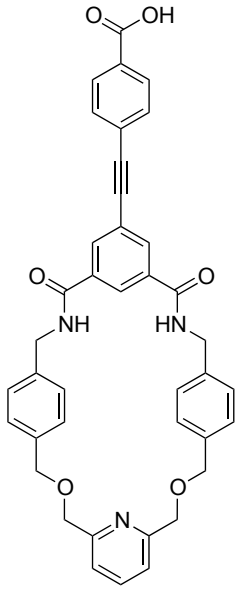

To a solution of ester macrocycle **168** (0.28 g, 0.39 mmol) in CH_2Cl_2 (15 mL) was added at 0 ˚C trifluoroacetic acid in excess. Triethylsilane (0.12 mL, 0.77 mmol) was added dropwise into the resulting mixture. The resulting solution was left stirred at ambient temperature for 16 h. The solvent was reduced *in vacuo*, diluted with CH_2Cl_2 and washed with deionised H_2O. The aqueous layer was adjusted to pH 1 and extracted into CH_2Cl_2. The organic layers were dried over $MgSO_4$ and evaporated. The crude product was additionally purified by flash chromatography (EtOAc:Cyclohexane, 2:1) to yield the desired compound as colourless solid (160 mg, 63%). M.p. = 294.5 ˚C (decomposed); ^{1}H NMR (500.1 MHz, $CDCl_3$ + 3 drops of d_6-DMSO) : δ_H 8.23 (2H, s; 2×Ar*H*), 8.19 (1H, s; Ar*H*), 7.98 (2H, t, $^3J_{HH}$ 4.6 Hz; 2×N*H*), 7.92 (2H, d, $^3J_{HH}$ 8.3 Hz; 2×Ar*H*), 7.60 (1H, t, $^3J_{HH}$ 7.7 Hz, Ar*H*), 7.47 (2H, d, $^3J_{HH}$ 8.3 Hz; 2×Ar*H*), 7.24 – 7.19 (10H, m; 10×Ar*H*), 4.53 (4H, d, $^3J_{HH}$ 5.1 Hz; 2×CH_2), 4.49 (4H, s; 2×CH_2), 4.26 (4H, s; 2×CH_2); ^{13}C NMR (100.6 MHz, $CDCl_3$+ 3 drops of d_6-DMSO): δ_C 167.6 (*C*=O), 165.4 (*C*=O), 156.9 (Ar*C*), 138.2 (Ar*C*), 137.2 (Ar*C*H), 136.8 (Ar*C*), 134.3 (Ar*C*H), 134.1 (Ar*C*), 131.6 (Ar*C*), 131.3 (Ar*C*H), 130.4 (Ar*C*), 129.7 (Ar*C*H), 129.3 (Ar*C*H), 128.9 (Ar*C*H), 126.8 (Ar*C*), 124.0 (Ar*C*H), 120.8 (Ar*C*H), 90.6 (q*C*), 89.7 (q*C*), 72.4 (*C*H_2), 71.6 (*C*H_2), 43.9 (*C*H_2). MS (ES^-) *m/z* 650 ([M–H]$^-$, 100); HRMS (ES^-) *m/z* calculated for $C_{40}H_{32}N_3O_6$ [M–H]$^-$ 650.2291, found 650.2290.

Macrocycle 169

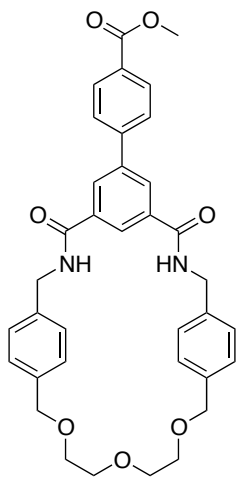

The 4-(methoxycarbonyl)phenylboronic acid (33 mg, 0.18 mmol) and potassium carbonate (37 mg, 0.27 mmol) were dissolved in the mixture of THF and H_2O (10 mL). Following this, $PdCl_2(PPh_3)_2$ (7 mg, 0.009 mmol) was added together with macrocycle **161** (50 mg, 0.09 mmol), all under the Ar atmosphere. The reaction mixture was left stirred for 16 h. The reaction was filtered through a pad of Celite and the solvent was then removed in *vacuo*. The crude was washed with water and extracted into $CHCl_3$, dried ($MgSO_4$), filtered, and concentrated before column chromatography was used to purify to give the product as colorless solid (48 mg, 87%). M.p. = 275.6 – 279.6 ˚C; ^{1}H NMR (400.1 MHz, $CDCl_3$) : δ_H 8.28 (2H, s; 2×Ar*H*), 8.05 (2H, d, $^3J_{HH}$ 8.5 Hz; 2×Ar*H*), 7.86 (1H, s; Ar*H*), 7.66 (2H, d, $^3J_{HH}$ 8.4 Hz; 2×Ar*H*), 7.24 (8H, s; 8×Ar*H*), 6.86 (2H, br s; 2×N*H*), 4.52 (4H, d, $^3J_{HH}$ 5.3 Hz; 2×CH_2), 4.45 (4H, s; 2×CH_2), 3.86 (3H, s; CH_3), 3.67 – 3.57 (8H, m; 4×CH_2); ^{13}C NMR (100.6 MHz, $CDCl_3$) : δ_C 167.0 (*C*=O), 166.6 (*C*=O), 143.6 (Ar*C*), 141.4 (Ar*C*), 137.8 (Ar*C*), 137.2 (Ar*C*), 135.5 (Ar*C*), 130.4 (Ar*C*H), 130.1 (Ar*C*H), 129.9 (Ar*C*H), 129.8 (Ar*C*), 128.7 (Ar*C*H), 127.4 (Ar*C*H), 123.4 (Ar*C*H), 73.2 (*C*H_2), 70.8 (*C*H_2), 69.7 (*C*H_2), 52.4 (*C*H_3), 44.5 (*C*H_2); MS (ES$^+$) *m/z* 631 ([M+Na]$^+$, 100); HRMS (ES$^+$) *m/z* calculated for $C_{36}H_{36}N_2O_7Na$ [M+Na]$^+$ 631.2420, found 631.2410.

Macrocycle APMDG

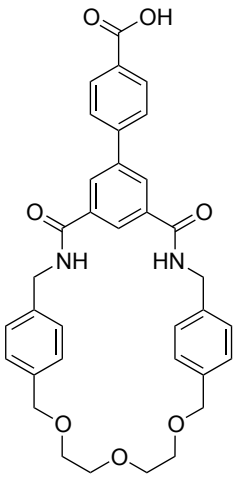

To a suspension of ester macrocycle **169** (0.15 g, 0.24 mmol) in dry THF (10 mL), potassium trimethyl silanolate (37 mg, 0.24 mmol) was added. The reaction mixture was refluxed at 75 ˚C for 16 h. After the resulting solution was evaporated to dryness, distilled water was added to residue. HCl conc. was added dropwise until the pH reached 3.0. The suspension was then filtered and the residue was washed with water, and dried under high vacuum to a constant mass to give the product as colourless solid (100 mg, 70%). M.p. = 292.6 – 295.8 ˚C; ^{1}H NMR (500.1 MHz, $CDCl_3$ + 3 drops of d_6-DMSO): δ_H 8.35 (2H, s; 2×Ar*H*), 8.19 (1H, s; Ar*H*), 8.02 (2H, d, $^{3}J_{HH}$ 8.4 Hz; 2×Ar*H*), 7.94 (2H, t, $^{3}J_{HH}$ 4.8 Hz; 2×N*H*), 7.66 (2H, d, $^{3}J_{HH}$ 8.4 Hz; 2×Ar*H*), 7.24 – 7.18 (8H, m; 8×Ar*H*), 4.53 (4H, d, $^{3}J_{HH}$ 4.7 Hz; 2×CH_2), 4.30 (4H, s; 2×CH_2), 3.45 (8H, s; 4×CH_2); ^{13}C NMR (100.6 MHz, $CDCl_3$ + 3 drops of d_6-DMSO): δ_C 168.1 (*C*=O), 166.2 (*C*=O), 143.5 (Ar*C*), 140.4 (Ar*C*), 137.8 (Ar*C*), 137.1 (Ar*C*), 134.4 (Ar*C*), 130.2 (Ar*C*), 130.1 (Ar*C*H), 130.1 (Ar*C*H), 129.3 (Ar*C*H), 128.6 (Ar*C*H), 126.8 (Ar*C*H), 123.6 (Ar*C*H), 73.3 (*C*H_2), 70.4 (*C*H_2), 69.2 (*C*H_2), 44.1 (*C*H_2); MS (ES$^+$) *m/z* 617 ([M+Na]$^+$, 100); HRMS (ES$^+$) *m/z* calculated for $C_{35}H_{34}N_2O_7Na$ [M+Na]$^+$ 617.2264, found 617.2254.

Macrocycle 170

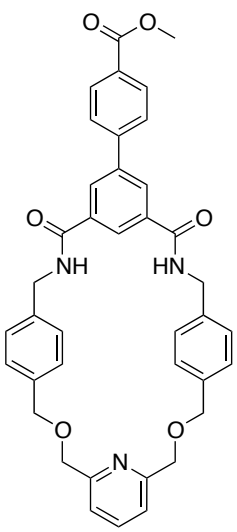

The 4-(methoxycarbonyl)phenylboronic acid (36 mg, 0.20 mmol) and potassium carbonate (41 mg, 0.30 mmol) were dissolved in the mixture of THF and H_2O (10 mL). Following this, $PdCl_2(PPh_3)_2$ (7 mg, 0.009 mmol) was added together with macrocycle **162** (53 mg, 0.09 mmol) all under the Ar atmosphere. The reaction mixture was left stirred for 16 h. TLC showed consumption of the starting materials and so the reaction was filtered through a pad of Celite and the solvent was

then removed in *vacuo*. The crude material was washed with water and extracted into $CHCl_3$, dried ($MgSO_4$), filtered, and concentrated before column chromatography was used to purify to give the product as colorless solid (45 mg, 78%). M.p. = 255.7 – 259.7 ˚C; ^{1}H NMR (400.1 MHz, $CDCl_3$) : δ_H 8.31 (2H, d, $^3J_{HH}$ 1.5 Hz; 2×Ar*H*), 8.13 (2H, d, $^3J_{HH}$ 8.6 Hz; 2×Ar*H*), 7.84 (1H, br s; Ar*H*), 7.77 (1H, t, $^3J_{HH}$ 7.8 Hz; Ar*H*), 7.72 (2H, d, $^3J_{HH}$ 8.6 Hz; 2×Ar*H*), 7.39 (2H, d, $^3J_{HH}$ 7.7 Hz; 2×Ar*H*), 7.31 (8H, s; 8×Ar*H*), 6.58 (2H, br s; 2×N*H*), 4.65 (4H, s; 2×CH_2), 4.60 (4H, d, $^3J_{HH}$ 5.5 Hz; 2×CH_2), 4.43 (4H, s; 2×CH_2), 3.95 (3H, s; CH_3); ^{13}C NMR (100.6 MHz, $CDCl_3$) : δ_C 167.0 (*C*=O), 166.5 (*C*=O), 157.3 (Ar*C*), 143.7 (Ar*C*), 141.3 (Ar*C*), 137.8 (Ar*C*H), 137.6 (Ar*C*), 137.2 (Ar*C*), 135.6 (Ar*C*), 130.0 (Ar*C*H), 129.9 (Ar*C*H), 129.8 (Ar*C*), 129.4 (Ar*C*H), 128.8 (Ar*C*H), 127.2 (Ar*C*H), 123.3 (Ar*C*H), 120.4 (Ar*C*H), 72.2 (*C*H_2), 71.0 (*C*H_2), 52.1 (*C*H_3), 44.2 (*C*H_2); MS (ES$^+$) *m/z* 664 ([M+Na]$^+$,15), 301 (100); HRMS (ES$^+$) *m/z* calculated for $C_{39}H_{35}N_3O_6Na$ [M+Na]$^+$ 664.2424, found 664.2429.

Macrocycle APMP

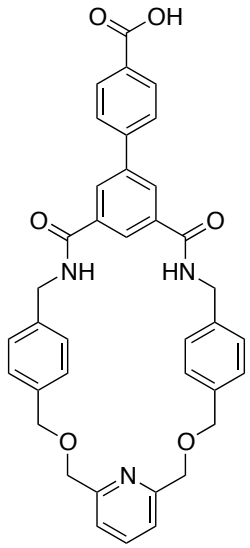

To a suspension of ester macrocycle **170** (0.30 g, 0.47 mmol) in dry THF (10 mL), potassium trimethyl silanolate (72 mg, 0.56 mmol) was added. The reaction mixture was refluxed at 75 ˚C for 16 h. After the resulting solution was evaporated to dryness, distilled water was added to residue. HCl conc. was added dropwise until the pH reached 3.0. The suspension was filtered and the residue was washed with water, and dried under high vacuum to a constant mass to give the product as colourless solid (0.22 g, 76%). M.p. = 312.8 – 315.4 ˚C; ^{1}H NMR (500.1 MHz, $CDCl_3$ + 3 drops of d_6-DMSO): δ_H 8.39 (2H, d, $^3J_{HH}$ 1.3 Hz; 2×Ar*H*), 8.23 (1H, s; Ar*H*), 8.03 (2H, d, $^3J_{HH}$ 8.4 Hz; 2×Ar*H*), 7.99 (2H, t, $^3J_{HH}$ 5.1 Hz; 2×N*H*), 7.68 (2H, d, $^3J_{HH}$ 8.4 Hz; 2×Ar*H*), 7.61 (1H, t, $^3J_{HH}$ 7.6 Hz; Ar*H*), 7.25 – 7.21 (10H, m; 10×Ar*H*), 4.57 (4H, d, $^3J_{HH}$ 5.1 Hz; 2×CH_2), 4.50 (4H, s; 2×CH_2), 4.28 (4H, s; 2×CH_2); ^{13}C NMR (100.6 MHz, $CDCl_3$ + 3 drops of d_6-DMSO): δ_C 168.2 (*C*=O), 166.1 (*C*=O), 156.9 (Ar*C*), 143.6 (Ar*C*), 140.6 (Ar*C*), 138.4 (Ar*C*), 137.2 (Ar*C*H), 136.9 (Ar*C*), 134.4 (Ar*C*), 130.2 (Ar*C*H), 130.2 (Ar*C*), 130.0 (Ar*C*H), 129.3 (Ar*C*H), 128.6 (Ar*C*H), 126.9 (Ar*C*H), 123.5 (Ar*C*H), 120.7 (Ar*C*H), 72.4 (*C*H_2), 71.7 (*C*H_2), 43.9 (*C*H_2); MS (ES$^+$) *m/z* 628 ([M+H]$^+$, 100); HRMS (ES$^+$) *m/z* calculated for $C_{38}H_{34}N_3O_6$

$[M+H]^+$ 628.2448, found 628.2452.

1,3-Di-tert-butyl-5-(2,2-dibromovinyl)benzene 172[273]

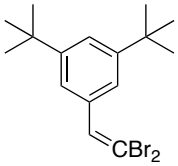

PPh_3 (26.2 g, 0.10 mol) and zinc powder (6.54 g, 0.10 mol) were dissolved in dry CH_2Cl_2 (120 mL). Tetrabromoethane, CBr_4 (33.2 g, 0.10 mol) was added at 0 ˚C. After 2 h, 3,5-di-tert-butylbenzaldehyde **171** (10.92 g, 50.0 mmol) was added neat to the solution and the reaction was left to stir for another 2 h at ambient temperature before cyclohexane (180 mL) was added. Filtration through a short plug of silica using cyclohexane as eluent and removal of the solvent in *vacuo* yielded the intermediate **172** and was used without further purification (15.2 g, 81%). ^{1}H NMR (300.1 MHz, $CDCl_3$): δ_H 7.53 (1H, s; C*H*), 7.42 (3H, m, 3×Ar*H*), 1.36 (18H, s; 6×CH_3); ^{13}C NMR (75.5 MHz, $CDCl_3$): δ_C 150.8 (Ar*C*), 137.8 (Ar*C*H), 134.5 (Ar*C*), 122.8 (Ar*C*H), 122.7 (Ar*C*H), 88.5 (*C*H), 34.9 (q*C*), 31.4 (*C*H_3).

1,3-Di-tert-butyl-5-ethynylbenzene 173[273]

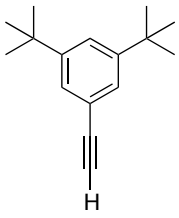

1,3-di-*tert*-butyl-5-(2,2-dibromovinyl)benzene **172** (1.0 g, 2.67 mmol) in dry THF (70 mL) was treated with *N*-butyllithium (2.5 M, 2.25 mL, 5.61 mmol). The solution was kept at –78 ˚C for 1.5 h before being allowed to warm up to ambient temperature and left stirred for 16 h. The following day, the reaction was quenched with sat. NH_4Cl solution and the mixture was extracted with CH_2Cl_2. The combined organic layers were dried over $MgSO_4$, filtered and concentrated *in vacuo* to directly yield the terminal alkyne **173** as a colourless solid (0.33 g, 58%). M.p. = 88.3 – 89.2 ˚C (lit.[274] 84 – 85 ˚C). ^{1}H NMR (300.1 MHz, $CDCl_3$): δ_H 7.43 (1H, dd, $^4J_{HH}$ 1.9 and $^4J_{HH}$ 1.9 Hz; Ar*H*), 7.37 (2H, d, $^4J_{HH}$ 1.9 Hz; 2×Ar*H*), 3.04 (1H, s; *CH*), 1.33 (18H, s; 6×CH_3). ^{13}C NMR (75.5 MHz, $CDCl_3$): δ_C 151.0 (Ar*C*), 126.5 (Ar*C*H), 123.4 (Ar*C*H), 121.2 (Ar*C*), 85.0 (*C*H), 75.9 (*C*H), 34.9 (q*C*), 31.4 (*C*H_3). MS (EI^+) *m/z* 214.2 ($[M+H]^+$, 10); HRMS (ES^+) *m/z* calculated for $C_{16}H_{22}$ $[M+H]^+$ 214.1722, found 214.1725.

1,3-Di-*tert*-butyl-5-((4-nitrophenyl)ethynyl)benzene 174

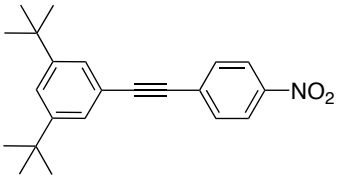

1-iodo-4-nitrobenzene (0.53 g, 2.12 mmol) was suspended in Et_3N (50 mL). PPh_3 (56 mg, 0.21 mmol), CuI (32 mg, 0.17 mmol) and $PdCl_2(PPh_3)_2$ (120 mg, 0.17 mmol) were added neat and the mixture was degassed with Ar for 40 min. Alkyne **173** (0.50 g, 2.33 mmol) was added *via* syringe under a protective Ar atmosphere and the mixture was heated at 50 ˚C for 16 h. The occurring brown solution was filtered through Celite, concentrated and purified by silica gel column chromatography (Hexane:EtOAc, 10:1) affording the nitro compound **174** as a yellow solid (0.63 g, 81%). M.p. = 161.3 – 162.9 ˚C; ^{1}H NMR (300.1 MHz, $CDCl_3$): δ_H 8.22 (2H, d, $^3J_{HH}$ 8.9 Hz; 2×Ar*H*), 7.68 (2H, d, $^3J_{HH}$ 8.9 Hz; 2×Ar*H*), 7.47 (1H, t, $^4J_{HH}$ 1.8 Hz; Ar*H*), 7.42 (2H, d, $^4J_{HH}$ 1.8 Hz; 2×Ar*H*), 1.35 (18H, s; 6×CH_3); ^{13}C NMR (75.5 MHz, $CDCl_3$): δ_C 151.3 (Ar*C*), 147.0 (Ar*C*H), 132.4 (Ar*C*H), 130.7 (Ar*C*), 126.2 (Ar*C*H), 124.0 (Ar*C*H), 123.8 (Ar*C*H), 121.2 (Ar*C*), 96.2 (*C*H), 86.6 (*C*H), 35.0 (q*C*), 31.5 (*C*H_3); MS (ES^+) *m/z* 358.03 ($[M+Na]^+$, 100); HRMS (ES^+) *m/z* calculated for $C_{22}H_{25}NO_2Na$ $[M+Na]^+$ 358.1783, found 358.1785.

(*Z*)-4-((3,5-Di-*tert*-butylphenyl)ethynyl)-*N*-(4-((4,6-dimethylpyridin-2-yl)carbamoyl)benzylidene)aniline oxide 176

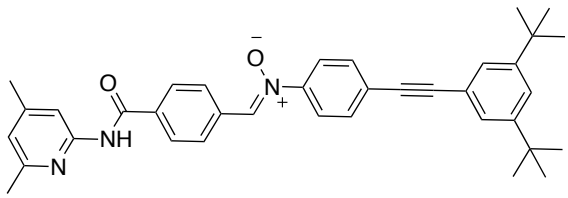

Nitro compound **174** (100 mg, 298 µmol) was dissolved in THF (10 mL). Rhodium (36 mg, 5 wt.% on carbon, wet) and hydrazine monohydrate (20 mg, 400 µmol) were added and the reaction was followed by TLC (Hexane:EtOAC, 3:1). After completion, the solution was filtered through Celite and concentrated *in vacuo* to obtain the desired intermediate hydroxylamine **175** product as a yellow oil, which was directly used in the next step without further purification. The obtained hydroxylamine (286 µmol) was dissolved in EtOH (15 mL) and aldehyde **117** (58 mg, 229 µmol) was added neat. The solution was left to stand in the dark for 3 days at ambient temperature before the resulting precipitate was filtered to give the nitrone **176** as

yellow solid (50 mg, 39% over 2 steps). M.p. = 211.8 - 213.4 ˚C; ^{1}H NMR (300.1 MHz, $CDCl_3$): δ_H 8.52 (2H, d, $^{3}J_{HH}$ 8.5 Hz; 2×Ar*H*), 8.49 (1H, s; N*H*CO), 8.05 (3H, s; 3×Ar*H*), 8.02 (1H, s; C*H*), 7.81 (2H, d, $^{3}J_{HH}$ 8.7 Hz; 2×Ar*H*), 7.68 (2H, d, $^{3}J_{HH}$ 8.7 Hz; 2×Ar*H*), 7.45 (1H, s; Ar*H*), 7.41 (2H, d, $^{4}J_{HH}$ 1.7 Hz; 2×Ar*H*), 6.80 (1H, s; Ar*H*), 2.45 (3H, s; CH_3), 2.38 (3H, s; CH_3), 1.35 (18H, s; 6×CH_3); ^{13}C NMR (100.6 MHz, $CDCl_3$): δ_C 164.7 (*C*=O), 156.8 (Ar*C*), 151.2 (Ar*C*), 150.8 (Ar*C*), 150.5 (Ar*C*), 148.1 (Ar*C*), 136.0 (Ar*C*), 134.0 (Ar*C*), 133.4 (*C*H), 132.5 (Ar*C*H), 129.3 (Ar*C*H), 127.7 (Ar*C*H), 126.2 (Ar*C*), 126.1 (Ar*C*H), 123.5 (Ar*C*H), 121.8 (Ar*C*H), 121.7 (Ar*C*), 121.0 (Ar*C*H), 111.8 (Ar*C*H), 93.4 (q*C*), 86.9 (q*C*), 35.3 (q*C*), 31.3 (*C*H_3), 24.0 (*C*H_3), 21.5 (*C*H_3); MS (ES^+) *m/z* 558.29 ([M+H]$^+$, 100); HRMS (ES^+) *m/z* calculated for $C_{37}H_{40}N_3O$ [M+H]$^+$ 558.3121, found 558.3126.

(Anthracen-9-ylethynyl)trimethylsilane 178[259]

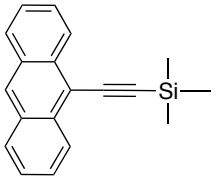

A solution of 9-bromoanthracene **177** (4.0 g, 15.6 mmol), CuI (237 mg, 1.24 mmol), $PdCl_2(PPh_3)_2$ (0.87 g, 1.24 mmol) and PPh_3 (0.60 g, 2.63 mmol) in Et_3N (110 mL) was reacted (110 mL) with (trimethylsilyl)acetylene (7.66 g, 11.0 mL, 78.0 mmol) under Ar atmosphere at 80 ˚C for 24 h. The solution obtained was filtered through a pad of Celite and concentrated *in vacuo*. The crude was purified by column chromatography (Cyclohexane) affording a yellow solid of **178** (3.72 g, 87%). M.p. = 82.1 – 84.4 ˚C; ^{1}H NMR (300.1 MHz, $CDCl_3$): δ_H 8.57 (2H, dd, $^{4}J_{HH}$ 1.1 and $^{3}J_{HH}$ 8.7 Hz; 2×Ar*H*), 8.42 (1H, s; Ar*H*), 8.00 (2H, dt, $^{4}J_{HH}$ 0.6 and $^{3}J_{HH}$ 8.4 Hz; 2×Ar*H*), 7.59 (2H, ddd, $^{4}J_{HH}$ 1.4, $^{3}J_{HH}$ 6.6 and $^{3}J_{HH}$ 8.6 Hz; 2×Ar*H*), 7.50 (2H, ddd, $^{4}J_{HH}$ 1.4, $^{3}J_{HH}$ 6.7, $^{3}J_{HH}$ 8.2 Hz; 2×Ar*H*), 0.44 (9H, s; 3×CH_3); ^{13}C NMR (75.5 MHz, $CDCl_3$): δ_C 133.0 (Ar*C*), 131.2 (Ar*C*), 128.8 (Ar*C*H), 128.0 (Ar*C*H), 126.9 (Ar*C*H), 126.8 (Ar*C*H), 125.8 (Ar*C*H), 117.2 (Ar*C*), 106.3 (q*C*), 101.7 (q*C*), 0.4 (*C*H_3); MS (CI^+) *m/z* 275.1 ([M+H]$^+$, 100); HRMS (CI^+) *m/z* calculated for $C_{19}H_{19}Si$ [M+H]$^+$ 275.1256, found 275.1249.

9-((4-Nitrophenyl)ethynyl)anthracene 180[275]

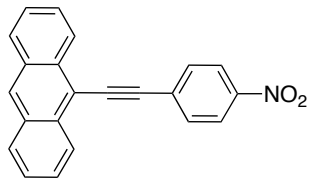

The protected acetylene **178** (1.20 g, 7.29 mmol) was dissolved in a 1:1 mixture of dry THF and MeOH (50 mL).

Potassium carbonate (5.04 g, 36.5 mmol) was added to the solution, which was stirred under Ar atmosphere for 4 h at ambient temperature, before quenched with distilled water (80 mL). The aqueous phase was extracted with CH_2Cl_2. The organic fractions were collected, dried ($MgSO_4$), filtered and concentrated to 10% of the original volume to give[259] the terminal alkyne **179**. Et_3N (100 mL) were then added as a solvent for the subsequent conversion. CuI (101 mg, 0.53 mmol), $PdCl_2(PPh_3)_2$ (372 mg, 0.53 mmol), PPh_3 (174 mg, 0.66 mmol) and 1-iodo-4-nitrobenzene (1.65 g, 6.63 mmol) were added to the solution simultaneously under Ar atmosphere, which was stirred at 50 ˚C for 24 h. The solution was filtered through a pad of Celite, concentrated and purified by column chromatography (Hexane:EtOAc, 10:1) to yield the product as a red solid (1.59 g, 67%). M.p. = 203.4 – 205.7 ˚C; ^{1}H NMR (300.1 MHz, $CDCl_3$): δ_H 8.59 (2H, dd, $^4J_{HH}$ 1.0 and $^3J_{HH}$ 8.6 Hz; 2×Ar*H*), 8.50 (1H, s; Ar*H*), 8.28 (2H, d, $^3J_{HH}$ 9.0 Hz; 2×Ar*H*), 8.05 (2H, dt, $^4J_{HH}$ 0.6 and $^3J_{HH}$ 8.4 Hz; 2×Ar*H*), 7.86 (2H, d, $^3J_{HH}$ 9.0 Hz; 2×Ar*H*), 7.64 (2H, ddd, $^4J_{HH}$ 1.5, $^3J_{HH}$ 6.8 and $^3J_{HH}$ 8.5 Hz; 2×Ar*H*), 7.55 (2H, ddd, $^4J_{HH}$ 1.3, $^3J_{HH}$ 6.7 and $^3J_{HH}$ 8.2 Hz; 2×Ar*H*); ^{13}C NMR (75.5 MHz, $CDCl_3$): δ_C 147.1 (Ar*C*-NO_2), 133.0 (Ar*C*), 132.3 (Ar*C*H), 131.2 (Ar*C*), 130.6 (Ar*C*), 129.3 (Ar*C*H), 129.1 (Ar*C*H), 127.3 (Ar*C*H), 126.5 (Ar*C*H), 126.0 (Ar*C*H), 123.9 (Ar*C*H), 115.9 (Ar*C*), 98.9 (q*C*), 92.0 (q*C*); MS (ES^+) *m/z* 346.84 ([M+Na]$^+$, 100).

(Z)-4-(Anthracen-9-ylethynyl)-N-(4-((4,6-dimethylpyridin-2-yl)carbamoyl)benzylidene)aniline oxide 182

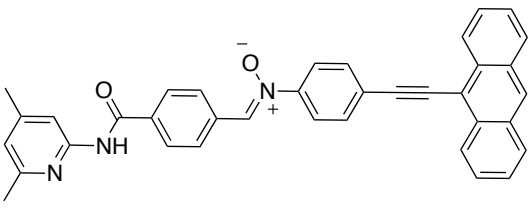

9-((4-nitrophenyl)ethynyl)anthracene **180** (0.20 g, 0.62 mmol) in THF (20 mL) was reacted with Rhodium (40 mg, 10 wt. % on carbon, wet), before being slowly reacted with hydrazine monohydrate (0.12 mL, 0.74 mmol). The reaction was stirred for 2 h and monitored by TLC until the disappearance of the starting material. The solution was filtered through a pad of Celite and the solvent was then removed to give the intermediate red solid hydroxylamine (0.62 mmol), which was sufficiently pure to carry out to the next step. The hydroxylamine **181** was subsequently dissolved in EtOH (4 mL) and added to a solution of aldehyde **117** (157 mg, 0.62 mmol) in EtOH (15 mL). The reaction mixture was kept in the dark for 3 days at ambient temperature. The resulting precipitate was filtered, washed with hexane and dried in

vacuum to give nitrone **182** (0.27 g, 81%). M.p. = 196.4 – 199.2 ˚C; ^{1}H NMR (400.1 MHz, $CDCl_3$): δ_H 8.63 (2H, d, $^{3}J_{HH}$ 8.6 Hz; 2×Ar*H*), 8.59 (1H, br s; N*H*), 8.55 (2H, d, $^{3}J_{HH}$ 8.5 Hz; 2×Ar*H*), 8.49 (1H, s; Ar*H*), 8.09 (1H, s; C*H*), 8.06 (3H, s; 3×Ar*H*), 8.04 (2H, m; 2×Ar*H*), 7.91 (2H, d, $^{3}J_{HH}$ 9.1 Hz; 2×Ar*H*), 7.88 (2H, d, $^{3}J_{HH}$ 9.0 Hz; 2×Ar*H*), 7.66 – 7.62 (2H, m; 2×Ar*H*), 7.56 – 7.53 (2H, m; 2×Ar*H*), 6.80 (1H, s; Ar*H*), 2.45 (3H, s; CH_3), 2.38 (3H, s; CH_3); ^{13}C NMR (100.6 MHz, $CDCl_3$): δ_C 164.7 (*C*=O), 156.4 (Ar*C*), 150.5 (Ar*C*), 150.4 (Ar*C*), 148.3 (Ar*C*), 136.0 (Ar*C*), 133.9 (Ar*C*), 133.1 (*C*H), 132.9 (Ar*C*), 132.2 (Ar*C*H), 131.3 (Ar*C*), 128.9 (Ar*C*H), 128.7 (Ar*C*H), 128.2 (Ar*C*H), 127.4 (Ar*C*H), 126.8 (Ar*C*H), 126.4 (Ar*C*H), 126.2 (Ar*C*), 125.6 (Ar*C*H), 121.7 (Ar*C*H), 120.6 (Ar*C*H), 116.5 (Ar*C*), 111.5 (Ar*C*H), 99.3 (q*C*), 89.2 (q*C*), 23.6 (*C*H_3), 21.2 (*C*H_3); MS (ES$^+$) *m/z* 568 ([M+Na]$^+$, 100); HRMS (ES$^+$) *m/z* calculated for $C_{37}H_{28}N_3O_2$ [M+H]$^+$ 546.2182, found 546.2183.

5-Iodo-6-ethylpyridin-2-amine 184[276]

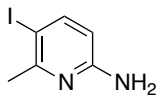

2-Amino-6-picoline **183** (5.4 g, 50.0 mmol) was dissolved in CH_3COOH (50 mL) and H_2SO_4 conc. (7.5 mL) and stirred at 60 ˚C for 0.5 h before addition of HIO_4 (1.63 g, 7.1 mmol) and iodine (5.4 g, 21.3 mmol). The reaction solution was then stirred at 60 ˚C for 20 h and upon completion, the solvent was removed under reduced pressure and the residues were dissolved in water (100 mL). The pH was adjusted to 14 with 5M KOH solution and extracted into CH_2Cl_2. The combined organic fractions were dried ($MgSO_4$), filtered and the solvent was removed *in vacuo* to yield the crude product, which was recrystallised in CH_2Cl_2 to yield the product **184** (9.98 g, 85%) as a colourless powder. M.p. = 98.8 – 100.2 ˚C (lit.[276] 100 ˚C); ^{1}H NMR (400.1 MHz, $CDCl_3$): δ_H 7.66 (1H, d, $^{3}J_{HH}$ 8.7 Hz; Ar*H*), 6.09 (1H, dd, $^{3}J_{HH}$ 8.5 Hz and $^{4}J_{HH}$ 0.6 Hz; Ar*H*), 4.75 – 4.35 (2H, br s; NH_2), 2.52 (3H, s; CH_3); ^{13}C NMR (100.6 MHz, $CDCl_3$): δ_C 158.1 (Ar*C*), 157.6 (Ar*C*), 147.4 (Ar*C*H), 108.0 (Ar*C*H), 80.6 (Ar*C*), 28.5 (*C*H_3); MS (ES$^+$) *m/z* 234.9 ([M+H]$^+$, 100); HRMS (ES$^+$) *m/z* calculated for $C_6H_8N_2I$ [M+H]$^+$ 234.9732, found 234.9734.

4-Formyl-N-(5-iodo-6-methylpyridin-2-yl)benzamide 185

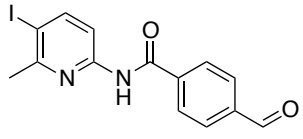

5-iodo-6-methylpyridin-2-amine **184** (6.56 g, 28.0 mmol) and

Et_3N (7.5 mL, 53.0 mmol) were dissolved in CH_2Cl_2 (20 mL) and stirred under N_2 atmosphere at 0 ˚C. A solution of 4-formylbenzoyl chloride **116** (4.5 g, 26.7 mmol) in CH_2Cl_2 (30 mL) was added in a dropwise manner and the solution was slowly allowed to rise to ambient temperature and stirred for 48 h. The reaction was quenched by addition of sat. solution of $NaHCO_3$ (100 mL) and the product was extracted into CH_2Cl_2. The combined organic fractions were washed with 1M HCl, dried ($MgSO_4$), filtered and the solvent removed to give the crude which was purified by recrystallisation in CH_2Cl_2 and yield compound **185** (9.52 g, 93 %) as a colourless solid. M.p. = 180.6 – 181.5 ˚C; ^{1}H NMR (400.1 MHz, $CDCl_3$): δ_H 10.1 (1H, s; C*H*O), 8.50 (1H, br s; N*H*), 8.11 – 8.05 (3H, m; 3×Ar*H*), 8.02 (2H, d, $^3J_{HH}$ 8.5 Hz; 2×Ar*H*), 7.95 (1H, dd, $^3J_{HH}$ 8.6 Hz and $^4J_{HH}$ 0.5 Hz; Ar*H*), 2.65 (3H, s; CH_3); ^{13}C NMR (100.6 MHz, d_6-DMSO): δ_C 192.9 (*C*HO), 165.4 (NH*C*O), 157.9 (Ar*C*), 151.1 (Ar*C*), 147.9 (Ar*C*H), 138.9 (Ar*C*), 138.1 (Ar*C*), 129.2 (Ar*C*H), 128.8 (Ar*C*H), 113.8 (Ar*C*H), 89.4 (Ar*C*-I), 27.9 (*C*H_3); MS (ES^-) *m/z* 365 ([M–H]$^-$, 100); HRMS (ES^-) *m/z* calculated for $C_{14}H_{10}N_2O_2I$ [M–H]$^-$ 364.9787, found 364.9790.

N-(5-(4-(tert-Butyl)phenyl)-6-methylpyridin-2-yl)-4-formylbenzamide 186

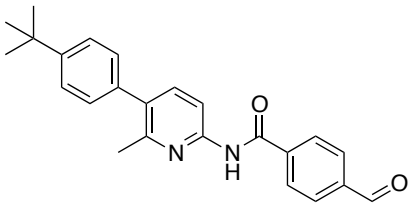

tert-butyl boronic acid (0.48 g, 2.73 mmol) and potassium carbonate (0.57 g, 4.11 mmol) were dissolved in the solvent mixture of THF and H_2O (20 mL). $PdCl_2(PPh_3)_2$ (98 mg, 0.14 mmol) and aldehyde **185** (0.5 g, 1.37 mmol) were added under Ar atmosphere and heated at 70 ˚C for 16 h. The solution was filtered through a pad of Celite and wash thoroughly with THF and extracted into $CHCl_3$. The organic layers were washed twice with distilled water, dried ($MgSO_4$) and the solvents were evaporated under reduced pressure. The residue was purified with a column chromatography using (Hexane:EtOAC, 5:1) yielded the product **186** as yellow solid (0.5 g, 98%). M.p. = 163.7 – 167.5 ˚C; ^{1}H NMR (300.1 MHz, $CDCl_3$): δ_H 10.1 (1H, s; C*H*O), 8.77 (1H, s; N*H*), 8.24 (1H, d, $^3J_{HH}$ 8.4 Hz; Ar*H*), 8.10 (2H, d, $^3J_{HH}$ 8.3 Hz; 2×Ar*H*), 8.01 (2H, d, $^3J_{HH}$ 8.3 Hz; 2×Ar*H*), 7.64 (1H, d, $^3J_{HH}$ 8.4 Hz; Ar*H*), 7.46 (2H, d, $^3J_{HH}$ 8.3 Hz; 2×Ar*H*), 7.26 (2H, d, $^3J_{HH}$ 8.3 Hz; 2×Ar*H*), 2.45 (3H, s; CH_3), 1.37 (9H, s; 3×CH_3); ^{13}C NMR (75.5 MHz, $CDCl_3$): δ_C 191.5 (*C*HO), 164.6 (NH*C*O,), 154.5 (Ar*C*), 150.6 (Ar*C*), 149.3 (Ar*C*), 140.2 (Ar*C*H), 139.6 (Ar*C*), 138.7 (Ar*C*), 136.4 (Ar*C*), 133.9

(Ar*C*), 130.1 (Ar*C*H), 128.9 (Ar*C*H), 128.1 (Ar*C*H), 125.5 (Ar*C*H), 111.6 (Ar*C*H), 34.7 (q*C*), 31.5 (*C*H$_3$), 23.1 (*C*H$_3$); MS (ES$^-$) *m/z* 371 ([M–H]$^-$, 100); HRMS (ES$^-$) *m/z* calculated for $C_{24}H_{23}N_2O_2$ [M–H]$^-$ 371.1760, found 371.1752.

1-Ethynyl-4-nitrobenzene 189[261]

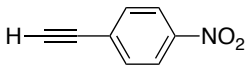

Activated MnO_2 (4.87 g, 56.0 mmol) and KOH (1.58 g, 28.2 mmol) were added to a stirred solution of compound **188** (1.0 g, 5.64 mmol) in CH_2Cl_2 (50 mL). After completion, the mixture was filtered through a pad of Celite, and the filtrate dried over $MgSO_4$ and evaporated to dryness under reduced pressure affording the terminal alkyne **189** as yellow solid (0.67 g, 81%). M.p. = 138.7 – 139.6 ˚C (lit.[277] 140 -142 ˚C); ^{1}H NMR (400.1 MHz, $CDCl_3$): δ_H 8.20 (2H, d, $^3J_{HH}$ 8.9 Hz; 2×Ar*H*), 7.64 (2H, d, $^3J_{HH}$ 8.9 Hz; 2×Ar*H*), 3.36 (1H, s; C*H*); ^{13}C NMR (75.5 MHz, $CDCl_3$): δ_C 147.5 (Ar*C*), 133.1 (Ar*C*H), 129.0 (Ar*C*), 123.7 (Ar*C*H), 82.5 (q*C*), 81.7 (*C*H); MS (CI$^+$) *m/z* 148.04 ([M+H]$^+$, 100); HRMS (CI$^+$) *m/z* calculated for $C_8H_6NO_2$ [M+H]$^+$ 148.0399, found 148.0399.

(*Z*)-*N*-(4-((5-(4-(*tert*-Butyl)phenyl)-6-methylpyridin-2-yl)carbamoyl)benzylidene)-4-(naphthalen-2-ylethynyl)aniline oxide 192

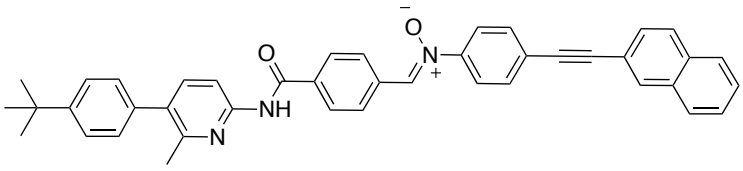

Nitro compound **190** (100 mg, 366 µmol) was dissolved in THF (7 mL). Rhodium (42 mg, 5 wt. % on carbon, wet) and hydrazine monohydrate (21 mg, 439 µmol) were added and the reaction was followed by TLC (Hexane:EtOAC, 3:1). After completion, the solution was filtered through Celite and concentrated *in vacuo* to obtain the intermediate hydroxylamine **191** as a light yellow solid, which was directly used in the next step without further purification. The obtained hydroxylamine **191** (366 µmol) was dissolved in EtOH (15 mL) and aldehyde **186** (109 mg, 293 µmol) was added neat. The solution was left to stand in the dark for 3 days at ambient temperature before the resulting precipitate was filtered to give the nitrone **192** as yellow solid (100 mg, 44% over 2 steps). M.p.= 205.6 ˚C (decomp.); ^{1}H NMR (400.1 MHz, $CDCl_3$): δ_H 8.65 (1H, s; N*H*), 8.54 (2H, d, $^3J_{HH}$ 8.46 Hz; 2×Ar*H*), 8.26 (1H, d, $^3J_{HH}$ 8.34 Hz; Ar*H*), 8.10 (1H, s; Ar*H*), 8.07 (2H, d,

$^4J_{HH}$ 3.37 Hz; 2×Ar*H*), 8.06 (1H, s; C*H*), 7.85 – 7.83 (5H, m; 5×Ar*H*), 7.70 (2H, d, $^3J_{HH}$ 8.58 Hz; 2×Ar*H*), 7.64 (1H, d, $^3J_{HH}$ 8.35 Hz; Ar*H*), 7.60 (1H, d, $^3J_{HH}$ 8.47 Hz; Ar*H*), 7.53 (2H, dd, $^3J_{HH}$ 6.19 and $^4J_{HH}$ 3.23 Hz; 2×Ar*H*), 7.46 (2H, d, $^3J_{HH}$ 8.24 Hz; 2×Ar*H*), 7.28 (2H, d, $^3J_{HH}$ 8.27 Hz; 2×Ar*H*), 2.47 (3H, s; CH_3), 1.38 (9H, s; 3×CH_3); ^{13}C NMR (100.6 MHz, $CDCl_3$): δ_C 164.7 (NH*C*O), 154.5 (Ar*C*), 150.5 (Ar*C*), 149.5 (Ar*C*), 148.2 (Ar*C*), 140.1 (Ar*C*H), 136.5 (Ar*C*), 136.0 (Ar*C*), 133.9 (Ar*C*), 133.6 (Ar*C*), 133.5 (*C*H), 133.2 (Ar*C*), 133.1 (Ar*C*), 132.6 (Ar*C*H), 132.0 (Ar*C*H), 129.3 (Ar*C*H), 129.0 (Ar*C*H), 128.4 (Ar*C*H), 128.3 (Ar*C*H), 128.1 (Ar*C*H), 128.0 (Ar*C*H), 127.7 (Ar*C*H), 127.1 (Ar*C*H), 126.9 (Ar*C*H), 125.9 (Ar*C*), 125.5 (Ar*C*H), 121.9 (Ar*C*H), 120.0 (Ar*C*), 115.1 (CH), 92.6 (q*C*), 88.4 (qC), 34.8 (q*C*), 31.5 (*C*H_3), 23.1 (*C*H_3); MS (ES^+) *m/z* 636.16 ($[M+Na]^+$, 100); HRMS (ES^+) *m/z* calculated for $C_{42}H_{36}N_3O_2$ $[M+H]^+$ 614.2808, found 614.2819.

(*Z*)-*N*-(4-((5-(4-(*tert*-Butyl)phenyl)-6-methylpyridin-2-yl)carbamoyl)benzylidene)-4-((3,5-di-*tert*-butylphenyl)ethynyl)aniline oxide 193

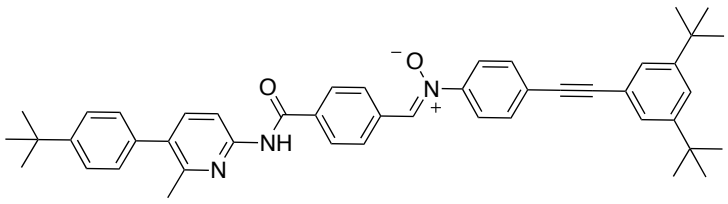

Nitro compound **174** (100 mg, 298 µmol) was dissolved in THF (10 mL). Rhodium (40 mg, 5 wt. % on carbon, wet) and hydrazine monohydrate (30 mg, 596 µmol) were added and the reaction was followed by TLC (Hexane:EtOAC, 3:1). After completion, the solution was filtered through celite and concentrated *in vacuo* to obtain the desired intermediate hydroxylamine **175** product as a yellow solid, which was directly used in the next step without further purification. The obtained hydroxylamine **175** (299 µmol) was dissolved in EtOH (15 mL) and aldehyde **186** (89 mg, 239 µmol) was added neat. The solution was left to stand in the dark for 3 days at ambient temperature before the resulting precipitate was filtered to give the nitrone **193** as yellow solid (0.2 g, 40% over 2 steps). M.p. = 225.8 – 226.7 ˚C; ^{1}H NMR (300.1 MHz, $CDCl_3$): δ_H 8.66 (1H, s; N*H*CO), 8.56 – 8.53 (2H, m; 2×Ar*H*), 8.26 (1H, d, $^3J_{HH}$ 8.4 Hz; Ar*H*), 8.08 (1H, s; C*H*), 8.06 (2H, s; 2×Ar*H*), 7.82 (1H, d, $^3J_{HH}$ 8.7 Hz; Ar*H*), 7.69 – 7.66 (2H, m; 2×Ar*H*), 7.63 – 7.60 (1H, m; Ar*H*), 7.48 – 7.41 (5H, m; 5×Ar*H*), 7.28 (3H, m; 3×Ar*H*), 2.48 (3H, s; CH_3), 1.38 (9H, s; 3×CH_3), 1.35 (18H, s; 6×CH_3); ^{13}C NMR (75.5 MHz, $CDCl_3$): δ_C 164.7 (NH*C*O), 154.4 (Ar*C*), 151.2 (Ar*C*), 151.0 (Ar*C*), 149.3 (Ar*C*), 140.1

(Ar*C*H), 139.4 (Ar*C*), 136.5 (Ar*C*), 134.0 (Ar*C*), 132.8 (Ar*C*H), 132.5 (*C*H), 129.3 (Ar*C*H), 129.0 (Ar*C*H), 127.8 (Ar*C*H), 126.2 (Ar*C*), 126.1 (Ar*C*H), 125.5 (Ar*C*H), 122.3 (Ar*C*), 121.8 (Ar*C*H), 121.7 (Ar*C*), 121.3 (Ar*C*H), 111.5 (Ar*C*H), 91.4 (q*C*), 86.9 (q*C*), 35.0 (q*C*), 34.8 (q*C*), 31.5 (*C*H_3), 31.5 (*C*H_3), 23.1 (*C*H_3); MS (ES^+) *m/z* 698.21 ([M+Na]$^+$, 100); HRMS (ES^+) *m/z* calculated for $C_{46}H_{49}N_3O_2Na$ [M+Na]$^+$ 698.3722, found 698.3728.

(Z)-4-(Anthracen-9-ylethynyl)-N-(4-((5-(4-(tert-butyl)phenyl)-6-methylpyridin-2-yl)carbamoyl)benzylidene)aniline oxide 194

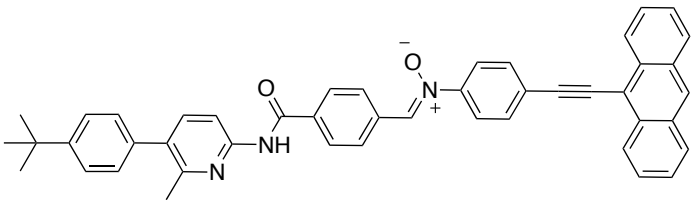

Compound **180** (0.20 g, 0.62 mmol) in THF (10 mL) was reacted with Rh/C (118 mg, 50 wt. %), before being slowly reacted with hydrazine monohydrate (0.24 mL, 1.24 mmol). The reaction was stirred for 3 h and monitored by TLC until the disappearance of the starting material. The solution was filtered through a pad of Celite and the solvent was removed to give the intermediate red solid hydroxylamine, which was carried out to the next step without further purification. The hydroxylamine **181** (0.62 mmol) was subsequently dissolved in EtOH (10 mL) and and added to a solution of aldehyde **186** (190 mg, 0.43 mmol) in EtOH (15 mL). The reaction mixture was left to stand in the dark for 3 days before the resulting precipitate was filtered, washed with hexane and dried in *vacuo* to afford nitrone **194** (0.27 g, 94% over 2 steps). M.p. = 218.3 ˚C (decomp.); ^{1}H NMR (300.1 MHz, $CDCl_3$): δ_H 8.72 (1H, s; N*H*), 8.63 (2H, d, $^3J_{HH}$ 8.4 Hz; 2×Ar*H*), 8.56 (2H, d, $^3J_{HH}$ 8.6 Hz; 2×Ar*H*), 8.48 (1H, s; Ar*H*), 8.26 (1H, d, $^3J_{HH}$ 8.5 Hz; Ar*H*), 8.09 – 8.03 (5H, m; 4×Ar*H* + C*H*), 7.92 – 7.87 (4H, m; 4×Ar*H*), 7.64 (2H, d, $^3J_{HH}$ 8.5 Hz; 2×Ar*H*), 7.63 (1H, d, $^3J_{HH}$ 7.4 Hz; Ar*H*), 7.54 (2H, t, $^3J_{HH}$ 7.2 Hz; 2×Ar*H*), 7.46 (2H, d, $^3J_{HH}$ 8.4 Hz; 2×Ar*H*), 7.28 (2H, d, $^3J_{HH}$ 8.4 Hz; 2×Ar*H*), 2.48 (3H, s, CH_3), 1.36 (9H, s, 3×CH_3); ^{13}C NMR (75.5 MHz, $CDCl_3$) : δ_C 164.7 (*C*=O), 154.4 (Ar*C*), 150.5 (Ar*C*), 149.6 (Ar*C*), 148.3 (Ar*C*), 140.1 (Ar*C*H), 136.5 (Ar*C*), 136.0 (Ar*C*), 133.9 (Ar*C*), 133.6 (Ar*C*), 133.5 (*C*H), 132.9 (Ar*C*), 132.5 (Ar*C*H), 131.3 (Ar*C*), 129.4 (Ar*C*H), 129.1 (Ar*C*H), 129.0 (Ar*C*H), 128.6 (Ar*C*H), 127.7 (Ar*C*H), 127.1 (Ar*C*H), 126.7 (Ar*C*H), 126.2 (Ar*C*), 126.0 (Ar*C*H), 125.5 (Ar*C*H), 122.1 (Ar*C*H), 116.5 (Ar*C*), 111.5 (Ar*C*H), 99.3 (q*C*), 89.2 (q*C*), 34.8 (q*C*), 31.5 (*C*H_3), 23.1 (*C*H_3); MS (ES^+) *m/z* 687 ([M+Na]$^+$, 10); HRMS

(ES$^+$) *m/z* calculated for $C_{46}H_{38}N_3O_2$ $[M+H]^+$ 664.2964, found 664.21959.

4-Formyl-*N*-(5-iodo-4,6-dimethylpyridin-2-yl)benzamide 195

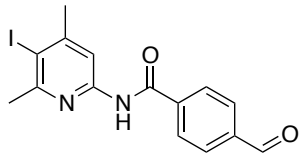

5-iodo-4,6-dimethylpyridin-2-amine **194** (1.0 g, 4.03 mmol) and Et_3N (1.02 g, 10.1 mmol) were dissolved in CH_2Cl_2 (30 mL) and the solution was cooled to 0 ˚C. 4-formylbenzoyl chloride **116** (1.02 g, 6.05 mmol) in dry CH_2Cl_2 (5 mL) was added dropwise at 0 ˚C and under vigorous stirring. Once the addition was finished, the reaction mixture was allowed to get to rt and was left stirred for 48 h before it was washed with 1M HCl and extracted with sat. aqueous $NaHCO_3$. The combined organic extracts were dried ($MgSO_4$) and evaporated *in vacuo*. The residue was purified by column chromatography (Hexane:EtOAc, 5:1) to afford the desired aldehyde **195** (0.58 g, 38%) as colorless solid. M.p.= 158.3 – 159.6 ˚C; ^{1}H NMR (400.1 MHz, $CDCl_3$): δ_H 10.1 (1H, s; CO*H*), 8.57 (1H, s; N*H*CO), 8.10 (1H, s; Ar*H*), 8.06 (2H, d, $^3J_{HH}$ 8.3 Hz; 2×Ar*H*), 8.00 (2H, d, $^3J_{HH}$ 8.3 Hz; 2×Ar*H*), 2.67 (3H, s; CH_3), 2.50 (3H, s; CH_3); ^{13}C NMR (100.6 MHz, $CDCl_3$): δ_C 191.4 (*C*OH), 164.6 (NH*C*O), 159.2 (Ar*C*), 154.1 (Ar*C*), 150.0 (Ar*C*), 139.3 (Ar*C*), 138.8 (Ar*C*), 130.1 (Ar*C*H), 128.0 (Ar*C*H), 112.5 (Ar*C*H), 97.2 (Ar*C*-I), 29.7 (*C*H_3), 29.5 (*C*H_3); MS (ES$^-$) *m/z* 378.87 ([M–H]$^-$, 100); HRMS (ES$^-$) *m/z* calculated for $C_{15}H_{12}N_2O_2I$ $[M–H]^-$ 378.9944, found 378.9934.

***N*-(5-((3,5-Di-*tert*-butylphenyl)ethynyl)-4,6-dimethylpyridin-2-yl)-4-formylbenzamide 196**

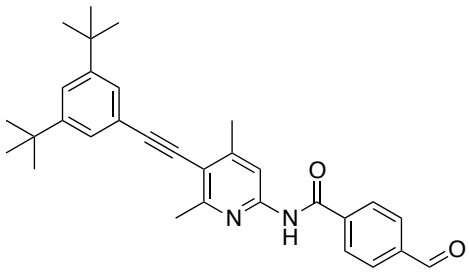

Aldehyde **195** (0.49 g, 1.28 mmol) was dissolved in Et_3N (40 mL). PPh_3 (37 mg, 140 µmol), CuI (21 mg, 112 µmol) and $PdCl_2(PPh_3)_2$ (79 mg, 112 µmol) were added neat and the mixture was degassed with Ar for 40 min. The previous alkyne **173** (0.33 g, 1.54 mmol) were added *via* syringe under a protective Ar atmosphere and the mixture was heated at 60 ˚C and vigorously stirred for 24 h. The occurring brown solution was filtered through a plug of Celite. The solvent was evaporated and the reaction crude was purified by flash chromatography (Hexane:EtOAc, 5:1) to afford the desired aldehyde **196** (0.15 g,

25%) as yellow solid. M.p. = 152.9 - 154.5 ˚C; ^{1}H NMR (300.1 MHz, $CDCl_3$): δ_H 10.1 (1H, s; C*H*O), 8.95 (1H, br s; N*H*CO), 8.17 (1H, br s; Ar*H*), 8.08 (2H, d, $^{3}J_{HH}$ 8.2 Hz; 2×ArH), 7.98 (2H, d, $^{3}J_{HH}$ 8.2 Hz; 2×Ar*H*), 7.45 (1H, t, $^{4}J_{HH}$ 1.7 Hz; Ar*H*), 7.39 (2H, d, $^{4}J_{HH}$ 1.7 Hz; 2×Ar*H*), 2.63 (3H, s; CH_3), 2.57 (3H, s; CH_3), 1.36 (18H, s, 6×CH_3); ^{13}C NMR (75.5 MHz, $CDCl_3$): δ_C 191.4 (*C*HO), 164.5 (NH*C*O), 158.9 (Ar*C*), 152.2 (Ar*C*), 151.1 (Ar*C*), 148.8 (Ar*C*), 139.4 (Ar*C*), 138.7 (Ar*C*), 130.0 (Ar*C*H), 128.1 (Ar*C*H), 125.7 (Ar*C*H), 123.2 (Ar*C*H), 122.3 (Ar*C*), 116.4 (Ar*C*), 112.0 (Ar*C*H), 100.2 (q*C*), 83.7 (q*C*), 34.9 (q*C*), 31.4 (*C*H_3), 23.4 (*C*H_3), 21.4 (*C*H_3); MS (ES^-) *m/z* 465.10 ([M–H]$^-$, 100); HRMS (ES^-) *m/z* calculated for $C_{31}H_{33}N_2O_2$ [M–H]$^-$ 465.2542, found 465.2543.

(*Z*)-4-((3,5-Di-*tert*-butylphenyl)ethynyl)-*N*-(4-((5-((3,5-di-*tert*-butylphenyl)ethynyl)-4,6-dimethylpyridin-2-yl)carbamoyl)benzylidene)aniline oxide 197

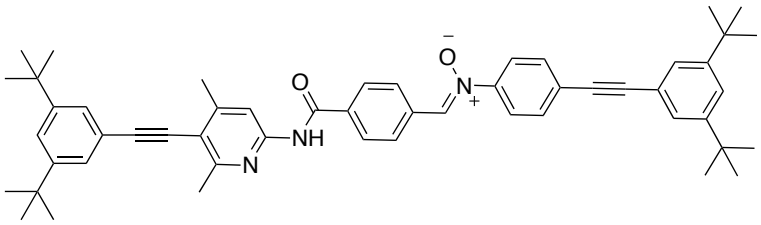

Nitro compound **174** (100 mg, 298 µmol) was dissolved in THF (10 mL). Rhodium (40 mg, 5 wt.% on carbon, wet) and hydrazine monohydrate (30 mg, 596 µmol) were added and the reaction was followed by TLC (Hexane:EtOAC, 3:1). After completion, the solution was filtered through Celite and concentrated *in vacuo* to obtain the desired intermediate hydroxylamine **175** as a yellow oil, which was directly used in the next step without further purification. The obtained hydroxylamine **175** (96 mg, 298 µmol) was dissolved in EtOH (7 mL) and aldehyde **196** (130 mg, 268 µmol) was added neat. The solution was left to stand in the dark for 48 h at ambient temperature before the resulting precipitate was filtered to give the desired product as yellow solid (50 mg, 24% over 2 steps). M.p. = 235.7 – 236.3 ˚C; ^{1}H NMR (400.1 MHz, $CDCl_3$): δ_H 8.57 (1H, br s; N*H*CO), 8.54 (2H, d, $^{3}J_{HH}$ 8.5 Hz; 2×Ar*H*), 8.18 (1H, s; Ar*H*), 8.06 – 8.05 (2H, m; 2×Ar*H*), 8.04 (1H, s, CH_3), 7.81 (2H, d, $^{3}J_{HH}$ 8.7 Hz; 2×Ar*H*), 7.68 (2H, d, $^{3}J_{HH}$ 8.7 Hz; 2×Ar*H*), 7.45 (2H, s; 2×Ar*H*), 7.41 (2H, d, $^{4}J_{HH}$ 1.8 Hz; 2×Ar*H*), 7.39 (2H, d, $^{4}J_{HH}$ 1.8 Hz; 2×Ar*H*), 2.70 (3H, s; CH_3), 2.58 (3H, s; CH_3), 1.36 (18H, s; 6×CH_3), 1.35 (18H, s; 6×CH_3); ^{13}C NMR (100.6 MHz, $CDCl_3$): δ_C 164.6 (NH*C*O), 158.6 (Ar*C*), 152.1 (Ar*C*), 151.2 (Ar*C*), 147.8 (Ar*C*), 135.7 (Ar*C*), 134.0 (Ar*C*), 133.4 (*C*H), 132.5 (Ar*C*H), 129.3 (Ar*C*H), 127.7

(Ar*C*H), 126.2 (Ar*C*), 126.1 (Ar*C*H), 125.7 (Ar*C*H), 123.5 (Ar*C*H), 123.3 (Ar*C*H), 123.2 (Ar*C*H). 122.4 (Ar*C*), 121.8 (Ar*C*H), 121.7 (Ar*C*), 116.1 (Ar*C*), 111.9 (Ar*C*H), 99.9 (q*C*), 93.2 (q*C*), 35.0 (q*C*), 31.5 (*C*H_3), 23.6 (*C*H_3), 21.7 (*C*H_3); MS (ES^+) *m/z* 770.17 ($[M+H]^+$, 100); HRMS (ES^+) *m/z* calculated for $C_{53}H_{60}N_3O_2$ $[M+H]^+$ 770.4686, found 770.4672.

4-((4-Nitrophenyl)ethynyl)aniline 206[278]

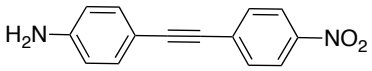

4-iodoaniline **187** (1.0 g, 4.57 mmol) was dissolved in Et_3N (50 mL). PPh_3 (120 mg, 457 µmol), CuI (70 mg, 366 µmol) and $PdCl_2(PPh_3)_2$ (260 mg, 366 µmol) were added and the reaction mixture was degassed with Ar for 40 min. The alkyne **189** (0.74 g, 5.02 mmol) were added *via* syringe under a protective Ar atmosphere and the mixture was heated at 65 °C and vigorously stirred for 16 h. The occurring brown solution was filtered through a plug of celite. The solvent was evaporated and the reaction crude was purified by flash chromatography (Cyclohexane:EtOAc, 3:1) to afford the desired aniline **206** (0.30 g, 28%) as an orange solid. M.p. = 189.2 – 192.3 °C (lit.[278] = 190 °C); ^{1}H NMR (300.1 MHz, $CDCl_3$): δ_H 8.19 (2H, d, $^3J_{HH}$ 8.9 Hz; 2×Ar*H*), 7.60 (2H, d, $^3J_{HH}$ 8.9 Hz; 2×Ar*H*), 7.36 (2H, d, $^3J_{HH}$ 8.6 Hz; 2×Ar*H*), 6.66 (2H, d, $^3J_{HH}$ 8.6 Hz; 2×Ar*H*), 3.92 (2H, br s; NH_2); ^{13}C NMR (75.5 MHz, $CDCl_3$) : δ_C 147.7 (Ar*C*), 146.8 (Ar*C*), 133.6 (Ar*C*H), 131.9 (Ar*C*H), 131.3 (Ar*C*), 123.8 (Ar*C*H), 114.8 (Ar*C*H), 111.6 (Ar*C*), 96.6 (q*C*), 86.6 (q*C*); MS (ES^-) *m/z* 236.96 ($[M-H]^-$, 100); HRMS (ES^-) *m/z* calculated for $C_{14}H_9N_2O_2$ $[M-H]^-$ 237.0664, found 237.0668.

3,5-Dichloro-*N*-(4-((4-nitrophenyl)ethynyl)phenyl)benzamide 207

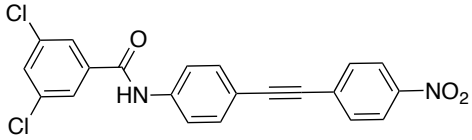

4-((4-nitrophenyl)ethynyl)aniline **206** (100 mg, 420 µmol) and Et_3N (85 mg, 840 µmol) were dissolved in CH_2Cl_2 (30 mL). 3,5- dichlorobenzoyl chloride (85 mg, 420 µmol) was added dropwise at 0 °C under vigorous stirring. Once the addition was finished, the reaction mixture was allowed to get to room temperature and was left stirred for 16 h. The resulting precipitate formed was filtered, washed with chilled CH_2Cl_2 and dried. The title compound **207** (96 mg, 56%) was obtained as yellow solid. M.p. =

286.2 – 287.1 ˚C; ^{1}H NMR (300.1 MHz, d_6-DMSO): δ_H 10.6 (1H, s; CON*H*), 8.26 (2H, d, $^{3}J_{HH}$ 8.8 Hz; 2×Ar*H*), 7.98 (2H, d, $^{4}J_{HH}$ 1.8 Hz; 2×Ar*H*), 7.89 (1H, s, Ar*H*), 7.88 (2H, d, $^{3}J_{HH}$ 8.8 Hz; 2×Ar*H*), 7.80 (2H, d, $^{3}J_{HH}$ 8.8 Hz; 2×Ar*H*), 7.64 (2H, d, $^{3}J_{HH}$ 8.6 Hz; 2×Ar*H*); ^{13}C NMR (75.5 MHz, d_6-DMSO) : δ_C 163.0 (*C*ONH), 146.7 (Ar*C*), 139.9 (Ar*C*), 137.8 (Ar*C*), 134.3 (Ar*C*), 132.5 (Ar*C*H), 132.4 (Ar*C*H), 131.1 (Ar*C*H), 129.3 (Ar*C*), 126.6 (Ar*C*H), 123.9 (Ar*C*H), 120.3 (Ar*C*H), 116.5 (Ar*C*), 94.5 (q*C*), 87.4 (q*C*); MS (ES$^-$) *m/z* 408.89 ([M–H]$^-$, 100); HRMS (ES$^-$) *m/z* calculated for $C_{21}H_{11}N_2O_3Cl_2$ [M–H]$^-$ 409.0147, found 409.0151.

N-(4-Iodophenyl)-3,5-bis(trifluoromethyl)benzamide 208

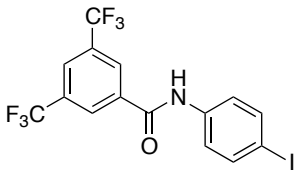

4-iodoaniline **187** (1.90 g, 8.68 mmol) and Et_3N (1.46 g, 14.46 mmol) were dissolved in CH_2Cl_2 (25 mL) and the solution was cooled at 0 ˚C. 3,5-bis(trifluoromethyl) benzoyl chloride **124** (2.0 g, 7.23 mmol) was added dropwise at 0 ˚C under vigorous stirring. Once the addition was finished, the reaction mixture was allowed to get room temperature and stirred for 1 h. The resulting precipitate formed was filtered, washed with chilled CH_2Cl_2 and dried. The title compound **208** (1.28 g, 38%) was obtained as colorless solid. M.p. = 218.6 – 219.8 ˚C; ^{1}H NMR (300.1 MHz, $CDCl_3$): δ_H 10.2 (1H, s; N*H*CO), 8.47 (2H, s; 2×Ar*H*), 7.90 (1H, s; Ar*H*), 7.55 (2H, d, $^{3}J_{HH}$ 8.9 Hz; 2×Ar*H*), 7.47 (2H, d, $^{3}J_{HH}$ 8.9 Hz; 2×Ar*H*); ^{13}C NMR (75.5 MHz, $CDCl_3$ + 3 drops of d_6-DMSO): δ_C 163.0 (*C*ONH), 138.2 (Ar*C*), 137.5 (Ar*C*H), 136.8 (Ar*C*), 131.0 (q, $^{2}J_{CF}$ 34.0 Hz, Ar*C*), 128.4 (m, Ar*C*H), 124.7 (m, Ar*C*H), 123.1 (*C*F_3), 87.9 (ArC-*I*); ^{19}F NMR (282.4 MHz, $CDCl_3$ + 3 drops of d_6-DMSO): δ_F –63.2 (ArC*F*$_3$); MS (ES$^-$) m/z 457.72 ([M–H]$^-$, 100), HRMS (ES$^-$) m/z calculated for $C_{15}H_7NOF_6I$ [M–H]$^-$ 457.9477, found 457.9477.

N-(4-((4-Nitrophenyl)ethynyl)phenyl)-3,5-bis(trifluoromethyl)benzamide 209

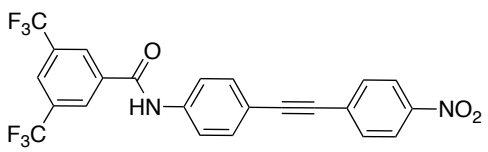

The iodo derivative **208** (1.25 g, 2.72 mmol) was suspended in a mixture of Et_3N:THF (50 mL: 10 mL). PPh_3 (71 mg, 272 µmol), CuI (50 mg, 218 µmol) and $PdCl_2(PPh_3)_2$ (153 mg, 218 µmol) were added neat and the mixture was degassed with Ar for 40 min. The alkyne **189** (0.48 g, 3.27 mmol) were

added *via* syringe under a protective Ar atmosphere and heated at 60 ˚C for 16 h. The brown solution was filtered through a plug of Celite, concentrated and purified by column chromatography (Hexane:EtOAc, 20:1) to afford the desired nitro compound **209** (1.0 g, 75%) as a bright yellow powder. M.p. = 223.3 – 224.0 ˚C; ^{1}H NMR (300.1 MHz, $CDCl_3$): δ_H 8.33 (2H, s; 2×Ar*H*), 8.23 (2H, d, $^{3}J_{HH}$ 8.8 Hz; 2×Ar*H*), 8.08 (1H, s; Ar*H*), 8.02 (1H, s; N*H*CO), 7.68 (4H, dd, $^{2}J_{HH}$ 14.8 and $^{3}J_{HH}$ 8.7 Hz; 4×Ar*H*), 7.60 (2H, d, $^{3}J_{HH}$ 8.6; 2×Ar*H*); ^{13}C NMR (75.5 MHz, $CDCl_3$): δ_C 162.9 (Ar*C*O), 147.1 (Ar*C*), 144.2 (Ar*C*), 138.0 (Ar*C*), 136.8 (Ar*C*), 133.1 (Ar*C*H), 132.7 (q, $^{2}J_{CF}$ 34.1 Hz, Ar*C*), 132.4 (Ar*C*H), 130.3 (Ar*C*), 127.5 (m, Ar*C*H), 125.8 (m, Ar*C*H), 123.8 (Ar*C*H), 120.4 (Ar*C*H), 119.1 (Ar*C*), 94.3 (qC), 88.0 (q*C*); ^{19}F (282.4 MHz, $CDCl_3$): δ_F –63.4 (ArC*F*$_3$); MS (ES^-) *m/z* 477.0 ([M–H]$^-$, 100); HRMS (ES^-) calculated for $C_{23}H_{11}N_2O_3F_6$ [M–H]$^-$ 477.0674, found 477.0672.

3,5-Bis(octyloxy)benzoic acid 211[264]

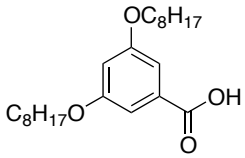

To a dry *N*,*N*-dimethylformamide (80 mL) solution of 3,5-dihydroxybenzoic acid **210** (1.54 g, 10.0 mmol) were added 1-bromooctane (2.89 g, 2.60 mL, 15.0 mmol) and K_2CO_3 (13.8 g, 0.1M) and the mixture was heated at 65 ˚C for 16 h under N_2 atmosphere. After cooling down to room temperature, aqueous 5% HCl solution (80 mL) and hexane (80 mL) were added to the reaction mixture under vigorous stirring at room temperature. The separated organic phase was washed with sat. $NaHCO_3$ solution and brine and dried over $NaSO_4$. Purification by flash column chromatography (CH_2Cl_2:Hexane, 1:1) and recrystallisation with MeOH gave the corresponding ester as white powder. Ester (0.64 g, 1.30 mmol) was dissolved in EtOH (60 mL) and water (20 mL), to which KOH (0.73 g, 13.0 mmol) was added and refluxed at 88 ˚C for 16 h under N_2. After cooling down to ambient temperature, the solvent was removed under vacuum and the product extracted into CH_2Cl_2 and washed with 1M HCl. All the solvents were evaporated and the resulting solids were dried *in vacuo* and crystallised to give the desired corresponding acid compound **211** (1.50 g, 40% over two steps). M.p. = 53.9 – 55.2 ˚C; ^{1}H NMR (300.1 MHz, $CDCl_3$): δ_H 7.23 (2H, d, $^{4}J_{HH}$ 2.30 Hz; 2×Ar*H*), 6.69 (1H, t, $^{4}J_{HH}$ 2.28 Hz; Ar*H*), 3.98 (4H, t, $^{3}J_{HH}$ 6.54 Hz; 2×C*H*$_2$), 1.79 (4H, quintet, $^{3}J_{HH}$ 7.13 Hz; 2×C*H*$_2$), 1.51 – 1.41 (4H, m; 2×C*H*$_2$), 1.41 –1.29 (16H, m; 8×C*H*$_2$), 0.91 – 0.87 (6H, m; 2×C*H*$_3$); ^{13}C NMR (100.6 MHz, $CDCl_3$): δ_C

171.8 (*C*OOH), 160.2 (Ar*C*), 147.6 (Ar*C*), 130.9 (Ar*C*), 108.2 (Ar*C*H), 107.5 (*ArCH*), 68.4 (CH_2), 31.8 (CH_2), 29.4 (CH_2), 29.3 (CH_2), 29.2 (CH_2), 26.0 (CH_2), 22.7 (CH_2), 14.1 (CH_3); MS (ES^+) *m/z* 401.40 ($[M+Na]^+$, 100); HRMS (ES^+) *m/z* calculated for $C_{23}H_{38}O_4Na$, $[M+Na]^+$ 401.2668, found 401.2665.

3,5-Bis(octyloxy)benzoyl chloride 212[279]

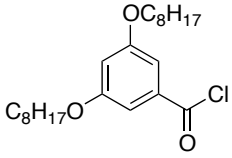

3,5-bis(octyloxy)benzoic acid **211** (1.0 g, 2.64 mmol) was dissolved in toluene (20 mL). Thionyl chloride (1.56 g, 1.02 mL, 13.0 mmol) was added and the mixture was refluxed at 110 ˚C for 16 h. Removing all solvents *in vacuo* yielded the desired product **212** as a colourless oil that was used directly without further purification (1.02 g, 97%). ^{1}H NMR (300.1 MHz, $CDCl_3$): δ_H 7.22 (2H, d, $^4J_{HH}$ 2.26 Hz; 2×Ar*H*), 6.73 (1H, t, $^4J_{HH}$ 2.25 Hz; Ar*H*), 3.97 (4H, t, $^3J_{HH}$ 6.51 Hz; 2×CH_2), 1.79 (4H, quintet, $^3J_{HH}$ 7.13 Hz; 2×CH_2), 1.51 – 1.41 (4H, m; 2×CH_2), 1.32 – 1.29 (16H, m; 8×CH_2), 0.91 – 0.87 (6H, m; 2×C*H3*); ^{13}C NMR (75.5 MHz, $CDCl_3$): δ_C 168.5 (*C*OCl), 160.5 (Ar*C*), 134.9 (Ar*C*), 109.6 (Ar*C*H), 108.8 (*ArCH*), 68.7 (CH_2), 32.0 (CH_2), 29.5 (CH_2), 29.4 (CH_2), 29.2 (CH_2), 26.1 (CH_2), 22.8 (CH_2), 14.3 (CH_3).

***N*-(4-((4-Nitrophenyl)ethynyl)phenyl)-3,5-bis(octyloxy)benzamide 213**

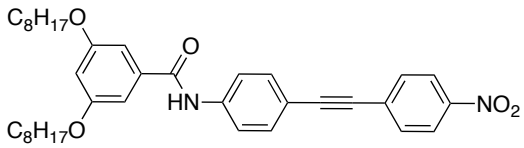

4-((4-nitrophenyl)ethynyl)aniline **206** (200 mg, 839 µmol) and Et_3N (0.21 g, 2.10 mmol) were dissolved in CH_2Cl_2 (15 mL). 3,5-bis(octyloxy)benzoyl chloride **212** (0.40 g, 1.01 mmol) was added dropwise at room temperature under vigorous stirring for 1 h. Once the addition was finished, the reaction mixture was heated under reflux for 10 h. The solvent was evaporated and the crude was purified by flash chromatography (Hexane:EtOAc, 5:1) to afford the desired nitro compound **213** (0.3 g, 60%) as yellow solid. M.p.= 147.7 – 148.2 ˚C; ^{1}H NMR (400.1 MHz, $CDCl_3$): δ_H 8.22 (2H, d, $^3J_{HH}$ 8.5 Hz; 2×Ar*H*), 7.88 (1H, s; CON*H*), 7.69 (2H, d, $^3J_{HH}$ 8.4 Hz; 2×Ar*H*), 7.66 (2H, d, $^3J_{HH}$ 8.7 Hz; 2×Ar*H*), 7.56 (2H, d, $^3J_{HH}$ 8.5 Hz; 2×Ar*H*), 6.95 (2H, d, $^4J_{HH}$ 1.5 Hz; 2×Ar*H*), 6.62 (1H, s; Ar*H*), 3.99 (4H, t, $^3J_{HH}$ 6.5 Hz; 2×CH_2), 1.79 (4H, quintet, $^3J_{HH}$ 7.1 Hz; 2×CH_2), 1.46 (4H, dt, $^3J_{HH}$ 7.0 Hz and $^2J_{HH}$ 14.1; 2×CH_2), 1.42 – 1.29 (16H, m; 8×CH_2), 0.91 – 0.87 (6H, m; 2×CH_3); ^{13}C

NMR (100.6 MHz, $CDCl_3$): δ_C 165.7 (*C*ONH), 160,8 (Ar*C*), 147.0 (Ar*C*), 139.0 (Ar*C*), 136.7 (Ar*C*), 133.0 (Ar*C*H), 132.3 (Ar*C*H), 130.5 (Ar*C*), 123.8 (Ar*C*H), 119.8 (Ar*C*H), 117.9 (Ar*C*), 105.5 (Ar*C*H), 104.9 (Ar*C*H), 94.8 (q*C*), 87.6 (q*C*), 68.6 (CH_2), 31.9 (CH_2), 29.5 (CH_2), 29.4 (CH_2), 29.3 (CH_2), 26.2 (CH_2), 22.8 (CH_2), 14.2 (CH_3); MS (ES^+) *m/z* 621.20 ($[M+Na]^+$,100); HRMS (ES^+) *m/z* calculated for $C_{37}H_{46}N_2O_5Na$ $[M+Na]^+$ 621.3304, found 621.3304.

References

1. Desiraju, G. R. *Nature* **2001**, *412*, 397.
2. Reinhoudt, D. N. *Science* **2002**, *295*, 2403.
3. Lehn, J. M. *Chem. Scripta* **1988**, *28*, 237.
4. Cram, D. J. *Angew. Chem., Int. Ed.* **1988**, *27*, 1009.
5. Philp, D.; Stoddart, J. F. *Angew. Chem., Int. Ed.* **1996**, *35*, 1155.
6. Mascal, M. *Contemp. Org. Synth.* **1994**, *1*, 31.
7. Shakhnovich, E.; Abkevich, V.; Ptitsyn, O. *Nature* **1996**, *379*, 96.
8. Hof, F.; Rebek, J. *Proc. Natl. Acad. Sci. USA* **2002**, *99*, 4775.
9. Amabilino, D.; Stoddart, J. F. *New Scientist* **1994**, *141*, 25.
10. Anderson, S.; Anderson, H. L.; Sanders, J. K. M. *Acc. Chem. Res.* **1993**, *26*, 469.
11. Hoss, R.; Vögtle, F. *Angew. Chem., Int. Ed.* **1994**, *33*, 375.
12. Bryant, J. A.; Knobler, C. B.; Cram, D. J. *J. Am. Chem. Soc.* **1990**, *112*, 1254.
13. Cram, D. J. *Angew. Chem., Int. Ed.* **1986**, *25*, 1039.
14. Bryant, J. A.; Ericson, J. L.; Cram, D. J. *J. Am. Chem. Soc.* **1990**, *112*, 1255.
15. Knowles, P. F. *Biochem. Educ.* **1995**, *23*, 224.
16. Lindoy, L. F.; Atkinson, I. M. *Self-assembly in supramolecular systems*; The Royal Society of Chemistry, Cambridge, **2000**, p 47.
17. Pedersen, C. J. *J. Am. Chem. Soc.* **1967**, *89*, 2495.
18. Frensdorff, H. K. *J. Am. Chem. Soc.* **1971**, *93*, 600.
19. von Kiedrowski, G. *Angew. Chem., Int. Ed.* **1986**, *25*, 932.
20. Hoffmann, S. *Angew. Chem., Int. Ed.* **1992**, *31*, 1013.
21. Andreu, C.; Beerli, R.; Branda, N.; Conn, M.; Demendoza, J.; Galan, A.; Huc, I.; Kato, Y.; Tymoschenko, M.; Valdez, C.; Wintner, E.; Wyler, R.; Rebek, J. *Pure Appl. Chem.* **1993**, *65*, 2313.
22. Watson, J. D.; Crick, F. H. C. *Nature* **1953**, *171*, 737.
23. von Kiedrowski, G. *Bioorg. Chem. Front.* **1993**, *3*, 113.
24. Howell, S. J.; Spencer, N.; Philp, D. *Tetrahedron* **2001**, *57*, 4945.
25. Bennes, R.; Babiloni, M. S.; Hayes, W.; Philp, D. *Tetrahedron Lett.* **2001**, *42*, 4595.
26. Soai, K.; Shibata, T.; Sato, I. *Acc. Chem. Res.* **2000**, *33*, 382.
27. Bennes, R. I.; Philp, D.; Spencer, N.; Kariuki, B. M.; Harris, K. D. M. *Org. Lett.* **1999**, *1*, 1087.
28. Philp, D.; Robertson, A. *Chem. Commun.* **1998**, 879.
29. Robertson, A.; Philp, D.; Spencer, N. *Tetrahedron* **1999**, *55*, 11365.
30. Sadownik, J. PhD thesis, University of St. Andrews, 2009.
31. Allen, V. C.; Philp, D.; Spencer, N. *Org. Lett.* **2001**, *3*, 777.
32. Quayle, J. M.; Slawin, A. M. Z.; Philp, D. *Tetrahedron Lett.* **2002**, *43*, 7229.
33. Vidonne, A.; Philp, D. *Eur. J. Org. Chem.* **2009**, 593 and references therein.
34. Orgel, L. E.; Lohrmann, R. *Acc. Chem. Res.* **1974**, *7*, 368.
35. Issac, R.; Ham, Y. W.; Chmielewski, J. *Curr. Opin. Struct. Biol.* **2001**, *11*, 458.
36. Askew, B.; Ballester, P.; Buhr, C.; Jeong, K. S.; Jones, S.; Parris, K.; Williams, K.; Rebek, J. *J. Am. Chem. Soc.* **1989**, *111*, 1082.
37. Patzke, V.; von Kiedrowski, G. *Arkivoc* **2007**, 293.

38. von Kiedrowski, G.; Wlotzka, B.; Helbing, J. *Angew. Chem., Int. Ed.* **1989**, *28*, 1235.
39. von Kiedrowski, G.; Wlotzka, B.; Helbing, J.; Matzen, M.; Jordan, S. *Angew. Chem., Int. Ed.* **1991**, *30*, 423.
40. Achilles, T.; von Kiedrowski, G. *Angew. Chem., Int. Ed.* **1993**, *32*, 1198.
41. Sievers, D.; von Kiedrowski, G. *Nature* **1994**, *369*, 221.
42. Joyce, G. F. *Nature* **1989**, *338*, 217.
43. Cech, T. R. *Proc. Natl. Acad. Sci. USA* **1986**, *83*, 4360.
44. Paul, N.; Joyce, G. F. *Proc. Natl. Acad. Sci. USA* **2002**, *99*, 12733.
45. Severin, K.; Lee, D.; Martinez, J.; Ghadiri, M. *Chem. -Eur. J.* **1997**, *3*, 1017.
46. Lee, D. H.; Granja, J. R.; Martinez, J. A.; Severin, K.; Ghadiri, M. R. *Nature* **1996**, *382*, 525.
47. Lee, D.; Severin, K.; Yokobayashi, Y.; Ghadiri, M. *Nature* **1997**, *390*, 591.
48. Severin, K.; Lee, D.; Martinez, J.; Vieth, M.; Ghadiri, M. *Angew. Chem., Int. Ed.* **1998**, *37*, 126.
49. Lee, D. H.; Severin, K.; Yokobayashi, Y.; Ghadiri, M. R. *Nature* **1998**, *394*, 101.
50. Dawson, P.; Muir, T.; Clark-Lewis, I.; Kent, S. *Science* **1994**, *266*, 776.
51. Issac, R.; Chmielewski, J. *J. Am. Chem. Soc.* **2002**, *124*, 6808.
52. Paul, N.; Joyce, G. F. *Curr. Opin. Chem. Biol.* **2004**, *8*, 634.
53. Li, X.; Chmielewski, J. *J. Am. Chem. Soc.* **2003**, *125*, 11820.
54. Nowick, J. S.; Feng, Q.; Tjivikua, T.; Ballester, P.; Rebek, J. *J. Am. Chem. Soc.* **1991**, *113*, 8831.
55. Menger, F. M.; Eliseev, A. V.; Khanjin, N. A. *J. Am. Chem. Soc.* **1994**, *116*, 3613.
56. Conn, M. M.; Wintner, E. A.; Rebek, J. *J. Am. Chem. Soc.* **1994**, *116*, 8823.
57. Wintner, E. A.; Tsao, B.; Rebek, J. *J. Org. Chem.* **1995**, *60*, 7997.
58. Menger, F. M.; Eliseev, A. V.; Khanjin, N. A.; Sherrod, M. J. *J. Org. Chem.* **1995**, *60*, 2870.
59. Reinhoudt, D. N.; Rudkevich, D. M.; deJong, F. *J. Am. Chem. Soc.* **1996**, *118*, 6880.
60. Rotello, V.; Hong, J. I.; Rebek, J. *J. Am. Chem. Soc.* **1991**, *113*, 9422.
61. Park, T. K.; Feng, Q.; Rebek, J. *J. Am. Chem. Soc.* **1992**, *114*, 4529.
62. Feng, Q.; Park, T. K.; Rebek, J. *Science* **1992**, *256*, 1179.
63. Terfort, A.; von Kiedrowski, G. *Angew. Chem., Int. Ed.* **1992**, *31*, 654.
64. Wang, B.; Sutherland, I. O. *Chem. Commun.* **1997**, 1495.
65. Kindermann, M.; Stahl, I.; Reimold, M.; Pankau, W. M.; von Kiedrowski, G. *Angew. Chem., Int. Ed.* **2005**, *44*, 6750.
66. Blackmond, D. G. *Proc. Natl. Acad. Sci. USA* **2004**, *101*, 5732.
67. Booth, C. A.; Philp, D. *Tetrahedron Lett.* **1998**, *39*, 6987.
68. Pearson, R. J.; Kassianidis, E.; Philp, D. *Tetrahedron Lett.* **2004**, *45*, 4777.
69. Pearson, R. J.; Kassianidis, E.; Slawin, A. M. Z.; Philp, D. *Org. Biomol. Chem.* **2004**, *2*, 3434.
70. Kassianidis, E.; Pearson, R. J.; Philp, D. *Chem. -Eur. J.* **2006**, *12*, 8798.
71. Pearson, R. J.; Kassianidis, E.; Slawin, A. M. Z.; Philp, D. *Chem. -Eur. J.* **2006**, *12*, 6829.
72. Kassianidis, E.; Pearson, R. J.; Wood, E. A.; Philp, D. *Faraday Discuss.* **2010**, *145*, 235.
73. Kassianidis, E.; Philp, D. *Angew. Chem., Int. Ed.* **2006**, *45*, 6344.
74. del Amo, V.; Slawin, A. M. Z.; Philp, D. *Org. Lett.* **2008**, *10*, 4589.

75. Amabilino, D. B.; Stoddart, J. F. *Chem. Rev.* **1995**, *95*, 2725.
76. Amabilino, D. B. *Encyclopedia of Supramolecular Chemistry*; Marcel Dekker Inc.; New York **2004**.
77. Lipatov, Y.; Lipatova, T.; Kosyanchuk, L. In *Speciality Polymers/Polymer Physics*; Springer Berlin / Heidelberg: **1989**; Vol. 88, p 49.
78. Breault, G. A.; Hunter, C. A.; Mayers, P. C. *Tetrahedron* **1999**, *55*, 5265.
79. Frisch, H. L.; Wasserman, E. *J. Am. Chem. Soc.* **1961**, *83*, 3789.
80. Walba, D. M. *Tetrahedron* **1985**, *41*, 3161.
81. Siegel, J. S. *Science* **2004**, *304*, 1256.
82. Schill, G. *Catenanes, Rotaxanes and Knots; Academic Press, New York,* **1971**.
83. Dietrich-Buchecker, C. O.; Sauvage, J.-P. *Angew. Chem., Int. Ed.* **1989**, *28*, 189.
84. Pentecost, C. D.; Chichak, K. S.; Peters, A. J.; Cave, G. W. V.; Cantrill, S. J.; Stoddart, J. F. *Angew. Chem., Int. Ed.* **2007**, *46*, 218.
85. Chichak, K. S.; Cantrill, S. J.; Pease, A. R.; Chiu, S.-H.; Cave, G. W. V.; Atwood, J. L.; Stoddart, J. F. *Science* **2004**, *304*, 1308.
86. Cantrill, S. J.; Chichak, K. S.; Peters, A. J.; Stoddart, J. F. *Acc. Chem. Res.* **2005**, *38*, 1.
87. Amabilino, D. B.; Ashton, P. R.; Reder, A. S.; Spencer, N.; Stoddart, J. F. *Angew. Chem., Int. Ed.* **1994**, *33*, 1286.
88. Williams, A. R.; Northrop, B. H.; Chang, T.; Stoddart, J. F.; White, A. J. P.; Williams, D. J. *Angew. Chem., Int. Ed.* **2006**, *45*, 6665.
89. Lüttringhaus, A.; Cramer, F.; Prinzbach, H.; Henglein, F. M. *Justus Liebigs Ann. Chem.* **1958**, *613*, 185.
90. Harrison, I. T.; Harrison, S. *J. Am. Chem. Soc.* **1967**, *89*, 5723.
91. Safarowsky, O.; Windisch, B.; Mohry, A.; Vögtle, F. *J. Prakt. Chem.* **2000**, *342*, 437.
92. Wasserman, E. *J. Am. Chem. Soc.* **1960**, *82*, 4433.
93. Stoddart, J. F. *Chem. Soc. Rev*. **2009**, 38, 1802.
94. Stoddart, J. F.; Tseng, H. R. *Proc. Natl. Acad. Sci. USA* **2002**, *99*, 4797.
95. Griffiths, K. E.; Stoddart, J. F. *Pure Appl. Chem.* **2008**, *80*, 485.
96. Anderson, S.; Anderson, H. L.; Sanders, J. K. M. *Acc. Chem. Res.* **1993**, *26*, 469.
97. Stoddart, J. F. *Nat. Chem.* **2009**, *1*, 14.
98. Ashton, P. R.; Chrystal, E. J. T.; Glink, P. T.; Menzer, S.; Schiavo, C.; Spencer, N.; Stoddart, J. F.; Tasker, P. A.; White, A. J. P.; Williams, D. J. *Chem. -Eur J.* **1996**, *2*, 709.
99. Asakawa, M.; Janssen, H. M.; Meijer, E. W.; Pasini, D.; Stoddart, J. F. *Eur. J. Org. Chem.* **1998**, 983.
100. Loeb, S. J.; Wisner, J. A. *Angew. Chem., Int. Ed.* **1998**, *37*, 2838.
101. Anelli, P. L.; Ashton, P. R.; Spencer, N.; Slawin, A. M. Z.; Stoddart, J. F.; Williams, D. J. *Angew. Chem., Int. Ed.* **1991**, *30*, 1036.
102. Ashton, P. R.; Philp, D.; Spencer, N.; Stoddart, J. F. *J. Chem. Soc., Chem. Commun.* **1991**, 1677.
103. Wisner, J. A.; Beer, P. D.; Drew, M. G. B. *Angew. Chem., Int. Ed.* **2001**, *40*, 3606.
104. Kavallieratos, K.; de Gala, S. R.; Austin, D. J.; Crabtree, R. H. *J. Am. Chem. Soc.* **1997**, *119*, 2325.
105. Kavallieratos, K.; Bertao, C. M.; Crabtree, R. H. *J. Org. Chem.* **1999**, *64*, 1675.

106. Ashton, P. R.; Ballardini, R.; Balzani, V.; Boyd, S. E.; Credi, A.; Gandolfi, M. T.; Gomez-Lopez, M.; Iqbal, S.; Philp, D.; Preece, J. A.; Prodi, L.; Ricketts, H. G.; Stoddart, J. F.; Tolley, M. S.; Venturi, M.; White, A. J. P.; Williams, D. J. *Chem. -Eur. J.* **1997**, *3*, 152.
107. Asakawa, M.; Ashton, P. R.; Iqbal, S.; Quick, A.; Stoddart, J. F.; Tinker, N. D.; White, A. J. P.; Wiliams, D. J. *Isr. J. Chem.* **1996**, *36*, 329.
108. Ashton, P. R.; Johnston, M. R.; Stoddart, J. F.; Tolley, M. S.; Wheeler, J. W. *J. Chem. Soc., Chem. Commun.* **1992**, 1128.
109. Johnston, A.; Leigh, D.; Murphy, A.; Smart, J.; Deegan, M. *J. Am. Chem. Soc.* **1996**, *118*, 10662.
110. Leigh, D.; Murphy, A.; Smart, J.; Slawin, A. *Angew. Chem., Int. Ed.* **1997**, *36*, 728.
111. Cardenas, D. J.; Gaviña, P.; Sauvage, J.-P. *Chem. Commun.* **1996**, 1915.
112. Chambron, J.-C.; Sauvage, J.-P.; Mislow, K. *J. Am. Chem. Soc.* **1997**, *119*, 9558.
113. Armaroli, N.; Diederich, F.; Dietrich-Buchecker, C. O.; Flamigni, L.; Marconi, G.; Nierengarten, J.-F.; Sauvage, J.-P. *Chem. -Eur. J.* **1998**, *4*, 406.
114. Wenz, G.; von der Bey, E.; Schmidt, L. *Angew. Chem., Int. Ed.* **1992**, *31*, 783.
115. Gibson, H. W.; Liu, S.; Lecavalier, P.; Wu, C.; Shen, Y. X. *J. Am. Chem. Soc.* **1995**, *117*, 852.
116. Raymo, F. M.; Stoddart, J. F. *Pure Appl. Chem.* **1997**, *69*, 1987.
117. Fyfe, M. C. T.; Stoddart, J. F. *Acc. Chem. Res.* **1997**, *30*, 393.
118. Ashton, P. R.; Belohradsky, M.; Philp, D.; Stoddart, J. F. *J. Chem. Soc., Chem. Commun.* **1993**, 1269.
119. Stoddart, J. F. *Chem. Br.* **1991**, *27*, 714.
120. Ashton, P. R.; Glink, P. T.; Stoddart, J. F.; Tasker, P. A.; White, A. J. P.; Williams, D. J. *Chem. -Eur. J.* **1996**, *2*, 729.
121. Vögtle, F.; Händel, M.; Meier, S.; Ottens-Hildebrandt, S.; Ott, F.; Schmidt, T. *Liebigs Ann.* **1995**, *1995*, 739.
122. Ashton, P. R.; Ballardini, R.; Balzani, V.; Belohradsky, M.; Gandolfi, M. T.; Philp, D.; Prodi, L.; Raymo, F. M.; Reddington, M. V.; Spencer, N.; Stoddart, J. F.; Venturi, M.; Williams, D. J. *J. Am. Chem. Soc.* **1996**, *118*, 4931.
123. Asakawa, M.; Ashton, P. R.; Ballardini, R.; Balzani, V.; Belohradsky, M.; Gandolfi, M. T.; Kocian, O.; Prodi, L.; Raymo, F. M.; Stoddart, J. F.; Venturi, M. *J. Am. Chem. Soc.* **1997**, *119*, 302.
124. Raymo, F. M.; Houk, K. N.; Stoddart, J. F. *J. Am. Chem. Soc.* **1998**, *120*, 9318.
125. Arico, F.; Badjic, J. D.; Cantrill, S. J.; Flood, A. H.; Leung, K. C. F.; Liu, Y.; Stoddart, J. F. *Templates in Chemistry II* **2005**, *249*, 203.
126. Ashton, P. R.; Belohradsky, M.; Philp, D.; Spencer, N.; Stoddart, J. F. *J. Chem. Soc., Chem. Commun.* **1993**, 1274.
127. Thompson, M. C.; Busch, D. H. *J. Am. Chem. Soc.* **1962**, *84*, 1762.
128. Busch, D. H. *J. Inclusion Phenom. Macrocyclic Chem.* **1992**, *12*, 389.
129. Schill, G.; Lüttringhaus, A. *Angew. Chem., Int. Ed.* **1964**, *3*, 546.
130. Vetter, W.; Schill, G. *Tetrahedron* **1967**, *23*, 3079.
131. Schill, G.; Schweickert, N.; Fritz, H.; Vetter, W. *Chem. Ber.* **1988**, *121*, 961.
132. Schill, G.; Doerjer, G.; Logemann, E.; Fritz, H. *Chem. Ber.* **1979**, *112*, 3603.
133. Dietrich-Buchecker, C. O.; Sauvage, J. P.; Kintzinger, J. P. *Tetrahedron Lett.* **1983**, *24*, 5095.
134. Bickelhaupt, F. *J. Organomet. Chem.* **1994**, *475*, 1.

135. Sauvage, J. P. *Acc. Chem. Res.* **1990**, *23*, 319.
136. Whang, D.; Park, K.-M.; Heo, J.; Ashton, P.; Kim, K. *J.Am. Chem. Soc.* **1998**, *120*, 4899.
137. Fujita, M.; Ogura, K. *Coord. Chem. Rev.* **1996**, *148*, 249.
138. Amabilino, D. B.; Stoddart, J. F. *Pure Appl. Chem.* **1993**, *65*, 2351.
139. Hamilton, D. G.; Davies, J. E.; Prodi, L.; Sanders, J. K. M. *Chem. -Eur. J.* **1998**, *4*, 608.
140. C. Try, A.; M. Harding, M.; G. Hamilton, D.; K. M. Sanders, J. *Chem. Commun.* **1998**, 723.
141. Hunter, C. A. *Chem. Soc. Rev.* **1994**, *23*, 101.
142. Johnston, A. G.; Leigh, D. A.; Pritchard, R. J.; Deegan, M. D. *Angew. Chem., Int. Ed.* **1995**, *34*, 1209.
143. Glink, P. T.; Schiavo, C.; Stoddart, J. F.; Williams, D. J. *Chem. Commun.* **1996**, 1483.
144. Leigh, D. A.; Moody, K.; Smart, J. P.; Watson, K. J.; Slawin, A. M. Z. *Angew. Chem., Int. Ed.* **1996**, *35*, 306.
145. Ottens-Hildebrandt, S.; Meier, S.; Schmidt, W.; Vögtle, F. *Angew. Chem., Int. Ed.* **1994**, *33*, 1767.
146. G. Kolchinski, A.; A. Roesner, R.; H. Busch, D.; W. Alcock, N. *Chem. Commun.* **1998**, 1437.
147. Fyfe, M. C. T.; Stoddart, J. F. *Coord. Chem. Rev.* **1999**, *183*, 139.
148. Sauvage, J. *Acc. Chem. Res.* **1998**, *31*, 611.
149. Collin, J.-P.; Dietrich-Buchecker, C.; Gaviña, P.; Jimenez-Molero, M. C.; Sauvage, J.-P. *Acc. Chem. Res.* **2001**, *34*, 477.
150. Poleschak, I.; Kern, J.-M.; Sauvage, J.-P. *Chem. Commun.* **2004**, 474.
151. Odell, B.; Reddington, M. V.; Slawin, A. M. Z.; Spencer, N.; Stoddart, J. F.; Williams, D. J. *Angew. Chem., Int. Ed.* **1988**, *27*, 1547.
152. Hernandez, R.; Tseng, H. R.; Wong, J. W.; Stoddart, J. F.; Zink, J. I. *J. Am. Chem. Soc.* **2004**, *126*, 3370.
153. Ashton, P. R.; Goodnow, T. T.; Kaifer, A. E.; Reddington, M. V.; Slawin, A. M. Z.; Spencer, N.; Stoddart, J. F.; Vicent, C.; Williams, D. J. *Angew. Chem., Int. Ed.* **1989**, *28*, 1396.
154. Philp, D.; Slawin, A. M. Z.; Spencer, N.; Stoddart, J. F.; Williams, D. J. *J. Chem. Soc., Chem. Commun.* **1991**, 1584.
155. Hunter, C. A.; Sanders, J. K. M. *J. Am. Chem. Soc.* **1990**, *112*, 5525.
156. Hunter, C. A. *Angew. Chem., Int. Ed.* **1993**, *32*, 1584.
157. Jeppesen, J. O.; Nielsen, K. A.; Perkins, J.; Vignon, S. A.; Di Fabio, A.; Ballardini, R.; Gandolfi, M. T.; Venturi, M.; Balzani, V.; Becher, J.; Stoddart, J. F. *Chem. -Eur. J.* **2003**, *9*, 2982.
158. Raehm, L.; Hamilton, D. G.; Sanders, J. K. M. *Synlett.* **2002**, 1743.
159. Hunter, C. A. *J. Am. Chem. Soc.* **1992**, *114*, 5303.
160. Vögtle, F.; Meier, S.; Hoss, R. *Angew. Chem., Int. Ed.* **1992**, *31*, 1619.
161. Adams, H.; Carver, F. J.; Hunter, C. A. *J. Chem. Soc., Chem. Commun.* **1995**, 809.
162. Altieri, A.; Gatti, F. G.; Kay, E. R.; Leigh, D. A.; Martel, D.; Paolucci, F.; Slawin, A. M. Z.; Wong, J. K. Y. *J. Am. Chem. Soc.* **2003**, *125*, 8644.
163. Lane, A. S.; Leigh, D. A.; Murphy, A. *J. Am. Chem.Soc.* **1997**, *119*, 11092.
164. Gatti, F. G.; Leigh, D. A.; Nepogodiev, S. A.; Slawin, A. M. Z.; Teat, S. J.; Wong, J. K. Y. *J. Am. Chem. Soc.* **2001**, *123*, 5983.

165. Asakawa, M.; Brancato, G.; Fanti, M.; Leigh, D. A.; Shimizu, T.; Slawin, A. M. Z.; Wong, J. K. Y.; Zerbetto, F.; Zhang, S. *J. Am. Chem. Soc.* **2002**, *124*, 2939.
166. Da Ros, T.; Guldi, D. M.; Morales, A. F.; Leigh, D. A.; Prato, M.; Turco, R. *Org. Lett.* **2003**, *5*, 689.
167. Altieri, A.; Bottari, G.; Dehez, F.; Leigh, D. A.; Wong, J. K. Y.; Zerbetto, F. *Angew. Chem., Int. Ed.* **2003**, *42*, 2296.
168. Keaveney, C. M.; Leigh, D. A. *Angew. Chem., Int. Ed.* **2004**, *43*, 1222.
169. Rowan, S. J.; Cantrill, S. J.; Stoddart, J. F. *Org. Lett.* **1999**, *1*, 129.
170. Rowan, S. J.; Stoddart, J. F. *J. Am. Chem. Soc.* **2000**, *122*, 164.
171. Chiu, S. H.; Rowan, S. J.; Cantrill, S. J.; Stoddart, J. F.; White, A. J. P.; Williams, D. L. *Chem. -Eur. J.* **2002**, *8*, 5170.
172. Hübner, G. M.; Gläser, J.; Seel, C.; Vögtle, F. *Angew. Chem. Int. Ed.* **1999**, *38*, 383.
173. Reuter, C.; Wienand, W.; Hübner, G. M.; Seel, C.; Vögtle, F. *Chem. -Eur. J.* **1999**, *5*, 2692.
174. Schmieder, R.; Hübner, G.; Seel, C.; Vögtle, F. *Angew. Chem., Int. Ed.* **1999**, *38*, 3528.
175. Mahoney, J. M.; Shukla, R.; Marshall, R. A.; Beatty, A. M.; Zajicek, J.; Smith, B. D. *J. Org. Chem.* **2002**, *67*, 1436.
176. Ghosh, P.; Mermagen, O.; Schalley, C. A. *Chem. Commun.* **2002**, 2628.
177. Linnartz, P.; Bitter, S.; Schalley, Christoph A. *Eur. J. Org. Chem.* **2003**, *2003*, 4819.
178. Pease, A. R.; Jeppesen, J. O.; Stoddart, J. F.; Luo, Y.; Collier, C. P.; Heath, J. R. *Acc. Chem. Res.* **2001**, *34*, 433.
179. Sauvage, J.-P.; Dietrich-Buchecker, C. *Molecular Catenanes, Rotaxanes and Knots : A Journey Through the World of Chemical Topology*; Wiley-VCH, Weinheim, Germany **1999**.
180. Gomez-Lopez, M.; Preece, J. A.; Stoddart, J. F. *Nanotechnology* **1996**, *7*, 183.
181. Balzani, V.; Gomez-Lopez, M.; Stoddart, J. F. *Acc. Chem. Res.* **1998**, *31*, 405.
182. Schalley, C.; Beizai, K.; Vögtle, F. *Acc. Chem. Res.* **2001**, *34*, 465.
183. Raehm, L.; Kern, J.-M.; Sauvage, J.-P. *Chem. -Eur. J.* **1999**, *5*, 3310.
184. Martinez-Diaz, M. V.; Spencer, N.; Stoddart, J. F. *Angew. Chem., Int. Ed.* **1997**, *36*, 1904.
185. Kelly, T. R.; De Silva, H.; Silva, R. A. *Nature* **1999**, *401*, 150.
186. Elizarov, A. M.; Chiu, S. H.; Stoddart, J. F. *J. Org. Chem.* **2002**, *67*, 9175.
187. Gaviña, P.; Sauvage, J.-P. *Tetrahedron Lett.* **1997**, *38*, 3521.
188. Armaroli, N.; Balzani, V.; Collin, J.-P.; Gaviña, P.; Sauvage, J.-P.; Ventura, B. *J. Am. Chem. Soc.* **1999**, *121*, 4397.
189. Ashton, P. R.; Ballardini, R.; Balzani, V.; Credi, A.; Dress, K. R.; Ishow, E.; Kleverlaan, C. J.; Kocian, O.; Preece, J. A.; Spencer, N.; Stoddart, J. F.; Venturi, M.; Wenger, S. *Chem. -Eur. J.* **2000**, *6*, 3558.
190. Blanco, M.-J.; Consuelo Jimenez, M.; Chambron, J.-C.; Heitz, V.; Linke, M.; Sauvage, J.-P. *Chem. Soc. Rev.* **1999**, *28*, 293.
191. Mulder, A.; Jukovic, A.; Lucas, L. N.; van Esch, J.; Feringa, B. L.; Huskens, J.; Reinhoudt, D. N. *Chem. Commun.* **2002**, 2734.
192. Tseng, H. R.; Wu, D. M.; Fang, N. X. L.; Zhang, X.; Stoddart, J. F. *Chemphyschem* **2004**, *5*, 111.
193. Raehm, L.; Kern, J.-M.; Sauvage, J.-P.; Hamann, C.; Palacin, S.; Bourgoin, J.-P. *Chem. -Eur. J.* **2002**, *8*, 2153.

194. Beckman, R.; Beverly, K.; Boukai, A.; Bunimovich, Y.; Choi, J. W.; Delonno, E.; Green, J.; Johnston-Halperin, E.; Luo, Y.; Sheriff, B.; Stoddart, J. F.; Heath, J. R. *Faraday Discuss.* **2006**, *131*, 9.
195. Collier, C. P.; Mattersteig, G.; Wong, E. W.; Luo, Y.; Beverly, K.; Sampaio, J.; Raymo, F. M.; Stoddart, J. F.; Heath, J. R. *Science* **2000**, *289*, 1172.
196. Collier, C. P.; Jeppesen, J. O.; Luo, Y.; Perkins, J.; Wong, E. W.; Heath, J. R.; Stoddart, J. F. *J. Am. Chem. Soc.* **2001**, *123*, 12632.
197. Diehl, M. R.; Steuerman, D. W.; Tseng, H.-R.; Vignon, S. A.; Star, A.; Celestre, P. C.; Stoddart, J. F.; Heath, J. R. *ChemPhysChem* **2003**, *4*, 1335.
198. Luo, Y.; Collier, C. P.; Jeppesen, J. O.; Nielsen, K. A.; Delonno, E.; Ho, G.; Perkins, J.; Tseng, H. R.; Yamamoto, T.; Stoddart, J. F.; Heath, J. R. *Chemphyschem* **2002**, *3*, 519.
199. Green, J. E.; Choi, J. W.; Boukai, A.; Bunimovich, Y.; Johnston-Halperin, E.; Delonno, E.; Luo, Y.; Sheriff, B. A.; Xu, K.; Shin, Y. S.; Tseng, H.-R.; Stoddart, J. F.; Heath, J. R. *Nature* **2007**, *445*, 414.
200. Vidonne, A. PhD thesis, University of St. Andrews, 2009.
201. Garcia-Tellado, F.; Goswami, S.; Chang, S. K.; Geib, S. J.; Hamilton, A. D. *J. Am. Chem. Soc.* **1990**, *112*, 7393.
202. Garcia-Tellado, F.; Albert, J.; Hamilton, A. D. *J. Chem. Soc., Chem. Commun.* **1991**, 1761.
203. Goodman, M. S.; Weiss, J.; Hamilton, A. D. *Tetrahedron Lett.* **1994**, *35*, 8943.
204. Huisgen, R. *J. Org. Chem.* **1976**, *41*, 403.
205. Huisgen, R.; Weinberger, R. *Tetrahedron Lett.* **1985**, *26*, 5119.
206. Tufariello, J. J.; Puglis, J. M. *Tetrahedron Lett.* **1986**, *27*, 1265.
207. Vidonne, A.; Philp, D. *Tetrahedron* **2008**, *64*, 8464.
208. Illuminati, G.; Mandolini, L. *Acc. Chem. Res.* **1981**, *14*, 95.
209. Lindoy, L. F. *The Chemistry of Macrocyclic Ligand Complexes*; Cambridge University Press, England **1989**.
210. Steed, J. W.; Atwood, J. L. *Supramolecular Chemistry*; John Wiley & Sons, Ltd; England **2000**.
211. Alvarez-Pérez, M.; Goldup, S. M.; Leigh, D. A.; Slawin, A. M. Z. *J. Am. Chem. Soc.* **2008**, *130*, 1836.
212. Altieri, A.; Aucagne, V.; Carrillo, R.; Clarkson, G. J.; D'Souza, D. M.; Dunnett, J. A.; Leigh, D. A.; Mullen, K. M. *Chem. Sci.* **2011**.
213. Fioravanti, G.; Haraszkiewicz, N.; Kay, E. R.; Mendoza, S. M.; Bruno, C.; Marcaccio, M.; Wiering, P. G.; Paolucci, F.; Rudolf, P.; Brouwer, A. M.; Leigh, D. A. *J. Am. Chem. Soc.* **2008**, *130*, 2593.
214. Serreli, V.; Lee, C. F.; Kay, E. R.; Leigh, D. A. *Nature* **2007**, *445*, 523.
215. Berna, J.; Brouwer, A. M.; Fazio, S. M.; Haraszkiewicz, N.; Leigh, D. A.; Lennon, C. M. *Chem. Commun.* **2007**, 1910.
216. Chatterjee, M. N.; Kay, E. R.; Leigh, D. A. *J. Am. Chem. Soc.* **2006**, *128*, 4058.
217. Radha Kishan, M.; Parham, A.; Schelhase, F.; Yoneva, A.; Silva, G.; Chen, X.; Okamoto, Y.; Vögtle, F. *Angew. Chem., Int. Ed.* **2006**, *45*, 7296.
218. Chmielewski, M. J.; Jurczak, J. *Chem. -Eur. J.* **2005**, *11*, 6080.
219. Vögtle, F.; Jager, R.; Handel, M.; OttensHildebrandt, S. *Pure Appl. Chem.* **1996**, *68*, 225.
220. Li, Qian Y.; Vogel, E.; Parham, Amir H.; Nieger, M.; Bolte, M.; Fröhlich, R.; Saarenketo, P.; Rissanen, K.; Vögtle, F. *Eur. J. Org. Chem.* **2001**, *2001*, 4041.
221. Murray-Rust, P.; Glusker, J. P. *J. Am. Chem. Soc.* **1984**, *106*, 1018.

222. Fairlamb, I. J. S.; Bauerlein, P. S.; Marrison, L. R.; Dickinson, J. M. *Chem. Commun.* **2003**, 632.
223. Karplus, M. *J. Am. Chem. Soc.* **1963**, *85*, 2870.
224. Simonis, H. *Chem. Ber.* **1912**, *45*, 1584.
225. P. W. Oxley, B. M. A., M. J. Sasse, and M. A. Forth *Org. Synth.* **1993**, *8*, 16.
226. Rocha, G. B.; Freire, R. O.; Simas, A. M.; Stewart, J. J. P. *J. Comput. Chem.* **2006**, *27*, 1101.
227. Leigh, D. A.; Perez, E. M. *Chem. Commun.* **2004**, 2262.
228. Zehnder, D.; Smithrud, D. *Org. Lett.* **2001**, *3*, 2485.
229. Oku, T.; Furusho, Y.; Takata, T. *Org. Lett.* **2003**, *5*, 4923.
230. Craig, M. R.; Hutchings, M. G.; Claridge, T. D. W.; Anderson, H. L. *Angew. Chem., Int. Ed.* **2001**, *40*, 1071.
231. Hassan, N. I.; del Amo, V.; Calder, E.; Philp, D. *Org. Lett.* **2011**, *3*, 458.
232. Furusho, Y.; Matsuyama, T.; Takata, T.; Moriuchi, T.; Hirao, T. *Tetrahedron Lett.* **2004**, *45*, 9593.
233. Leigh, D. A.; Thomson, A. R. *Org. Lett.* **2006**, *8*, 5377.
234. Huang, Y.-L.; Hung, W.-C.; Lai, C.-C.; Liu, Y.-H.; Peng, S.-M.; Chiu, S.-H. *Angew. Chem., Int. Ed.* **2007**, *46*, 6629.
235. Fyfe, M. C. T.; Raymo, F. M.; Stoddart, J. F. In *Stimulating Concepts in Chemistry*; Wiley-VCH; Weinheim, Germany **2005**.
236. del Amo, V.; Philp, D. *Org. Lett.* **2009**, *11*, 301.
237. Ito, J.-i.; Miyakawa, T.; Nishiyama, H. *Organometallics* **2006**, *25*, 5216.
238. Vickers, M. S.; Beer, P. D. *Chem. Soc. Rev.* **2007**, *36*, 211.
239. Sambrook, M. R.; Beer, P. D.; Wisner, J. A.; Paul, R. L.; Cowley, A. R.; Szemes, F.; Drew, M. G. B. *J. Am. Chem. Soc.* **2005**, *127*, 2292.
240. Koulov, A. V.; Mahoney, J. M.; Smith, B. D. *Org. Biomol. Chem.* **2003**, *1*, 27.
241. Ema, T.; Hamada, K.; Sugita, K.; Nagata, Y.; Sakai, T.; Ohnishi, A. *J. Org. Chem.* **2010**, *75*, 4492.
242. Zhao, L.; Davis, J. J.; Mullen, K. M.; Chmielewski, M. Ç. J.; Jacobs, R. M. J.; Brown, A.; Beer, P. D. *Langmuir* **2009**, *25*, 2935.
243. Wessendorf, F.; Hirsch, A. *Tetrahedron* **2008**, *64*, 11480.
244. Taylor, E. C.; Ray, P. S. *J. Org. Chem.* **1988**, *53*, 35.
245. Kidd, T. J.; Leigh, D. A.; Wilson, A. J. *J. Am. Chem. Soc.* **1999**, *121*, 1599.
246. Kidd, T.; Loontjens, T.; Leigh, D.; Wong, J. *Angew. Chem., Int. Ed.* **2003**, *42*, 3379.
247. Zhou, W.; Zhang, S.; Li, G.; Zhao, Y.; Shi, Z.; Liu, H.; Li, Y. *ChemPhysChem* **2009**, *10*, 2066.
248. Hannam, J. S.; Kidd, T. J.; Leigh, D. A.; Wilson, A. J. *Org. Lett.* **2003**, *5*, 1907.
249. Mullen, K. M.; Davis, J. J.; Beer, P. D. *New J. Chem.* **2009**, *33*, 769.
250. Zhao, L.; Mullen, K. M.; Chmielewski, M. J.; Brown, A.; Bampos, N.; Beer, P. D.; Davis, J. J. *New J. Chem.* **2009**, *33*, 760.
251. Lovric, M.; Cepanec, I.; Litvic, M.; Bartolincic, A.; Vinkovic, V. *Croat. Chem. Acta* **2007**, *80*, 109.
252. Aucagne, V.; Leigh, D.; Lock, J.; Thomson, A. *J. Am. Chem. Soc.* **2006**, *128*, 1784.
253. Aucagne, V.; Berná, J.; Crowley, J. D.; Goldup, S. M.; Hänni, K. D.; Leigh, D. A.; Lusby, P. J.; Ronaldson, V. E.; Slawin, A. M. Z.; Viterisi, A.; Walker, D. B. *J. Am. Chem. Soc.* **2007**, *129*, 11950.
254. Seel, C.; Parham, A. H.; Safarowsky, O.; Hübner, G. M.; Vögtle, F. *J. Org. Chem.* **1999**, *64*, 7236.

255. Heim, C.; Affeld, A.; Nieger, M.; Vogtle, F. *Helv. Chim. Acta* **1999**, *82*, 746.
256. Ashton, P. R.; Fyfe, M. C. T.; Hickingbottom, S. K.; Stoddart, J. F.; White, A. J. P.; Williams, D. J. *J. Chem. Soc. Perkin Trans. 2* **1998**, 2117.
257. Ashton, P. R.; Baxter, I.; Fyfe, M. C. T.; Raymo, F. M.; Spencer, N.; Stoddart, J. F.; White, A. J. P.; Williams, D. J. *J. Am. Chem. Soc.* **1998**, *120*, 2297.
258. Bottero, I. Unpublished results, University of St. Andrews, 2010.
259. Nierth, A.; Kobitski, A. Y.; Nienhaus, G. U.; JaÃàschke, A. *J. Am. Chem. Soc.* **2010**, *132*, 2646.
260. Carroll, F. I.; Lee, J. R.; Navarro, H. n. A.; Brieaddy, L. E.; Abraham, P.; Damaj, M. I.; Martin, B. R. *J. Med. Chem.* **2001**, *44*, 4039.
261. Robinson, J. M. A. PhD Thesis, University of Birmingham 2000.
262. Huck, J. PhD Thesis, University of St. Andrews, 2011.
263. Isaacs, N. S. *Physical organic chemistry*; Longman Scientific & Technical ; England **1987**.
264. Tamiaki, H.; Ogawa, K.; Enomoto, K.; Taki, K.; Hotta, A.; Toma, K. *Tetrahedron* **2010**, *66*, 1661.
265. Boiocchi, M.; Del Boca, L.; Gomez, D. E.; Fabbrizzi, L.; Licchelli, M.; Monzani, E. *J. Am. Chem.Soc.* **2004**, *126*, 16507.
266. Armarego, W. L. F.; Chia, C. *Purification of Laboratory Chemicals*; Butterworth-Heinemnann, Oxford **2009**.
267. Stewart, J. J. P. *J. Comput. Chem.* **1989**, *10*, 221.
268. Stewart, J. J. P. MOPAC2009, Stewart Computational Chemistry, Colorado Springs, CO, USA, http://openmopacnet. 2007.
269. Latyshev, G. V.; Baranov, M. S.; Kazantsev, A. V.; Averin, A. D.; Lukashev, N. V.; Beletskaya, I. P. *Synthesis* **2009**, *15*, 2605.
270. Hall, A.; Billinton, A.; Bristow, A. K.; Brown, S. H.; Chowdhury, A.; Cutler, L.; Giblin, G. M. P.; Goldsmith, P.; Hayhow, T. G.; Kilford, I. R.; Naylor, A.; Passingham, B.; Rawlings, D. A. *Bioorg. Med. Chem. Lett.* **2008**, *18*, 4027.
271. Evans, N. H.; Beer, P. D. *Org. Biomol. Chem.* **2011**, *9*, 92.
272. Taylor, E. C.; Wong, G. S. K. *J. Org. Chem.* **1989**, *54*, 3618.
273. Philp, D.; Gramlich, V.; Seiler, P.; Diederich, F. *J. Chem. Soc. Perkin Trans. 2* **1995**, 875.
274. Hwang, S.-H.; Moorefield, C. N.; Cha, H.-C.; Wang, P.; Newkome, G. R. *Des. Monomers Polym.* **2006**, *9*, 413.
275. Akiyama, S.; Tajima, K.; Nakatsuji, S; Nakashima, K.; Abiru, K.; Watanabe, M. *Bull. Chem. Soc. Jpn.* **1995**, *68*, 2043.
276. Sun, Z.; Ahmed, S.; McLaughlin, L. W. *J. Org. Chem.* **2006**, *71*, 2922.
277. Branca, M.; Gamba, A.; Saba, A.; Barzaghi, M.; Simonetta, M. *J. Chem. Soc., Perkin Trans. 2* **1982**, 349.
278. Graham, E. M.; Miskowski, V. M.; Perry, J. W.; Coulter, D. R.; Stiegman, A. E.; Schaefer, W. P.; Marsh, R. E. *J. Am. Chem. Soc.* **1989**, *111*, 8771.
279. Bao, C.; Lu, R.; Jin, M.; Xue, P.; Tan, C.; Xu, T.; Liu, G.; Zhao, Y. *Chem. -Eur. J.* **2006**, *12*, 3287.

Appendixes

A1. Crystal data and structure refinement for macrocycle MEU

Empirical formula	$C_{94}\ H_{103}\ Cl_{12}\ N_{15}\ O_{15}$	
Formula weight	2108.31	
Temperature	93(2) K	
Wavelength	0.71073 Å	
Crystal system	Triclinic	
Space group	P-1	
Unit cell dimensions	a = 13.462(4) Å	a= 84.36(3)°
	b = 15.659(4) Å	b= 79.435(19)°
	c = 29.611(8) Å	g = 80.75(3)°
Volume	6041(3) $Å^3$	
Z	2	
Density (calculated)	1.159 Mg/m^3	
Absorption coefficient	0.333 mm^{-1}	
F(000)	2192	
Crystal size	0.18 x 0.06 x 0.02 mm^3	
Theta range for data collection	1.86 to 25.36°	
Index ranges	-16<=h<=14, -18<=k<=14, -29<=l<=35	
Reflections collected	37771	
Independent reflections	20910 [R(int) = 0.1473]	
Completeness to theta = 25.00°	95.0 %	
Absorption correction	Multiscan	
Max. and min. transmission	1.00000 and .8763	
Refinement method	Full-matrix least-squares on F^2	
Data / restraints / parameters	20910 / 834 / 1189	
Goodness-of-fit on F^2	0.884	
Final R indices [I>2sigma(I)]	R1 = 0.1977, wR2 = 0.4395	
R indices (all data)	R1 = 0.4225, wR2 = 0.5393	
Largest diff. peak and hole	0.876 and –0.479 $e.Å^{-3}$	

A2. Publication

Low Temperature Capture of Pseudorotaxanes

Nurul Izzaty Hassan, Vicente del Amo, Ewen Calder, and Douglas Philp

EaStCHEM and Centre for Biomolecular Sciences, School of Chemistry, University of St Andrews, North Haugh, St Andrews, Fife KY16 9ST, United Kingdom

Organic Letters 2011, Vol. 13, No. 3 458-461
doi: 10.1021/ol1027915